THE PHYSICAL REVIEW

A journal of experimental and theoretical physics established by E. L. Nichols in 1893

Published by the American Institute of Physics for the

AMERICAN PHYSICAL SOCIETY

Officers

President

C. C. LAURITSEN
California Institute of Technology
Pasadena, California

Vice-President

J. H. VAN VLECK
Harvard University
Cambridge, Massachusetts

Secretary

K. K. DARROW
Bell Telephone Laboratories
Office:
Columbia University
New York 27, New York

Treasurer

G. B. PEGRAM
Columbia University
New York 27, New York

Local Secretary for the Pacific Coast

J. KAPLAN
University of California at Los Angeles
Los Angeles, California

Managing Editor

S. A. GOUDSMIT
Brookhaven National Laboratory
Upton, Long Island
New York

BOARD OF EDITORS

Editor

S. A. Goudsmit — Brookhaven National Laboratory

Associate Editors

J. Barnes	Harvey Brooks	H. Margenau
T. Bonner	R. F. Christy	H. Primakoff
R. G. Herb	C. L. Critchfield	A. H. Rose
W. E. Lamb, Jr.	M. Deutsch	A. Tonomura
A. J. F. Siegert	T. H. Johnson	H. Tompkins
W. E. Stephens	Bruno Rossi	C. H. Townes

Manuscripts for publication should be submitted to S. A. Goudsmit, Brookhaven National Laboratory, Upton, Long Island, New York. Authors' institutions are requested to pay a publication charge of $20 per page which, if honored, entitles them to 100 free reprints. Instructions will be sent with galley proofs.

Proof and all correspondence concerning papers in the process of publication should be addressed to the Publication Manager, American Institute of Physics, 57 East 55 Street, New York 22, New York.

Subscription Price

United States and Canada $15.00
Elsewhere $17.00

Back Numbers

Yearly back number rate when complete year is available:
Prior to 1949: $20.00
Thereafter: $27.00
Single copies: $2.00 each, prior to July, 1929;
$1.00 each, July, 1929–December, 1941;
$2.00 each, January, 1942–December, 1946;
$1.00 each, January, 1947–December, 1948;
$1.25 each, thereafter.
General index, 1893–1920: $4.00.

Subscriptions, renewals, and orders for back numbers should be addressed to the American Institute of Physics, 57 East 55 Street, New York 22, New York.

Changes of address in the case of members of the American Physical Society should be addressed to the Treasurer; in the case of other subscribers, to the American Institute of Physics.

[The Secretary is at Physics Department, Cornell University, Ithaca, New York.]

This [illegible] published semi-monthly at Prince and Lemon Streets, Lancaster, Pennsylvania.

Entered as second-class matter August 6, 1947, at the Post Office at Lancaster, Pennsylvania, under the Act of March 3, 1879.

Acceptance for mailing at special rate of postage provided for in paragraph (d-2), section 34.40, P. L. & R. of 1948, authorized August 21, [illegible]

THE
PHYSICAL REVIEW

A journal of experimental and theoretical physics established by E. L. Nichols in 1893

SECOND SERIES, VOL. 82, NO. 2 APRIL 15, 1951

Proton-Proton Scattering at 5 Mev*

K. B. MATHER†
Department of Physics, Washington University, St. Louis, Missouri
(Received December 8, 1950)

A scattering chamber has been constructed which employs a number of radial slit units arranged at various angles with respect to the collimated beam of protons. A photographic plate is placed behind each slit unit and the tracks of protons which are scattered into the plate can be counted. To obtain cross sections from this apparatus the number of tracks per unit area must be determined. Protons were scattered from hydrogen gas at approximately 1.5-cm Hg pressure. Advantages of the design were relatively simple geometry, data obtained simultaneously at all angles, almost complete freedom from impurity-scattering, and short cyclotron running times. The differential cross sections were measured for 5.07-Mev protons from 14° to 150° in the center-of-mass system. The results indicate an *S*-wave phase shift of 54.5±0.6° and a repulsive *P*-wave phase shift of 0.05±0.09°. They are therefore quite consistent with pure *S*-wave scattering.

I. INTRODUCTION

HIGH precisions have been reached in proton–proton scattering experiments at energies attainable in van de Graaff type ion accelerators. In the present work it was desired to extend the results to energies of 5 Mev and at the same time maintain a high order of precision. It was accordingly necessary to use a cyclotron as the accelerator and to determine the energy of the beam from it with considerable accuracy. Furthermore, because of the danger of fluctuating performance of the cyclotron, the beam energy measurement had properly to be made during the actual scattering runs. Finally, it was felt that a large angle range should be studied in the hope of observing effects of *P*-wave scattering.

The use of nuclear photographic emulsions to record the tracks of scattered particles provides many advantages. These include in particular the recording of data simultaneously at all the angles studied and a discriminating power between real and spurious tracks.

The 45-inch cyclotron at Washington University, producing 5.1-Mev protons was the source of the high energy particles.

II. APPARATUS

A semi-schematic diagram of the scattering chamber is shown in Fig. 1. Details of the construction can be read from the figure. The beam from the cyclotron enters the chamber through a collimator, and the protons not scattered end their flight in a Faraday cage collector located diametrically across the circular chamber from the collimator. The principal scattering of the proton beam occurs in the gas in the open region seen in the figure in the center of the ring-shaped element which occupies the larger part of the scattering chamber. This element contains a series of radial holes fitted with slit systems so that particles scattered near the center of the ring at the requisite angles will pass through the appropriate holes. By careful machining and measurement, the angle-ranges covered by each slit system were determined with good precision. At the outer end of each hole, a block was mounted, tilted at a small angle, on which a nuclear emulsion plate could be placed to record as an emulsion track each particle that emerged from the corresponding slits at the given angle.

Extensive tests were necessary to establish a collimator design which would reduce adequately the number of particles scattered from slit edges and other metal surfaces. Some such scattering continued to appear at the small scattering angles, and a negligible amount resulting from multiple scattering from the walls at higher angles. The final design is shown in Fig. 2.

The angles at which scattering could be observed were, on one side, at 7°, 11°, 16°, 21°, 30°, 40°, 50°, 60°,

* Assisted by the joint program of the ONR and AEC.
† Now at Birmingham University, Birmingham, England.

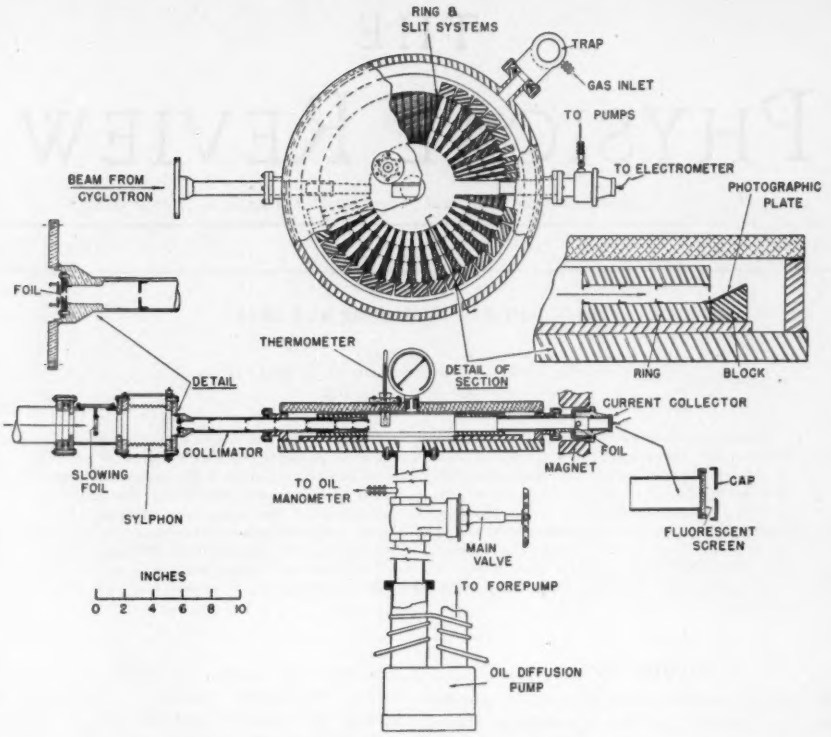

FIG. 1. Plan and side elevation of photographic scattering chamber.

and 70°. On the other side, the slits were equally spaced at 10° intervals from 15° to 165°. Comparison readings of scattering to the right and left, respectively, at the same angle value served to disclose any discrepancies in alignment or machining.

The apparatus was initially aligned relative to the incoming beam from the cyclotron by removing the bottom of the Faraday cage and replacing it with a glass window coated with fluorescent material. When a fluorescing spot appeared accurately centered, the alignment was satisfactory. During actual runs, the Faraday cage was also fitted with an external permanent magnet providing approximately 500 gauss in the cage.

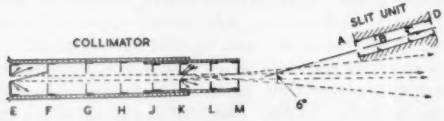

FIG. 2. Schematic of collimator and typical slit unit showing defining slits EK and baffle system FGHJLM designed to minimize slit scattering. Baffle M limits the cone of particles spraying from the edges of slit K to ~6°.

This arrangement served to prevent escape of secondary electrons from the cage.

A trap containing dry ice and acetone was attached to the main chamber. Its chief function was to freeze out the water vapor released by the photographic plates. A schematic of the vacuum system and gas filling controls is shown in Fig. 3.

The use of silicone oil was an essential feature of the present design. No bypass for the diffusion pump was incorporated. Operation of the chamber involved cycles of loading, pumping out, exposing, and unloading. Hence, the oil was always hot when air was admitted. (Frequently the heaters were not even switched off.) In spite of this ruthless treatment over a period of several months, the silicone oil showed no deterioration. (It was, however, found necessary to use the Distillation Products Ion Gauge, Type VG-1A. Several other types of gauge were poisoned by silicone oil vapor.)

With no plates present the chamber could be evacuated to 2×10^{-6} mm Hg after several days of pumping. In order to keep plate background (gamma- and neutron-induced) as low as possible the cyclotron was never operated between loading the chamber and

commencing the scattering run. Hence, in the interest of economy of cyclotron time the prepumping period was kept as short as possible. With plates present, the trap filled and, allowing about three hours for pumping, the chamber vacuum was usually $1-3\times10^{-5}$ mg Hg. The vacuum in the current collector space was $\sim10^{-6}$ mg Hg.

Theory

Figure 4 represents an idealized geometry of one slit unit. Here it is assumed that the beam is of infinitesimal cross section, that scattering is studied in a plane bisecting the slit height and containing the beam axis, and that scattering occurs at exactly angle Θ. Then it can be shown that

$$\sigma(\Theta)=n_a Rh\sin\Theta/N_{ee}N_i 2b\sin\Theta=n_a Rh\cdot F/N_{ee}N_i,$$

where $\sigma(\Theta)$ is the differential cross section in the laboratory system, for scattering plus recoil at angle Θ, n_a is the number of proton tracks per unit area as determined from an element of area situated at distances h and R, respectively, from the slit A and the midpoint of the scattering length, Φ is the angle between the surface of the photographic plate and the plane of the figure, $2b$ the width of slit A, N_{ee} the number of scattering protons per unit volume, and N_i the number of incident protons. F could be calculated for each slit unit. (h and R are more conveniently dealt with as $h'+\Delta h$ and $R'+\Delta R$, where h' is the distance between slits A and D and R' is the distance from scattering volume to slit D.)

During the design of the chamber the magnitudes of $2b$ and Φ were juggled so as to maintain n_a comparable at all Θ, thereby avoiding having to give different exposures for different ranges of Θ. Moreover, as scattering of charged particles is always so much more intense in the forward direction, this criterion did not clash with the desire to keep $2b$ small there in order to preserve good resolution. Another factor which influenced Φ was the range in photographic emulsions of protons at angle Θ because it was highly desirable that the protons come to rest in the emulsion, (Sec. V).

When the particles have equal masses, as in the present case, the energy of a particle scattered or recoiling at an angle Θ is related to the initial energy E_0 by the relation $E=E_0\cos^2\Theta$. Hence, E for each slit was calculated and the expected range in emulsion read from a range-energy curve.[1] Energies and ranges are listed in Table I for $E_0=5$.

The experimental cross sections were converted to cross sections in the center-of-mass system by

$$\sigma(\theta)=\sigma(\Theta)/4\cos\Theta,$$

where θ is the center-of-mass angle and $\theta=2\Theta$. (Relativistic effects are negligible at the energy of this experiment, $\beta=0.1035$.)

[1] Lattes, Fowler, and Cuer, Proc. Phys. Soc. (London) **59**, 883 (1947).

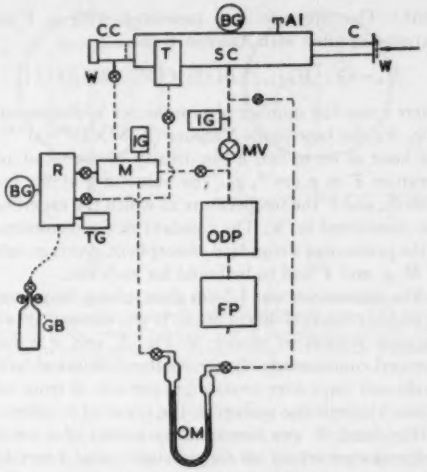

FIG. 3. Schematic of vacuum system and gas-filling controls. SC, scattering chamber; C, collimator; CC, current collector; BG, Bourdon gauge; AI, air inlet; T, trap; W, window; MV, main valve; M, manifold; R, reservoir; GB, gas bottle; OM, oil manometer; ODP, oil diffusion pump; FP, forepump; IG, ion gauge; TG, thermogauge. All valves except the main valve were Hoke sylphon-sealed, needle valves.

III. GAS SUPPLY AND MEASUREMENT OF N_{ee}

Hydrogen was contained in a small cylinder connected to the vacuum system as shown in Fig. 3. It was admitted to the reservoir at a few pounds per square inch and thence to the chamber via a needle valve. No attempt was made to purify the gas. Highest purity commercially available hydrogen (99.8 percent) was purchased from the Matheson Company, Joliet, Illinois. It was one of the principal advantages of the photographic chamber that preliminary purification was unnecessary, since spurious tracks were distinguishable at most angles.

N_{ee} is the number of scattering protons per unit volume at the pressure and temperature of the experi-

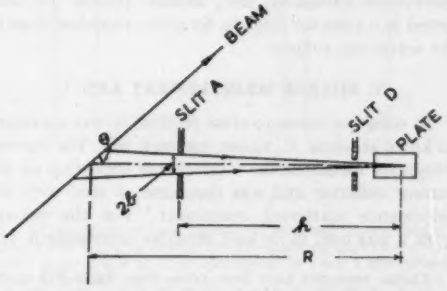

FIG. 4. Idealized geometry of a slit unit for angle of scattering Θ. Slit A defines (together with R and h) the length of the beam which can be seen by an infinitesimal area of plate.

ment.[2] The pressure was measured with a U-tube manometer filled with Apiezon B oil.

$$N_{cc}=rN_L\{H\rho g_{SL}/1.01325\times10^6\}\cdot\{273.18/T\},$$

where r was the number of protons per hydrogen molecule, N_L the Loschmidt Number (2.687×10^{19} cm^{-3}), H the head of oil in cm, ρ the density of the oil at temperature T in g cm^{-3}, g_{SL} the value of g at St. Louis (980.0), and T the temperature at which the experiment was conducted in °K. The constant in the denominator is the pressure of a standard atmosphere. Average values of H, ρ, and T had to be found for each run.

The manometer was 1.5-cm glass tubing, long enough to register heads of 40 cm of oil. It was connected to the vacuum system as shown in Fig. 3, one side being pumped continuously. Large volume cylindrical ballast flasks and traps were provided to prevent oil from being blown through the system in the event of accident.

The head H was measured by means of a vertical cathetometer set up on a rigid stand some 4 feet from the manometer and sighting through a vertical slit in the concrete fort surrounding the scattering equipment. Obvious checks were made for verticality of the cathetometer travel and horizontality of its telescope line of sight. Vertical travel of the cathetometer was 100 cm, its vernier read to 0.01 cm without interpolation, and with the oil meniscus properly illuminated settings were repeatable to 0.005 cm.

The density ρ was measured as a function of temperature by weighing a known volume of oil in a specific gravity bottle at a temperature controlled by a water bath. The volume of the bottle was obtained over the same temperature range by weighing it filled with distilled water whose density is known accurately as a function of temperature. ρ for Apiezon B was found to be fitted, to three-figure accuracy, by the following:[3]

$$\rho=0.882\{1-0.00070(T-273.18)\}.$$

Oil temperatures were measured during each run by an ordinary 0–100° mercury thermometer. The gas temperature was measured to 0.1° by a 20–35°C mercury thermometer manufacture and certified by the Parr Instrument Company, Inc., Moline, Illinois. Its bulb rested in a tube set into the lid of the chamber close to the scattering volume.

IV. CHARGE MEASUREMENT AND N_i

To compute absolute cross sections it was necessary to know absolute N_i values for each run. The current integrator measured the total charge appearing on the current collector and was the same as used with the coincidence scattering equipment.[4] For the present work it was used in its least sensitive arrangement, i.e., potential applied to the 1-μf condenser shunted by the 0.1 and 0.01 μf in series, the potential developed across the 0.1-μf condenser being measured by a Compton electrometer. The capacitances of all three condensers were measured by the Bureau of Standards for various charging rates in order to simulate the conditions of the experiment as closely as possible. The 1- and 0.01-μf condensers were charged to ~6 v and the 0.1 μf to ~0.6 v in an interval ranging from 1300 to 1600 sec. Actual values of the capacitances were more nearly 1.30, 0.108, and 0.0118 μf, respectively. (Exact values used for each run differed slightly according to the charging rate and were derived in each case from calibration charts based on the Bureau of Standards report.)

Various checks were made on the corrections applied to the current integrator system (see Sec. VI of reference 4). In addition, an independent check was made with the chamber loaded in the usual way but with the magnet removed from the current collector. Several plates were scanned and apparent cross sections derived. These appeared to be about 3 percent higher, presumably because of secondary electron effects. It has been assumed that the magnet eliminated this effect entirely.

The value of e used when computing N_i from the total charge collected was 1.608×10^{-19} coulomb.

V. PHOTOGRAPHIC PLATES AND SCANNING

Ilford C2 plates were used, either 50 or 100μ thick, the thicker emulsions being used at small angles where the proton range was greatest. The tracks formed a swath down the center of each plate, the blackening being just visible to the naked eye. Scanning was carried out by the writer with a Cooke binocular microscope at magnifications ranging from 500× to 1400×. The most useful objective for this work proved to be a 45× fluorite of N.A.=0.95.

The aim in scanning was threefold: (1) to determine the average number n_a of proton tracks (of correct length) per unit area of surface of each plate; (2) to measure accurately a few hundred tracks in order to find the proton energy (Sec. VII); (3) to determine the number of spurious tracks per unit area of each plate.

At most angles *bona fide* and spurious tracks could be distinguished at sight and (1) and (3) proceeded simultaneously and rapidly. Under best conditions approximately 3000 tracks were counted per day. At intermediate angles, e.g., 21, 25, and 30°, tracks could be distinguished; but it was found advisable to measure the length of every track and plot a histogram. This was a tedious task requiring about one day per 500 tracks. At still smaller angles the tracks could not be distinguished, so the total number was counted (Sec. VI) and this could again be done rapidly.

To obtain n_a it was necessary to count the number of tracks entering known area of the surface of the emulsion. A known area was established in two ways (Fig. 5).

[2] Atomic constants have been taken from Table VII of the article by J. W. M. DuMond and E. R. Cohen, Revs. Modern Phys. **20**, 82 (1948).
[3] O. Beeck, Rev. Sci. Instr. **6**, 399 (1935).
[4] Karr, Bondelid, and Mather, Phys. Rev. **81**, 37 (1951).

(1) The simplest procedure was to calibrate a convenient fraction of the field of view of the microscope and count the tracks in that area, repeated many times. This was ideal when there were no spurious tracks or when they were much longer than *bona fide* tracks (Fig. 5A). An eyepiece graticule with a 7-mm square was used with a 10× Kellner eyepiece for much of the present work.

(2) When *bona fide* tracks were too long for that setup a simple graticule (Fig. 5B) having a scale across one diameter was used. This scale was used in conjunction with the screw micrometer which moved the stage of the microscope in order to define an area of plate. By means of the X screw micrometer, the swath was made to move across the field of view so that each track could be examined, recorded, and (if necessary) measured as it passed the scale. This arrangement was conveniently flexible. The Y dimension could be selected and the magnification adjusted so that all tracks originating within the strip also ended in the field of view.

Where possible both methods of counting were applied to the same plate and the results averaged. In (1) the area XY was found by calibration against a stage micrometer. In (2) the scale Y was calibrated against the stage micrometer, dimension X being the length of sweep as read from the screw micrometer.

In the early stages of work with the photographic chamber some trouble was experienced because of the emulsions peeling off the glass plates when in vacuum, especially in the case of the 100-μ plates. Ilford plates were found to be much less susceptible to this fault than Kodak plates and were used exclusively for the p–p work. Peeling, when it did occur, usually began with the lifting of the emulsion at the edges. Two devices were found helpful in minimizing trouble from this source: first, painting around the edges of each plate with lacquer to bind the emulsion firmly to the glass, and second, a "preselection" procedure. If in a preliminary pumping a plate did not peel within the first 20 hours or so, then in general it would not peel during the run.

VI. CORRECTION FOR IMPURITY SCATTERING

The number of impurity tracks per unit area was determined at every angle where they were sufficiently longer than the *bona fide* tracks to be counted separately. This could be done completely reliably for $\Theta=21°$, where the difference of track lengths was $\sim 28\mu$. Hence all cross sections for angles greater than 21° (Tables I and II) can be regarded as free from impurity scattering. However, corrections had to be applied at all smaller angles.

Two control runs were made, the first with the chamber evacuated to $\sim 10^{-5}$ mm Hg and the second with a small quantity of air deliberately admitted to the chamber. The first established the amount and kind of slit scattering at each angle, *viz.*, a continuous spectrum (Fig. 6) having an end point sufficiently shorter than the *bona fide* tracks to avoid any confusion. The second established the shape of the scattering curve for air plus any organic vapors and water vapor present. (Absolute values were not obtained, merely the shape of the curve.) A plausible correction for impurity scattering at the smaller angles, 7° to 16°, could then be determined by comparison with the observations at larger angles. At the larger angles ($\Theta \geqslant 21°$) impurity tracks could be distinguished and counted separately, so that their absolute number was known. If the ratio of the number of impurity tracks at larger angles to that at smaller angles follows the same rule that governs the shape of the scattering curve deliberately taken in air,[5] the actual magnitude of the impurity scattering could be calculated for each of the small angles. This has been done for the cross sections listed in Tables I and II.

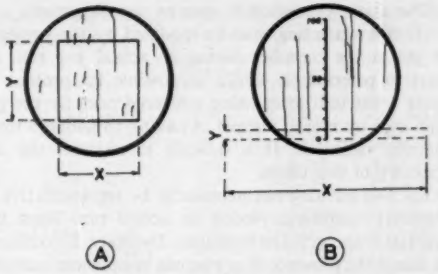

FIG. 5. Typical fields of view showing how *bona fide* and spurious tracks were counted separately when the former were (A) much shorter than the spurious tracks, (B) of comparable length. The unit area for counting was XY in each case. (Protons are supposed to have traveled in the direction 0→100 of the scale.)

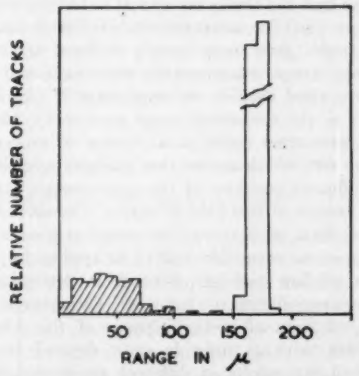

FIG. 6. Histogram of *bona fide* and slit scattered (shown shaded) tracks at $\Theta=7°$. On an average run slit scattered tracks were ~14 percent of the whole at 7°, 7.5 percent at 11°, and a few percent or less thereafter.

[5] Over the range $\Theta=7$ to 25° in the air scattering was very close to the Rutherford form: $\sigma(\Theta) \propto (\sin\frac{1}{2}\Theta)^{-4}$ although the method of application of the correction does not depend on this.

The above procedure is open to two objections.

(1) Slit scattering may be modified by the presence of gas in the chamber during an actual p–p run. At least in principle it would be possible for protons to enter a slit unit after being scattered once by the gas and once by metal, instead of having to undergo three metallic collisions. It is difficult to estimate the importance of this effect.

(2) The air may not necessarily be representative of impurity conditions during an actual run. Some impurities enter with the hydrogen. However, it is difficult to image the presence of any atoms in sufficient numbers which would change the shape of the impurity curve; and this is the only way in which an error could be introduced.

VII. BEAM ENERGY MEASUREMENT

The ranges of scattered protons in photographic emulsions were measured to give the beam energy. Ranges were converted to energies by means of the Rotblat curve[6] which supersedes the original data of Lattes, Fowler, and Cuer[1] (actually there is no significant difference between the two sets of data at 5 Mev).

(1) The beam at the end of the slit system was measured by scattering protons from a thin platinum foil into an Ilford C2 plate, and the ranges measured. This led to an energy of 5.11 Mev after correction for recoil of the platinum nucleus and loss of energy in the foil. (2) The beam energies assumed in the present work were based on measurements made on plates exposed to protons scattered by hydrogen during the actual p–p run, thereby removing the suspicion that the beam energy may have changed slightly between different runs and from day to day. The plate at $\Theta=45°$ had $\Phi=3°$ so that the tracks lay almost flat in the emulsion and were ideal for measurement. (3) Plates placed at other angles gave more steeply inclined tracks, but horizontal range measurements were made and a correction applied to give the true range R ($R=l/\tan\Phi$, where l is the horizontal range measured). Measurements were thus made at a variety of angles from $\Theta=7$ to $60°$, which meant that energies were inferred from different positions of the range-energy curve.

The beauty of this kind of energy measurement was twofold. First, it measured the energy at the scattering volume, so no correction had to be applied for energy loss in window and gas. Second, it determined the *average* energy during the run itself. The average energy calculated from all determinations of this kind was 5.07 Mev with a probable error derived from the spread of the results at different angles and runs of ± 0.02 Mev.

However, it must be emphasized that this does not include any systematic errors which may be involved in the use of the Rotblat curve. After correspondence with Dr. Rotblat it has been decided that 5.07 ± 0.04 Mev is a safe statement of energy.

[6] J. Rotblat, Nature **165**, 337 (1950).

VIII. EXPERIMENTAL ERRORS

The following is a review of every kind of measurement which had to be made, the instrument used, the standard the instrument was checked against and the probable error estimate of each measurement. It will be noticed that a large number of length measurements had to be made. Those on the chamber and concerning the apparatus were made at Washington University, St. Louis, U.S.A., while those on the plates were made at Birmingham University, Birmingham, England; and both sets had to be coordinated and related to a standard of length. Measurements on the chamber were based on a large Gaertner Comparator, capable of measuring to 10^{-4} cm, while those on the plates were based on a glass stage micrometer (by Cooke, Troughton, and Simms, Ltd.) having a 1-mm scale subdivided into 100 parts. This scale[7] was calibrated at the National Physical Laboratory, Teddington, England.

Slit Widths ($2b$)

For the p–p work 16 brass slits had to be measured accurately ($\Theta=7$ to $75°$). These were set on a Vee block, illuminated diffusely from behind and measured to 0.0001 cm with a small Gaertner traveling microscope. Each was measured from both sides; and if any bevel was detected on the slit jaws, the smaller dimension was taken. The probable errors, calculated from about 10 measurements on each slit, were $\sim$0.2 percent, except in the case of the 7° slit, where it was about double this. The microscope was also used to check the centering of all defining slits with respect to their brass cylinders.

Ring

Internal and external diameters of the ring were measured with standard screw micrometers. The width of the ring was checked at a number of places with vernier calipers. (Micrometer and calipers were checked against the large comparator.) These measurements led to values of R' and h' for all but the 7° and 11° slit units, where a special micrometer had to be employed to measure the position of slit A. Estimated probable errors in R' and h' were each $\sim$0.06 percent.[8]

Head of Oil (H)

The cathetometer (Sec. III) was checked against the large comparator over its full travel. Other sources of systematic error in H are difficult to assess. What independent checks could be made indicated a probable error not greater than 0.1 percent.

Density of Oil (P)

The formula given in Sec. III has a probable error of about 0.15 percent including the effects of the probable error in temperature measurement.

Gas Temperature (T)

T was measured at frequent intervals to 0.1°C and an average calculated for the run. However, there may have been a small

[7] All comparator measurements made in St. Louis were ultimately referred to this scale, which therefore becomes the final length standard for the present experiment. The distance between two scratches on a glass plate was measured, initially in St. Louis with the comparator and subsequently in Birmingham relative to the 1-mm standard.

[8] Some higher order errors caused by the geometry may have persisted. It is very difficult to estimate residual errors of this kind, but they are believed to be of the order only of 0.01 percent or less.

TABLE I. Measured cross-section values.

Θ	θ	E in (Mev)	R in μ	$\sigma(\theta)\times10^{25}$ cm² steradian⁻¹ Run 1: April 7, 1949		Run 2: April 8, 1949		Run 3: April 9, 1949	
7°	11°	4.93	168	···		7.86(?)	(2699)	7.21(?)	(1523)
11	22	4.82	162	1.53	(2736)	1.59	(1491)	···	
15	30	4.67	154	0.961	(2597)	0.990	(1403)	0.983	(2672)
16	32	4.62	152	0.912	(1875)	0.944	(1703)	···	
21	42	4.36	139	0.856(?)	(116)	0.920	(1996)	0.904	(1015)
25	50	4.11	126	0.913	(2353)	0.947	(910)	0.945	(1616)
30	60	3.75	108	0.914	(1046)	0.947	(858)	0.906	(1198)
35	70	3.36	90	0.952	(2160)	0.938	(990)	1.00	(1276)
40	80	2.93	72	0.921	(1165)	0.996	(952)	0.992	(1713)
45	90	2.50	56	1.02	(219)	0.94	(132)	···	
50	100	2.07	42	0.955	(2460)	0.996	(1100)	0.906	(1377)
55	110	1.64	30	0.930	(2080)	0.988	(991)	0.963	(1414)
60	120	1.25	20	0.971	(1262)	0.946	(1029)	1.01	(1069)
65	130	0.893	12	0.906	(1255)	0.955	(852)	0.867	(988)
70	140	0.585	7	0.900	(989)	0.883	(622)	···	
75	150	0.335	~3	0.86(?)	(510)	···		···	

The figures in parentheses are number of tracks.

TABLE II. Final values of the cross section with statistical errors.

θ	$\sigma(\theta)\times10^{25}$		Standard deviation (percent)	$p_1(E,\theta)$	δ_a
14°	7.62(?)	(4222)	1.52	−20.68	56.3 ±4.2
22	1.56	(4227)	1.54	−7.516	54.81±0.81
30	0.976	(6672)	1.22	−3.715	54.95±0.41
32	0.928	(3578)	1.67	−3.185	54.45±0.55
40	0.892	(1611)	2.48	−1.784	54.30±0.77
42	0.911	(3127)	1.79	−1.553	54.86±0.55
50	0.921	(7974)	1.12	−0.8931	54.58±0.35
60	0.949	(6462)	1.24	−0.4254	54.77±0.41
70	0.957	(8911)	1.06	−0.1696	54.50±0.36
80	0.958[1]	(8787)	1.07	−0.0399	54.24±0.37
90	0.99(?)	(351)	5.3	···	55.3 ±1.8

systematic difference between the temperature at the thermometer and that at the scattering volume. A discrepancy of 0.3°C in the average temperature would correspond to an error in N_m of 0.1 percent.

Measurement of Angles

Two sets of angles Θ and Φ had to be measured accurately. A probable error of 0.07° has been assigned to Θ and 0.02° to Φ. Since it is sinΦ which enters, this could introduce probable errors in σ of 0.12, 0.10, and 0.07 percent for Φ=14, 17, and 25°, respectively.

Plate Scanning

A purely statistical error entered at each angle due to the finite number of tracks counted (Table I). Standard deviations of the final figures (Table II) were between 1.1 and 2.5 percent. A systematic error could also enter in calibration of the microscope. The probable error in absolute magnitude of n_a from this source was believed to be not greater than 0.5 percent. Relative n_a values should be much less influenced by this error, possibly by 0.1 or 0.2 percent because of small day to day variations in microscope calibration which seem to occur (presumably associated with small thermal changes affecting the microscope magnification).

N_i Measurement

This introduced the largest single error in absolute cross sections, chiefly contributed by uncertainty in capacitance values. The probable error assigned to N_i was 1 percent. However, as all plates were exposed simultaneously, relative cross sections are independent of this error.

Combination of Errors

The above errors have been combined in the usual way $(\Sigma\Delta^2)^{\frac{1}{2}}$. Some of them affect only absolute cross sections, but others affect relative cross sections also. The probable error in relative values, excluding the statistical error, is ~0.3 percent, which must be combined with the statistical error at each angle. The probable error in absolute value of each cross section was ~1.2 percent apart from the effect of the statistical error.

Multiple Scattering Effects

The gas pressure in the chamber was kept low deliberately in order to avoid multiple scattering corrections. Two aspects were examined carefully. (1) Spread of the beam through the chamber. If this became large enough, it endangered collection of the total charge by the Faraday cup. (2) A proton which has suffered a large angle collision so as to cause it to enter one of the photographic plates may be multiply scattered and lost. This process has a probability which varies as E^{-2}, where E is the energy of the scattered proton and so should become important at large Θ. Calculations showed both (1) and (2) to be unimportant for the present design of chamber, energy, and gas pressure. Consideration (2) might have become important if angles beyond Θ=70° had been studied; but proton tracks were, in any case too short to count reliably beyond this angle, so that the question did not arise. The situation is helped, so far as (2) is concerned, by the fact that the multiple scattering process is self-compensating. There is an equal probability (to a good approximation) that protons which should have entered the plate have been multiply scattered out and lost and that protons which should not have entered the plate do enter because of multiple scattering into it.

IX. RESULTS AND DISCUSSION

The results of each plate scanned, after all corrections have been applied, are displayed in Table I. The total number of tracks counted was 56412. Cross sections were examined for symmetry about the $\theta=90°$ angle and found to be satisfactory. Data at θ were then combined with those at $\pi-\theta$, and the final cross sections listed as a function of θ in Table II together with their statistical errors.

In order to facilitate comparison with other low energy and medium energy p–p work, the present results have been treated along the lines adopted by Jackson and Blatt.[9] Apparent S-wave phase shifts δ_a (defined by $\delta_a=\delta_0+p_1\delta_1+p_2\delta_2$, where δ_0, δ_1, δ_2, are the S-, P-, and D-wave phase shifts, respectively, and $p_n=(\partial\sigma/\partial\delta_n)/(\partial\sigma/\partial\delta_0)$ were calculated from

$$2\delta_a=\sin^{-1}[\sin w-Q\cos w((\sigma(\theta)/\sigma_M(\theta))-1)]-w,$$

where the notation is that of Jackson and Blatt. δ_a-values are listed in Table II. p_1-values were calculated for each θ of the experiment, and Fig. 7 is a graph of δ_a as a function of p_1. In this figure the limits of error drawn about each point were obtained by combining the statistical error with the probable error computed from all sources which affect *relative* cross sections.

It is apparent that the data are consistent with pure S-wave scattering. The point at $\theta=14°$ is of too low accuracy to contribute to the conclusions. The δ_a-values

[9] J. D. Jackson and J. M. Blatt, Revs. Modern Phys. 22, 77 (1950).

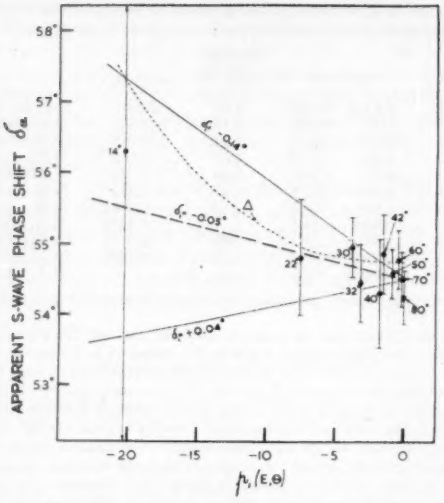

FIG. 7. Apparent S-wave phase shifts vs $p_1(E,\theta)$ for $E=5.07$ Mev. The value at $\theta=14°$ is too uncertain to be of any use, and the value at 90° has been omitted because of poor statistics. The remaining points are fitted best by a small repulsion in the $3p$ state, viz., as indicated by the broken line $\delta_1=-0.05°$. The data could be fitted, however, by any δ_1-value between the extremes, also drawn in, $\delta_1=-0.14°$ and $+0.04°$, and is obviously consistent with no P-state interaction. Curve Δ indicates the distortion in δ_a which would result if scattering were pure S-wave, but the energy had been overestimated by 0.8 percent when computing δ_a.

at other angles have been examined by the method of least squares and found to be represented best by a slight P-wave (repulsive) as follows: $\delta_1=-0.05°$; but the uncertainty on this is $\pm 0.09°$. There is little doubt that the P-wave effect is zero at 5 Mev, especially in view of the recent work at 340 Mev (and lower energies) carried out at Berkeley, none of which indicates any departure from isotropy. The best value for the S-wave phase shift at 5.07 Mev, as derived from the above data, is 54.5° with a probable error of $\pm 0.6°$. This result is in good agreement with that of Meagher[10] ($54.7\pm 1.0°$ at 4.94 Mev).

At the small angles studied in the present experiment considerable error could result in δ_a from small systematic errors in energy measurement. The probable error in E claimed in Sec. VII is 0.8 percent. $\Delta_E=0.008E(\partial\delta_a/\partial E)_\theta$ (see Jackson and Blatt[1]), is the change in δ_a due to a 0.8 percent change in E. Δ_E has been calculated for the various θ-values and is represented by the dotted curve (Δ) of Fig. 7. It is thus seen that overestimating the energy by the probable error quoted could easily account for the slight negative δ_1-value suggested by the data.

The interest of Professor A. L. Hughes in this and other projects was encouraging stimulus to the writer during his stay at Washington University. The successful operation of the chamber was due largely to the skill of Mr. O. Retzloff and his workshop staff. Thanks are due also to the cyclotron crew for continued cooperation and especially to Mr. B. Phillips for the considerable amount of unscheduled operating time given to the project.

In particular the writer wishes to express his appreciation to Professors Oliphant and Moon for their courtesy in permitting this work to be completed at the University of Birmingham, England while the writer was there on an Imperial Chemical Industries Fellowship.

[10] R. E. Meagher, Phys. Rev. **78**, 667 (1950).

Electric Excitation and Disintegration of Nuclei. I. Excitation and Disintegration of Nuclei by the Coulomb Field of Positive Particles*

CHARLES J. MULLIN AND EUGENE GUTH
University of Notre Dame, Notre Dame, Indiana
(Received September 11, 1950)

General formulas for the cross section for the 2^l-pole excitation (or disintegration) of a nucleus by the electric field of a non-relativistic positively charged projectile have been obtained by using the Born approximation; the finite size of the nucleus has been taken into account. For electric dipole and quadrupole excitation a more accurate evaluation has been made in which the initial and final states of the charged projectile are described by the exact coulomb field wave functions.

The cross section for electric 2^l-pole excitation of a nucleus by the field of a charged projectile is proportional to the corresponding photo-excitation cross section; the proportionality factor may be interpreted as the number of virtual electric 2^l-pole quanta in the field of the charged projectile. In the electric dipole case, the cross section for the inelastic scattering of a charged projectile is shown to be proportional to the cross section for the production of continuous x-rays by deflection of the projectile in a coulomb field. Thus a relation is established between the virtual quanta representing the coulomb field of the projectile and the real quanta of the x-ray spectrum corresponding to the scattering process.

The theory of electric transitions has been applied, in some detail, in a discussion of two cases in which it seems likely that these transitions play a significant role. These two cases are (1) the inelastic scattering of deuterons and (2) the electric break-up of the deuteron when it "collides" with a target nucleus.

I. INTRODUCTION

WHEN target nuclei are bombarded with positively charged projectiles, nuclear excitation or disintegration may take place by either of two competing processes: (1) A direct nuclear interaction may take place in which the projectile enters the nucleus, thereby forming an excited compound nucleus which decays by the emission of a γ-ray or a particle; or (2) the target nucleus may be excited or disintegrated by the electromagnetic field of the charged projectile. Under conditions most favorable for electromagnetic excitation, the cross section for process (2) should be given roughly by the product of the fine structure constant ($e^2/\hbar c = 1/137$) and the photo-excitation cross section.

Thus, generally speaking, we may expect the excitation by direct nuclear interaction to be more probable than excitation by electromagnetic interaction. However, we may expect transitions induced by electromagnetic interaction to play a significant role if either of the two following conditions is fulfilled: (1) The transition energy is small compared to the coulomb barrier energy. In this case the excitation energy can be supplied by electric interaction even though the projectile misses the nucleus by several nuclear diameters. (2) Because of special conditions the probability of excitation by direct nuclear interaction is small.

The smallness of the cross section for the "electric excitation" of nuclei by positively charge projectiles has made experimental detection difficult, with the result that although the electric excitation process has been looked for in the past[1] only recently has rather clear-cut evidence for the occurrence of this process been obtained. This evidence has been obtained in the inelastic scattering of deuterons.[2,3] In this case electric transitions may be expected to play the major role because once a deuteron enters the nucleus, the probability that a deuteron will be emitted is very small; and the much more probable event in which a single nucleon is evaporated from the excited compound nucleus does not yield an inelastically scattered deuteron. We shall show that the angular distribution of the inelastically scattered deuterons obtained experimentally agrees with that to be expected on the basis of electric transitions. A second example of a reaction involving deuterons in which electric transitions may play a significant role is the stripping process. This process, in which one of the nucleons is stripped off the deuteron as it passes the nucleus, may be due to electric interaction or to direct nuclear encounter of one of the nucleons of the deuteron with the target nucleus.

The excitation of a nucleus by the electromagnetic field of a charged projectile is very closely related to the corresponding photo-excitation. This relation is seen readily if one uses the quantum-mechanical analog to the semiclassical method of virtual quanta.[4] The cross section, σ_e, for excitation by the electromagnetic field of a charged projectile can be written in terms of the photo-excitation cross section, $\sigma^{(\gamma)}$, as follows:

$$\sigma_e(E_i, E) = N(E_i, E)\sigma^{(\gamma)}(E), \qquad (1)$$

where E is the excitation energy, E_i the energy of the incident projectile, and $N(E, E_i)$ is the number of virtual quanta (per unit energy) of energy E in the electromagnetic field of the charged projectile which are available for producing the transition. If the final energy level lies in an energy continuum (as in the case, for example, when a disintegration is produced), the cross section for the transition is obtained by integrating

* Supported in part by the ONR.

[1] Lark-Horovitz, Risser, and Smith, Phys. Rev. **55**, 878 (1939). E. H. Rhoderick, Nature **163**, 848 (1949). H. V. Halban, private communication (unpublished).

[2] Greenlees, Kempton, and Rhoderick, Nature **164**, 663 (1949).

[3] J. R. Holt and C. T. Young, Nature **164**, 1000 (1949).

[4] The quantum mechanical analog of the method of virtual quanta has been used by E. Guth and C. J. Mullin [Phys. Rev. **76**, 234 (1949)] to describe the disintegration of nuclei by electrons in the Born approximation. A general diacussion of the method, also in the Born approximation, has been given by M. Lax and H. Feshbach (unpublished).

over all permissible transition energies:

$$\sigma_s=\int N\sigma^{(\gamma)}dE. \tag{2}$$

The number of quanta, $N(E, E_i)$, is given by a matrix element involving only the projectile's coordinates and, therefore, is independent of specific assumptions made in choosing a model for the nucleus.

In the past, recognition of electric excitation has been hampered by the lack of an adequate theory. Crude estimates of the cross section for electric excitation have been given by Landau[6] and Weisskopf.[6] An exact formula for the total cross section in a special case has been given by Guth[7] who employed Ehrenfest's theorem to reduce the rather complicated electric matrix element to the matrix element for the production of bremsstrahlung by a particle deflected by a coulomb field.

The principal objective of the present paper is to give a detailed treatment of the excitation and disintegration of nuclei by the electric field of nonrelativistic, positively charge particles. This treatment should facilitate comparison of theory with experiment. In Sec. II-A formulas for the cross sections for electric 2^l-pole excitation are developed using the Born approximation. Since the coulomb deflection of the projectile should decrease the overlap of the projectile's wave functions occuring in the electric matrix element. the Born approximation should yield an upper limit for the correct electric excitation cross section. In Sec. II-B, cross sections for electric dipole and quadrupole excitation are developed by using the exact coulomb wave functions to describe the initial and final states of the charged projectile. The quantum mechanical analog of the method of virtual quanta is applied to the electric excitation of nuclei by nonrelativistic positively charged projectiles in Sec. III of this paper; expressions for the numbers of electric dipole, quadrupole, and octupole quanta in the electric field of the charged projectile are derived. In the electric dipole case, the relationship is established between the virtual quanta representing the coulomb field of the charged projectile and the real quanta of the x-ray spectrum corresponding to the scattering process. In Sec. IV the theory of electric excitation is applied to the electric break-up of the deuteron in flight. In Sec. V the theory of electric transitions is applied in a detailed discussion of two cases in which it seems likely that these transitions play a significant role. These two cases are (1) the inelastic scattering of deuterons and (2) the electric break-up of the deuteron when it "collides" with a target nucleus.

[6] L. Landau, Physik. Z. U.S.S.R. **1**, 88 (1932).
[6] V. Weisskopf, Phys. Rev. **53**, 1018 (1938). Weisskopf assumes the projectile's wave functions to be constant over the region extending from the classical turning point to infinity.
[7] E. Guth, Phys. Rev. **68**, 280 (1945).

II. CROSS SECTIONS FOR ELECTRIC EXCITATION

In this section we shall develop the theory of the excitation of a nucleus by the coulomb field of an incident, nonrelativistic, charged projectile.

Cross sections for the excitation of a nucleus through the interaction of the electromagnetic field of relativistic electrons with the electric dipole, magnetic dipole, and the electric quadrupole moments of the nucleus have been obtained by Wick.[8] In the nonrelativistic limit Wick's results differ from ours because he neglected the finite size of the nucleus. We shall assume that all projectiles which penetrate into the nucleus give rise to nonelectric processes. Since we wish to exclude all nonelectric processes from our considerations, we shall set the interaction between the projectile and the nucleus equal to zero when the projectile is within a certain distance, r_0, from the center of the nucleus. This distance will be taken as the sum of the "radii" of the nucleus and the projectile. The extended range of nuclear forces also modifies the projectile's wave functions outside the nucleus. This latter effect plays a significant role only in the angular distributions of particles scattered through rather large angles and will be neglected here.

We neglect the nonzero extension of the charge distribution of the projectile. This procedure is correct when the projectiles are protons, but is an approximation when deuterons or α-particles are used. Thus the interaction between the nucleus of charge Ze and the projectile of charge ze is given by

$$\begin{aligned} V&=0 && r\leqslant r_0,\\ V&=\sum_{\mu=1}^{Z}\frac{ze^2}{|\mathbf{r}-\mathbf{R}_\mu|} && r\geqslant r_0, \end{aligned} \tag{3}$$

where $\mathbf{r}$ is the coordinate of the projectile, and $\mathbf{R}_\mu$ is the coordinate of the μth of the Z protons in the nucleus. Making the multipole expansion:

$$V=\sum_{\mu=1}^{Z}\sum_{n=0}^{\infty}(ze^2/r)(R_\mu/r)^n P_n[\cos(\mathbf{r},\mathbf{R}_\mu)]=\sum_l V_l, \tag{4}$$

where $(\mathbf{r}, \mathbf{R}_\mu)$ is the angle between the vectors $\mathbf{r}$ and $\mathbf{R}_\mu$. The $n=l$ term of this series gives the interaction between the projectile and the electric 2^l-pole moment of the nucleus and gives rise to electric 2^l-pole transitions. If we assume that the nuclear states are classified by parity and angular momentum, the terms in the series can be considered separately.

We shall work in the center-of-mass coordinate system. Using first-order perturbation theory, the cross section for an electric 2^l-pole transition is

$$d\sigma/d\Omega=[2\pi/\hbar(2j_A+1)]\sum_{a,b}|(\chi_2 b|V_l|\chi_1 a)|^2, \tag{5}$$

where V_l is the interaction between the projectile and the electric 2^l-pole moment of the nucleus, χ_1 and χ_2

[8] G. C. Wick, Ricerca Scient. **XI**, 49 (1940).

are the initial and final states of the projectile (normalized, respectively, to unit flux and unit energy), a is one of the $2j_A+1$ initial nuclear states belonging to the initial level A, and b is one of the $2j_B+1$ final nuclear states belonging to the final level B. The integrals over the projectile's coordinates extend from r_0 to infinity.

In the usual case, in which the nuclear moments are randomly oriented, the angular distribution of the inelastically scattered particles is symmetric about the direction of incidence of the projectiles. In all cases which we shall consider it is possible to choose a direction in terms of which the product $\chi_2^*\chi_1$ has axial symmetry. Taking this axis of symmetry in, say, the $\mathbf{n}$ direction, and using the addition theorem for the Legendre polyomials, the matrix element occuring in Eq. (5) can be factored, and we obtain

$$d\sigma/d\Omega=[2\pi/\hbar(2j_A+1)]M_{AB}^2M_{12}^2, \tag{6}$$

where

$$M_{AB}^2=\sum_{a,b}|(b|\sum_{\mu=1}^{Z}R_\mu^lP_l[\cos(\mathbf{n},\mathbf{R}_\mu)]|a)|^2$$

and

$$M_{12}^2=|(\chi_2|ze^2P_l[\cos(\mathbf{n},\mathbf{r})]/r^{l+1}|\chi_1)|^2.$$

The electric 2^l-pole photo-excitation cross section $\sigma_l^{(\gamma)}$ is proportional to M_{AB}^2. Writing $\sigma_l^{(\gamma)}=\beta M_{AB}^2/(2j_A+1)$

$$\sigma_l=(2\pi\sigma_l^{(\gamma)}/\hbar\beta)\int M_{12}^2d\Omega.$$

The number of virtual electric 2^l-pole quanta in the electric field of the projectile is thus given by

$$N_l=(2\pi/\hbar\beta)\int M_{12}^2d\Omega. \tag{7}$$

(A) Cross Sections in the Born Approximation

In the Born approximation the incident and scattered particles are represented by plane waves with wave numbers $\mathbf{k}_1$ and $\mathbf{k}_2$, respectively. The cross section for an electric 2^l-pole transition is given by

$$\frac{d\sigma}{d\Omega}=\left(\frac{n_1}{2\pi Z}\right)^2\frac{k_1k_2}{2j_A+1}M_{AB}^2M_{12}^2 \tag{8}$$

with

$$M_{12}^2=\left|\int\frac{\exp(i\mathbf{K}\cdot\mathbf{r})\cdot P_l[\cos(\mathbf{K},\mathbf{r})]}{r^{l+1}}d\mathbf{r}\right|^2,$$

$$M_{AB}^2=\sum_{a,b}\left|\sum_{\mu=1}^{Z}(b|R_\mu^lP_l[\cos(\mathbf{K},\mathbf{R}_\mu)]|a)\right|^2,$$

$$n_1=zZe^2/\hbar v_1,$$

$$\mathbf{K}=\mathbf{k}_1-\mathbf{k}_2,\quad K=|\mathbf{K}|=[k_1^2+k_2^2-2k_1k_2\cos\theta]^{\frac{1}{2}},$$

where θ is the scattering angle in the center-of-mass system. The integral over the particles coordinates can be carried out readily and yields

$$M_{12}^2=16\pi^2K^{2(l-2)}[\,j_{l-1}(Kr_0)/(Kr_0)^{l-1}]^2.$$

$j_q(x)$ is the spherical bessel function of order q.

The cross section for electric 2^l-pole excitation is then

$$\frac{d\sigma}{d\Omega}=4\left(\frac{n_1}{Z}\right)^2\frac{k_1k_2}{2j_A+1}K^{2(l-2)}\left[\frac{j_{l-1}(Kr_0)}{(Kr_0)^{l-1}}\right]^2M_{AB}^2. \tag{9}$$

The angular distribution is given by the factor $K^{2(l-2)}[\,j_{l-1}(Kr_0)/(Kr_0)^{l-1}]^2$. The effect of the finite size of the nucleus on the angular distribution shows up in the factor in brackets. If one allows r_0 to go to zero, this factor becomes a constant, and the angular distribution is given simply by the factor $K^{2(l-2)}$.

On integrating over all angles of scattering, one has

$$\sigma=8\pi(n_1/Z)^2M_{AB}^2B_l/(2j_A+1), \tag{10}$$

where

$$B_l=\frac{1}{r_0^{2l-2}}\int_{(k_1-k_2)r_0}^{(k_1+k_2)r_0}\frac{j_{l-1}^2(y)}{y}dy.$$

The integration for B_l can be carried out, but the general result is rather complicated and will not be given here. For $l=1$, 2, and 3 we shall obtain relatively simple expressions for B_l.

From the transformation properties of $P_l[\cos(\mathbf{K},\mathbf{R})]$ it is evident that the square of the nuclear matrix element (M_{AB}^2) is proportional to the sum of the squares of the elements of the irreducible (traceless) multipole moment tensor for the 2^l-pole transition $A\rightarrow B$. In the following paragraphs we shall evaluate M_{AB}^2 in terms of the multipole moments for dipole, quadrupole, and octupole interactions.

(1) *Electric Dipole Transitions*

We introduce the electric dipole moment of the nucleus, $\mathbf{D}$, which has the cartesian components

$$D_i=x_i=\sum_{\mu=1}^{Z}x_{i\mu}.$$

The cross section for electric dipole transitions is obtained by setting $l=1$ in Eq. (9). If we average over all directions of $\mathbf{R}_\mu$ we obtain

$$\left\{\left[\sum_{\mu=1}^{Z}R_\mu P_1[\cos(\mathbf{K},\mathbf{R}_\mu)]\right]^2\right\}_{\text{Av}}=\tfrac{1}{3}|\mathbf{D}|^2.$$

Hence, for randomly oriented nuclear moments

$$M_{AB}^2=D_{AB}^2/3,$$

where

$$D_{AB}^2=\sum_{a,b}\sum_i|(b|D_i|a)|^2$$

is the square of the electric dipole moment of the

nucleus for the transition $A\rightarrow B$. Thus, for electric dipole transitions

$$\frac{d\sigma}{d\Omega}=\frac{4}{3}\left(\frac{n_1}{Z}\right)^2\frac{D_{AB}{}^2}{2j_A+1}\frac{k_1k_2}{K^2}j_0{}^2(Kr_0), \tag{11}$$

$$\sigma=\frac{8\pi}{3}\left(\frac{n_1}{Z}\right)^2\frac{D_{AB}{}^2}{2j_A+1}B_1, \tag{12}$$

where

$$B_1=f[2(k_1+k_2)r_0]-f[2(k_1-k_2)r_0],$$

$$f(x)=Ci(x)+(\cos x-x\sin x-1)x^2.$$

$Ci(x)$ is the cosine integral:

$$Ci(x)=-\int_x^\infty(\cos t/t)dt.$$

The relatively complicated function B_1 can be approximated in a very simple way in certain cases of physical interest. Thus in the case that $2(k_1+k_2)r_0$ is small compared to unity,

$$B_1\cong\ln[(k_1+k_2)/(k_1-k_2)].$$

In the physically important case that $2(k_1-k_2)r_0\ll1$ and $2(k_1+k_2)r_0\gg1$,

$$B_1\cong\ln[\epsilon/2\gamma(k_1-k_2)r_0],$$

where ϵ=base for natural logarithms, $\ln\gamma$=Euler's constant: $\gamma=1.781$. It is interesting to note that the last formula yields a total cross section which differs very little from that which is obtained by using a point nucleus in performing the integrations over the projectile's configuration space and taking account of the nonzero size of the nucleus by limiting the recoil momentum imparted to the nucleus to values $\leqslant\hbar/r_0$. This latter procedure, which has been used by Dancoff[9] in describing the electric break-up of the deuteron, yields the result

$$B_1=\ln[1/(k_1-k_2)r_0],$$

which is just slightly larger than our value of B_1.

(2) *Electric Quadrupole Transitions*

The differential and total cross sections for electric quadrupole transitions are obtained by setting $l=2$ in Eqs. (9) and (10). We introduce the quadrupole moment tensor Q which has elements $Q_{ij}=x_ix_j$ and the irreducible quadrupole moment tensor Q' which has elements $Q_{ij}'=Q_{ij}-\frac{1}{3}I\delta_{ij}$, where $I=x^2+y^2+z^2$ is the trace of the quadrupole moment tensor. From the transformation properties of $P_2[\cos(\mathbf{K},\mathbf{R})]$ it is evident that the square of the nuclear matrix element, $M_{AB}{}^2$, is proportional to $Q_{AB}{}'^2$, that is, proportional to the square of the traceless quadrupole moment for the transition $A\rightarrow B$.

[9] S. M. Dancoff, Phys. Rev. **72**, 1017 (1947).

The elements of the quadrupole moment tensor satisfy the equation:

$$\sum_{ij}|Q_{ij}'|^2=\tfrac{3}{5}\sum_{ij}|Q_{ij}|^2.$$

Since averaging over all directions of the vector $\mathbf{R}$ yields

$$[\{R^2P_2[\cos(\mathbf{K},\mathbf{R})]\}^2]_{\text{Av}}=\tfrac{1}{5}\sum_{ij}|Q_{ij}|^2=\tfrac{3}{10}\sum_{ij}|Q_{ij}'|^2,$$

it follows that for randomly oriented nuclear moments

$$M_{AB}{}^2=3Q_{AB}{}'^2/10,$$

where

$$Q_{AB}{}'^2=\sum_{a,b}\sum_{ij}|(b|Q_{ij}'|a)|^2$$

is the square of the traceless quadrupole moment for the transition $A\rightarrow B$. Consequently, from Eq. (9) we obtain

$$\frac{d\sigma}{d\Omega}=\frac{6}{5}\left(\frac{n_1}{Z}\right)^2k_1k_2\frac{Q_{AB}{}'^2}{2j_A+1}\left[\frac{j_1(Kr_0)}{Kr_0}\right]^2, \tag{13}$$

and

$$\sigma=\frac{12\pi}{5}\left(\frac{n_1}{Z}\right)^2\frac{Q_{AB}{}'^2}{2j_A+1}B_2 \tag{14}$$

with

$$B_2=F[2(k_1+k_2)r_0]-F[2(k_1-k_2)r_0],$$

$$F(x)=(2/r_0{}^2x^4)[\cos x+x\sin x-1-\tfrac{1}{2}x^2].$$

In certain cases of physical interest, simple approximations for B_2 can be obtained. Thus, if $2(k_1+k_2)r_0<1$, $B_2\cong2k_1k_2/9$. If $2(k_1-k_2)r_0<1$ but $2(k_1+k_2)r_0\gg1$, $B_2\cong1/4r_0{}^2$. Use of a cutoff in momentum space rather than in configuration space leads to the value $B_1\cong1/18r_0{}^2$ in this latter case.

It is of interest to note that our quadrupole cross section is proportional to the square of the traceless quadrupole moment, $Q_{AB}{}'^2$. Wick,[8] on the other hand, obtains a cross section which contains a term proportional to $Q_{AB}{}'^2$ and a second term proportional to the square of the trace of the quadrupole moment tensor $(I_{AB}{}^2)$. This latter term, which corresponds to a "monopole" interaction, and which gives rise to $j=0\rightarrow j=0$ transitions, occurs nowhere in our cross sections because we have deleted the region occupied by the nucleus from the projectile's configuration space. The manner in which the monopole term enters into the cross sections can be seen easily by extending our integrations over the projectile's configuration space to include the region occupied by the nucleus. In this case the cross section is

$$\frac{d\sigma}{d\Omega}=\frac{4}{2j_A+1}\left(\frac{n_1}{Z}\right)^2\frac{k_1k_2}{K^4}\sum_{a,b}\left|\left(b\left|\sum_{\mu=1}^{Z}\exp(i\mathbf{K}\cdot\mathbf{R}_\mu)\right|a\right)\right|^2.$$

The exponential can be expanded in a Taylor series or in a series of spherical harmonics. The Taylor series classifies terms according to powers of $\mathbf{K}\cdot\mathbf{R}$. The

$(\mathbf{K}\cdot\mathbf{R})^l$ term mixes together terms corresponding to electric 2^l-pole, 2^{l-2}-pole, 2^{l-4}-pole, etc., interactions. Thus

$$(\mathbf{K}\cdot\mathbf{R})^2=\tfrac{1}{3}K^2R^2\{2P_2[\cos(\mathbf{K},\mathbf{R})]+P_0[\cos(\mathbf{K},\mathbf{R})]\}$$

yields a term which corresponds to quadrupole interaction (P_2) and a term which corresponds to a monopole interaction (P_0). The pure quadrupole interaction yields a cross section proportional to $Q_{AB}'^2$; the monopole interaction gives a cross section proportional to I_{AB}^2. Similarly,

$$(\mathbf{K}\cdot\mathbf{R})^3=\tfrac{1}{5}K^3R^3\{2P_3[\cos(\mathbf{K},\mathbf{R})]+3P_1[\cos(\mathbf{K},\mathbf{R})]\}$$

mixes octupole and dipole interactions. The pure electric 2^l-pole interaction always yields a cross section expressible in terms of the elements of the irreducible 2^l-pole moment tensor. If the exponential $\exp(i\mathbf{K}\cdot\mathbf{R})$ is expanded in a series of spherical harmonics:

$$\exp(i\mathbf{K}\cdot\mathbf{R})=\sum_{l=0}^{\infty} i^l(2l+1)P_l[\cos(\mathbf{K},\mathbf{R})]j_l(KR),$$

the lth-order term of the series corresponds to the pure electric 2^l-pole interaction. In this series the monopole transitions arise from the $l=0$ term, the dipole transitions from the $l=1$ term, etc.

(3) *Electric Octupole Transitions*

The differential and total cross sections for electric octupole transitions are obtained by setting $l=3$ in Eqs. (9) and (10). We introduce the octupole moment tensor S with elements $S_{ijk}=x_ix_jx_k$, and the irreducible octupole moment tensor S' with elements $S'_{ijk}=x_ix_jx_k-\frac{1}{5}(x_i\delta_{jk}+x_j\delta_{ki}+x_k\delta_{ij})$. From the transformation properties of $P_3[\cos(\mathbf{K},\mathbf{R})]$ it is evident that the square of the nuclear matrix element, M_{AB}^2, is proportional to $S_{AB}'^2$, where

$$S_{AB}'^2=\sum_{a,b}\sum_{i,j,k}|(b|S'_{ijk}|a)|^2$$

is the square of the irreducible octupole moment tensor for the transition $A\rightarrow B$. The elements of the octupole moment tensor satisfy the equation

$$\sum_{ijk}|S'_{ijk}|^2=\tfrac{2}{5}\sum_{ijk}|S_{ijk}|^2.$$

Since averaging over all directions of $\mathbf{R}$ yields

$$[\{R^3P_3[\cos(\mathbf{K},\mathbf{R})]\}^2]_{\text{Av}}=(1/7)\textstyle\sum_{ijk}|S_{ijk}|^2=(5/14)\sum_{ijk}|S'_{ijk}|^2,$$

we obtain, for randomly oriented nuclear moments,

$$M_{AB}^2=(5/14)S_{AB}'^2.$$

Thus from Eq. (9)

$$\frac{d\sigma}{d\Omega}=\frac{10}{7}\left(\frac{n_1}{Z}\right)^2 k_1k_2\frac{S_{AB}'^2}{2j_A+1}K^2\left[\frac{j_2(Kr_0)}{(Kr_0)^2}\right]^2 \tag{15}$$

and

$$\sigma=\frac{20\pi}{7}\left(\frac{n_1}{Z}\right)^2\frac{S_{AB}'^2}{2j_A+1}B_2 \tag{16}$$

with

$$B_2=\phi[2(k_1+k_2)r_0]-\phi[2(k_1-k_2)r_0],$$

$$\phi(x)=\frac{48}{r_0^4x^6}\left[\left(1-\frac{3}{8}x^2\right)\cos x+\left(1-\frac{x^2}{24}\right)x\sin x-\left(1+\frac{x^2}{8}+\frac{x^4}{48}\right)\right].$$

In certain cases of physical interest simple approximations for B_2 can be obtained. Thus if $2(k_1+k_2)r_0<1$, $B_2\cong(2/225)k_1k_2(k_1^2+k_2^2)$. If $2(k_1-k_2)r_0<1$, but

$$2(k_1+k_2)r_0\gg1,\quad B_2\cong 1/12r_0^4.$$

(B) Electric Dipole and Quadrupole Excitation Using Coulomb Field Wave Functions

(1) *Electric Dipole*

In this section we shall give a more accurate treatment of electric dipole excitation, using the exact Coulomb wave functions to describe the motion of the projectile.[10] The motion of the incident projectile is described by a coulomb wave asymptotic to a plane wave moving in the direction $\mathbf{k}_1$ plus an outgoing spherical wave; this wave function is normalized to unit flux. The scattered projectile's wave function is taken as a Coulomb wave asymptotic to a plane wave moving in the $\mathbf{k}_2$ direction plus an incoming spherical wave; this wave function is energy normalized. The wave functions are

$$\begin{aligned}&\chi_1=N_{f1}\exp(i\mathbf{k}_1\cdot\mathbf{r})L_{in_1}(\rho_1)=N_{f1}U_1,\\&N_{f1}=[2\pi mn_1/\hbar k_1(e^{2\pi n_1}-1)]^{\frac{1}{2}},\\&\chi_2=N_E\exp(i\mathbf{k}_2\cdot\mathbf{r})L_{-in_2}(-\rho_2)=N_EU_2,\\&N_E=[mk_2n_2/(2\pi)^2\hbar^2(e^{2\pi n_2}-1)]^{\frac{1}{2}},\end{aligned} \tag{17}$$

with $\rho_1=i(kr-\mathbf{k}\cdot\mathbf{r})$, and $\rho_2=i(kr+\mathbf{k}\cdot\mathbf{r})$. $L_q(x)$ is the Laguerre function (S-119) and is a special case of a confluent hypergeometric function: $L_q(x)=F(-q,1,x)$.

Using these wave functions, the cross section for an electric dipole transition may be obtained from Eq. (5):

$$\frac{d\sigma}{d\Omega}=\frac{2\pi}{\hbar}\frac{D_{AB}^2}{3(2j_A+1)}\sum_i\left|\left(\chi_2\left|\frac{ze^2x_i}{r^3}\right|\chi_1\right)\right|^2. \tag{18}$$

To simplify the calculations we shall neglect the extension of the nucleus in the integration over the projectile's

[10] A. Sommerfeld, *Atombau und Spektrallinien* (II Band, F. Vieweg and Sohn, Braunschweig, 1939). Hereafter, references to this book will be given as S followed by the appropriate page number.

configuration space. However, we shall take this extension into account after integration.

The matrix elements occurring in (18) can be simplified by use of the equation of motion (Ehrenfest's theorem) for a particle moving in a Coulomb field. The force acting on such a particle is given by

$$F_{x_i}=m\ddot{x}_i=-\partial(zZe^2/r)/\partial x_i=zZe^2x_i/r^3.$$

Using this relation and the relation between the operator x_i and its time derivative, we have

$$\left(\chi_2\left|\frac{ze^2x_i}{r^3}\right|\chi_1\right)=-\frac{1}{Z}\left(\chi_2\left|\frac{\partial}{\partial x_i}\frac{zZe^2}{r}\right|\chi_1\right)=\frac{m}{Z}(\chi_2|\dot{x}_i|\chi_1)$$
$$=-\frac{m}{Z}\left(\frac{E_2-E_1}{h}\right)^2(\chi_2|x_i|\chi_1).$$

Thus the matrix elements in (18) can be reduced to the well-known matrix elements for the production of bremsstrahlung by a charged particle scattered in a coulomb field.

In terms of the wave functions

$$U_1=\exp(i\mathbf{k}_1\cdot\mathbf{r})L_{in_1}(\rho_1),\quad U_2=\exp(i\mathbf{k}_2\cdot\mathbf{r})L_{-in_2}(-\rho_2)$$

and the matrix elements

$$M_{x_i}=(U_2|x_i|U_1),$$

the cross section can be written as

$$\frac{d\sigma}{d\Omega}=\frac{A_1A_2}{3(2\pi)^2}\left(\frac{m}{h^2}\right)^4\frac{k_2}{k_1}\frac{(E_2-E_1)^4}{Z^2}\exp[-2\pi(n_1+n_2)]$$
$$\times\frac{D_{AB}^2}{2j_A+1}\sum_i|M_{x_i}|^2,$$

where

$$A_{(1,2)}=2\pi n_{(1,2)}/1-\exp(-2\pi n_{(1,2)}).$$

The matrix elements, M_{x_i}, have been evaluated by Sommerfeld. Taking the x-axis in the $\mathbf{k}_1$ direction and θ as the scattering angle, the results are (S-502 and 509)

$$M_x=C\{i(n_2-n_1\cos\theta)F+(1-\cos\theta)(1-x)F'\}(1-x)^{-in_1-in_2-1},\tag{19}$$

$$M_{(z,y)}=-C\left\{\begin{matrix}\cos\phi\\ \sin\phi\end{matrix}\right\}\sin\theta[in_1F+(1-x)F']$$
$$\times(1-x)^{-in_1-in_2-1},$$

where $F=F(-in_1,-in_2,1,x)$ is the hypergeometric function,

$$F'=dF/dx,\quad x=-[4k_1k_2/(k_1-k_2)^2]\sin^2\tfrac{1}{2}\theta$$

and

$$C=-16\pi e^{\pi n_1}\frac{k_1k_2}{(k_1^2-k_2^2)^2(k_1-k_2)^2}\left(\frac{k_1+k_2}{k_1-k_2}\right)^{i(n_1+n_2)}.$$

Hence the cross section is given by

$$\frac{d\sigma}{d\Omega}=\frac{4}{3}\frac{A_1A_2e^{-2\pi n_2}}{Z^2}\frac{k_2}{k_1}\frac{k_1^2k_2^2}{(k_1-k_2)^4}\frac{D_{AB}^2}{2j_A+1}$$
$$\cdot\{|i(n_2-n_1\cos\theta)F+(1-\cos\theta)(1-x)F'|^2$$
$$+\sin^2\theta|in_1F+(1-x)F'|^2\}.\tag{20}$$

Still disregarding the finite size of the nucleus, this expression can be integrated over all angles of scattering (S-526), yielding the total cross section:

$$\sigma=\frac{2\pi}{3}\frac{A_1A_2e^{-2\pi n_2}}{Z^2}\frac{k_2}{k_1}\frac{D_{AB}^2}{2j_A+1}\frac{d}{dx_0}|F(x_0)|^2,\tag{21}$$

where $x_0=-4k_1k_2/(k_1-k_2)^2$ and

$$F(x_0)=F(-in_1,-in_2,1,x_0).$$

The general expressions for the cross sections given by (20) and (21) are rather complicated functions of energy and scattering angle. In certain limiting cases they reduce to much simpler expressions. We shall consider three limiting cases which are of some physical interest.

(*a*) *Cross Sections When n_1 Is Small.*—We shall consider the case $n_1\to0$, with n_2 arbitrary. For small n_1, $F\cong g$, $F'\cong0$, where $g=1$ if n_2/n_1 is not approximately equal to unity and $g=\sinh\pi n_1/\pi n_1$ if n_2/n_1 is approximately equal to unity.[11] Thus for small n_1,

$$\frac{d\sigma}{d\Omega}=\frac{4}{3}\left(\frac{n_1}{Z}\right)^2A_1A_2e^{-2\pi n_2}g^2\frac{D_{AB}^2}{2j_A+1}\frac{k_1k_2}{K^2}f^2,\tag{22}$$

$$K^2=k_1^2+k_2^2-2k_1k_2\cos\theta,$$

$$g=\left\{\begin{matrix}\sinh\pi n_1/\pi n_1 & \text{if } n_2\cong n_1\\ 1 & \text{otherwise}\end{matrix}\right\}.$$

The factor f^2 has been included to take account of the finite size of the nucleus. The value of f may be obtained readily in the limiting cases of small and large n_2. Thus if n_2 is small, Eq. (22) gives the first order coulomb corrections to the Born formula. Consequently for small n_2 we may take for f the value obtained in the Born approximation: $f=j_0(Kr_0)$. If, on the other hand, n_2 is large (i.e., v_2 is small), the angular distribution should be isotropic; for this case we may therefore take $f=1$. Thus we have the results

$$\begin{matrix}f=j_0(Kr_0) & \text{if } n_2 \text{ is small,}\\ f=1 & \text{if } n_2 \text{ is large.}\end{matrix}$$

[11] As $n_1\to0$ and $n_2/n_1\neq1$, then x is small and one can expand F and retain only the first term, namely, unity. As $n_1\to0$ and $n_2/n_1\cong1$, x is large (except for $\theta=0$) and one can express $F(x)$ in terms of $F(1/1-x)$; expanding $F(1/1-x)$ and retaining only the first term leads to the value $g=(\sinh\pi n_1)/\pi n_1$ in this case.

Integration over all angles then leads to the results:

$$\sigma=\frac{8\pi}{3}\left(\frac{n_1}{Z}\right)^2 g^2A_1A_2e^{-2\pi n_2}\frac{D_{AB}^2}{2j_A+1}C_i, \qquad (23)$$

where

$C_1=\ln[(k_1+k_2)/(k_1-k_2)]$ if n_2 is large (k_2 small),
$C_1=B_1$ of Eq. (12) if n_2 is small.

(*b*) *Cross Sections for Strong Coulomb Field.*—We consider next the case in which the influence of the coulomb field is very large. In particular, we consider the case $n_2\to\infty$ and $n_1\gg1$. Let

$$|P|^2=|i(n_2-n_1\cos\theta)F+1(1-\cos\theta)(1-x)F'|^2,$$
$$|Q|^2=|in_1F+(1-x)F'|^2,$$
$$\rho=n_1/n_2 \text{ so that } 0\leqslant\rho\leqslant1.$$

Again we take the x-axis along the $\mathbf{k}_1$ direction. Then as $n_2\to\infty$ and $n_1\gg1$, the majority of the particles are scattered backwards, and we need consider values of $\theta\cong\pi$ only. We then obtain (S-806)

$$\left\{\begin{matrix}|P|^2\\|Q|^2\end{matrix}\right\}=\frac{1}{64}\frac{n_2^2}{3}e^{2\pi n_1}\left\{\begin{matrix}\alpha^2e^{5\pi i/6}H_{2/3}^{(1)}(is)\\\alpha e^{2\pi i/3}H_{1/3}^{(1)}(is)\end{matrix}\right\}^2,$$

where

$$s=\frac{n_2\alpha^3\rho(1-\rho)}{6(1+\rho)^2},\quad \alpha=\pi-\theta,$$

and $H_q^{(1)}$ is the (cylindrical) hankel function. Hence

$$\left\{\begin{matrix}|M_x|^2\\|M_y|^2\\|M_z|^2\end{matrix}\right\}=\frac{4\pi^2}{3}\left(\frac{a}{Z}\right)^8\frac{n_1^{12}e^{4\pi n_1}}{(1-\rho^2)^3(1+\rho)^8}\alpha^4$$
$$\times\left\{\begin{matrix}e^{5\pi i/6}H_{2/3}^{(1)}(is)\\\cos\phi\ e^{2\pi i/3}H_{1/3}^{(1)}(is)\\\sin\phi\ e^{2\pi i/3}H_{1/3}^{(1)}(is)\end{matrix}\right\}^2, \qquad (24a)$$

where $a=\hbar^2/me^2$. Thus

$$\frac{d\sigma}{d\Omega}=\frac{A_1A_2}{144}\frac{k_2k_1^3}{(k_1-k_2)^4}\left(\frac{n_1}{Z}\right)^2\frac{D_{AB}^2}{2j_A+1}\exp[-2\pi(n_2-n_1)]\alpha^4$$
$$\cdot\{|e^{5\pi i/6}H_{2/3}^{(1)}(is)|^2+|e^{2\pi i/3}H_{1/3}^{(1)}(is)|^2\}. \qquad (24)$$

It is readily seen that the cross section is very small unless n_1 is quite large. For large n_1, the projectiles are not likely to penetrate into the nucleus, and it seems unnecessary, therefore, to make any correction for the finite size of the nucleus.

Integrating over all angles of scatter, we obtain (S-560)

$$\sigma=\frac{8\pi^2}{3\sqrt3}\left(\frac{n_1}{Z}\right)^2\frac{D_{AB}^2}{2j_A+1}\exp[-2\pi(n_2-n_1)]. \qquad (25)$$

(*c*) *Cross Sections for $n_2\cong n_1$, with n_1 Arbitrary.*—A case of considerable physical interest is that in which the energy transferred to the nucleus is small. For this case we write

$$k_1-k_2=\epsilon$$

so that,

$$n_2-n_1=n_1\epsilon/k_2.$$

The hypergeometric functions occurring in Eq. (20) can then be evaluated by use of the theorems:

$$\frac{d}{dx}F(a,b,c,x)=\frac{ab}{c}F(a+1,b+1,c+1,x),$$

$$(1-x)^{a+b-c}F(a,b,c,x)=F(c-a,c-b,c,x),$$

$$\lim_{\epsilon\to0}\epsilon^{-1}F(1+in_1,1+in_2,1,x)=0,$$

$$\lim_{\epsilon\to0}\epsilon^{-2}|F(1+in_1,1+in_2,1,x)$$
$$+in_1F(1+in_1,1+in_2,2,x)|^2=\frac{1}{K^2|\Gamma(1+in_1)|^2}.$$

Consequently, for this case

$$|M_x|^2\cong\frac{|c|^2n_1^2(k_1-k_2)^4}{|\Gamma(1+in_1)|^4}\cdot\frac{(1-\cos\theta)^2}{K^4},$$
$$|M_y|^2=|M_z|^2\cong\frac{|c|^2n_1^2(k_1-k_2)^4}{|\Gamma(1+in_1)|^4}\cdot\frac{\sin^2\theta}{K^4}. \qquad (26a)$$

On substitution of these results into Eq. (20) one obtains

$$\frac{d\sigma}{d\Omega}\cong\frac{4}{3}\exp[-2\pi(n_2-n_1)]n_1^2\frac{k_1k_2}{K^2}\frac{D_{AB}^2}{2j_A+1}j_0^2(Kr_0). \qquad (26)$$

The factor $j_0^2(Kr_0)$ has been included in (26) to take account of the finite size of the nucleus. Since the case $n_2\cong n_1$ corresponds to small effective interaction between projectile and nucleus we may expect this factor, which was obtained by the Born approximation [compare Eq. (11)] to be approximately correct here.

Integration over angles yields for the total cross section:

$$\sigma=\frac{8\pi}{3}\left(\frac{n_1}{Z}\right)^2\exp[-2\pi(n_2-n_1)]\frac{D_{AB}^2}{2j_A+1}B_1. \qquad (27)$$

(2) *Electric Quadrupole*

If the motion of the projectile is described by the coulomb wave functions U_1 and U_2 given in the preceding section, the matrix element for electric quadrupole transitions may be evaluated rather easily if the finite size of the nucleus is neglected in the integration over the projectile's coordinates. The effects of the finite size of the nucleus may be included, in limiting cases, by the procedures used in the preceding Section (II-B-1).

If the coulomb wave functions are expanded in terms of momentum functions[12]

$$U_1=\int \psi_k \exp(i\mathbf{k}\cdot\mathbf{r})d\mathbf{k}, \quad U_2^*=\int \psi_{k'} \exp(-i\mathbf{k}'\cdot\mathbf{r})d\mathbf{k}', \tag{28}$$

the electric matrix element, M, for 2^l-pole transitions can be written as

$$M_l=\langle U_2|\,V_l\,|U_1\rangle=\int\int \psi_{k'}\psi_k M_{l(\mathrm{Born})}(\mathbf{k},\mathbf{k}')d\mathbf{k}d\mathbf{k}', \tag{29}$$

where $M_{l(\mathrm{Born})}(\mathbf{k},\mathbf{k}')$ is the matrix element in the Born approximation. In the quadrupole ($l=2$) case, $M_{l(\mathrm{Born})}$ is independent of $\mathbf{k}$ and $\mathbf{k}'$. Thus,

$$M_2=M_{2(\mathrm{Born})}\cdot\int\int \psi_{k'}\psi_k d\mathbf{k}d\mathbf{k}'$$

$$=M_{2(\mathrm{Born})}\cdot U_2^*(0)U_1(0),$$

where $U_1(0)$ and $U_2(0)$ are the coulomb wave functions evaluated at the origin. Consequently, the use of coulomb field wave functions modifies the differential and total cross sections only by the factor

$$[2\pi n_1/(e^{2\pi n_1}-1)]\cdot[2\pi n_2/(e^{2\pi n_2}-1)]. \tag{30}$$

(C) Elastic Scattering

If both elastic and inelastic scattering cross sections are measured at an angle for which the elastic scattering is relatively independent of the properties of the target nucleus, the elastic scattering cross section can be used as a convenient normalization. The well-known formula for the elastic scattering cross section[13] can be simplified by making use of the semiclassical approximation that those projectiles for which the angular momentum l is greater than $l_c=kr_0(1-Ze^2/Er_0)^{\frac{1}{2}}$ miss the nucleus; these projectiles suffer no phase shift. The coulomb phase shift, η_l, can be evaluated by use of the relation

$$\eta_l=\arg\Gamma(l+1+in)=\arg\prod_{s=0}^{l-1}(l-s+in)\Gamma(1+in)$$

$$=\eta_0+\beta_l,$$

where

$$\beta_l=\sum_{s=1}^{l}\tan^{-1}n/s.$$

A case of particular simplicity is that in which projectiles which penetrate into the nucleus ($l\lesssim l_c$) are not likely to be elastically scattered. These projectiles may be omitted from the elastic scattering by setting their phase shifts equal to $i\infty$. In this case the elastic scattering cross section is given by

$$\frac{d\sigma}{d\Omega}=\left|\frac{n}{2k}\csc^2\tfrac{1}{2}\theta\exp[-2in\ln(\sin\tfrac{1}{2}\theta)]\right.$$

$$\left.+\frac{1}{2ik}\left\{1+\sum_{l=1}^{l_c}(2l+1)e^{2i\beta_l}P_l(\cos\theta)\right\}\right|^2. \tag{31}$$

This expression is independent of all properties of the nucleus except its radius and charge.

III. COMPARISON BETWEEN PARTICLE CROSS SECTIONS AND PHOTO CROSS SECTIONS: NUMBER OF ELECTRIC 2^l-POLE QUANTA

In Sec. II [Eq. (6)] we have seen that if the nuclear moments are randomly oriented, the cross section for the electric 2^l-pole excitation of a nucleus by the field of a nonrelativistic charged projectile may be factored into a product of the number of virtual electric 2^l-pole quanta in the field of the projectile and the photo-excitation cross section for the transition. We shall now give an explicit formulation of this "method of virtual quanta" for the coulomb field excitation of nuclei. We shall give explicitly the numbers of virtual electric dipole, quadrupole, and octupole quanta in the field of the charged projectile; and in the electric dipole case we establish the relation between the number of virtual and the number of real quanta (bremsstrahlung) associated with the deflection of the projectile. In the present discussion we shall give the results for a "point" target nucleus; the effects of the finite size of the nucleus may be taken into account, at least approximately, by the method discussed in Sec. II.

In order to obtain the number of virtual quanta, we must obtain an expression for the electric 2^l-pole photo-excitation cross section. The interaction between the radiation electric field $\boldsymbol{\varepsilon}$ and the electric 2^l-pole moment of the nucleus is taken as

$$U_l=\frac{1}{l!}e(\mathbf{E}\cdot\mathbf{R})(\mathbf{k}_\nu\cdot\mathbf{R})^{l-1}, \tag{32}$$

where $\mathbf{R}$ stands for the coordinates of the protons in the nucleus, $\mathbf{k}_\nu$ is the wave number of the incident radiation ($k_\nu=|\mathbf{k}_\nu|=2\pi/\lambda=E/hc$; E= transition energy); and $\boldsymbol{\pi}$ is a unit vector in the direction of polarization of the incident radiation. Thus

$$\sigma_l^{(\gamma)}=4\pi^2\frac{e^2}{hc}\frac{E}{2j_A+1}\sum_{a,b}\left|\left(b\left|\frac{(\boldsymbol{\pi}\cdot\mathbf{R})(\mathbf{k}_\nu\cdot\mathbf{R})^{l-1}}{l!}\right|a\right)\right|^2. \tag{33}$$

(1) *Electric Dipole Excitation*

Setting $l=1$ in Eq. (33) yields for the electric dipole photo-excitation cross section:

$$\sigma_1^{(\gamma)}=\frac{4\pi^2e^2k_\nu}{2j_A+1}\sum_{a,b}|(b|\,\boldsymbol{\pi}\cdot\mathbf{R}\,|a)|^2=\frac{4\pi^2}{3}e^2k_\nu\frac{D_{AB}^2}{2j_A+1}. \tag{34}$$

[12] This procedure was suggested to one of us by R. Serber in connection with another problem.

[13] L. I. Schiff, *Quantum Mechanics* (McGraw-Hill Book Company, Inc., New York, 1949), pp. 116 ff.

Thus from Eqs. (21) and (1) the cross section for electric dipole excitation of the nucleus by the field of a positively charged projectile is given by

$$\sigma_1 = N_1 \sigma_1^{(\gamma)},$$

where N_1, the number of virtual electric dipole quanta in the field of the charged projectile, is given by

$$N_1 dE = \frac{dE}{E} \frac{A_1 A_2}{2\pi Z^2} \frac{1}{e^2/\hbar c} \frac{k_2}{k_1} e^{-2\pi n_2 x_0} \left| \frac{d}{dx_0} F(x_0) \right|^2, \quad (35)$$

where E is the transition energy.

It is interesting to note that the cross section for the production of real quanta (bremsstrahlung), when the charged particle makes the transition due to deflection in a pure coulomb field, is expressible in terms of N_1 in a simple way. In the electric dipole approximation, the cross section for the production of bremsstrahlung in dE is (S-527 and 564)

$$\sigma_x dE = \frac{dE}{E} \frac{e^2}{\hbar c} \left(\frac{\hbar}{mc} \right)^2 \frac{n_1}{n_2} A_1 A_2 e^{-2\pi n_2 x_0} \left| \frac{d}{dx_0} F(x_0) \right|^2. \quad (36)$$

Comparison with (35) shows that the bremsstrahlung cross section may be written:

$$\sigma_x dE = 2\pi z^2 Z^2 (e^2/mc^3)^2 N_1 dE. \quad (37)$$

This simple result is of the form to be expected on the basis of semi-classical arguments.

In certain limiting cases the rather formidable expression (35) for N_1 may be replaced with relatively simple approximate expressions. Thus, from Eqs. (23), (27), and (25) we have

$$N_1 dE = \frac{dE}{E} \frac{2z^2}{\pi} \frac{e^2}{\hbar c} \left(\frac{c}{v_1} \right)^2 A_1 A_2 \times e^{-2\pi n_2} \ln \left(\frac{k_1 + k_2}{k_1 - k_2} \right), \quad \begin{matrix} n_1 \to 0 \\ n_2 \text{ arbitrary} \end{matrix} \quad (38)$$

$$N_1 dE = \frac{dE}{E} \frac{2z^2}{\pi} \frac{e^2}{\hbar c} \left(\frac{c}{v_1} \right)^2 \frac{A_2}{A_1} \times e^{-2\pi(n_2 - n_1)} \ln \left(\frac{k_1 + k_2}{k_1 - k_2} \right), \quad n_1 \cong n_2 \quad (39)$$

$$N_1 dE = \frac{dE}{E} \frac{2z^2}{\sqrt{3}} \frac{e^2}{\hbar c} \left(\frac{c}{v_1} \right)^2 e^{-2\pi(n_2 - n_1)}, \quad \begin{matrix} n_1 \gg 1 \\ n_2 \neq n_1 \end{matrix}. \quad (40)$$

The Born approximation result can be obtained from the first or second of these limiting cases by setting $A_1 = A_2 = 1 = e^{-2\pi n_2}$. The Born result is essentially the same as that obtained by the semi-classical method.

(2) *Electric Quadrupole Transitions*

Setting $l = 2$ in Eq. (33) gives for the electric quadrupole photo-excitation cross section:

$$\sigma_2^{(\gamma)} = \frac{\pi^2 e^2 k_\nu}{(2j_A + 1)} \sum_{a,b} |(b|(\boldsymbol{\pi} \cdot \mathbf{R})(\mathbf{k}_\nu \cdot \mathbf{R})|a)|^2$$

$$= \frac{\pi^2 e^2 k_\nu}{(2j_A + 1)} \sum_{a,b} \left| \sum_{i,j} (b|Q_{ij}|a) \pi_i k_{\nu j} \right|^2.$$

From a theorem which is given in Part 1 of the appendix to this paper it follows that

$$\sum_{a,b} \left| \sum_{i,j} (b|Q_{ij}|a) \pi_i k_{\nu j} \right|^2 = k_\nu^2 Q_{AB}'^2/10 \quad (41)$$

and, therefore,

$$\sigma_2^{(\gamma)} = (\pi^2 e^2/10) Q_{AB}'^2/(2j_A + 1) k_\nu^3. \quad (42)$$

Writing $\sigma_2 = N_2 \sigma_2^{(\gamma)}$ and using Eq. (14), one has for the number of electric quadrupole quanta

$$N_2 dE = (dE/E)(16z^2 e^2/3\pi\hbar c)(c/v_1)^2 k_1 k_2/k_\nu^2. \quad (43)$$

(3) *Electric Octupole Transitions*

Setting $l = 3$ in Eq. (33) yields for the electric octupole photo-excitation cross section:

$$\sigma_3^{(\gamma)} = \frac{\pi^2}{9} \frac{e^2}{\hbar c} \frac{E}{2j_A + 1} \sum_{a,b} |(b|(\boldsymbol{\pi} \cdot \mathbf{R})(\mathbf{k}_\nu \cdot \mathbf{R})^2|a)|^2$$

$$= \frac{\pi^2}{9} \frac{e^2}{\hbar c} \frac{E}{2j_A + 1} \sum_{a,b} \left| \sum_{ijk} (b|S_{ijk}|a) \pi_i k_{\nu i} k_{\nu k} \right|^2.$$

From a theorem given in Part 2 of the appendix it follows that

$$\sum_{a,b} \left| \sum_{ijk} (b|S_{ijk}|a) \pi_i k_{\nu j} k_{\nu k} \right|^2 = \frac{4k_\nu^4}{105} [S_{AB}'^2 + (7/20)(R^2 D)_{AB}^2], \quad (44)$$

where

$$(R^2 D)_{AB}^2 = \sum_i |(b|R^2 x_i|a)|^2.$$

Consequently

$$\sigma_3^{(\gamma)} = \frac{4\pi^2}{945} e^2 k_\nu^5 \frac{S_{AB}'^2 + (7/20)(R^2 D)_{AB}^2}{2j_A + 1}. \quad (45)$$

The $(R^2 D)_{AB}^2$ term results from an interaction between the radiation and the electric dipole moment of the nucleus, and should be added as a second order term to the electric dipole cross section. Since this term does not correspond to an octupole transition, we shall drop it from our expression for $\sigma_3^{(\gamma)}$. Thus we take

$$\sigma_3^{(\gamma)} = (4\pi^2 e^2/945) S_{AB}'^2 k_\nu^5/(2j_A + 1). \quad (46)$$

Writing $\sigma=N_\gamma\sigma_2^{(\gamma)}$ and using Eq. (16) for σ_2 we obtain, for the distribution of octupole quanta in the electric field of the charged projectile,

$$N_\gamma dE=\frac{dE}{E}\frac{6z^2}{\pi}\left(\frac{e^2}{\hbar c}\right)\left(\frac{c}{v_1}\right)^2\frac{k_1k_2(k_1^2+k_2^2)}{k_\rho^4}. \quad (47)$$

IV. ELECTRIC BREAK-UP OF THE DEUTERON

When a beam of deuterons strikes a target the deuterons may be disintegrated and emergent beams of neutrons and protons thus obtained. In a number of experiments the angular and energy distributions of the neutrons and protons have been studied. Helmholz, McMillan, and Sewell[14] have studied the angular and energy distributions of the neutrons obtained by bombarding targets with 190-Mev deuterons. Angular and energy distributions of the neutrons obtained when various targets are bombarded with 14- to 18-Mev deuterons have been studied by Falk, Creutz, and Seitz,[15] Roberts and Abelson,[16] and Ammiraju.[17] Angular and energy distributions of the protons obtained by bombarding thin targets with 14-kev deuterons have been studied by the M.I.T. group.[18] The results of all these experiments seem to indicate that the deuteron break-up which yields the protons or neutrons is due to stripping or to electric break-up. In the stripping process one of the nucleons of the deuteron strikes the target nucleus and is stripped off the deuteron; the other nucleon misses the nucleus and continues its flight. This process has been discussed for high energy deuterons by Serber,[19] and for low energy deuterons by Falk and Wolfenstein[20] and by French.[21] In the electric break-up process, the deuteron misses the nucleus but is disintegrated by its electric field. The possibility of electric break-up of the deuteron was first discussed by Oppenheimer.[22] A detailed theory of the process for high energy deuterons has been given by Dancoff,[9] using the Born approximation. The results of Dancoff and Serber show that for high energy deuterons nuclear stripping is considerably more probable than is electric break-up. However, at somewhat lower deuteron energies the electric process may play a significant role. Consequently, in this section we shall apply the results of Sec. II to the electric break-up of the deuteron.

In our discussion we include the effects of the coulomb field on the motion of the center of gravity of the deuteron, but we neglect the effects of the coulomb field on the outgoing proton. This procedure is probably adequate for a description of the behavior of the outgoing neutrons, but does not give an adequate description of the outgoing protons unless the deuteron energy is very high. We confine our attention to the outgoing neutrons.[23]

We describe the motion of the c.g. of the deuteron by means of the wave functions χ_1 and χ_2 of Eq. (17). The initial and final states of the deuteron's relative motion we shall describe by the "zero-range" wave functions:[24]

$$D_1=(\alpha/2\pi)^{\frac{1}{2}}e^{-\alpha\rho}/\rho, \quad \alpha=(M\epsilon_0/\hbar^2)^{\frac{1}{2}},$$
$$D_2=N_2\exp(i\mathbf{k}_\rho\cdot\boldsymbol{\rho}), \quad N_f=[Mk_\rho/(2\pi)^32\hbar^2]^{\frac{1}{2}}, \quad (48)$$

where $\epsilon_0\cong 2.2$ Mev is the deuteron's binding energy, M is the nucleon mass, $\boldsymbol{\rho}$ is the relative coordinate, and $\mathbf{k}_\rho$ is the wave number of the relative motion. In the electric dipole approximation, the cross section for deuteron break-up with disintegration energy in $d\epsilon$, the center of mass being scattered into the solid angle $d\Omega_2$, and the neutron ejected into $d\Omega_1$, is

$$\sigma d\epsilon d\Omega_1 d\Omega_2=\frac{2\pi}{\hbar}\left|\left(D_fX_f\left|\frac{Ze^2(\mathbf{r}\cdot\boldsymbol{\rho})}{2r^3}\right|D_iX_i\right)\right|^2 d\epsilon d\Omega_1 d\Omega_2$$
$$=\frac{\pi N_f^2|D|^2}{2\hbar k\rho^2}\left|\left(\chi_f\left|\frac{Ze^2(\mathbf{k}_\rho\cdot\mathbf{r})}{r^3}\right|\chi_i\right)\right|^2 d\epsilon d\Omega_1 d\Omega_2$$

with

$$|D|^2=\frac{1}{k_\rho^2}\left|\int\exp(-i\mathbf{k}_\rho\cdot\boldsymbol{\rho})(\mathbf{k}_\rho\cdot\boldsymbol{\rho})D_1d\rho\right|^2=\frac{32\pi\alpha k_\rho^2}{(k_\rho^2+\alpha^2)^4}.$$

Applying the equation of motion discussed in Sec. II-B we find

$$\sigma d\epsilon d\Omega_1 d\Omega_2$$
$$=\frac{2\pi}{\hbar}\frac{N_f^2|D|^2M^2}{k_\rho^2}\left(\frac{E_2-E_1}{\hbar}\right)^4|(\chi_2|\mathbf{k}_\rho\cdot\mathbf{r}|\chi_1)|^2 d\epsilon d\Omega_1 d\Omega_2$$
$$=(2\pi/\hbar)N_f^2N_E^2N_{fl}^2|D|^2M^2(E_2-E_1/\hbar)^4$$
$$\times\{\cos^2\theta_1\cdot|M_x|^2+\sin^2\theta_1\cdot\tfrac{1}{2}(M_y^2+M_z^2)\}d\epsilon d\Omega_1 d\Omega_2,$$

where θ_1 is the angle between the wave number vectors $\mathbf{k}_\rho$ and $\mathbf{k}_1$, with E_2 and E_1 as the final and initial energies of the motion of the center of mass, and with N_{fl}, N_E, $M_{x,y,z}$ as given by Eqs. (17) and (19). The x-direction has been chosen as the direction of the incident deuteron beam. When the intergrations over the

[14] Helmholz, McMillan, and Sewell, Phys. Rev. **72**, 1003 (1947).
[15] Falk, Creutz, and Seitz, Phys. Rev. **76**, 322 (1949). This publication gives only the preliminary results of the experiments. A complete account of the results is given by C. E. Falk, thesis, Carnegie Institute of Technology (1950). The authors wish to thank Dr. Falk for communicating his results to them.
[16] R. P. Roberts and P. H. Abelson, Phys. Rev. **72**, 76 (1947).
[17] P. Ammiraju, Phys. Rev. **76**, 1421 (1949).
[18] Progress Reports of the Laboratory for Nuclear Science and Engineering, M.I.T., January 1, 1950 and April 1, 1950, unpublished.
[19] R. Serber, Phys. Rev. **72**, 1008 (1947).
[20] C. E. Falk, thesis, reference 15.
[21] J. B. French, private communication (unpublished).
[22] J. R. Oppenheimer, Phys. Rev. **47**, 845 (1945).

[23] In an independent treatment of the electric break-up of the deuteron M. L. Goldberger (private communication) has taken into account in the influence of the coulomb field on the outgoing protons. M. L. Goldberger, Phys. Rev. **79**, 221 (1950). In all discussions the effects of polarization of the deuteron on the wave function of the incident deuteron are neglected.
[24] The finite range of the neutron-proton interaction can be included in an approximate way by using the factor $(1+\alpha b_t)$, where b_t is the range of the n–p interaction in the triplet ground state.

angles of scattering of the center of mass of the deuteron have been carried out we find that

$$\sigma d\epsilon d\Omega_1=(2\pi/\hbar)N_f{}^2N_E{}^2N_{fl}{}^2|D|^2M^2(E_2-E_1/\hbar)^2 \times\left\{\cos^2\theta_1\cdot\int|M_x|^2d\Omega_2+\sin^2\theta_1 \cdot\tfrac{1}{2}\int(M_y{}^2+M_z{}^2)d\Omega_2\right\}d\epsilon d\Omega_1. \quad (49)$$

This relatively complicated result can be simplified in certain limiting cases. Thus, if the deuteron moves in a strong coulomb field ($n_1\gg1$, $n_2\neq n_1$) we can use the approximate expressions given by Eq. (24a) for $M_{x,y,z}$. Then

$$\sigma d\epsilon d\Omega_1=\frac{8n_1{}^2\hbar^2(\epsilon_0\epsilon^2)^{\frac{1}{2}}}{3\sqrt{3}M(\epsilon+\epsilon_0)^4}\cdot\exp[-2\pi(n_2-n_1)] \cdot\{\cos^2\theta_1+\tfrac{1}{4}\sin^2\theta_1\}d\epsilon d\Omega_1. \quad (50)$$

A limiting case of importance from the experimental viewpoint is that in which the deuteron's initial energy exceeds the coulomb barrier energy by considerably more than the binding energy of the deuteron. We shall now investigate this case in detail. Inspection of the form of the factor $|D|^2$ shows that the cross section becomes small if the disintegration energy, ϵ, is large. Consequently the center of mass of the deuteron is not likely to lose more than a rather small fraction of its energy in the disintegration. For this reason we can substitute for M_x, M_y, and M_z the approximate values suitable for small energy transfer. From Eqs. (19) and (26a) we see that if n_2-n_1 is small, *or* if n_1 and n_2 are both small,

$$\begin{aligned}|M_x|^2&\cong|C|^2(k_1-k_2)^4(\sinh n_1\pi/n_1\pi)^2 \times(n_2-n_1\cos\theta_2)^2/K^4,\\ |M_y|^2+|M_z|^2&\cong|C|^2(k_1-k_2)^4 \times(\sinh n_1\pi/n_1\pi)^2\sin^2\theta_2/K^4.\end{aligned} \quad (51)$$

Substitution of these expressions into Eq. (49) yields:

$$\sigma d\epsilon d\Omega_1=\frac{2}{\pi}n_1{}^2\exp[-2\pi(n_2-n_1)]\frac{\hbar^2}{M}\frac{\epsilon_0{}^{\frac{1}{2}}\epsilon^{\frac{3}{2}}}{(\epsilon+\epsilon_0)^4} \times\left\{\frac{(k_1+k_2)^2+K_m{}^2}{4k_1{}^2}\left(1-\frac{1}{\Gamma^2}\right)P_2(\cos\theta_1) +\sin^2\theta_1\ln\Gamma\right\}d\epsilon d\Omega, \quad (52)$$

where $\Gamma=K_m/(k_1-k_2)$ and $\hbar K_m$ is the maximum recoil suffered by the center of gravity of the deuteron. If the finite size of the nucleus is neglected, $K_m=k_1+k_2$; the effects of the finite size of the nucleus can be taken into account by limiting the maximum recoil momentum to $\hbar K_m=1/r_0$, where r_0 is the sum of the "radii" of the deuteron and target nucleus. Apart from the "coulomb factor," $\exp[-2\pi(n_2-n_1)]$, the cross section given by Eq. (52) is equivalent to that obtained by Dancoff[9] by using the Born approximation.

To facilitate comparison with experiment, we shall carry out a transformation of variables from (ϵ,θ_1) to (E_n,θ), where E_n is the neutron's energy in the system of the center of mass of the target nucleus and deuteron, and θ is the angle between the direction of the outgoing neutron and the direction of the incident deuteron beam. We neglect the finite size of the target nucleus, taking $K_m=k_1+k_2$. This omission will tend to overemphasize the role of the neutrons at the upper and of the energy spectrum and will yield an upper limit for the total cross section. Since with $n_2\cong n_1$ the probability of large lateral deflection of the deuteron's center of gravity is small (see Eq. (26)), we shall assume that the deuteron's center of gravity moves in a straight line. With these approximations one can take

$$\epsilon/E_D'\cong f^2+\theta^2,\quad(\epsilon/E_D')\sin^2\theta_1\cong\theta^2$$

so that

$$(\epsilon/E_D')P_2(\cos\theta_1)\cong f^2-\tfrac{1}{2}\theta^2.$$

The jacobian of the transformation is

$$J\cong2\cos\theta/[f^2+\theta^2]^{\frac{1}{2}},$$

where $E_D'=E_D-E_B$; $E_D=$initial deuteron energy; $E_B=$coulomb barrier energy of the deuteron at the time of break-up and

$$f=[E_N-\tfrac{1}{2}(E_D'-\epsilon_0)]/E_D'. \quad (53)$$

Consequently the cross section for electric break-up, with the neutron being ejected into the solid angle $d\Omega$ with energy in dE_N

$$\sigma d\Omega dE_N\cong\frac{8Z^2e^4C_1}{\pi E_DE_D'{}^2}\left(\frac{\epsilon_0}{E_D'}\right)^{\frac{1}{2}}\frac{[f^2+\frac{1}{2}\theta^2(\ln\lambda-1)]}{[f^2+\theta^2+(\epsilon_0/E_D')]^4}d\Omega dE_N \quad (54)$$

with

$$\begin{aligned}C_1&=\exp\{-(\pi n_1E_D'/E_D)[f^2+\theta^2+(\epsilon_0/E_D')]\},\\ &=4/[f^2+\theta^2+(\epsilon_0/E_D')].\end{aligned}$$

The angular and energy distributions can be obtained from Eq. (55) by integration. In general, these integrations cannot be carried out analytically, and we shall perform them explicitly only for the case that n_1 is sufficiently small that $\pi n_1\epsilon_0/E_D\ll1$, so that $C_1\cong1$. Since the logarithm is a slowly varying function of the angle, the integrals of the type

$$I=\int f(x)\ln\phi(x)dx,$$

in which $f(x)$ is a rather rapidly varying function of x which is appreciably different from zero only over a limited range of x, can be evaluated by the following approximation

$$I\cong\ln\phi_M\cdot\int f(x)dx,$$

where

$$\phi_{Av}=\int \chi(x)f(x)dx \Big/ \int f(x)dx.$$

Furthermore, since the cross section diminishes rapidly to zero as θ becomes large, or as $[E_N-\frac{1}{2}(E_D'-\epsilon_0)]$ becomes large, the limits of the integral can be taken to be zero and infinity. Carrying out the integrations for $C_1\cong 1$ we find for the angular and energy distributions of the outgoing neutrons

$$\sigma d\Omega=\frac{Z^2e^4}{2E_DE_D'}\left(\frac{\epsilon_0}{E_D'}\right)^{\frac{1}{2}} \times\frac{[(\epsilon_0/E_D')+\frac{1}{2}\theta^2(5\ln\xi_1-3)]}{[(\epsilon_0/E_D')+\theta^2]^{7/2}}\cdot\cos\theta\cdot d\Omega, \quad (55)$$

$$\sigma dE_N=\frac{2Z^2e^4}{3E_DE_D'^2}\left(\frac{\epsilon_0}{E_D'}\right)^{\frac{1}{2}} \times\frac{[(3+\ln\xi_2)f^2+(\ln\xi_2-1)\epsilon_0/E_D']}{[f^2+(\epsilon_0/E_D')]^3}dE_N \quad (56)$$

with

$$\xi_1=10/3(\theta^2+\epsilon_0/E_D'), \quad \xi_2=4/3(f^2+\epsilon_0/E_D').$$

The total cross section can be obtained by an integration of (56) over all neutron energies. We thus find

$$\sigma=(\pi Z^2e^4/3\epsilon_0E_D)\ln(E_D'/3^{\frac{1}{2}}\epsilon_0). \quad (57)$$

The total cross section can also be obtained by a direct integration of Eq. (52). In case the exponential member is taken to be unity this yields

$$\sigma=\frac{16Z^2e^4\epsilon_0^{\frac{1}{2}}}{3E_D}\int_0^{\epsilon_{\max}}\frac{\epsilon^{\frac{1}{2}}}{(\epsilon+\epsilon_0)^4}\ln\Gamma\cdot d\epsilon \cong\frac{16Z^2e^4\epsilon_0^{\frac{1}{2}}}{3E_D}\ln\Gamma_{Av}\cdot\int_0^{\infty}\epsilon^{\frac{1}{2}}/(\epsilon+\epsilon_0)^4d\epsilon$$

or

$$\sigma=(\pi Z^2e^4/3\epsilon_0E_D)\ln\Gamma_{Av}, \quad (58)$$

where

$$\Gamma=(k_1+k_2)/(k_1-k_2)\cong 4E_D/(\epsilon+\epsilon_0).$$

We then have from our definition of average values

$$\Gamma_{Av}=\frac{\int_0^{\infty}\Gamma(\epsilon)\epsilon^{\frac{1}{2}}/(\epsilon_0+\epsilon)^4d\epsilon}{\int_0^{\infty}\epsilon^{\frac{1}{2}}/(\epsilon_0+\epsilon)^4d\epsilon}=2E_D/3\epsilon_0.$$

The very slight difference between the cross section formulas (57) and (58) arises from the approximations used in the transformation to the laboratory system of coordinates.

V. DISCUSSION OF THE RESULTS

We shall now apply the theory developed in the preceding sections to a discussion of two processes in which electric transitions may play a significant role.

(A) Inelastic Scattering of Deuterons

We have pointed out that the inelastic scattering of deuterons should take place primarily through electric transitions. Experimental data on the deuterons scattered inelastically on aluminum and magnesium targets have been obtained by Greenlees, Kempton, and Rhoderick,[2] and by Holt and Young.[3] The angular distribution of the inelastically scattered deuterons offers the best criterion for the determination of the type of interaction responsible for the transition. Transitions occuring as a result of compound nucleus formation should yield an almost isotropic distribution of the inelastically scattered deuterons. Electric dipole interaction, on the other hand, leads to the differential cross section [see Eq. (26)]:

$$\frac{d\sigma}{d\Omega}=\frac{4}{3}\left(\frac{n_1}{Z}\right)^2\exp[-2\pi(n_2-n_1)]\frac{D_{AB}^2}{2j_A+1}\frac{k_1k_2}{K^2}j_0^2(Kr_0). \quad (59)$$

In making quantitative use of Eq. (59) for deuterons it must be remembered that to the approximations used in the derivation of this equation we must add the following: (1) the finite extension of the projectile's charge distribution is neglected; the deuteron's charge is assumed to be concentrated at the deuteron's center of mass, (2) the polarization (stretch) of the deuteron in the field of the target nucleus is neglected.

Because of the approximations used, we can expect Eq. (59) to have only semi-quantitative significance at large angles. However, the angular distributions predicted by Eq. (59) on the one hand, and by the theory of compound nucleus formation on the other, differ so greatly that despite the omission of the second-order effects involved in our approximations we should be able to distinguish readily between the two types of angular distribution.

The angular distribution obtained by Holt and Young for 7.5-Mev deuterons cattered inelastically on magnesium is reproduced for convenience in Fig. 1(a). The excitation energy is 1.36 Mev. The angular distribution for elastically scattered deuterons (7.5-Mev deuterons on the same magnesium target) is also given in this figure.

The theoretical angular distribution given by Eq. (59) depends somewhat upon the choice of the "cut-off" radius, r_0. We may write

$$r_0=1.5(24)^{\frac{1}{3}}\times 10^{-13}+R_D \text{ cm}$$

where R_D is the mean radius of the deuteron. The choice of R_D is certainly not unambiguous; and we have chosen it so that the theoretical angular distribution has its second minimum at $\theta=60°$ as required by the experimental results. This requires that $Kr_0=2\pi$ at $\theta=60°$; thus, $r_0=7.58\times 10^{-13}$ cm, and $R_D=3.25\times 10^{-13}$ cm.

The value of the nuclear dipole moment,

$$D_{AB}[=(D_{AB}^2)^{\frac{1}{2}}],$$

for the transition which causes the inelastic scattering

may be obtained by comparison of the experimental and theoretical ratios of inelastic and elastic scattering. Since compound nucleus formation is not likely to play a significant role in the elastic scattering of deuterons, the appropriate expression for the elastic scattering cross section is given by Eq. (31). Since the elastic scattering at a given angle depends rather critically on the choice of the ambiguous quantity l_e, we have integrated the differential cross sections over all angles from 75° to 135° and then equated the theoretical and experimental ratios of inelastic to elastic cross sections. One obtains $D_{AB}=7.5\times10^{-13}$ cm; this is about 1.74 R_N, where R_N is the nuclear radius ($R_N=1.5\times(24)^{\frac{1}{3}}\times10^{-13}=4.33\times10^{-13}$ cm) of $_{12}Mg^{24}$. In view of the approximations involved, this result is not unreasonable. The theoretical angular distribution ($d\sigma/d\Omega$) for the inelastic scattering of 7.5-Mev deuterons on Mg^{24} is given in Fig. 1(b). The total cross section for inelastic scattering is given by

$$\sigma=0.041D_{AB}^2=2.1\times10^{-26}\text{ cm}^2.$$

Comparison of the theoretical angular distribution with the experimental one seems to indicate rather clearly that the inelastic scattering is due to electric interaction.†

The experimental data obtained by Rhoderick[1] on the total cross sections for protons scattered inelastically on aluminum and magnesium targets seem to indicate that the energy transfer takes place primarily by compound nucleus formation. Unfortunately, no angular distributions are given in the published results of these experiments.

(B) Electric Break-Up of the Deuteron in Flight

First of all we shall give a comparison of the cross sections for the competitive processes of stripping and electric break-up. In both processes, we shall restrict ourselves to the case in which the escaping *neutron* is observed. In the computation of the electric break-up cross section, we shall neglect the finite size of the target nucleus;[25] this procedure yields an upper limit for the cross section. In the point nucleus approximation, the cross section for electric break-up may be obtained by setting $K_m=k_1+k_2$ in Eq. (52). We shall assume that in the majority of the disintegrations, the energy lost by the center of gravity of the deuteron is small compared

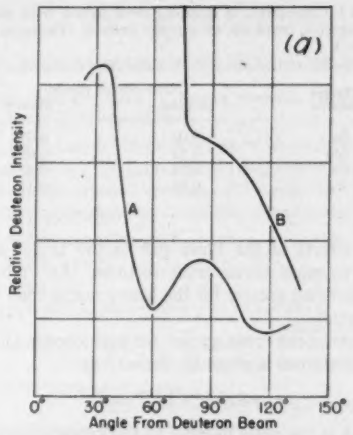

FIG. 1(a). Empirical results obtained by Holt and Young for the angular variation of the intensity of deuterons scattered inelastically (curve *A*) and elastically (curve *B*) on magnesium.

to the initial energy of the deuteron; consequently, we may make the approximations: $k_1-k_2\cong2E_1/(\epsilon+\epsilon_0)$, $k_1+k_2\cong2k_1$. Setting $x=\epsilon/\epsilon_0$, the total cross section for electric break-up is given by

$$\sigma=\frac{16Z^2e^4}{3\epsilon_0E_1}e^{-\pi\eta_1\epsilon_0/E_1}\int_0^{x_m}\frac{x^3}{(1+x)^4}\times e^{-\pi\eta_2\epsilon_0/E_1}\ln\left[\frac{4E_1}{E_0(1+x)}\right]dx.$$

The upper limit, x_m, is determined by energy conservation; for deuterons having energy of 15 Mev or more, no appreciable error is incurred by taking $x_m=\infty$. The electric break-up cross section has been evaluated by numerical integration for 15-Mev deuterons for four values of Z; the results are given in Table I. Inclusion

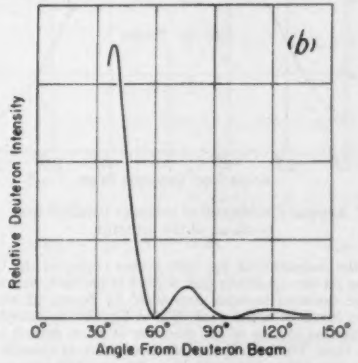

FIG. 1(b). Theoretical angular variation of intensity of deuterons scattered inelastically from magnesium.

† If the electric dipole moment, D_{AB}, is very small, the scattering may be due to electric quadrupole interaction.

[25] For 200-Mev deuterons, Dancoff has taken the finite size of the nucleus into account by limiting the recoil momentum of the deuteron's center of gravity to values less than or equal to $\hbar/r_0$, where r_0 is the sum of the radii of the deuteron and target nucleus. For high energies this cutoff in momentum space is approximately equivalent to the more exact procedure of modifying (in configuration space) the interaction between the target nucleus and the deuteron to take account of the nuclear forces. For the much lower energies (~15 Mev) in which we shall be interested, the momentum space cutoff is a very poor approximation, and the more exact procedure must be used. Modification of the interaction to include the effects of nuclear forces leads to very complicated integrations and cumbersome formulas; we believe that that the labor involved in these computations is not warranted at the present time.

TABLE I. Comparison of stripping cross section with cross section for electric break-up on a point nucleus. (Deuteron energy = 15 Mev.)

Target nucleus	Cross section (barns) Stripping	Electric
Be	0.09	0.016
Mg	0.12	0.094
Cu	0.14	0.22
Au	0.08	0.17

of the effects of the finite size of the target nucleus would decrease these cross sections, the amount of decrease being greater for the heavy nuclei than for the light nuclei.

The stripping cross section for high energy ($E_1 \cong 200$ Mev) deuterons is given by Serber[19] as

$$\sigma_s \cong 5.4 A^{\frac{1}{3}} \times 10^{-26} \text{ cm}^2, \tag{60}$$

where A is the mass number of the target nucleus. For lower deuteron energies an estimate of the (d,n) stripping cross section can be obtained by modifying Eq. (60) to include the effect of the coulomb repulsion on the incident deuteron.[26] This modification may be achieved in an approximate way by multiplying the right hand side of Eq. (60) by a factor $\rho(R)$ which takes

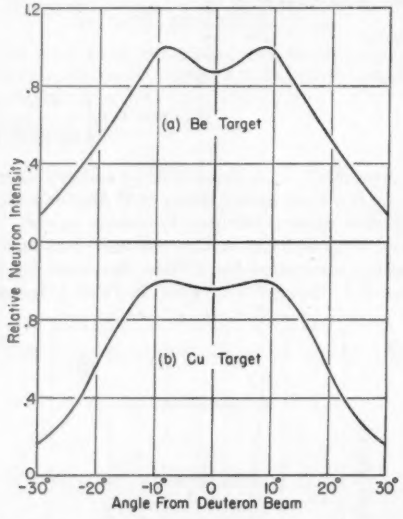

FIG. 2. Angular distribution of neutrons obtained from electric break-up of the deuteron.

[26] In the derivation of Eq. (60) Serber neglected the Coulomb repulsion on the deuteron; this neglect is justified, of course, for the large deuteron energies considered by Serber. A second assumption involved in the derivation of Eq. (60) is that the period of the internal motion of the deuteron is much greater than the collision time. The validity of this assumption is questionable for deuteron energies as low as 15 Mev, but we shall assume that no large errror is introduced in the total cross section by the use of this assumption.

account of the decrease in the density of protons at the nuclear surface due to the coulomb repulsion.[27] This density factor has been evaluated by Konopinski and Bethe.[28] For the target nuclei ${}_4\text{Be}^9$, ${}_{12}\text{Mg}^{24}$, ${}_{29}\text{Cu}^{63}$, and ${}_{79}\text{Au}^{197}$ one obtains the values $\rho = 0.9$, 0.8, 0.72, and 0.28, respectively. Values of the stripping cross sections for the four nuclei are given in Table I. Since we have assumed tacitly the proton's sticking probability to be unity in each case, the values listed in the table really give upper limits for the stripping cross sections.

The results given in Table I indicate that cross sections for the electric break-up process may be large enough, in some cases, to enable this process to compete favorably with the stripping process.

The theoretical angular and energy distributions for the neutrons obtained by electric break-up of the deuteron in flight are given by Eqs. (54), (55), and (56). Plots of the angular distributions obtained with 15-Mev deuterons incident on Be and Cu targets are given in Fig. 2. In the consideration of the theoretical distributions it should be remembered that a "point nucleus" model has been used. Furthermore, spreading of the deuteron beam because of coulomb deflection and multiple scattering has been neglected; this spreading of the beam will widen the angular distribution somewhat. It should be noted that in the angular distributions given in Fig. 2, neutrons of all permitted energies are counted. In most of the experiments, neutron detectors having rather high threshold energies have been employed. At the high end of the neutron spectrum our expressions are not quantitatively valid, for we have assumed the loss of energy of the deuteron's center of gravity to be small compared to the deuteron's initial energy.

The predictions of the electric break-up theory seem to be consistent with the experimental results. Thus, neglecting the spreading of the deuteron beam, the theoretical angular distribution (for neutrons of all permitted energies) has a half width of about 40° for both Be and Cu targets. Thus, at least up to $Z = 30$, the half-width is roughly independent of the atomic number of the target nucleus. And, again in agreement with experiment, the theory predicts that the yield of neutrons from a heavy target such as gold is less than the yield from a light target such as magnesium.

The electric break-up of the deuteron seems to lead characteristically to a "double-peaked" angular distribution for the escaping neutrons if neutrons of all energies are counted. If, however, one counts only the neutrons at the upper end of the energy spectrum, the theory yields a "single-peaked" distribution; it must be remembered, however, that our expressions do not have quantitative validity for the extreme energies of the neutron spectrum.

Lack of sufficient experimental data in the range of

[27] D. C. Peaslee, Phys. Rev. **74**, 1001 (1948).

[28] E. J. Konopinski and H. A. Bethe, Phys. Rev. **54**, 130 (1938). In the notation of these authors $\rho = l_0^2/l_0^2$.

neutron energies for which our theory has quantitative significance, and lack of an adequate theory of the stripping process for "low" energy deuterons make it impossible to assess, at present, the relative contributions of stripping and electric break-up to the observed neutron intensities. Of course, any neutrons observed to have energy greater than $E_1-\epsilon_0$ ($\cong$12.8 Mev for 15 Mev deuterons) cannot result from electric break-up and must be attributed to stripping or to compound nucleus formation in which the target nucleus absorbs the incident deuteron and subsequently emits a neutron.

APPENDIX

(A). The result given in Eq. (41) of the text follows from the more general theorem[29]

$$\sum_{a,b}|\sum_{ij}(b|Q_{ij}|a)u_iv_j|^2=(Q_{AB}'^2/10)[u^2v^2+\tfrac{1}{2}(\mathbf{u}\cdot\mathbf{v})^2]+I_{AB}^2(\mathbf{u}\cdot\mathbf{v})^2/9, \quad (61)$$

where $\mathbf{u}$ and $\mathbf{v}$ are arbitrary vectors. We shall now prove this theorem.

We introduce the tensor T which has elements $T_{ij}=u_iv_j+u_jv_i$. And we introduce the spherical harmonics Y_2^m defined by

$$Y_2^0(Q)=(\tfrac{5}{4})^{\frac{1}{2}}(3z^2-r^2), \qquad Y_2^0(T)=(\tfrac{5}{4})^{\frac{1}{2}}(3u_zv_z-\mathbf{u}\cdot\mathbf{v}),$$
$$Y_2^{\pm1}(Q)=\mp 2s(x\pm iy), \qquad Y_2^{\pm1}(T)=\mp\{u_z(v_x\pm iv_y)+v_z(u_x\pm iu_y)\},$$
$$Y_2^{\pm2}(Q)=(x\pm iy)^2, \qquad Y_2^{\pm2}(T)=(u_x\pm iu_y)(v_x\pm iv_y).$$

We then have the following relations

$$\sum_m|Y_2^m(Q)|^2=4\sum_{ij}|Q_{ij}|^2,$$
$$\sum_{a,b}|(b|Y_2^m(Q)|a)|^2=\tfrac{1}{5}Q_{AB}'^2 \text{ for all } m,$$
$$\sum_m|Y_2^m(T)|^2=2[u^2v^2+\tfrac{1}{2}(\mathbf{u}\cdot\mathbf{v})^2],$$
$$\sum_m Y_2^m(Q)Y_2^{m*}(T)=2\sum_{ij}Q_{ij}'(u_iv_j+u_jv_i-\tfrac{2}{3}\mathbf{u}\cdot\mathbf{v}\delta_{ij}).$$

Consequently,

$$\sum_{a,b}|\sum_{ij}(b|Q_{ij}|a)u_iv_j|^2$$
$$=\sum_{a,b}|\sum_{ij}\{(b|Q_{ij}'|a)+\tfrac{1}{5}(b|I|a)\delta_{ij}\}\tfrac{1}{2}(u_iv_j+u_jv_i)|^2$$
$$=\sum_{a,b}|\tfrac{1}{2}\sum_{ij}(b|Q_{ij}'|a)(u_iv_j+u_jv_i-\tfrac{2}{3}\mathbf{u}\cdot\mathbf{v}\delta_{ij})+\tfrac{1}{10}\mathbf{u}\cdot\mathbf{v}(b|I|a)\delta_{ij}|^2$$
$$=\sum_{a,b}|\tfrac{1}{2}\sum_m(b|Y_2^m(Q)|a)Y_2^{m*}(T)+\tfrac{1}{10}\mathbf{u}\cdot\mathbf{v}(b|I|a)|^2$$
$$=\sum_{a,b}|\tfrac{1}{16}\sum_m|(b|Y_2^m(Q)|a)|^2|Y_2^m(T)|^2+[(\mathbf{u}\cdot\mathbf{v})^2/9]|(b|I|a)|^2\}$$
$$=(Q_{AB}'^2/10)[u^2v^2+\tfrac{1}{2}(\mathbf{u}\cdot\mathbf{v})^2]+(I_{AB}^2/9)(\mathbf{u}\cdot\mathbf{v})^2.$$

The special choice $\mathbf{u}=\mathbf{k}_p$, $\mathbf{v}=\boldsymbol{\pi}$ yields the result given in Eq. (41) of the text.

(B). The result given in Eq. (44) of the text follows from the more general theorem

$$\sum_{a,b}|\sum_{ijk}(b|S_{ijk}|a)u_iv_jw_k|^2$$
$$=\frac{S_{AB}'^2}{210}\{5u^2v^2w^2-2(\mathbf{u}\cdot\mathbf{v})(\mathbf{v}\cdot\mathbf{w})(\mathbf{w}\cdot\mathbf{u})$$
$$+3[(\mathbf{u}\cdot\mathbf{v})^2w^2+(\mathbf{v}\cdot\mathbf{w})^2u^2+(\mathbf{w}\cdot\mathbf{u})^2v^2]\}$$
$$+\frac{(r^2D)_{AB}^2}{75}\{6(\mathbf{u}\cdot\mathbf{v})(\mathbf{v}\cdot\mathbf{w})(\mathbf{w}\cdot\mathbf{u})$$
$$+[(\mathbf{u}\cdot\mathbf{v})^2w^2+(\mathbf{v}\cdot\mathbf{w})^2u^2+(\mathbf{w}\cdot\mathbf{u})^2v^2]\}, \quad (62)$$

where

$$(r^2D)_{AB}=\sum_{a,b}\sum_i|(b|r^2z_i|a)|^2$$

and $\mathbf{u}$, $\mathbf{v}$, and $\mathbf{w}$ are arbitrary vectors. We shall now prove this theorem.

We introduce the tensor T having elements $T_{ijk}=\sum_P u_iv_jw_k$ and the tensor T' having elements

$$T_{ijk}'=\sum_P\{u_iv_jw_k-\tfrac{1}{5}\delta_{ij}[u_k(\mathbf{v}\cdot\mathbf{w})+v_k(\mathbf{w}\cdot\mathbf{u})+w_k(\mathbf{u}\cdot\mathbf{v})]\},$$

where the sums are extended over all permutations of ijk. And we introduce the spherical harmonics Y_3^m defined by

$$Y_3^0(S)=(\tfrac{7}{4})^{\frac{1}{2}}(5z^3-3r^2z),$$
$$Y_3^{\pm1}(S)=\mp(\tfrac{7}{8})^{\frac{1}{2}}(5z^2-r^2)(x\pm iy),$$
$$Y_3^{\pm2}(S)=(6)^{\frac{1}{2}}z(x\pm iy)^2,$$
$$Y_3^{\pm3}(S)=\mp(x\pm iy)^3,$$
$$Y_3^0(T)=(4/45)^{\frac{1}{2}}\{u_z(5v_zw_z-3\mathbf{v}\cdot\mathbf{w})+v_z(5w_zu_z-3\mathbf{w}\cdot\mathbf{u})$$
$$+w_z(5u_zv_z-3\mathbf{u}\cdot\mathbf{v})\},$$
$$Y_3^{\pm1}(T)=\mp(1/15)^{\frac{1}{2}}\{(5u_zv_z-\mathbf{u}\cdot\mathbf{v})(w_x\pm iw_y)$$
$$+(5v_zw_z-\mathbf{v}\cdot\mathbf{w})(u_x\pm iu_y)+(5w_zu_z-\mathbf{w}\cdot\mathbf{u})(v_x\pm iv_y)\},$$
$$Y_3^{\pm2}(T)=(\tfrac{7}{8})^{\frac{1}{2}}\{u_z(v_x\pm iv_y)(w_x\pm iw_y)$$
$$+v_z(w_x\pm iw_y)(u_x\pm iu_y)+w_z(u_x\pm iu_y)(v_x\pm iv_y)\},$$
$$Y_3^{\pm3}(T)=\mp(u_z\pm iu_y)(v_x\pm iv_y)(w_x\pm iw_y).$$

We then have the following relations:

$$\sum_{ijk}S_{ijk}'T_{ijk}'=\tfrac{3}{4}\sum_m Y_3^m(S)Y_3^{m*}(T),$$
$$\sum_m|Y_3^m(S)|^2=8\sum_{ijk}|S_{ijk}'|^2,$$
$$\sum_{a,b}|(b|Y_3^m(S)|a)|^2=(8/7)S_{AB}'^2 \text{ for all } m,$$
$$\sum_m|Y_3^m(T)|^2=(4/15)\{5u^2v^2w^2-2(\mathbf{u}\cdot\mathbf{v})(\mathbf{v}\cdot\mathbf{w})(\mathbf{w}\cdot\mathbf{u})$$
$$+3[(\mathbf{u}\cdot\mathbf{v})^2w^2+(\mathbf{v}\cdot\mathbf{w})^2u^2+(\mathbf{w}\cdot\mathbf{u})^2v^2]\},$$
$$\sum_i[(\mathbf{u}\cdot\mathbf{v})w_i+(\mathbf{v}\cdot\mathbf{w})u_i+(\mathbf{w}\cdot\mathbf{u})v_i]^2$$
$$=6(\mathbf{u}\cdot\mathbf{v})(\mathbf{v}\cdot\mathbf{w})(\mathbf{w}\cdot\mathbf{u})+[(\mathbf{u}\cdot\mathbf{v})^2w^2+(\mathbf{v}\cdot\mathbf{w})^2u^2+(\mathbf{w}\cdot\mathbf{u})^2v^2].$$

Consequently,

$$\sum_{a,b}|\sum_{ijk}(b|S_{ijk}|a)u_iv_jw_k|^2$$
$$=\frac{1}{36}\sum_{a,b}|\sum_{ijk}(b|S_{ijk}|a)\sum_P u_iv_jw_k|^2$$
$$=\frac{1}{36}\sum_{a,b}|\sum_{ijk}\{(b|S_{ijk}'|a)+\frac{1}{10}(b|r^2\sum_P x_i\delta_{jk}|a)\}\sum_P u_iv_jw_k|^2$$
$$=\frac{1}{36}\sum_{a,b}|\sum_{ijk}(b|S_{ijk}'|a)T_{ijk}'+\frac{1}{10}(b|r^2\sum_P x_i\delta_{jk}|a)\sum_P u_iv_jw_k|^2$$
$$=\frac{1}{36}\sum_{a,b}|\tfrac{3}{4}\sum_m(b|Y_3^m(S)|a)Y_3^{m*}(T)$$
$$+\frac{1}{10}\sum_{ijk}(b|r^2\sum_P x_i\delta_{jk}|a)\sum_P u_iv_jw_k|^2$$
$$=\frac{1}{36}\sum_{a,b}|\tfrac{3}{4}\sum_m(b|Y_3^m(S)|a)Y_3^{m*}(T)$$
$$+(6/5)\Sigma_i(b|r^2x_i|a)[(\mathbf{u}\cdot\mathbf{v})w_i+(\mathbf{v}\cdot\mathbf{w})u_i+(\mathbf{w}\cdot\mathbf{u})v_i]|^2$$
$$=\frac{1}{64}\sum_{a,b}\sum_m|(b|Y_3^m(S)|a)|^2|Y_3^m(T)|^2$$
$$+\frac{(r^2D)_{AB}^2}{75}\sum_i[(\mathbf{u}\cdot\mathbf{v})w_i+(\mathbf{u}\cdot\mathbf{w})v_i+(\mathbf{w}\cdot\mathbf{u})v_i]^2$$
$$=\frac{S_{AB}'^2}{210}\{5u^2v^2w^2-2(\mathbf{u}\cdot\mathbf{v})(\mathbf{v}\cdot\mathbf{w})(\mathbf{w}\cdot\mathbf{u})$$
$$+3[(\mathbf{u}\cdot\mathbf{v})^2w^2+(\mathbf{v}\cdot\mathbf{w})^2u^2+(\mathbf{w}\cdot\mathbf{u})^2v^2]\}$$
$$+\frac{(r^2D)_{AB}^2}{75}\{6(\mathbf{u}\cdot\mathbf{v})(\mathbf{v}\cdot\mathbf{w})(\mathbf{w}\cdot\mathbf{u})$$
$$+[(\mathbf{u}\cdot\mathbf{v})^2w^2+(\mathbf{v}\cdot\mathbf{w})^2u^2+(\mathbf{w}\cdot\mathbf{u})^2v^2]\}.$$

The special choice $\mathbf{u}=\mathbf{v}=\mathbf{k}_p$, $\mathbf{w}=\boldsymbol{\pi}$ leads to the result given in Eq. (44).

[29] This theorem is used by G. C. Wick, reference 8. A similar theorem has been proved by D. L. Falkoff (thesis, University of Michigan, 1948). Our proof is based on the method used by Falkoff.

Statistical Theory of Pressure Broadening*

HENRY MARGENAU
Sloane Physics Laboratory, Yale University, New Haven, Connecticut
(Received December 4, 1950)

The statistical theory of pressure broadening is developed for any interaction law in which the potential energy is inversely proportional to some power of the distance between the molecules, including cases in which the forces change sign. Markoff's method is used. Special attention is given to the broadening produced by dipoles and by quadrupoles.

I. INTRODUCTION

TO calculate the contour of a spectral line under the most general conditions is a very difficult task. It is customary to use the phase integral method because of its analogy with the classical Lorentz treatment, although this method is sometimes not exact. The statistical theory,[1] on the other hand, has its own major shortcomings, being correct only for slow perturbations among the molecules. However, since it represents a limiting case of both the correct theory and the phase-integral method, its simplicity makes it often a useful guide.

II. THEORY

The statistical theory is based on the following considerations. The distance between the two energy levels involved in a spectral transition is a function, E_0+V, of the position of all perturbing molecules, since the perturbation $V=\sum_i V_i$, which is present in addition to the normal energy difference, E_0, depends on the configuration of all molecules surrounding the radiating one. According to the statistical theory, the intensity of the spectral line at an energy V (i.e., a frequency V/h) to one side of its undisturbed position, E_0, equals the probability of those configurations of perturbers which yield the value V. Our problem is, thus, one of calculating the relative volume of configuration space in which $\sum_{i=1}^{N} V_i$ equals some given V, N being the number of molecules interacting with the emitter.

The potential, V_i, due to the ith molecule depends on r_i, its distance from the radiating molecule, and a set of other variables like angles and spins. Usually the latter, here to be denoted by ξ_i, are separable, and V_i depends on r_i in accordance with a simple power law. We, therefore, set

$$V_i = c r_i^{-m} u(\xi_i).$$

The function $u(\xi)$ has a vanishing mean. When this characteristic is satisfied, the precise form of $u(\xi)$ is relatively unimportant, leading only to different numerical factors than we shall encounter by putting

$$u(\xi)=\begin{cases}-1, & \xi\leqslant 0\\ +1, & \xi>0\end{cases} \qquad -1\leqslant\xi\leqslant 1.$$

If the volume occupied by the gas is $4\pi R^3/3$, the probability density with respect to r is

$$p(r)dr = 3r^2dr/R^3,$$

and that with respect to ξ,

$$p(\xi)d\xi = \tfrac{1}{2}d\xi.$$

It is desired to find the probability $W_N(V)$ that, in the presence of N perturbing molecules, the potential energy $\sum_i^N V_i$ shall have the value V. This is most easily determined by the use of Markoff's method.[2] The calculation is analogous to Holtsmark's evaluation of the probability for a given electric field strength at a point in a gas.[3]

According to Markoff's analysis,

$$W_N(V) = (1/2\pi)\int_{-\infty}^{\infty} e^{-i\rho V} A_N(\rho)d\rho, \tag{1}$$

where

$$A_N(\rho) = \left\{\int p(\xi)d\xi \int p(r)dr \exp[i\rho c r^{-m} u(\xi)]\right\}^N.$$

The last expression can be written

$$A_N(\rho) = [1-3B(\rho)/2R^3]^N,$$

provided

$$B(\rho) = \int_{-1}^{1} d\xi \int_0^R \{1-\exp[i\rho c r^{-m} u(\xi)]\} r^2 dr.$$

If the number density of molecules is n, so that $N = 4\pi n R^3/3$, the limit of A_N as $R\to\infty$ is

$$A(\rho) = \exp[-2\pi n B(\rho)],$$

and Eq. (1) becomes in this limit

$$W(V) = (1/2\pi)\int_{-\infty}^{\infty} \exp[-i\rho V - 2\pi n B(\rho)]d\rho.$$

We now turn to the evaluation of $B(\rho)$.

* Assisted by the ONR.
[1] T. Holstein, Phys. Rev. **79**, 744 (1950); H. Margenau and S. Bloom, Phys. Rev. **79**, 213 (1950).
[2] S. Chandrasekhar, Revs. Modern Phys. **15**, 1 (1943).
[3] J. Holtsmark, Ann. Physik **58**, 577 (1919).

After integrating over ξ,

$$B(\rho)=2\int_0^\infty (1-\cos\rho v)r^2dr, \quad \text{with} \quad v=cr^{-m}. \qquad (2)$$

On expressing the volume element in terms of $\rho r\equiv t$, we have

$$B=\tfrac{2}{3}(c|\rho|)^{3/m}\int_0^\infty (1-\cos t)d(t^{-3/m})$$

$$=\tfrac{2}{3}(c|\rho|)^{3/m}\int_0^\infty t^{-3/m}\sin t dt$$

provided $m>\frac{3}{2}$. In fact, B does not exist unless this inequality is satisfied, and W fails to have meaning in that case.

Let

$$\frac{4\pi}{3}c^{3/m}\int_0^\infty t^{-3/m}\sin t dt$$

$$=\frac{4\pi}{3}c^{3/m}\sin\left[\left(1-\frac{3}{m}\right)\frac{\pi}{2}\right]\Gamma\left(1-\frac{3}{m}\right)=g_m.$$

Then

$$2\pi B(\rho)=g_m|\rho|^{3/m},$$

and

$$W(V)=\frac{1}{\pi}\int_0^\infty \exp(-ng_m\rho^{3/m})\cos\rho V d\rho.$$

For $V=0$, this integral can be evaluated directly. The probability that the total potential shall be zero, is

$$W(0)=(m/3\pi)\Gamma(m/3)/(ng_m)^{m/3}.$$

The intensity at the center of a "statistically" broadened line, therefore, decreases with $n^{-m/3}$.

For finite V, our result can be written in the form

$$W(V)=(1/\pi|V|)I_m(V/V_0), \qquad (3)$$

the function I_m being defined by

$$I_m(x)=\int_0^\infty \exp[-(u/x)^{3/m}]\cos u du,$$

and $V_0=(ng_m)^{m/3}$ represents a convenient unit for measuring the energy; it is a measure of the potential energy of two molecules at their mean distance of separation.

III. APPLICATIONS

Interesting cases are, (a) broadening by permanent dipoles ($m=3$, e.g., ammonia) and, (b) broadening by quadrupoles ($m=5$; e.g., oxygen). These have usually been considered from the point of view of impact theories.[4] The present considerations become applicable to these cases at high pressures and, possibly, at low temperatures. But since the statistical effect is always basically present and yields a lower limit for all observations on the broadening of lines, these results may not be without interest.

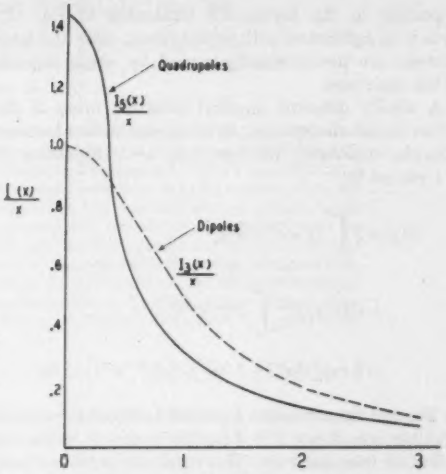

FIG. 1. Line contours for dipoles and quadrupoles. The ordinates are proportional to the intensities, and x is proportional to the frequency displacement.

For $m=3$ (dipole broadening)

$$V_0=\tfrac{2}{3}\pi^2 nc, \quad I_3(x)=x/(1+x^2),$$

and

$$W(V)=V_0/\pi(V^2+V_0^2).$$

This represents the usual dispersion curve with half-width V_0. In an earlier publication[5] the fact that the statistical theory yields a distribution of this form when many perturbers cooperate was merely stated, but the statement was met with some doubt.[6]

For other values of m the integrals must be evaluated by numerical computation or series expansion. This has been done for a number of instances. As an example, $I_5(x)/x$ is plotted, together with $I_3(x)/x$, in Fig. 1. Note that $x=V/V_0=\Delta\nu/\Delta\nu_0$ in terms of frequencies, where $\Delta\nu_0$ is the frequency displacement at the mean distance of separation of the molecules.

For large values of V, $W(V)$ becomes proportional to $V^{-1-3/m}$. If one considers only binary interactions, $W(V)\propto d\tau_i/dV_i$, where $\tau_i=4\pi r_i^3/3$. This also leads to $V^{-1-3/m}$, but with a somewhat different factor than that

[4] W. V. Smith and R. Howard, Phys. Rev. **79**, 132 (1950); R. Beringer and J. G. Castle, Phys. Rev. **81**, 82 (1950); M. Mizushima, unpublished work. More general considerations may be found in P. Anderson, Phys. Rev. **76**, 647 (1949).

[5] H. Margenau, Phys. Rev. **76**, 121 (1949).

[6] See the comments relating to this point by Smith and Howard, reference 4.

appearing in the asymptotic expansion of Eq. (3). This is in agreement with expectations, since the large energies are predominantly caused by single impacts of the molecules.

A wholly different physical situation arises if the forces do not change sign, as in the interaction between nonpolar molecules. We then take $u=1$. Equation (2) is replaced by

$$B(\rho)=2\int_0^\infty (1-e^{-i\rho v})r^2dr$$

$$=i^{\frac{2}{3}}(c|\rho|)^{3/m}\int_0^\infty t^{-3/m}e^{it}dt$$

$$=\tfrac{2}{3}\exp[i\tfrac{1}{2}\pi(2-3/m)](c|\rho|)^{3/m}\Gamma(1-3/m).$$

The last step involves a partial integration which is possible only if $m>3$. For smaller values of m the distribution does not exist. This condition is more drastic than in the case of forces which change sign.

Now define

$$g\equiv g'+ig''\equiv(i4\pi/3)c^{3/m}\int_0^\infty t^{-3/m}e^{it}dt.$$

Then, since $B(-\rho)=B^*(\rho)$, we have

$$W(V)=\frac{1}{\pi}\int_0^\infty \exp(-ng'\rho^{3/m})\cdot\cos(\rho V+g''\rho^{3/m})d\rho. \quad (4)$$

This distribution is not symmetric and has a mean different from zero. Indeed, as might have been expected,

$$\int W(V)VdV=4\pi n\int V_i r_i^2 dr_i.$$

The most interesting case for an application of Eq. (4) is to the broadening caused by Van der Waals forces, for which $m=6$ and $g'=g''$. The details of this problem have been worked out already[7] in a manner less compact than the present.

[7] H. Margenau, Phys. Rev. 48, 755 (1935).

Excited States of the Mirror Nuclei, Li^7 and Be^7

A. B. Brown, C. W. Snyder, W. A. Fowler, and C. C. Lauritsen
*Kellogg Radiation Laboratory, California Institute of Technology, Pasadena, California**
(Received December 28, 1950)

By studying the alpha-particles emitted in the disintegration of B^{10} by protons it has been shown that there exists an excited state in Be^7 at 434.4±4 kev which corresponds to the well-known first excited state in the mirror nucleus, Li^7. Measurements on the inelastic scattering of protons in Li^7 yield a value 479.0±1.0 kev for the energy of the Li^{7*}. The existence of these mirror states adds support to the equality of the p-p and n-n interactions exclusive of electrostatic and magnetic forces. The small difference, 45±4 kev, in the excitation energies is larger than second-order electric effects and is believed to be consistent with the order of magnitude of magnetic interactions in nuclei. The splitting of the ground and excited states must arise in some specific property of the nuclear interactions. In connection with the energy determinations, a detailed discussion is given of the precise measurements of the Q-values of nuclear reactions employing high resolution analyzers, electrostatic and magnetic, in the determination of particle energies. Experimental determinations of the cross sections for $B^{10}(p,\alpha)Be^7$, $B^{10}(p,\alpha')Be^{7*}(\gamma)Be^7$, $B^{10}(p,p)B^{10}$, $Li^7(p,p)Li^7$, and $Li^7(p,p')Li^{7*}(\gamma)Li^7$ are given.

I. INTRODUCTION

EARLY investigations[1] in this laboratory of the maximum kinetic energy of the positrons emitted by the light radioactive nuclei $_6C^{11}$, $_7N^{13}$, and $_8O^{15}$ showed that these nuclei differed in mass from their mirror isobars $_5B^{11}$, $_6C^{13}$, and $_7N^{15}$, respectively, by amounts which are quite simply calculable from the electrostatic energies[1a] of the nuclei and the small difference in the masses of neutron and proton. This indicated that the intrinsic nuclear interactions among any group of nucleons is unchanged if the neutrons are replaced by protons and vice versa. On the assumption of two body forces, this indicated further that the force between pairs of neutrons is equal to that between pairs of protons except for the repulsive electrostatic interaction. This equality had been suggested by the approximately linear variation of the binding energy of nuclei with atomic weight[2] and explained, in a very straightforward way, the fact that the stable nuclei consist of approximately equal numbers of neutrons and protons, the small excess of neutrons being directly attributable to the repulsive electrostatic forces between protons.

In subsequent investigations[3] it was found that the same conclusions could be drawn from measurements on the positron energy of all the radioactive transitions involving the mirror nuclei with $A=2Z+1$ up to $A=41$. For $Sc^{41}(\beta^+)Ca^{41}$ the maximum positron energy of 4.94 Mev can be accurately calculated even though the total nuclear binding is of the order of 400 Mev for $A=41$, showing that the nuclear binding must be the same for Sc^{41} and Ca^{41} within very narrow limits. Additional strong evidence is afforded by the difference in mass of Be^7 and Li^7 and of H^3 and He^3 in which cases the electrostatic effects are small and K-capture and electron emission, rather than positron emission, occur. Recent experimental determinations[4] of the mass differences of the radioactive mirror nuclei for which $A=2Z\pm2$ can be summarized as follows: $_5B^9-{}_3Li^9=2.0$ Mev, $_6C^{10}-{}_4Be^{10}=3.5$ Mev, $_7N^{12}-{}_5B^{12}=4.2$ Mev, $_8O^{14}-{}_6C^{14}=4.9$ Mev, $_{11}Na^{20}-{}_9F^{20}=8.3$ Mev. These are consistent with the conclusions discussed above, but the mass-energy differences have not been as precisely determined as those for $A=2Z\pm1$.

The electrostatic energy of a nucleus arising from the mutual repulsion of the protons in the nucleus can be expressed[1] as

$$U_E=\tfrac{1}{2}Z(Z-1)e^2\langle 1/r\rangle, \quad (1)$$

where $\langle 1/r\rangle$ is the average of the reciprocal of the distance between all possible pairs of protons in the nucleus. It is usually assumed that the effect of the relatively weak electrostatic forces can be calculated by perturbation methods using the proton distribution determined by the nuclear forces only and that the electrostatic energy can be superimposed on the intrinsic nuclear energy without higher order corrections. On the additional assumption of constant nuclear density out to a radius $R=R_0A^{\frac{1}{3}}$, which is indicated by numerous other nuclear phenomena, one can also write

$$U_E=3Z(Z-1)e^2/5R=3Z(Z-1)e^2/5A^{\frac{1}{3}}R_0. \quad (1')$$

The difference in electrostatic energy for mirror nuclei for which $A=2Z\pm n$ is then given by[4a]

$$\delta U_E=\tfrac{1}{2}n(A-1)e^2\langle 1/r\rangle=3n(A-1)e^2/5A^{\frac{1}{3}}R_0. \quad (2)$$

* This work was assisted by the joint program of ONR and AEC.

[1] Fowler, Delsasso, and Lauritsen, Phys. Rev. **49**, 561 (1936).

[1a] It was assumed that magnetic terms were small.

[2] L. A. Young, Phys. Rev. **47**, 972 (1935); **48**, 913 (1935).

[3] White, Delsasso, Fox, and Creutz, Phys. Rev. **56**, 512 (1939). White, Creutz, Delsasso, and Wilson, Phys. Rev. **59**, 63 (1941). L. D. P. King and D. R. Elliott, Phys. Rev. **58**, 846 (1940); **59**, 403 (1941).

[4] Sherr, Muether, and White, Phys. Rev. **75**, 282 (1949). L. Alvarez, University of California Radiation Lab. Report 739, May 31 (1950); Phys. Rev. **75**, 1815 (1949).

[4a] We include only the term in δU_E arising from $\delta Z=n$ and neglect any contribution from a difference in $\langle 1/r\rangle$ for the two nuclei. Such contributions will be small and require, in calculation, detailed attention to symmetry properties and higher order effects of the coulomb perturbation.

All of the results discussed in the preceding paragraphs are consistent with the values $e^2/R_0 \approx 2m_0c^2$ or $R_0 \approx 1.4 \times 10^{-13}$ cm. Detailed theoretical calculations have been given by numerous authors.[5]

It has been emphasized by Inglis[6] that because of the Larmor and Thomas precessions there will be a small magnetic contribution to the energy of a nucleus. For an unpaired proton or neutron with orbital angular momentum $l\hbar$ and spin $s\hbar=\frac{1}{2}\hbar$, a very elementary calculation shows that this energy is linear in the nuclear density, $\rho=(4\pi R_0^3/3)^{-1}$, and is given by

$$U_M \sim -(g'e^2\hbar^2/4R_0^3M_p^2c^2)(\mathbf{l}\cdot\mathbf{s}) \sim -5g'(\mathbf{l}\cdot\mathbf{s}) \text{ kev}, \quad (3)$$

where $g'=g_p-1=4.587$ for a proton and $g'=g_n=-3.827$ for a neutron. This expression yields, as an example, a contribution in the separation of ${}_3Li^{7*}-{}_3Li^7$, on the assumption that they are ^2P states, of approximately 30 kev, as was first noted by Inglis. There is some indication that the nuclear density is anomalously low in Li^7 and that the true value for the magnetic splitting may be somewhat smaller. Spin-orbit forces of an intrinsic nuclear nature such as those discussed recently by Case and Pais[7] may account for the much larger observed splitting which is discussed in this paper.

The difference in magnetic energy for mirror nuclei with $A=2Z\pm1$ is given by

$$\delta U_M \sim \pm\tfrac{1}{2}(g_p-g_n-1)\left(\frac{e^2\hbar^2}{R_0^3M_p^2c^2}\right)\mathbf{l}\cdot\mathbf{s} \sim \pm 50\mathbf{l}\cdot\mathbf{s} \text{ kev}, \quad (4)$$

the plus sign holding for an unpaired proton in the nucleus with $A=2Z+1$ and the minus sign for an unpaired neutron in this nucleus. The magnetic interactions are treated in considerably more detail in the paper by Inglis which follows this one.[7a] The total interaction energy difference for corresponding low lying states of mirror nuclei will be given by $\delta U=\delta U_E+\delta U_M$. Additional complications in states of high excitation are discussed briefly in Sec. VII.

In addition to the equality of neutron-neutron and proton-proton forces, it has been known for some time, from scattering experiments, that the singlet s-wave interaction between neutron and proton was approximately equal to that between pairs of protons if ranges and shapes are assumed to be identical.[8] There exists, however, a small difference, the neutron-proton potential depth exceeding that of two protons by several percent.[9] It has been shown recently[10] that the magnetic interaction between nucleons accounts adequately for this difference if the nuclear potential resembles that of Yukawa. It has also been shown that the anomalous scattering results at very high energies,[11] which seemed to demand inequality in the p-p and singlet n-p forces, can be explained by the introduction of a spin-orbit velocity dependent interaction[7] or by a very short range repulsive interaction between nucleons.[12] There would thus seem to be, at the present time, no conclusive evidence against the hypothesis that nuclear forces are fundamentally charge independent. Complications arising from the exclusion principle, which excludes certain interactions for like particles, must, of course, always be taken into account.

From the charge independence of nuclear forces, and in particular from the equality of neutron-neutron and proton-proton forces it follows that mirror nuclei should have corresponding series of excited quantum states as long as electromagnetic perturbations are not too large. Not only should the difference in energy of the ground states of mirror nuclei be given by a simple electrostatic and magnetic calculation but so also should the differences in energy of the low-lying excited states of these nuclei, with proper allowance being made for the fact that the excited states might have different radii than do the ground states and also different spin-orbit values and orientations. With the publication in 1948 of a summary of the energy levels of light nuclei,[13] it became clear that very little information was available on the excited states of mirror nuclei. In general, one or both of the pairs fell in the class of nuclei whose energy levels had not been investigated experimentally for one or more of the large variety of reasons which were emphasized in a discussion[14] of the methods of investigating the excited states of light nuclei. It was realized that a definite solution of the problem would await a complete investigation of the level structure of a number of mirror pairs, but it was decided that a start could best be made by a search for an unknown level in one member of a pair corresponding to a well-known level in the other member of the pair.

The most carefully and completely investigated excited state in light nuclei is the excited state of Li^7 at 479 kev. This is illustrated in Table I where we list the numerous measurements which have been made on the energy of this state. We give, in the table, a complete list of references on determinations of the energy of this state, some of which will be discussed further in the following. The existence of this state was first indicated by the detection of gamma-rays from the non-capture excitation of lithium with alpha-particles

[5] E. Feenberg and E. Wigner, Phys. Rev. **51**, 95 (1937); E. Wigner, Phys. Rev. **51**, 106, 947 (1937), **56**, 519 (1939); H. A. Bethe, Phys. Rev. **54**, 436 (1938); and E. Feenberg and G. Goertzel, Phys. Rev. **70**, 597 (1946).

[6] D. R. Inglis, Phys. Rev. **50**, 783 (1936).

[7] K. M. Case and A. Pais, Phys. Rev. **79**, 185 (1950).

[7a] D. R. Inglis, Phys. Rev. **82**, 181 (1951).

[8] Breit, Condon, and Present, Phys. Rev. **50**, 825 (1936).

[9] Breit, Hoisington, Share, and Thaxton, Phys. Rev. **55**, 1103 (1939).

[10] J. Schwinger, Phys. Rev. **78**, 135 (1950).

[11] R. S. Christian and E. W. Hart, Phys. Rev. **77**, 441 (1950); **79**, 85 (1950).

[12] R. Jastrow, Phys. Rev. **79**, 389 (1950).

[13] W. F. Hornyak and T. Lauritsen, Revs. Modern Phys. **20**, 191 (1948). T. Lauritsen, N.R.C. Preliminary Report No. 5 (1949), and Hornyak, Lauritsen, Morrison, and Fowler, Revs. Modern Phys. **22**, 291 (1950).

[14] Lauritsen, Fowler, and Lauritsen, Nucleonics **2**, No. 4, 18 (1948).

TABLE I. Measurements of the excitation energy of Li^{7*}.

Investigators	Reference	Reaction	Method	Energy (kev)
Bothe and Becker	Z. Physik **66**, 289 (1930).	$Li^7(\alpha,\alpha')Li^{7*}$	detected γ-rays	—
Webster	Proc. Roy. Soc. (London) **136**, 428 (1932).	$Li^7(\alpha,\alpha')Li^{7*}$	γ-absorption	600±100
Savel	Comptes rend. **198**, 1404 (1934).	$Li^7(\alpha,\alpha')Li^{7*}$	γ-absorption	500
Schnetzler	Z. Physik **95**, 302 (1935).	$Li^7(\alpha,\alpha')Li^{7*}$	γ-absorption	500
Delsasso, Fowler and Lauritsen	Phys. Rev. **48**, 848 (1935).	$Li^6(d,p')Li^{7*}$	detected p-groups	—
Bothe	Z. Physik **100**, 273 (1936).	$Li^7(\alpha,\alpha')Li^{7*}$	γ-spectrometer	200?, 390, 590
Rumbaugh, Roberts and Hafstad	Phys. Rev. **50**, 681 (1936). Phys. Rev. **54**, 657 (1938).	$Li^6(d,p')Li^{7*}$	p-group ranges	455±15
Speh	Phys. Rev. **50**, 689 (1936).	$Li^7(\alpha,\alpha')Li^{7*}$	γ-absorption	700±70
Haxel	Z. Physik **104**, 540 (1937).	$B^{10}(n,\alpha')Li^{7*}$	α-group ranges	900
Williams, Shepherd, and Haxby	Phys. Rev. **52**, 390 (1937).	$Li^6(d,p')Li^{7*}$	γ-absorption	400±25
Livingston and Hoffman	Phys. Rev. **53**, 227 (1938).	$B^{10}(n,\alpha')Li^{7*}$	α-group ranges	480
Maier-Leibnitz	Naturwiss. **26**, 614 (1938). Z. Physik **112**, 569 (1939).	$Be^7(K)Li^{7*}$	γ-cloud chamber	425±20
Roberts, Heydenburg, and Locher	Phys. Rev. **53**, 1016 (1938).	$Be^7(K)Li^{7*}$	γ-absorption	425±25
Bower, Bretscher and Gilbert	Proc. Cambridge Phil. Soc. **34**, 290 (1938).	$B^{10}(n,\alpha')Li^{7*}$	α-group ranges	500
O'Ceallaigh and Davies	Proc. Roy. Soc. (London) **167**, 81 (1938).	$B^{10}(n,\alpha')Li^{7*}$	α-group ranges	550±150
Mauer and Fisk	Z. Physik **112**, 436 (1939).	$B^{10}(n,\alpha')Li^7$	total ionization	200, 410, 640, 840?
Fowler and Lauritsen	Phys. Rev. **56**, 841 (1939).	$Li^7(p,p')Li^{7*}$	γ-absorption	495±25
Hudson, Herb, and Plain	Phys. Rev. **57**, 587 (1940).	$Li^7(p,p')Li^{7*}$	γ-absorption	459
Graves	Phys. Rev. **57**, 855 (1940).	$Be^9(d,\alpha)Li^{7*}$	α-group ranges	494±16
Wilson	Proc. Roy. Soc. (London) **177**, 382 (1941).	$B^{10}(n,\alpha')Li^{7*}$	total ionization	420±50
Zlotowski and Williams	Phys. Rev. **62**, 29 (1942).	$Be^7(K)Li^{7*}$	γ-coincidence counters	485±5
Bøggild	Kgl. Danske. Videnskab Selskab Math.-fys. Medd. **23**, No. 4 (1945).	$B^{10}(n,\alpha')Li^{7*}$	total range	420
Rubin	Phys. Rev. **69**, 134 (1946).	$Be^7(K)Li^{7*}$	γ-absorption	476±10
Siegbahn and Slätis	Arkiv. f. Ast. Math-Fys. **34A**, No. 15 (1946).	$Li^7(\alpha,\alpha')Li^{7*}$	γ-spectrometer	462
Siegbahn	Arkiv. f. Ast. Math-Fys. **34B**, No. 6 (1946).	$Be^7(K)Li^{7*}$	γ-spectrometer	453±5
Gilbert	Proc. Cambridge Phil. Soc. **44**, 447 (1948).	$B^{10}(n,\alpha')Li^{7*}$	α-Li^7 group ranges	500±40
Zaffarano, Kern and Mitchell	Phys. Rev. **74**, 105 (1948).	$Be^7(K)Li^{7*}$	γ-spectrometer	474±4
Kurie and Ter-Pogossian	Phys. Rev. **74**, 677 (1948).	$Be^7(K)Li^{7*}$	γ-spectrometer	485±5
Buechner, *et al.*	Phys. Rev. **74**, 1569 (1948).	$Be^9(d,\alpha')Li^{7*}$	α-spectrometer	482±3
Buechner, *et al.*	Phys. Rev. **74**, 1569 (1948).	$Li^6(d,p)Li^{7*}$	p-spectrometer	483±6
Elliott and Bell	Phys. Rev. **74**, 1869 (1948).	$B^{10}(n,\alpha')Li^{7*}$	γ-spectrometer	478.5±1.5
Stebler, Huber and Bicksel	Helv. Phys. Acta. **22**, 362 (1949).	$B^{10}(n,\alpha')Li^{7*}$	total ionization	490±20
Rasmussen, Hornyak and Lauritsen	Phys. Rev. **76**, 581 (1949).	$Be^7(K)Li^{7*}$	γ-spectrometer	476.6±0.8
Rasmussen, Hornyak and Lauritsen	Phys. Rev. **76**, 581 (1949).	$Be^9(d,\alpha')Li^{7*}$	γ-spectrometer	472
Hornyak, Lauritsen and Rasmussen	Phys. Rev. **76**, 731 (1949).	$Li^7(p,p')Li^{7*}$	γ-spectrometer	478.3±0.6[a]
Ter-Pogossian, Robinson, and Goddard	Phys. Rev. **76**, 1407 (1949).	$Be^7(K)Li^{7*}$	γ-spectrometer	478.5±0.5
Thomas and Lauritsen	Phys. Rev. **78**, 88 (1950).	$Li^6(d,p')Li^{7*}$	γ-spectrometer	478.5±1[a]
Burcham and Freeman	Phil. Mag. **41**, 337 (1950).	$B^{10}(n,\alpha')Li^{7*}$	α-spectrometer	490±70
This report	—	$Li^7(p,p')Li^{7*}$	p-spectrometer	479.0±1

[a] No correction for Doppler shifts.

by Bothe and Becker, Webster, Savel, and Schnetzler. The latter two investigators each measured the energy of the gamma-rays as approximately 0.5 Mev and correctly inferred their origin. Two groups of protons were observed in the bombardment of natural lithium targets by Delsasso, Fowler, and Lauritsen. The state was shown to be in the nucleus Li^7 by Rumbaugh and Hafstad, who detected two groups of protons from the reactions $Li^6(d,p)Li^7$ and $Li^6(d,p')Li^{7*}$, using a separated Li^6 target.

Several energy determinations of increased precision were made later, one being made in this laboratory by Rubin, who found an energy of 476±10 Mev by a comparison of the absorption coefficient of the radiation from $Be^7(K)Li^{7*}(\gamma)Li^7$ with that of the annihilation radiation of positrons. In 1949, two methods were used in this laboratory to measure the energy of this state with high precision. A magnetic lens gamma-ray spectrometer was used to measure the energy of the radiation following the inelastic scattering of protons by Li^7. In addition, a double focusing particle spectrometer[15] was employed to measure the difference in energy of the elastically and inelastically scattered protons. A preliminary estimate[16] for the excitation energy was reported. These latter measurements will be discussed in detail as a part of this paper. With these experiments as background, it was considered appropriate to search for a corresponding level in Be^7, the mirror nucleus of Li^7. As Be^7 is not readily available as a target for nuclear disintegration experiments, the most straightforward investigation, namely that of the inelastic scattering of protons by Be^7, was ruled out. It was decided to study the reaction $B^{10}(p,\alpha)Be^7$ and to look for evidence for $B^{10}(p,\alpha')Be^{7*}$. The alpha-particles produced in the bombardment of B^{10} by protons are of

[15] Snyder, Rubin, Fowler, and Lauritsen, Rev. Sci. Inst. **21**, 852 (1950).

[16] Fowler, Lauritsen, and Rubin, Phys. Rev. **75**, 1471 (1949).

TABLE II. Measurements of the excitation energy of Be^{7*}.

Investigators	Reference	Reaction	Method	Energy (kev)
Grosskreutz and Mather	Phys. Rev. 77, 580, 747 (1950).	$Li^7(p,n)Be^{7*}$	n-groups	205, 470, 745, all ±70
Hall	Phys. Rev. 77, 411 (1950).	$Li^7(p,n)Be^{7*}$	n-groups	420 to 480
Johnson, Laubenstein and Richards	Phys. Rev. 77, 413 (1950).	$Li^7(p,n)Be^{7*}$	n-groups	435±15
Whaling and Butler	Phys. Rev. 78, 72 (1950).	$Li^6(d,n)Be^{7*}$	n-groups	about 400
Hamermesh and Hummel	Phys. Rev. 78, 73 (1950).	$Li^7(p,n)Be^{7*}$	n-groups	428±20
Lauritsen and Thomas	Phys. Rev. 78, 88 (1950).	$Li^6(d,n)Be^{7*}$ $B^{10}(p,\alpha)Be^{7*}$	γ, spectrometer	429±5
Gibson and Green	Proc. Phys. Soc. (London) 63, 494 (1950).	$Li^6(d,n)Be^{7*}$	n-groups	450±60
Burcham and Freeman	Phil. Mag. 41, 337 (1950).	$B^{10}(p,\alpha)Be^{7*}$	α-groups	about 400
Freier, Rosen, and Stratton	Phys. Rev. 79, 721 (1950).	$Li^7(p,n)Be^{7*}$	n-groups	428±15
Van Patter, Sperduto, Strait, and Buechner	Phys. Rev. 79, 900 (1950).	$B^{10}(p,\alpha)Be^{7*}$	α-groups	431±5
Keepin	Phys. Rev. 80, 768 (1950)	$Li^7(p,n)Be^{7*}$	n-groups	433±26
This report		$B^{10}(p,\alpha)Be^{7*}$	α-groups	434.4±4

low energy and could be analyzed easily in the double focusing magnetic spectrometer mentioned above, with which observations on alpha-particles up to 2 Mev in energy can be made. Furthermore, these reactions are of considerable interest because of their correspondence with the well-known neutron reactions, $B^{10}(n,\alpha)Li^7$ and $B^{10}(n,\alpha')Li^{7*}$. Preliminary results[17] of the investigation of these proton reactions have been presented. Similar results have been obtained at the Massachusetts Institute of Technology.[18] Numerous investigators (Table II) have shown that the excited state occurs in the reaction $Li^6(d,n')Be^{7*}$, and Grosskreutz and Mather have reported evidence for the occurrence of two additional low energy excited states of Be^7 in this reaction. In this laboratory, a careful comparison[19] has been made of the energy of the gamma-rays from the two excited mirror states produced in the mirror reactions $Li^6(d,p')Li^{7*}$ and $Li^6(d,n')Be^{7*}$. These results will be reported in detail separately.

II. THE EXPERIMENTAL ARRANGEMENT

The apparatus used in these experiments has been described previously in detail. The protons for the bombardment were accelerated in the 1.7-Mev electrostatic accelerator[20] of the Kellogg Radiation Laboratory. The energy of these incident protons was determined accurately by passing the beam through a 90°, one meter radius, electrostatic analyzer[21] whose energy resolution is 2×10^{-4} of the bombarding energy. This resolution has been recently ascertained by measurements on the narrow resonance in $Al(p,\gamma)$ at 993 kev. The electrostatic analyzer was calibrated against the resonance at 873.5 kev in the gamma-ray yield from the proton bombardment of fluorine. In making the calibration, corrections were made for relativistic mass changes, for the positive guard potential on the target which was used to avoid the effects of secondary electron emission, for the change of the target potential during bombardment, and for the presence of contamination layers of carbon and oxygen on the target. This last effect was minimized by the use of an auxiliary pumping system and liquid air trap on the target chamber. It is believed that the energy of the protons actually incident on the relevant target material was known to about 0.1 percent on an absolute scale, and for comparison experiments it could be held to 0.02 percent.

The energy of the scattered particles and of the reaction products was measured by a 180°, 26.7-cm radius, double focusing magnetic spectrometer.[15] The spectrometer was calibrated by using protons of known energy leaving the electrostatic analyzer scattered at a known angle into the spectrometer by copper or gold targets. Details of the calibrations are given in the reference cited. The method of determination of the angle of observation of the spectrometer is also discussed in this reference. It is believed that the energy of the products of a reaction could be determined to ±0.1 percent and that the angle was known to ±0.3°. The particles were detected after leaving the magnetic spectrometer by either an ionization chamber or by a scintillation counter.[22] The scintillation counter was found to be especially convenient because it was not necessary to use thin vacuum tight foils before it, as was the case with the ionization chamber.

In those cases in which protons and alpha-particles of the same energy passed through the spectrometer, at a given field setting, into the detector, it was necessary to use auxiliary absorption techniques to distinguish them. Aluminum foils thick enough to stop the alpha-particles but thin enough to pass the protons could be interposed between the spectrometer and the counter, and readings were taken with and without the foils in place. The first reading gave the number of protons, with some small correction for scattering and straggling in the foil, while the difference gave the number of alpha-particles.

[17] Chao, Lauritsen, and Tollestrup, Phys. Rev. 76, 586 (1949). Brown, Chao, Fowler, and Lauritsen, Phys. Rev. 78, 88 (1950).
[18] Van Patter, Sperduto, Strait, and Buechner, Phys. Rev. 79, 900 (1950).
[19] C. C. Lauritsen and R. G. Thomas, Phys. Rev. 78, 88 (1950).
[20] Lauritsen, Lauritsen, and Fowler, Phys. Rev. 59, 241 (1941).
[21] Fowler, Lauritsen, and Lauritsen, Rev. Sci. Instr. 18, 818 (1947).
[22] A. V. Tollestrup, Phys. Rev. 74, 1561 (1948).

The gamma-radiation produced during the various bombardments was monitored with a Geiger-Müller counter made by the Radiation Counter Laboratories of Chicago. The wall of the counter was glass weighing 30 mg/cm² and the cathode was a thin silver deposit on the wall. The effective length of the counter was $3\frac{5}{8}$ inches and its diameter was 23/32 inch. The counter was mounted axially in a lead cylinder $2\frac{1}{8}$ inches in diameter with a slot the width and length of the counter cut to admit the radiation. The hole for the counter was lined with an aluminum cylinder whose wall thickness was 3/32 inch.

III. EXCITATION ENERGY OF Li^{7*}

The excitation energy of the state is determined directly by measuring the energies of incident and inelastically scattered protons and solving for the reaction energy Q by the usual formula of nuclear dynamics.[23a] The excitation energy is equal to $-Q^*$, where Q^* applies to the inelastic scattering process in which Li^{7*} is produced. The entire procedure involves three separate measurements. First, the energy scale of the electrostatic accelerator is calibrated. The resulting datum is a conversion factor between the potentiometer reading for the voltage on the electrostatic analyzer and the absolute energy in kev of the bombarding protons. Second, the magnetic spectrometer is calibrated against the electrostatic analyzer. In the present instance, since the magnetometer reading is inversely proportional to the magnetic field of the spectrometer, the resulting datum is a constant which is to be divided by the square of the magnetometer reading to give the energy of the scattered protons. Third, with a fixed bombarding energy, the energy of protons, inelastically scattered from a lithium target, is measured. Details of the calibrations, including small relativistic corrections, are given in Appendix A.

For calibration of the spectrometer, curves which we have termed "profiles" were run for thick targets of copper and lithium and for the thin contamination layers of carbon and oxygen which appear on the surface of the lithium. These profiles are shown in Fig. 1 and Fig. 2. All were taken with a bombarding energy of 1237.3 kev, and observations were made at an angle of 81.1 degrees relative to the beam with the target symmetrically placed relative to incident and outgoing beams. A copper scattering curve using HH^+ ions (mass 2 beam) was also obtained in order to calibrate the spectrometer in the region intermediate between the elastic and inelastic protons scattered by lithium. In the calculations a small correction for surface layer losses was made on E_1. For the thick targets, the magnetometer reading corresponding to the midpoint in the rise for a given group of particles plus a correction

[23a] We have incorporated all mathematical details in the appendices. The expression for Q is given in Appendix A, Eq. (11) and an expression for the difference in two Q-values is given in Appendix C, Eq. (3).

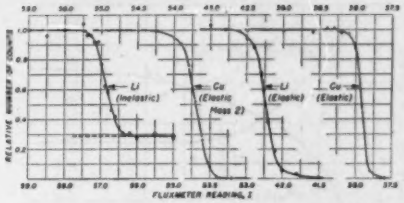

FIG. 1. Spectrometer profiles of the protons scattered at $\theta_{lab} = 81.1°$ by thick lithium and copper targets. The energy of the incident protons was 1237.3 kev (618.3 kev for the individual protons in the mass 2 or HH^+ beam), and the energy of the scattered protons is given non-relativistically by $E_0 = 1738I^{-2}$ Mev, where I is the fluxmeter reading.

for surface layers was taken as a measure of the scattered energy, and for the thin targets, the centroid of the observed particles, plus one-half the surface layer, was used. These procedures are discussed in Appendix B. In addition, a correction for the isotope Li^6 was made in the lithium case. A major uncertainty in the data is the thickness of contamination layers on the surface of the thick targets. This was minimized by making the bombardments as short as possible consistent with good statistics and by using high energy protons which lose relatively little energy in traversing the film. That the error is quite small was attested by the agreement (see Tables I and II of reference 15) between the calculated values of the spectrometer constant for the various scattering targets and scattered beams.

In the detection of the inelastically scattered protons one must use a semi-thin lithium target on a semi-thin backing. By "semi-thin" is meant a thickness measured in energy units that is greater than the resolution width of the spectrometer but much less than the energy of the incident protons. Actually, the backing foil should

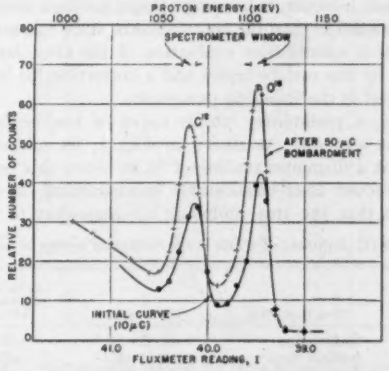

FIG. 2. Spectrometer profiles of the protons scattered at $\theta_{lab} = 81.1°$ by thin carbon and oxygen targets. The energy of the incident protons was 1237.3 kev and the energy of the scattered protons is given non-relativistically by $E_0 = 1738I^{-2}$ Mev, where I is the fluxmeter reading.

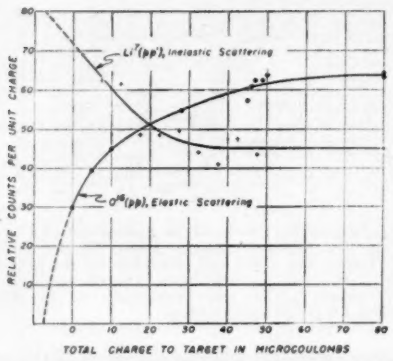
$Li^7(pp)$, Inelastic Scattering
$O^{16}(pp)$, Elastic Scattering
RELATIVE COUNTS PER UNIT CHARGE
TOTAL CHARGE TO TARGET IN MICROCOULOMBS

FIG. 3. Dependence of the number of protons scattered by a surface layer of oxygen increasing with amount of bombardment and the corresponding effect on the number of protons inelastically scattered at a given spectrometer setting by the underlying lithium target.

be as thin as possible. The lithium targets were made by evaporation in an "oven" directly below the target chamber and a beryllium foil (~10 kev energy loss for 1 Mev protons) was used as backing. The tail of the elastic scattering from the beryllium and lithium extends, because of straggling and scattering, down to the energy of the inelastic protons, giving a large background count, as is shown by the dashed line in Fig. 1. The background is so large because the cross sections for elastic scattering in lithium and beryllium exceed the lithium inelastic scattering cross section by factors of 10 and 40, respectively. With available foils of higher atomic number than beryllium, the background was found to be even larger.

With the long bombardments required to get sufficient numbers of inelastic protons, the surface contamination became a serious source of error. We were fortunate, however, to be using a target having a smaller atomic number than the contaminants, since this made possible a quantitative evaluation of the error introduced by the surface layers and a correction for it as discussed in the following paragraphs.

First, a preliminary profile curve of the inelastic protons was run. As shown in Fig. 1, its midpoint came at a fluxmeter reading of 56.88. Since this point was reached after considerable bombardment, it was certain that the true midpoint lay somewhat to the right of this one (i.e., at higher energy, smaller fluxmeter reading). Numerous trials with freshly evaporated targets indicated that the midpoint for very short bombardment lay at 56.70. Profile curves of the carbon and oxygen contamination after various lengths of bombardment (Fig. 2) showed definitely that the surface layers increased with bombardment. Consequently, a fresh layer of lithium was deposited, and with the bombarding voltage fixed at 1237.3 kev, points were taken with the spectrometer set alternately at 56.70 (the assumed midpoint for inelastic scattering from lithium) and at 39.50 (the oxygen peak). The latter required only about one-tenth of the bombardment time of the former to give sufficient counts. The resulting data are shown in Fig. 3. As the thickness of the surface layer built up, the lithium profile moved gradually to the left so that the point 56.70 slid gradually down the profile until it reached the background plateau, after which the yield flattened out as shown in the curve. The shape of the two curves was such that extrapolation seemed feasible. It was apparent that a contamination layer existed on the lithium even before the bombardment began. The oxygen curve was therefore extrapolated down to the horizontal axis, and the corresponding value of the extrapolated lithium curve (80 counts per unit charge) was taken as the number of counts which would have been obtained in the absence of any contamination layer. Actually, 80 counts was slightly more than half-way up the edge of the lithium profile curve, and the fluxmeter reading finally decided upon was 56.60, corresponding to a scattered proton energy of 539.3 kev. Putting this value and the bombarding energy 1237.3 kev into the nuclear dynamics equation with the relativistic corrections discussed in the appendices gave for the reaction energy $Q^*=-479.0$ kev.

The validity of the extrapolation was checked by calculating the Q^* in another way. From the oxygen and carbon profiles in Fig. 3 for minimum bombardment, one can calculate, using formulas discussed later in this paper, the number of nuclei in the contamination layer. It was found that the thickness of the minimum layer was $0.42/\cos 50°=0.65$ kev for the incident protons (1237.3 kev) and $0.75/\cos 50°=1.16$ kev for the inelastically scattered protons (537.4 kev, corresponding to a magnetometer reading of 56.7). On correcting the two energies by these amounts, the calculated value of Q^* was -479.3. In the calculation of the layer thickness we used the Rutherford scattering formula, so that the agreement is a good check that the scattering cross sections for carbon and oxygen are not markedly different from the Rutherford values at these energies even though reactions other than scattering do occur.

The inelastic scattering energy was also measured at 137.8° to the beam. The observed lithium edge midpoint was 68.0 for approximately the same amount of bombardment as that of the 56.88 point above. The actual

TABLE III. Estimate of errors in the excitation energy of Li^{7*}.

Quantity	Source of error	Direct error	Error in $E_x=\Delta Q$ (kev)
E_1, E_2	Calibration	$\delta E/E=10^{-3}$	±0.5
	Surface layer	$\delta\xi/\xi=0.2$	±0.1
E_2	Location of E_{2B}'	$\delta E_2/E_2=10^{-3}$	±0.6
θ	Measurement of θ	$\delta\theta=0.3°$	±0.4
E_x	Statistical	$\Delta E_x/E_x=10^{-3}$	±0.5
Final value and probable error			479.0±1 kev

layer thickness was not measured, but assuming it to give the same percentage correction as in the first case, it yielded a value of -479.1 kev for the value of Q, but with considerably greater probable error.

The statistical probable error of the above determinations was reduced, by numerous trials with freshly evaporated targets, to a relative value of 0.1 percent of the final result. There are several systematic errors of this same order of magnitude. They are discussed in detail in Appendix C and are tabulated in Table III. The final result and estimated probable error for the excitation energy of Li^{7*} or for $-Q^*$ of the inelastic scattering process, $Li^7(p,p')Li^{7*}$, is 479.0 ± 1.0 kev.

The most accurate of the recent measurements of the gamma-ray energy (Table I) is 478.5 ± 0.5 kev. Our value of 479.0 ± 1.0 is in substantial agreement with this. Since our value is proportional to the original energy scale calibration of the accelerator, the agreement gives an independent check on this scale. In order

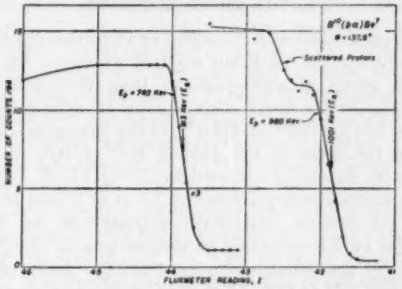

FIG. 4. Spectrometer profiles for the alpha-particles produced at $\theta_{lab}=137.8°$ in the reaction $B^{10}(p,\alpha)Be^7$ by protons of energy 742 kev and 989 kev bombarding a thick B^{10} target. The alpha-particle energy is given non-relativistically by $E_\alpha=1750I^{-2}$ Mev, where I is the fluxmeter reading.

to make the two values coincide, the energy of the $F(p,\alpha'\gamma)O^{16}$ resonance would have to be 872.6 ± 2.0 kev, in agreement within the probable errors with the determination of Herb, 873.5 ± 0.9. We feel that this constitutes an indirect but completely independent check of the current nuclear energy scale.

IV. EXCITATION ENERGY OF Be^{7*}

In order to obtain an accurate value for the difference of the Q-values of the reactions to the ground state and to the excited state of Be^7, the alpha-particles from the two reactions, $B^{10}(p,\alpha)Be^7$ and $B^{10}(p,\alpha')Be^{7*}$, were observed at different bombarding energies, so chosen that the energies of the alpha-particles were approximately the same. In this way the determination of the excitation energy of Be^{7*} was insensitive to errors of calibration of the magnetic spectrometer and to the relatively large energy losses of the alpha-particles in surface layers.

The targets used in this part of the experiment were B^{10} or $(B^{10})_2O_3$ evaporated on aluminum leaf. The B^{10}

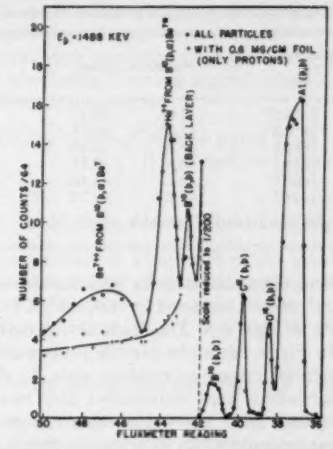

FIG. 5. Spectrometer profiles for alpha-particles, Be^{7++} ions, and scattered protons observed at $\theta_{lab}=137.8°$ from a thin $(B^{10})_2O_3$ target on aluminum bombarded by 1488-kev protons.

isotope was obtained from the Atomic Energy Commission. The target had to be thin enough to keep too many elastically scattered protons and alpha-particles of the main group from deep in the target from entering the spectrometer when the reaction $B^{10}(p,\alpha')Be^{7*}$ was being observed. The subtraction technique, which was used to distinguish between protons and alpha-particles, resulted in large uncertainties whenever the number of protons was equal to or larger than the number of alpha-particles.

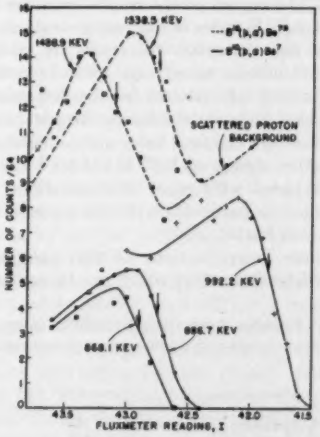

FIG. 6. Spectrometer profiles for the alpha-particles produced in the reactions $B^{10}(p,\alpha')Be^{7*}$ and $B^{10}(p,\alpha)Be^7$ at $\theta_{lab}=137.8°$ by protons of the indicated energies. The target was B^{10} evaporated in a thin layer on Al. The alpha-particle energies are given non-relativistically by $E_\alpha=1750I^{-2}$ Mev, where I is the fluxmeter reading.

TABLE IV. Measurements on the excitation energy of Be^{7*}.

Bombarding proton energy (kev) E_1	E_1'	Fluxmeter reading I	I'	ΔQ (kev)
992.2	1488.9	41.85	43.10	435.4
992.2	1538.5	41.85	42.75	441.0
868.1	1488.9	42.88	43.10	429.7
868.1	1538.5	42.88	42.75	435.2
886.7	1488.9	42.73	43.10	429.8
886.7	1538.5	42.73	42.75	435.3
Mean value and statistical probable error				434.4±3

Profiles of the alpha-particles from the two reactions and of the protons scattered by B^{10}, Al^{27}, C^{12}, and O^{16} are shown in Figs. 4–6. The angle of observation was 137.8°. In Fig. 6 the alpha-particle profiles are shown on an extended inverse momentum scale. In the series of measurements here represented the two alpha-particle groups have about the same energy. It was these measurements which were used to obtain ΔQ, and the results are tabulated in Table IV. The calculation of ΔQ was made using Eq. (3) of Appendix C. An estimate of the target thickness from the shape of the curves indicated that the point which most probably represented the energy of the alpha-particles from the front surface of the target was that at which the yield was 0.6 times the maximum. This choice is particularly uncertain in the case of the alpha-particles accompanying the production of Be^{7*} because of the large background of scattered protons.

Each of the three readings for the main group was combined with each of the two readings for the second group in order to give, as nearly as possible, equal weight to each, and the resulting six values of ΔQ were averaged. The scatter of the results indicates that the statistical probable error of the average is about ±3 kev. This error and the systematic errors are tabulated in Table V. It will be noted that we have estimated a relative error of 0.15 percent for the determination of E_{2B}' and that this contributes the largest part of the systematic error. The final value and probable error for the excitation energy of Be^{7*} is 434.4±4 kev. This is to be compared with other determinations given in Table II and in particular with the value 431±5 kev given by Van Patter, *et al.*[18]

The three determinations of the energies of the alpha-particles from $B^{10}(p,\alpha)Be^7$ can be used to obtain three measurements of the Q of this reaction, and these have been combined with eight determinations by Chao, Lauritsen, and Tollestrup,[17] using the same apparatus and methods as described in this report to yield an average value $Q=1.148\pm0.006$ Mev. This can be combined with our value for the ΔQ to give $Q^*=0.714\pm0.008$ Mev for the $B^{10}(p,\alpha')Be^{7*}$ reaction. These results are to be compared with those of Van Patter, *et al.*[18] which are $Q=1.152\pm0.004$ and $Q^*=0.721\pm0.006$ Mev.

TABLE V. Estimate of errors in the excitation energy of Be^{7*}.

Quantity	Source of error	Direct error	Error in $E_\alpha=\Delta Q$ (kev)
E_1, E_1'	Calibration	$\delta E/E=10^{-3}$	±0.4
	Surface layer	$\delta\xi/\xi=0.2$	±0.1
E_2	Location of E_{2B}'	$\delta E_1/E_2=1.5\times10^{-3}$	±2.7
θ	Measurement of θ	$\delta\theta=0.3°$	±0.6
E_α	Statistical	$\delta E_\alpha/E_\alpha=7\times10^{-3}$	±3.0
	Final value and probable error		434.4±4

The average of the two values for $Q=1.150\pm0.003$ can be employed with the value[22] $Q=-1.645\pm0.002$ Mev for $Li^7(p,n)Be^7$ to give a value for the Q of the reaction $B^{10}(n,\alpha)Li^7$ equal to 2.795±0.004 Mev. From this one can calculate that Q^* for $B^{10}(n,\alpha')Li^{7*}$ is equal to 2.316±0.004 Mev, which is in excellent agreement with the value 2.310±0.010 Mev which has been recently determined by careful ionization measurements.[24]

V. THE CROSS SECTIONS

Cross sections were measured as a function of proton energy for the following reaction products: (a) the main group of alpha-particles from $B^{10}(p,\alpha)Be^7$ at 137.8°, (b) the lower energy group of alpha-particles from $B^{10}(p,\alpha')Be^{7*}$ at 137.8°, (c) the gamma-radiation from the decay of the residual Be^{7*} at 90°, (d) the protons elastically scattered by B^{10} at 137.8°, (e) the protons elastically scattered by Li^7 at 81.1° and 137.8°, (f) the protons inelastically scattered at the same angles by Li^7 according to the reaction $Li^7(p,p')Li^{7*}$, and (g) the gamma-radiation from the decay of the residual Li^{7*} at 90°. All the angles listed above are in the laboratory system of coordinates and are measured relative to the direction of the incident proton beam.

(A) The Cross Section of $B^{10}(p,\alpha)Be^7$

The cross section of the main group of alpha-particles was measured for proton energies from 615 kev to 1114 kev and from 1208 kev to 1585 kev. It was necessary to use different target arrangements in the two energy ranges to avoid scattered protons. Between 1114 kev and 1208 kev, with either target arrangement, large numbers of protons were scattered into the spectrometer with energies such as to be counted, and reliable data for the alpha-particles could not be obtained.

For bombarding energies between 615 kev and 1114 kev, the target was made by evaporating on a copper strip a layer of $(B^{10})_2O_3$ thick enough to stop all incident protons. At these bombarding energies, protons scattered elastically by heavy backing material had approximately the same energy as the alpha-particles from the reaction being studied, and it was necessary to absorb them in the target. The upper limit on the bombarding energy was the energy at which the protons scattered

[22] Herb, Snowdon, and Sala, Phys. Rev. **75**, 246 (1949). Shoupp, Jennings, and Jones, Phys. Rev. **76**, 502 (1949).
[24] Jesse, Forstat, and Sadauskis, Phys. Rev. **77**, 782 (1950).

from oxygen had nearly the same energy as did the alpha-particles from the reaction.

In these measurements the energy loss in the target for the reaction products is greater than the energy interval accepted by the spectrometer window. The cross section in the center-of-mass system is thus given by[15]

$$\sigma(\theta_c)=4\pi/\Omega_c(R_c\epsilon_{eff}/2E_{20})fY(He^{++}) \quad (5)$$

$$=(R_c\epsilon_{eff}/q\Omega_cE_{20})fN(He^{++})\times10^{-8}\text{ barns}, \quad (5')$$

where $\sigma(\theta_c)$ is 4π times the cross section per unit solid angle observed at an angle θ_c in the center of mass coordinates with the incident proton beam. $Y(He^{++})$ is the number of doubly-charged helium ions observed per incident proton. It is given by $(1/q)N(He^{++})\times1.602\times10^{-13}$, where $N(He^{++})$ is the number of doubly-charged helium ions observed for q microcoulombs of protons incident on the target. The factor $f=1+Y(He^{+})/Y(He^{++})$ corrects for those helium nuclei which are produced in the reaction but are not counted because they are only singly charged when they leave the target, having captured an electron. The correction for singly-charged helium ions was obtained from a curve prepared by R. G. Thomas of this laboratory using data of Henderson,[25] Briggs,[26] and Rutherford.[27] No correction was made for neutral particles, their number being very small at the energies encountered in these experiments. The quantity $2E_{20}/R_c\epsilon_{eff}$ is the number of effective target nuclei per square centimeter perpendicular to the beam; this is shown in Appendix B. In (5') $\epsilon_{eff}=\epsilon_1(\partial E_2/\partial E_1+\eta)$ must be in the customary units, 10^{-15} ev-cm^2 and E_{20} the energy of the observed particles must be in electron-volts; Ω_c is the solid angle in the center-of-mass system in steradians.

The cross section given by Eq. (5) is not the cross section at the energy E_{1B}, of the incident particles leaving the electrostatic analyzer and impinging on the top layer of the target. In Appendix B it is shown that the energy of the incident particles actually producing the observed particles is given by Eq. (3'). In this equation E_{2B} is the energy of the outgoing particles produced when the incident particles do have energy E_{1B}. The quantity E_{2B} can be calculated for each analyzer setting, E_{1B}, from Eq. (12) of Appendix A once the Q of the process has been determined, as by the methods discussed previously in this paper. We have, in general, prepared extensive tables of E_{2B} *vs* E_{1B} as aids during the actual determination of cross section data. The magnetic spectrograph is set at each determination at a "following" energy E_{20}, just enough below E_{2B} to fill the spectrograph window or to avoid surface layer effects. From time to time complete profiles were run to check the entire procedure. As noted above the energy E_1 was determined from the calculated E_{2B}, and the measured values of E_{1B} and E_{20} using (3') of Appendix B.

The solid angle correction from laboratory to center-of-mass coordinates was made according to the following non-relativistic expression:

$$\Omega_c/\Omega\approx d\Omega_c/d\Omega=[(1-\alpha^2\sin^2\theta)^{\frac{1}{2}}+\alpha\cos\theta]^2/(1-\alpha^2\sin^2\theta)^{\frac{1}{2}}\approx1+2\alpha\cos\theta \quad (6)$$

where

$$\alpha=\{M_1M_3E_1/[(M_2+M_3)M_3Q+M_0M_3E_1]\}^{\frac{1}{2}}, \quad (7)$$

Ω is the solid angle of acceptance of the spectrometer, and E_1 is the energy of the bombarding particle in laboratory coordinates at the point where the reaction takes place. It is true that θ_c is a variable depending on E_1 given by

$$\cos\theta_c=\cos\theta(1-\alpha^2\sin^2\theta)^{\frac{1}{2}}-\alpha\sin^2\theta\approx\cos\theta-\alpha\sin^2\theta. \quad (8)$$

The variation is small, however, and the results are essentially the cross section in center of mass coordinates over a range of angles slightly greater than θ, the angle of observation in laboratory coordinates.

The factor R_c/Ω which enters Eq. (5) when (6) is applied, is a constant of the spectrometer and can be determined from any reaction whose cross section is already known. In this case the elastic scattering of 1488 kev protons from copper was used. The cross section was calculated from the Rutherford formula and R_c/Ω was found to be 23,400 steradian^{-1} with a statistical uncertainty of about ½ percent and an uncertainty arising from lack of knowledge of the stopping cross section of copper of about 5 percent.

In measuring the cross section for bombarding energies between 615 kev and 1114 kev numerous complications were encountered because of the background of low energy singly charged alpha-particles produced in deep layers of the target and of protons which had suffered large energy losses in the target (straggling). These backgrounds were assumed to vary slowly with the energy of the observed particles and were evaluated at several bombarding energies by observations at magnetic fields just slightly higher than those at which the He^{++} groups appeared. Correction factors for the penetration of the aluminum foils before the counter by protons and alpha-particles were also determined empirically.

For bombarding energies between 1208 and 1585 kev, the targets were thin layers of $(B^{10})_2O_3$ evaporated on aluminum leaf. The targets were oriented with the $(B^{10})_2O_3$ on the back side of the aluminum, so that both the protons and alpha-particles passed through the aluminum foil. Thus, the alpha-particles appeared with much lower energy than did the scattered protons. The upper limit to the bombarding energy was set by breakdown of the stabilizer of the electrostatic analyzer; the lower limit was the energy at which protons scattered by the boron came from the target with the same energy as the alpha-particles. There were at all bom-

[25] Henderson, Proc. Roy. Soc. (London) **A109**, 157 (1925).
[26] Briggs, Proc. Roy. Soc. (London) **A114**, 341 (1927).
[27] Rutherford, Phil. Mag. **47**, 277 (1924).

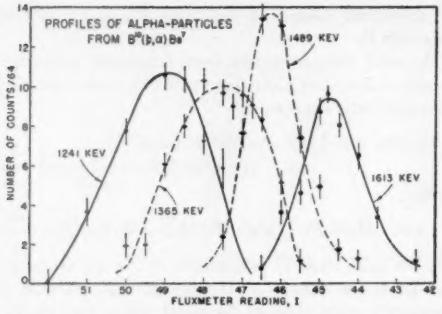

FIG. 7. Spectrometer profiles of alpha-particles observed at $\theta_{lab}=137.8°$ from $B^{10}(p,\alpha)Be^7$ at the bombarding energies indicated. The target was a thin layer of $(B^{10})_2O_3$ on the back side of an 0.2 mg/cm² Al foil.

barding energies some protons of the same energy as the alpha-particles, but at the alpha-particle energies encountered, the aluminum foils in front of the counter could be used to distinguish protons from alpha-particles as long as the protons were not too numerous.

Three runs were made, one with one target set with θ_1 in Fig. 17 equal to 28°, the other two with another target on a thinner aluminum leaf, which was set perpendicular to the proton beam to make the loss of energy by the alpha-particles in the aluminum leaf the same as in the other case. Because the alpha-particles exhibited straggling when they emerged from the aluminum leaf, the spectrometer would not select those from any particular lamina of the target, so all of them produced in the whole target thickness were counted.

Complete profiles were taken at four bombarding energies. These profiles were used to determine the integrals which appear in the cross section for thin target measurements, which is[15]

$$\sigma(\theta_c)=\frac{4\pi R_c}{nt\Omega_c}\int\frac{fY(\mathrm{He}^{++})}{I}dI \tag{9}$$

$$=\frac{2R_c}{q\Omega_c}\left(\frac{10^{12}}{nt}\right)\int\frac{fN(\mathrm{He}^{++})}{I}dI \text{ barns}, \tag{9'}$$

where $Y(\mathrm{He}^{++})=(1/q)N(\mathrm{He}^{++})\times1.602\times10^{-13}$ is the number of alpha-particles per incident proton counted at a fluxmeter reading I, n is the disintegrable nuclei per cc in the target, and t is the thickness of the target parallel to the incident beam.

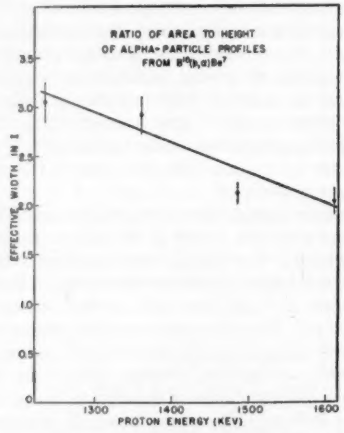

FIG. 8. Effective width of the alpha-particle profiles shown in Fig. 7.

At the four bombarding energies chosen, the ratio of the integral in Eq. (9) to the maximum value of the integrand, $fY(\mathrm{He}^{++})/I$, was found, and this ratio was used to find equivalent values of the integral at intermediate bombarding energies from the maximum values of the integrand at those energies. The profiles of the alpha-particles are shown in Fig. 7, and the four points and the curve used for the ratio are shown in Fig. 8. The ratio of the integral to the maximum value of the integrand was used for both targets, although measured for only one, because the energy loss of the alpha-particles was the same for the two targets and the straggling was therefore also the same.

The value of nt used was found from elastic scattering of protons from the B^{10} nuclei, using the proton scattering cross section of boron found as described in part (D) of this section. The two targets were of nearly the same thickness, and the value used for both was 4.18×10^{17} B^{10} nuclei/cm²; the uncertainty in each value was larger than the difference.

It was also necessary to correct the bombarding energy for the energy lost by the protons in passing through the aluminum foil. Using the arguments discussed in Appendix B, one has

$$E_1=E_{1B}-(\epsilon_1/\epsilon_{\mathrm{eff}})(E_{2B}-E_{20}), \tag{10}$$

where E_{1B} = energy of protons from accelerator, E_{20} = energy of alpha-particles observed with B_2O_3 on back side of foil, and E_{2B} = energy of alpha-particles calculated for B_2O_3 on front side of foil using Q from preceding section and the measured E_{1B} in Eq. (12) of Appendix A.

The cross section for $B^{10}(p,\alpha)Be^7$ is plotted as a function of bombarding energy in the laboratory system in Fig. 9. There is, in addition to statistics, an uncertainty of 20 percent in the scale of the ordinate, due principally to poor knowledge of the boron stopping cross section on which nt depends, to statistical uncertainty in the determination of N, to uncertainty in the ratio of the integral in Eq. (9) to the maximum value of the integrand, to uncertainty in background corrections, and to uncertainty in the factor f. When corrected for barrier penetration factors for the incoming protons and outgoing alpha-particles, the excitation curve indi-

cates resonances at 1.0 and 1.5 Mev superimposed on a continuous background.

(B) The Cross Section of $B^{10}(p,\alpha')Be^{7*}$

The target used for the excitation curve was a thin layer of B^{10} evaporated on aluminum leaf. It was necessary that the target be thin in order to keep alpha-particles of the main group and scattered protons from deep in the target from interfering with the observations, and that it be thick enough so that the alpha-particles would fill the spectrometer window. Equation (5) was used to determine the cross section with $Y(He^{++})$ determined by the subtraction technique using a foil before the counter to differentiate protons and alpha-particles. Figure 10 shows the two curves obtained. At proton energies above 1488 kev, some of the alpha-particles were counted through the foils in front of the counter. For the final calculations, the proton counts were considered to be constant above 1488 kev as shown by the dotted portion of the curve. This extrapolation probably indicates too high values for the proton counts so that the calculated cross section may be low, relative to the rest of the curve, by as much as 20 percent.

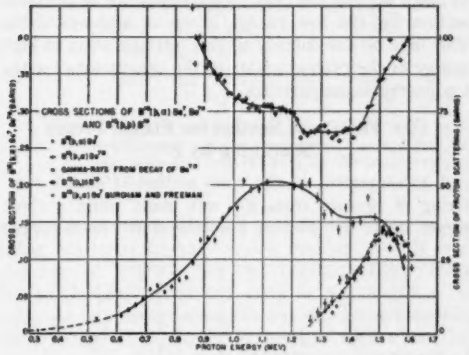

FIG. 9. Cross sections per 4π steradians in the center-of-mass system at $\theta_{cm}\sim140°$ ($\theta_{lab}=137.8°$) for various $B^{10}+H^1$ reactions *vs* laboratory proton energy. The upper curve is for $B^{10}(p,p)B^{10}$; the intermediate curve is for $B^{10}(p,\alpha)Be^7$; the lower curve is for $B^{10}(p,\alpha')Be^{7*}(\gamma)Be^7$. The gamma-rays from the decay of Be^{7*} were measured at $\theta_{lab}=90°$.

The composition of the B^{10} target was determined by a comparison of its yield for the alpha-particles from $B^{10}(p,\alpha)Be^7$ at 1488-kev proton energy with that of two $(B^{10})_2O_3$ targets. Since $(B^{10})_2O_3$ evaporates at a few hundred degrees centigrade, presumably little pump oil vapor is decomposed and such a target is fairly pure. The ϵ_{eff} for the B^{10} target was found at one energy in this way. Proton scattering showed that the impurities were principally carbon and oxygen, in large amounts, distributed throughout the target layer. The stopping cross sections of oxygen and carbon vary in the same way with energy, so the target could be considered as B^{10} plus a single contaminant. The effective stopping power of the target for the reaction $B^{10}(p,\alpha')Be^{7*}$ was computed for all of the bombarding energies used. The uncertainty in the composition leads to an uncertainty in ϵ_{eff} of 10 percent.

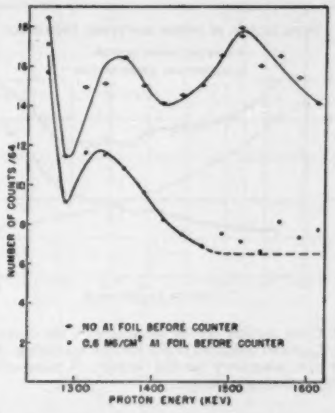

FIG. 10. Curves from which the excitation curve for $B^{10}(p,\alpha')Be^{7*}$ was determined. In the upper curve both scattered protons and the alpha-particles were counted; in the lower curve only the protons were counted.

The curve for the cross section in the center of mass system at $\sim140°$ is shown in Fig. 9 and Fig. 11. In addition to statistics there are the uncertainties in the target composition and the uncertainty in ϵ_{eff}, making the scale of ordinates uncertain by 20 percent. It was remarked earlier that the high energy end of the curve may be low with respect to the remainder of the curve. A marked resonance is indicated near 1.52 Mev with a breadth, $\Gamma\sim250$ kev.

(C) The Cross Section for $B^{10}(p,\alpha')Be^{7*}(\gamma)Be^7$

The gamma-radiation from a B^{10} target bombarded by protons was shown[19] by Lauritsen and Thomas to

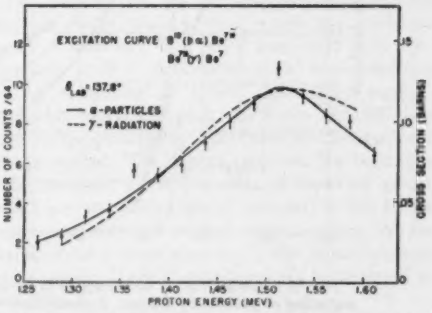

FIG. 11. Cross section per 4π steradians in the center-of-mass system at $\theta_{cm}\sim140°$ ($\theta_{lab}=137.8°$) for $B^{10}(p,\alpha')Be^{7*}$ *vs* laboratory proton energy.

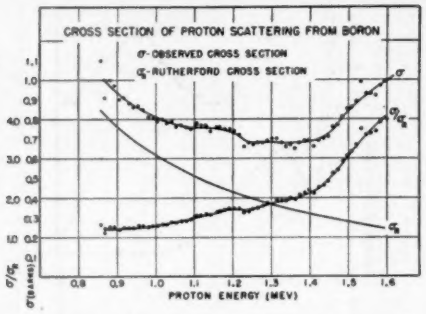

FIG. 12. Cross section per 4π steradians in the center-of-mass system at $\theta_{cm}\sim 140°$ ($\theta_{lab}=137.8°$) for the scattering of protons by B^{10} as a function of the laboratory proton energy. A comparison with Rutherford scattering is shown.

have an energy 429 ± 4 kev, and its origin is thus the decay of the Be^{7*}. Using the techniques described in detail previously,[28] the cross section for this radiation was determined. A thin layer of $(B^{10})_2O_3$ evaporated on copper was used as target.

The thickness of the target was found by a comparison of the yield from the $(B^{10})_2O_3$ target with the differentiated yield from a thick B^{10} target, made by pressing amorphous boron on a copper strip. The thickness of the $(B^{10})_2O_3$ target was found to be 14.1 kev for 1.5-Mev protons, or 1.45×10^{18} boron atoms/cm^2.

The counts arising from background radiation from protons striking the copper target backing were found by measuring the yield from proton bombardment of a copper strip. The background radiation from copper was measured at six proton energies, and the values at intermediate energies were found by graphical interpolation. The background counts were, at most, about 25 percent of the total counts.

The cross section for the gamma-radiation from $B^{10}(p,\alpha')Be^{7*}(\gamma)Be^7$ at 90° to the incident beam is plotted in Fig. 9 and Fig. 11. Uncertainty in the calculated value of target thickness, which depends on the differentiation of a thick target curve and on the stopping cross section of boron and oxygen for protons, makes the scale of the ordinates uncertain by 20 percent. The agreement with the curve for alpha-particles from $B^{11}(p,\alpha')Be^{7*}$ is good, but it is to be noted that the cross section for the gamma-radiation does not fall off as much beyond the peak of the resonance as the cross section for the low energy group of alpha-particles. This may be due entirely to poor extrapolation to high energy of the proton counts in the calculations for the low energy alpha-particles.

(D) The Cross Section for Elastic Proton Scattering by B^{10}

A measurement of the cross section of elastic scattering of protons from B^{10} was made using a thick target made by pressing amorphous B^{10} on a copper

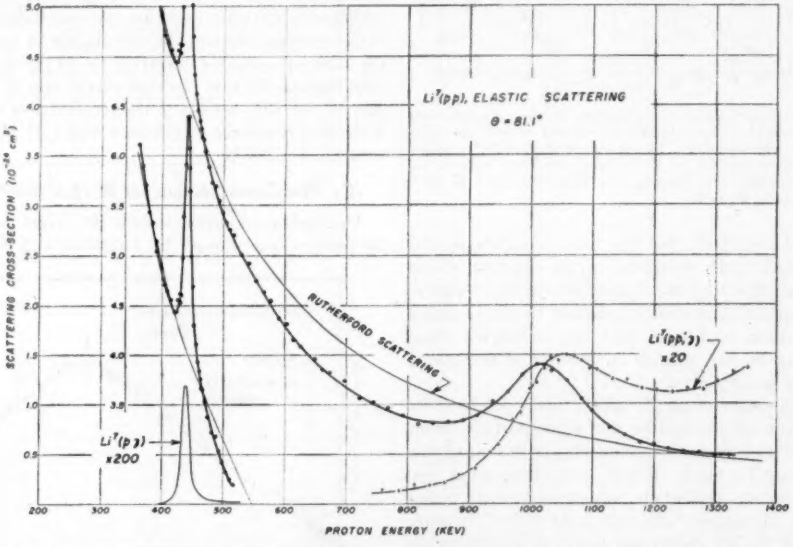

FIG. 13. Cross section per 4π steradians in the center-of-mass system at $\theta_{cm}\sim 85°$ ($\theta_{lab}=81.1°$) for the elastic scattering of protons by lithium. A comparison with Rutherford scattering is shown. It will be noted that anomalies occur at 441 kev, the resonance energy for $Li^7(p,\gamma)$ and near 1050 kev, the resonance energy for $Li^7(p,p'\gamma)$.

[28] Fowler, Lauritsen, and Lauritsen, Revs. Modern Phys. **20**, 236 (1948).

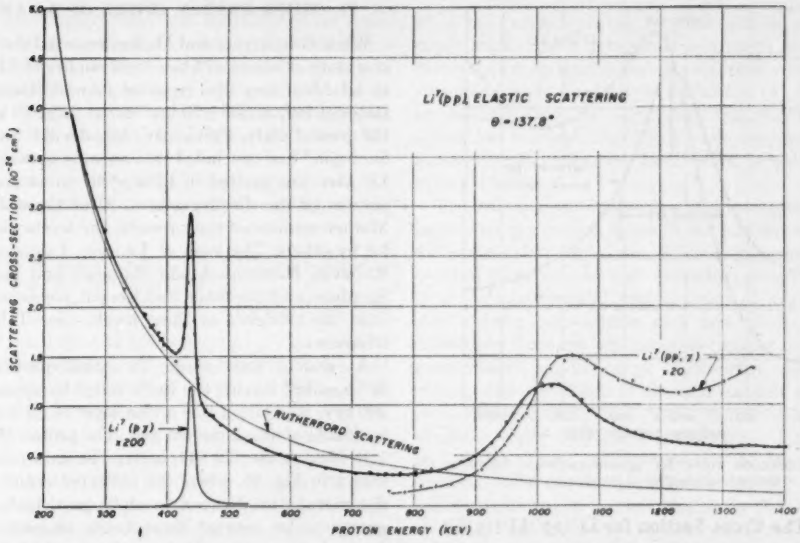

FIG. 14. Cross section per 4π steradians in the center-of-mass system at $\theta_{cm} \sim 145°$ ($\theta_{lab} = 137.8°$) for the elastic scattering of protons by lithium. A comparison with Rutherford scattering is shown. It will be noted that anomalies occur at 441 kev, the resonance energy for $Li^7(p,\gamma)$ and near 1050 kev, the resonance energy for $Li^7(p,p'\gamma)$.

strip. Protons were absorbed in the thick target before being scattered by the copper backing, and it was possible to correct, for the alpha-particles from $B^{10}(p,\alpha)Be^7, Be^{7*}$ produced deep in the target. The alpha-particle cross sections do not change very rapidly with energy, and the alpha-particle counts can be subtracted after measuring them with the spectrometer set for a slightly higher energy than possessed by the scattered protons. Their number was the order of 5 percent that of the number of protons. Again Eq. (5) was used to determine the cross section with $fN(He^{++})$ replaced by $N(H^+)$. No correction was made for neutral hydrogen atoms, their number being very small.

The cross section is plotted in Fig. 9, for comparison with the others, and in Fig. 12, where the ratio to Rutherford scattering is also shown. There is an uncertainty of 10 percent in the scale of ordinates owing principally to ϵ_{eff}. There is a strong anomaly in the neighborhood of the resonances in $B^{10}(p,\alpha)Be^7$ and $B^{10}(p,\alpha')Be^{7*}$ at 1.5 Mev, and a small anomaly at about 1.15 Mev, near the resonance in $B^{10}(p,\alpha)Be^7$.

(E) The Cross Section for Elastic Proton Scattering by Li^7

Measurement of the cross section for the elastic scattering of protons from Li^7 at 81.1° and 137.8° was performed in the manner described in (D) over the energy interval 300 to 1300 kev. Freshly evaporated deposits of lithium (natural isotopic ratio) were used throughout the experiments. The results are shown in Figs. 13 and 14, where the Rutherford scattering is also indicated. It will be noted that a marked anomaly occurs at 441 kev, where $Li^7(p,\gamma)Be^8$ is known to exhibit a strong resonance. This anomaly was first observed by Creutz.[29] Another anomaly will be noted near 1 Mev at which point the inelastic scattering discussed in the next paragraph shows resonance. A detailed discussion of these results will be given in a forthcoming publication after measurements over a wider range of angles have been performed.

(F) The Cross Section for $Li^7(p,p')Li^{7*}$

The cross section for the protons inelastically scattered by Li^7 was measured directly only at a bombarding energy of 1240 kev. The result was 0.036 barn per 4π steradians at 81.1° (laboratory angle) and 0.065 barns per 4π steradians at 137.8° (laboratory angle) in reasonable agreement with the value of 0.057 barns given by the gamma-ray measurements discussed in the next paragraph. The gamma-radiation has been shown to be isotropic by Littauer[30] and thus the gamma-radiation cross section should be equal to the inelastic proton cross section averaged over all angles. We have also observed a large anomaly in the elastic scattering in this region. These observations will be reported at a later date.

[29] E. C. Creutz, Phys. Rev. **55**, 819 (1939).
[30] S. Littauer, Proc. Phys. Soc. (London) **63**, 244 (1950).

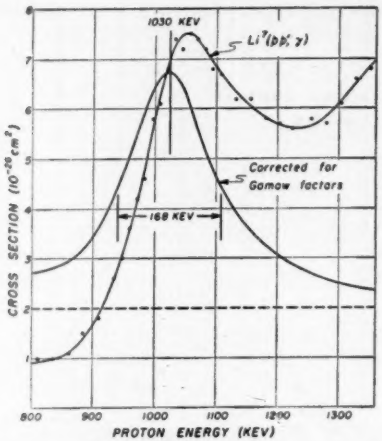

FIG. 15. Excitation curve for gamma-radiation following the inelastic scattering of protons by Li^7.

(G) The Cross Section for $Li^7(p,p')Li^{7*}(\gamma)Li^7$

The cross section for the production of the gamma-radiation following the inelastic scattering of protons by Li^7 has been measured at 90° in the laboratory system over the interval of bombarding proton energies from 800 to 1400 kev. The results are shown in Fig. 15 where we also show the cross section corrected for the barrier penetration factors[31] for the incoming and inelastically scattered protons. This curve indicates a resonance at 1030±5 kev with a full width at half-maximum of 168 kev superimposed on a relatively constant background. The thick target yield (92.6 percent Li^7) was measured at 1350 kev and was found to be 1.2×10^{-5} quanta/proton.

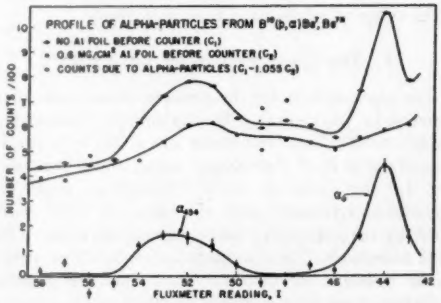
PROFILE OF ALPHA-PARTICLES FROM $B^{10}(p,\alpha)Be^7, Be^{7*}$
NO Al FOIL BEFORE COUNTER (C_1)
0.6 MG/CM^2 Al FOIL BEFORE COUNTER (C_2)
COUNTS DUE TO ALPHA-PARTICLES (C_1-1.055 C_2)
NUMBER OF COUNTS / 100
α_{434}
α_0
FLUXMETER READING, I

FIG. 16. Alpha-particle groups observed at $\theta_{lab}=137.8°$ from the bombardment of B^{10} by 1460 kev protons. A thin layer of $(B^{10})_2O_3$ evaporated on the back side of a thin Al leaf was used as the target. The groups corresponding to the formation of Be^7 in the ground and 434-kev states are evident. No evidence for a group leaving Be^7 in a state at 205 kev is indicated.

[31] R. F. Christy and R. Latter, Revs. Modern Phys. **20**, 185 (1948).

VI. OTHER ENERGY LEVELS OF Be^7 AND Li^7

When Grosskreutz and Mather reported the existence of a state at about 470 kev from studies of $Li^7(p,n)Be^7$ at 5.1 Mev, they also reported two additional excited states of Be^7, at 205±70 kev and at 745±70 kev above the ground state. Previously, Mandeville, Swann, and Snowdon[32] had concluded that no state between 0.5 and 1.0 Mev was excited in $Li^6(d,n)Be^7$ in as much as 10 percent of the disintegrations. After Grosskreutz and Mather announced their results, the levels were looked for by others. The work of Johnson, Laubenstein, and Richards, Hamermesh and Hummel, and Van Patter, Sperduto, and Buechner, and Keepin, yields no evidence from the existence of these levels. (See Table II for references.)

A search was made for alpha-particles from $B^{10}(p,\alpha)Be^{7*}$ leaving the Be^{7*} excited by approximately 200 kev. The target was a thin layer of $(B^{10})_2O_3$ on the back side of an aluminum leaf. The proton energy was 1.46 Mev at the $(B^{10})_2O_3$ layer. The data obtained are shown in Fig. 16, where the indicated errors are those due to statistics. None of the alpha-particles had enough energy to be counted through the aluminum foils in front of the counter. The energies at which the groups of alpha-particles appeared agree with calculations based on the foil thickness. The data indicate that in the reaction $B^{10}(p,\alpha)Be^7$ at a proton energy of 1.46 Mev, the residual Be^7 is not left in any excited state near 200 kev as much as one-tenth as often as in either the ground state or the state at 434 kev. Excitation of the state at 745 kev was not attempted, since if the state exists, the barrier penetration factor for the alpha-particles would be so low that the reaction could not have been observed at the proton energy available. It must be pointed out that Grosskreutz and Mather used proton energies of 5.1 Mev, which is higher than employed by other investigators. All that is indicated by the null results here reported is a choice of two possibilities; either the state does not exist or it cannot be produced in the range of excitations available in these experiments.

Careful studies of the reactions $Be^9(d,\alpha)Li^7$ by several investigators[33] have revealed no additional states in Li^7 up to 2-Mev excitation energy. The next known state in Li^7 occurs at an excitation of 7.38 Mev and was first observed as a resonance[34] at $E_n=0.27$ Mev in $Li^6(n,\alpha)H^3$. The mirror state has been recently found in Be^7 at 7.1 Mev from resonances[35] in $Li^6(p,\alpha)He^3$ and $Li^6(p,p)Li^6$.

VII. CONCLUSIONS

From these experiments it is concluded that there exist excited states in Li^7 and Be^7 at 479.0±1 kev and

[32] Mandeville, Swann, and Snowdon, Phys. Rev. **76**, 980 (1949).
[33] W. W. Buechner and E. N. Strait, Phys. Rev. **76**, 1547 (1949). D. R. Inglis, Phys. Rev. **78**, 104 (1950).
[34] Goldsmith, Ibser, and Feld, Revs. Modern Phys. **19**, 259 (1947) quotes unpublished results of Blair, *et al.*
[35] Bashkin, Ajzenberg, Browne, Goldhaber, Laubenstein, and Richards, Phys. Rev. **79**, 238 (1950).

434.4±4 kev, respectively, and no evidence for additional low-lying states has been found. Additional states do not exist or *they cannot be excited* in the reactions used in these experiments with available excitations. The Q-value for $B^{10}(p,\alpha)Be^7$ has been measured as 1.148±0.006 Mev and for $B^{10}(p,\alpha')Be^{7*}$, as 0.714 ±0.008 Mev.

For the reaction $Li^7(p,n)Be^7$, the Q-value is −1.645 ±0.001 Mev and thus, using $M(n)-M(H^1)=0.782$ ±0.001 Mev,

$$\delta Mc^2=[M(Be^7)-M(Li^7)]c^2=0.863\pm0.002 \text{ Mev}$$
$$\delta M^*c^2=[M(Be^{7*})-M(Li^{7*})]c^2=0.818\pm0.004 \text{ Mev}$$

$\delta(M-M^*)c^2=479-434$ kev$=45\pm4$ kev.

The difference in the splitting of the Be^7 levels and the Li^7 levels is more than ten times the error of measurement and amounts to about 10 percent of the energy splitting between the excited and ground states. There is now considerable evidence for the assumption that the excited state in Li^7 (and presumably in Be^7) has $I=\frac{1}{2}$ forming a ^2P-doublet with the ground state for which $I=\frac{3}{2}$ by direct measurement. This evidence is given by the γ-α angular correlation measurements[36] in $B^{10}(n,\alpha')Li^{7*}(\gamma)Li^7$ and the angular distribution measurements[30] in $Li^7(p,p')Li^{7*}(\gamma)Li^7$. The observed splitting difference reported here is of considerable significance in connection with this probable doublet structure. The over-all separation of the levels is perhaps to be attributed to a new term in the ultimate nuclear forces, such as seems to be manifest in the *jj*-coupling shell model for medium and heavy nuclei, and in the spin-orbit forces of Case and Pais.[7] However, the splitting *difference* in these mirror levels must be sought in terms of electrostatic and magnetic effects, it not being possible to neglect the latter in calculating the small difference.

The matter is discussed in the following paper[7a] by Inglis who first calculated[6] the magnetic contributions to nuclear energies. In regard to the electrostatic effects, it can be expected that the excited states will have slightly larger radii than do the ground states, thus reducing their first-order electrostatic energy difference ($\sim 1/R$). However, a reasonable estimate based on Feenberg's analysis[37] of nuclear compressibility yields $\delta R/R\sim 0.2$ percent and a splitting difference of at most 3 kev. It also can be expected that the larger radii of the Be^7 states relative to the Li^7 states arising from their larger positive electrostatic energies would reduce any reasonable spin-orbit interaction ($\sim 1/R^3$). According to Inglis, a reasonable estimate of the two terms together yields only 10 kev. Furthermore, it does not seem reasonable to ascribe large differences between the ground and excited states to the $\langle 1/r\rangle$ term in Eq. (2). Some contribution to the difference must then arise from the magnetic effects, and in his paper Inglis finds a reasonable agreement between the theoretical expectations and the observed value. Rough agreement is obtained by the use of Eq. (4). It is to be emphasized that the sign (and magnitude) of the separation is correct for $I^*=\frac{1}{2}$ while the sign is given incorrectly, for example, for $I^*=5/2$ in a ^2D-doublet with $I=3/2$.

The calculations lend considerable support to the belief that the excited states in Be^7 and Li^7 at 434 and 479 kev are "mirror" states. Their displacement by the order of 10 percent of their excitation energy indicates that the experimental identification of mirror states may require considerable care and study. At high excitations the mean separation of protons may change substantially, giving large differential electrostatic effects, and for states with high enough energy of excitation to be subject to decay by proton or neutron emission, there may be a considerable displacement (~1 Mev) of the relative position of the states. A detailed discussion of this effect in the $N^{13}-C^{13}$ case will be published in the near future by R. G. Thomas of this laboratory.

It will remain for additional experimental evidence to confirm in a variety of cases the correspondence of the excited states of mirror nuclei. As indicated in the paper by Inglis, it may be necessary to make detailed calculations of fine structure effects, such as electrostatic and magnetic contributions to the energy of the state, in order to clarify apparent deviations in the excitation energies. Just the fact that a reasonable calculation involving a few tens of kilovolts can be made with some confidence in the case of Be^{7*} and Li^{7*}, constitutes substantial evidence for the equality of the nuclear *pp* and *nn* forces within very narrow limits.

VIII. DISCUSSION OF THE $B^{10}(p,\alpha)Be^7$ CROSS SECTIONS

The $B^{10}(p,\alpha)Be^7$ cross sections measured in these experiments have some bearing on the important question of the spin of the excited states of Be^7 and Li^7. The analysis of the cross section requires first the elimination of barrier factor effects for the incoming protons and outgoing alpha-particles. This has been done by one of us.[38] The analysis indicates that there is probably a resonance in $B^{10}(p,\alpha)Be^7$ at 1.0 Mev superimposed on a broad continuous background extending over the entire range of excitations used in these experiments. The yields are consistent with reasonable values (~1 Mev) for the widths without barrier of both the protons and alpha-particles on the assumptions that the background arises from *s*-wave capture into a broad state of C^{11} with $I=5/2^+$ and that the resonance arises from *p*-wave capture into a state of C^{11} with $I=3/2^-$. The assumption of $I(Be^{7*})=1/2^-$ along with $I(B^{10})=3^+$ makes it reasonable that the

[36] B. Rose and A. R. W. Wilson, Phys. Rev. **78**, 68 (1950).
[37] E. Feenberg, Revs. Modern Phys. **19**, 239 (1947).
[38] A. B. Brown, PhD. thesis "Excited states of the mirror nuclei, Be^7 and Li^7," California Institute of Technology (1950).

yield of the low energy alpha-particles should be very small in this region since the angular momentum of the outgoing α'-particle must be large, and the barrier factors markedly reduce the yield. On the other hand, the resonance yield for $B^{10}(p,\alpha')Be^{7*}$ at 1.5 Mev is anomalously large compared to $B^{10}(p,\alpha)Be^{7}$ in the same way that the slow neutron yield for $B^{10}(n,\alpha')Li^{7*}$ is large compared to that for $B^{10}(n,\alpha)Li^{7}$.[39] Only for f-wave capture of protons into a C^{11} state with $I=1/2^-$ is the emission of the α' favored (s-wave) by barrier factors over that for the α (d-wave), and in this case the detailed calculations indicate an impossibly large and unobserved partial width for the proton scattering. In the case of s-capture into a C^{11} state with $I=7/2^+$, or of p-capture into $I=5/2^-$, the outgoing waves can have the same minimum value (f and d, respectively), and the widths without barrier for α' are about 10 times those for α. It is true that this factor can be reduced by assuming $I(Be^{7*})=5/2$ or $7/2$, but it must be emphasized that we have found just such variations in widths without barrier in a considerable number of cases of proton induced reactions.[28] Furthermore, considerable confidence is lent to the assignment $I(Be^{7*})=1/2^-$ by the relative yields in the region below 1.3 Mev where, as expected on this assignment, the reaction $B^{10}(p,\alpha')Be^{7*}$ is highly improbable.

In conclusion, we wish to thank Sylvan Rubin and C. Y. Chao, who aided in many of the observations reported here, and R. F. Christy for valuable discussions of the theoretical aspects. We are grateful to D. R. Inglis for communication of his results prior to publication.

APPENDIX A. METHODS OF CALCULATING NUCLEAR Q-VALUES

In the experiments described in this report the excitation energies of Li^{7*} and Be^{7*} are essentially determined as the differences in the Q-values for reactions in which the ground states and excited states are involved. The experiments thus reduced to the determination of reaction Q-values. In the lithium case in which the reactions are the special cases of scattering, the Q-value of one of the processes, the elastic scattering, is of course equal to zero, and some advantage can be taken of this fact in ascertaining the over-all accuracy of the methods employed. In this appendix we discuss certain points involved in the accurate determination of the release of energy in nuclear reactions. In addition to a general treatment of the methods of calculating Q-values from the experimental data, we wish to consider small effects arising from special relativity, from thermal motion of the target nuclei, and from the choice of masses—nuclear, atomic, or integral. In Appendix B we consider the effects of energy losses and straggling in the target material and in surface contamination layers. In Appendix C we attempt to ascertain the error produced in the final result by errors made in the evaluation of the directly determined quantities. Throughout these appendices we calculate, as examples, appropriate correction terms, δQ, to illustrate the order of magnitude of the corrections necessary to account for small effects. In actual calculations we have applied the corrections straight-forwardly in an exact manner.

The Q-value of a nuclear reaction is by definition the difference in rest mass in energy units of the initial and final nuclei involved. For two initial and two final nuclei this becomes:

$$Q=(M_0+M_1-M_2-M_3)c^2, \tag{A1}$$

where we use the usual subscript notation, *zero* for the target nucleus, *one* for the bombarding particle, *two* for the observed particle, and *three* for the residual nucleus or particle. To avoid duplication, we do not use an additional subscript to designate rest mass when a subscript is already employed to identify the mass. Strictly, it is only correct to use nuclear masses in (A1), but atomic masses can be used if positron emission is not involved and if electronic binding energies are neglected. The neglect of electronic binding energies involves an error in Q if calculated from atomic masses of the order of

$$\delta Q\approx 36(Z_0+Z_1)^{4/3}(Z_1-Z_2)\text{ ev} \tag{A1'}$$

for $Z_0>Z_1$ and $Z_3>Z_2$. If atomic masses are employed in (A1) then Q should be replaced on the left-hand side by $Q+\delta Q$ with δQ given by (A1'). To derive (A1') we employ $E_b\approx 15.6Z^{7/3}$ ev as a rough estimate of total atomic binding energies. The error is -0.4 kev for the reaction $B^{10}(p,\alpha)Be^{7}$, for which $Z_0+Z_1=6$ and $Z_1-Z_2=-1$. In general, the masses are not known accurately enough to make any correction necessary. In the experiments described here the determination of Q from mass spectroscopic values is not possible at the present time, and nuclear methods must be employed. When Q-values determined by nuclear methods are employed to determine an unknown *atomic* mass from known ones, the Q-value should first be corrected by a small amount equal to that given by (A1').

The determination by nuclear methods[40,41] depends on the expression:

$$Q=E_3+E_2-E_0-E_1=E_3+E_2-E_1, \tag{A2}$$

where the E's designate kinetic energies. This can be derived from (A1) by using the conservation of the total energy, mass plus kinetic, before and after the reaction. It will be noted that (A2) is relativistically correct. In the second equality we neglect the thermal energy of the target nuclei. This is certainly valid in Eq. (A2) since $E_0\sim 0.025$ ev at ordinary temperatures, and at the present time, under the best circumstances, it is not possible to reduce errors in the measurement of E_1, E_2, and E_3 to less than several hundred electron volts. The determination of Q thus can be reduced to the determination of the energies E_1, E_2, and E_3. In actual practice the energy of only one of the outgoing particles is measured directly and that of the other is calculated using the conservation of momentum.

In the most accurate early investigations the energy of the incident particle was determined by a direct measurement of the high potential on the accelerating device. The energy of the emitted particle was usually determined by range or ionization measurements. Recently, these methods have been supplanted by the use of electrostatic,[42] velocity,[43] and magnetic[44] analyzers or spectrometers. For energies exceeding 1 Mev, direct measurements of the accelerating potential are impractical, and range measurements have not proven sufficiently precise, the accuracy being limited to $\sim$1 percent. In the experiments described in this paper a 90° cylindrical electrostatic analyzer[42] has been used to measure E_1, and a 180° double focusing magnetic spectrometer[44] has been used to measure E_2.

[28] D. R. Inglis, Phys. Rev. **74**, 1876 (1948).

[40] M. S. Livingston and H. A. Bethe, Revs. Modern Phys. **9**, 245 (1937).

[41] C. E. Mandeville, J. Franklin Inst. **244**, 385 (1947).

[42] Allison, Frankel, Hall, Montague, Morrish, and Warshaw, Rev. Sci. Instr. **20**, 735 (1950); Herb, Snowdon, and Sala, Phys. Rev. **75**, 246 (1949); Fowler, Lauritsen, and Lauritsen, Rev. Sci. Instr. **18**, 818 (1947).

[43] Shoup, Jennings, and Jones, Phys. Rev. **76**, 502 (1949).

[44] Snyder, Rubin, Fowler, and Lauritsen, Rev. Sci. Instr. **21**, 852 (1950); Burcham and Freeman, Phil. Mag. **40**, 807 (1949); Buechner, Strait, Stergiopoulos, and Sperduto, Phys. Rev. **74**, 1569 (1948).

The Electrostatic Analyzer

In an electrostatic analyzer the "electric rigidity" of the particle trajectory (field×radius of curvature) is used as a measure of the particle's energy. The kinetic energy of the particle is given relativistically by

$$E=E_0-M_0c^2+(M_0^2c^4+E_0^2)^{\frac{1}{2}} \approx E_0(1+E_0/2M_0c^2) \quad \text{for} \quad E_0\ll M_0c^2. \tag{A3}$$

Here E_0 is the energy calculated on the basis of simple proportionality to the centrifugal force and thus to the measured potential V across the analyzer plates (symmetrically charged). It is given by

$$E_0=\tfrac{1}{2}Mv^2=E(M_0c^2+\tfrac{1}{2}E)/(M_0c^2+E)=ZeV/2\ln(\rho_1/\rho_2) =ZeV\rho/2d[1+(1/24)(d^2/\rho^2)+\cdots]\approx ZeV\rho/2d=C_eZR. \tag{A4}$$

In Eq. (A4), ρ_1 and ρ_2 are the radii of the plates, $d=\rho_1-\rho_2$ is the plate separation, and $\rho=(\rho_1\rho_2)^{\frac{1}{2}}$ is the geometric mean of the radii of curvature. Ze, M_0, and P are the charge, rest mass, and momentum of the particle, respectively. R is the reading of the device by which V is measured, usually a potentiometer across a portion of the plate resistor stacks, and C_e is a constant of the apparatus. Small corrections for edge effects, misalignment of entrance and exit slits, superimposed magnetic fields, and other factors have been adequately discussed previously.[45a, b] The focal properties which make energy measurements with the analyzer independent of the entrance angle in the plane of curvature and of the angle of deflection have also been completely treated. In the experiments described here the constant C_e was determined by measurements on the strong gamma-ray resonance in the reaction $F^{19}(p,\alpha\gamma)$ at a proton energy of 873.5 kev.[46] Rough measurements of ρ and d checked the value obtained. The linearity was checked by measurements on H^+, HH^+, and HHH^+ ions using for detection a magnetic spectrometer at a fixed field setting. Relativistically correct results were given conveniently by using the approximate form of (A3). Numerically, for R in millivolts and E_0 in Mev, $C_e=0.12368$.

The Magnetic Spectrometer

In a magnetic spectrometer the "magnetic rigidity" is measured and gives directly the relativistically correct momentum of the particle. The energy is thus given by

$$E=(M_0^2c^4+2E_0M_0c^2)^{\frac{1}{2}}-M_0c^2 \approx E_0(1-E_0/2M_0c^2) \quad \text{for} \quad E_0\ll M_0c^2 \tag{A5}$$

where E_0 is the energy calculated on the basis of a simple quadratic dependence on the measured magnetic induction B. It is given by

$$E_0=P^2/2M_0=(B\rho Ze)^2/2M_0c^2=0.4827(ZB\rho)^2/M_0\times10^{-10}\ \text{Mev} =C_mZ^2/M_0I^2. \tag{A6}$$

The numerical value is for $B\rho$ in gauss-cm and M_0 in atomic mass units. Here I is the reading of a fluxmeter of the type used for some time in this laboratory.[45b] The constant C_m was determined by measurements on particles of known energy after scattering off targets of Li, Be, C, O, Al, Cu, and Au. Linearity in I^{-2} was checked by measurements on H^+, HH^+, and HHH^+ ions of the same energy as determined by the electrostatic analyzer at a fixed setting. Relativistically correct results were given conveniently by using the approximate form of (A5). Numerically, $E_0=1738I^{-2}$ Mev for protons and $E_0=1750I^{-2}$ Mev for alpha-particles. These expressions hold for I in the units used in all of the figures of this paper.

Equations for Q

As noted previously, only one of the energies, E_3 and E_4, is measured directly, and usually the energy of the lighter particle is measured rather than that of the heavier. In general, this gives the higher precision in the final result although, if the emitted particle is a neutron, more precise results may be obtained by measurements on the other nucleus which, because of its charge, can be deflected in a magnetic or electric field. In any case, the energy not measured directly is determined by measuring the angle of emission, θ, with the direction of bombardment as well as the energy of the one product and then using the relativistically correct expression for the conservation of momentum in the over-all process, namely

$$P_3^2=P_4^2-2P_3P_1\cos\theta+P_1^2. \tag{A7}$$

Here θ is the angle of emission of particle 2 with the original direction of particle 1. In writing Eq. (A7) we have neglected P_0, the momentum of the target nucleus arising from its thermal motion. It is true that this motion will cause an observed spread[46] in either P_3 or P_4 at any given angle of observation. However, if we employ appropriately averaged values of P_3 and P_4 in Eq. (A7), we can neglect terms in P_0. This is because terms linear in P_0 yield zero when averaged over all possible directions of motion, and those quadratic in P_0 are of the order of $E_0=0.025$ ev and are thus negligible.

At this point it is usually considered sufficiently accurate in the customary Q-value determinations to employ the non-relativistic relation between the energy, momentum, and rest mass of each particle, namely:

$$P^2=2EM_0. \tag{A8}$$

Upon substitution of (A8) in (A7) one obtains

$$E_3=(M_4E_4/M_3)+(M_1E_1/M_3)-2\mathcal{S}\cos\theta, \tag{A9}$$

where

$$\mathcal{S}=(M_1M_4E_1E_4/M_3^2)^{\frac{1}{2}}. \tag{A10}$$

Then using (A2),

$$Q=\frac{M_3+M_4}{M_3}E_3-\frac{M_3-M_1}{M_3}E_1-2\mathcal{S}\cos\theta, \tag{A11}$$

or

$$Q=\frac{M_3+M_4}{2M_3M_4}P_3^2-\frac{M_3-M_1}{2M_3M_1}P_1^2-\frac{1}{M_4}P_1P_3\cos\theta, \tag{A11'}$$

and in a convenient form for application in the experiments described in this report

$$Q=\frac{M_3+M_4}{2M_3M_4}P_3^2-\frac{M_3-M_1}{M_3}E_1-\frac{1}{M_4}(2M_1E_1)^{\frac{1}{2}}P_3\cos\theta. \tag{A11''}$$

Equation (A11) can be solved for E_3 as a function of E_1, Q, and θ to yield

$$E_3^{\frac{1}{2}}=\frac{(M_1M_4E_1)^{\frac{1}{2}}}{M_3+M_4}\cos\theta \pm\left(\frac{M_4}{M_3+M_4}Q+\frac{M_3-M_1}{M_3+M_4}E_1+\frac{M_1M_4}{(M_3+M_4)^2}E_1\cos^2\theta\right)^{\frac{1}{2}}. \tag{A12}$$

In (A12) the negative sign is only used when the first term is numerically larger than the second and in this case E_3 is a double-valued function of θ, and the angle within which the particle can be observed is limited to a value less than 90°. A form involving $\sin^2\theta$ in the second bracket can be derived using $M_0+M_1\approx M_3+M_4$, but the approximation is of the same order as certain relativistic corrections to be considered later.

Dependence of Q on the Independent Variables

In our further discussion we will be interested in $\delta Q=\Sigma_X(\partial Q/\partial X)\delta X$, where X represents the independent variables

[45] C. C. Lauritsen and T. Lauritsen, Rev. Sci. Instr. **19**, 916 (1948).

[46] In the most common cases where $(M_3+M_4)M_4Q>(M_1M_4-M_3M_4)E_1$, it can be shown that the full spread in E_3 for a given target energy E_0 is given by

$$\delta E_3=4(M_4M_0/M^2)^{\frac{1}{2}}E_0E_3.$$

For the reaction $B^{10}(p,\alpha)Be^7$ this yields $\delta E_3=0.5$ kev when the alpha-particles are observed with $E_3=2$ Mev and when one takes $E_0=0.025$ ev.

in (A11), (A11′), or (A11″) and thus we will need the following partial derivatives:

$$\frac{\partial Q}{\partial\theta}=2\mathcal{E}\sin\theta\rightarrow 2\mathcal{E} \text{ at } 90°, \tag{A13}$$

$$\frac{\partial Q}{\partial E_1}=-\frac{M_3-M_1}{M_3}-\frac{\mathcal{E}}{E_1}\cos\theta\rightarrow-\frac{M_3-M_1}{M_3} \text{ at } 90°, \tag{A14}$$

and

$$\frac{\partial Q}{\partial E_2}=\frac{M_3+M_3}{M_3}-\frac{\mathcal{E}}{E_2}\cos\theta\rightarrow\frac{M_3+M_3}{M_3} \text{ at } 90°. \tag{A15}$$

If the energies are determined we have from (A11)

$$\frac{\partial Q}{\partial M_1}=\frac{E_1}{M_3}-\frac{\mathcal{E}}{M_1}\cos\theta\rightarrow\frac{E_1}{M_3} \text{ at } 90°, \tag{A16}$$

$$\frac{\partial Q}{\partial M_2}=\frac{E_2}{M_3}-\frac{\mathcal{E}}{M_2}\cos\theta\rightarrow\frac{E_2}{M_3} \text{ at } 90°, \tag{A17}$$

and

$$\partial Q/\partial M_3=-E_3/M_3. \tag{A18}$$

If the momenta are determined we have from (A11′)

$$\partial Q/\partial M_1=E_1/M_1, \tag{A16′}$$

$$\partial Q/\partial M_2=-E_2/M_2, \tag{A17′}$$

and

$$\partial Q/\partial M_3=-E_3/M_3. \tag{A18′}$$

From (A12)

$$\frac{\partial E_2}{\partial\theta}=-\frac{2M_3\mathcal{E}\sin\theta}{M_2+M_3-(M_3\mathcal{E}/E_2)\cos\theta}\rightarrow-\frac{2M_3}{M_2+M_3}\mathcal{E} \text{ at } 90°, \tag{A19}$$

$$\frac{\partial E_2}{\partial E_1}=\frac{M_3-M_1+(M_3\mathcal{E}/E_1)\cos\theta}{M_2+M_3-(M_3\mathcal{E}/E_2)\cos\theta}\rightarrow\frac{M_3-M_1}{M_2+M_3} \text{ at } 90°, \tag{A20}$$

and

$$\frac{\partial E_2}{\partial Q}=\frac{M_3}{M_2+M_3-(M_3\mathcal{E}/E_2)\cos\theta}\rightarrow\frac{M_3}{M_2+M_3} \text{ at } 90°. \tag{A21}$$

The Relativistic Solution for Q

In seeking a relativistic solution for Q we must use instead of (A8) the relativistic relation

$$P^2=2EM_0+E^2/c^2. \tag{A8′}$$

An explicit solution using (A8′) involves algebraic expressions of considerable complexity.[47] It will be noted, however, that (A8) is identical with (A8′) if M_0 in (A8) is replaced by an effective mass given by

$$M_{eff}=M_0+E/2c^2. \tag{A8″}$$

The derivation of (A9), (A11), and (A12) will be as before but with each mass replaced by this effective mass. *Thus the usual non-relativistic expressions involving nuclear Q values can be employed relativistically if only each mass involved is replaced by its effective value which is the rest mass plus one-half the kinetic energy in mass units.* It will be noted that this effective mass is not the relativistic total mass corresponding to the rest mass plus all of the kinetic energy in mass units. It is true that one does not obtain an explicit solution for Q since the effective value of M_3 and thus E_3 appears in (A11). However, when the relativistic corrections are small it is sufficiently accurate to estimate E_3 non-relativistically from (A9), and even for large relativistic effects the method of successive approximations, using (A8″), (A9), (A10), and (A11) is often convenient. When quanta are involved, as in photoeffect reactions and capture-radiation reactions, the substitution $Mc^2=h\nu/2$ makes possible the direct use of these equations.

It is possible to estimate relativistic and other small corrections by using the appropriate partial derivations from (A13) to (A18′). There are three relativistic effects to be taken into account; first, in the determination of the incident particle energy; second, in the determination of the observed emitted particle energy; and third, in the dynamical equation for the Q-value. We calculate $\delta Q=\Sigma_X(\partial Q/\partial X)\delta X$, where X runs through E_1, E_2, M_1, M_2, and M_3, as an example. We obtain the δE from (A3) or (A5) and set each $\delta M=E/2c^2$. The relativistic corrections are then combined into an over-all correction factor, δQ, which will, in general, depend on the methods of energy determination and on the angle of observation. If the energies are known correctly and it is wished to estimate the relativistic correction necessary if rest masses are used in (A11), then the result is particularly simple for 90° observation being given by

$$\delta Q=(E_1^2+E_2^2-E_3^2)/2M_3c^2, \tag{A22}$$

or for large $Q\approx E_2+E_3\gg E_1$

$$\delta Q/Q\approx Q(M_3-M_3)/2M_3c^2(M_3+M_3). \tag{A22′}$$

This was first shown by Livingston and Bethe.[40] In general, the correction is at most of the order of 0.1 percent. Another case is of special interest. If the particle momenta are determined in a relativistically correct manner, as by the use of magnetic analyzers for *both* incoming and outgoing particles, then the momentum of the residual nucleus is correctly given by (A3). The error in a non-relativistic calculation involves only the E-values used in (A2). Hence, the correction to be made to such a calculation can be implicitly written independently of the angle of observation as

$$\delta Q=\tfrac{1}{2}[(E_1^2/M_1c^2)-(E_2^2/M_2c^2)-(E_3^2/M_3c^2)]. \tag{A23}$$

In the case of the techniques used in the experiments reported here, where an electrostatic analyzer was used to measure E_1 and a magnetic analyzer was used to measure E_2, one finds

$$\delta Q\approx-\tfrac{1}{2}[(E_1^2/M_1c^2)+(E_2^2/M_2c^2)+(E_3^2/M_3c^2)]. \tag{A24}$$

This equation holds strictly only for $M_3E_3=M_2E_2$, which will be approximately true for $Q>E_1$. For 90° observation the expression is exact if E_1^2/M_2c^2 is added to the right-hand side.

The Rest Masses

The question arises concerning the correct rest mass to use in Eqs. (A8′) or (A8″)—nuclear or atomic—in transforming Eq. (A6) into Eq. (A9). That the nuclear rather than the atomic mass for the target nucleus should be used seems reasonable from the fact that a nuclear collision happens in a time short compared with characteristic atomic times. A calculation by Christy[47a] indicates that the nuclear mass is indeed the one to use in the usual case in which the excitation energy, which can be imparted to the atom, is so small as to be unresolvable by the spectrometer employed and in which the excitation of the atom to various electronic states results in only small changes in momenta. The tabulated atomic masses are, of course, convenient to use, and for light nuclei,

$$\delta M/M=(M_{\text{nuclear}}-M_{\text{atomic}})/M_{\text{nuclear}}=-Z/1800\text{A}. \tag{A25}$$

Thus, in the experiments reported here we have

$$\delta Q=1/1800[(Z_1E_1/A_3)-(Z_1\mathcal{E}\cos\theta/A_1)-(Z_2E_2/A_2)-(Z_3E_3/A_3)]. \tag{A26}$$

For $Z/A\sim1/2$ and $Q\approx E_2+E_3>E_1$ we have

$$\delta Q\sim Q/3600, \tag{A26′}$$

which is a negligible correction in all but a few special cases. On the other hand, the use of integral rather than exact atomic weights introduces mass errors of the order of $\delta M/M\sim0.001$ and hence

$$\delta Q\sim Q/1000. \tag{A27}$$

This error is comparable to the precision obtainable is present Q-measurements and thus the use of integral atomic weights is not advisable. As long as non-integral numbers are to be used,

[47] R. H. Bacon, Am. J. Phys. **8**, 154, 354 (1940).

[47a] We are indebted to Professor Christy for communicating his conclusions to us.

we find it just as convenient to use nuclear masses with relativistic corrections as it is to use the tabulated atomic masses.

Energy of Nuclei in Ions

In some instances ions other than the stripped nucleus are used as bombarding agents or are measured as the reaction product. In either case, the fraction of the energy attributable to the nucleus can be calculated on the simple basis of proportionality to rest mass. For example, if HH^+ ions are used in bombardment, each proton has 0.49986 of the total energy of the ion. In the case of capture and loss of electrons in the target we assume that any energy transfers are covered by the empirical or theoretical estimates of the over-all energy losses in the target and contamination layers.

APPENDIX B. ANALYSIS OF ENERGY RELATIONS IN THE TARGET PROCESSES

The use of high resolution devices in the determination of the energy of the incident and emitted particles in a nuclear reaction necessitates a detailed analysis of the reaction events in the target. Figure 17 illustrates the general situation in experiments, such as described in this report, in which the Q-value or the cross section of a nuclear reaction is determined. In practically every calculation involved in such determinations one needs to know the relations between the bombarding energy, E_{1B}, the observed energy of the emitted particles, E_{20}, the average energy, E_1, of the incident particles which actually produce the observed particles, and the energy, E_2, of the emitted particles at production.

In Q-value measurements these relations must be understood in actually determining from the observations the energy, E_{2B}, of the emitted particles produced at the surface of the target by the bombarding particles with their full energy. Neglecting contamination layers to be discussed later, E_{1B} and E_{2B} or E_1 and E_2 but not E_{1B} and E_{20} are the energies which must be substituted into (A11) to yield Q. In cross-section measurements the cross section determined is that for the incident particles with energy E_1. Thus the measurements involve not only the usual counting procedures but also the calculation of E_1 from E_{1B} and E_{20}.

It is clear that these relations will depend primarily on the energy loss of the incident and emitted particles in the target material and secondarily on the scattering and straggling which they undergo. We give here a very elementary discussion in which energy loss considerations are emphasized.

Energy Loss Considerations

For observation of the emitted particles on the same side of the target on which the incident particles impinge, as illustrated in Fig. 17, we have

$$\Delta E_2/\Delta E_1=(E_2-E_{20})(E_{1B}-E_1)=\epsilon_2\cos\theta_1/\epsilon_1\cos\theta_2\equiv\eta, \quad \text{(B1)}$$

where θ_1 and θ_2 are the angles with the normal to the target drawn on the side of the incident beam, and ϵ_1 and ϵ_2 are the stopping cross sections[48] in the target for the incident and emitted particles, respectively. We define η in Eq. (B1) for brevity in what follows. We also have in first approximation

$$E_{2B}-E_2=(\partial E_2/\partial E_1)(E_{1B}-E_1), \quad \text{(B2)}$$

[48] Throughout the calculations using the methods described here we have used stopping cross sections computed from data given by H. A. Bethe, BNLT-7 (1949) (unpublished); C. B. Madsen and P. Venkateswarlu, Phys. Rev. **74**, 648 (1948); C. M. Crenshaw, Phys. Rev. **62**, 54 (1942); R. Wilson, Phys. Rev. **60**, 749 (1941); S. D. Warshaw, Phys. Rev. **76**, 1759 (1949). We have used interpolation methods for elements for which measurements have not been made. This is satisfactory in the evaluation of small correction terms in energy measurements but does constitute a source of error of ~10 percent in cross-section measurements. Following the practice of M. S. Livingston and H. A. Bethe, Revs. Modern Phys. **9**, 270 (1937), we have used ϵ in units of 10^{-15} ev cm^2.

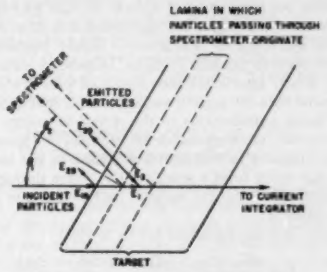

FIG. 17. Analysis of energy relations in the target processes taking into account only energy loss effects and neglecting scattering and straggling.

where $\partial E_2/\partial E_1$, is given by Eq. (A20). From these two equations we obtain:

$$\frac{\Delta E_1}{\Delta E_{20}}=\frac{E_{1B}-E_1}{E_{2B}-E_{20}}=\frac{\epsilon_1}{\epsilon_{eff}}=\left(\eta+\frac{\partial E_2}{\partial E_1}\right)^{-1} \quad \text{(B3)}$$

$$\frac{\Delta E_2}{\Delta E_{20}}=\frac{E_2-E_{20}}{E_{2B}-E_{20}}=\frac{\epsilon_2\cos\theta_1}{\epsilon_{eff}\cos\theta_2}=\left(1+\frac{1}{\eta}\frac{\partial E_2}{\partial E_1}\right)^{-1}. \quad \text{(B4)}$$

In these equations we have defined an effective over-all stopping cross section as

$$\epsilon_{eff}=\epsilon_1(\partial E_2/\partial E_1)+\epsilon_2\cos\theta_1/\cos\theta_2. \quad \text{(B5)}$$

These equations reflect in the spread of the energy of the observed particles, ΔE_{20} not only their loss of energy, ΔE_2, in the target, but also the variation in their energies at production arising from the loss of energy, ΔE_1, of the incident particles in the target. We place ΔE_{20} in the denominator of (B3) and (B4), as it will be the observable from which ΔE_1 and ΔE_2 can be calculated. A similar derivation for the case of the particles being observed after transmission through the target leads to the same result if θ_2 is measured as before and if E_{2B} is the observed energy of those particles produced at the front surface of the target *after* their passage through the target with consequent energy loss. Our results (B3) and (B4) thus hold in general.

Equations (B3) and (B4) are useful in determining E_1 and E_2 if E_{1B}, E_{2B}, and E_{20} are measured. At this point we wish to discuss the determination of E_{2B}. In the case illustrated we note that $\cos\theta_1$ and $\cos\theta_2$ are both positive. Then since $\partial E_2/\partial E_1$ is usually positive, E_{2B} will be the maximum energy observed for the emitted particles and, aside from some complications arising from the finite resolution of the spectrometer, it can be readily measured experimentally. In fact, in either method of observation E_{2B} will be the maximum E_{20} for $\epsilon_{eff}>0$. However, in the transmission case the absolute energy losses must be ascertained to complete the Q-value calculations. In case $\epsilon_{eff}<0$, then E_{2B} will be the minimum E_{20}, while for $\epsilon_{eff}=0$, all the observed particles will have the same energy. These last two cases may arise in transmission observations when $\cos\theta_2<0$ or in observations at certain angles on residual nuclei when $\partial E_2/\partial E_1<0$. In these cases, however, straggling in energy plays an important role. In the case $\epsilon_{eff}=0$, straggling will determine completely the spread in energy of the emitted particles, while for $\epsilon_{eff}<0$, straggling will make it difficult to choose E_{2B} from the observations, especially in the transmission case. It might be argued that the maximum observed energy should always be employed with appropriate treatment in the calculations. However, for $\epsilon_{eff}<0$, the maximum energy particles observed will be those produced at the back side of the target, and their energy will depend on energy losses in the target. Straggling in this loss and errors in its measurement will contribute considerable uncertainty to such a determination.

For the reasons just discussed, in the experiments reported in this paper, observations have been made on the side of the target on which the incident particles impinge and on the lighter of the

two reaction products, so that $\epsilon_{eff}>0$. In this way it has been possible to use thick targets for mechanical and other reasons and to use the spectrometer resolution to isolate reaction products from determinable lamina in these targets. A case in which $\partial E_2/\partial E_1<0$ and $\epsilon_{eff}\approx 0$ has been discussed previously.[49] It must also be noted that for $\epsilon_{eff}\approx 0$, variations in ϵ_1 and ϵ_2 with energy will also make contributions to the spread in energy of the observed particles, it being possible for particles of a given observed energy to originate in two separate lamina in the target if, for example, ϵ_{eff} varies from a small positive value through zero to a small negative one over the range of particle energies involved in the target events.

Equation (B3) can be solved for E_1 to yield

$$E_1=\frac{\eta E_{1B}+E_{20}+[E_{1B}(\partial E_2/\partial E_1)-E_{2B}]}{\eta+(\partial E_2/\partial E_1)}, \qquad \text{(B3')}$$

where the term in brackets is zero in the case of elastic scattering and in any case is a constant for a given reaction over any small range of energies. The independent variables in the experiments are E_{1B} and E_{20} and convenient relations in certain calculations are

$$\partial E_1/\partial E_{1B}=(1+\eta^{-1}\partial E_2/\partial E_1)^{-1} \qquad \text{(B6)}$$

$$\partial E_1/\partial E_{20}=(\eta+\partial E_2/\partial E_1)^{-1}. \qquad \text{(B7)}$$

These partial derivatives make it possible to determine numerically any interval or fluctuation in E_1 in terms of the corresponding intervals or fluctuations in E_{1B} and E_{20}. This will be important, for example, in determining the energy resolution or errors in cross section *vs* energy measurements (excitation curves).

The Effective Target Thickness in Thick Target Measurements

The application of the above energy loss arguments to any thin lamina in the target leads to relations similar to (B3) and (B4). For example, if δE_{20} represents the energy interval over which the spectrometer accepts particles because of its finite exit window, then the energy loss of the incident particles in the lamina from which the observed particles are emitted is

$$\xi_1=\epsilon_1 nl=\frac{\epsilon_1\delta E_{20}}{|\epsilon_{eff}|}=\frac{\delta E_{20}}{|\eta+\partial E_2/\partial E_1|}=\frac{2E_{20}}{R_c|\eta+\partial E_2/\partial E_1|}, \qquad \text{(B8)}$$

where R_c is the resolution (in momentum) calculated, taking into account only the exit (or collector) slit width. It is given by

$$R_c=2(1+M)r_0/\delta r_c, \qquad \text{(B8')}$$

where M is the magnification of the instrument (0.8 in these experiments), δr_c is the collector slit width, and r_0 is the radius of curvature of the particle orbit. As long as the actual target is thicker than ξ_1, other sources of finite resolution do not enter into the probability of detection and in any case integrals over the thin target distribution depend only on R_c. Expression (B8) is useful for determining nl in cross-section measurements where n is the number of nuclei per cubic centimeter of target and l is the effective target thickness parallel to the incident beam. Again considerable caution must be observed when $|\epsilon_{eff}|\approx 0$ since then, straggling and variations in ϵ_1 and ϵ_2 with energy play dominant roles in determining the effective target thickness.

Corrections for Contamination Surface Layers

In the body of this report we have reported our finding of thin layers of carbon and oxygen on certain types of targets even with liquid air traps and diffusion pumps connected directly to the target chambers. We have emphasized that the use of the magnetic spectrometer in the detection of reaction and scattering products has made it possible to ascertain the thickness of these layers throughout the observations and to make appropriate corrections for them. We here wish to discuss the magnitude of these corrections.

The thickness of the layers is usually most directly expressed in terms of the energy loss of the incident particles in them. This is because observations on the amount of scattering by the layers and on the change in energy of the particles scattered by the true target under the layers can be accomplished so conveniently with the spectrometer. In the experiments described in this report we have used protons as incident particles and have found the energy loss in the layers in one traversal normal to the target to be, in general, of the order of 0.5 kev for 1-Mev protons. As the layers are about equally carbon and oxygen, it is sufficiently accurate to use the readily available stopping cross sections for air in calculations of the thickness. For 1-Mev protons the value is 5×10^{-15} ev-cm^2, so $nl\approx 10^{17}$ atoms/cm^2 where l is the thickness of the layer. Using a density of one, it is found that these layers are the order of 100 atoms thick or $l\approx 3\times 10^{-6}$ cm.

The correction for surface layers to be applied to Q, if the bombarding incident energy and the observed product energy are used in the preliminary calculations, is

$$\delta Q=\frac{\epsilon_2 nl}{\cos\theta_2}\frac{\partial Q}{\partial E_2}-\frac{\epsilon_1 nl}{\cos\theta_1}\frac{\partial Q}{\partial E_1}$$

$$\approx 0.1\left(\frac{\epsilon_2}{\cos\theta_2}\frac{\partial Q}{\partial E_2}-\frac{\epsilon_1}{\cos\theta_1}\frac{\partial Q}{\partial E_1}\right)\text{ kev}$$

$$\approx 0.1\left(\frac{\epsilon_2}{\cos\theta_2}\frac{M_2+M_3}{M_3}+\frac{\epsilon_1}{\cos\theta_1}\frac{M_3-M_1}{M_3}\right)\text{ kev at 90°}. \qquad \text{(B9)}$$

In the approximate expressions the ϵ are in the usual units employed, namely 10^{-15} ev cm^2 or 10^{-18} kev cm^2. The partial derivatives can be obtained from (A14, 15). As an example, the correction for $B^{10}(\dot{p},\alpha)Be^7$, where $\theta=138°$, $\theta_1=28°$, $\theta_2=14°$, and $E_1\sim E_2\sim 1$ Mev is

$$\delta Q\approx 0.1[(46\times 1.77/0.97)+(5\times 0.66/0.88)]\approx 8.8\text{ kev}. \qquad \text{(B9')}$$

Because of the large value of this correction, E_1 and E_2 were carefully corrected before substitution in the Q-equation for layers measured before and after the direct observations. Also, in determining the excitation energy of Be^{7*}, the incident proton energy was adjusted so that the two alpha-particle groups had about the same energy and thus their large losses approximately cancelled in calculating the excitation energy.

The Effects of Straggling

In the previous discussion we have emphasized that the straggling in the energy loss of the incident and outgoing particles introduces considerable uncertainty in the results of transmission experiments and even in the reflection experiments when $\partial E_2/\partial E_1$ is negative enough to make $\epsilon_{eff}<0$. Fortunately, in the experiments here discussed $dE_2/dE_1>0$, and we have observed at angles for which the reflection method is convenient. Here, we wish to discuss straggling effects in somewhat more detail for this case.

The mean square deviation in energy loss is given with sufficient accuracy for our purposes by the early formula of Bohr:

$$\langle(dE-\Delta E)^2\rangle=4\pi e^4 z^2 Znl$$
$$=260 z^2 Z\Delta E/\epsilon\text{ (ev)}^2, \qquad \text{(B10)}$$

where ze is the charge of the incident particle, Z is the atomic number of the target material, $\Delta E=\langle dE\rangle$ is the mean energy loss in ev, and ϵ is the stopping cross section in units 10^{-15} ev cm. In measurements on the straggling of 1 Mev protons in Be we find this expression gives a value for the root-mean-square deviation low by only 30 percent and, since this is an extreme case, (B10) is accurate enough for use in small correction terms. Using the customary approximate expression[40] for ϵ we have

$$\langle(dE-\Delta E)^2\rangle=E\Delta E[2m_0/M\ln(4m_0E/MI)], \qquad \text{(B11)}$$

or

$$[\langle(dE-\Delta E)^2\rangle]^{\frac{1}{2}}=1/30(E\Delta E/M)^{\frac{1}{2}}(\ln E/5200MZ)^{-\frac{1}{2}}. \qquad \text{(B12)}$$

[49] Tollestrup, Jenkins, Fowler, and Lauritsen, Phys. Rev. **75**, 1947 (1949).

In (B12) the mass of the particle M is in atomic mass units and the average ionization potential, $\bar{I}$, of the stopping material has been evaluated as $11.5Z$ ev. In the logarithm term, E must be in ev. In the region of usual interest ($E\sim1$ Mev for protons) the slowly varying logarithmic term ~3 and

$$[\langle(dE-\Delta E)^2\rangle]^{\frac{1}{2}}\sim0.02(E\Delta E/M)^{\frac{1}{2}}. \tag{B13}$$

The straggling will be in the same units as E and the energy loss ΔE. In our estimates of the straggling effects we add, linearly, the mean square deviations in energy loss for the incident and outgoing particles, using coefficients determined in the section on energy relations in the target.

In the reflection experiments, when $\epsilon_{eff}>0$, there is little effect of straggling on the energy of the particles produced at the front surface of the target. The ideal step function is of course rounded off slightly but this rounding off occurs completely in an energy interval which is at most of the order of the maximum energy transfer in a single collision to atomic electrons by the particles involved. This transfer is just $4m_0/M$ times the energy of the particle and even for protons is only ~0.002 of the proton's energy. This is well obscured by other sources of finite resolution in the experiments here described, and, in any case, the effect on the average behavior of the particles at the surface can be expected to be smaller. As a consequence, straggling can be neglected in the determination of E_{2B} except in so far as contamination layers are important.

In a surface contamination layer in which the apparent shift in the observed energy of the outgoing particles is

$$\Delta E_{20}=(\partial E_2/\partial E_1)\Delta E_1+\Delta E_2, \tag{B14}$$

the straggling will be given by summing the squares of the contribution of the incident and outgoing particles, *viz.*:

$$\delta E_{20}^2=[(\partial E_2/\partial E_1)\delta E_1]^2+\delta E_2^2, \tag{B15}$$

where δE_1 and δE_2 can be any arbitrary measures of the straggling. They will always be proportional to the root mean square deviation in energy loss given by (B10 to 13). Neglecting other sources of finite resolution the rise at the high energy end of the observed energy distribution will be given by the integral of the error function and a tangent line drawn through the midpoint will rise to the full value in $(2\pi)^{\frac{1}{2}}\sim2.5$ times the root mean square deviation. Using this as a measure of the straggling we have

$$\begin{aligned}\delta E_{20}^2&=1600Z[(z_1\partial E_2/\partial E_1)^2(\Delta E_1/\epsilon_1)+z_2^2(\Delta E_2/\epsilon_2)](\text{ev})^2\\&=1600Z(\Delta E_{20}/\epsilon_{eff})[(z_1\partial E_2/\partial E_1)^2+z_2^2\cos\theta_1/\cos\theta_2](\text{ev})^2\end{aligned} \tag{B16}$$

for ϵ_{eff} in 10^{-15} ev-cm^2. We note that

$$\Delta E_{20}/\epsilon_{eff}=\Delta E_1/\epsilon_1=nl/\cos\theta_1\times10^{-15}$$

$nl\approx10^{17}$ cm^{-2} for the observed layers, and $Z=7.22$ if we use ϵ for air. Hence,

$$\delta E_{20}=1.1[(z_1\partial E_2/\partial E_1)^2/\cos\theta_1+z_2^2/\cos\theta_2]^{\frac{1}{2}}\text{ kev}_1. \tag{B17}$$

For the $B^{10}(p,\alpha)Be^7$ example of the preceding section we have $\Delta E_{20}=4.9$ kev and $\delta E_{20}=3.2$ kev. Since $\delta E_{20}<\Delta E_{20}$, this small straggling effect is a symmetrical one, and the method of determination of E_{2B} is not effected.

The straggling in the target itself has its major effect on the low energy side of the distribution of observed particles. If ΔE_{20} is the average apparent energy loss in the target then Eq. (B16) gives the interval δE_{20} over which the tangent to the midpoint of the low energy side falls from the maximum reading to zero. As long as $\delta E_{20}<\Delta E_{20}$, as is the case for even the thinnest targets we have used, the straggling is symmetrical about the mean loss, and the distribution in energy of the observed particles has a flat maximum extending over the interval $\sim\Delta E_{20}-\frac{1}{2}\delta E_{20}$ followed by a drop to zero over the interval $\sim\delta E_{20}$. This is illustrated in Fig. 7 of reference 15 which shows the scattering of protons by a Be foil using very high resolution in the spectrometer. It can be shown that the maximum number of processes detected is just that to be expected in the ideal case neglecting straggling, and thus in calculating reaction cross sections it is justifiable to use the stopping cross sections, which are based on average energy losses, in Eq. (5) of the main body of this report. The straggling in the target is also a source of finite resolution in energy determinations in excitation curve measurements. The effects of straggling in this connection will be discussed in a forthcoming paper on scattering measurements.

Determination of E_{2B} in Thin Target Measurements

When thin targets are employed in Q-determinations the position in the observed energy distribution of the particles produced at the target surface depends on the effective target thickness for the emitted particles and the over-all resolution of the spectrometer. It is clear that E_{2B} is given by the average energy of the observed particles plus one-half the effective target thickness for those particles in energy units. This effective thickness will just be the energy loss of the incident particles in the target multiplied by $\partial E_2/\partial E_1$ plus the energy loss of the emitted particles in traversing the target. It is most directly obtained by weighing the target and determining its area and then using the empirical values of the stopping cross sections and the angles of traversal. This is not always feasible, however, and measurements on the energy distribution of the incident particles scattered by the target can be employed readily to yield its thickness for a given energy of the incident particle. Only the variation of the stopping cross section with energy and not the absolute values need be used in such a calculation. Similarly, to obtain the energy loss of the emitted particles and the effective thickness for them, it is only necessary to know the ratio of the stopping cross sections ϵ_2/ϵ_1. When it is possible to do so, the effective thickness is most easily determined by comparing the integrated yield for the target with the maximum yield for a thick target of the same material. From Eqs. (5) and (9) of the text one has directly

$$\xi_{eff}=\frac{E_{20}}{N_{max}}\int\frac{NdE}{E}=\frac{2E_{2B}}{N_{max}}\int\frac{NdI}{I}, \tag{B18}$$

where N_{max} represents the maximum number of counts obtainable with a thick target and is the N appearing in Eq. (5').

The determination of the average energy of the observed particles involves the use of particles which have suffered large losses, and it is sometimes preferable to estimate the instrumental spread[10] in the energy of the observed particles and to use the ratio of ξ_{eff} to δE_{20} to predict the relative number of counts at E_{2B}. As an illustration we consider the instrumental spread to be gaussian, and in keeping with our practice we take $(2\pi)^{\frac{1}{2}}$ times the root-mean-square deviation as δE_{20}. We let the effective energy loss be spread uniformly over ξ_{eff} without straggling. Then if $T=(2\pi)^{\frac{1}{2}}\xi_{eff}/\delta E_{20}$, we have

$$\frac{N(I_B)}{N_{max}}=\frac{1}{2}\left(\int_{-T}^{T}\exp(-t^2/2)dt\right)\Big/\left(\int_{-T/2}^{T/2}\exp(-t^2/2)dt\right), \tag{B19}$$

where I_B is the fluxmeter reading from which E_{2B} is calculated. For $\xi_{eff}\gg\delta E_{20}$, this approaches $\frac{1}{2}$, as expected for a thick target, while for $\xi_{eff}\ll\delta E_{20}$, it approaches unity, as expected for a very thin target. For $\xi_{eff}=\delta E_{20}$, $N(I_B)/N_{max}=0.63$ and for $\xi_{eff}=\delta E_{20}/2$, $N(I_B)/N_{max}=0.84$. The determination of the point at which $N(I_B)/N_{max}$ has its calculated value can often be done with considerable precision on the front side of the observed curve, and E_{2B} is thus given accurately.

The Determination of E_{2B} in Thick Target Measurements

We have found that the most precise determinations are yielded by thick target curves. In this case, to the approximation discussed above, $N(I_B)/N_{max}=\frac{1}{2}$, but in some cases it is worthwhile to consider additional effects. These are the effects of the

[10] We use δE_{20} for the instrumental spread in E_{20} in this section while we used it for the straggling in E_{20} in the preceding section.

dependence of the cross section of the process, the stopping cross sections, and the probability of detection of the emitted particle on energy. For no instrumental spreads other than that arising from the width of the exit slit, the number of counts at the fluxmeter reading I_0 corresponding to the energy, E_{20}, is proportional to the following energy dependent terms:

$$N(I_0)\sim nl\sigma(E_1)\sim E_{20}\sigma(E_1)/\epsilon_{eff}(E_1, E_2), \tag{B20}$$

where σ must be evaluated at E_1, the energy of the incident particles at which the reaction actually occurs (Fig. 17) and ϵ_{eff} must be evaluated at appropriate average energies in the intervals E_{1B} to E_1 and E_2 to E_{20}. As an illustration we consider the behavior of this function in the case of Rutherford elastic scattering for which $\sigma\sim E_1^{-2}$. If we assume the scattering nuclei are heavy compared to the incident particles, we have $\partial E_2/\partial E_1=1$ and $E_1=E_2=\frac{1}{2}(E_{2B}+E_{20})$. The stopping cross section can be taken as inversely proportional to the square root of the energy (Geiger's law) and hence

$$N\sim E_{20}\Big/\left(\frac{E_{2B}+E_{20}}{2}\right)^{\frac{1}{2}}. \tag{B21}$$

For E_{20} not too far below E_{2B}, this becomes

$$N\sim E_{20}^{\frac{1}{2}}/E_{2B}^{\frac{1}{2}}\sim I_B^{\frac{1}{2}}/I_0^{\frac{1}{2}}\to I_B \quad \text{for} \quad I_0=I_B. \tag{B22}$$

The observed number drops away slowly from a maximum number which is proportional to $E_{2B}^{-\frac{1}{2}}=E_{1B}^{-\frac{1}{2}}$ or to I_B. We have verified this experimentally in considerable detail in the scattering of protons by copper.

Returning to the general expression (B20) we now consider the effect of the instrumental spread in energy which, for convenience in calculation, we now assume to be rectangular in distribution with width $\delta E_{20}=2E_{20}/R$ in energy or with width $\delta I=I/R$ on the fluxmeter scale. In the energy range of interest we approximate the yield by

$$N\sim E_{20}{}^{n/2}\sim I_0{}^{-n},$$

where by comparison with (B20) we have

$$n=2+a+(2d\sigma/\sigma dE_1)(\epsilon_1 E_{20}/\epsilon_{eff}).$$

In this expression the member a is a complicated term arising from the dependence of (B20) on ϵ_{eff} and is given by

$$\begin{aligned} a&=0, \quad \epsilon_2\cos\theta_1/\cos\theta_2\gg\epsilon_1\partial E_2/\partial E_1\\ a&\sim\tfrac{1}{2}, \quad \epsilon_2\cos\theta_1/\cos\theta_2\sim\epsilon_1\partial E_2/\partial E_1\\ a&=1, \quad \epsilon_2\cos\theta_1/\cos\theta_2\ll\epsilon_1\partial E_2/\partial E_1. \end{aligned}$$

To determine n, the relation σ *vs* E_1 must be known or must be measured, independently. Then the effect of the finite resolution yields

$$N(I_B)/N_{\max}=\tfrac{1}{2}(1+n/4R).$$

Alternatively, I_B from which E_{2B} is calculated can be found by adding $n\delta I_B/8=nI_B/8R$ to the reading at half-maximum. Whaling and Li have found this correction to be appreciable in the $Li^7(p,\alpha)He^4$ reaction.[51]

APPENDIX C. ERRORS OF THE MEASUREMENTS

Sources which contribute to errors in measurements of E_1, E_2, and θ and hence of Q have been enumerated previously.[15] As is customary, they can be classified as either systematic or statistical errors. It has been our experience in performing measurements with the electrostatic analyzer and magnetic spectrometer discussed in this paper that the statistical errors in a Q-value, determined under widely differing conditions (different bombarding energies, targets, and angles of observation) over long periods of time, could be reduced to very small values compared to realistic estimates of the systematic errors. Fluctuations in the incident beam energy, in the measurement of the fluxmeter reading, in the relative values of the field over the particle path, in the target, collector, and stop positions have apparently contributed statistical probable errors of 0.1 percent.

We have not attempted to make absolute energy measurements but have depended on the standard nuclear energy scale established through the careful work of Herb and his collaborators at the University of Wisconsin.[42b] One systematic error is as follows: (1) the published probable error in the energy of the resonance used directly in the calibration of the electrostatic analyzer and indirectly in the calibration of the magnetic spectrometer. Others are, (2) the nonlinearity of the scales of the analyzer and spectrometer, (3) the uncertainty in the interpretation of the line shape of the observed particles as reflected in the choice of E_{2B}, (4) errors in the estimate of surface layer corrections arising from uncertainty in the scattering and stopping cross sections and, (5) the error in measurement of the angle of observation.

If the errors in E_1, E_2, and θ are completely independent, then the error in Q can be calculated from

$$\delta Q^2=\left(\frac{\partial Q}{\partial E_1}\delta E_1\right)^2+\left(\frac{\partial Q}{\partial E_2}\delta E_2\right)^2+\left(\frac{\partial Q}{\partial\theta}\delta\theta\right)^2 \tag{C1}$$

with the partial derivatives being found in Eqs. (A13 to 15). In our method of calibration of the spectrometer, however, part of the error in E_2 is dependent on the errors in E_1 and θ. By the use in these calibrations of scattering materials such as Cu, for which $M_2\gg M_1$, we made the contribution of any error in θ to the error in E_2 practically negligible. We also used high energy particles so that layer errors were minimized. On the other hand, the relative error in E_2 is equivalent to that in E_1 of the calibrating particles, since $\partial E_2/\partial E_1=E_2/E_1$ in scattering processes [see (A12) and (A20) for $Q=0$]. It is then easy to show that $(\partial Q/\partial E_1)$ in (C1) must be replaced by Q/E_1, and δE_2 must be taken as just the independent errors in E_2. Since Herb gives the probable error of his determinations of the $F^{19}(p,\alpha'\gamma)$ and $Al(p,\gamma)$ resonances as 0.1 percent, a contribution to the first term in (C1) is $(0.001Q)^2$.

Another interdependent error in E_1 and E_2 is number (4) above, the surface layer error. The correction we make for surface layers can be in error by $\delta\xi/\xi\sim 20$ percent just because scattering and stopping cross sections are uncertain to about this amount. The error is thus about 0.1 kev for 1-Mev protons or 0.01 percent. The contribution to the error in Q is $(-\partial Q/\partial E_1+\eta\partial Q/\partial E_2)\delta\xi_1\sim(1+\eta)E_1\times 10^{-4}$. Note that the terms in the coefficient of $\delta\xi_1$ are usually of the same sign, since $\delta E_1=-\delta\xi_1$ and $\delta E_2=\eta\delta\xi_1$.

Careful measurements with H^+, HH^+, and HHH^+ ions, as described previously,[15] have not revealed any indication of a systematic nonlinearity in the scales of the analyzer and spectrometer. One possible source of nonlinearity—the stray field of the magnetic spectrometer—has been shown by Mr. William Warters of this laboratory to be closely proportional to the field in the magnetic gap over the full range of fields used in these experiments. We have, in addition, attempted to perform calibration experiments at the same energies as in the direct measurements.

The determination of E_{2B} from the observed distribution in E_{20} has been discussed in Appendix B. In clean-cut cases in which the cross sections are known, the backgrounds are small, and the surface layer effects are small, the location of E_{2B} involves only negligible error. This is the case for $Li(p,p)Li^7$ and $B^{10}(p,\alpha)Be^7$. In the cases $Li^7(p,p')Li^{7*}$ and $B^{10}(p,\alpha')Li^{7*}$, the background and layers were especially troublesome, and we estimate the systematic independent probable error from this cause to be $0.001E_2$ in the first case and $0.0015E_2$ in the second case. Multiplication by $\partial Q/\partial E_2$ yields the contribution to the error in Q.

The error in Q arising from the error in the measurement of the angle of observation can be relatively large. For E_1 and E_2 in Mev we have from (A10) and (A13)

$$\partial Q/\partial\theta=35(M_1M_2E_1E_2/M_3^2)^{\frac{1}{2}}\sin\theta \text{ kev/degree}. \tag{C2}$$

The corrections can be minimized by observations near 0° or 180° but this is often not practical for other reasons. In these experiments we have been primarily interested in the excitation energies of Li^{7*} and Be^{7*}. By measurements of the Q's involving the ground and excited states without changing the position of the spectrom-

[51] W. Whaling and C. W. Li, Phys. Rev. **81**, 150 (1951).

eter and thus without changing θ, we have been able to minimize the effect of the systematic error in θ. We actually compute $E_x = \Delta Q = Q - Q^*$ from

$$\Delta Q = \frac{M_3+M_2}{M_3}(E_2-E_2') - \frac{M_3-M_1}{M_3}(E_1-E_1') - 2\cos\theta\frac{(M_1M_2)^{\frac{1}{2}}}{M_3}[(E_1E_2)^{\frac{1}{2}}-(E_1'E_2')^{\frac{1}{2}}], \quad \text{(C3)}$$

where the unprimed quantities are determined in $Li^7(p,p)Li^7$ or $B^{10}(p,\alpha)Be^7$ and the primed ones in $Li^7(p,p')Li^{7*}$ or $B^{10}(p,\alpha')Be^{7*}$. It is clear that the systematic error in θ can even be reduced to zero by appropriate choices (not independent) of the E's such that $(E_1E_2)^{\frac{1}{2}}-(E_1'E_2')^{\frac{1}{2}}=0$. Also, it can be shown that if the scales for E_1 and E_2 are calibrated against the same primary standard, $\delta\Delta Q=(\Delta Q/E_1)\delta E_1=(\Delta Q/E_2)\delta E_2$. In the Be^{7*} case, we choose $E_2'\sim E_2$ in order to minimize the large errors arising from uncertainty in the energy losses of the outgoing alpha-particles. This also reduced the error from θ to 30 percent of its effect on the main Q-value. In the Li^{7*} case, for intensity reasons, we choose $E_1=E_1'$. It should be emphasized that the systematic error in the location of E_{12} is large only in determining Q^* and so this error is not reduced in the calculation of ΔQ. The various errors and the final values are discussed and tabulated in the text (Tables III and V).

PHYSICAL REVIEW VOLUME 82, NUMBER 2 APRIL 15, 1951

Spin-Orbit Coupling in Li^7 and Be^7

D. R. INGLIS
Argonne National Laboratory, Chicago, Illinois
(Received January 2, 1951)

The magnetic spin-orbit coupling of the p-shell nucleons is shown to have the correct sign and about half the magnitude to account for the 45-kev difference of the first excitation energies, 479 kev in Li^7 and 434 kev in Be^7, if these are interpreted as doublet splittings arising mainly from a spin-orbit coupling term of the same form as the Thomas term but stronger and presumably of mesonic origin, such as seems to be responsible for the appearance of (jj) coupling in heavy nuclei. Be^7 is expected to be slightly larger than Li^7 because of the added coulomb repulsion, so that the average value of the main term is expected to be smaller for Be^7, and it is estimated that this coulomb expansion explains another one-fourth to the splitting difference, leaving about one-forth unaccounted for. These estimates are made both very simply by means of the droplet model and more reliably by minimizing the energy obtained with exchange interactions and three-dimensional isotropic oscillator wave functions. Energies attributed to spin-orbit coupling in other nuclei indicate that the main term should make the Li^7 and Be^7 doublet splittings about 50 percent larger than observed. This suggests that second-order perturbations may reduce both by nearly the same amount, leaving their estimated difference significant. The possibility of more drastic perturbations and their relation to the quadrupole-moment problem are discussed. The agreement of the estimated splitting difference in sign and order of magnitude is consistent with other evidence favoring the (LS)-coupling interpretation that the two low states form a ^2P.

I. INTRODUCTION

ONE very interesting feature of the 434-kev state in Be^7 is that its excitation energy is approximately[1] but not exactly equal to that of the 479-kev state in the mirror nucleus Li^7. One, of course, assumes that they are mirror states,[2] or that they differ only in isotopic spin and coulomb energy, and the current experimental situation[3] favors the conclusion that they have nuclear spin $I=\frac{1}{2}$ in spite of the intensity-ratio difficulty in the thermal reaction $B^{10}(n,\alpha)Li^{7*}$, Li^7. This permits one to assume[4] that this state, together with the ground state, forms a ^2P. The magnitude of the 479-kev doublet splitting has long presented a problem of interpretation in terms of nuclear spin-orbit coupling, and now the 45-kev difference between the two doublet splittings enriches the opportunity for testing simultaneously the interactions responsible for spin-orbit coupling, the theory of nuclear structure, and the ^2P assignment. The original interpretation[4] of this splitting was given in terms of the picture of a nucleus consisting of nucleons as its fundamental constituents, with their binding forces treated phenomenologically, and with no attention paid to the source of these forces. The relativistic kinematic effect known as the Thomas precession was seen as the primary source of the splitting, modified by the magnetic effect. This simple theory automatically gives the correct sign of spin-orbit coupling to account for the nuclear spins of the ground states of most fairly simple nuclei (whereas subsequent theories of spin-orbit coupling unfortunately leave an arbitrary choice of sign). For this reason it remained attractive even after it became increasingly apparent that it was inadequate to account for the magnitude of the 479-kev splitting in Li^7, because of the possibility that a narrower doublet might be hidden in the rather broad ground-state group of the range measurements, until rather recent magnetic analysis[5] showed the ground state to be single within a few kev. The recent success of the (jj) coupling shell model[6] indicates the presence of strong spin-orbit coupling in heavy nuclei

[1] Brown, Snyder, Fowler, and Lauritsen, Phys. Rev. **82**, 159 (1951).
[2] As is verified by the approximately equal gamma-ray intensities in the mirror reactions.
[3] B. Rose and A. R. W. Wilson, Phys. Rev. **78**, 68 (1950); B. T. Feld, Phys. Rev. **75**, 1618 (1949); S. Devons, Proc. Phys. Soc. (London) **62A**, 580 (1949); D. R. Inglis, Phys. Rev. **81**, 914 (1951).
[4] D. R. Inglis, Phys. Rev. **51**, 783 (1936).
[5] Buechner, Strait, Stergiopoulos, and Sperduto, Phys. Rev. **74**, 1569 (1948).
[6] M. G. Mayer, Phys. Rev. **78**, 16, 22 (1950); D. Kurath, Phys. Rev. **80**, 98 (1950); Haxel, Jensen, and Suess, Naturwiss. **36**, 155 (1949).

of the same sign and order of magnitude as required to account for the 479 kev excitation in Li^7 as a ^2P splitting. It is impressive that in quite another branch of nuclear physics, the high energy nucleon-nucleon scattering, strong spin-orbit coupling of a compatible order of magnitude has recently appeared[7] as a possible means of preserving the symmetry of the interactions.

Both the Thomas term and the magnetic term in the spin-orbit coupling satisfy, and indeed arise from, the requirements of relativistic invariance, as does the spin itself (apart from the rather abitrarily introduced anomalous nucleon gyromagnetic ratios), and Furry[8] has shown how they are related to the introduction of electromagnetic or scalar potentials in the Dirac equation for a single particle. They are not the only Lorentz-invariant types of spin-orbit coupling: Breit[9–11] has shown that, with ordinary non-exchange interactions (or with Heisenberg interactions that are also spin-independent in the isotopic-spin language), invariance to order v^2/c^2 is obtained with a spin-orbit coupling between two nucleons of the form $Q_{kl}+Q_{lk}$ with

$$Q_{kl}=(\hbar/4M^2c^2)[-a\boldsymbol{\sigma}_k+(1-a)\boldsymbol{\sigma}_l]\cdot\mathbf{p}_k\times\nabla_k J_{kl}, \quad (1)$$

where a is arbitrary. The special case $a=-1$ gives the spin-orbit coupling for Dirac particles interacting through an electromagnetic field, $\nabla_k J_{kl}$ then corresponding to the (charge times the) electric field, the time component of a four-vector, which transforms into a magnetic field plus an electric field in the coordinate system of a moving particle (of which the magnetic field gives the magnetic term and the electric field contributes to the Thomas term in the spin-orbit coupling). The term containing $2\sigma_l$ is the purely magnetic term for the particle whose motion is not represented, corresponding to having the other particle circulate around it. The term containing σ_k is the magnetic term reduced by a factor $\frac{1}{2}$ by the Thomas term for the moving particle k, corresponding to the Thomas precession[12] introduced by the acceleration arising from $\nabla_k J_{kl}$. When arbitrarily multiplied by $g/2$ (where g is the gyromagnetic ratio, which is 2 for a Dirac particle) to account for the anomalous magnetic moment, the magnetic term for a nucleon (k) due to its own motion is

$$H_m=(\hbar g/4M^2c^2)\boldsymbol{\sigma}_k\cdot\mathbf{p}_k\times\nabla_k J_{kl}$$
$$=-(\hbar^2 ge/2M^2c^2)(1/r)(dU/dr)\mathbf{l}\cdot\mathbf{s}. \quad (1a)$$

Here the last member is written for the case of a central electric potential energy $J_{kl}\rightarrow eU(r_k)=eU(r)$, as though the other particle were effectively at rest as in an average over a closed shell, the angular momentum is $\mathbf{l}\hbar=\mathbf{r}\times\mathbf{p}_k$ and the spin $s=\sigma/2$. This term arises directly from the charge and magnetic moments of the nucleons involved, which we consider to be intrinsic properties of the nucleons in addition to any other effects related to the exchange nature of the forces, so that we assume this term to be present in any case. The Thomas term is

$$H_T=-(\hbar/4Mc^2)\boldsymbol{\sigma}_k\cdot\mathbf{v}_k\times\nabla_k J_{kl}$$
$$=(\hbar^2/2M^2c^2)(1/r)(dV/dr)\mathbf{l}\cdot\mathbf{s}, \quad (1b)$$

where $v_k=p_k/M$ and V is a central non-electromagnetic potential which simply transforms into itself and enters the Dirac equation of a single particle as a scalar[8] added to the mass term. Although this is too small to account for the large spin-orbit coupling appearing in nuclei, it is of interest here because of its form. Breit also showed that there are still other possibilities with a space-exchange (Majorana) interaction, for example, and that with "reasonable" choice of the arbitrary constant (that is, with the constant analogous to a having order of magnitude unity) one can obtain[10] a sufficiently large spin-orbit coupling. The effect of the exchange nature of nuclear forces, which was thus treated phenomenologically with this promising result, has been studied more recently from the point of view of the meson origin of nuclear forces. Dancoff[13] has shown by a perturbation theory treating the nucleons relativistically that a scalar coupling to a field of neutral vector mesons gives only a term which is essentially the same as the Thomas term, too small, but of determinate and correct sign (as may be associated with the concept that it corresponds to the centripetal acceleration of mesons as the Thomas term does to that of the nucleon, the nucleon with spin up being part of the time a nucleon with spin down and a meson with spin up). Møller and Rosenfeld (reference 11, Sec. 17.43) have shown that a mixed vector and tensor coupling may, with appropriate choice of the arbitrary constant, give rise to a coupling of the form (1b) but with $\pm 1/\mu$, the reciprocal of the meson mass, in place of $1/M$ in the second member of (1b), which makes it sufficiently large and leaves its sign arbitrary. In a later discussion of essentially the same theory, Gaus[14] has brought out more clearly the simplification that can be introduced in the spin-orbit coupling problem by treating the saturation of forces as arising from a saturation of the meson field. In an evaluation of the expression $\Delta V/\Delta r$ at the edge of the nucleus, that is, dV/dr in (1b), this allows one to identify the energy increment ΔV for the meson with the familiar

[7] K. M. Case and A. Pais, Phys. Rev. **80**, 203 (1950). The terminology of this very important paper, unfortunately, adds to the current confusion, with rebirth of interest, in the use of the word "coupling" as taken from atomic physics: it erroneously uses the term "LS coupling" as an abbreviation for "spin-orbit coupling (energy)" whereas "(LS) coupling" has traditionally meant "Russell-Saunders coupling (scheme)" in which L and S are approximately diagonal.

[8] W. Furry, Phys. Rev. **51**, 784 (1936).

[9] G. Breit, Phys. Rev. **51**, 248 (1937).

[10] G. Breit and G. R. Stehn, Phys. Rev. **53**, 459 (1938).

[11] L. Rosenfeld, *Nuclear Forces* (North-Holland Publishing Company, Amsterdam, 1948).

[12] S. Dancoff and D. R. Inglis, Phys. Rev. **51**, 784 (1936). Errata. The following nearly obvious misprints in this pedagogical note have not been previously recorded: In the equation for $d\alpha$ and dt the numerator, and in the equations for u_x and u_y the denominator should have $+$ in place of $-$. In the first equation of the second column, δ_T should be ω_T.

[13] S. Dancoff, Phys. Rev. **78**, 382 (1950).

[14] H. Gaus, Z. Naturforsch. **4A**, 721 (1949).

ΔV for a nucleon. This is a theory which applies perhaps better to heavy nuclei than to light nuclei because it assumes a full realization of the saturation property of nuclear forces. A still newer consideration of the problem by Heisenberg[15] discusses the interaction between individual nucleons in terms of an analogy with the coupling of electrons to the photon field, purposefully avoiding any further specification of the nature of the meson field than is necessary for the discussion of this analogy in general terms. Because it treats the interaction of individual nucleons, this formulation seems to be better suited to the discussion of Li^7 and Be^7, where the saturation of the forces is not fully realized. His argument consists simply in pointing out that the coupling of two electrons to the photon field leads not only to the coulomb force but also to a spin-orbit coupling and a spin-spin coupling as well. The analogous coupling of the nucleons to the meson field is known to give rise to a Yukawa force, and in the analysis of the properties of the deuteron, to a spin-spin, or tensor force between nucleons. By analogy it may be expected to give rise to a spin-orbit coupling as well. By a careful comparison of the constants involved in the two cases, including dimensional arguments, Heisenberg makes it plausible that the spin-orbit coupling for a circulating nucleon (k), which in analogy to the spin-orbit coupling for an electron $[(M/m)^2$ times (1) with $a=-1]$ is taken to have the form (1b), has the magnitude

$$H_d=\pm(\hbar/\mu c^2)\boldsymbol{\sigma}_k\cdot\mathbf{v}_k\times\nabla_k J_{kl} \rightarrow -(2\hbar^2/\mu M c^2)(1/r)(dV/dr)(\mathbf{l}\cdot\mathbf{s}), \quad (1c)$$

with the meson mass μ in the denominator. The negative sign of the last member is determined empirically from the Li^7 ground state.

One may prefer to look on the existence of a large spin-orbit coupling merely as an empirical fact.[6-7] From invariance considerations we have interactions of the general form of (1) available, and with $a=\frac{1}{2}$, which corresponds to a scalar or non-electromagnetic J_{kl}, it includes a factor $\mathbf{L}\cdot(\mathbf{s}_l+\mathbf{s}_k)$, where in the case of just two nucleons $\mathbf{L}$ is their angular momentum. This it what is needed in the high energy scattering problem,[7] an interaction in a triplet state and none in a singlet state so the Pauli principle may make a large difference between like-nucleon and unlike-nucleon scattering. Such an interaction (or (1) with any $a\neq 1$), although it contains two spins, still reduces to a simple spin-orbit coupling of the form (1b) when applied to a single nucleon (k) circulating under the influence of other nucleons (l) in closed shells or pairs (since in the sum over l the opposing σ_l cancel) and this is consistent with the needs of the (jj) coupling shell model.

In discussing the magnitude of the first excitation energies of Li^7 and Be^7, we wish to test the possibility of attributing the spin-orbit coupling to a main term H_d (which may be considered to include H_T), of the order of magnitude given by (1c), whose exact magnitude we determine only empirically in terms of the average excitation energy of the two nuclei, and the magnetic term H_m which contains no arbitrary parameter. The main term, H_d, even though it does not have any direct connection with the coulomb energy, can be expected to contribute more to the doublet splitting in Li^7 than in Be^7 because of the larger size of Be^7 arising from its additional coulomb repulsion. The magnetic term, though very much smaller, contributes more directly to the difference of excitation energies, being positive for Li^7 and negative for Be^7 because of the opposite signs of the proton and neutron magnetic moments. We shall show that the two effects together have the right order of magnitude as well as the right sign to account for the 45 kev Li^7-Be^7 difference.

Evaluation of the energy resulting from the assumed interactions involves use of a nuclear model, so we are forced to test the adequacy of the interactions and the model at the same time. Because it may help to show how much uncertainty arises from the model and for the sake of a presentation in steps of decreasing simplicity, we shall discuss the question separately in terms of two models. The first is the very simple uniform-density or droplet model of the nucleus which suffices for puposes of preliminary orientation, even though seven particles are too few for the valid application of statistical methods. The second is a simple variation calculation based on the use of a phenomenological exchange interaction and oscillator wave functions, which presumably more adequately represents the contention between potential and kinetic terms in determining the relevant nuclear properties, but which also falls far short of a complete treatment of the seven-body problem.

II. COULOMB EXPANSION

In calculating the effect on H_d of the added coulomb expansion in Be^7 one considers the balance between kinetic and potential energies which determines the stiffness against expansion, or the compressibility of the nuclei. In either model one obtains, as functions of a nuclear size parameter such as R, the mean kinetic energy $T(R)$, the mean potential energy $V(R)$ arising from the specific nuclear interactions, and the average coulomb energy for Li^7, $U_{Li}(R)$, and for Be^7, $U_{Be}(R)=U_{Li}(R)+E_c(R)$, E_c being the *coulomb* difference. The main term H_d in the spin-orbit coupling contributes an averaged value $E_d(R)$ to the *doublet* splitting, and at the equilibrium value R_0 is assumed to be $E_d(R_0)\approx 450$ kev. Of this, according to the Lande interval rule, $-(1/3)E_d$ belongs to the energy of the ground state and $(2/3)E_d$ to the excited state. The zeroth-order energy for the ground state of Li^7 is taken to be $E_0(R)=T+V+U_{Li}$ (here $-E_d/3$ is neglected). The equilibrium value R_0 for Li^7 is found from the minimization process $E'(R_0)=0$. The equilibrium values for Li^{7*}, Be^7, and Be^{7*} may be called R_1, R_2 and R_3, respectively. For the excited state Be^{7*}, for example, the minimizing

[15] W. Heisenberg (unpublished lectures).

value R_3 is found from the Taylor expansion

$$E_{\mathrm{Be}}^*(R)=E_0+\tfrac{1}{2}(R-R_0)^2E_0''+E_c(R_0)+(R-R_0)E_c'+E_d(R_0)+(R-R_0)E_d'+\cdots \quad (2)$$

as

$$R_3-R_0=-(E_c'+E_d')/E_0'' \quad (3)$$

and thus one has the equilibrium value $E_{\mathrm{Be}}^*(R_3)$. Here E_0'' represents the compressibility. Similarly, one has $E_{\mathrm{Be}}(R_2)$ and $E_{\mathrm{Li}}^*(R_1)$ at their individual minima by omitting E_d' or E_c', respectively. Then the difference in doublet splittings of Li^7 and Be^7 is

$$E_{\mathrm{dif}}=[E_{\mathrm{Li}}^*(R_1)-E_0(R_0)]-[E_{\mathrm{Be}}^*(R_3)-E_{\mathrm{Be}}(R_2)]=E_c'E_d'/E_0''. \quad (4)$$

The result is the same as would be obtained by considering only the effect of the coulomb expansion caused by E_c' on the evaluation of the spin-orbit term E_d, the effect[16] on E_c of the expansion brought about by E_d' having disappeared in taking differences.

III. THE DROPLET MODEL

In the uniform-droplet model the kinetic energy is

$$T=k/R^2=(3/10)(9\pi)^{\frac{1}{3}}(137^2/1837)A\ \mathrm{mc}^2=28.5A\ \mathrm{mc}^2 \quad (5)$$

with the equilibrium value of the nuclear radius

$$R=R_0=A^{\frac{1}{3}}e^2/2\ \mathrm{mc}^2. \quad (6)$$

We may assume that the only lack of saturation of the nuclear forces is found on the surface and thus that the change of potential energy on expansion of the nucleus is the change of the surface energy, which is proportional to the surface area,

$$E_s=sR^2. \quad (7)$$

The nuclear equilibrium size is determined by the vanishing of the derivative

$$d(E_s+\bar{T})/dR=2(E_s-\bar{T})/R=0. \quad (8)$$

We may take $E_0=\bar{T}+E_s$, neglecting the coulomb term, $\bar{U}_{\mathrm{Li}}$, and at the equilibrium radius have

$$E_0'=2(E_s-\bar{T})/R=0, \quad (9)$$

and

$$E_0''=2(E_s+3\bar{T})/R^2=8\bar{T}/R^2. \quad (10)$$

The main term in the doublet splitting, E_d, contains a factor $\langle(1/r)(dV/dr)\rangle_{\mathrm{Av}}$ according to (1c), and the method of averaging used by Gaus[14] is appropriate for the droplet model: The probability that the nucleon is in the surface layer of thickness Δr over which the potential drop ΔV takes place is proportional to the relative volumes, $3\Delta r/R$, so $E_d(R)\sim R^{-3}$, or $E_d'=-2E_d/R$ with $E_d=450$ kev$=0.9$ mc^2. The coulomb energy of a uniformly charged sphere is

$$\bar{U}=C/R=(6/5)Z(Z-1)A^{-1}\ \mathrm{mc}^2; \quad (11)$$

the latter for the usual equilibrium radius (6), and thus the coulomb difference E_c has the equilibrium value $(36/5)7^{-1}$ mc^2, and $E_c'=-E_c/R$. From (4) we then have the coulomb-expansion part of the Li^7-Be^7 difference in excitation energy

$$E_{\mathrm{dif}}=E_cE_d/4\bar{T}=(9/5)(0.9/28.5)7^{-4/3}\ \mathrm{mc}^2=2.2\ \mathrm{kev}. \quad (12)$$

This is very small compared to the observed difference 45 kev, but this simplified estimate is unreliable because of the use of the surface energy, as is discussed further below.

The magnetic term in the spin-orbit coupling, H_m, contains a factor $\mathbf{l}\cdot\mathbf{s}$ the evaluation of which depends on the angular properties of the ^2P states or the way in which the individual-nucleon vectors $\mathbf{l}$ and $\mathbf{s}$ are compounded to make the nuclear vectors $\mathbf{L}$ and $\mathbf{S}$. The simple spin-independent symmetric hamiltonian discussed by Feenberg and Wigner[17] gives a well-isolated ^2P having maximum symmetry, an appropriate combination of $^1S^2p$ and $^1D^2p$ in which the neutrons, in the case of Li^7, are in singlet states and do not contribute to $\mathbf{S}$, although the three p nucleons contribute equally to $\mathbf{L}$. It appears that the only simple way one can obtain a ^2P as well isolated from other multiplets, as required by experiment, is to have an approximation to this state of maximum symmetry. For this ^2P we have for the expectation values,

$$\mathbf{l}\cdot\mathbf{s}=(1/3)\mathbf{L}\cdot\mathbf{S} \quad (13)$$

because the proton which has the spin carries only one-third of the orbital angular momentum.[10] $\mathbf{L}\cdot\mathbf{S}$ is of course -1 for the $^2P_{\frac{1}{2}}$ and $\frac{1}{2}$ for the $^2P_{\frac{3}{2}}$, the difference being $-(L+\frac{1}{2})=-\frac{3}{2}$. The difference E_m of the proper values of the magnetic energy H_m then contains a factor $-(\frac{3}{2})/3=-\frac{1}{2}$ in place of $\mathbf{l}\cdot\mathbf{s}$ in (1a), for the ^2P of maximum symmetry.

The odd neutron in Be^7 in the droplet model moves in the parabolic electric potential of the uniform spherical distribution of charge Ze representing the four protons,

$$U=(3-(r/R)^2)Ze/2R \quad (14)$$

for which the factor $(1/r)(dU/dr)$ appearing in H_m has the value $-Ze/R^3$. The magnetic contribution to the doublet splitting is then

$$E_m=(4/A)(137/1837)^2Zg\ \mathrm{mc}^2=0.0061Z(g/2)\ \mathrm{mc}^2, \quad (15)$$

where $(g/2)$ is -1.91 for the neutron in Be^7 and 2.78 for the proton in Li^7. For Li^7 only the other protons contribute to U, and Z is to be replaced by $Z-1$. Thus, we find $E_d=17.5$ kev for Li^7 and -24 kev for Be^7. The difference 41 kev (when augmented by 2 kev from (12)) agrees exactly with the experimental difference 45 ± 4

[16] E. Feenberg, Revs. Modern Phys. **19**, 239 (1947), in the neighborhood of Eq. (20), in a rather similar treatment of nuclear compressibility, discusses the effect of the state of excitation in a different manner.

[17] E. Feenberg and E. Wigner, Phys. Rev. **51**, 95 (1937); E. Feenberg and M. Phillips, Phys. Rev. **51**, 597 (1937).

kev, which of course should not have been expected of so rough a model, and indeed the agreement is not so good with the more refined oscillator estimate.

IV. THE CENTRAL MODEL WITH OSCILLATOR FUNCTIONS

The treatment of the problem in terms of oscillator wave functions permits the following improvements over the crudity of the droplet model: (1) introduction of a reasonable radial and angular density dependence, (2) allowance for exchange, and (3) determination of nuclear size from binding energy and the range of forces given by scattering, rather than by the rough assumption that the density is the same as in heavy nuclei. The compressibility is again given as the result of a competition between kinetic and potential energies, but these quantities are presumably expressed more nearly correctly in this more refined model.

The single-nucleon oscillator wave functions are[18,19]

$$\begin{aligned}\psi_s &= s = \pi^{-\frac{1}{4}}\exp(-\rho^2/2),\\ \psi_{p,z} &= p_z = 2^{\frac{1}{2}}\pi^{-\frac{1}{4}}\xi\exp(-\rho^2/2),\end{aligned} \tag{16}$$

where $\rho^2=\sigma\alpha r^2$, $\xi^2=\sigma\alpha z^2$. Here α is the inverse-square range parameter which appears in the simple Majorana interaction $-BP^q\exp(-\alpha r^2)$ which is introduced into the calculation, and σ gives the size of the wave function relative to this range.

The simplest wave function we can write for the Li^7 nucleus is then the product

$$\langle s^+s^-p_z^+p_z^-\rangle_\nu\langle s^+s^-p_z^+\rangle_\pi, \tag{17}$$

where the superscripts refer to spin direction and the subscripts ν and π to neutron and proton. Such a product is to be thought of as antisymmetric in exchange of like nucleons, and the effect of the space-exchange operator of the Majorana interaction is to introduce a negative exchange term for each like-spin like-nucleon pair. The sum of the interactions within the s shell and between the s and p shells can then be written, in the notation of reference 19,

$$\begin{aligned}-B(6f_{0000}+12f_{1001}-3f_{1010})(\sigma/\tau)^{\frac{1}{2}}&\\ =-3B(\sigma/\tau)^{\frac{1}{2}}(1+5/\tau).&\end{aligned} \tag{18}$$

Here $\tau=\sigma+2$. This part is valid for any state of the configuration s^4p^3, not just for (17). The interaction in the p shell for the simplified wave function (17) is

$$-3f_{1111}B(\sigma/\tau)^{\frac{1}{2}}=-3B(\sigma/\tau)^{\frac{1}{2}}(1-2/\tau+3/\tau^2). \tag{19}$$

A more complete calculation[17] which takes into account the angle and symmetry relations of the p-nucleons in the ^2P of maximum symmetry gives, as an improved evaluation of the Majorana interaction between them,

$$\begin{aligned}3L+2K&=-B(\sigma/\tau)^{\frac{1}{2}}(3f_{1111}+2f_{1100^2})\\ &=-3B(\sigma/\tau)^{\frac{1}{2}}(1-2/\tau+11/3\tau^2).\end{aligned} \tag{20}$$

TABLE I. Coulomb energies.

	Li^7	Be^7	
s-shell	2	2	(23)
s–p	13/4	13/2	
p-shell	0	17/10	
U	5.25	10.2	

This is seen to differ very little from (19). (It appears that the failure to symmetrize the space wave function of the two neutrons is approximately compensated by the excessive angular concentration of the p-nucleons in (17).) The potential energy $V(\sigma)$ is the sum of (19) and (20). The kinetic energy corresponding to (17) is $(3+21/2)\alpha\sigma/2$, the zero-point energy of 21 one-dimensional harmonic oscillators, plus one unit of excitation each for three of them. This includes a small erroneous contribution from the zero-point fluctuations of the center of mass in (17), and the corrected value[20] is slightly lower

$$T=6\alpha\sigma \tag{21}$$

n units $\hbar^2m/M$, or mc^2 including the unit $mMc^2/\hbar^2$ of α. The coulomb energy is, of course, larger for Be^7 than for Li^7. In calculating the coulomb interaction within the s-shell and the direct interaction between s and p shells, the integrations are elementary radial ones making use of the constant potential within a thin spherical shell. The exchange part of the s–p interaction and both parts of the interaction within the p shell involve angular integrals over the expansion which appears in the theory of atomic spectra,

$$1/r=\sum_{k,m}(k+\tfrac{1}{2})^{-1}\Theta_k^m(\theta)\Theta_k^m(\theta')r^k_{\text{smaller}}/r^{k+1}_{\text{larger}}, \tag{22}$$

the Θ's being normalized to unity. The interaction within the p-shell depends, of course, on the nature of the ground-state ^2P, whether it is purely the $^2P_{\frac{1}{2}}$ state of maximum symmetry[17] or whether it contains a large admixture of higher states in this representation. In seeking to attribute the first excitation energy to spin-orbit coupling we are in a sense trying to get along with a simple ^2P since large admixtures of higher states would contribute independently to the separation, as has been proposed as an alternative mechanism by Feingold and Wigner[21] (discussed in (*d*) below). For the simple ^2P the coulomb interaction between the two p-protons in Be^7 has been given[17] as $L_c+(2/3)K_c$, where L_c can be written briefly as $(zz|e^2/r|zz)=(49/30)(\sigma\alpha/2\pi)^{\frac{1}{2}}e^2$ and K_c as the exchange integral $(yz|e^2/r|zy)=(1/15)\times(\sigma\alpha/2\pi)^{\frac{1}{2}}e^2$. The exchange contribution is positive because of the high space symmetry in the two protons and small because of cancellation of positive and negative parts of the overlapping function. In units $(\sigma\alpha/2\pi)^{\frac{1}{2}}e^2$, the various coulomb energies are given in

[18] W. Heisenberg, Z. Physik **96**, 473 (1935).
[19] D. R. Inglis, Phys. Rev. **51**, 531 (1937).
[20] D. R. Inglis, Phys. Rev. **53**, 880 (1938), reference 17.
[21] A. M. Feingold and E. Wigner, Phys. Rev. **79**, 221 (1950).

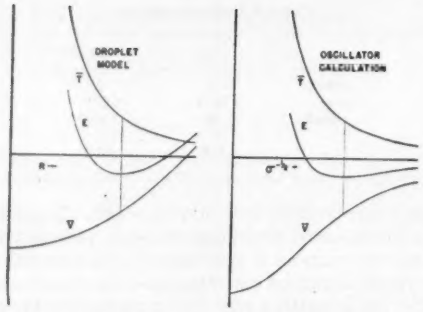

FIG. 1. The artificial treatment of the potential energy $\bar{V}$ in the droplet model makes the curvature of the energy E at equilibrium greater than in the oscillator calculation, and the nucleus stiffer.

Table I. For[22] $\alpha=22mMc^2/\hbar^2$, these totals are $U_{\mathrm{Li}}=3.08\sigma^{\frac{1}{3}}mc^2$ and $U_{\mathrm{Be}}=5.98\sigma^{\frac{1}{3}}mc^2$. The difference of these is the coulomb difference, $E_c=2.9\sigma^{\frac{1}{3}}mc^2$.

It is important that the arbitrary constants be determined in such a way as to give as good an account as possible of the competition between kinetic and potential energies in determining the nuclear compressibility. It is well known[17–19] that such a first-order calculation is quite inadequate to give a correct account of the binding energy of the nucleus, partly because the binding energy is a rather small difference between two larger quantities neither of which is estimated sufficiently accurately by this method, perhaps partly also because of inadequacy of the interactions. Yet the nuclear radius given by the calculation is very sensitive to the binding energy, a fault which may plausibly be remedied by increasing the nuclear interactions beyond their presumed actual strength by an amount just sufficient to give the correct binding energy. This procedure should give the size and stiffness of the nucleus as nearly correct as can be expected from any available simple approximation.

The actual specific nuclear interaction between two nucleons is taken to be specified by the parameters[22]

$$B\approx 50mc^2, \quad \alpha=22mMc^2/\hbar^2. \tag{24}$$

The first-order energy $E_0(\sigma)$, the sum (18)+(20)+(21)+(23), the latter for Li^7, is found to have a minimum at $\sigma_0=1.355$ and to give the binding energy 75.4 mc^2, thus matching sufficiently closely the experimental value 77 mc^2, if B in E_0 is increased to 104 mc^2. (So large an increase of B would not be required if a combination of exchange operators were used, so chosen as barely to satisfy the saturation requirement; but this added refinement would not greatly alter the way in which the potential energy varies with σ, in which the variation of the inevitable factor $(\sigma/\tau)^{\frac{1}{2}}$ is most important.)

[22] Breit, Thaxton, and Eisenbud, Phys. Rev. **55**, 1018 (1939); R. D. Hatcher and G. Breit, Phys. Rev. **75**, 1389 (1949). We have rounded out their numbers $A=51.44\ mc^2$ and $\alpha=21.59\ mMc^2/\hbar^2$.

The curvature of $E_0(\sigma)$ at the minimum is $E_0''(\sigma_0)=85.5\ mc^2$.

The oscillator wave functions are generated by a fictitious three-dimensional oscillator potential

$$V=(\hbar^2/2M)(\alpha\sigma)^2r^2$$

which in a perturbation theory similar to the Hartree procedure is taken to approximate the actual potential experienced by the nucleons throughout most of the range of their wave functions, so we may conveniently use this V in (1c). We then have[23]

$$\langle(1/r)(dV/dr)\rangle_{\mathrm{Av}}\sim\sigma^2\sim E_d=(\sigma/\sigma_0)^2\ 0.9\ mc^2. \tag{25}$$

Thus, with $E_d'=1.8\sigma_0^{-1}\ mc^2$, $E_c'=1.45\sigma_0^{-\frac{1}{3}}\ mc^2$, and $E_0''=85.5\ mc^2$, we have from (4) the expansion contribution to the excitation difference

$$E_{\mathrm{dif}}=0.019\ mc^2=9.7\ \mathrm{kev}. \tag{26}$$

This is much larger than the value given by the cruder droplet model but still only about one-fourth of the observed difference of 45 kev. The reason for the discrepancy between the two models is displayed in Fig. 1. In using the droplet model we have gone beyond the usual comparison of situations in which the density remains constant, as in the elongation leading to fission, and have treated the saturation as so complete in the interior that the only lack of saturation is found in an idealized surface layer even when the density changes. This artificial treatment makes the potential energy V quadratic in the radius, whereas in the more realistic oscillator calculation it tails off to zero for large radii and indeed has negative curvature at the equilibrium radius. The positive curvature of V in the droplet model thus makes the curvature of the total energy at the equilibrium radius unduly large and makes the nucleus much too stiff.

This estimate is to be considered as an upper limit in the sense that it is based on the very favorable assumption of equal sizes of neutron and proton distributions: if the neutron in Be^7 were not expanded as much as its fellow protons, which are directly affected by the coulomb force, the effect would be smaller (or might even reverse its sign).

V. MAGNETIC SPIN-ORBIT COUPLING

In the usual approximate treatment of magnetic spin-orbit coupling, the electric potential $U(r)$ in (1a) is considered to be already averaged over the positions of the ("other") protons. In Li^7 the other protons are in the s-shell so U has spherical symmetry and the

[23] Keeping the constants of (1c) and (13), we have

$$E_d=(\hbar^4/2\mu Mc^2)(\alpha\sigma)^2=242(m/\mu)\sigma^2mc^2,$$

which is about 1.6 mc^2. This shows that Heisenberg's evaluation of the constant, with the present estimate of σ, gives too large a spin-orbit coupling by about 70 percent even with the factor $\frac{1}{2}$ from (13) included.

evaluation is straightforward:

$$\langle(1/r)(dU/dr)\rangle_{av}$$

$$= 2(\alpha\sigma)^{\frac{1}{2}}e\frac{\int_{\varrho}^{\infty}\rho^4 d\rho\exp(-\rho^2)\int_0^{\varrho}\rho^2 d\rho\exp(-\rho^2)}{\int_0^{\infty}\rho^4 d\rho\exp(-\rho^2)\int_0^{\infty}\rho^2 d\rho\exp(-\rho^2)}$$

$$= (4/3)(2\pi)^{-\frac{1}{2}}(\alpha\sigma)^{\frac{1}{2}}e. \quad (27)$$

With $\alpha = 22\,mMc^2/\hbar^2$, this with (13) in (1a) gives the magnetic splitting for Li^7

$$E_{m,\,Li} = 0.0047(g/2)\sigma^{\frac{1}{2}}mc^2 = 10.5 \text{ kev}. \quad (28)$$

Here we have assumed that $\mathbf{l}\cdot\mathbf{s}$ contributes the factor $-\frac{1}{2}$ appropriate to a ^2P of maximum symmetry, and have put $g/2 = 2.78$, $\sigma = 1.35$.

For completeness, one should also take into account the electrostatic Thomas term, as has been suggested privately by Professor Gregory Breit, but it merely has the effect of reducing (28) by a fraction $1/g$ of itself, which we neglect. It is absent in Be^7.

This calculation by use of (1a) ignores exchange. Actually, there is, in addition, a small exchange term of opposite sign corresponding to the reduced probability that the s and p protons with parallel spin find themselves close together, the nuclear wave function tending to be antisymmetrical in their space coordinates. This exchange term appears to be of the order of magnitude 10 percent of the direct term (for $a \approx \frac{1}{2}$ in (1)), so it is not very significant in the comparison with experiment in view of the other uncertainties in the calculation and is here neglected, but it is considered that its evaluation both in the s–p and the p-shell cases might merit further investigation at a later time.

In Be^7 the calculation of the magnetic spin-orbit coupling is essentially more complicated than in Li^7 because in this case there are four protons, rather than just two "other" protons, to give rise to the field at the neutron, and two of them are p-protons having an angular correlation with the neutron's position rather than the spherical symmetry which allows one in the s–p case to use the simplicity of the electrostatic potential of a spherical shell. We may think of the correlation as having two aspects (though it is not clear that they would be separately calculable): first, a geometrical "flattening" of the mass distribution corresponding to the composition of the three vectors $\mathbf{l}$ into $L = 1$ and second, an increased probability that the p-neutron finds itself close to one of the p-protons because of the symmetry of the nuclear wave function in the space coordinates of these three nucleons. Both effects are expected to increase the calculated coupling. Neglecting them, we estimate the p-shell contribution to the spin-orbit coupling of Be^7, by use of (13) and (1a) with a spherically symmetric p-shell, to be

$$(\hbar^2 ge^2/2M^2c^2)(2/3)(2\pi)^{-\frac{1}{2}}(\alpha\sigma)^{\frac{1}{2}}(1/2)$$
$$= 0.00235(g/2)\sigma^{\frac{1}{2}}mc^2 = -3.6 \text{ kev}, \quad (29)$$

with the same substitutions again, except $\frac{1}{2}g = -1.91$. This together with the s–p contribution, which from (28) is just twice as great, gives for the magnetic splitting in Be^7, $E_{m,\,Be} = -10.8$ kev. In this treatment the Li^7 and Be^7 splittings are almost equal in absolute magnitude. This ratio is not the same as in the droplet model because in the oscillator treatment the added p-protons in Be^7 are only half as effective as the more centrally clustered s-protons, an effect reminiscent of the partial self-shielding of electron shells in atoms. The magnetic contribution to the Li^7–Be^7 difference as thus estimated is 21.3 kev, only about half of the estimate made with the rougher uniform-droplet model. Only the small contribution (29) would be expected to be increased by inclusion of exchange and angular correlations in the calculation, and this by probably not more than about 2 kev. Any such increase is at least partly compensated by the corresponding decrease in the s–p contribution. Even if exchange were taken into account, we would thus expect our best estimate of the Li^7–Be^7 difference based on these premises, with the expansion term included, to be rather close to 21.3 kev +9.7 kev = 31 kev, to be compared with the experimental difference 45 kev ± 4 kev.

VI. DISCUSSION

The magnetic term estimated with the oscillator functions is thus too small to give agreement with the observed difference of 45 kev even when augmented by the expansion term (26). Among the possible shortcomings of the calculation or initial assumptions, which might be responsible for the discrepancy, are (*a*) the nuclear size parameter given by the fit to the binding energy may be too large; (*b*) the phenomenological treatment of the saturation properties of the interactions may make the nucleus too stiff; (*c*) the states discussed may be more complicated than the ^2P with maximum space symmetry having a factor $\frac{1}{3}$ in the spin-orbit coupling; (*d*) higher order perturbations may make a direct contribution to the difference of excitation energies by depressing one ^2P state more than the other. These we discuss in order.

(*a*) The nuclear size parameter may be adjudged also by its success in accounting for the coulomb energy difference between isobars, since one is prone to assume an otherwise symmetrical hamiltonian. In fact, this criterion has provided one of the principal justifications for taking the density of heavy nuclei to apply approximately also to light nuclei. The Be^7–Li^7 coulomb energy difference given by the oscillator calculation, from (23) with $\sigma = 1.35$, is 1.72 Mev, only about 5 percent greater than the experimental value of 1.645 Mev, known from the $Li^7(p,n)Be^7$ threshold. This agreement is rather impressive as nuclear physics goes,

since no special parameter was introduced to bring it about. An increase of nuclear size is required to bring about more exact agreement with the coulomb energy, whereas a smaller nucleus is required to make the magnetic spin-orbit coupling strong enough. A decrease of radius by about 19 (or at least 15 percent) is needed to bring about agreement with the experimental difference 45 kev (or at least 41 kev) and this would increase the calculated coulomb difference to 2.05 Mev (or at least 1.98 Mev). (The cruder droplet model, which gives large enough spin-orbit coupling, gives a colomb difference of 1.93 Mev.) It thus seems unlikely that the nuclei can be small enough to make a sufficiently strong magnetic spin-orbit coupling.

(*b*) The introduction of a Majorana interaction with a gaussian radial dependence must be recognized as a rather desperate attempt to represent a phenomenon about which we know very little, the nuclear saturation mechanism. We have seen in the discussion of Fig. 1 that the stiffness comes about as a balance between the curvature of the kinetic energy and of the potential energy when plotted as a function of nuclear size, $\sigma^{-\frac{1}{2}}$. If instead we consider $T(\sigma)$ and $V(\sigma)$, functions of σ itself, the curvature comes entirely from $V(\sigma)$. The factor $(\sigma/\tau)^{\frac{1}{2}}$ in (18), for example, is characteristic of the gaussian radial dependence introduced for mathematical convenience, and the other factor is characteristic also of the exchange operator. While these two assumptions give a rather good account of some significant nuclear phenomena, it is not inconceivable that the mesonic calculation which they are intended to approximate would in effect reduce the curvature of $V(\sigma)$ by about a factor two, which would make the expansion term about equal to the magnetic contribution and bring about agreement.

(*c*) Apart from the success of the simple exchange interactions[17] (along with the accepted sign of nucleon spin-orbit coupling)[4] in accounting for the spins of the *p*-shell nuclei, the main bits of evidence for the interpretation of the low ^2P in Li^7 as the simple one of maximum space symmetry are (1) the remarkable isolation of this doublet—the lack of other low excited states[24]—and (2) the need for the factor $\frac{1}{3}$ in the main term of the spin-orbit coupling in order to make the small splitting in Li^7 and Be^7 compatible with the large doublet splittings in heavy nuclei. The isolation of the ground doublet is a result of the symmetry with any attractive two-nucleon interactions. There are two other ^2P of lower symmetry in the ground configuration s^4p^3. In general, an admixture of higher multiplets would depress the two states of the ground doublet by different amounts and thus contribute directly to the splitting as discussed in (*d*), but certain interactions not containing spin-orbit coupling could admix the higher doublets ^2P without doing this. A strong admixture would lower the symmetry of the ground doublet and by altering the factor $\frac{1}{3}$ might increase the magnetic term enough to bring about agreement with the Li^7-Be^7 difference. Mixtures, in general, are expected to remove the isolation of the ground doublet by complicating the spectrum,[25] but such a special admixture might not—considered as a second-order perturbation it would depress the ground doublet, perhaps more than the next ^2F because there is only one ^2F in the configuration.

Interpretation of the ground doublet as a simple ^2P state of maximum symmetry requires that one ignore evidence for the positive quadrupole moment Q of Li^7 deduced from careful measurements of qQ by Kusch[26] on the basis of uncertain estimates of the molecular coupling constant q. If, instead, we should accept the positive quadrupole moment, it might be due to an admixture of states of maximum symmetry from other configurations,[27] in which case some modification of the present interpretation of the Li^7-Be^7 difference might apply, or it might be due to an admixture of states of other symmetries from the ground configuration,[28] in which case the two low states would be so complex that nothing could be said at present about the expected sign and order of magnitude of the Li^7-Be^7 difference. In either case, enormous admixtures of higher states are needed to obtain a positive quadrupole moment of reasonable magnitude (mostly ^2P from the configurations p^2p' and p^2f with only 12 percent left of the ground configuration p^3 is suggested in reference 27, and mostly states of lower symmetries with only 6 percent from the ^2P of maximum symmetry is suggested in reference 28), so large as to seem completely incompatible with any vestigial validity of a nuclear shell model with its single-nucleon first approximation which has been so useful, particularly in heavier nuclei. If the quadrupole moment really should be proved to be positive, perhaps the most reasonable evaluation of the situation would be as follows: Li^7 and Be^7, although particularly light, might be particularly complex (rather than simple as has been thought) because the field of the *s*-shell core is not of an appropriate shape to define the *p*-shell. The shell structure might thus develop again toward the end of the *p*-shell and be increasingly valid for heavier nuclei because of a tendency of the larger number of particles to approximate a nuclear fluid with the square-well potential of the droplet model. This could leave Li^7 and Be^7 with strong configuration interaction, perhaps still symmetrical between them, and with a ground state ^2P split at least partly by the same H_d responsible for (jj) coupling in heavy nuclei. The sign of the magnetic contribution to the Li^7-Be^7 difference would remain unchanged and it would in most

[24] W. W. Buechner and E. N. Strait, Phys. Rev. **76**, 1547 (1949); D. R. Inglis, Phys. Rev. **78**, 68 (1950); S. S. Hanna and R. W. Gelinas, Bull. Am. Phys. Soc. **26**, 1, C3 (1951); G. R. Keepin, Jr., Phys. Rev. **80**, 768 (1950).

[25] H. H. Hummel and D. R. Inglis, Phys. Rev. **81**, 910 (1951).
[26] P. Kusch, Phys. Rev. **76**, 138 (1949).
[27] R. D. Present, Phys. Rev. **80**, 43 (1950).
[28] R. Avery and C. H. Blanchard, Phys. Rev. **78**, 704 (1950).

possibilities be larger because of an increase of the factor $\frac{1}{3}$ in (10). The present estimate of the expansion term could also retain some significance. Through the middle of the p-shell would be found nuclei of a complexity compatible with the rather dense spectra of low states observed, in which some of the agreement of nuclear spins with simple models might be fortuitous or might be significant in the manner discussed for Li^7. This interpretation based on the possibility of a positive Q seems so complicated, when compared to the empirical success of a much simpler theory, that one is reluctant to accept it until the determination of the relevant q can be based on more reliable molecular (or atomic) electron distributions than are available at present.

(*d*) As an alternative to a theory of spin-orbit coupling based on the introduction of a term such as (1) into the hamiltonian, Feingold and Wigner[21] have proposed that the tensor interaction responsible for the deuteron quadrupole moment has the effect of admixing excited states by a different amount in the two states of the ground doublet, depressing the $^2P_{\frac{1}{2}}$ more than the $^2P_{\frac{3}{2}}$ if excited configurations are taken into account, *vice versa* with the p^3 configuration only. In spite of the possible complexity of such effects, Feingold and Wigner suggest the preponderance of the matrix elements of single-nucleon excitations as a reason for considering this mainly a single-nucleon effect, so that it might not only apply to these light nuclei but also be a source of apparent (jj) coupling in heavy nuclei. With such a complicated mechanism one might expect that almost anything could happen, but the simplest guess concerning the Li^7-Be^7 difference gives the wrong sign. The more compact low states of Be^7 are raised more by the extra coulomb energy than are the highly excited states, so the "resonance denominators" of the second-order perturbation theory are smaller in Be^7 than in Li^7, which tends to make the splitting greater in Be^7. If this effect and possibly any contrary effects among the matrix elements could merely be shown to be small, we would again have the correct sign and order of magnitude given by the magnetic term, which is present also with this mechanism. The present investigation is an exploration, but is thus not necessarily a criterion, of the possibility (and hope) that a simpler mechanism is mainly responsible for the phenomena considered and that the second-order perturbations play only a secondary role. The judgment must be reached by comparison of successes and failures in a number of nuclei, of which Li^7 and Be^7 are among the lightest and perhaps among the simplest.

VII. COMPARISON WITH OTHER NUCLEI

That second-order effects are playing a considerable role is suggested by the failure to find a consistent indication of the magnitude of spin-orbit coupling among the various nuclei. Such a comparison involves averaging the expression $(1/r)(dV/dr)$ for various nuclei, and the method used by Gaus, which places the entire increment ΔV in a thin surface layer, gives a doublet splitting varying as $(l+\frac{1}{2})/R^2$, or $(l+\frac{1}{2})A^{-\frac{1}{3}}$, as we have seen. This neglects the tendency for nucleons with large angular momentum to be concentrated toward the outside, a tendency which is taken into account in an extreme fashion in the estimate which uses the centripetal-acceleration relation

$$(dV/dr)=l(l+1)\hbar^2/Mr^3. \tag{30}$$

This, when applied to the relevant wave functions with no radial nodes which correspond roughly to circular orbits with radii approximating the nuclear radius, gives a doublet splitting proportional to $l(l+\frac{1}{2})(l+1)A^{-\frac{4}{3}}$. The comparison of a few typical nuclei made in Table II is based on the assumption that the contribution of the main term H_d to Li^7 and Be^7 is 450 kev and that the single-nucleon splitting is three times this, 1.35 Mev. The single-nucleon splittings expected from both modes of variation are listed. If the true variation lies between the two estimates, then an increase of the doublet splittings by about 50 percent is needed to obtain agreement with the roughly known needs of He^5 and the heavy nuclei. The simplest way to obtain this would be to assume that second-order effects reduce the doublet splitting in Li^7 (this is the sign of contributions[21] from the ground configuration s^4p^3) by this amount without much affecting the Li^7-Be^7 difference, and that second-order effects are relatively unimportant in He^5 because of its paucity of excited states (stability of the alpha) and in heavy nuclei for some unknown reason (such a similarity to a degenerate electron gas in a metal) contributing to the success of the (jj) coupling shell model. This leaves the lack of states in N^{15} between the ground state and 5.3 Mev as an enigma, perhaps associated with a growing validity of the shell model as one gets up to this and heavier nuclei. It may be that almost-closed-shell nuclei are both exceptionally compact and have exceptionally large nucleon affinity (or, as in the discussion of Gaus, "meson affinity") ΔV, making an unusually large spin-orbit coupling which could also contribute to the sharpness of the "magic numbers."

TABLE II. Comparison of single-nucleon doublet splittings according to two simple estimates.

Nucleus	He^5	Li^7	N^{15}	Zr^{90}	Ce^{140}	Pb^{206}
N	1	1	1	4 50	5 82	6 126
$E\sim(l+\frac{1}{2})A^{-\frac{4}{3}}$	1.68	(1.35)	0.8	1.1	1.0	0.9 Mev
$E\sim l(l+\frac{1}{2})(l+1)A^{-\frac{4}{3}}$	2.11	(1.35)	0.49	1.34	1.35	1.33 Mev
E "observed"[a]	3	(1.35)	5.3		2	2 Mev

[a] R. K. Adair, Phys. Rev. **81**, 310 (1950) (He^5); R. E. Malm and W. W. Buechner, Phys. Rev. **78**, 337 (1950) (N^{15}); see reference 6.

I wish to thank Professor William A. Fowler and his associates at the California Institute of Technology for suggesting the preparation of this discussion to accompany their paper, and for constructive criticism of the manuscript.

Neutron-Proton Scattering at 27 Mev*

J. E. Brolley, Jr., J. H. Coon, and J. L. Fowler
Los Alamos Scientific Laboratory, University of California, Los Alamos, New Mexico

(Received January 2, 1951)

Monoenergetic neutrons of energy 27.2 Mev were produced by 10-Mev deuterons incident on a gaseous tritium target. Protons recoiling from the neutrons were observed in a fourfold coincidence proportional counter telescope. The angular distribution of neutrons scattered through angles in the range from 180° to 76° in the CM system was measured. The observed ratio of scattering at 180° to that at 90° was 1.28±0.10.

I. INTRODUCTION

IT is thought that experimental study of the scattering of neutrons by protons will yield fruitful information about the nature of nuclear forces. For neutrons having an energy of 14 Mev or less, measurements[1,2] indicate that the scattering is isotropic in the center-of-mass system, though the accuracy of the experiments does not preclude the possibility of there being a 5 percent anisotropy. For 40- and 90-Mev neutrons, however, the experiments indicate a definite anisotropy with a minimum in the intensity of scattering at 90° and approximate symmetry around 90° over the angular region investigated.[3,4] In the present experiment, the scattering of 27.2-Mev neutrons has been studied by observation of the recoil protons emerging from a hydrogenous radiator into a fourfold coincidence counter telescope. A preliminary report of the results of this investigation has been given previously.[5]

II. EXPERIMENT

For the present measurements neutrons were produced by the reaction

$$D+T^3=He^4+n+17.6 \text{ Mev}.$$

Deuterons, accelerated by the cyclotron, entered a tritium-filled gas target cell (Fig. 1), and the neutrons emitted in the forward direction were used. The cyclotron beam was brought to a focus by a wedge-shaped magnet and limited by a series of circular apertures to an angular divergence of ±0.5°. The region in which the experiment was performed was 15 feet from the cyclotron exit port and was shielded from the cyclotron by a wall of water and paraffin three feet thick.[6] After passing through a 0.952-cm diameter hole in a gold diaphragm, the beam entered the target cell through a dural window of thickness 15.6 mg/cm². The gas cell was filled to a pressure of 4.2 atmos with a mixture of 83 percent tritium and 17 percent hydrogen gas. After passing through the target gas, the beam was stopped by a gold disk to minimize neutron background. Accurate alignment of the axis of the gas cell with the direction of the beam was accomplished by use of a similar cell with a transparent end, so that the position of the beam could be determined by burning photographic film. Relative neutron yield was monitored by integrating the deuteron beam current (0.2 to 1 μamp). Handling of the tritium gas was facilitated by using a small stainless steel vessel containing uranium, in which the tritium was absorbed whenever it was desirable to empty the target cell. Tritium was evolved from the uranium by heating.

Prior to the installation of the gas target, the energy of the cyclotron beam was measured to be 11.0±0.2 Mev by deflection in a magnetic field.[6] During the course of the experiment the energy of the neutrons produced both by the *D–D* reaction and the *D–T* reaction was measured by determining aluminum absorption curves for the recoil protons. The results of these measurements agreed with the conclusion that the incident deuteron energy was 11.0 Mev within the precision of the data (about 4 percent).

Principally because of the loss of energy of the deuterons in passing through the tritium gas, the neutrons were not strictly monoenergetic. After penetrating the dural window, the deuterons had an energy of 10.1 Mev. The average deuteron energy in the tritium target was 9.76 Mev, with a maximum spread in energy of about 0.8 Mev. If one uses 17.6 Mev for the reaction energy, it follows that the energy of the 0° neutrons from the *D–T* reaction was 27.2±0.6 Mev, where the ±0.6 Mev includes the effect of the uncertainty in deuteron energy, and the neutron energy spread resulting from target thickness.

The proportional counter telescope and recording system was a modification of the type used for the determination of the angular distribution of 14-Mev neutrons scattered by protons.[2] Proton recoils were produced in polyethylene foils mounted in the counter telescope shown in Fig. 1. These foils had a total thickness of 45.9 mg/cm² and an exposed diameter of 1.613 cm. The recoil protons passed through four platinum-lined proportional counters. At the end of the third counter the recoil protons passed through a 7 mg/cm² Dural window into a 3.0-cm air gap in which could be inserted

* Work done under the auspices of the AEC.

[1] J. S. Laughlin and P. G. Kruger, Phys. Rev. **73**, 197 (1948).
[2] H. H. Barschall and R. F. Taschek, Phys. Rev. **75**, 1819 (1949).
[3] Hadley, Kelly, Leith, Segrè, Wiegand, and York, Phys. Rev. **75**, 351 (1949).
[4] Brueckner, Hartsough, Hayward, and Powell, Phys. Rev. **75**, 555 (1949).
[5] Brolley, Coon, and Fowler, Phys. Rev. **79**, 227 (1950).
[6] Curtis, Fowler, and Rosen, Rev. Sci. Instr. **20**, 388 (1949).

aluminum absorbers, and then through a second 7 mg/cm² Dural window into the fourth proportional counter. For each angular setting of the counter telescope a thickness of aluminum absorber was used (column 2, Table II) such that the lowest energy recoil proton had sufficient residual range to pass through the fourth counter. The purpose of the aluminum absorbers was to reduce the number of background coincidence counts and to increase the height of pulses originating in the fourth counter. In choosing the aluminum absorber thickness, allowance was made for errors in determining proton energy and for straggling in range. The counters were filled with 0.40 atmos argon containing approximately 2 percent CO_2. Ionization pulses produced in the counters were amplified by Los Alamos Model 500 amplifiers with a rise time of about 0.1 μsec and *RC* clipping time constant of 0.2 μsec. The amplifiers drove discriminators, from which the pulses were fed into a coincidence circuit which recorded coincidences between the first three channels as well as coincidences between all four channels. Each discriminator also drove a scaler to ascertain the number of counts in each channel. To facilitate background determinations the platinum holder which held the polyethylene foil could be rotated to expose the back side, on which was mounted a disk of graphite containing the same amount of carbon as was contained in the polyethylene radiator.

Since the energy loss of the recoil protons in a single counter was in some instances only 40 kev, special care was required to ascertain at what level the pulse-height discriminators should be set. A preliminary set of measurements was made to determine the dependence of coincidence counting rate on the bias setting in each channel. To obtain these bias curves, all the biases were set (by trial and error) sufficiently low to detect recoil protons, and the number of quadruple coincidence counts per μcoulomb of beam charge was observed as a function of bias setting in one channel. This procedure was repeated for each of the four channels, and was done with the counter telescope set to receive protons recoiling at 0° and at 45°. The subsequent operating bias setting for each channel was selected to be approximately 25 percent below the end of the bias curve plateau. For taking data at intermediate angles, the operating biases were selected by means of a linear interpolation between the values determined for 0° and 45°. For 52° the same settings were used as for 45°. In order to reproduce bias settings from day to day, a small gamma-ray source was placed next to a counter in a reproducible position, and the counting rate used as an indication of a change in bias.

Two series of neutron–proton scattering measurements were made: one with the center of the polyethylene radiator at a distance of 14.7 cm from the center of the tritium target ("near geometry"), and the other in which the radiator was 38.8 cm from the center of the tritium target ("far geometry"). To detect

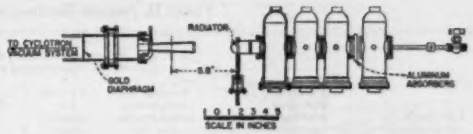

FIG. 1. Target and fourfold coincidence counter telescope. The tritium target cell is shown attached to the port through which the deuteron beam emerges. The polyethylene radiator in the counter telescope receives neutrons emerging from the target in the forward direction.

protons at different angles, the counter telescope was mounted to rotate about a vertical axis through the polyethylene foil. The plane of the foil was maintained perpendicular to the axis of the telescope. During the first series of runs ("near geometry"), proton recoils were counted at angles of 0, 15, 30, and 45 degrees in the laboratory system. In the second series of runs ("far geometry"), measurements were made at 0, 15, 30, 37.5, 45 and 52 degrees. For a given angular setting, the coincidence count per μcoulomb of deuteron current was determined for a variety of conditions as tabulated in Table I. As is indicated in this table, run (a) measured the number R_T, of proton recoils produced in the polyethylene radiator by the *D–T* neutrons, together with certain background effects which could be evaluated from runs (b), (c), (d), and (e). The aluminum absorber used in run (b) was sufficient to absorb all protons, whether recoiling from neutrons or originating from (n,p) disintegrations. Therefore, the counts observed in run (b) were due to accidental coincidences between triple coincidence counts (real or accidental) in the first three counters and single pulses in the fourth counter. The resolving time (approximately 0.5 μsec) calculated from the observed number of accidentals was used to calculate the number of accidental coincidences to be subtracted as background from runs (a), (c), (d), and (e). The results of run (e) indicated that in every case D_H was a negligible background of less than one-half percent. By reference to Table I, one can conclude therefore that the desired quantity R_T is obtained by a subtraction of the sum of runs (c) and (d) from run (a). The magnitude of these background corrections

TABLE I. Operating conditions under which coincidence counts were recorded.

Run type	Target	Radiator	Aluminum absorber	Number of coincidence counts of specified origin*
(a)	*T*	CH_2	see Table II	$R_T+R_H+D_T+D_H$
(b)	*T*	CH_2	1.10 g/cm²	only accidentals
(c)	*T*	C	see Table II	D_T+D_H
(d)	*H*	CH_2	see Table II	R_H+D_H
(e)	*H*	C	see Table II	D_H

* R_T = number of protons recoiling from *D–T* neutrons and originating in the CH_2.
D_T = number of disintegration protons arising from (n,p) reactions induced by *D–T* neutrons.
R_H = number of protons recoiling from background neutrons and originating in the CH_2.
D_H = number of disintegration protons arising from (n,p) reactions induced by background neutrons.

TABLE II. Angular distribution data and average corrections.

Lab angle for recoil proton (1)	Thickness of Al absorber including windows g/cm² (2)	Percentage correction applied to uncorrected values: Average for accidental coincidences, run (b) (3)	Average for counting losses (4)	Background D–T, from run (c) (5)	Background R_H, from run (d) (6)	Corrected number of quadruples per microcoulomb: Un-normalized data (7)	Near geometry normalized to far geometry (8)
Near geometry							
0°	0.70	−9.6	+38.4	0	0	4.03±0.13	0.517±0.017
15°	0.43	−5.5	+25.0	0	0	3.95±0.10	0.507±0.013
30°	0.18	−6.4	+14.2	−9.0	−4.7	3.14±0.10	0.403±0.013
45°	0.027	−1.6	+7.9	−17.2	−18.4	2.24±0.08	0.287±0.010
Far geometry							
0°	0.70	−6.5	+16.7	0	−1.1	0.516±0.017	
15°	0.43	−6.0	+11.2	−1.7	−1.3	0.469±0.019	
30°	0.25	−3.8	+7.4	−6.1	−4.0	0.383±0.017	
37.5°	0.15	−2.5	+7.6	−12.5	−4.8	0.341±0.020	
45°	0.055	−0.6	+2.6	−17.3	−9.9	0.273±0.020	
45° (0° bias)	0.055	−2.5	+11.7	−17.0	−12.1	0.276±0.034	
52°	0.014	−0.4	+2.9	−18.6	−17.4	0.246±0.015	

is given in Table II, columns 3, 5, and 6. The tabulated number is an average of the corrections applied to individual runs and represents the average percentage of the uncorrected value applied as correction.

Counting losses occurred because of the short but finite recovery time of the pulse shaping circuits and because of the high counting rate which in some cases was as high as 2×10^4 per sec per channel. The background pulses were due to argon recoils from the D–T neutrons, argon recoils from background neutrons, gamma-rays, etc. To make it possible to correct for losses, "near geometry" data were taken with various values of cyclotron beam current. The true coincidence count Q, which would occur in the absence of losses, is related to the observed coincidence count Q', by the formula

$$Q=Q'/(1-\tau\Sigma),$$

where τ is the average recovery time and Σ is the sum of the counting rates in the four channels. According to this relation a plot of Q' *versus* Σ will yield a straight line with $Q'=Q$ at $\Sigma=0$. "Near geometry" data were plotted in this way and a graphical extrapolation made to determine the corrected coincidence count.

When a complete set of data at the "near geometry" position had been obtained, the counters were moved to the "far geometry" position to improve the angular resolution and also to increase the angular range over which measurements could be made. Correction of "far geometry" data for the relatively small counting losses was done by extrapolation to zero counting rate with the same slope as determined from the "near geometry" data. The average counting loss corrections are listed in Table II, column 4. Because of variation in beam current, corrections for counting losses as well as corrections for accidental coincidences varied by a factor of three for different runs. After these corrections were applied, however, data taken at different times were consistent within the standard deviation expected to arise from the statistics of counting, from random errors in beam measurement, and from fluctuations of the number of target atoms in the gas cell which was frequently emptied and refilled.

It seemed advisable to check on the possibility of systematic error being introduced by the method of bias setting, since the biases were changed with angle in a systematic way in order to minimize backgrounds. For this reason data were taken at 45° with the bias settings normally used for 0° runs. As is indicated in Table II, the data taken in this fashion agreed quite well with the data taken using normal biases. This result also furnished evidence that the counting loss corrections were applied correctly, since the counting loss for the lower bias settings was 4.5 times that for the higher bias settings.

To avoid the possibility of the data being affected by long time drifts in the characteristics of the apparaus, relatively short runs (long enough to obtain about 100 quadruple coincidence counts) were taken at a given angular setting, whence the angle was changed to a new value selected at random. This procedure was continued until about 1000 counts were accumulated at each angle. When the final data were assembled for this series of runs, which occurred over a period of six weeks, no systematic trend of the values for a given angular setting could be discerned. The results of separate runs at a given angle varied around their mean in approximately a gaussian distribution. The standard errors were slightly larger than the statistical errors, which is to be expected because of errors in beam measurement, variation in gas target density, etc.

A measurement of the efficiency of the detector system was performed by using 14-Mev D–T neutrons from the Los Alamos Cockcroft-Walton accelerator, from which the neutron flux is known approximately. The efficiency so measured was in agreement with that calculated from the known geometry of the detector and the n–p total scattering cross section value of Ageno

et al.[7] The purpose of this measurement was to increase confidence that the behavior of the apparatus was well understood.

A minor correction was applied to account for multiple Rutherford scattering[8] of protons in the aluminum absorbers inserted between the third and fourth counters. An approximate calculation of the effect introduced a maximum correction of 1.3 percent. The method of calculation was checked experimentally, by use of the Cockcroft-Walton 14-Mev neutron source. For this check recoil protons were counted under conditions such that the Rutherford scattering was negligible; i.e., no scattering medium was present except the counter gas and the polyethylene radiator. Data were also taken with an aluminum absorber between the second and third counters under conditions such that the observed quadruple coincidence count was reduced by 18±4 percent. The approximate calculation applied to this case gave a reduction of 20 percent in agreement with the measurement.

III. RESULTS AND CONCLUSIONS

Table II gives a summary of results. The final corrected number of proton recoils is tabulated in column 7. The "near geometry" data are normalized to the "far geometry" data by the ratio of solid angles (0.1283) and are given in column 8. Tabulated errors represent the standard errors as calculated from the deviation of the different runs from the mean. In Fig. 2 these data, converted to the center-of-mass system (small effects of relativity are included), are plotted as a function of the angle of scattering of the neutron in the center-of-mass system. The vertical spread indicated on the plotted points is standard error. The horizontal spread indicated on the plot defines an angular range such that about 70 percent of the detected recoil protons appeared within this range. An experimental curve through the points has been drawn assuming symmetry around 90° as suggested by data at 40 and 90 Mev.[3,4] Only relative values of the differential cross section as a function of angle were measured in this experiment. However, with the assumption of symmetry about 90°, the data in Fig. 2 can be normalized so that integration over all angles gives the total cross section. A smooth curve through the experimental values of the total cross section as a function of energy gives a value[9] of 0.36 barn at 27 Mev. The differential cross section determined by means of this normalization is 32 mb per unit solid angle at 180° and 25 mb at 90°. For the ratio of the scattering at 180° to that at 90°, the present experiment yields a value of 1.28 with an over-all estimated

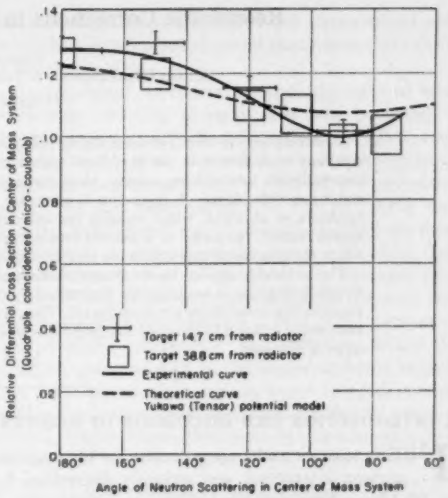

FIG. 2. Relative intensity of scattered neutrons *versus* angle of scattering of the neutron in the center-of-mass system. Standard errors are indicated by the vertical height of the symbols, while instrumental angular resolution is indicated by the width of the symbols.

error of ±8 percent. Of this error, 4 percent is the computed standard error, and the remaining 4 percent is a guess as to the systematic uncertainties arising from error in bias setting, Rutherford scattering, counting loss corrections, etc.

The dashed curve shown in Fig. 2 is calculated in the manner of Christian and Hart[10] using a Yukawa potential with a range of 1.35×10^{-13} cm and with inclusion of a tensor force. Comparison of this theory to experimental data at 40 and 90 Mev is shown in Fig. 17 of reference 10. At 40 Mev this theory predicts the ratio at 180° to that at 90° to be 1.45, which is in fair agreement with, though less than, the experimental value of 1.55±0.2 measured by Hadley *et al.*[3] At 27.2 Mev the theory predicts a value of 1.15 which is also less than the experimental value of 1.28±0.10.

We wish to acknowledge the contribution of Dr. R. S. Christian of the University of California Radiation Laboratory who has made the theoretical calculations reported here. We wish also to acknowledge the assistance of H. T. Gittings, Jr., and R. J. Watts in connection with the electronic problems and the aid of R. M. Potter in handling the tritium. Thanks also are due to Dr. H. H. Barschall for his interest in this problem and his suggestions with regard to the preparation of this paper.

[7] Ageno, Amaldi, Bocciarelli, and Trabacchi, Phys. Rev. **71**, 20 (1947).
[8] H. S. Snyder and W. T. Scott, Phys. Rev. **76**, 220 (1949).
[9] Robert K. Adair, Revs. Modern Phys. **22**, 249 (1950).
[10] R. W. Christian and E. W. Hart, Phys. Rev. **77**, 441 (1950).

Relativistic Corrections in High Energy n-p Scattering*

ARMAND SIEGEL†
Massachusetts Institute of Technology, Cambridge, Massachusetts
(Received July 28, 1950)

A method, due to Breit, of generalizing phenomenological nuclear interactions to give a relativistically invariant cross section in the first Born approximation, has been extended to apply to a broad class of nonrelativistic interactions; namely, those containing isotopic spin operators and any kind of Pauli spin and space dependence. A procedure is given for obtaining an equivalent Pauli operator for the Dirac operators so obtained, which reduces the calculation of the relativistic cross section (in the first Born approximation), formally, to a nonrelativistic calculation. The cross section is then obtained in a form in which the relativistic corrections are explicitly split off from the nonrelativistic terms.

The method is applied to the symmetric-exchange interaction with tensor forces. The form of the relativistic interaction is not uniquely determined by that of the nonrelativistic one, but a number of the more conservative possibilities are investigated. The corrections to the 90-Mev n-p scattering thus obtained are analyzed in relation to the data. The possibility of exploiting these corrections to adjust the theory to experiment is discussed.

I. INTRODUCTION AND DISCUSSION OF RESULTS

THE symmetric exchange postulate for the nucleon-nucleon interaction was seriously discredited by the 90-Mev neutron–proton scattering experiments of Segrè and his co-workers.[1] It was shown by Christian and Hart[2] that the angular distribution of the 90-Mev cross section is incompatible with the relatively large proportion of space exchange in the symmetric exchange factor $\frac{1}{4}(\sigma_1\cdot\sigma_2)(\tau_1\cdot\tau_2)$ if the scattering is treated on a nonrelativistic basis. On the other hand, the symmetric exchange is an attractive theoretical concept because it accounts for the saturation of nuclear binding energies and embodies the charge symmetry of nuclear forces (which is at least approximately demonstrable at low energies). This is probably not the case[3] with the half-exchange, half-ordinary force found by Christian and Hart to give the best fit of the 90-Mev scattering results.

The true explanation of nuclear saturation is of course not necessarily to be found entirely in an exchange effect in the two-nucleon interaction. It may originate in some part from many-body forces, for example, or the nucleon–nucleon interaction may not be expressible by a quantum-mechanical potential operator at all. Nevertheless, one is not yet compelled to abandon the two-body force as the phenomenological interaction. Specifically, one might suppose that the nonrelativistic interaction is something similar to the symmetric exchange interaction, correct at nonrelativistic energies, and explaining saturation. The 90-Mev scattering would then deviate from that predicted by this interaction through effects that become important only at appreciably relativistic energies. (Reconciling the symmetric exchange theory with the deviations from charge equivalence shown by the 32-Mev p–p scattering[4] might, of course, require additional postulates).

That such a point of view is not necessarily incompatible with at least the meson theory of nuclear forces is shown by the field theory calculations of Watson and Lepore.[5] *A priori*, the main objection to attributing the deviations from the scattering results to relativistic corrections alone is that the deviations are too large[5a] compared with the nominal figure of 5 percent at 90 Mev obtained by assuming the magnitude of such corrections to be v^2/c^2 times the nonrelativistic cross section. In contrast with this, Watson and Lepore find relativistic contributions of the order of magnitude of the nonrelativistic cross section itself. There seems to be nothing, therefore, in current theory that rules out the possibility of relativistic corrections much greater than the nominal v^2/c^2.

In the present paper the relativistic corrections obtainable with symmetric exchange are investigated from a phenomenological point of view. The cross section in the Born approximation is generalized to a relativistically covariant form. The interaction potential is a Dirac operator, whose matrix elements are required to fit those of the nonrelativistic interaction at low energies. (Two phenomenologically adjusted nonrelativistic interactions are used, a square well, and a Yukawa well). The low energy fitting requirement does not yield a unique Dirac interaction operator. The corrections to the cross section obtained by utilizing several of the more conservative possibilities allowed by this non-uniqueness have been calculated. Each appears as a function that can be added to the differential cross section with a more or less arbitrary multiplicative coefficient. We say "more or less arbitrary" for the

* Supported in part by the joint program of the ONR and AEC.
† During the writing of this paper the author was at Worcester Polytechnic Institute, Worcester, Massachusetts. Present address: Boston University, Boston, Massachusetts.
[1] Hadley, Kelley, Leith, Segrè, Wiegand, and York, Phys. Rev. 75, 351 (1949).
[2] R. S. Christian and E. W. Hart, Phys. Rev. 77, 441 (1950).
[3] E. Gerjuoy, Phys. Rev. 77, 568 (1950).
[4] H. P. Noyes, Phys. Rev. 78, 90 (1950).
[5] K. M. Watson and J. V. Lepore, Phys. Rev. 76, 1157 (1949).
[5a] 46 percent of the theoretical value with respect to total cross section, using the square well with Rarita-Schwinger constants, or 21 percent with a Yukawa well (Born approximation triplet, exact singlet). See Table II, and Section VII of this paper.

following reason. Each such coefficient appears in the Dirac interaction potential as the multiplier of a term whose matrix elements are of order v^2/c^2 compared to the leading term (the latter has matrix elements of zero order, which reduce to those of the nonrelativistic interaction in the limit $v/c=0$). Thus, if the only fitting requirement is agreement of the relativistic interaction with the nonrelativistic one in the *zero*-energy limit, these coefficients are entirely arbitrary.

Actually, of course, since the relativistic interaction must fit the experimental data at all energies, not only in the zero-energy limit, the following difficulty arises. If the nonrelativistic approximation is to be considered to be correct for the low and moderate-energy phenomena to which it has been adjusted (and this would be the simplest and hence most desirable situation), the v^2/c^2 terms must not be allowed to become appreciable at these energies. This sets an upper limit to the values of the multiplicative coefficients under discussion. As is shown in detail in the last section, if we are to be able to adjust the 90-Mev cross section by means of these coefficients, without exceeding this upper limit, then since the discrepancies are so much greater than v^2/c^2 in their ratio to the nonrelativistic cross section, a very favorable combination of properties is needed in the purely relativistic contributions to the cross section; namely, (1) a fair degree of coincidence of their values as functions of angle with the values of the discrepancies and (2) a substantial amount of constructive interference at 90 Mev in the amplitudes that combine to give these contributions, so that they will have an actual numerical ratio greater than their formal ratio v^2/c^2 to the nonrelativistic terms at this energy, but not at the low and moderate energies.

In the last section of this paper, the numerical results obtained are analyzed to see how close they come to satisfying these requirements. Requirement (1) is satisfied surprisingly well for the Yukawa interaction, at least, but requirement (2) is so far from being satisfied that it is impossible to have any confidence in the justifiability of handling either interaction along the lines desired. This means that, if the program originally proposed, that of utilizing relativistic terms to adjust the symmetric theory to experiment at 90 Mev, is to be carried out, the form of the nonrelativistic interaction cannot be treated as given, but must instead undergo some further adjustment along with the relativistic coefficients even at low and moderate energies. (We are assuming here that the more radical possibilities in generalizing the nonrelativistic interaction either lead to the same result or are to be rejected, at least tentatively, as excessively speculative). Although such a method is not as simple as could be desired, nevertheless the favorable qualitative behavior of the relativistic corrections [satisfaction of requirement (1)] obtained with the Yukawa interaction indicates that agreement with experiment might be obtainable with a relativistic interaction containing only a very few parameters in addition to those contained in the conventional nonrelativistic interactions. Further research on this subject is now in progress.

An important difference between the case of large coefficients and that of small ones may be noted. If requirements (1) and (2) are met, so that small coefficients can be used, the relativistic contributions to scattering would be expected to level off with increasing energy, as the disappearance of the fortuitous constructive interference counteracts the increase in these terms due to the increase of the ratio v/c, on which they depend more or less monotonically in the near-relativistic region. If these requirements are not met, and large coefficients are required, a very rapid increase of the peculiarly relativistic contributions would be expected, going as v^2/c^2 in the near-relativistic region; thus these terms might rapidly come to predominate, making the scattering at moderate relativistic energies entirely different from that given by the nonrelativistic interaction.

II. GENERAL PROCEDURE

Entirely apart from detailed considerations involving meson theory, there are two very general conditions on the relativistic generalization of a given nucleon–nucleon interaction. These are: (a) Relativistic covariance of physical quantities obtained from it, and (b) reduction of these quantities, in the zero velocity limit, to the corresponding quantities obtained from the given nonrelativistic interaction. Breit[6] has devised a simple procedure, satisfying these conditions, for generalizing the nucleon–nucleon interaction with respect to those matrix elements that appear in the Born approximation cross section. In the same paper he presents explicit generalizations, along these lines, of certain types of nonrelativistic interactions. We adopt his method here, adapting it to the case of symmetric forces and Pauli spin operators of general type.

In order to obtain a covariant cross section, certain terms of purely kinetic origin (i.e., common to all interactions) must be revised. But the essential quantity with which we are concerned is the dynamic one, namely the transition matrix element of the interaction operator of the neutron–proton system. Assume a nonrelativistic interaction V depending on the relative position vector $\mathbf{r}=\mathbf{r}_1-\mathbf{r}_2$ of the two particles, and in addition on the Pauli and isotopic spins. The initial and final momenta of the particles are $\mathbf{p}_{1i}$, $\mathbf{p}_{2i}$ and $\mathbf{p}_{1f}$, $\mathbf{p}_{2f}$, respectively. After elimination of the motion of the center of mass, the transition matrix element is

$$\mathfrak{M}=\langle \mathbf{p}_f, S_f, T_f | V | \mathbf{p}_i, S_i, T_i \rangle, \tag{2.1}$$

in which

$$\mathbf{p}_i=\tfrac{1}{2}(\mathbf{p}_{1i}-\mathbf{p}_{2i}), \quad \mathbf{p}_f=\tfrac{1}{2}(\mathbf{p}_{1f}-\mathbf{p}_{2f}); \tag{2.2}$$

S and T are the Pauli and isotopic spin quantum numbers of the two-nucleon system.

[6] G. Breit, Phys. Rev. 53, 153 (1938).

Requirement (a) above, when applied to the Born approximation cross section, was shown by Breit[6] to be equivalent to the requirement that under Lorentz transformations of the state vectors (including densities) and the relativistic potential operator, the relativistic generalization of $\mathfrak{M}$ must be invariant. In the paragraphs that follow, we present the general procedure for satisfying conditions (a) and (b), starting with a nonrelativistic interaction containing very general space and Pauli and isotopic spin dependence.

Since isotopic spin state vectors and operators are relativistically invariant, it is sufficient to consider the relativistic generalization of operators of the form

$$(\text{Pauli spin operator})\times(\text{space operator}). \quad (2.3)$$

The most general interaction of the type described above will be a sum of operators of the form (2.3), with isotopic spin operators as coefficients. The relativistic interaction is thus obtainable by replacing (2.3) by its relativistic counterpart in each term.

Let U denote an operator of the form (2.3), i.e., not containing isotopic spin. We seek a relativistic generalization, U_{rel}, of U, satisfying conditions (a) and (b). The difficulties standing in the way of a formulation of a relativistically invariant interaction in configuration space can be avoided by using a momentum representation of U. The factor (space operator) in (2.3) is then replaced by the equivalent operator in terms of the momenta. This operator factor, when the interaction is diagonal in the space variable $\mathbf{r}$, can be written in the explicit form

$$U_p=\int\int|\mathbf{p}_f\rangle\mathbf{dp}_f\mathfrak{U}_p(\mathbf{p}_{if})\mathbf{dp}_i\langle\mathbf{p}_i|, \quad (2.4)$$

where

$$\mathbf{p}_{if}\equiv\mathbf{p}_i-\mathbf{p}_f; \quad (2.5)$$

$\mathfrak{U}_p(\mathbf{p}_{if})$ is a c-quantity (in general a tensor with c-numbers as components) equal to the matrix elements of U_p between the state vectors $\langle\mathbf{p}_f|$ and $|\mathbf{p}_i\rangle$:

$$\mathfrak{U}_p(\mathbf{p}_{if})=\langle\mathbf{p}_f|U_p|\mathbf{p}_i\rangle. \quad (2.6)$$

At this point, for later convenience, we introduce the notation

$$\{f(\mathbf{p})\}_{\text{op}}\equiv\int|\mathbf{p}_f\rangle\mathbf{dp}_f f(\mathbf{p}_{if})\mathbf{dp}_i\langle\mathbf{p}_i|; \quad (2.7)$$

in words, $\{f(\mathbf{p})\}_{\text{op}}$ is the operator whose matrix element between $\langle\mathbf{p}_f|$ and $|\mathbf{p}_i\rangle$ is $f(\mathbf{p}_{if})$. $f(\mathbf{p}_{if})$ may be a scalar or tensor, or tensor component.

The spin factor of (2.3), to be denoted by U_σ, will be left in the customary representation. The factored form of U is now

$$U=U_pU_\sigma. \quad (2.8)$$

The transition to the relativistic domain will be made by constructing a mapping which defines the correspondence between nonrelativistic and relativistic state vectors, and by characterizing the relativistic interactions whose matrix elements between these relativistic states satisfy conditions (a) and (b).

III. RELATIVISTIC NOTATION

We shall use, throughout, the very advantageous scheme of expressing the Dirac operators in terms of dichotomic variables.[7] If we write $|\rho_-'\rangle$ for the eigenvector of ρ_3 having the eigenvalue -1, we obtain a basic set of one-particle solutions of the Dirac equation in the form

$$|E,\mathbf{p},(\sigma)\rangle=C\left(1-\frac{c\boldsymbol{\alpha}\cdot\mathbf{p}}{E+\mu c^2}\right)|\rho_-'\rangle|\sigma\rangle|\mathbf{p}\rangle, \quad (3.1)$$

where $|\sigma\rangle$ is any σ-spin state vector, $|\mathbf{p}\rangle$ is a momentum eigenvector normalized to one particle per unit volume. C is a normalization constant:

$$C=[1+c^2p^2/(E+\mu c^2)]^{-\frac{1}{2}}. \quad (3.2)$$

E and $\mathbf{p}$ are related by

$$E=\pm(c^2p^2+\mu^2c^4)^{\frac{1}{2}}. \quad (3.3)$$

Four mutually orthogonal vectors are obtained by using the two signs of the energy and any pair of orthogonal σ state vectors.

We use henceforth the notation

$$G_{E,\mathbf{p}}(i)\equiv 1-c\boldsymbol{\alpha}(i)\cdot\mathbf{p}/(E+\mu c^2). \quad (3.4)$$

The argument i designates the particle on whose dichotomic variables G operates. The normalization constant C is a function of the sign and magnitude of the energy only; since all our calculating will be done in the center-of-mass system with particles of equal mass and equal positive energies, it will never be necessary to use distinguishing subscripts with C.

For a system of two particles, linear combinations of products of state vectors of the form (3.1), one for each particle, are solutions of the Dirac equation for two free particles. These have the form

$$|E_1,E_2,\mathbf{p}_1,\mathbf{p}_2,(S_{\text{rel}}(1,2))\rangle$$
$$=C^2G_{E_1,\mathbf{p}_1}(1)G_{E_2,\mathbf{p}_2}(2)|\rho_-'(1)\rangle|\rho_-'(2)\rangle$$
$$\times|S_{\text{rel}}(1,2)\rangle|\mathbf{p}_1(1)\rangle|\mathbf{p}_2(2)\rangle, \quad (3.5)$$

in which $|S_{\text{rel}}(1,2)\rangle$ is *any* linear combination of two-particle σ-spin state vectors. As in the nonrelativistic case,

$$|\mathbf{p}(1)\rangle|\mathbf{p}(2)\rangle=|\mathbf{P}\rangle|\mathbf{p}\rangle, \quad (3.6)$$

where $\mathbf{P}$ and $\mathbf{p}$ are the momenta conjugate to $\mathbf{R}=\frac{1}{2}(\mathbf{r}_1+\mathbf{r}_2)$ and $\mathbf{r}=\mathbf{r}_1-\mathbf{r}_2$ respectively; i.e. $\mathbf{P}=\mathbf{p}_1+\mathbf{p}_2$,

[7] L. Rosenfeld, *Theory of Nuclear Forces* (Interscience Publishers, Inc., New York, 1949). The notation we use is given in Rosenfeld's Chapter IV, particularly Sec. 4.2. However, the representation in which we write the Dirac equation differs from Rosenfeld's; it is obtained from his by transforming with the unitary operator ρ_1, i.e., essentially by the interchange of large and small components of the state vectors.

$\mathbf{p}=\frac{1}{2}(\mathbf{p}_1-\mathbf{p}_2)$. Thus, putting also $|\rho_-'(1)\rangle|\rho_-'(2)\rangle=|\rho_-\rangle$:

$$|E_1, E_2, \mathbf{p}_1, \mathbf{p}_2, (S_{\rm rel}(1,2))\rangle$$
$$=|E_1, E_2, \mathbf{p}, \mathbf{P}, (S_{\rm rel}(1,2))\rangle$$
$$=C^2 G_{E_1,\mathbf{p}_1}(1) G_{E_2,\mathbf{p}_2}(2)|\rho_-\rangle|S_{\rm rel}(1,2)\rangle|\mathbf{P}\rangle|\mathbf{p}\rangle. \quad (3.7)$$

The form of the relativistic state vector that replaces the nonrelativistic one $|\mathbf{P}\rangle|\mathbf{p}\rangle|S\rangle$ follows from the customary formulation of the assumption that the Pauli-Schrödinger mechanics is the nonrelativistic limiting form of the Dirac mechanics, *viz.*: The Dirac operator $\mathbf{p}(i)$ corresponds to the observable, relativistic momentum of a particle; and the Dirac operator $\boldsymbol{\sigma}(i)$ corresponds to the Pauli operator $\boldsymbol{\sigma}(i)$ in the limit $v/c=0$. The values of the relativistic momenta $\mathbf{P}$ and $\mathbf{p}$ are determined by the experimental situation. The correspondence of the $\boldsymbol{\sigma}$ operators requires that $|S_{\rm rel}\rangle$ be chosen equal to the nonrelativistic $|S\rangle$, to within a unitary transformation; we put $|S_{\rm rel}\rangle=|S\rangle$. The signs of the energies E_1 and E_2 will, of course, in our case be positive (*first* Born approximation).

IV. COVARIANT INTERACTION FORMS

The relativistic generalization of U_p [Eq. (2.4)] that we shall use will be the simplest one satisfying conditions (a) and (b): On the right-hand side of (2.4), the vectors $\mathbf{p}_i$ and $\mathbf{p}_f$ in the state vectors $|\mathbf{p}_f\rangle$ and $\langle\mathbf{p}_i|$, and $\mathbf{dp}_i$ and $\mathbf{dp}_f$, are replaced by their relativistic *three*-vector counterparts; the normalization of the nonrelativistic state vectors is retained, and the integration over all values of the vectors $\mathbf{p}_i$ and $\mathbf{p}_f$ is also retained. In $\mathfrak{U}_p(\mathbf{p}_{if})$ considered as a function of $\mathbf{p}_{if}$, on the other hand, $\mathbf{p}_{if}$ is replaced by $(\mathbf{p}_{if}, iE_{if}/c)$, with

$$E_{if}=\tfrac{1}{2}[(E_{1i}-E_{2i})-(E_{1f}-E_{2f})], \quad (4.1)$$

to yield the relativistic function $\mathfrak{U}_{p\,\rm rel}(\mathbf{p}_{if})$; whatever the form of $\mathfrak{U}_p(\mathbf{p}_{if})$, whether scalar or tensor in $\mathbf{p}_{if}$, this replacement is straightforward for positive energy states. (It will be noted that this procedure gives a four-vector for $\mathfrak{U}_{p\,\rm rel}$ when $\mathfrak{U}_p$ is a three-vector, and similarly for higher rank tensors. Symbolically, if $U_p=\{T(\mathbf{p})\}_{\rm op}$, where $T(\mathbf{p})$ is a scalar, vector, dyadic, etc., function of $\mathbf{p}$, this gives for the relativistic generalization of U_p (to be called $U_{p\,\rm rel}$):

$$U_{p\,\rm rel}=\{T((\mathbf{p}, iE/c))\}_{\rm op}).$$

The invariance of all matrix elements (between state vectors of the form $|\mathbf{p}\rangle$) of $U_{p\,\rm rel}$ follows from the invariance of $\mathfrak{U}_{p\,\rm rel}(\mathbf{p}_{if})$, provided normalization of all state vectors of the form $|\mathbf{p}\rangle$ to one particle per unit volume is retained under Lorentz transformations. It will be noted that the change in normalization of actual solutions of the free-particle Dirac equation under Lorentz transformations is incorporated in the factor C^2 of Eq. (3.5).

The lack of uniqueness of the above choice of $U_{p\,\rm rel}$ is quite apparent. In particular, $\mathfrak{U}_{p\,\rm rel}(\mathbf{p}_{if})$ as above defined could be multiplied by any scalar function of $(\mathbf{p}_i, iE_i/c)$ and $(\mathbf{p}_f, iE_f/c)$ that reduces to unity in the nonrelativistic limit, without violating conditions (a) and (b).

We now turn to the matter of the relativistic generalization of U_σ [Eq. (2.8)], to be denoted to $U_{\sigma\,\rm rel}$. The necessary invariance of the matrix elements of $U_{\sigma\,\rm rel}$ when taken between the spinor parts of the state vectors (3.5) (the factor C, giving the Lorentz density change, being taken as included in the spinor part) restricts us to the operators $S=\beta=\rho_3$, $V=(\boldsymbol{\alpha}, -i)$, $T=\beta(\boldsymbol{\sigma}, \boldsymbol{\alpha})$, $A=(\boldsymbol{\sigma}, -i\rho_1)$, $P=\rho_2$, S being a scalar, V a polar four-vector, T an antisymmetric tensor, A an axial four-vector, and P a pseudoscalar.

The forms of U_pU_σ that appear in the nonrelativistic interactions with which we are concerned are invariant combinations of the Pauli operators $\mathbf{1}$ and $\boldsymbol{\sigma}$ and momentum operators of the form $\{f(|\mathbf{p}|)\}_{\rm op}$ or $\{f(|\mathbf{p}|)p_jp_k\}_{\rm op}$ (j, k being tensor indices). The corresponding relativistic operators will be obtained by combining the Dirac operators S, V, T, A, P with momentum operators obtained from the nonrelativistic momentum operators in the manner described previously. We shall retain in the relativistic domain the restriction that the latter be tensors of not higher than second rank in the momentum.

The desired operators will be written down systematically[8] in a way that exhibits the completeness of the collection subject to the above restrictions. For simplicity, we put f_0 for a scalar operator function of $(\mathbf{p}_{if}, iE_{if}/c)$; f_1 for the corresponding four-vector; and f_2 for a tensor. Of the two Dirac operators in each product, one belongs to one of the particles, and one to the other; some have to be symmetrized between the particles and this is indicated by the operator "s" appearing in front of such expressions. The factor i (square root of minus one) that appears in some cases is for the purpose of making the operator hermitian.

The two-particle operators are then (a) SSf_0, (b) $isSVf_1$, (c) $sSTf_2$, (d) VVf_0, (e) $sVVf_2$, (f) $iVTf_1$, (g) TTf_0, (h)[9] TTf_2, (i) AAf_0, (j) AAf_2, (k) $isAPf_1$, (l) PPf_0, (m) $isAT(\text{dual})f_1$. In all cases the operators are to be combined by summation of indices in such a way as to give an invariant; where this summation is ambiguous, it is uniquely defined by requiring that the result does not duplicate the form of another operator included in the list.

We note that three of the above operators, while included for completeness, could have been omitted, at least for our present purposes: (c) vanishes identically,

[8] The cases involving a sum over the indices of T by itself are omitted; this sum vanishes, since T is an antisymmetrical tensor.

[9] A Møller type calculation [Z. Physik **70**, 686 (1931)] of the interaction matrix element between momentum eigenstates for two Dirac particles leads to just this operator (h), if instead of using the complete charge-current density four-vectors one uses the parts of these that refer to the magnetization-polarization densities alone. Thus this operator is physically the relativistic form of the dipole-dipole potential energy interaction.

since T is an antisymmetric tensor and f_2 is symmetric, and (b) and (e) can be shown, by use of the one-particle Dirac equation, to have matrix elements which vanish between states of positive energy.

The Pauli operators to which the above operators reduce may be found by setting the Dirac operators α, ρ_1, and ρ_2 equal to zero and $\rho_3=1$. We then obtain, since E_{if} vanishes in the nonrelativistic limit (particles of equal mass): (a) $\rightarrow f_0$, (c) $=0$, (d) $\rightarrow -f_0$, (g) $\rightarrow \boldsymbol{\sigma}_1\cdot\boldsymbol{\sigma}_2 f_0$, (h) $\rightarrow \{[|\mathbf{p}_{if}|^2\boldsymbol{\sigma}_1\cdot\boldsymbol{\sigma}_2-\boldsymbol{\sigma}_1\cdot\mathbf{p}_{if}\boldsymbol{\sigma}_2\cdot\mathbf{p}_{if}]f(|\mathbf{p}_{if}|^2)\}_{\text{op}}$, (i) $\rightarrow \boldsymbol{\sigma}_1\cdot\boldsymbol{\sigma}_2 f_0$, (j) $\rightarrow \{\boldsymbol{\sigma}_1\cdot\mathbf{p}_{if}\boldsymbol{\sigma}_2\cdot\mathbf{p}_{if}f(|\mathbf{p}_{if}|^2)\}_{\text{op}}$ while all others approach zero. These equivalences hold, of course, only in the positive energy subspace.

V. DERIVATION OF THE RELATIVISTIC CORRECTIONS TO THE CROSS SECTION

We take as our relativistic interaction

$$V_{\text{rel}}=\boldsymbol{\tau}_1\cdot\boldsymbol{\tau}_2 U_{\text{rel}}, \tag{5.1}$$

where U_{rel} operates on momentum, ρ- and σ-spin coordinates only. In obtaining the relativistic matrix element, it is convenient to make an explicit separation of the three types of inner product corresponding to the three types of coordinates of U_{rel}. We define

$$\mathfrak{U}_{\text{rel}}=\langle \mathbf{p}_f|U_{\text{rel}}|\mathbf{p}_i\rangle, \tag{5.2}$$

and further

$$U_{\text{rel}}'=\langle \rho_-|G_f(1)G_f(2)\mathfrak{U}_{\text{rel}}G_i(1)G_i(2)|\rho_-\rangle, \tag{5.3}$$

in which the G_i and G_f are operators of the form (3.4) appropriate for the description of the initial and final states. $\mathfrak{U}_{\text{rel}}'$ is, formally, a Pauli operator, and will be called the *Pauli* equivalent operator of $\mathfrak{U}_{\text{rel}}$, since in terms of it the relativistic first Born approximation cross section (for positive energy states) is formally the same as the nonrelativistic one, except for constant factors. We shall use the prime and the term "Pauli equivalent operator" for any operator of this type.

To order v^2/c^2, the neutron–proton cross section for unpolarized initial and final particles is found to be[9a]

$$\sigma(\theta)=\sigma_{NR}(\theta)+\frac{\mu^2}{32\pi^2\hbar^4}Tr(V\mathfrak{U})(YH^{(2)}). \tag{5.4}$$

The unfamiliar terms in this expression are defined as follows:

$$\sigma_{NR}(\theta)=\frac{\mu^2}{64\pi^2\hbar^4}Tr(V\mathfrak{U})^2 \tag{5.5}$$

is the nonrelativistic cross section,

$$\mathfrak{U}=\mathfrak{U}(\mathbf{p}_{if})=\langle \mathbf{p}_f|U|\mathbf{p}_i\rangle \tag{5.6}$$

being the momentum matrix element of the nonrelativistic interaction. $H^{(2)}$ is that part of $\mathfrak{U}_{\text{rel}}'$ which is hermitian in σ-spin and of second order in v/c; we shall henceforth, where necessary, use superscripts in parentheses to indicate the order in v/c of any operator. The trace Tr is to be taken over a complete set of two-particle spin states. The dictates of the Pauli principle, and the effect of the operator $\boldsymbol{\tau}_1\cdot\boldsymbol{\tau}_2$, are contained in the operator

$$Y=-\tfrac{1}{2}(1+P_pP_\sigma), \tag{5.7}$$

where P_σ is the σ-spin exchange operator, and P_p interchanges $\mathbf{p}_{1i}$ and $\mathbf{p}_{1f}$ wherever they occur in $\mathfrak{U}$.

The way in which terms of higher than zero order in v/c are separated off, can be seen as follows. If the expression (3.4) is used explicitly for all the G's in (5.3) and the multiplication then carried out, one obtains a sum of terms of zero to fourth order in $cp/(E+\mu c)$, or, essentially, in v/c. The zero-order term must be just $\mathfrak{U}$. The first-order term vanishes for all operators that we shall use (see Sec. VI for criteria of selection of these operators). The second-order term produces the v^2/c^2 contribution, i.e., the second term of (5.4), which is seen to have the form of an interference term between the nonrelativistic scattering amplitude and that due to the "hermitian" part of the second-order Pauli equivalent operator of the interaction.

VI. APPLICATION TO TWO NONRELATIVISTIC INTERACTIONS; RESULTS

The nonrelativistic interactions that we shall deal with in this paper can be written in the general form

$$V(\mathbf{r})=\tfrac{1}{3}\boldsymbol{\sigma}_1\cdot\boldsymbol{\sigma}_2\boldsymbol{\tau}_1\cdot\boldsymbol{\tau}_2 V_0[(1-\tfrac{1}{2}g)f_0(r)+\tfrac{1}{2}g\boldsymbol{\sigma}_1\cdot\boldsymbol{\sigma}_2 f_0(r)+\gamma S_{12}(\mathbf{r})f_2(r)], \tag{6.1}$$

where V_0, g and γ are constants; r means $|\mathbf{r}|$; and

$$S_{12}(\mathbf{r})=3[(\boldsymbol{\sigma}\cdot\mathbf{r})(\boldsymbol{\sigma}_2\cdot\mathbf{r})/r^2]-\boldsymbol{\sigma}_1\cdot\boldsymbol{\sigma}_2. \tag{6.2}$$

$f_0(r)$ and $f_2(r)$ embody the spatial dependence of the central and tensor parts of the interaction respectively; these are so far abitrary.

In order to investigate the relativistic corrections, we need $\mathfrak{U}(\mathbf{p}_{if})$ (defined in Sec. V). For convenience in the relativistic work we break up the tensor force into its two components, defining

$$s(\mathbf{p}_{if})=(\boldsymbol{\sigma}_1\cdot\mathbf{p}_{if}\boldsymbol{\sigma}_2\cdot\mathbf{p}_{if})/p_{if}^2. \tag{6.3}$$

Then

$$\mathfrak{U}(\mathbf{p}_{if})=\frac{4\pi}{3}V_0\{\tfrac{3}{2}g\varphi_0(p_{if})+[(1-\tfrac{3}{2}g)\varphi_0(p_{if})+\gamma\varphi_2(p_{if})]\boldsymbol{\sigma}_1\cdot\boldsymbol{\sigma}_2-3\gamma s(\mathbf{p}_{if})\varphi_2(p_{if})\}, \tag{6.4}$$

[9a] *Note added in proof:* It will be noted that in the present formulation, the relativistic correction [second term of Eq. (5.4)] is dynamically independent of the nonrelativistic cross section since it contains the factor $H^{(2)}$ in the trace. The normalization factor C^2 [see Eq. (3.2)] coming from the Dirac state vectors cancels, to order v^2/c^2, the relativistic corrections contained in the density-of-states factor common to all terms in the cross section. The net result is that $\sigma_{NR}(\theta)$ of (5.4) would, if $\sigma(\theta)$ were calculated exactly, be multiplied by a factor differing from unity only in terms of order v^4/c^4, these terms amounting to only 0.03 percent at 90 Mev. This wholly negligible amount is the entire "kinematic" correction in our interpretation, which we think is recommended by the natural way in which it emerges from the above analysis (a completely non-arbitrary definition of the "kinematic" correction is evidently impossible). It has, of course, been customary to omit the C^2 factor in defining the correction; this explains the difference between our result and that of Case and Pais [K. M. Case and A. Pais, Phys. Rev. **80**, 203 (1950)].

where

$$\varphi_n(p_{ij})=\int_0^\infty j_n(p_{ij}r/\hbar)f_n(r)r^2dr;$$

j_0 and j_2 are spherical bessel functions,

$$j_n(x)=(\pi/2x)^{\frac{1}{2}}J_{n+\frac{1}{2}}(x).$$

We regard $\mathfrak{U}(\mathbf{p}_{ij})$ as a linear combination of the Pauli operators **1**, $\boldsymbol{\sigma}_1\cdot\boldsymbol{\sigma}_2$, $s(\mathbf{p}_{ij})$, and 0, with coefficients depending on $\mathbf{p}_{ij}$ and on the constants g and γ. Then the relativistic generalization of $\mathfrak{U}(\mathbf{p}_{ij})$ will be obtained by (a) replacing $\mathbf{p}_{ij}$ by the magnitude of its corresponding four-vector (this four-vector has zero fourth component in the CM system, and its space part is equal to the nonrelativistic $\mathbf{p}_{ij}$ and (b) making the operator replacements, for each Pauli operator,

Pauli operator → linear combination of relativistic equivalent Pauli operators;

where the "relativistic equivalent Pauli operators" are deduced from invariant operators (a) to (m), Sec. IV. Formally, the coefficients of all the relativistic operators on the right-hand side that reduce to the Pauli operator on the left-hand side must add up to unity, and the coefficients of relativistic operators that reduce to zero may have arbitrary magnitude (so far as the zero-energy limit is concerned; see Sec. I).

It did not seem worth while at present to attempt an exhaustive investigation, such as would consist of incorporating all the operators (a) to (m) into the generalized interaction in all allowable combinations, for example. The criterion of choice was to omit zero-reducing operators, with the exception of PPf_0, which is a particularly simple and fundamental case, and to replace each Pauli operator by a linear combination of only those two operators of the list which reduce to it. The operators that are omitted, other than those that vanish identically or have vanishing matrix elements between positive energy states, are *differences* between operators that reduce to the same Pauli equivalent operator, and (f), (k), and (m), all linear in the momentum. The last three operators have Pauli equivalent operators with nonvanishing terms of first order in v/c. In general, they will thus yield relativistic corrections to the cross section of order v/c, while the operators that we include yield corrections of order v^2/c^2. This v/c cross-section contribution turns out to be zero for (m), but is not zero for (f) and (k). So long as one hopes to adjust relativistic terms to fit theory to experiment at 90 Mev, without introducing appreciable relativistic effects in the moderate and low energy regions, operators that contribute to first order in v/c are substantially less important than those which contribute only in higher orders, since their relativistic terms decrease more slowly with decreasing energy. If the desired type of adjustment cannot be achieved with v^2/c^2 corrections, the same should hold still more strongly with v/c corrections.

Instead of writing down the Dirac spin-momentum operators that will be used, we shall give just the momentum matrix elements, derived from them, which are to be used as spin operators in $\mathfrak{U}_{\tau\sigma 1}$. We use the following notation. The subscript u refers to a Dirac operator reducing to the unit Pauli operator; σ to the Pauli $\boldsymbol{\sigma}_1\cdot\boldsymbol{\sigma}_2$; s to the Pauli $s(\mathbf{p}_{ij})$; and n to the Pauli null operator. Further subscripts are used to distinguish between Dirac operators both of which reduce to the same Pauli operator. The operators to be used are then

$$\begin{aligned}
&\zeta_{u1}=\beta(1)\beta(2),\\
&\zeta_{u2}=1-\boldsymbol{\alpha}(1)\cdot\boldsymbol{\alpha}(2),\\
&\zeta_{\sigma 1}=\beta(1)\beta(2)[\boldsymbol{\sigma}(1)\cdot\boldsymbol{\sigma}(2)+\boldsymbol{\alpha}(1)\cdot\boldsymbol{\alpha}(2)],\\
&\zeta_{\sigma 2}=\boldsymbol{\sigma}(1)\cdot\boldsymbol{\sigma}(2)-\rho_1(1)\rho_1(2),\\
&\zeta_{s1}=\beta(1)\beta(2)[s(\mathbf{p}_{ij})-\rho_1(1)\rho_1(2)s(\mathbf{p}_{ij})+\boldsymbol{\alpha}(1)\cdot\boldsymbol{\alpha}(2)],\\
&\zeta_{s2}=s(\mathbf{p}_{ij}),\\
&\zeta_n=\rho_2(1)\rho_2(2).
\end{aligned}\tag{6.5}$$

These are the forms obtained in the CM system for two particles of equal mass, i.e., with the fourth component of the momentum-energy vector $(\mathbf{p}_{ij}, iE_{ij}/c)$ equal to zero, from the following operators of Sec. IV, respectively: (a), (d), (g), (i), (g) minus (h), (*j*), and (l). (In the case of ζ_{s1} and ζ_{s2}, the original operators have been divided by $|\mathbf{p}_{ij}|^2$.)

With our restrictions, the equivalent Pauli $\mathfrak{U}_{\tau\sigma 1}'(\mathbf{p}_{ij})$ corresponding to the $\mathfrak{U}(\mathbf{p}_{ij})$ of (6.4) is

$$\begin{aligned}
\mathfrak{U}_{\tau\sigma 1}'(\mathbf{p}_{ij})=\frac{4\pi}{3}V_0\{&\tfrac{3}{2}g[a_{u1}\zeta_{u1}'+a_{u2}\zeta_{u2}']\varphi_0(p_{ij})\\
&+[1-\tfrac{3}{2}g][a_{\sigma 10}\zeta_{\sigma 1}'+a_{\sigma 20}\zeta_{\sigma 2}']\varphi_0(p_{ij})\\
&+\gamma[a_{\sigma 12}\zeta_{\sigma 1}'+a_{\sigma 22}\zeta_{\sigma 2}']\varphi_2(p_{ij})\\
&-3\gamma[a_{s1}\zeta_{s1}'+a_{s2}\zeta_{s2}']\varphi_2(p_{ij})\\
&+a_{n0}\zeta_n'\varphi_0(p_{ij})+a_{n2}\zeta_n'\varphi_2(p_{ij})\},
\end{aligned}\tag{6.6}$$

with the condition that the sum of the a's in any bracket is equal to unity. The ζ' in (6.6) are primed to indicate that equivalent Pauli operators are meant. Expressions for the equivalent Pauli operators of the ζ' are given in the Appendix. Note that the coefficients of $\zeta_{\sigma 1}'$ and $\zeta_{\sigma 2}'$ that are coupled with $\varphi_0(p_{ij})$ are treated independently of those that are coupled with $\varphi_2(p_{ij})$.

The cross section in the Born approximation [Eq. (5.4)] can be written as

$$\sigma(\theta)=\sigma_{NR}(\theta)+\sum_i a_i\sigma_i^{(2)}(\theta),\tag{6.7}$$

where $\sigma_i^{(2)}(\theta)$ is the second-order-in-v/c contribution due to the operator ζ_i with all factors that appear with it in Eq. (6.6) *except* the factor $a_i=a_{u1}, a_{u2}, a_{\sigma 10}, \cdots$; e.g.,

$$\begin{aligned}
\sigma_{u1}^{(2)}(\theta)=(\mu^2/64\pi^2\hbar^4)\cdot&\tfrac{3}{2}g\cdot 2Tr[(V\mathfrak{U})\\
&\cdot(4\pi/3)V_0\cdot VH^{(2)}(\zeta_{u1}')\varphi_0(p_{ij})].
\end{aligned}\tag{6.8}$$

Simplified expressions for evaluating the traces are given in the Appendix. The expression for $\sigma_{NR}(\theta)$ is also given for reference.

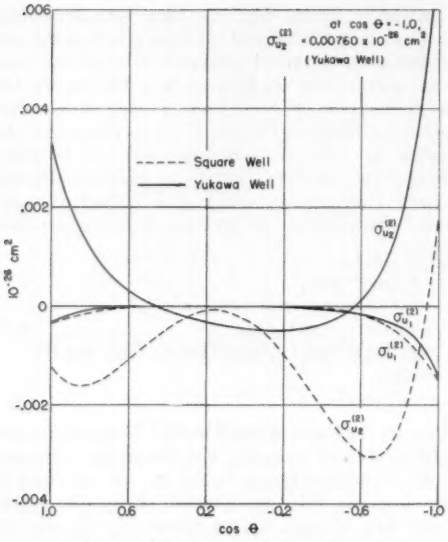

FIG. 1. Relativistic corrections $\sigma_{u1}^{(2)}$, $\sigma_{u2}^{(2)}$.

As stated in Sec. I, relativistic corrections have been calculated for two nonrelativistic interactions of the form (6.1): (1) The Rarita-Schwinger square-well interaction,[10] and (2) a Yukawa interaction with constants computed by Feshbach[11] for "best" fit of the low-energy data.

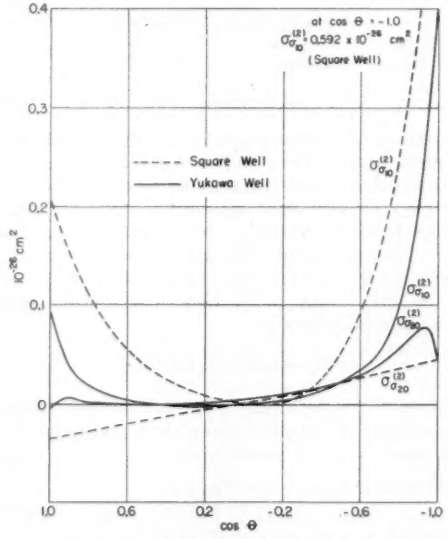

FIG. 2. Relativistic corrections $\sigma_{\sigma 10}^{(2)}$, $\sigma_{\sigma 20}^{(2)}$.

[10] W. Rarita and J. Schwinger, Phys. Rev. **59**, 436 (1941).
[11] Private communication (to be published).

The numerical results for the second-order contributions $\sigma_i^{(2)}(\theta)$ that appear in Eq. (6.7) are plotted in Figs. 1 to 5 for the two interactions. It will be noted that the $\sigma_i^{(2)}(\theta)$ are much more sensitive to the nonrelativistic interaction than is the nonrelativistic cross section. For purposes of comparison, the nonrelativistic cross sections given by the two interactions are plotted in Fig. 6; the experimental points are also shown. The nonrelativistic cross section for interaction (1) was obtained by extrapolation from the 100-Mev calculations of Ashkin and Wu,[12] using the 90- and 100-Mev Born approximation results to give the proportion. In this way a considerable improvement over the straight Born approximation should be obtainable. For interaction (2), the nonrelativistic cross section was obtained by combining a Born approximation calculation for the triplet scattering with an exact calculation for singlet scattering.[13] In the latter case a substantial error probably still remains, although, as will be argued later, it should not affect our conclusions. The nonrelativistic total cross sections obtained are

$$\sigma_{NR}=14.1\times10^{-26}\text{ cm}^2\text{ (Square well)},$$
$$\sigma_{NR}=9.59\times10^{-26}\text{ cm}^2\text{ (Yukawa well)};$$

these are to be compared with the experimental value[1] of 7.6×10^{-26} cm².

VII. ANALYSIS OF RESULTS

In this section we analyze the properties of the relativistic corrections obtained, by comparing them quantitatively with the discrepancies in total cross section

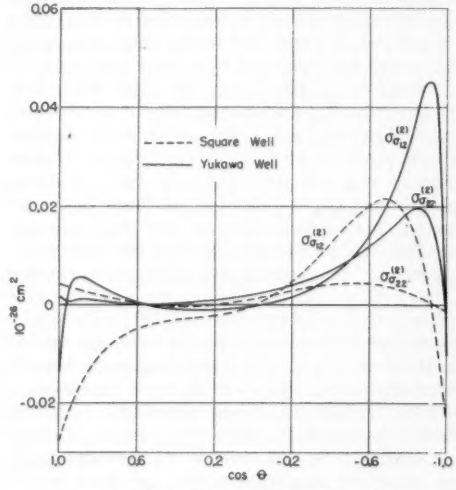

FIG. 3. Relativistic corrections $\sigma_{\sigma 12}^{(2)}$, $\sigma_{\sigma 22}^{(2)}$.

[12] Ashkin and Wu, Phys. Rev. **73**, 973 (1948).
[13] The author is indebted to Professor Feshbach for the results of the singlet scattering calculation. Its use eliminates the substantial error that would result from the very large repulsive singlet odd potential if the Born approximation were used.

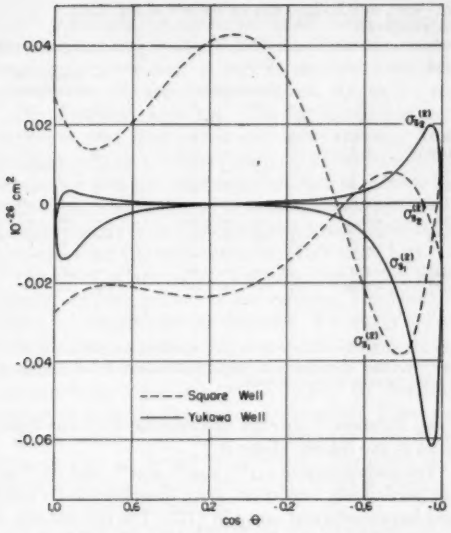

FIG. 4. Relativistic corrections $\sigma_{s1}^{(2)}$, $\sigma_{s2}^{(2)}$.

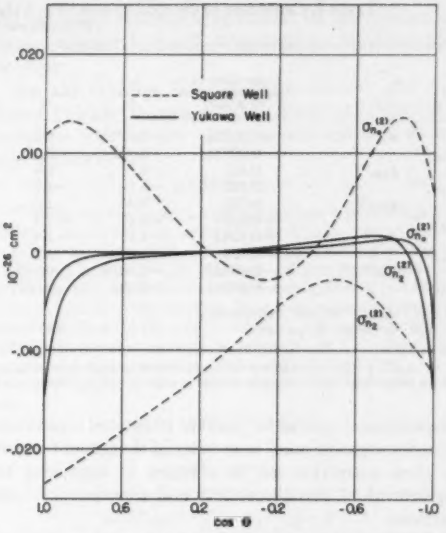

FIG. 5. Relativistic corrections $\sigma_{n0}^{(2)}$, $\sigma_{n2}^{(2)}$.

and angular distribution between nonrelativistic theory and experiment.

The shape characteristics of n–p scattering curves are usually expressed through the ratio of the 180° value to that at the minimum of the curve, and to that at 0°. In this case the point $\cos\theta=0.8$ will be used instead of $\theta=0°$, because the data do not extend to 0°. Furthermore, the Yukawa curves fluctuate very greatly in the immediate neighborhood of 180°, so that the point $\cos\theta=-0.9$, where they behave more quietly, will be used instead; this will result in a better measure of their effect in the back-scattering portion of the curve (any very rapid fluctuations of this kind if they occurred in nature, would of course be smoothed out in the experimental results, due to finite resolution).

The required shape improvements can now be summed up:

(a) Reduction of the ratio $\sigma(-0.9)/\sigma(0.2)$.
Experimental value: 2.6.
Square well, nonrel.: 7.9.
Yukawa well, nonrel.: 5.7 (Born approx. triplet, exact singlet).

(b) Reduction of the ratio $\sigma(-0.9)/\sigma(+0.8)$.
Experimental value: 1.4.
Square well, nonrel.: 3.0.
Yukawa well, nonrel.: 3.6 (Born approx. triplet, exact singlet).

A convenient criterion for the shape-improving characteristics of the relativistic corrections in these two respects is the following: Let

$$R_i(\cos\theta)=\sigma_i^{(2)}(\cos\theta)/\sigma_{NR}(\cos\theta).$$

Then we have the following conditions on the sign of any a_i in Eq. (6.7) for shape improvement with respect to the desiderata (a) and (b), respectively:

(a) $R_i(0.2)>(<)R_i(-0.9)$ requires $a>(<)0$. (7.1)
(b) $R_i(+0.8)>(<)R_i(-0.9)$ requires $a>(<)0$.

The correlation of the signs required for shape improvement with that required for total cross-section

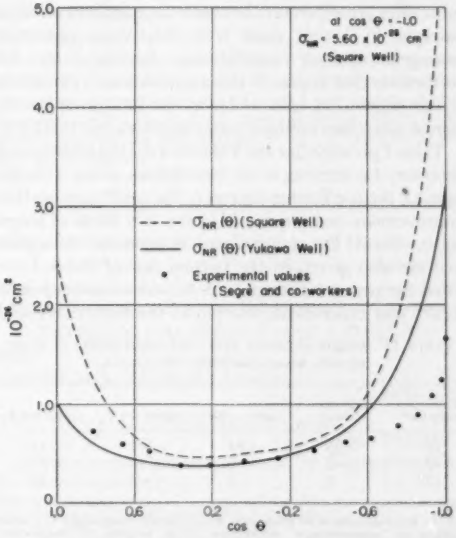

FIG. 6. Nonrelativistic cross sections.

TABLE I. Corrections to the total cross section. Values of $R_i(-0.9)$, $R_i(0.2)$, $R_i(+0.8)$ for the $\sigma_i^{(2)}$ of Eq. (7.2); $R_i(\text{total})=\sigma_i^{(2)}(\text{total})/\sigma_{NR}(\text{total})$.

		Corrections to total cross section (10^{-28} cm^2)	Yukawa well R_i(total) %	$R_i(-0.9)$ %	$R_i(0.2)$ %	$R_i(+0.8)$ %	Correlations[a] a	b	c	d	Square-well correlations[a] a	b	c	d
$\sigma_{u-}^{(2)}$	$\sigma_{u1}^{(2)}$	−0.00183	−0.019	−0.035	0.0017	−0.014	+	+	+	+	+	+	+	+
		0.00934	0.097	0.21	−0.089	0.22	−	−	−	+?	+	−	−	−
$\sigma_{\sigma 0-}^{(2)}$	$\sigma_{\sigma 10}^{(2)}$	0.427	4.5	8.0	−0.44	3.2	−	*	−	−	−	−	−	−
	$\sigma_{\sigma 12}^{(2)}$	−0.240	−2.5	−4.6	0.84	−2.9	+	+	+	+	+	?	+	−
$\sigma_{\sigma 2-}^{(2)}$		0.090	0.96	2.0	−0.27	0.66	−	−	−	−	−	−	−	−
	$\sigma_{s1}^{(2)}$	−0.0259	−0.27	−1.1	0.53	−0.52	+	+	+	+	−	+	+	+
$\sigma_{s-}^{(2)}$		−0.1045	−1.1	−2.4	−0.085	−1.2	+	+	+	+	−	+	+	+
	$\sigma_{n0}^{(2)}$	0.138	1.4	3.2	0.11	1.5	−	−	−	−	+	−	−	−
$\sigma_{n2}^{(2)}$		−0.000327	−0.0034	0.036	−0.0051	−0.12	+	−	−	−	−	?	−	+
		−0.00817	−0.085	−0.067	−0.021	−0.35	+	?	+	−	+	−	−	−
$N-R$ theory minus experiment, ratio to theory (in percent)			21	53	0	−21								

[a] Column a: Sign of coefficient for improvement of total cross section. Column b: Net sign of coefficient for shape improvement. Column c: Sign for shape improvement with respect to ratio $\sigma(-0.9)/\sigma(+0.2)$. Column d: Same as c, but for ratio $\sigma(-0.9)/\sigma(+0.8)$.

improvement (minus for positive integrated corrections, plus for negative ones) is an index of the extent to which a given correction can be effective in improving the agreement of the theoretical and experimental cross sections.

For the present purpose it is convenient to eliminate the necessity of referring to the condition that the two a's of any pair add up to unity, by replacing a_{u1} by $1-a_{u2}$, $a_{\sigma 10}$ by $1-a_{\sigma 20}$, etc., in Eq. (6.7). We then obtain for the summation in (6.7):

$$\sum a_i\sigma_i{}^{(2)}=\sigma_{u1}{}^{(2)}+a_{u2}\sigma_{u-}{}^{(2)}+\sigma_{\sigma 10}{}^{(2)}+a_{\sigma 20}\sigma_{\sigma 0-}{}^{(2)}+\sigma_{\sigma 12}{}^{(2)}+a_{\sigma 22}\sigma_{\sigma 2-}{}^{(2)}+\sigma_{s1}{}^{(2)}+a_{s2}\sigma_{s-}{}^{(2)}+a_{n0}\sigma_{n0}{}^{(2)}+a_{n2}\sigma_{n2}{}^{(2)}, \quad (7.2)$$

where the second-order σ's with minus signs in the subscripts are *differences* between the members of those pairs in (6.7) that come from relativistic operators having a common nonrelativistic limiting form. All coefficients that appear in this expression are completely at our disposal at least as far as the limit $v=0$ is concerned, since they multiply terms that vanish in this limit.

Table I presents (for the Yukawa well) the information necessary for arriving at all correlations, along with the signs of the coefficients necessary for total cross-section improvement and [from (7.1)] the two kinds of shape improvement. For comparison, the signs for the square well are also given. In the bottom row of Table I are listed the percent discrepancies between nonrelativistic theory and experiment, referred to the theory. Each of these numbers is directly comparable with the quantities in the column above it.

The correlations of $\sigma_{u1}{}^{(2)}$, $\sigma_{\sigma 10}{}^{(2)}$, $\sigma_{\sigma 12}{}^{(2)}$, and $\sigma_{s1}{}^{(2)}$ are not particularly important, since these are mostly small and have coefficient unity in (7.2). The correlations of principal importance are those of $\sigma_{u-}{}^{(2)}$, $\sigma_{\sigma 0-}{}^{(2)}$, $\sigma_{\sigma 2-}{}^{(2)}$, $\sigma_{s-}{}^{(2)}$, $\sigma_{n0}{}^{(2)}$ and $\sigma_{n2}{}^{(2)}$; a perfect correlation for any of these consists in having the *same* sign, either plus or minus, across the last four columns of the table.

It will be seen that for the square-well interaction most of the correlations are rather poor, though not entirely unfavorable. Much better correlations are obtained with the Yukawa interaction; these are, in fact, qualitatively almost perfect except for $\sigma_{n0}{}^{(2)}$ and $\sigma_{n2}{}^{(2)}$.

We can utilize Table I to obtain a rough idea of the magnitudes of the coefficients needed to adjust the nonrelativistic cross sections to experiment. These estimates will contain errors from several sources, to be described later, but arguments will be given to show that the errors do not interfere with an order of magnitude estimate. Only a few of the most favorable corrections will be used; since the coefficients required with these are already large enough to introduce substantial relativistic corrections at low energies, it is not necessary to go any further.

The procedure used in estimating the magnitudes of the coefficients will become clear on considering Table II, in which the results are presented. The first row of the table shows the percent discrepancies *after* the addition of $\sigma_{u1}{}^{(2)}+\sigma_{\sigma 10}{}^{(2)}+\sigma_{\sigma 12}{}^{(2)}+\sigma_{s1}{}^{(2)}$ (termed "nonarbitrary" corrections) to the nonrelativistic cross section, these being necessarily included in the cross section, formally speaking, if we use (7.2). These discrepancies are obtained by adding the percent R_i's for these corrections to the percent discrepancies in the last row of Table I; the resulting numbers are percent discrepancies referred to the uncorrected nonrelativistic theoretical cross section. If we now add $12\sigma_{\sigma 0-}{}^{(2)}$ to this result, we reduce the discrepancies to the amounts shown in row 2, Table II. If, instead, we subtract 18

TABLE II. Results obtained with trial adjustments of cross section, using relativistic corrections.

Discrepancy for*	Total cross section	$\cos\theta=-0.9$	$\cos\theta=+0.2$	$\cos\theta=+0.8$
(1)	+25	+61	−1	−18
(2)	−5	+6	+10	−53
(3)	0	+3	−3	−45

* (1) Discrepancies with respect to $N-R$ theory [Interaction (2)] after addition of "non-arbitrary" corrections. All in percent. (2) Same after addition of "non-arbitrary" corrections plus $12\sigma_{\sigma 0-}{}^{(2)}$. (3) Same after addition of "non-arbitrary" corrections minus $18\sigma_{s-}{}^{(2)}$.

$\sigma_{s-}{}^{(2)}$, the remaining discrepancies are those in row 3. The two corrections $\sigma_{s0-}{}^{(2)}$ and $\sigma_{s-}{}^{(2)}$ are the largest relativistic corrections, as well as the best individual ones for over-all curve-fitting purposes.

The difficulty with the Yukawa interaction corrections is that their values at $\cos\theta=-0.9$ and $+0.8$, although such as to correct the *ratio* $\sigma(-0.9)/\sigma(+0.8)$ in harmony with the other ratios, are such as to lower the $+0.8$ value, while it should be at least unchanged, if not actually raised a little. This is not a large effect absolutely, however, since the cross section is itself small here.

The effect of relativistic contributions of the magnitudes obtained above, at low energies, can be illustrated by considering the deuteron. For the Yukawa well, the mean value of v^2/c^2 for either particle in the deuteron is about 0.016. The coefficients twelve and eighteen then imply relativistic effects on deuteron properties of about 20 percent or 30 percent. These are quite substantial, and could of course turn out to be even greater in actual calculations. Moreover, the estimates given are, if anything, lower limits on the basis of the available information.

In emphasizing the largeness of the coefficients, it is well not to lose sight of one aspect of our results, already mentioned in the introductory section, which is highly favorable to the construction of a workable phenomenological interaction incorporating relativistic corrections; namely, the strikingly consistent correlations shown by Table I for the Yukawa corrections. These will contribute greatly to simplifying any eventual interaction of this type.

The errors due to the method of calculating the relativistic corrections remain to be discussed in relation to their possible effect on the above conclusions. In the first place, there is the use of the Born approximation. Guided by the form of the calculation, we might expect this error, relatively, to be of the same order as the relative error of the nonrelativistic Born approximation, a high estimate of which is perhaps 100 percent. This amount would not change our qualitative conclusions. There is also the neglect of terms of order higher than v^2/c^2; but since these are of order v^4/c^4, the relative error involved is nominally only 5 percent at 90 Mev.

A gross error in the relativistic corrections might occur if some components of the imaginary part of the Born nonrelativistic amplitude had the wrong sign [v. N. F. Mott and H. W. S. Massey, *Theory of Atomic Collisions*, 2d Ed. (Oxford University Press, London, 1949), p. 24]. This can easily occur, without making the Born *intensity* wrong, if any phase shifts are close to 90°. The only available information in this is the values of the phase shifts at 80 Mev for a square well and central forces, but with symmetric exchange.[14] These are all well under 90°.

The author is indebted to Professor Herman Feshbach for his original suggestion of this problem, for his understanding guidance during the entire course of the work, and for many concrete suggestions. He also wishes to thank Professor Victor F. Weisskopf for his interest in the work.

The aid of Mrs. Barbara Siegle Levine, and the Misses Patricia Boland, Hannah Paul, and Elizabeth Campbell, who did the computational work, is gratefully acknowledged.

[14] Bethe and Camac, Phys. Rev. **73**, 191 (1948).

APPENDIX

(1) When the Dirac spin-momentum operators, from which the ζ of (6.5) are derived, are substituted for U_{rel} in (5.2), and (3.4) is used for the G's in (5.3), the resulting operators are of zero to fourth order in $c\mathfrak{p}_{ij}/(E+\mu c^2)$. We shall here give the second-order part in $c\mathfrak{p}_{ij}/(E+\mu c^2)$ of the momentum matrix element [see (5.3)] of the operator obtained when the Dirac spin-momentum operator related to each of the ζ is substituted for U_{rel} in (5.2); this will be a Pauli spin operator, and will be designated by $\zeta'^{(2)}$, along with the subscript of the particular ζ from which it is obtained.

Much simplicity is gained by working in the CM system, in which

$$\mathfrak{p}_{2i}=-\mathfrak{p}_{1i}, \quad \mathfrak{p}_{2f}=-\mathfrak{p}_{1f};$$

hence also [see Eq. (2.2)]

$$\mathfrak{p}_i=\mathfrak{p}_{1i}, \quad \mathfrak{p}_f=\mathfrak{p}_{1f}.$$

The momentum exchange operator P_p turns $\mathfrak{p}_i$ into $-\mathfrak{p}_i$; we define

$$\mathfrak{p}_{if}=P_p\mathfrak{p}_{if}=P_p(\mathfrak{p}_i-\mathfrak{p}_f)=-\mathfrak{p}_i-\mathfrak{p}_f.$$

With energy conservation, $|\mathfrak{p}_i|=|\mathfrak{p}_f|$, and $\mathfrak{p}_{if}\cdot\mathfrak{p}_{if}=0$. The following expressions are then obtained in the CM system, for transitions in which energy is conserved ($D=c^2/(E+\mu c^2)^2$):

$$\zeta_{s1}'^{(2)}=D[\tfrac{1}{2}(\mathfrak{p}_{ij}^2-\mathfrak{p}_{if}^2)+i(\boldsymbol{\sigma}_1+\boldsymbol{\sigma}_2)\cdot\mathfrak{p}_i\times\mathfrak{p}_f],$$

$$\zeta_{s2}'^{(2)}=D[-\tfrac{1}{2}\mathfrak{p}_{ij}^2+\tfrac{3}{2}\mathfrak{p}_{if}^2-\mathfrak{p}_{ij}^2\boldsymbol{\sigma}_1\cdot\boldsymbol{\sigma}_2+\mathfrak{p}_{if}{}^2s(\mathfrak{p}_{ij}) -3i(\boldsymbol{\sigma}_1+\boldsymbol{\sigma}_2)\cdot\mathfrak{p}_i\times\mathfrak{p}_f],$$

$$\zeta_{\sigma1}'^{(2)}=D[-\mathfrak{p}_{ij}^2+(\tfrac{3}{2}\mathfrak{p}_{if}^2-\tfrac{1}{2}\mathfrak{p}_{ij}^2)\boldsymbol{\sigma}_1\cdot\boldsymbol{\sigma}_2+\mathfrak{p}_{if}{}^2s(\mathfrak{p}_{ij}) -2\mathfrak{p}_{if}{}^2s(\mathfrak{p}_{ij})-3i(\boldsymbol{\sigma}_1+\boldsymbol{\sigma}_2)\cdot\mathfrak{p}_i\times\mathfrak{p}_f],$$

$$\zeta_{\sigma2}'^{(2)}=D[\tfrac{1}{2}(\mathfrak{p}_{ij}^2-\mathfrak{p}_{if}^2)\boldsymbol{\sigma}_1\cdot\boldsymbol{\sigma}_2-\mathfrak{p}_{if}{}^2s(\mathfrak{p}_{if}) +2\mathfrak{p}_{if}{}^2s(\mathfrak{p}_{if})+i(\boldsymbol{\sigma}_1+\boldsymbol{\sigma}_2)\cdot\mathfrak{p}_i\times\mathfrak{p}_f],$$

$$\zeta_{s1}'^{(2)}=D[\mathfrak{p}_{if}{}^2\boldsymbol{\sigma}_1\cdot\boldsymbol{\sigma}_2+\tfrac{1}{2}(\mathfrak{p}_{ij}^2+\mathfrak{p}_{if}^2)s(\mathfrak{p}_{if})-\mathfrak{p}_{if}{}^2s(\mathfrak{p}_{if}) -\mathfrak{p}_{if}{}^2s(\mathfrak{p}_{if}\times\mathfrak{p}_{if})],$$

$$\zeta_{s2}'^{(2)}=-2D\mathfrak{p}_i{}^2s(\mathfrak{p}_{if}),$$

$$\zeta_{n}'^{(2)}=D\mathfrak{p}_{if}{}^2s(\mathfrak{p}_{if}).$$

(2) The second-order contributions to the cross section associated with any of the operators (6.5) are given by expressions constructed analogously to Eq. (6.8). We give here a compact expression for the result of the trace calculation, which is sufficiently general to be used with any of the $\zeta'^{(2)}$ listed in the first part of this Appendix.

Let

$$\mathfrak{IC}=\frac{4\pi}{3}V_0D\{f_1+\boldsymbol{\sigma}_1\cdot\boldsymbol{\sigma}_2f_2+s_+f_3+s_-f_4+s_\times f_5\}$$

where $f_1\cdots f_5$ are arbitrary functions of $\mathfrak{p}_{if}$ and $\mathfrak{p}_{if}$; and

$$s_+=\tfrac{1}{2}(1+P_p)s(\mathfrak{p}_{if}); \quad s_-=\tfrac{1}{2}(1-P_p)s(\mathfrak{p}_{if}); \quad s_\times=s(\mathfrak{p}_{if}\times\mathfrak{p}_{if}).$$

Then if $\mathfrak{U}$ is given by (6.4), the following expression holds in the CM system ($\mathfrak{p}_{ij}$, $\mathfrak{p}_{if}$, and $\mathfrak{p}_{if}\times\mathfrak{p}_{if}$ being mutually perpendicular):

$$Tr(V\mathfrak{IC})(V\mathfrak{U})=(4\pi/3)^2V_0{}^2D(A+4P_pA+2B+2P_pB),$$

where

$$A=2\{[3gf_1+(2-3g)(3f_2+f_3+f_5)]\varphi_0(\mathfrak{p}_{if}) +\gamma[-f_2-3f_4+2f_5]\varphi_2(\mathfrak{p}_{if})\},$$

$$B=2\{[3(1-g)f_1+(-1+3g)(3f_2+f_3+f_5)]\varphi_0(\mathfrak{p}_{if}) +\gamma[-f_2+3f_4+2f_5]\varphi_2(\mathfrak{p}_{if})\}.$$

(3) The nonrelativistic cross section in the Born approximation for the interaction (6.1) is

$$\sigma_{NR}(\theta)=\frac{\mu^2V_0{}^2}{3\hbar^4}\{[1-3g+3g^2][\varphi_0{}^2(\mathfrak{p}_{if})+4\varphi_0{}^2(\mathfrak{p}_{if})] +2[-1+6g-6g^2]\varphi_0(\mathfrak{p}_{if})\varphi_0(\mathfrak{p}_{if})+2\gamma^2[\varphi_2{}^2(\mathfrak{p}_{if}) -2\varphi_2(\mathfrak{p}_{if})\varphi_2(\mathfrak{p}_{if})+4\varphi_2{}^2(\mathfrak{p}_{if})]\}.$$

Cosmic-Ray Bursts and the Nucleonic Cascade*†

G. N. WHYTE
Palmer Physical Laboratory, Princeton University, Princeton, New Jersey
(Received November 13, 1950)

The cosmic-ray burst rate has been measured as a function of altitude at geomagnetic latitudes of 0°, 29°, and 35°N by means of a thin-walled spherical ionization chamber. The burst rate at an atmospheric depth of 20 g/cm² increases by a factor of 6 between 0° and 52°. When the data are corrected for the effects of heavy primary nuclei, the residual rates, believed due almost entirely to nuclear disintegrations, show maxima below the top of the atmosphere. The maxima at 0°, 29°, 35°, and 52° occur at depths of approximately 100, 70, 60, and 50 g/cm² respectively.

I. INTRODUCTION

THE establishment of the fact that, at mountain altitudes and above, a thin-walled ionization chamber can be used as a detector of the radiation producing nuclear disintegrations[1,2] has led to the use of such chambers for the investigation of the altitude dependence of this "star-producing" component. The work of Bridge and Rossi[3] at mountain and B-29 altitudes, of Hulsizer,[4] Coor,[5] and McClure and Pomerantz[6] at balloon altitudes, and of Tatel and Van Allen[7] at rocket altitudes gives the variation of the burst rate in thin-walled ion chambers through the entire atmosphere in the neighborhood of 52°N. These results indicate an exponential decrease in the lower atmosphere with an absorption length close to 140 g/cm², in good agreement with the value for stars in photographic emulsions.[8] At high altitudes the data appear to differ somewhat from the simple absorption of an isotropic primary component,[9] and, in fact, when the rates are corrected for the contribution of heavy primary nuclei,[6,10] they show an initial build-up below the top of the atmosphere.

The purpose of the experiments to be described was to extend the investigation to higher average primary energies by making high altitude burst measurements at lower latitudes. To this end, five balloon flights were made from the *U. S. S. Norton Sound* in the Pacific during the summer of 1949.

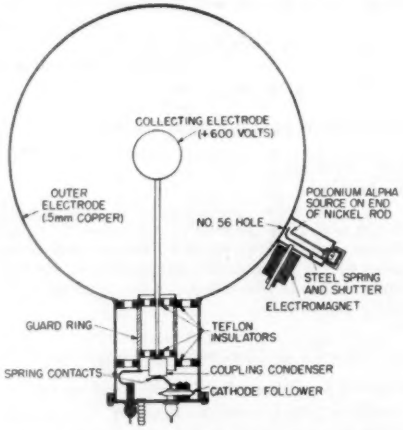

FIG. 1. Cross section through ionization chamber.

II. EXPERIMENTAL METHOD

The experimental equipment was substantially the same as that used by Coor and described in detail by him.[11] It was comprised of the ion chamber with its associated amplifier and telemetering equipment mounted in a light balloon-borne gondola, and a receiving and recording station on the ship.

The chamber (Fig. 1) consisted of a spherical copper shell, 30 cm in diameter and 0.054 cm in wall thickness,

TABLE I. Schedule of flights. The two flights made by Coor at 52° are included.

Date	Geographic point of launching	Geomagnetic latitude	Maximum altitude (ft)	g/cm²	Duration (hr)
July 11, 1949	00°11′N 160°03′W	0°	103,000	9	3
July 16, 1949	01°30′N 157°30′W	2°	95,000	14	4.7
July 20, 1949	00°01′N 158°21′W	0°	85,000	22	7
August 9, 1949	27°40′N 148°10′W	29°	88,000	19	6
August 13, 1949	30°25′N 129°52′W	35°	93,000	15	9
January 27, 1948	Princeton, N. J.	52°	92,000	16	3.8
March 1, 1948	Princeton, N. J.	52°	50,000	120	3.5

* This work was assisted by the joint program of the ONR and AEC.

† This article is based upon a thesis submitted to Princeton University in partial fulfilment of the requirements for the degree of Doctor of Philosophy.

[1] H. S. Bridge, Phys. Rev. **72**, 172 (1947).
[2] Bridge, Hazen, Rossi, and Williams, Phys. Rev. **74**, 1083 (1948).
[3] H. S. Bridge and B. Rossi, Phys. Rev. **71**, 379 (1947).
[4] R. I. Hulsizer, Phys. Rev. **73**, 1252 (1948).
[5] T. Coor, Princeton University thesis (1948), (to be published).
[6] G. W. McClure and M. A. Pomerantz, Phys. Rev. **79**, 911 (1950).
[7] H. E. Tatel and J. A. Van Allen, Phys. Rev. **73**, 87 (1948).
[8] Bernardini, Cortini, and Manfredini, Phys. Rev. **74**, 845 (1948); **74**, 1878 (1948).
[9] B. Rossi, Revs. Modern Phys. **20**, 537 (1948).
[10] G. N. Whyte, Phys. Rev. **78**, 321 (1950); **78**, 630 (1950).
[11] Coor, Snow, and Darago, Rev. Sci. Instr. (to be published).

and a concentric spherical collecting electrode, 5 cm in diameter, maintained at 600 volts positive with respect to the shell. The use of pure argon at 1.4 atmos pressure as the chamber gas permitted electron collection to be employed. Periodic calibration of the over-all response of the system was provided by a polonium source mounted on the chamber; a number of alpha-particles from this source were allowed to dissipate approximately 5.2 Mev each in the gas every 15 minutes. Burst sizes between 0.7 and 20 Po-alpha could be detected.

Pulses due to ionization taking place in the chamber gas were magnified by a linear amplifier (rise time 3 μsec, decay time 50 μsec), before being fed to the telemetering circuit. Here they were converted to a form

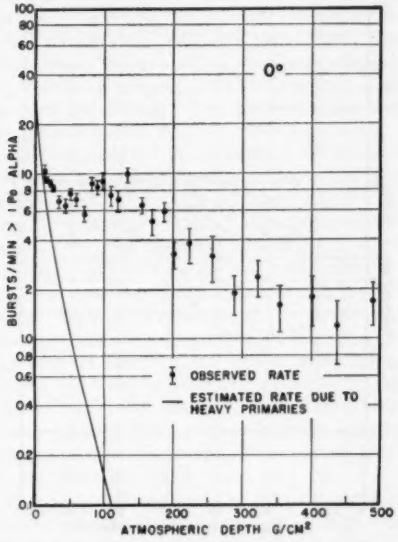

FIG. 2. Burst rate vs atmospheric depth at 0° geomagnetic.

more suitable for transmission and allowed to modulate an audiofrequency signal. A second audiofrequency channel carried pressure information from an aneroid barometer and temperature information from a temperature-sensitive resistor. The two audio channels finally frequency-modulated an rf channel which transmitted the information to the receiving station on the ship. There it was decoded and recorded on a moving strip of photographic paper.

The contents of the gondola were protected from extremes of temperature by a cellophane wrapping, the chamber being shielded from the direct rays of the sun by a layer of aluminum foil. The gondola was lifted by a cluster of Dewey and Almy J-2000 balloons which gave a rate of rise around 500 ft/min to a maximum altitude between 80,000 and 100,000 ft. In some flights

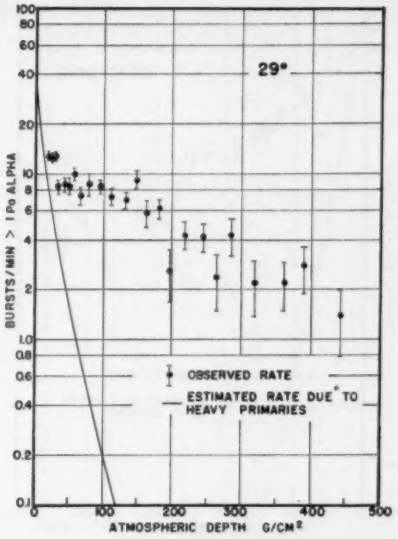

FIG. 3. Burst rate vs atmospheric depth at 29° geomagnetic.

data were obtained during the descent as well as the ascent.

III. EXPERIMENTAL RESULTS

Three flights were carried out at the geomagnetic equator, one at 29°N, and one at 35°N. A summary of information pertaining to these five flights is presented

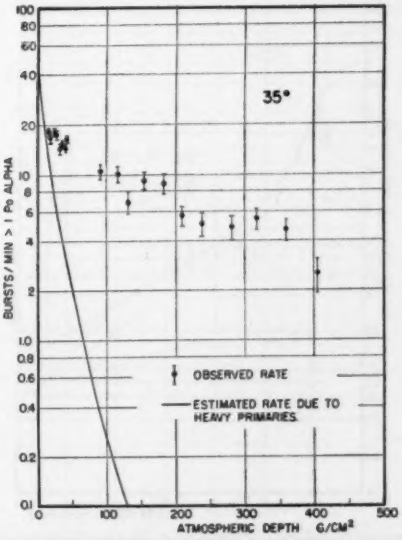

FIG. 4. Burst rate vs atmospheric depth at 35° geomagnetic.

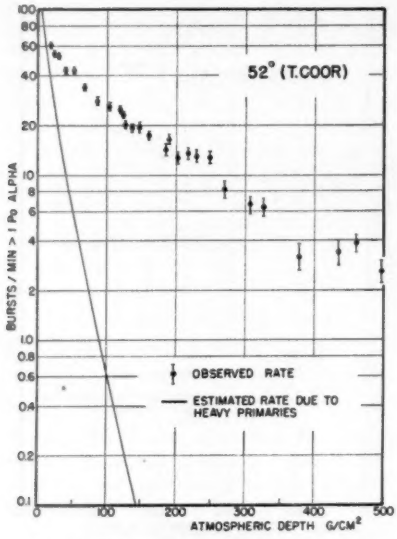

FIG. 5. Burst rate vs atmospheric depth at 52° geomagnetic (T. Coor, reference 5).

in Table I, together with the corresponding data for the two flights made with an identical chamber by Coor at 52°.

Figures 2 to 5 show the variation of the burst rate with atmospheric depth. The rates given are for all bursts greater than 1 Po-alpha in size, averaged over one or more 5-min intervals. In the 0°-latitude case the results for the three flights, which show no significant differences, have been averaged together. All rates have been corrected for the background rate at sea level, due principally to alpha-particles from radioactive materials in the chamber walls.

Despite the poor statistics, the most noticeable feature of Figs. 2 to 5 is the apparent maximum in the burst rate at 0° at a depth of about 100 g/cm². At 29° there appears to be a plateau in this region, while at 35° the data between 40 and 80 g/cm² are uncertain, so that it is difficult to determine the shape of the curve. At 52° there is no sign of either a maximum or a plateau. A check on the sizes of the Po calibration pulses showed that the effect at 0° could not be due to changes in the gain of the equipment, a fact supported by the reproducibility of the results in different flights. Pulse-size distributions plotted around the minimum at 50 g/cm² and around the maximum at 100 g/cm² show that the rate at the latter depth was consistently greater over the range of burst sizes observed (Fig. 6). Thus, the effect cannot be due to spurious pulses of one particular size, nor is it likely to be the result of a statistical fluctuation. The data at the lower latitudes, thus, indicate a real maximum in the cosmic-ray burst rate well below the top of the atmosphere.

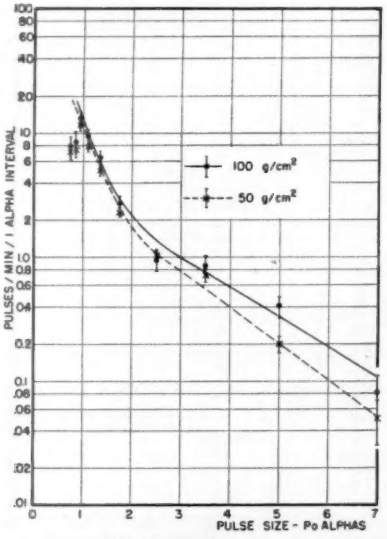

FIG. 6. Comparison of differential pulse size distributions at 50 and 100 g/cm² at 0° geomagnetic.

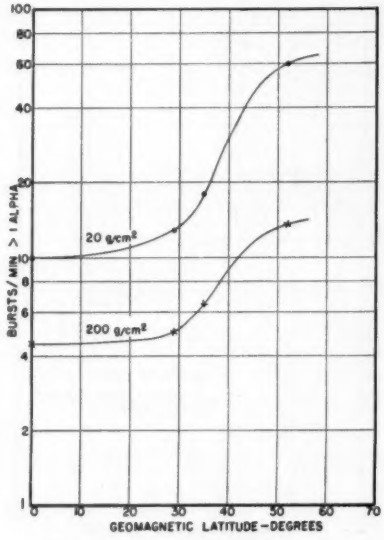

FIG. 7. Latitude variation of burst rate.

Figure 7 shows the latitude variation of the burst rate at two different altitudes. It is of interest to note that at high altitudes (20 g/cm²) the rate increases by a factor of 6 between 0° and 52°, whereas at a depth of 200 g/cm² this factor is only 3.

IV. DISCUSSION

Three types of phenomenon should be able to produce detectable bursts in the chambers used: electron showers, heavy primary nuclei, and nuclear disintegrations in or near the chamber walls. Of these, the contribution of the first is negligible[1,2,5] and that of the second can be estimated from other measurements; therefore, the rate due to nuclear disintegrations can be found.

In order to estimate the rate due to heavy primary nuclei, one needs to know what charge a relativistic nucleus must have before it can cause a burst greater that 1 Po-alpha by ionization in passing through the chamber. On the assumption that all δ-rays of energies less than about 200 kev dissipate most of their energies in the chamber gas, the Bethe-Bloch formula gives a mean energy loss of 70 kev for singly charged primaries crossing the chamber. (A mean path length through the chamber of 20 cm has been used here.) Taking the energy loss to be proportional to Z^2, one finds that primary particles of charge 9 or greater should produce bursts greater than 1 Po-alpha. The flux of such particles at the top of the atmosphere at 52° can be estimated from the measurements of Bradt and Peters[12] to be $0.55\pm0.16\times10^{-3}$ nuclei cm^{-2} sec^{-1} sterad^{-1}; the resulting burst rate is 150/min. Assuming isotropic incidence, so that the variation with depth, t, is of the form $N(t)=N(0)[e^{-t/L}+E_1(-t/L)]$, and using for L the collision mean free paths measured as a function of charge by Bradt and Peters, one arrives at the curve of burst rate *vs* altitude shown in Fig. 5 (solid line). From the preliminary energy spectrum for heavy primaries calculated by Vallarta[13] and the geomagnetic cut-off energies[14,15] at 0°, 29°, and 35°, one can now estimate the heavy-primary fluxes at these latitudes and thence obtain the corresponding curves of burst rate *vs* altitude. These are shown in Figs. 2, 3, and 4.

It may be worth emphasizing that the burst rates just calculated arise from particles of such high specific ionization that they cause bursts greater than 1 Po-alpha simply in passing through the chamber. Such particles are detected with 100 percent efficiency, in contrast to ordinary star-producing particles which are detected with an efficiency of the order of 1 percent. Thus, at the altitudes where heavy primaries exist in appreciable numbers their contribution to the burst rate is disproportionately large.

The results of subtracting the estimated heavy primary rates from the observed total rates are shown in Figs. 8 to 11. (The errors shown include the statistical errors in the burst measurements and in the heavy-primary fluxes, and an estimate of the possible error due to approximations in the calculation of the heavy-primary rates.) The burst rate now exhibits a maximum

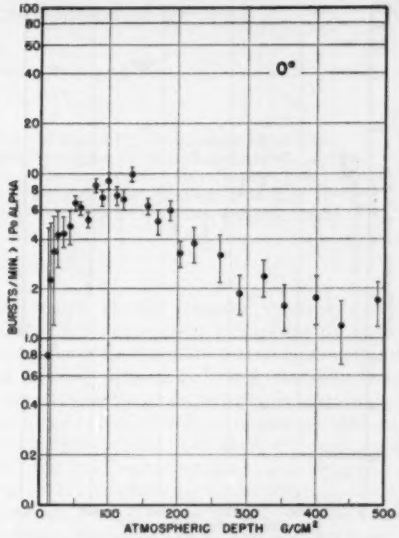

FIG. 8. Nuclear disintegration rate *vs* atmospheric depth at 0° geomagnetic.

at all latitudes, the position of this maximum being nearer the top of the atmosphere at higher latitudes. The depths of the maxima at 0°, 29°, 35°, and 52° respectively are approximately 100, 70, 60, and 50 g/cm^2. Because of the rather large uncertainties in the heavy-particle correction, these positions become progres-

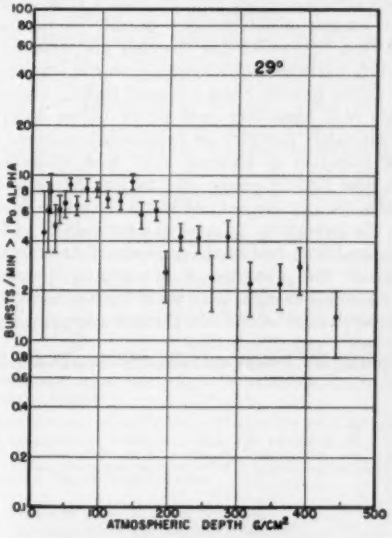

FIG. 9. Nuclear disintegration rate *vs* atmospheric depth at 29° geomagnetic.

[13] H. L. Bradt and B. Peters, Phys. Rev. **77**, 54 (1950).
[14] M. S. Vallarta, Phys. Rev. **77**, 419 (1950).
[14] M. S. Vallarta, Phys. Rev. **74**, 1837 (1948).
[15] G. Lemaitre and M. S. Vallarta, Phys. Rev. **43**, 87 (1933).

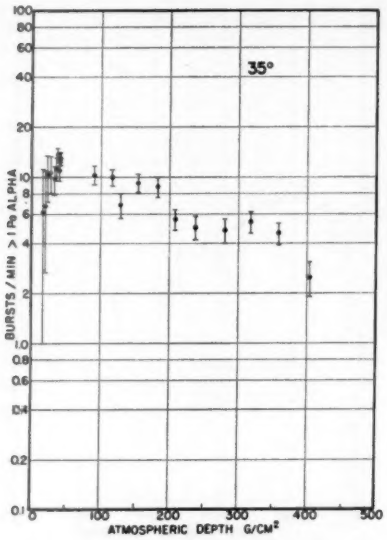

FIG. 10. Nuclear disintegration rate *vs* atmospheric depth at 35° geomagnetic.

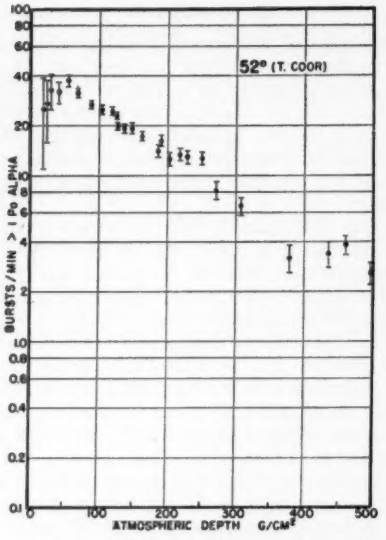

FIG. 11. Nuclear disintegration rate *vs* atmospheric depth at 52° geomagnetic.

sively less well defined with increasing latitude, until at 52° the data are not inconsistent with a mere leveling off of the star rate at the top of the atmosphere. On the other hand, the maximum at 0° appears even before the heavy-particle correction is made, so that its position depends but slightly on that correction.

These results indicate strongly that a large fraction of the nuclear disintegrations capable of producing bursts in a thin-walled ion chamber are initiated by secondary particles which multiply in the atmosphere by a cascade process. Since π-mesons travel a negligible fraction of a mean free path in air before decaying, these secondary particles are presumably nucleons.

The variation of latitude effect with atmospheric depth now finds a ready explanation. At very high altitudes the cascade has not had a chance to develop fully; the increase by a factor of 6 between 0° and 52° is comparable to that of the primaries.[16] At a depth of 200 g/cm² the primaries at the equator, possessing higher average energies than those farther north, have given rise to more secondaries through a longer cascade; the increase between 0° and 52° is only 3. This latter value is comparable to that found for bursts and fast neutrons at 300 g/cm² by Simpson[17] and rather less than that found by Yuan[18] for slow neutrons. It provides another indication of the close connection between bursts and the nucleonic component.

A comparison of these results with nucleonic cascade theory will be made in a forthcoming paper by S. Schweber and A. S. Wightman.

It is a pleasure to thank Mr. D. B. Davis and the shop staff of the Princeton Cosmic Ray Laboratory for their assistance with the construction of the equipment, Captain John Quinn, USN, and the officers and men of the *U. S. S. Norton Sound* for their cooperation throughout the expedition, Mr. Robert Price for his help in the preparation and execution of the flights, Miss H. Maginnis for assistance in the reduction of the data, and Dr. G. T. Reynolds for his continuing encouragement and advice.

[16] Winckler, Stix, Dwight, and Sabin, Phys. Rev. **79**, 656 (1950).

[17] J. A. Simpson and R. B. Uretz, Phys. Rev. **76**, 569 (1949); J. A. Simpson and E. Hungerford, Phys. Rev. **77**, 847 (1950).

[18] L. C. L. Yuan, Phys. Rev. **78**, 325 (1950).

Interpretation of the Decay Scheme of K^{40}

P. MORRISON
Department of Physics, Cornell University, Ithaca, New York
(Received December 11, 1950)

The three ground states and one excited state of the three nuclei involved in the disintegration of K^{40} are assigned parity and angular momentum values which are essentially unique. The rates of all measured transitions and such energy differences as are well known are used for the assignment, which depends on the *j–j* coupling shell model, the Gamow-Teller selection rules, and certain empirical groupings of beta-ray lifetimes. Appreciable *K*-capture directly to the ground state of A^{40} can be excluded on these quasi-theoretical grounds.

I. INTRODUCTION

THE decay scheme of the natural radioactive isotope, K^{40}, has received very extensive study both because of the inherent interest of its unusual nuclear properties and because of its high importance for the history of the earth. From data now available, using very plausible assumptions based on the shell model and on general beta-decay theory, a consistent interpretation of the decay scheme is given, with an identification of the quantum numbers of the three ground states and the one excited state involved. This interpretation also serves as an aid in the examination of certain experimental results which are still ambiguous.

II. ANALYSIS OF THE DATA

The experimental data adopted are presented in Fig. 1. The experimental errors in the energy measurements are indicated. The assignment of the gamma-ray to the excited state, **e**, of the A^{40} nucleus is made both because no beta-rays have energies higher than that of the gamma-ray, and because of the experimental absence of beta-gamma coincidences.[1] The partial transition probabilities are given in Table I.

The two data most uncertain are the amount of *K*-capture to the A^{40} ground state, and the mass difference, δ, which, with the well-known gamma-ray energy, determines the energy of the excited state $(A^{40})_e$. Both of these numbers will be fixed more reliably on the basis of the present interpretation.

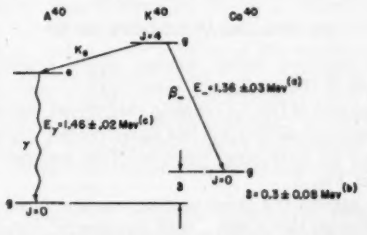

FIG. 1. The observed decay of K^{40}. The energies given are the measured values. (a) D. Alburger, Phys. Rev. **78**, 629 (1950); (b) T. Roberts and A. O. Nier, Phys. Rev. **79**, 198A (1950); (c) P. Bell and J. Cassidy, Phys. Rev. **79**, 173 (1950).

[1] Meyer, Schwachheim, and de Souza Santos, Phys. Rev. **71**, 908 (1947).

The shape of the beta-ray spectrum has been measured fairly accurately;[2] it is apparently, that to be expected for a third-forbidden transition of Greuling's types 3A or 3T. (Fourth-forbidden transitions involving the non-Gamow-Teller coupling types may lead to the same shape.) The lifetime is consistent with an empirically third-forbidden transition, although again this could arise from vector coupling, depending on parity changes.[3] In an interesting communication, which was unfortunately based on preliminary and now evidently misleading experimental data, Fireman[4] has shown how the ratio, λ_{K_g}/λ_+, which is almost independent of any nuclear matrix elements, depends on the total energy, E_+, which is available for positron emission. A recalculation of this ratio, using the approximation[3] for low values of Z, yields the results given in Table II, which differ slightly from those of Fireman.

Now from the shell model, say, in the *j–j* coupling form,[5] we can write the configurations for the three ground states concerned very plausibly as shown in Table III, using an obvious notation.

The change of parity indicated justifies the use of the Gamow-Teller coupling, assigning the transitions to the terms 3A or 3T. No way is available in this decay scheme for distinguishing between tensor and axial vector. Both shape and empirical lifetime fit well; and the transitions thus satisfy the selection rules: $\Delta J=3$, parity changes. The ground-state characters are then: Ca^{40} and A^{40}, $J=0$, *even*; and K^{40}, $J=4$, *odd*. The

TABLE I. Partial transition probabilities.

$K^{40}\rightarrow(Ca^{40})_g+\beta_-$, $\lambda_-=(1.54\pm0.06)\times10^{-17}$ sec^{-1}.[a]
$K^{40}\rightarrow(A^{40})_g+\beta_+$, λ_+: (not observed, less than $5\times10^{-6}\lambda_-$).[b]
$K^{40}+(e^-)_K\rightarrow(A^{40})_e$, $\lambda_{K_e}/\lambda_-=0.13\pm0.01$, from the observed gamma-ray yield.[a]
$K^{40}+(e^-)_K\rightarrow(A^{40})_g$, $\lambda_{K_e}+\lambda_{K_g}$, the total *K*-capture, is given by the measurement of Auger electrons,[a] and by the abundance of radiogenic argon. $(\lambda_{K_e}+\lambda_{K_g})/\lambda_-=0.13\pm0.04$. λ_{K_g} is not observed separately.

[a] G. Sawyer and M. Wiedenbeck, Phys. Rev. **79**, 490 (1950).
[b] Private communication from Mr. S. Colgate. The very low limit $(\lambda_+/\lambda_-<2\times10^{-6})$ given in reference c to Fig. 1 could not be confirmed by recalculation from the published data.

[2] D. Alburger, Phys. Rev. **78**, 629 (1950).
[3] E. Greuling, Phys. Rev. **61**, 568 (1942).
[4] E. Fireman, Phys. Rev. **75**, 1447 (1949).
[5] M. Mayer, Phys. Rev. **78**, 16 (1950).

TABLE II. Dependence of λ_{K_g}/λ_+ on E_+.

$E_+(mc^2)$	λ_{Kg}/λ_+
2.1	100
2.3	60
2.5	30

$[(E_+)_{obs}=1.17\pm0.08$ Mev$]$.

transitions can be assigned to the change of a single particle state as follows:

(a) β_-: $f_{7/2}{}^n \rightarrow d_{3/2}{}^p$; (b) β_+(or K_g): $d_{3/2}{}^p \rightarrow f_{7/2}{}^n$.

It is now almost inescapable that one sets the nuclear matrix elements of these two similar transitions equal, or at least nearly so. Under this assumption we can compute quantities, A, which are proportional to the transition probabilities, as shown in Table IV.

From Tables II and IV and the observed energies it follows that the value of λ_{K_g}/λ_+ lies between 0.01 and 0.08. Since experiment[6,7] indicates that within the rather sizable error the total branching ratio to K-capture does not differ from that to gamma-emission, one infers that the lower value of around 0.01 is correct, and that the $K^{40}-(A^{40})_g$ atomic energy difference is

TABLE III. Ground state of configurations.

Nucleus	Z	$N(=A-Z)$	Configuration
Ca^{40}	20	20	closed shell
K^{40}	19	21	$(d_{3/2})^{-p}(f_{7/2})^{+n}$
A^{40}	18	22	$(d_{3/2})^{-2p}(f_{7/2})^{+2n}$

close to $3.1mc^2$. We conclude then that direct K-capture to the ground state *cannot* contribute heavily to the decay of K^{40}. At most, the process can give a few percent of all transitions. This conclusion is confirmed by the latest experiments,[8] and seems to provide an additional basis for disregarding the high upper limits given by several experimenters for possible K-capture. This conclusion is so decisive for certain geophysical problems that it is very satisfactory to find some theoretical argument to bolster the difficult experiments.

Now consider the K-capture to the excited state (even here, L_I electrons and those of all higher shells are unimportant), using the energy difference obtained

TABLE IV. Transition probabilities (unnormalized).

$E_+(mc^2)$	λ_+ A_+	$E_-(mc^2)$	λ_- A_-
2.1	2.4	3.6	8.2×10^3
2.3	6.7	3.7	1.15×10^4
2.5	21.2	3.8	1.8×10^4

[6] Hess, Brown, Patterson, and Ingraham, Phys. Rev. **81**, 298A (1951).
[7] G. Sawyer and M. Wiedenbeck, Phys. Rev. **79**, 490 (1950).
[8] T. Gráf, Phys. Rev. **79**, 1014 (1950), and the references given there.

from the smallness of capture to the ground state. Assuming only as a zeroth approximation that the nuclear matrix elements are the same for the two K-capture transitions, we can write a relation for their lifetimes, in which the nuclear radius $R=1.4\times10^{-13}\cdot A^{\frac{1}{3}}$ cm enters:

$$\log_{10}(\lambda_{K_e}/\lambda_{K_g}) = 2\log_{10}N(n)+(2n+2)\log(E_{K_g}/E_{K_e})-1.4(2n-6).$$

Here n is the degree of forbiddenness for the excited state K-capture, and $N(n)=1\cdot3\cdots(2n+1)/1\cdot3\cdot5\cdot7$. Evaluating this expression for various choices of n, we can conclude that the transition is at least first forbidden, and not as slow as second forbidden. It is very slow among transitions with $n=1$; it is in fact about intermediate between $n=1$ and $n=2$. The value of the familiar product $\log_{10}(ft_{1/2})$ is about 8, with f calculated as for an allowed transition. Nordheim[9] and Shull and Feenberg[10] have pointed out that a whole set of beta-transitions exists with values of $ft_{1/2}$ in this range. Such transitions correspond to $\Delta J=2$, but with parity change, which can be described in the language of the j–j coupling model as $\Delta J=2$, $\Delta L=1$. Now, if the first

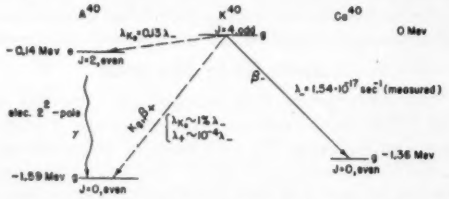

FIG. 2. Complete decay scheme and level assignments for K^{40}. The estimated atomic mass differences are shown.

excited state in A^{40} belongs to the same configuration as does the ground state, as one might expect, the transition is just $d_{3/2}\rightarrow f_{7/2}$ with $\Delta L=1$. One of the possible equivalent levels in this configuration, indeed one of the most plausible, is that with $J=2$, *even*. This assignment then fulfills the empirical requirements of the beta-decay theory, $\Delta J=2$, $\Delta L=1$.

III. THE DECAY SCHEME OF K^{40}

The proposed decay scheme, which satisfies all demands of the beta-decay theory with Gamow-Teller coupling and of the j–j coupling shell model, allows the assignment of all four nuclear states and determines all lifetimes at least approximately. This assignment is given in Fig. 2.

The gamma-ray is an ordinary electric quadrupole transition on this scheme, with an expected lifetime of about 10^{-12} second. It is known empirically only that its lifetime is short compared with the time required for diffusion of argon out of a beaker full of boiling KOH,

[9] L. Nordheim, Phys. Rev. **78**, 294 (1950).
[10] F. Shull and E. Feenburg, Phys. Rev. **75**, 1768 (1949).

say, a few seconds.[11] This is enough to exclude the possible assignment $J=6$ for the level e, which would otherwise be acceptable. The internal conversion of the quadrupole gamma-ray by electron or pair emission is very improbable. No positrons have yet been observed in spite of fairly careful search. Further confirmation of the scheme seems possible but not easy, either by looking still more closely for the predicted positrons or by improving the accuracy of the K-capture and gamma-ray yield measurements considerable.

[11] See reference b of Table I.

It is a pleasure to acknowledge interesting discussion with Professor E. P. Wigner, and the computational assistance of Mr. J. Goldstein.

PHYSICAL REVIEW VOLUME 82, NUMBER 2 APRIL 15, 1951

On Fermi's Theory of the Origin of Cosmic Radiation

CHANG-YUN FAN
Institute for Nuclear Studies, University of Chicago, Chicago, Illinois
(Received September 14, 1950)

Starting from Fermi's theory of the origin of cosmic radiation, an explanation of the observed shape of the energy spectrum of the proton component is suggested. On this basis there seems to be some indication that the majority of the protons originate from the nucleus of our galaxy. Assuming that the nucleus of the galaxy is a cluster of stars, the origin of the heavier nuclear components and protons of cosmic radiation can be explained on the same basis providing that an ordinary star can eject high energy particles (up to one Bev per nucleon). The observation of the effect of the sun on the heavier nuclear components may give a critical test of the theory.

The trapping magnetic field, if any, of the galaxy has a negligible effect on the energy spectra of cosmic radiation observed on the earth. The age of the galaxy is estimated to be greater than two billion years.

I. INTRODUCTION

RECENT measurements of the proton component of the cosmic radiation[1,2] show that the differential energy spectrum indicates a maximum at the low energy end with a gradually increasing slope toward high energies. In this paper, which is based on Fermi's theory of the origin of cosmic radiation,[3] an explanation of this effect is suggested and a hypothetical picture describing the origin of cosmic radiation is then deduced.

Fermi's theory is based on the assumed existence of wandering magnetic clouds in interstellar space. According to this theory a charged particle will gain energy by a "head-on collision" with a magnetic cloud and will lose energy by an "over-taking collision;" but since the chance of a collision of the first type is larger than one of the second type, there is an average energy gain per collision. This is given by $\delta w = B^2 w$, where w is the energy of the particle (including rest energy) before the collision, and B is the velocity of the wandering cloud in units of the velocity of light. If the initial energy of the particle exceeds a certain threshold value so that the loss of energy in passing through the interstellar medium between collisions can be compensated by the gain, the particle will be accelerated and will become a cosmic-ray particle.

The wandering magnetic clouds are presumably eddies in interstellar space. They are stirred up by the rotation of the galaxy. Recent reports on the polarization of starlight when passing through interstellar clouds seem to support the existence of the magnetic nature of these clouds.[4–6] The existence of the wandering magnetic clouds indicates that Fermi's mechanism must account for at least a part of the cosmic radiation. We shall start with Fermi's mechanism as a fundamental basis and investigate the spatial distribution of sources of protons which will produce the observed spectrum of the primary proton component.

Assume that protons originate from some source at a distance r from the earth and that some of them reach the earth after many collisions. Applying the principle of random flight, we are able to deduce the energy distribution of these protons as a function of r. Thus, the energy spectrum of the proton component is determined by the spatial distribution of the proton sources. Several types of spatial distribution were investigated, and it was found that the observed energy spectrum seems to indicate that the majority of cosmic-ray particles originate from the nucleus of our galaxy.

The nucleus of our galaxy is presumably a cluster of stars. If stars are able to eject high energy particles (up to one Bev per nucleon), as proposed by different authors,[7,8] then our finding might mean that cosmic-ray particles originate from stars and are then accelerated in interstellar space according to Fermi's mechanism. However, if normal stars are unable to eject high energy particles, we are forced to assume that a series of some

[1] Winckler, Stix, Dwight, and Sabin, Phys. Rev. **79**, 656 (1950).
[2] J. A. Van Allen and S. F. Singer, Phys. Rev. **78**, 819 (1950).
[3] E. Fermi, Phys. Rev. **75**, 1169 (1949).
[4] J. S. Hall, Science **109**, 166 (1949).
[5] W. A. Hiltner, Science **109**, 165 (1949).
[6] L. Spitzer and J. W. Tukey, Science **109**, 461 (1949).
[7] F. Hoyle, Monthly Notices Roy. Astron. Soc. **106**, 384 (1947).
[8] K. Kiepenheuer, Phys. Rev. **78**, 809 (1950).

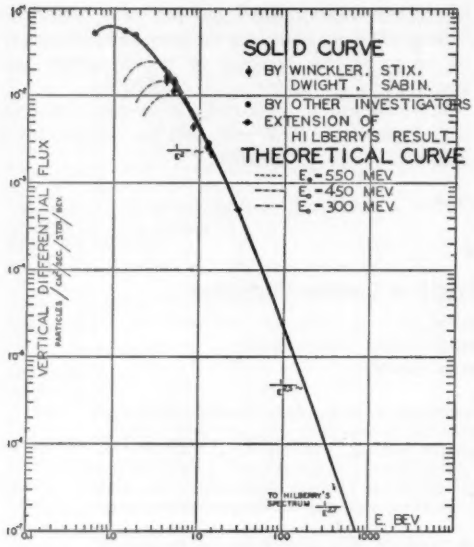

FIG. 1. Differential energy spectrum.

sort of explosions occurred in the nucleus many ages ago. It is hard, at present, to tell which possibility is closer to the truth, but if we assume that primarily the heavier elements are ejected from stars and that protons are the break-up products of these elements by collisions with the interstellar gases, then the first mechanism would give the correct relative abundances of the different components in cosmic radiation and the day-night difference of the intensities of the heavier nuclear components would follow as a direct consequence.[9] Detailed discussions will be given in Secs. IV and V.

The following data concerning our galaxy and solar system are used for calculations and for comparison:

(1) Radii of our galaxy: $R_1=4.63\times10^{22}$ cm, $R_2=R_1/5$.
(2) Average distance between stars: 1.7×10^{17} cm.
(3) Average density of the interstellar matter: 10^{-24} g/cm^3.
(4) Solar system: Near meridian plane of the galaxy and 3.09×10^{22} cm from the center.

II. THE MECHANISM OF ACCELERATION OF THE PROTON COMPONENT

The mechanism of acceleration of the proton component is described in Fermi's paper.[3] In order to use it as a basis for further deductions, we reproduce it here with some slight alterations.

A charged particle gains energy by "collisions" with wandering magnetic clouds in interstellar space. The *average* energy gain per "collision" is given by:

$$\delta w=B^2w, \tag{1}$$

where w is the energy (including the rest energy) of the particle before "collision," and B is the average velocity of the magnetic clouds in units of the velocity of light. The value of B is taken to be of the order of 10^{-4} in accordance with the value given in Fermi's paper. If ϵ is the energy loss in passing through the interstellar matter between collisions, then the energy of the particle after N collisions is given by:

$$w(N)=(1+B^2)[w(N-1)-\epsilon], \tag{2}$$

if it is not eliminated by nuclear collisions with interstellar gases.

Let ρ be the average density of the interstellar matter, D be the *average length of path* traversed by a proton between collisions, and q be the energy loss of a proton per g/cm^3 of material traversed. Then $\epsilon=q\rho D$.

The value of q is tabulated in Fermi's paper and can also be deduced from Smith's results.[10] *For high energy protons* it is easy to show that the energy dependence of q can be represented adequately by the following form:

$$q=a+b/(w-ah)^x, \tag{3}$$

where $h=D\rho/B^2$ and a, b, and x are three adjustable constants. This form enables us to integrate Eq. (2) exactly. Agreement with the results of Fermi and Smith is achieved by suitably altering the three constants a, b, and x, after we determine the value of h in the next section.

On inserting the value of ϵ in Eq. (2) and then performing the integration, we get:

$$\{[w(N)-ah]^{x+1}-bh\}=\{[w(0)-ah]^{x+1}-bh\}\exp[(x+1)B^2N], \tag{4}$$

if we neglect unity as compared with $1/B^2$.

It is clear from Eq. (4) that a particle will undergo an acceleration or a deceleration according to whether $w(0)$ is greater or less than $[(bh)^{1/(x+1)}+ah]$. Thus, $[(bh)^{1/(x+1)}+ah]$, is the minimum initial energy for subsequent acceleration, and this value minus the rest energy of the proton is called the injection energy of the proton in Fermi's paper

If we put

$$y=\left\{\frac{[w(N)-ah]^{x+1}-bh}{[w(0)-ah]^{x+1}-bh}\right\}^{1/(x+1)}, \tag{5}$$

then Eq. (4) becomes simply

$$y=\exp(B^2N). \tag{6}$$

III. THE SPECTRUM OF THE PROTON COMPONENT

Recently, Winckler, Stix, Dwight, and Sabin[1] analyzed the spectrum of the proton component. They combined their measurements in the range of $E\approx4$ Bev to $E\approx14$ Bev with Hilberry's spectrum[11] in the high energy region and with other measurements in the low energy region in order to produce a smooth curve over the entire range. Modifying their curve slightly at the junction of their results and the extension of Hilberry's

[9] J. J. Lord and M. Schein, Phys. Rev. **80**, 304 (1950).

[10] J. H. Smith, Phys. Rev. **71**, 32 (1947).
[11] N. Hilberry, Phys. Rev. **60**, 1 (1941).

spectrum to make a smoother connection, and converting the integral energy spectrum to a differential energy spectrum, we have the solid curve given in Fig. 1. The slope of each section of the curve is shown in the same figure. Using Fermi's acceleration mechanism as basis, we now investigate the nature of the proton source which will produce this spectrum.

Let Sdt protons of $w(0)$ greater than the minimum initial energy be injected at some point at a distance r from the earth in a time interval dt at $t=0$. Some of them will reach the earth after many collisions with the wandering magnetic clouds. If r is much larger than the average linear distance, L, traversed between collisions, so that the principle of random flight is valid, then the probability density of finding those protons at time t on the earth is

$$P_0(r, t)dt=[Sdt/(2\pi\xi^2)^{\frac{3}{2}}]\exp(-r^2/2\xi^2)$$

provided the loss of protons caused by nuclear collisions with interstellar gases is neglected. Here $\xi^2=2NL^2/3$, and N is the total number of collisions in $(0, t)$.

The absorption cross section of a fast proton per nucleon due to nuclear collision is $\sigma_p\approx 2.5\times 10^{-26}$ cm^2. Let $\lambda=M/\sigma_p\rho$ be the absorption mean free path and $T=\lambda/\bar{v}$ be the absorption lifetime, where M is the mass of proton, ρ is the average density of the interstellar matter, and $\bar{v}$ is the average velocity of the proton. Then the probability of finding a proton of life greater than t is $\exp(-t/T)$. Taking this factor into account, the probability density of finding the protons which originated from a distance r at $t=0$ on the earth is then equal to

$$P(r, t)dt=\frac{dt}{(2\pi\xi^2)^{\frac{3}{2}}}\exp(-r^2/2\xi^2)\exp(-t/T) \qquad (7)$$

for $S=1$.

Putting $s=\sigma_p h/M$ and $R^2=4L^2/3B^2$ for simplicity, we have from Eq. (6) and the relation $\bar{v}t=ND$,

$$P(r, y)dy=\frac{sT}{(\pi R^2\ln y)^{\frac{3}{2}}}\exp(-r^2/R^2\ln y)\frac{dy}{y^{1+s}}. \qquad (8)$$

The spectrum of the primary proton component depends, therefore, on the position of the source from which protons originated.

(A)

Case 1. The source is uniformly distributed throughout the whole galaxy and ejects gases at a constant rate.

The spectrum of the proton component observed on the earth for *a source ejecting gases at a constant rate* is given roughly by:

$$f(E)dE=\left[\int_{E_i}^{E}\int_V S(E_0)P(r, y)(dy/dE)dE_0d\tau\right]dE, \qquad (9)$$

where $S(E_0)dE_0d\tau$ is the number of protons of kinetic energy between E_0 and E_0+dE_0 ejected from $d\tau$ per unit time, E_i is the minimum initial kinetic energy, and V is the volume of the galaxy. *If the distribution of the sources is uniform throughout the whole galaxy*, as is the case, for instance, with the randomly distributed supernovae, the value of Eq. (9) is then approximately:

$$f(E)dE=(TsdE/E^{1+s})\int_{E_i}^{E}E_0{}^sS(E_0)dE_0, \qquad (10)$$

when we put $y=E/E_0$ (see next Section) and neglect the small difference in the high energy region due to the finiteness of the dimension of the galaxy.

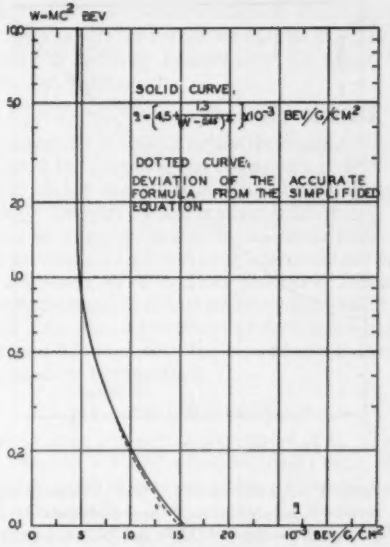

FIG. 2. Plot of q from Eq. (11).

As far as present knowledge goes, the mechanism of ejection of high energy particles from stars (being similar to the explosions in supernovae, according to the most recent speculations) gives, at maximum, energies up to only a few Bev per nucleon. For $E\gtrsim$ the maximum initial kinetic energy per nucleon, Eq. (10) becomes simply

$$f(E)dE=(K/E^{1+s})dE,$$

where K is a constant. This is the well-known inverse power law, which is a good approximation only in the high energy region.

It must be noticed that a uniform source, even if it is very weak, yet may make an important contribution to the low energy region. This can be seen from the rapid increase of $f(E)$ with decreasing E in Eq. (10).

(B)

Case 2. "Point source." Equation (8) gives the spectrum of the proton component if the protons originate from a *"point source" emitting at a constant rate with a definite initial energy.* It is clear that Eq. (8) consists of two factors: the first contains $(\ln y)$ as an argument and is important for small values of y, while the other is

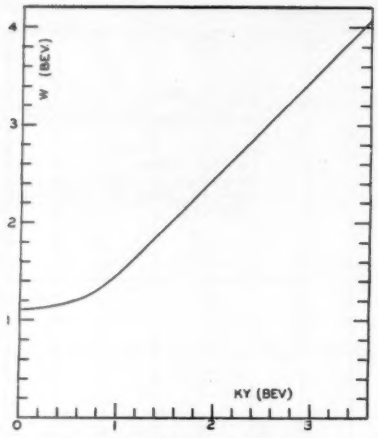

FIG. 3. Plot of $W(N)$ *vs* y, for $k=1$.

important for large values of y. $P(r, y)$ increases rapidly from zero to a maximum and then decreases. It varies as $1/y^{1+s}$ when $y=\exp(2r^2/3R^2)$ and becomes gradually steeper than $1/y^{1+s}$ with increasing y. This feature, together with the shape of the experimental energy spectrum, suggests $s=1.5$ in Eq. (8). From this value of s $(=\sigma_p h/M)$, the following results can be obtained:

(a) $h=D\rho/B^2=100$ g/cm^2; $D\approx 10^{13}$ cm.

(b) By adjusting the constants a, b, and x in Eq. (3) to fit Fermi's and Smith's results, the energy loss of a *high energy* proton per g/cm^2 of material traversed in the interstellar space can be represented by:

$$q=[4.5+1.3/(w-0.45)^4]\times 10^{-3}\ \text{Bev/g/cm}^2. \quad (11)$$

The comparison of Eq. (11) and the exact results is shown in Fig. 2.

(c) The minimum value of $w(0)$, denoted by $w(0)_i$, is given by $[(w(0)_i-0.45)^5-0.31]=0$ which gives $w(0)_i=1.12$ Bev. *The injection energy is, therefore, about* 0.2 Bev.

(d) The value of y is then

$$y=\left[\frac{(w(N)-0.45)^5-0.13}{(w(0)-0.45)^5-0.13}\right]^{1/5}. \quad (12)$$

For large $w(N)$,

$$y\approx k(w(N)-0.45)\approx kE,$$

where $k=1/[(w(0)-0.45)^5-0.31]^{1/5}$. If $w(0)$ is also large, y is simply equal to E/E_0, where E_0 is the initial kinetic energy. The dependence of $w(N)$ on y for $k=1$ is given in Fig. 3.

The adjustment of Eq. (8) to fit with the experimental curve is facilitated by the fact that when we plot Eq. (8) on log-log paper the shape of the curve is not altered if we assume a different initial energy or multiply by an arbitrary constant. Therefore, taking k to be unity and fitting our curve with two arbitrary points of the experimental result (we take $E=7.4$ Bev and 20 Bev), we get:

$$P_\perp(r, y)=[115/(\ln y)^4]e^{-7.4/\ln y}(1/y^{2.5}). \quad (13)$$

The comparison with the experimental results is shown in Fig. 1, where the theoretical curves of different initial energies are obtained by mere linear translations. A change of the parameter $w(0)$ causes a horizontal translation, and an arbitrary multiplier is introduced to effect a vertical linear translation, which brings the high energy portion of the curves to coincidence except for a small discrepancy which is not indicated.

The above results indicate that a "point source" seems to be a close guess. If this is not merely a coincidence, then the assumed source is probably *the nucleus of our galaxy because it is the only place*, as far as we know, *which can supply the necessary energy*. Assume that $D\approx L$ and $\rho\approx 10^{-24}$ g/cm^3, we find from the value of h and of r^2/R^2 that the distance of our assumed source is just the distance of the center of our galaxy from the earth, 3.1×10^{22} cm.

(C)

Discussion—the low energy end of the spectrum. Before we give a detailed discussion of Case 2, we should emphasize one point which is, perhaps, the weakest part of the whole picture presented in this paper.

Our speculations have been based on the experimental results of Winckler *et al.*,[1] and we have indicated that the most probable spatial distribution of proton sources is that which would most closely produce these results. But we have ignored the possibility that the observed spectrum may be distorted. Thus, the following facts, for instance, have not been considered: (1) the spectrum may be distorted by the magnetic field of the sun; (2) the observed cosmic-ray protons are presumably mixed up with the protons produced through nuclear collisions by cosmic-ray protons which we have considered as lost in our calculations. The dipole magnetic field of the sun probably affects only low energy particles,[12] but the secondary protons will distort the spectrum even up to the high energies. The purpose of the following discussions is to show that *the distortion seems unlikely to be large except at the low energy end.*

The protons produced through nuclear collisions by cosmic-ray protons tend to distribute themselves uniformly throughout the whole galaxy. These protons will be again accelerated according to Fermi's mechanism. Thus, we may consider these secondary protons as a uniformly distributed source, and, therefore, Eq. (10) is applicable for this case except that E does not have a definite maximum.

Differentiating Eq. (10) with respect to E, we have:

$$S(E)=(1/Ts)[(1+s)f(E)+Ef'(E)].$$

Let us put

$$f(E)=kK/E^s.$$

[12] The dipole magnetic field of the sun was proposed in 1939 as an explanation of the cut-off of the energy spectrum below 4 Bev. Now it is believed that the magnetic field is perhaps much weaker than thought before.

Here K is a constant, and k and x are *slowly-varying* functions of E; x varies from some negative value to $1+s$, and k varies from 0 to 1. Then

$$S(E)\approx(1+s-x)f(E)/Ts.$$

The last equation shows that if the secondary protons are principal sources, $S(E)$ would have a maximum at $E\approx 1$ Bev as $f(E)$. This seems unlikely to be the possible energy spectrum of the protons produced by cosmic-ray protons through nuclear collisions. Arguing on this basis, the turning-off of the primary energy spectrum indicates perhaps that $S(E)$ is rather small. It is, therefore, considered together with supernovae as a source which plays an important part only in the low energy region and will not be mentioned in the next section.

IV. GENERAL DISCUSSION OF THE SOURCE

The nucleus of our galaxy is presumably a cluster of stars. The density of stars in our galaxy might be put in the following form:

$$D(a)=(D_0/a)\exp(-a^2/a_0^2), \tag{14}$$

where a is the distance measured from the center of our galaxy, and D_0 and a_0 are two constants (a simplified form of Oort's description of our galaxy). If stars are able to eject high energy particles (up to 1 Bev per nucleon) as proposed by different authors,[7,8] then our result would mean that the cosmic radiation originates from stars and is then accelerated according to Fermi's mechanism in interstellar space. In fact, if we integrate Eq. (8) over the whole space with the weight function (14), we obtain a curve similar to that of Fig. 1 except that the maximum of the spectrum shifts toward lower energies. This is to be expected since the distribution (14) is highly concentrated. When we choose $E_0=1$ Bev and $a_0=r^2/7.4$ for simplicity (r is the distance from the earth to the nucleus), the maximum occurs at $E\approx 2$ Bev.

On the other hand, if stars are unable to eject high energy particles, our result would mean that something corresponding to a series of explosions occurred in the nucleus of the galaxy over an extended period of time many ages ago. Our galaxy belongs to the late stage of the normal spiral type. A normal spiral type has its arms fully developed before condensation occurs. This could be understood if the latter hypothetical mechanism were correct, because the ejection of a large amount of gas would result in the reduction of the mass of the nucleus, causing the arms to be developed by centrifugal force.

At the present time it is hard to tell which of the hypothesis discussed above is the more nearly correct, but the author favors the first one, because it would solve the problem of the heavier nuclear components of cosmic radiation, as will be shown in the next section.

V. THE HEAVIER NUCLEAR COMPONENTS OF COSMIC RADIATION

(A) The Relative Abundances

In dealing with the heavier nuclear components we encounter one difficulty; namely, the high minimum initial energies required for subsequent acceleration. Let $w(N)$ now denote the energy per nucleon of a nucleus A just after N collisions. Integration of Eq. (2), with ϵ as a constant, yields:

$$[Aw(N)-\epsilon/B^2]=[Aw(0)-\epsilon/B^2]\exp(B^2N). \tag{15}$$

ϵ/B^2 (denoted by $Aw(0)_i$), is then the required minimum energy of the nucleus under consideration. If Z is the nuclear charge, the minimum initial kinetic energy per nucleon[13] (denoted by E_i), is about $0.2Z^2/A$.

Now let us *assume that mostly heavier nuclei of charge $Z\geqslant 6$ are originally ejected from the source and that protons and α-particles are the break-up products of such nuclei, resulting from collisions with the interstellar gases.*[14] *If the source is far from the earth* and protons and α-particles exist in equilibrium with the heavier nuclei, then two cases must be distinguished:

$$(I)\ w(0)\geqslant w(0)_i$$

Let us start originally with 6 nuclei of C, N, and O and 2 heavier nuclei of average atomic weight, $A=30$. The ratio 6:2 is that existing among these gases in the interstellar medium. Assume that the break-up fragments of a nucleus A consist of $\frac{1}{4}A$ α-particles and $\frac{1}{4}A$ protons and neutrons (which will decay to be protons).[15] Take the absorption cross section of He as

$$\sigma_{\mathrm{He}}=(4)^{\frac{2}{3}}\sigma_p=6.3\times10^{-26}\ \mathrm{cm}^2,$$

and the cross sections of the C, N, O group as[16]

$$\sigma_{\mathrm{C,N,O}}=20\times10^{-26}\ \mathrm{cm}^2,$$

and that of $A\geqslant 30$ as[16]

$$\sigma_M=30\times10^{-26}\ \mathrm{cm}^2.$$

Then the number of α-particles (N_{He}) when in equilibrium with nuclei of charge $Z\geqslant 6$ is

$$N_{\mathrm{He}}=\frac{14}{6}\frac{\sigma_{\mathrm{C,N,O}}}{\sigma_{\mathrm{He}}}N_{\mathrm{C,N,O}}+\frac{30}{6}\frac{\sigma_M}{\sigma_{\mathrm{He}}}N_M\approx 90,$$

and the number of fast protons (N_p) is

$$N_P=\frac{14}{3}\frac{\sigma_{\mathrm{C,N,O}}}{\sigma_P}N_{\mathrm{C,N,O}}+\frac{30}{3}\frac{\sigma_M}{\sigma_P}N_M+4\frac{\sigma_{\mathrm{He}}}{\sigma_P}N_{\mathrm{He}}\approx 1400.$$

Thus, on the assumption that only nuclei of charge $Z\geqslant 6$ are ejected, we predict that the ratio of elements in cosmic radiation *with energies above a certain minimum energy per nucleon* should be

$$\mathrm{H:He:(C,N,O):}(Z\geqslant 10)=1400:90:6:2.$$

This is of the order of magnitude of the observed ratio, as first pointed out by Bradt and Peters.[16]

[13] Gases ejected from stars are presumably only partially ionized. The stripping cross section per electron by collision is about 10^{-20} cm^2, so that we can assume that all of the nuclei are bare except those coming directly from the sun.

[14] The absorption cross sections of the heavier elements are sufficiently large so that no serious errors are introduced if we assume that the protons originate directly from a star in calculating the spectrum of the proton component.

[15] J. B. Harding, Phil. Mag. **11**, 530 (1949).

[16] H. L. Bradt and B. Peters, Phys. Rev. **77**, 54 (1950).

(2) $w(0)_i \geqslant w(0) \geqslant 1.12$ Bev

In this case the heavier nuclei under consideration are unable to be accelerated, but the break-up products, protons and α-particles, have their energies still above the minimum required energy 1.12 Bev per nucleon. Because the source is far away from the earth, heavier nuclei will be slowed down and absorbed before they reach the earth.

Thus, a distant source, as the nucleus of our galaxy would be, for instance, gives too low abundances for heavier nuclear components. This difficulty can be overcome if we adopt the first mechanism discussed in the last section; that is, if we assume that stars are the original source of cosmic radiation.

The closer stars give much higher relative abundances for heavier nuclei for the following two reasons: (1) the equilibrium condition has not been reached, and (2) low energy nuclei still have a chance to reach the earth. Specifically, the sun would give an important contribution to the low energy heavier nuclear components, and, therefore, the day-night difference of intensities of these particles[9] would follow as a direct consequence.

(B) The Energy Spectra of The Heavier Nuclear Components

The energy spectrum of the α-particles can be obtained by the same argument as that by which we obtained the spectrum of the proton component. It is practically:

$$P(r, y)dy = \frac{KS(E_0)}{(\ln y)^{\frac{1}{2}}} e^{-7.4/\ln y} \frac{dy}{y^{4.8}} \tag{16}$$

for a given initial energy, where y stands for $[4w(N) - \epsilon/B^2]/[4w(0) - \epsilon/B^2]$, K is a constant and $S(E_0)$ is the number of α-particles ejected per sec with initial kinetic energy E_0, ($\approx (4w(0) - \epsilon/B^2)$).

Equation (16) has a maximum at $y \approx 3$. The value of the maximum is $K'S(E_0)$ where K' is a constant. Because the spectrum for a given initial energy is so steep that the shape of the *observed* spectrum would be then roughly given by:

$$f(E)dE = (dE/E)K'S(E/3)$$

when we write $y \approx E/E_0$. This resembles more or less the initial energy spectrum except that the observed spectrum may have a steep "tail" in the high energy region.

From considerations similar to the above discussion, the energy spectra of the heavier nuclear components would all resemble the initial energy spectra.[17]

It is interesting to notice that by a comparison of Eq. (8) with Eq. (13) we are able to estimate the total number of nucleons of kinetic energy $\geqslant 0.2$ Bev ejected from each stars if our hypothetical mechanism is correct. Let S be the total number of nucleons of $w(0) \geqslant w(0)_i$ ejected per second. Then

$$SsT\bar{v}/3(\pi R^2)^{\frac{1}{2}} \approx 115\pi.$$

This gives $S \approx 10^{44}$ particles per second. There are 10^{11} stars in our galaxy. The number of nucleons of kinetic energy $\geqslant 0.2$ Bev ejected from each stars is then 10^{33} per second. This is about 10^{-24} of the mass of the sun, and the energy is about 10^{-4} of the total electromagnetic energy emitted per second from the sun.

VI. THE EFFECT OF THE "REFLECTIVITY" OF THE GALACTIC BOUNDARY

In this section we shall estimate the effect of the boundary condition of our galaxy. The question is: How much does the trapping magnetic field of our galaxy, if it exists at all, affect the spectra of cosmic radiation? If there is such a magnetic field and if it is strong, we can consider the boundary of the galaxy to be a perfect reflector. On the other hand, if there is no magnetic field to trap cosmic radiation, we can consider the boundary to be a perfect absorber. The theory of random flight with a reflecting boundary and with an absorbing boundary provides an easy way of estimating this effect.

In order to give only the qualitative features for the two cases, we simplify the condition as follows: We suppose the galaxy to be a sphere of radius a and assume that cosmic radiation originates only from the center of the galaxy. For a given initial energy, the spectrum of the cosmic radiation (say the proton component), is given by:

$$P(r, y)dy = \frac{Ts}{(\pi R^2 \ln y)^{\frac{1}{2}}} \times \exp\left(-\frac{r^2}{R^2 \ln y}\right)\left\{1 \pm \exp\left[-\frac{4a(a-r)}{R^2 \ln y}\right]\right\}\frac{dy}{y^{2.5}},$$

where the notation is the same as in Eq. (8). The plus sign is for a perfectly reflecting boundary, and the minus sign is for a perfectly absorbing boundary. For a perfect reflector, the spectrum will be flatter in the high energy region, and for a perfect absorber, it will be steeper. But the effect is so small that it could not be shown in Fig. 1.

VI. THE TIME SCALE OF THE GALAXY

If we assume that the state of interstellar space has not changed since the "birth" of the galaxy and that the protons of the highest energy in the cosmic radiation have been accelerated ever since, then Fermi's theory serves as a new method for estimating the age of our galaxy. The highest proton energy observed is about 10^9 Bev. Assuming that such a particle had an initial kinetic energy of 2 Bev, then the life of this particle is 6×10^{16} sec, which is about two billion years, from which we conclude that the age of the galaxy is greater than two billion years.

[17] M. S. Vallarta, Phys. Rev. **77**, 419 (1950).

Overlapping Divergences and the S-Matrix

ABDUS SALAM
St. John's College, Cambridge, England
(Received September 29, 1950)

By extending considerations given by Dyson, general rules are obtained for isolating divergent parts from integrals corresponding to overlapping graphs, and a proof is obtained for the appearance of an extra factor Z_1^{-1} from "b divergences." In the last section the possibility of renormalization for scalar meson-nucleon interactions is demonstrated.

I. INTRODUCTION

IN his treatment of spinor electrodynamics Dyson[1] has defined operators Λ_μ, Σ^*, and Π^* corresponding to the three types of primitive divergent graphs in the theory. In the calculation of the contribution to Γ_μ arising from a reducible vertex part V_R it is possible to break V_R down unambiguously into an irreducible vertex part plus various inserted self-energy (S) and vertex (V) parts. The divergences introduced by the latter can be removed in a well-defined manner because any two of the insertions made in V_R are either completely non-overlapping or else are so arranged that one is completely contained in the other. This procedure fails, however, in the calculation of the contributions to Σ^* or Π^* from reducible self-energy graphs. Considering, for example, the electron self-energy, there is just one irreducible graph W_1 (Fig. 1). V parts inserted at one of the two end vertices a or b appear simultaneously as vertex insertions at the other vertex. Correspondingly, the contribution to Σ^* arising from a reducible part W_R is, in general, an integral which involves divergences corresponding to each of the ways in which W_R might have been built up by insertion of V parts at either or both vertices of W_1. Dyson has called these "b-divergences" and their expected effect is appearance of an extra factor Z_1^{-1} in his Eqs. (88) and (89). In order to demonstrate the possibility of renormalization, it is vital that this factor should appear; and it is the purpose of this paper to attempt a formal proof. The considerations presented here throw some light on the prospects of renormalization for scalar electrodynamics.

II. SEPARATION OF OVERLAPPING DIVERGENCES

Dyson[2] (unpublished) has defined a for.nal mathematical procedure for the isolation of the divergent part from an integral representing overlapping divergent graphs. This procedure is illustrated most readily by an example.

Figure 2 represents an electron self-energy graph which could be obtained by the insertion of a V part at vertex a or b of Fig. 1. Here

$$\Sigma(W_2, p)=e^4\int\int dt_1dt_2F_\mu(p, t_1)G_{\nu\mu}(p, t_1, t_2)H_\nu(p, t_2), \quad (1)$$

where

$$F_\mu(p, t_1)=\frac{1}{t_1^2}\gamma_\mu\frac{i\gamma(p-t_1)-\kappa}{(p-t_1)^2+\kappa^2},$$

$$G_{\nu\mu}(p, t_1, t_2)=\gamma_\nu\frac{i\gamma(p-t_1-t_2)-\kappa}{(p-t_1-t_2)^2+\kappa^2}\gamma_\mu,$$

$$H_\nu(p, t_2)=\frac{i\gamma(p-t_2)-\kappa}{(p-t_2)^2+\kappa^2}\gamma_\nu\frac{1}{t_2^2}.$$

Not only is the double integral over t_1t_2 linearly divergent, but it also diverges logarithmically if the integration is performed over either t_1 or t_2, while the other variable is held fixed. In order to isolate these divergences, we use (here and in the subsequent work) the invariant separation procedure outlined in Sec. VI of D II.

Rewrite Eq. (1) as follows:

$$\begin{aligned}\Sigma(W_2, p)=e^4\int\int dt_1dt_2[&F_\mu(p, t_1)G_{\nu\mu}(p, t_1, t_2)H_\nu(p, t_2)\\&-F_\mu(p_0, t_1)G_{\nu\mu}(p_0, t_1, 0)H_\nu(p, t_2)\\&-F_\mu(p, t_1)G_{\nu\mu}(p_0, 0, t_2)H_\nu(p_0, t_2)]\\&+e^4\left(\int dt_1F_\mu(p_0, t_1)G_{\nu\mu}(p_0, t_1, 0)\right)\\&\times\left(\int dt_2H_\nu(p, t_2)\right)+e^4\left(\int dt_1F_\mu(p, t_1)\right)\\&\times\left(\int dt_2G_{\nu\mu}(p_0, 0, t_2)H_\nu(p_0, t_2)\right), \quad (2)\end{aligned}$$

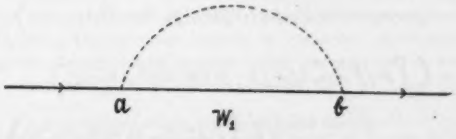

FIG. 1.

[1] F. J. Dyson, Phys. Rev. **75**, 1736 (1949), referred to as D II, in this paper.
[2] The only published calculation for an integral corresponding to an overlapping (fourth order) graph is that of R. Jost and J. M. Luttinger, Helv. Phys. Acta **23**, 201 (1949), who have followed Dyson's procedure.

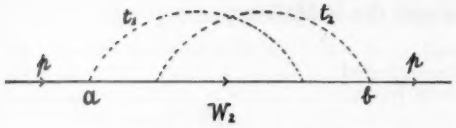

FIG. 2.

where $p_0^2+\kappa^2=0$, $i\gamma p_0+\kappa=0$. If

$$\int dt_1 F_\mu(p_0, t_1)G_{\nu\mu}(p_0, t_1, 0)=L_a\gamma_\nu,$$

$$\int dt_2 G_{\nu\mu}(p_0, 0, t_2)H_\nu(p_0, t_2)=L_b\gamma_\mu,$$

then we write

$$\Sigma(W_2, p)=e^4\int\int dt_1dt_2[R(p, t_1, t_2)]$$

$$+e^4L_a\int\gamma_\nu H_\nu(p, t_2)dt_2+e^4L_b\int F_\mu(p, t_1)\gamma_\mu dt_1, \quad (3)$$

where $R(p, t_1, t_2)$ is the expression within square brackets in Eq. (2).

The terms within the square bracket are such that if t_2 is held fixed, the integration over t_1 is convergent if the first and the second terms are combined—this second term being obtained by putting in those factors of $F_\mu(p, t_1)G_{\nu\mu}(p, t_1, t_2)H_\nu(p, t_2)$ which contain t_1, all momenta other than t_1 equal to their free particle values—while, if t_1 is held fixed, the first and the third terms in the square bracket combine to give a convergent t_2 integration.

Algebraically, it is impossible to find a single term which if subtracted might make the t_1 and t_2 integrations convergent simultaneously. Even as it stands, the expression within the square brackets, is, as a whole, convergent neither over t_1 nor over t_2, nor has this subtraction made any difference in its degree of divergence when the double integration is performed. However, when t_2 is held fixed and the integration over t_1 is performed, the third term in the square bracket

$$-\int\int dt_1dt_2F_\mu(p, t_1)G_{\nu\mu}(p_0, 0, t_2)H_\nu(p_0, t_2)$$

can be written

$$-\left\langle\int\int dt_1dt_2[F_\mu(p, t_1)-F_\mu(p_0, t_1)\right.$$

$$\left.-(p-p_0)(\partial/\partial p)F_\mu(p_0, t_1)](G_{\nu\mu}(p_0, 0, t_2)H_\nu(p_0, t_2))\right\rangle$$

$$-\left\langle\int dt_1(F_\mu(p_0, t_1)+(p-p_0)(\partial/\partial p)F_\mu(p_0, t_1))\right\rangle$$

$$\times\left\langle\int dt_2G_{\nu\mu}(p_0, 0, t_2)H_\nu(p_0, t_2)\right\rangle.$$

The integrand in the first angular bracket, $\langle\ \rangle$, above is absolutely convergent as far as the t_1 integration is concerned, while the second angular bracket, $\langle\ \rangle\langle\ \rangle$, is a product of a divergent constant L_b with a term of the form $A+B(\gamma p-i\kappa)$. Hence, with t_2 fixed, the integral of $R(p, t_1, t_2)$ over t_1 consists of an absolutely convergent part together with a divergent part, the latter being unambiguous and fully determinate. Since a similar result holds for t_2, we can say that the expression in the square bracket is "convergent" in a special sense over both the t_1 and t_2 integrations. It is to be emphasized that this has been made possible because, in the second (and also the third) term in the square bracket, the overlap factor G no longer appears as a function of two variables and so the integrand $F_\mu(p_0, t_1)G_{\nu\mu}(p_0, t_1, 0)H_\nu(p, t_2)$ splits into a product of two functions, each a function of a single variable.

In order to obtain the absolutely convergent (and physically significant) part of $\Sigma(W_2, p)$, we now perform the final separation. Thus,

$$\Sigma_c(W_2, p)=e^4\int\int dt_1dt_2[R(p, t_1, t_2)-R(p_0, t_1, t_2)$$

$$-(p-p_0)(\partial/\partial p)R(p_0, t_1, t_2)]. \quad (4)$$

If Eq. (4) is written out in full, we notice the basic point of this procedure. Whereas, in Eq. (4), we have subtracted terms with a view to securing convergence over the double integration, we have also succeeded, by the same step, in making $\Sigma_c(W_2, p)$ convergent for each of the two t_1 and t_2 integrations. The part which we designated above as the unambiguous and fully determinate divergent part of the t_1 integration, has in fact canceled out.[2a] The first subtraction in Eq. (2) made the expression "convergent" in our special sense over and t_2, the final subtraction in Eq. (4) made it absolutely convergent over all the t_1, t_2 and t_1t_2 integrations. With the final step we have succeeded in isolating from the integral, divergences corresponding to the inserted V parts as well as the divergence corresponding to the over-all S part.

III. GENERAL RULES FOR THE SEPARATION OF DIVERGENCES

The procedure of Sec. II for the separation of divergent parts can be generalized to apply to any divergent n-fold integral howsoever complicated by overlapping or non-overlapping insertions. Consider a graph having n basic[3] momentum-vectors t_i associated with internal lines, such that the momentum vectors of the remaining lines are expressed in terms of these n vectors. The contribution to the corresponding matrix element is an integral, I, over n variables.

In general the integral will consist of a product of functions of each variable t_i (and possibly of momenta corresponding to external lines) with overlap functions,

[2a] This has happened because the integrals multiplying L_a and L_b in Eq. (3) are themselves self-energy integrals.

[3] P. T. Matthews, Phil. Mag. 41, 185 (1950).

i.e., functions of two or more variables, t_i. If a set of variables $t_a t_b \cdots t_m$ is held fixed, the integration over the remaining variables will be called a "subintegration." To estimate the convergence of each subintegration we employ the considerations given in Sec. V of D II and merely count the powers of the relevant t in the numerator and the denominator of the integrand. An n-fold integral, I, will be absolutely convergent if, besides the final integration, the subintegrations over all of the smaller sets of variables t_i, $t_i t_j$, $t_i t_j t_k$, $\cdots$, are also absolutely convergent for all possible choices of the basic variables. If by merely counting the powers of t_i we find that an integral is itself convergent, while any one of the subintegrations is not, the integral will be called "superficially convergent."

In general in an n-fold integral over $t_1 t_2 \cdots t_n$ a subintegration over $t_1 t_2 \cdots t_r$ can be made convergent only if we subtract from the integrand terms in which those factors in the integrand which are functions of $t_{r+1}, \cdots t_n$ only are left unchanged, while in the remaining factors the external momenta (which now include $t_{r+1}, \cdots t_n$) are given their free-particle values. Thus, to fulfill the condition of convergence over all subintegrations, we must subtract from the integral divergent terms corresponding to each subintegration, the degree of divergence of the integrand for a particular subintegration, in general, being unaffected by subtractions corresponding to other subintegrations.

The considerations of Sec. II can now be generalized. We define true divergence over a subintegration $t_1 t_2 \cdots t_r$ as the divergent part finally to be subtracted corresponding to this subintegration, in order to make the subintegration absolutely convergent, after the terms involving divergences corresponding to t_i, $t_i t_j$, $t_i t_j t_k$, $\cdots$, $t_1 t_2 \cdots t_{r-1}$, $\cdots$ subintegrations have already been separated. Anticipating the procedure to be formulated, we shall find that the above-mentioned divergences, corresponding to these latter integrations over smaller number of variables are themselves their true divergences. Thus, for example, to obtain the true divergence over $t_1 t_2$ subintegration we hold, first, all variables except t_1 fixed and subtract from the integrand divergent terms corresponding to t_1, leaving the rest of the integrand unchanged; similarly, holding all variables except t_2 fixed, we subtract divergent terms corresponding to t_2. Finally, holding all variables except $t_1 t_2$ fixed in this *new* integrand, we subtract divergent terms corresponding to the double integration. These last constitute the true divergence over $t_1 t_2$ subintegration. The integrand after the separation of all these divergent parts is absolutely convergent as far as $t_1 t_2$ subintegration is concerned.

We can now give, in analogy with Sec. II, unambiguous rules for the separation of divergences from an n-fold integral. Before making the final subtraction corresponding to the n-fold integration which will make the remaining integral an absolutely convergent one, we subtract from the integrand divergent terms corresponding to each of the subintegrations t_i, $t_i t_j$, $t_i t_j t_k$, $\cdots$, $t_1 t_2 \cdots t_{n-1}$. The divergent term to be separated corresponding to the $t_i t_j$ subintegration would, for example, consist of an n-fold integral over $t_1 t_2 \cdots t_n$, in which the part of the integrand containing t_i or t_j is such as to give, on integration, the true divergence corresponding to $t_i t_j$ multiplied by those factors in the original integrand which contain neither t_i nor t_j and have thus been left unchanged. In this expression, the integration over all variables other than $t_i t_j$ will correspond to a graph which we shall call the "reduced graph," and the corresponding integral the "reduced integral." Thus, in Sec. II, $\int dt_2 \gamma_\nu H_\nu(p, t_2)$ and $\int dt_1 F_\mu(p, t_1)\gamma_\mu$ are reduced integrals.

Our final result can be stated thus. The entire divergence to be separated from an n-fold integral is equal to the true divergence over the t_1 integration multiplied by the reduced integral over $t_2 \cdots t_n$ plus the true divergence over the t_2 integration multiplied by the reduced integral over $t_1 t_3 \cdots t_n$ and so on, together with the true divergence over the $t_1 t_2$ integration multiplied by the reduced integral over $t_3 t_4 \cdots t_n$ and so on, together with similar sets of terms ending finally with the true divergence over the final $t_1 t_2 \cdots t_n$ integration. After all these divergent terms have been isolated, the remainder is an absolutely convergent integral.

The maximum possible number of terms which may need to be isolated is $2^n - 1$. Of course, not all of the subintegrations will be divergent, a considerable number being "superficially" convergent, so that no corresponding separations will need to be made.

It may be possible (and indeed as we shall see later, it is possible in some special cases) to secure the actual convergence of certain subintegrations before the true divergence of the n-fold integration is separated. However, that this last separation will always leave behind an absolutely convergent integral as remainder, would follow from a generalization of considerations given in Sec. II.[3a]

A few remarks on superficial convergence will be relevant at this stage.

(a) In spinor electrodynamics all graphs with four or more external lines (except graphs corresponding to scattering of light by light) are at least superficially convergent. The "scattering of light by light" itself is not a genuine primitive divergent on account of the gauge invariance of the theory. It should, therefore, always be possible to find other graphs which when combined with the graph in question should give a convergent result. We shall therefore treat the integrals corresponding to the "scattering of light by light" too, as being at least formally superficially convergent. Opening two or more lines in a connected self-energy graph always leads to superficial convergence in the connected[3b] part of the remainder and so does the

[3a] A general proof of this will be published elsewhere.

[3b] Any part of a connected graph is joined to the rest by at least two lines.

opening of one or more lines in a vertex part, unless, of course, so many lines are opened that the only connected graph left is a V part. These considerations will immediately give the number of superficially convergent integrations, when dealing with S or V parts.

If an internal line t in a graph contains a self-energy insertion with associated momenta $t_1, t_2, \cdots t_r$, then the subintegrations over tt_i, tt_it_j, $\cdots$, $tt_1t_2\cdots t_{r-1}$, $\cdots$ (but not $tt_1t_2\cdots t_r$) are superficially convergent. t, being an internal line, itself belongs to a loop, which at the very worst consists of two electron lines, with but two external photon lines, the whole forming as far as $tt_1\cdots t_r$ integration is concerned, a photon self-energy graph. Opening one single line belonging to the self-energy insertion inside t gives at worst a scattering of light by light graph. Thus the subintegrations tt_i, tt_it_j, $\cdots$, $tt_1\cdots t_{r-2}$, $\cdots$ are certainly superficially convergent, while with the convention adopted above for the scattering of light by light graphs, the subintegrations over the last set $tt_1t_2\cdots t_{r-1}$, $\cdots$ are also superficially convergent.

(b) If two sets of variables $(t_i\cdots t_j)$ and $(t_a\cdots t_b)$ are such that the corresponding graphs do not overlap and if the integration over each set has been made convergent, then the product of these convergent integrands is also convergent over the subintegrations t_i, t_a, t_it_a, $\cdots$, $t_i\cdots t_jt_a\cdots t_b$. For integration of functions with no overlap terms certain new features arise. Taking a simple example, the integral $\int\int dt_1dt_2F(p, t_1)G(p, t_2)$ has no overlap term, and thus, if both t_1 and t_2 subintegrations are divergent (in this example logarithmically),

$$\int\int dt_1dt_2[F(p, t_1)-F(p_0, t_1)][G(p, t_2)-G(p_0, t_2)]$$

is absolutely convergent. We notice that the divergent part separated is

$$\int\int dt_1dt_2[F(p, t_1)G(p_0, t_2) + F(p_0, t_1)G(p, t_2)-F(p_0, t_1)G(p_0, t_2)].$$

Although it loses its precise significance, we may still formally retain the expression "true divergence" over t_1 for $\int dt_1F(p_0, t_1)$, over t_2 for $\int dt_2G(p_0, t_2)$, and over t_1t_2 for $-\int\int dt_1dt_2F(p_0, t_1)G(p_0, t_2)$. The negative sign before the true divergence from t_1t_2 integration, when overlap does not occur, makes the use of our general rule inconvenient for non-overlapping graphs.

The above remarks do show, however, that for non-overlapping graphs it is immaterial in what order divergences are removed, while for divergences arising from graphs one of which is completely contained in the other, Dyson's prescription of successive removal starting from the innermost insertion is a particular case of the general rule given above. We shall illustrate this rather more fully by considering self-energy insertions.

(c) Suppose a line t, in a graph I, contains a self-energy insertion with momenta $t_1, t_2, \cdots t_r$. It will be convenient to remove divergent parts from the integral corresponding to subintegrations $t_1, \cdots t_1t_2, \cdots, t_1t_2\cdots t_r$. After the "true divergence" over $t_1t_2\cdots t_r$ has been removed, the subintegration over this set is left absolutely convergent. The momenta associated with the self-energy insertion in line t define (except for t), no overlap function with any other momentum variable t_a in I. According to Remark (b), if the integrand is made convergent over t_a, its convergence over t_at_1, $\cdots t_at_1t_2\cdots t_r$, is already assured. Remark (a) shows that the same result holds for the only variable (t) which does have overlap functions with these variables. At this stage the only integrations in which $t_1, t_2, \cdots t_r$ appear explicitly are the $tt_1t_2\cdots t_r$ subintegration, and other subintegrations in which these variables appear as a group. But from considerations given by Dyson we know already that, for questions of convergence, this group will behave precisely as though the line t had no insertion inside it. This shows that it is immaterial whether we retain the variables $t_1, t_2, \cdots t_r$ or perform the integration over them at this stage; the latter procedure implies replacing $S_F(t)$ by $S_c(t)S_F(t)/2\pi$, which is precisely the result one would get if one followed the procedure of successive removal as described in D II. By using results on superficially convergent subintegrations derived by applying Remark (a), a similar proof could be constructed to show the validity of the procedure of successive removal for divergence arising from V parts one of which is completely contained in the other.

IV. APPLICATION TO ELECTRON SELF-ENERGY GRAPHS

We shall now apply the above considerations to the case of electron self-energy graphs. According to the Dyson-Feynman procedure for obtaining the effective radiative corrections to any physical process, one draws the relevant irreducible graphs and then replaces S_F by S_{F1}', D_F by D_{F1}', and γ_μ by $\Gamma_{\mu 1}$ in the corresponding integrals. One already uses the same procedure for calculating $\Gamma_{\mu 1}$ itself (Sec. VII, D II); one draws all of the irreducible vertex graphs and then makes the above substitutions. We attempt to obtain a similar set of self-energy graphs in which these substitutions can be made unambiguously—only in this case this set of graphs will not be irreducible. For this purpose we establish the following categories of self-energy graphs.

Category [1] consists of the sole irreducible self-energy graph in Fig. 1.

Category [2] consists of all graphs formed by inserting[4] at the end vertex b in Fig. 1 all irreducible V parts of any order in e. The first end vertex of each category $[n]$ will be called a and the last b, although sometimes, for clarity, we use $a_{[n]}$ and $b_{[n]}$.

To obtain the graphs in category [3] insert at $b_{[2]}$ all

[4] End vertices of self-energy graphs, vertex graphs, or Compton graphs, are the vertices where the external electron line enters or leaves the graph.

irreducible vertex parts, and so on for all subsequent categories.

Continuing the above procedure we obtain an infinite number of categories, each (except [1]) containing an infinite number of graphs. Figure 2, for example, belongs to category [2]. All graphs in $[n]$ can, in fact, be built up in precisely n different ways from the graph in Fig. 1 by the insertion of vertex parts at $a_{[1]}$ or $b_{[1]}$ or both. Further, all graphs in $[n]$ could equally well have been built by insertions at $a_{[n-1]}$ rather than at $b_{[n-1]}$. This complete symmetry will be found to be important for the subsequent proof.

A graph belonging to $[n]$ will contain precisely $(n-2)$ photon lines such that if these are opened (i.e., their associated integration variables held fixed), the graph splits into two vertex parts. Given a graph in $[n]$ we denote by L_b^1 the divergent constant arising from the irreducible V part which was inserted at $b_{[n-1]}$ in order to obtain this particular graph in $[n]$, by L_b^2 the "true" divergent constant arising from the reducible part which was inserted at $b_{[n-2]}$ to obtain this graph in $[n]$, and so on. This last V part is reducible because its end vertex has as an insertion the V part with the divergent constant L_b^1. Similar definitions apply for $L_a^1, L_a^2, \cdots$. We shall now prove the following lemmas.

Lemma 1.—Denote by $[n]$ the integral corresponding to a particular graph in the category $[n]$. We have the following result.

$$[n]=\langle L_a^1[n-1]+L_a^2[n-2]+L_a^3[n-3]+\cdots+L_a^{n-1}[1]\rangle \\ +\langle L_b^1[n-1]+L_b^2[n-2]+L_b^3[n-3]+\cdots+L_b^{n-1}[1]\rangle \\ -\left\langle \begin{matrix} L_a^1L_b^1[n-2]+L_a^1L_b^2[n-3]+L_a^1L_b^3[n-4]+\cdots \\ +L_a^2L_b^1[n-3]+L_a^2L_b^2[n-4]+\cdots \end{matrix} \right\rangle \\ +\Sigma_{[n]}{}^*, \quad (5)$$

where

$$\Sigma_{[n]}{}^*=A_{[n]}+B_{[n]}(\gamma\beta-i\kappa)+\Sigma_{\sigma[n]}{}^*.$$

A and B characterize the true divergence from $[n]$, and $[n-r]$ stands for an integral corresponding to a certain graph in category $[n-r]$ obtained from $[n]$ by successive removal of V parts from a or b as the case may be.

Proof.—It is convenient to associate the basic variables with the photon lines in the graph. Suppose $[n]$ has k basic variables of which $n-2$ are critical. The photon line l_1 starts from $a_{[n]}$, while l_k ends at $b_{[n]}$.

For the proof we shall systematize our procedure as follows: we hold each one of the variables l_i initially fixed, in turn, and remove all of the divergent terms corresponding to all possible subintegrations over the remaining $(n-1)$ variables. Of course, in following this procedure we shall have to guard against subtracting a divergent term more than once. However, holding l_k fixed we make the removal unambiguously corresponding to the subintegrations $l_1, \cdots, l_{k-1}, l_1l_2, \cdots, l_1l_{k-1}, l_2l_3, \cdots, l_2l_{k-1}, \cdots, l_1l_2l_3, \cdots, l_1l_2\cdots l_{k-1}$. This immediately gives us the terms in the first bracket of Eq. (5) by our general rule. The constants $L_a^1, L_a^2, \cdots$, etc., come from the successive reduction of a reducible vertex parts. It is to be emphasized that the first line in Eq. (5) is the result of the removal of divergences, corresponding to all the above subintegrations, due regard being paid to those subintegrations which are superficially convergent [see Remark (a)]. Now holding l_1 fixed we remove divergent terms corresponding to all the possible subintegrations over subsets of variables $l_2, l_3, \cdots l_k$. A number of these terms (those, for example, corresponding to subintegrations over $l_2, l_2, \cdots l_{k-1}, l_2l_3, \cdots l_2l_{k-1}, \cdots$, etc.) have already been removed. However, the subintegrations from these subsets which still remain, i.e., over $l_k, l_kl_{k-1}, \cdots l_kl_2, \cdots l_kl_{k-1}l_{k-2}, \cdots$ (barring those which are superficially convergent), cover the successive divergent parts of the (reducible) vertex graph one obtains by opening the line l_1 and are just sufficient to give us the second bracket in Eq. (5). The maximum number of subintegrations corresponding to which divergent terms still remain to be separated is 2^{k-2} at this stage. These terms must be separated by holding each of the remaining $k-2$ basic variables initially fixed. Of these only $(n-2)$ are critical. As noted earlier, opening a critical line splits the graph into two disconnected segments with no overlap term between them. As an example, let us assume l_2 to be the first critical variable, occurring from the left. Holding it fixed, we notice that the only divergent terms yet to be separated are the true divergences corresponding to the subintegrations $l_1l_k, l_1l_kl_{k-1}, l_1l_kl_{k-2}, \cdots$, those corresponding to $l_1, l_k, l_kl_{k-1}, l_kl_{k-2}, \cdots$, etc., already having been removed. Since these are the true divergences for integrations over non-overlapping parts, we shall get a negative sign before the separated terms as noted in Remark (b). This leads to the isolation of divergent terms of the form $-L_a^2L_b^1[n-2]$. Starting from end a and opening all the critical lines, we shall get all the subtracted terms on the right-hand side of the Eq. (5). It remains to prove now that holding each one of the remaining $(k-n)$ lines fixed gives no further divergent terms to be separated. We notice that every other line, if opened, converts the graph into a C part,[5] which we know to be at least superficially convergent in spinor electrodynamics. If the C part obtained by opening a line is reducible, the only insertions its irreducible skeleton has are vertex parts, inserted at its end vertices. But the divergent terms corresponding to the subintegrations over the variables associated with these vertex insertions have already been removed by the successive removal performed by holding l_1 and l_k fixed initially. Thus, these C parts give no further contribution to Eq. (5). This establishes the lemma.

If we had started with basic variables associated with electron rather than with photon lines, opening a basic line would convert the graph into an M part[6]—again at least superficially convergent—and similar considerations would apply.

Lemma 2.—This is a restatement of Remark (c) for the particular case of graphs in these categories. The divergent separations after inserting S parts in all the lines or V parts in all the *internal* vertices (all vertices except a and b) of $[n]$ are given by the divergent parts corresponding to the subintegrations over the internal variables of the insertions [as in Remark (c)], together with the divergent terms to be separated from $[n]$, where $S_F(l)$ is replaced by $S_c(l)S_F(l)$, $D_F(l)$ by $D_F(l)D_c(l)$, and γ_μ by $\Lambda_{\mu c}(l, l')$. As a concrete example, we see that if a photon self-energy graph is inserted in a line l of $[n]$, such that $D_F(l)\Pi^*(l)=C+D_c(l)$, then the resulting integral is equal to $C[n]+[n]^\times$, where $[n]^\times$ is the integral obtained by replacing $D_F(l)$ by $D_c(l)D_F(l)$ in the integrand. The proof is exactly similar to that of Remark (c).

If we now desire to construct all self-energy graphs up to a given order e^{2k+2}, say, we draw all of the graphs in the various categories defined above up to this order. No graph belonging to category $[k+2]$ or higher will be needed, the lowest order graph belonging to the category $[k+2]$ being of the order e^{2k+4}. Taking each one of the graphs drawn above, V and S parts will be inserted in its internal vertices and all its lines. *No insertions are ever to be made in the end vertices of the graphs of any category.* If the graph in which insertions are being made is of order $2r$, these insertions need only consist of graphs up to the order $(2k-2r+2)$.

It is easy to verify now that the above procedure gives accurately all self-energy graphs up to order $(2k+2)$ and that no graph appears more than once. Among them we shall, of course, find all the graphs which could have been obtained by insertions of vertex parts up to order $2k$ at the vertices a (or b) of the fundamental self-energy graph in Fig. 1. To verify the appearance of all vertex parts, up to the given order, we notice, for example, that by the very principle of their construction the graphs of

[5] A Compton graph—a graph with 2 external photon and 2 external electron lines.

[6] Møller graph—a graph with four external electron lines.

category [3] represent the insertion of vertex parts in the end vertices of graphs of category [2], while the insertions in their own end vertices are given by the graphs of the higher categories.

Correspondingly, adopting the procedure in Sec. VII of D II of dropping the divergent constants when they appear, if we assume that S_{F1}', D_{F1}', $\Gamma_{\mu 1}$ are defined up to order e^{2k} by, respectively, S_F plus S_F multiplied by a finite sum of products of $S(W,l)$, D_F plus D_F multiplied by a finite sum of products of $D(W,l)$, and γ_μ plus a finite sum of $\Lambda_{\mu\epsilon}(l,l')$, we can obtain S_{F1}' up to the order e^{2k+2} by drawing all of the graphs in the various categories, up to the order e^{2k+2}, and then substituting in all lines S_{F1}', D_{F1}' (*defined as above*) instead of S_F and D_F, and $\Gamma_{\mu 1}$ in all internal vertices instead of γ_μ. The γ_μ occurring at the two end vertices are always to be left unchanged. Once again, in a graph of order $2r$ belonging to any one of the categories, it will only be necessary to substitute S_{F1}', etc., up to the order $(2k-2r+2)$.

Lemma 3.—If by the above changes in all of the lines and internal vertices of an integral arising from a graph in category $[n]$ we obtain an integral $[n]^\times$, then

$$[n]^\times = L_a^{1\times}[n-1]^\times + L_a^{2\times}[n-2]^\times + L_a^{3\times}[n-3]^\times + \cdots + L_b^{1\times}[n-1]^\times + L_b^{2\times}[n-2]^\times + L_b^{3\times}[n-3]^\times + \cdots - (L_a^{1\times}L_b^{1\times}[n-1]^\times + L_a^{1\times}L_b^{2\times}[n-3]^\times + \cdots) + \Sigma^*{}_{[n]}{}^\times,$$

where $L_a^{1\times}$ stands for the "true" divergent constant from the V part introduced at $a_{[n-1]}$ in $[n-1]^\times$ in order to obtain $[n]^\times$. The definition of the other constants is similar. Noticing that $S_{F1}'(l)$ and $D_{F1}'(l)$, and $\Gamma_{\mu 1}$, as defined above, behave precisely as do $S_F(l)$, $D_F(l)$, and γ_μ as far as the power of variables involved and the question of convergence are concerned, the proof follows from Lemma 1.

Lemma 3 immediately gives the following set of equations

$$\begin{aligned}
[1]^\times &= \Sigma^*{}_{[1]}{}^\times \\
[2]^\times &= (L_a^{1\times} + L_b^{1\times})[1]^\times + \Sigma^*{}_{[2]}{}^\times \\
[3]^\times &= (L_a^{1\times} + L_b^{1\times})[2]^\times + (L_a^{2\times} + L_b^{2\times})[1]^\times \\
&\qquad - L_a^{1\times}L_b^{1\times}[1]^\times + \Sigma^*{}_{[3]}{}^\times \\
&\cdots\cdots\cdots

wave functions, that such graphs are in fact not divergent.[7]

In the sequel we shall consider pseudoscalar (charged or neutral) and scalar (charged) theories. Thus, besides the primitive divergents in electrodynamics the only new feature would be the divergent graphs corresponding to the Møller scattering of two mesons (M-parts). Following a suggestion first given by Matthews, it will be proved that the divergences arising from these M parts can be canceled consistently by adding an appropriate δ-type interaction between mesons to the lagrangian. We consider in detail only the case of pseudoscalar neutral meson, the remaining cases being almost identical.

Following Matthews we write the interaction hamiltonian as

$$H_1(x)=if\bar{\psi}(x)\gamma_5\psi(x)\phi(x)-hc\delta\kappa_0\bar{\psi}(x)\psi(x) -\tfrac{1}{2}\delta\kappa^2\phi^2(x)-\delta\lambda\phi^4(x).$$

The corresponding graphs will have, besides the vertices with two nucleon and one meson line incident, also vertices with two nucleon, two meson, or four meson lines incident. These last will be called 4-vertices, while graphs formed entirely from 3-vertices will be called the "original graphs."

The following remark will apply to all except meson self-energy graphs, which will be considered later.

Corresponding to any original graph (formed entirely from 3-vertices), which itself represents a Møller scattering of mesons, or contains M parts inside itself, there exist in the theory graphs formed by replacing the M parts by 4-vertices *in all possible ways*. It is easy to verify that for a field theory with ϕ^4 as the only interaction term there are two primitive divergent graphs, graphs with two external meson lines (meson self-energy graphs), and graphs with four external meson lines (M parts).

We shall call a graph "simple" if it does not contain an M part inside itself, or is a Møller graph which cannot be formed by joining two or more M parts. We shall retain the definition of reducibility of a graph as adopted in electrodynamics. Thus, a graph may not be "simple" but may still be irreducible if it satisfies the criteria of irreducibility as in electrodynamics.

To choose the constant $\delta\lambda$ we proceed in three steps.

(1) Consider the category of all original M parts which are both "simple" and irreducible. If $\delta\lambda$ is chosen

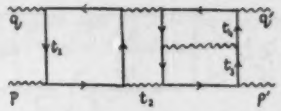

FIG. 3.

equal to the sum of their true divergences (the true divergence of an M part consists of a constant), the term $-\delta\lambda\phi^4$ suffices to cancel all divergences arising from the above graphs. $\delta\lambda$ is thus a power series in f.

(2) Now consider the category of all original irreducible M parts which are not simple. Before removing the true divergence from the over-all M part, divergent terms have to be removed corresponding to the M parts inside the graph in accordance with the procedure given in Sec. III. We illustrate the points involved with a simple example. Figure 3 represents an (irreducible) M part obtained by joining two simple M parts. The corresponding integral is given by[8]

$$f^{10}\int dt_1dt_2dt_3dt_4[\text{Trace }\gamma_5S(p+t_1)\gamma_5S(p+t_1-t_2) \times\gamma_5S(t_1-q)\gamma_5S(t_1)]\Delta(t_2)\Delta(p+q-t_2) \times[\text{Trace }\gamma_5S(p'+t_3)\gamma_5S(t_3)\gamma_5S(t_4)\gamma_5S(t_4-q') \times\gamma_5S(p'+t_4-t_2)\gamma_5S(p'+t_3-t_2)]\Delta(t_4-t_3).$$

The integral is logarithmically divergent with respect to the t_1, t_2t_4, and $t_1t_2t_4$ subintegrations, besides being logarithmically divergent with respect to the final 4-fold integration. The remaining subintegrations are at least superficially convergent.

The divergent terms to be separated before the true divergence over $t_1t_2t_3t_4$ is separated, in order to leave behind an absolutely convergent integral are

$$(\delta\lambda)_1f^8\int dt_2dt_3dt_4\Delta(t_2)\Delta(p+q-t_2) \times[\text{Trace }\gamma_5S(p'+t_3)\gamma_5S(t_3)\gamma_5S(t_4)\gamma_5S(t_4-q') \times\gamma_5S(p'+t_4-t_2)\gamma_5S(p'+t_3-t_2)]\Delta(t_4-t_3) +(\delta\lambda)_2f^4\int dt_1dt_2[\text{Trace }\gamma_5S(p+t_1)\gamma_5S(p+t_1-t_2) \times\gamma_5S(t_1-q)\gamma_5S(t_1)]\Delta(t_2)\Delta(p+q-t_2) -(\delta\lambda)_1(\delta\lambda)_2\int dt_2\Delta(t_2)\Delta(p+q-t_2),$$

where

$$(\delta\lambda)_1=f^4\int dt_1[\text{Trace }\gamma_5S(p_0+t_1)\gamma_5S(p_0+t_1-t_{20}) \times\gamma_5S(t_1-q_0)\gamma_5S(t_1)]$$

$$(\delta\lambda)_2=f^6\int dt_2dt_4[\text{Trace }\gamma_5S(p_0'+t_2)\gamma_5S(t_2) \times\gamma_5S(t_4)\gamma_5S(t_4-q_0')\gamma_5S(p_0'+t_4-t_{20}) \times\gamma_5S(p_0'+t_2-t_{20})]\Delta(t_4-t_2)$$

and

$$p_0=q_0=p_0'=q_0'=t_{20},\quad p_0^2+\kappa^2=0$$

[7] *Note added in proof.*—Dyson has, in fact, proved that the contribution $F(p_1, p_2, p_3)$ from any graph with just three meson lines (p_1, p_2, p_3) in neutral pseudoscalar theory vanishes identically. Let $\bar{p}$ be a vector obtained from p by space reflection. Since $\phi(p_1)\phi(p_2)\phi(p_3)F(p_1, p_2, p_3)$ is a scalar, $F(p_1, p_2, p_3)$ is a pseudoscalar function and therefore $F(\bar{p})=-F(p)$. (This can be demonstrated by a more explicit mathematical proof.) But $F(\bar{p})$ is invariant under a proper Lorentz transformation; for example, under a space rotation, through 180° about an axis in line perpendicular to p_1 and p_2, which transforms p_1 to $\bar{p}_1$ and p_2 to $\bar{p}_2$, and since $p_1+p_2+p_3=0$, also transforms p_3 to $\bar{p}_3$. Therefore, $F(\bar{p})=F(p)$. Hence, $F(p)$ must vanish identically.

The author is indebted to Mr. F. J. Dyson for kindly communicating the proof.

[8] S and Δ stand for Feynman's functions.

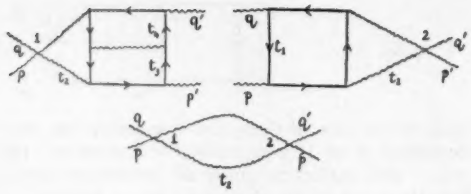

FIG. 4.

$(\delta\lambda)_1$, is the true divergence over t_1, $(\delta\lambda)_2$ over t_3t_4, and $-(\delta\lambda)_1\times(\delta\lambda)_2$ over $t_1t_3t_4$. The negative sign before the latter follows from the considerations about non-overlapping graphs given in Remarks in Sec. III.

Now we notice that on account of the presence of $-\delta\lambda\phi^4$ term in the hamiltonian with $\delta\lambda$ (for the present) chosen as the sum of true divergences from all irreducible simple M parts, there are three other graphs of order f^{10} in the theory, *viz.*, the graphs in Fig. 4. Since $\delta\lambda$ contains among other terms $(\delta\lambda)_1$ and $(\delta\lambda)_2$, we may assume that in the graphs drawn in Fig. 4 $-(\delta\lambda)_1\phi^4$ acts at the 4-vertex marked 1, and $-(\delta\lambda)_2\phi^4$ at the 4-vertex marked 2. Quite obviously the sum of contributions from these four graphs suffices to cancel all the divergent terms exhibited so far. The true divergence from the $t_1t_2t_3t_4$ integration $(\delta\lambda)_3$ which still remains to be separated from (1) to leave behind a convergent integral will now be added $\delta\lambda$ to already formed and we secure the cancellation of all divergences if for this process the graph consisting of a single 4-vertex $-(\delta\lambda)_3\phi^4$ is also taken into account. Thus if we consider all (irreducible) M parts which are not simple, only the true divergence over the final integration need be added to the $\delta\lambda$ term formed by adding the true divergences from all irreducible simple M parts. The result is of general validity and holds for the general case of an M part formed by joining any number of simple M parts.

It may be noticed that the operation of taking the trace does not interfere with the separation of divergences corresponding to an M part which is contained inside another. The reason is that nucleon lines run in loops while (in the case of original graphs) meson lines do not run continuously, thus making it possible to localize M parts unambiguously in this theory.

(3) $\delta\lambda$ so far has been obtained as a power series in f, and is equal to the sum of true divergences from all irreducible M parts. Considering reducible graphs now,

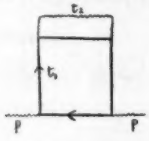

FIG. 5.

we have to consider the effect of inserting S and V parts in all the irreducible M parts. Since $S_F'=Z_2S_{F1}'(f_1)$, $\Delta_F'=Z_3\Delta_{F1}'(f_1)$, and $\Gamma^b=Z_1^{-1}\Gamma_1^b(f_1)$, we replace $S_F(p)$ by $S_{F1}'(p)$, $\Delta_F(p)$ by $\Delta_{F1}'(p)$, and γ_b by $\Gamma_1^b(p,p')$ in all the lines and the vertices of the original irreducible M parts. An irreducible M part of order $2r$ contains $2r$ 3-vertices, $2r$ nucleon lines, and $r-2$ meson lines. The above substitutions give $f^{2r}Z_1^{-2r}Z_2^{2r}Z_3^{r-2}=Z_3^{-2}f_1^{2r}$ as the f-factor outside the integral corresponding to this irreducible M part, while the integral itself can be written as the sum of divergent and convergent terms, both expressed as power series in f_1. Extending the arguments given above for irreducible graphs we readily see that finally $\delta\lambda(f_1)=Z_3^{-2}\times M_d(f_1)$, where $M_d(f_1)$ is a power series in f_1 (starting with a term f_1^4) each of whose terms corresponds to the true divergence of some original M part.

So far we have proved that with the above choice of $\delta\lambda$ not only can all divergent terms be separated from the integral corresponding to the original M parts to be canceled, but further that the new M graphs introduced into the theory because of the term $-\delta\lambda\phi^4$ in the hamiltonian are also accounted for.

Similar arguments prove that if we are considering graphs corresponding to any other process (except meson self-energy graphs) which contain M parts inside them, a combination of the original graphs for the process, with graphs obtained by replacing the M parts by 4-vertices *in all possible ways* will always lead to a cancellation of all divergences arising from the contained M parts, in the original graphs. The rest of the proof for the finiteness of the S-matrix follows D II.

(B) Meson Self-Energy Graphs

We now consider the case of meson self-energy graphs. By joining up an incoming meson line to an outgoing meson line in any M part we obtain a meson self-energy graph. Conversely, in a meson self-energy graph, if any meson line is opened, we obtain an M part. Just as it was impossible to make the substitution $\Gamma_{\mu 1}$ for γ_μ at the end vertices of a self-energy graph in electrodynamics unambiguously, similarly, it is impossible to make an unambiguous substitution Δ_{F1}' for Δ_F (or S_{F1}' for S_F) if we desire to obtain a higher order meson self-energy graph from one of lower order.

However, the procedure for isolating divergences from M parts, outlined in Sec. III, leads to an essential simplification. The principles involved can be illustrated once again by considering a simple example.

Figure 5 represents a meson self-energy graph, in one of the nucleon lines of which a nucleon self-energy graph is inserted. The corresponding integral is

$$\Pi(p)=f^4\int dt_1dt_2[\text{Trace }\gamma_bS(t_1-p)\gamma_bS(t_1)\times\gamma_bS(t_1-t_2)\gamma_bS(t_1)]\Delta(t_2).$$

The integral is logarithmically divergent for the t_1 subintegration, linearly divergent for the t_2 subintegration, and quadratically divergent for the t_1t_2 integration. The divergent terms to be separated in order to leave

behind an absolutely convergent integral are the following:

$$f^4\int dt_1dt_2\,\mathrm{Trace}\,[\gamma_b S(t_1-p_0)\gamma_b S(t_1)$$
$$\times\gamma_b S(t_1-t_{20})\gamma_b S(t_1)]\Delta(t_2)+f^4\int dt_1dt_2$$
$$\times\mathrm{Trace}\,[\gamma_b S(t_1-p)\gamma_b S(t_1)\{\gamma_b S(t_{10}-t_2)\gamma_b$$
$$+\langle(t_1-t_{10})\partial/\partial t_1\rangle_{t_1=t_{10}}(\gamma_b S(t_1-t_2)\gamma_b)\}S(t_1)\Delta(t_2)]$$
$$+\Big\{\Big\{f^4\int dt_1dt_2\,\mathrm{Trace}\,[\gamma_b S(t_1-p_0)\gamma_b S(t_1)$$
$$\times\gamma_b S(t_1-t_2)\gamma_b S(t_1)\Delta(t_2)-\gamma_b S(t_1-p_0)\gamma_b S(t_1)$$
$$\times\gamma_b S(t_1-t_{20})\gamma_b S(t_1)\Delta(t_2)-\gamma_b S(t_1-p_0)\gamma_b S(t_1)$$
$$\times\{\gamma_b S(t_{10}-t_2)\gamma_b+\langle(t_1-t_{10})\partial/\partial t_1\rangle_{t_1=t_{10}}$$
$$\times(\gamma_b S(t_1-t_2)\gamma_b)\}S(t_1)\Delta(t_2)]\Big\}\Big\}$$
$$+f^4\int dt_1dt_2\{(p-p_0)_\mu(\partial/\partial p_\mu)$$
$$+\tfrac{1}{2}(p-p_0)_\mu(p-p_0)_\nu(\partial/\partial p_\mu)(\partial/\partial p_\nu)\}^9{}_{p=p_0}$$
$$\times\mathrm{Trace}\,[\gamma_b S(t_1-p)\gamma_b S(t_1)\gamma_b S(t_1-t_2)$$
$$\times\gamma_b S(t_1)\Delta(t_2)-\gamma_b S(t_1-p)\gamma_b S(t_1)$$
$$\times\{\gamma_b S(t_{10}-t_2)\gamma_b+\langle(t_1-t_{10})\partial/\partial t_1\rangle_{t_1=t_{10}}$$
$$\times(\gamma_b S(t_1-t_2)\gamma_b)\}S(t_1)\Delta(t_2)]. \quad (10)$$

where

$$i\gamma t_{10}+K_0=t_{10}^2+K_0^2=0$$

and

$$t_{20}^2+K^2=p_0^2+K^2=0.$$

Let

$$f^4\int dt_1\,\mathrm{Trace}\,[\gamma_b S(t_1-p_0)\gamma_b S(t_1)$$
$$\times\gamma_b S(t_1-t_{20})\gamma_b S(t_1)]=\delta\lambda,$$
$$f^2\int dt_2,\quad \gamma_b S(t_{10}-t_2)\gamma_b\Delta(t_2)=A,$$

and let the expression in double brackets, $\{\{\ \ \}\}$, in Eq. (10) be equal to A'. Then among others the following are divergent terms separated:

$$\delta\lambda\int dt_2\Delta(t_2)+Af^2\int dt_1$$
$$\times\mathrm{Trace}\,[\gamma_b S(t_1-p)\gamma_b S(t_1)S(t_1)\gamma_b]+A'. \quad (11)$$

The integral with Af^2 as coefficient will be canceled by being combined with the integral arising from the nucleon mass renormalization term $-\delta\kappa_0\bar{\psi}\psi$ in the hamiltonian, while A' is similarly canceled by a proper choice of $\delta\kappa^2$ in the term $-\delta\kappa^2\phi^2$. To cancel $\delta\lambda\int dt_2\Delta(t_2)$ we can combine it with a meson self-energy graph obtained by replacing the M part by a 4-vertex as we have so far been doing; but now we notice that

$$A'=A''-\delta\lambda\int dt_2\Delta(t_2),$$

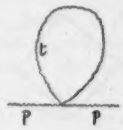

FIG. 6.

where A'' is that value of the meson mass renormalization constant which it would have if M parts were not divergent in the theory; i.e.

$$A''=f^4\int dt_1dt_2\,\mathrm{Trace}\,[\gamma_b S(t_1-p_0)\gamma_b S(t_1)$$
$$\times\gamma_b S(t_1-t_2)\gamma_b S(t_1)\Delta(t_2)-\gamma_b S(t_1-p_0)\gamma_b S(t_1)$$
$$\times\{\gamma_b S(t_{10}-t_2)\gamma_b+\langle(t_1-t_{10})\partial/\partial t_1\rangle_{t_1=t_{10}}$$
$$\times(\gamma_b S(t_1-t_2)\gamma_b)\}S(t_1)\Delta(t_2)],$$

so that (11) can be written as

$$A''+Af^2\int dt_1\,\mathrm{Trace}\,[\gamma_b S(t_1-p)\gamma_b S(t_1)S(t_1)].$$

Further, since $\delta\lambda$ is not a function of p, the divergent term separated corresponding to t_1 gives no contribution to the charge renormalization constant set out in the last integral in Eq. (10) as part of the coefficient of $(p-p_0)_\mu(p-p_0)_\nu$. The result is that the divergent terms to be separated in order to obtain an absolutely convergent integral from a meson self-energy graph are precisely the same as if M-parts were not divergent in the theory, this result holding for only those M parts which are obtained by opening a single meson line in a meson self-energy graph. A further consequence of this is that the self-energy graph in Fig. 6, unlike other graphs containing 4-vertices, has to be considered separately and is not like others a compensatory graph.

The reason why the result shown to hold true for the particular example can be generalized is this. Let us first consider a meson self-energy graph belonging to any category $[n]$. The meson and nucleon lines or the

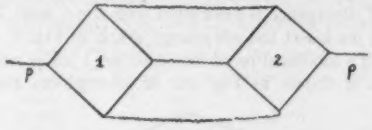

FIG. 7.

vertices in $[n]$ do not contain any S or V insertions so far. In order to remove the divergence from the M part formed by opening a meson line *we must associate one*

[9] The divergent terms shown here corresponding to t_1t_2 integration are of the form $A'+B(p^2+k^2)+C[p_0(p-p_0)]^2$ where C can be shown to be a finite constant. $C[p_0(p-p_0)]^2$ is thus properly to be included in the convergent part of Π^*.

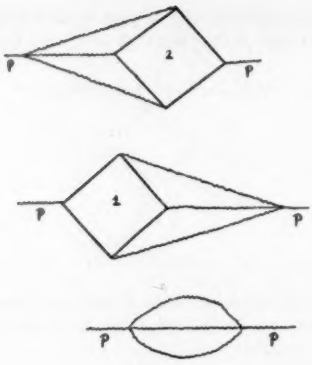

FIG. 8.

of the basic variables, say, t_1, with the particular meson line being opened. The true divergence corresponding to the subintegration $t_2 t_3 \cdots t_k$ is a constant $(\delta\lambda)$ and the reduced integral is necessarily $\int \Delta_F(t_1) d^4 t_1$. Thus, when the final true divergence over $t_1 t_2 \cdots t_k$ is separated, $\Delta_F(t_1)$ not containing the external momentum p, contributes $-\delta\lambda \int dt_1 \Delta_F(t_1)$ to A' and makes no contribution to the charge-renormalization constant at all, precisely as in the particular example. The effect is the same as if M parts were not divergent in the theory, and the mass renormalization constant were not A' but A''.

FIG. 9.

It must be emphasized that the above result holds only for those M parts obtained by opening one meson line. We shall call such M parts "final" M parts. Thus, for example, the self-energy graph shown in Fig. 7 containing the M parts with the loops marked 1 and 2 is necessarily to be combined with three other graphs in Fig. 8 just as in Sec. V(A).

So far we have restricted our considerations to graphs belonging to a category $[n]$ in which S and V parts have not been inserted. To bring out the new features involved we consider another example. Figure 9 shows a meson self-energy graph belonging to $[2]$ in which the M divergence is associated with the t_1 loop. In the line t_2 we insert the self-energy graph in Fig. 5, which is itself a modification of the graph in $[1]$. The resulting graph is shown in Fig. 10. M divergences are now

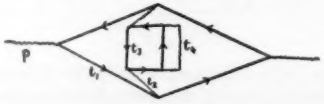

FIG. 10.

associated with the subintegrations over t_3, t_1, $t_1 t_3$, and $t_1 t_2 t_3$. Considering the line t_2 by itself, from the arguments given before it is obvious that we need not make an explicit separation of the M divergence corresponding to t_3. If now the "mass-renormalization constant" corresponding to the line p is considered, it will be seen that not only is it unnecessary to separate the divergence corresponding to $t_1 t_2 t_3$ subintegration (for which only one variable t_4 is held fixed), but the same applies for the t_1 and $t_1 t_3$ subintegrations. The reasoning for all cases is similar. For example, the true divergence over t_1 is obtained by putting, among other variables, p equal to p_0 *wherever* it occurs in the integrand. When the mass renormalization constant corresponding to line p is being separated, its part corresponding to t_1 is the same as above, no further change being necessary, since p has already been replaced by p_0. Thus, $A' = A'' -$ true divergence over $t_1 \times$ the reduced integral over $t_2 t_3 t_4$ $-$ true divergence over $t_1 t_3 \times$ reduced integral over $t_2 t_4$ $-$ true divergence over $t_1 t_2 t_3 \times$ reduced integral over t_4. Similarly, we can see that the *charge* renormalization constant is precisely the same as if these M parts were not divergent in the theory. From our definition, that M corresponding to the subintegration t_3 was the "final" M part contained in the meson self-energy graph (of Fig. 5) inserted in line t_2, while t_1 was the "final" M part for the line p in Fig. 9. Because of the insertion in t_2, new M divergences $t_1 t_3$, $t_1 t_2 t_3$ arise; since they can be associated with p, we shall call the divergences corresponding to t_1, $t_1 t_3$, and $t_1 t_2 t_3$ also "final" divergences associated with the line p in Fig. 10. This is an extension of the definition of "final" M-divergence.[10] In general, the result can be stated thus: given a meson self-energy graph of category $[n]$, the insertion of a meson self-energy graph with a number of final M divergences in any of its meson lines will increase the number (and complexity) of the M divergences in the entire graph. It will always be possible to associate these new divergences as the final M-divergences corresponding to some meson line, making it possible to prove that no explicit separation of corresponding M divergences is needed. We have the result that the mass and charge renormalization constants for meson self-energy graphs are precisely the same as if these "final" M parts were not divergent.

The same results (only simpler to prove) hold for insertions of S and V parts in the nucleon lines and vertices of graphs of categories $[n]$.

The only meson self-energy graph which still needs to be considered is the graph in Fig. 6. All other meson self-energy graphs with 4-vertices act as compensatory graphs like those in Fig. 8. The corresponding integral is

$$-\delta\lambda(f_1) \int \Delta_F'(t) dt = -M_d(f_1) Z_3^{-1} \int \Delta_{F1}'(t) dt,$$

[10] Analytically a final M-divergence inside a meson self-energy graph may be defined such that its reduced integral is independent of the external momentum of the meson line.

so that finally we choose

$$\delta\kappa^2 = -(1/\pi i)Z_2^{-1}(f_1)\left[A''(f_1) - M_d(f_1)\int \Delta_{F1}'(l, f_1)dl\right].$$

This completes the proof.

On account of the results above regarding "final" M-divergences, it will be found expedient to associate basic momenta with nucleon rather with meson lines in graphs belonging to any category $[n]$. This choice will remove all the significant divergences with a single choice of basic variables.

The case of the meson self-energy has been treated at length because it will serve as a prototype for renormalization in other theories such as scalar electrodynamics, where both C and M parts are divergent and it is not possible to make an unambiguous insertion of S parts in meson or photon lines.

The general rule for the separation of divergences given in Sec. III will also apply to other theories such as scalar electrodynamics; but the considerations given in the remarks will not, because both C and M parts are divergent in that theory, leading to overlaps of considerably greater complexity. It is, in fact, in scalar electrodynamics that the power of the general rule formulated in Sec. III exhibits itself. General considerations on that problem will be published shortly.

The author is deeply indebted to Mr. F. J. Dyson for indicating the considerations of Sec. II in an extremely helpful discussion, without which this work would not have been possible, and to Dr. N. Kemmer for continual help and encouragement. The tenure of a scholarship from the Education Department of the Government of Punjab, Pakistan is gratefully acknowledged.

PHYSICAL REVIEW VOLUME 82, NUMBER 2 APRIL 15, 1951

Emission of Protons from the Compound Nucleus F^{18*}

R. R. Roy
Centre de Physique Nucléaire, Université Libre de Bruxelles, Bruxelles, Belgium
(Received September 29, 1950)

The emission of protons from the reaction $N^{14}(\alpha,p)O^{17}$ was studied by photographic emulsion technique. Two groups of protons were observed, of Q values of about -1.16 Mev and -2.0 Mev for $E_\alpha = 3.6$ Mev and 4.2 Mev. The yield per million incident α-particles has been estimated at 0.348 and 0.409 for the two resonance levels, 3.6 Mev and 4.2 Mev, respectively. The angular distribution of protons in the CM system has a maximum at $\theta = 90°$ for the two ground states, and, for the excited states, it is isotropic.

I. INTRODUCTION

THE reaction $O^{16}(d,p)O^{17}$ and the reaction $N^{14}(\alpha,p)O^{17}$ both lead to the formation of the compound nucleus F^{18*}. It is known[1] that the former reaction yields two groups of protons. For $E_d = 0.575$ Mev, which corresponds to an excitation of 8 Mev in F^{18*}, these two groups had Q-values of 1.75 Mev and 0.8 Mev, according to the observation of Pollard and Davison.[2] At this excitation, which is provided by α-particles of energy about 3.6 Mev, only one group of protons has been observed in previous experiments for the second reaction, although two groups might be expected, unless forbidden by selection rule. The presence of two groups of protons in the reaction $N^{14}(\alpha,p)O^{17}$ has, in fact, been demonstrated by Pollard and Davison,[2] but in this case, the energy of the α-particles was about 5.2 Mev.

The purpose of the present experiment was to investigate, by emulsion technique; (A) the group structure of the protons, at low bombarding energies of the α-particles, arising from the reaction $N^{14}(\alpha,p)O^{17}$; (B) the yield of the process; and (C) the angular distribution of the protons.

II. EXPERIMENTAL DETAILS

The α-particles from polonium were channeled through a circular slit, the arrangement of which is shown in Fig. 1. It consists of two circular brass disks D, fitted with guard rings R, cut at sharp angles. The strength of the source is 1 mc deposited at one end of a wire W and introduced into the slit through the guide G which holds the source centrally between the two disks. The position of the source 0 can be viewed through holes H drilled at the center of each disk. The two supports S and the guide channel G subtend an equal angle at the center. This facilitated the calculation of the solid angle through which α-particles emerged.

TABLE I. Proton groups from $N^{14}(\alpha,p)O^{17}$.

E_α (Mev)	No. of protons	R_μ	E_p (Mev)	Q (Mev)	Ratio (II)/(I)
3.6	(I) 1986	54.5	2.45	(a) -1.15 ± 0.04	0.12
	(II) 245	28.5	1.60	(b) $-2.0\ \pm0.04$	
4.2	(I) 2321	75	3.02	(a) -1.18 ± 0.04	0.12
	(II) 291	46.2	2.20	(b) $-2.0\ \pm0.04$	

[1] J. D. Cockroft and W. B. Lewis, Proc. Roy. Soc. (London) **A130**, 463 (1936). Guggenheimer, Heitler, and Powell, Proc. Roy. Soc. (London) **A190**, 196 (1947).
[2] E. Pollard and Perry W. Davison, Phys. Rev. **72**, 736 (1947).

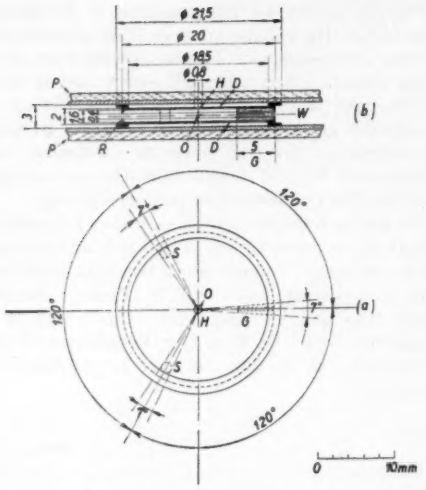

FIG. 1. (a) Sectional diagram of the slit arrangement together with the two plates P, one at the top, the other at the bottom of the slit. (b) Top view of the slit, the position of the supports S, the guide channel G, and the central hole H being indicated.

The angular dispersion of the α-beam calculated from the geometry of the slit was about 1°. This spread caused a dispersion in energy of the α-particles which was negligible in comparison with the width of the resonance levels investigated. The advantage of the slit was that, with the use of the two plates at each exposure, it permitted work with a low intensity source without sacrificing the yield. The location of the slit after development was possible because the geometry of the slit allowed α-particles from the source to strike the plates only through the central holes of the disks.

Ilford C2 50μ plates, 7 cm×5.5 cm, were used for the experiments and were exposed inside an airtight camera fitted with a manometer. Preliminary exposures were given in vacuum to study the effect of the slit and of the blackening of the plates due to γ-rays from the source, and, as a result, the upper time limit of exposure was fixed at 6 hours. However, in the final experiments an exposure of 2 hours was found sufficient to give the data required. The plates were developed by the discrimination method[3] in order to distinguish protons from any stray α-particles which might be present.

The measurement of angles was made by means of a goniometer calibrated at an interval of 0.5°. The total error in the measurement of angles, due partly to the small angular spread of the incident α-particles and partly to inaccuracy in measuring, was estimated to be less than 2°.

[3] M. Mortier and L. Vermaesen, Centre de Physique Nucléaire, Université Libre de Bruxelles, Note No. 5 (December, 1948).

III. RESULTS

(A) Structure of the Proton Groups

After measuring the coordinates, ranges, and angles of protons, it was found that there were altogether four groups of protons present; two for $E_\alpha = 4.2$ Mev and two for $E_\alpha = 3.6$ Mev. Protons originating from a disintegration must travel a certain distance in nitrogen before they strike the surface of the emulsion. This distance depends on the angle at which they are ejected with respect to the incident α-particles. In estimating the protons range this was taken into account. Table I gives the results.

It can be seen from Column 5 that the Q-value obtained for the ground state transition (a) is in agreement with the value -1.16 Mev derived from the mass data. The shorter range proton group from the excited state transition (b) gives a Q-value of -2.0 Mev for both the resonance levels. The ratio of the number of protons for the excited state and for the ground state is shown in the last column. The range of protons in micron is noted in Column 3 and its corresponding energy in Column 4.

(B) Yield of the Process

An estimate was made of the yield of protons per million incident α-particles for the two resonance levels. In order to calculate the yield, one must know how many protons are emitted for a given number of incident particles. The number of α-particles emerging from the slit during the course of the exposure was determined from the geometry of the slit and the strength of the source. Most of the disintegration protons were recorded, but some escaped through the gap between the two photographic plates. The number of these unrecorded protons was calculated according

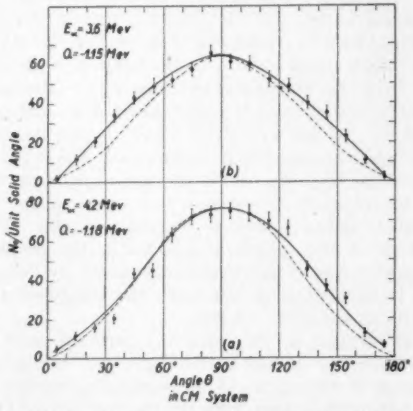

FIG. 2. (a) Angular distribution of the protons for the resonance level $E_\alpha = 4.2$ Mev and $Q = -1.18$ Mev. The distribution shows a maximum at $\theta = 90°$. (b) Distribution of the protons for the resonance level $E_\alpha = 3.6$ Mev and $Q = -1.15$ Mev. The maximum of the curve is at $\theta = 90°$.

to the method given in the Appendix. For $E_\alpha = 3.6$ Mev, the yield of protons for the ground and excited state transitions is 0.31 and 0.038, and for $E_\alpha = 4.2$ Mev it is 0.364 and 0.045.

(C) Angular Distribution

The angular distribution of protons for $E_\alpha = 3.6$ Mev and 4.2 Mev has been plotted in Figs. 2(a) and 2(b), respectively.

Both curves show a maximum at $\theta = 90°$ in the CM system. Figure 2(b) confirms the earlier observation of Champion and Roy,[4] who studied the angular distribution of protons from the reaction $N^{14}(\alpha,p)O^{17}$ for $E_\alpha = 3.6$ Mev by the cloud-chamber method. The experimental curves for the two ground state distributions can be fitted by the expression $1-\cos^2\theta$ (given in dotted lines).

Figures 3(a) and 3(b) illustrate the angular distribution of protons for the two excited states. No preferred direction in the emission of protons is evident. The curves are isotropic.

IV. CONCLUSIONS

The experimental results show the presence of two groups of protons for each resonance energy, 3.6 Mev and 4.2 Mev, corresponding to Q-values of about -1.16 Mev and -2.0 Mev. The difference between the Q-values, 0.84 Mev, reveals the presence of an excited level in O^{17}. This is approximately the value obtained from the reaction $O^{16}(d,p)O^{17}$ for the groups of protons at an excitation of 8 Mev above the ground state of the compound nucleus F^{18*}. The ratio of the number of protons from the two states is 0.12, which is smaller than the value 0.3 obtained by Pollard and Davison for the same reaction but with a higher incident energy of the α-particles. This difference might be explained by assuming that the yield from the excited state increases with increasing energy of incidence. The angular distribution of the ground state groups suggests that the probable value for the angular momentum is unity. It would seem that the P-wave is involved in this disintegration process.

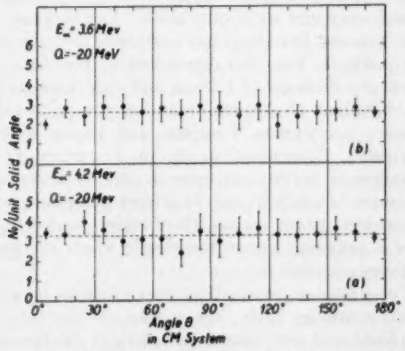

FIG. 3. Distributions for the two excited states, $E_\alpha = 4.2$ Mev and $E_\alpha = 3.6$ Mev, which are isotropic.

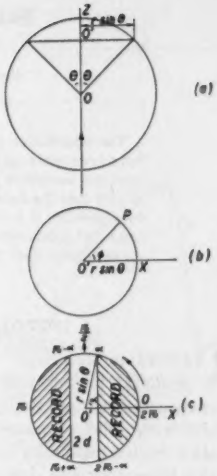

FIG. 4. Geometrical conditions of the experiment.

The author would like to express his thanks to Professor Max Cosyns for discussions on the design and construction of the slit and for his constant encouragement and interest in the progress of the experiment. He is also grateful to the other members of the staff of the Centre de Physique Nucléaire for their ever willing assistance in the course of the work.

APPENDIX

Method of Calculating the Total Number of Protons

Let r be the range of a proton ejected at an angle θ with the direction of incidence OZ. The protons will lie on a circle of latitude of the sphere, center O (the point where the disintegration occurs) and radius r. The vertical section can then be represented as in Fig. 4(a). All protons will be distributed on the circumference of the horizontal circle of latitude [Fig. 4(b)], which has a radius $r\sin\theta$. In Fig. 4(b), $O'X$ is any reference line drawn in the plane, and the point P on the circumference is specified by the angle ϕ made by $PO'X$. It is assumed that the intensity is independent of ϕ. If the total of the disintegrated protons be N, the number per unit angle of ϕ will be $N/2\pi$. Conversely, if we know the number of disintegrated particles over some definite range of ϕ, for instance β, then the total over the whole range will be

$$(2\pi/\beta)\times\text{no. of disintegrated particles in range } \beta. \qquad \text{(I)}$$

If $2d$ be the distance between the two plates, the particles whose paths end within the range of $2d$ are not recorded. The horizontal section in the plane of latitude is then represented as in Fig. 4(c). It can be seen from the figure that the particles are recorded for a range of ϕ which is 4α radians; those not recorded are of $(2\pi-4\alpha)$ radians. From the figure, we see that

$$\cos\alpha = d/r\sin\theta. \qquad \text{(II)}$$

Therefore, if, in (I), n be the number of particles recorded from the experiment, the total number present was $2\pi n/4\alpha$, where α is given by (II).

[4] F. C. Champion and R. R. Roy, Proc. Roy. Soc. (London) A191, 269 (1947).

Scintillations in Some Phosphor-Plastic Systems*

W. S. Koski
Department of Chemistry, Johns Hopkins University, Baltimore, Maryland
(Received December 26, 1950)

The scintillation properties of anthracene and stilbene dissolved in polystyrene, Lucite, and Paraplex have been investigated. The Lucite and Paraplex solutions were very poor counters, but the polystyrene solutions compared favorably in performance with pure anthracene. A study of the emission spectra indicates that the fluorescence bands of polystyrene overlap the absorption bands of anthracene and stilbene; consequently, it is possible to have an efficient energy transfer from the plastic to the phosphor in these cases and good counting systems result. This is not the case in the systems involving Lucite and Paraplex; consequently, their performance as counters is poor.

I. INTRODUCTION

RECENT publications[1–3] of results on scintillations produced in solutions of phosphors in organic solvents suggest the possibility of obtaining similar results with solid solutions of organic phosphors in plastics. Such a possibility has been under investigation in this laboratory and during the course of this work Schorr and Torney[4] published their preliminary results. In view of the fact that our investigation involved more than one plastic system and that the spectral studies which we have made shed some light on the mechanism of the energy transfer from plastic to the phosphor, it was considered worthwhile to make a report of the results.

The advantages of phosphor-plastic solid solution counters over both the liquid solution and the single crystal counter is obvious; however, it might be mentioned that, since one can form large clear masses of the plastics very simply, it might be expected that such counters could be utilized to count γ-rays and fast neutrons with higher efficiencies than is now possible.

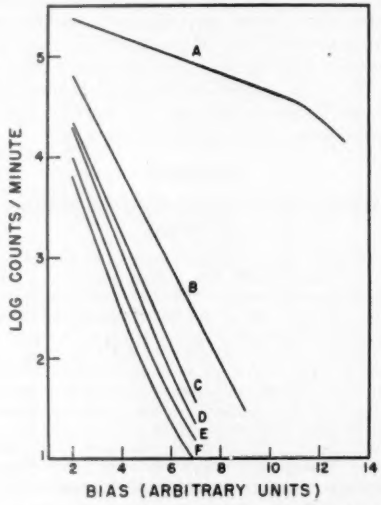

FIG. 1. Discriminator curves for some phosphor-plastic combinations using Co^{60} as a gamma-ray source: (A) single anthracene crystal, (B) 2 percent anthracene-polystyrene, (C) 10 percent stilbene-polystyrene, (D) 2 percent stilbene-polystyrene, (E) polystyrene, (F) background with the source in position but no phosphor present.

II. EXPERIMENTAL METHOD

The organic phosphors (anthracene and stilbene) used in this work were commercial products which had been recrystallized from appropriate solvents and then further purified by sublimation in high vacuums. When single crystals of these materials were needed, they were made in the usual manner, by slow cooling of the melt. In the preparation of the phosphor-plastic solid solution a weighed amount of the phosphor was dissolved in a weighed amount of the monomer of the plastic. To this solution about 0.5 percent catalyst (50–50 mixture of beyzoyl peroxide and tricresyl phosphate) was added. Then the material was frozen, the air was pumped out, and the glass vessel was sealed and heated overnight at about 125°C. The polymer was then removed from the glass container, cut into disks, and polished. The final dimensions of the disks consisted of a diameter of 1.28 cm and a thickness of 0.40 cm. Solutions of stilbene or anthracene in the three plastics, polystyrene, Paraplex, and Lucite were investigated. Concentrations up to 10 percent of the phosphor in polystyrene gave a clear colorless solid. Attempts to make 25 and 50 percent phosphor-plastics resulted in opaque masses. Overheating tended to produce a yellowish tint in the plastic which affected its performance efficiency.

The phosphor-plastic disks were mounted on a 5819 photo-multiplier tube. The output of this tube was amplified and sent into a pulse-height discriminator[5] using a Schmitt trigger-type circuit followed by a scale-of-1000 counter. Co^{60} was used as a γ-ray source and a

* This work was performed under the auspices of the AEC.
[1] Ageno, Chizzoto, and Querzoli, Atti. accad. nazl. Lincei **6**, 626 (1949).
[2] Reynold, Harrison, and Salvini, Phys. Rev. **78**, 488 (1950).
[3] H. Kallman, Phys. Rev. **78**, 621 (1950).
[4] M. G. Schorr and F. L. Torney, Phys. Rev. **80**, 474 (1950).
[5] Higinbotham, Gallagher, and Sands, Rev. Sci. Instr. **18**, 706 (1947).

discriminator bias curve was obtained for each phosphor-plastic system. These curves were compared with the curve for a single anthracene crystal of approximately the same geometry.

The spectrograms of the fluorescence in the various materials studied here were made with a small Hilger quartz spectrograph using Eastman 103-0 plates. Cu x-rays were used as a source of excitation. The material to be studied was fastened directly over the slit of the spectrograph. The slit width was 0.1 mm. The wavelengths were determined by comparison with a standard mercury spectrum.

III. DISCUSSION OF RESULTS

The results obtained for counting Co^{60} γ-rays are given in the discriminator curves of Fig. 1. The background without the source was practically negligible so is not included; however, the background with the source in place but with the phosphor removed is included, since it was appreciable. It is presumably due to the effect of the γ-rays on the tube envelope and components. It will be noted that the slope for the pure anthracene is considerably smaller than the slopes of any of the phosphor plastics, indicating a rather different distribution of pulse sizes; however, at the lower bias settings the performance of the 2 percent anthracene-polystyrene is comparable to that of the pure anthracene. The anthracene-plastic is superior to the stilbene-plastic, as might be expected. One reason for this is that the emission spectra and the spectral response of the 5819 are more evenly matched in the anthracene case.

The effect of concentration on the counting rate has not been studied exhaustively; but stilbene has been studied at three different concentrations, and the indications are that the counting rate begins to flatten out when the concentration is greater than a few percent. For example, in the bias curves in Fig. 1 it will be noticed that 10 percent stilbene is only slightly better than 2 percent stilbene. This fact appears to be compatible with the work of Schorr and Torney.[4]

The counting results obtained with the Lucite and the Paraplex solutions are not indicated, because their curves would hardly be distinguishable from the background curve. The counts for Paraplex and Lucite were only 150 and 200 counts/min, respectively, higher than the indicated background curve at the bias setting of 3.

The spectral data are summarized by the densitometer tracings in Fig. 2 and by Table I. These data indicate a 240A shift of the strong anthracene peak toward the blue and a considerably smaller shift of the corresponding stilbene peak. In view of the fact that polymerization in polystyrene takes place through the ethylemic linkage and the unsaturated benzene rings are left intact, the stilbene dissolved in polystyrene finds itself in an environment which is not too different from its crystal habitat so the effect of the solvent in shifting the stilbene peak might be expected to be small.

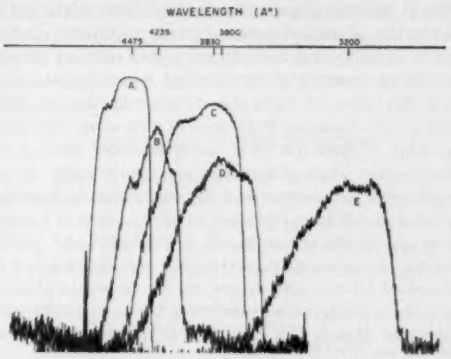

FIG. 2. Densitometer tracings of the emission spectrograms obtained for the following phosphor plastic combinations: (A) anthracene crystal, (B) 2 percent anthracene-polystyrene, (C) stilbene crystal, (D) 2 percent stilbene-polystyrene, (E) polystyrene. X-rays were used as a source of excitation.

This is not the case for anthracene, however, and consequently a larger solvent effect is observed. The emission spectra of polystyrene is of more interest and of greater significance as far as the subject of this investigation is concerned. It has been pointed out by several investigators[6,7] that scintillations in unsaturated organic crystals are intimately connected with the presence of conjugated double bonds; consequently, one would expect styrene to scintillate because of the presence of the benzene rings. Furthermore, since the wavelength[8] of the scintillations is determined by the extent over which the π electrons can migrate in the molecule, polystyrene would be expected to have an emission spectra in the region further shifted to the ultraviolet than anthracene, since the π electrons in polystyrene can migrate only over the extent of the benzene ring.

TABLE I. Wavelengths of emission bands of various phosphor-plastic systems excited by copper x-rays.

Material	Wavelength (A)
Anthracene crystal	4475 (strong) 4740
Two percent anthracene-polystyrene	4480 4235 (strong) 4090
Stilbene crystal	4035 3830 (strong)
Two percent stilbene-polystyrene	4000 (weak) 3800 (strong) 3640
Polystyrene	3350 (weak) 3200 3110

[6] Gittings, Taschek, Ronzio, Jones, and Masilum, Phys. Rev. **75**, 205 (1949).
[7] W. S. Koski and C. O. Thomas, Phys. Rev. **76**, 308 (1949).
[8] W. S. Koski and C. O. Thomas, Phys. Rev. **79**, 217 (1950).

This is not the situation in Lucite, since on the polymerization of methyl metacrylate no conjugated double bonds remain; and consequently, it would not be expected to fluoresce in the spectral region investigated here. We have not been able to ascertain the composition of the Paraplex P-43 used in this work; but presumably it does not have an appreciable amount of conjugation after polymerization, since there is no evidence of fluorescence on x-ray excitation. Anthracene in solution has been reported[9] to have a series of intense overlapping absorption bands in the 3500A and 2500A regions. Consequently, the polystyrene fluorescence is absorbed by the anthracene in the phosphor-plastic; and the anthracene in turn gives off its characteristic radiation when it falls from the excited state to a lower state. This interpretation is supported by the fact that even in long exposures where the anthracene emission is strongly overexposed there was no visible evidence of the polystyrene fluorescence on the plate, indicating that a large fraction of it had been absorbed by the solute molecules. A similar situation exists in the case of stilbene. In the case of Lucite and Paraplex the fluorescence is very weak, so there is very little energy transfer from the plastic to the phosphor; and as a result, such solid solutions make very poor counters.

The author wishes to acknowledge his indebtedness to Professor J. D. H. Donnay for the use of his x-ray machine, to Professor R. K. Witt for a sample of Paraplex, to Dr. Fred Kaufman for the densitometer tracings, and to Professor R. D. Fowler for several helpful suggestions.

[9] Radulecu and Ostrogovich, Ber. **64**, 2233 (1931).

PHYSICAL REVIEW VOLUME 82, NUMBER 2 APRIL 15, 1951

Plasma Oscillations in a Static Magnetic Field*

E. P. Gross
Laboratory for Insulation Research, Massachusetts Institute of Technology, Cambridge, Massachusetts
(Received December 4, 1950)

A theory of the small-amplitude oscillations of an ionized gas in a static magnetic field is developed, including the effects of temperature motions. The Boltzmann equation is solved for this problem, and exact expressions are obtained for the distribution function and dispersion relation. A general feature of the dispersion relation is the existence of gaps in the spectrum at frequencies which are approximately multiples of $\omega_c = eH/mc$. The magnitude of the gap depends on the temperature of the gas, being proportional to it for long wavelengths. This leads to the prediction of selective reflection of waves impinging on a plasma with frequency in the forbidden range.

For $ck \gg \omega_p$, ω_c the waves split into approximately longitudinal plasma waves and transverse waves. Detailed analysis is made of the plasma waves for ω_c small and ω_c large. At long wavelengths the frequency is $\omega^2 \simeq \omega_p^2 + \omega_c^2 + \beta(\kappa T/m)k^2$, where β depends on ω_p and ω_c. For waves near the Debye length the waves are heavily damped.

Two simplified treatments of plasma oscillations based on transport equations are compared with the above treatment. Expressions of the form $\omega^2 \simeq \omega_p^2 + \omega_c^2 + \beta(\kappa T/m)k^2$ are obtained where the factor β is independent of ω_c and ω_p. In addition, the transport treatments fail to predict the heavy damping near the Debye length and the existence of gaps in the frequency spectrum.

I. INTRODUCTION

THE small amplitude vibrations of a plasma oscillating in a static magnetic field are discussed in this paper. For the case in which the thermal velocities of the particles are negligible, or for the limiting case of zero wavelength, the customary[1] theory of the propagation of electromagnetic waves in the ionosphere provides a satisfactory treatment of the vibrations, including the longitudinal plasma oscillations. The customary theory is not adequate to take into account the effects of random thermal motions and to treat these it is necessary to make use of the general methods of kinetic theory. In this type of problem, one is generally interested, from the practical point of view, in the dispersion relation giving the frequency of the possible waves as a function of the wavelength and also in the polarization properties of the waves. From the theoretical viewpoint it is also of great interest to know the velocity distribution of the particles if it is possible to compute it exactly, since this allows one to see what part the individual particles play in sustaining the oscillation. Plasmas are of particular interest in this connection, since they display organized properties depending on the cooperative action of all members of the assembly, but are systems still so simple that one can follow mathematically the detailed motion of the individual members of the assembly to a great extent. A detailed physical picture of the mechanism of ordinary plasma oscillations has been given,[2-4] and in the present

* Sponsored by the ONR, the Army Signal Corps, and the Air Force.
[1] H. Lassen, Ann. Physik **1**, 415 (1947); H. R. Mimno, Revs. Modern Phys. **9**, 1 (1937).

[2] D. Bohm and E. P. Gross, Phys. Rev. **75**, 1851 (1949).
[3] D. Bohm and E. P. Gross, Phys. Rev. **75**, 1864 (1949).
[4] D. Bohm and E. P. Gross, Phys. Rev. **79**, 992 (1950).

paper we derive exact expressions for the distribution function and dispersion relation in the presence of a magnetic field.

The subject of plasma oscillations in static electric and magnetic fields has been of interest in experimental work with discharge tubes[5] and in the applications of trochotrons.[6] The instability of the oscillations in magnetic fields seems to have been observed, but there does not seem to be much precise information concerning the dependence of instabilities on the static electric fields and density gradients present in the plasma. Electric fields, density gradients, and beams of sharply defined energy provide sources from which energy can be taken to excite oscillations of the plasma. Theoretical calculations have been made on the basis of the gas discharge experiments. Bohm has carried out unpublished calculations showing excitation in magnetic fields when electric fields and drift arising from density gradients are present. Malmfors[7] has discussed the oscillations in a magnetic field of a simplified plasma consisting of electrons of a single velocity; and claims that the system is unstable. Later, we shall treat this case and show that, because of an error in his calculations, Malmfors's result is incorrect.

The same problems have arisen in the studies of electromagnetic propagation in ionized atmospheres, particularly in the explanations of the origin of solar radiation. For example, Bailey[8] has treated some of the problems, taking into account random motions by means of Maxwell's equations of transfer. His results show clearly that growing oscillations may occur in the presence of electric fields. The maxwell transfer equations, however, do not provide an exact description of the oscillating plasma, so that Bailey's results are not quantitatively exact. In view of this previous work it seems as though some of the conditions under which instability occurs are understood, so that we do not aim at a complete discussion of oscillations in electric fields and density gradients. We shall obtain an exact solution for the oscillations in the presence of a static magnetic field only and compare this treatment with approaches based on macroscopic transport equations such as the maxwell transfer equations. It will be shown that these lead to qualitatively correct conclusions, at least at long wavelengths. This is encouraging, since in the general case involving drift and collisions it is extremely difficult to give an exact treatment, while treatment by means of the transfer equations is a matter of a few lines of calculation. We must add, however, that there are some effects not predicted by the transport treatments. Among these are the existence of bands of forbidden frequencies at multiples of the cyclotron frequency, and the heavy damping at wavelengths near the Debye length. In addition the quantitative agreement is poor, particularly when magnetic fields are present.

[5] D. Bohm, in A. Guthrie and R. Wakerling, *Characteristics of Electrical Discharges in Magnetic Fields* (McGraw-Hill Book Company, Inc., New York, 1949), National Nuclear Energy Series, Vol. I, Paper No. 5.

[6] H. Alvén and co-workers, "Theory and applications of trochotrons," Kgl. Tekniska Högskolans Handlingar, No. 22 (1948).

[7] K. Malmfors, Arkiv Fysik **1**, 569 (1950).

[8] V. Bailey, Phys. Rev. **78**, 428 (1950).

II. EQUATIONS OF THE PROBLEM

The state of the plasma can be described by a distribution function[9] $f(\mathbf{x}, \mathbf{v}, t)$, giving the average number of particles in a small range of position and velocity at a time t. The distribution function changes with time in accordance with the Boltzmann equation

$$\frac{\partial f}{\partial t}+\mathbf{v}\cdot\nabla f+\frac{e}{m}\left(\mathbf{E}+\frac{\mathbf{v}\times\mathbf{H}_0}{c}\right)\cdot\frac{\partial f}{\partial \mathbf{v}}=\left(\frac{\delta f}{\delta t}\right)_{\text{coll}}. \quad (1)$$

The field $\mathbf{H}_0$ is the static magnetic field, while the field $\mathbf{E}$ includes fields arising from the particles of the system as well as impressed electric fields. To understand the physical assumptions[2-4,10] made in this treatment, we note that the forces acting on a given particle can be divided roughly into two types. One type is the ordinary short-range force acting on a particle when it makes a close collision involving a heavy momentum exchange with a neutral atom, and is taken into account by the collision term $(\delta f/\delta t)_{\text{coll}}$. In many low-density plasmas these collisions give rise to a minor damping effect, but in higher-density plasmas they may destroy many of the characteristic plasma properties. The second type of force is the long-range coulomb force, coming from other charged particles of the system. In this type of collision a very small momentum transfer is exchanged between two particles. A given electron is engaged in a many-body collision with a large number of distant particles, the effect of which is taken into account as a smoothed-out force. This latter force depends on the distribution function itself and gives rise to the characteristic plasma properties. The electric field is determined by Maxwell's equations, from which one can derive the equations

$$\nabla\times(\nabla\times\mathbf{E})=-(\partial^2\mathbf{E}/c^2\partial t^2)-(4\pi\partial\mathbf{j}/c^2\partial t); \quad (2)$$

$$\mathbf{j}=e\int\mathbf{v}f d\mathbf{v}.$$

Equations (1) and (2) are a set of coupled, nonlinear, integro-differential equations which determine $\mathbf{E}$ and f in a self-consistent field problem.[11]

[9] It is possible to give an alternative description of the plasma which has advantages in understanding the physical processes (reference 1). We shall use the distribution function treatment here, since it has the advantage of mathematical compactness.

[10] A. Vlasov, J. Phys. (U.S.S.R.) **9**, 25, 130 (1945).

[11] In the static magnetic field problem in general it is not correct to determine $\mathbf{E}$ from f by means of the Poisson equation. As will be seen, this procedure is correct at a limit ck much larger than ω_p and ω_c. In the general case the strong coupling of longitudinal and transverse motions makes it necessary to use the full set of Maxwell's equations, or equivalently, Eqs. (2). In Eq. (1) we have made the customary approximation of neglecting

Equations (1) and (2) are, in general, exceedingly difficult to solve; but, if one is concerned with only small amplitude oscillations, one can put $f=f_0(\mathbf{v})+f_1(\mathbf{x},\mathbf{v},t)$ with $f_1 \ll f_0$. The function f_0 represents the distribution in the absence of oscillations. One then neglects terms quadratic in f_1 and $\mathbf{E}$, so that the equations become linear.[12]

The linearized Boltzmann equation, in absence of collisions, is

$$\frac{\partial f_1}{\partial t}+\mathbf{v}\cdot\nabla f_1+\frac{e}{m}\mathbf{E}\frac{\partial f_0}{\partial \mathbf{v}}+\frac{e}{mc}(\mathbf{v}\times\mathbf{H}_0)\cdot\frac{\partial f_0}{\partial \mathbf{v}}+\frac{e}{mc}(\mathbf{v}\times\mathbf{H}_0)\cdot\frac{\partial f_1}{\partial \mathbf{v}}=0. \quad (1a)$$

Since $f_0(\mathbf{v})$ is the distribution function in the absence of oscillating electric fields, but in the presence of static magnetic fields, one must have $\mathbf{v}\times\mathbf{H}_0(\partial f_0/\partial \mathbf{v})=0$. If the static magnetic field $\mathbf{H}_0$ is considered to be in the z direction, this condition is $v_y(\partial f_0/\partial v_x)-v_x(\partial f_0/\partial v_y)=0$, so that we must have $f_0=f_0([v_x^2+v_y^2], v_z)$. The maxwellian velocity distribution is of this type.

The linearized equations may be used to treat various boundary problems, e.g., by means of laplace transformation methods.[13] If we confine ourselves to a discussion of the unbounded plasma, we find that, starting with an arbitrary initial distribution, the electric field has no simple form for small times; but the asymptotic behavior for long times for a wave of wave number k is $e^{i(kz-\omega t)}$, where $\omega(k)$ is, in general, complex. The distribution function has the asymptotic behavior $f\sim A(v)e^{-ikvt}e^{ikz}-e^{i(kz-\omega t)}$. The term $A(v)e^{ik(z-vt)}$ depends on the initial state and describes the "free particle" motions. If one is interested in the dispersion relation and in the part of the distribution function corresponding to the organized motions of particles, it is sufficient to study a very special initial distribution of electrons having the property that for all times the electric field and distribution function vary as $e^{i(kz-\omega t)}$. This solution does not contain the "free-particle" contributions and has been so chosen that all of the electrons are started with motions appropriate to an organized plasma wave.[2] The dispersion relation obtained with this solution is the same as that obtained in the more general case. In the treatment of the magnetic field problem we shall therefore restrict ourselves to a consideration of the special steady-state solutions.

Collisions may be taken into account in the present treatment by adding a term $(\delta f/\delta t)_{\text{coll}}=-(f-f_0)/\tau$ on the right-hand side of Eq. (1a). This represents a damping of the ordered (oscillatory) part of the distribution by collisions with heavy particles. The mean collision time is $\tau(v)$, and in the simplest case is a constant. Since we shall look for steady-state solutions of the type $e^{i(kz-\omega t)}$, collisions may be taken into account by replacing ω by $\omega+i/\tau$ in Eq. (1a). For the present we neglect collisions (see Sec. IV for a discussion of the modifications necessary to take collisions into account).

III. DETERMINATION OF THE DISTRIBUTION FUNCTION

Let us now attempt to solve Eqs. (1a) and (2) in the steady state for plane waves progressing in the x direction. The magnetic field couples motions in the x and y direction so that we expect both longitudinal and transverse components of the electric field. Steady-state solutions are found by setting electric field and distribution function proportional to $e^{i(kx-\omega t)}$, where ω and k are connected by means of the dispersion relation which will be found later. If one makes use of the vector identity $\nabla\times(\nabla\times\mathbf{E})\equiv\nabla(\nabla\cdot\mathbf{E})-\nabla^2\mathbf{E}$, one can write the equations describing the system as

$$i(kv_x-\omega)f_1+\frac{e}{m}\left(E_x\frac{\partial f_0}{\partial v_x}+E_y\frac{\partial f_0}{\partial v_y}\right)+\omega_c\left(v_y\frac{\partial f_1}{\partial v_x}-v_x\frac{\partial f_1}{\partial v_y}\right)=0, \quad (3a)$$

$$\omega^2E_x+4\pi i\omega e\int v_x f_1 d\mathbf{v}=0, \quad (3b)$$

$$(\omega^2-c^2k^2)E_x+4\pi i\omega e\int v_y f_1 d\mathbf{v}=0, \quad (3c)$$

where $\omega_c=eH_0/mc$.

Let us consider the Boltzmann equation first. It is possible to obtain the solution of this partial differential equation in v_x and v_y from the solution of an ordinary differential equation. We introduce new independent variables ρ, δ (polar coordinates in velocity space) defined by

$$\rho^2=v_x^2+v_y^2, \quad v_x=\rho\cos\delta, \qquad \tan\delta=v_y/v_x, \quad v_y=\rho\sin\delta. \quad (4a)$$

forces arising from time-varying magnetic fields, since these are of order v/c times the changing electric forces. In Eq. (2) we have neglected currents arising from the motion of the positive ions. To take into account the contribution of these ions one must define a distribution function $g(\mathbf{x},\mathbf{v},t)$ and write the additional equation

$$(\partial g/\partial t)+\mathbf{v}\cdot\nabla g-(e/M)(\mathbf{E}+\mathbf{v}\times\mathbf{H}_0/c)\cdot\partial g/\partial\mathbf{v}=(\delta g/\delta t)_{\text{coll}}.$$

In the present work the positive ions are considered as smeared out into a uniform positive charge continuum.

[12] The main condition of validity of the linear approximation is

$$\mathbf{E}\cdot\partial f_1/\partial\mathbf{v}\ll\mathbf{E}\cdot\partial f_0/\partial\mathbf{v}.$$

This condition holds for sufficiently small amplitudes, and for most particles continues to hold for rather large amplitudes. For particles moving with velocities close to the phase velocity of the oscillation the condition breaks down after a long time. These particles are connected with the excitation and damping of oscillations in the linear approximation, but cease to play this role for larger amplitudes. A discussion of these questions is given in reference 1.

[13] L. Landau, J. Phys. U.S.S.R. **10**, 25 (1946).

Then

$$\left.\begin{aligned}
&\frac{\partial}{\partial v_x}=\frac{v_x}{\rho}\frac{\partial}{\partial\rho}-\frac{v_y}{v_x^2}\cos^2\delta\frac{\partial}{\partial\delta}=\cos\delta\frac{\partial}{\partial\rho}-\frac{\sin\delta}{\rho}\frac{\partial}{\partial\delta}\\
&\frac{\partial}{\partial v_y}=\frac{v_y}{\rho}\frac{\partial}{\partial\rho}+\frac{\cos^2\delta}{v_x}\frac{\partial}{\partial\delta}=\sin\delta\frac{\partial}{\partial\rho}+\frac{\cos\delta}{\rho}\frac{\partial}{\partial\delta}\\
&v_y\frac{\partial f_1}{\partial v_x}-v_x\frac{\partial f_1}{\partial v_y}=-\frac{\partial f_1}{\partial\delta}
\end{aligned}\right\}. \quad (4b)$$

We also note that $E_x(\partial f_0/\partial v_x)+E_y(\partial f_0/\partial v_y)$ can be written as $(E_x\cos\delta+E_y\sin\delta(df_0/d\rho)$. Finally, on introducing the new quantities $F_x=E_x-iE_y$ and $F_y=E_x+iE_y$, the Boltzmann equation becomes

$$i(k\rho\cos\delta-\omega)f_1+\frac{e}{2m}\frac{df_0}{d\rho}(F_xe^{i\delta}+F_ye^{-i\delta})-\omega_c\frac{\partial f_1}{\partial\delta}=0. \quad (5)$$

This is an ordinary linear differential equation for δ in which ρ may be treated as a parameter. Thus, the solutions of the equation contain an arbitrary function of ρ which must be chosen so that the distribution function is periodic in δ with period 2π, as is required by physical considerations.

The general solution of the equation is

$$\begin{aligned}
f_1=A(\rho)\exp&\left[+i\left(\frac{k\rho\sin\delta-\omega\delta}{\omega_c}\right)\right]\\
&\times\exp\left[i\left(\frac{k\rho\sin\delta-\omega\delta}{\omega_c}\right)\right]\\
&\cdot\int_0^\delta\exp\left[-i\left(\frac{k\rho\sin\delta-\omega\delta}{\omega_c}\right)\right]\\
&\cdot\frac{e}{2m\omega_c}\frac{df_0}{d\rho}(F_xe^{i\delta}+F_ye^{-i\delta})d\delta. \quad (6)
\end{aligned}$$

In order to discuss this equation further and to obtain the periodic solutions, we make use of the expansion

$$e^{iz\sin\delta}=\sum_{n=-\infty}^{+\infty}J_n(z)e^{in\delta}.$$

The distribution function becomes

$$\begin{aligned}
f_1=A(\rho)\exp&\left[+i\left(\frac{k\rho\sin\delta-\omega\delta}{\omega_c}\right)\right]\\
&+\exp\left[i\left(\frac{k\rho\sin\delta-\omega\delta}{\omega_c}\right)\right]\frac{e}{2m\omega_c}\frac{df_0}{d\rho}\\
&\times\sum_{n=-\infty}^{+\infty}J_n\left(-\frac{k\rho}{\omega_c}\right)\left[\frac{F_x\exp[i(n+1+\omega/\omega_c)\delta]-1}{i(1+n+\omega/\omega_c)}\right.\\
&\left.+\frac{F_y\exp[i(n-1+\omega/\omega_c)\delta]-1}{i(n-1+\omega/\omega_c)}\right].
\end{aligned}$$

To select the solutions periodic in δ of period 2π, one puts

$$\begin{aligned}
A(\rho)=&\frac{e}{2m\omega_c}\frac{df_0}{d\rho}\sum_{n=-\infty}^{+\infty}J_n\left(-\frac{k\rho}{\omega_c}\right)\\
&\times\left\{\frac{F_x}{i(1+n+\omega/\omega_c)}+\frac{F_y}{i(n-1+\omega/\omega_c)}\right\}. \quad (7)
\end{aligned}$$

This gives for the velocity distribution

$$\begin{aligned}
f_1=&\frac{e}{2m\omega_c}\frac{df_0}{d\rho}\exp\left[i\frac{k\rho\sin\delta}{\omega_c}\right]\sum_{n=-\infty}^{+\infty}J_n\left(-\frac{k\rho}{\omega_c}\right)\\
&\times\left\{\frac{F_xe^{i(n+1)\delta}}{i(1+n+\omega/\omega_c)}+\frac{F_ye^{i(n-1)\delta}}{i(n-1+\omega/\omega_c)}\right\}. \quad (8)
\end{aligned}$$

We take Eq. (8) as the correct distribution function for an oscillating plasma in a static magnetic field. The distribution function may be expressed in terms of v_x and v_y by carrying out the transformation (4a); but the result is, in general, exceedingly complex.

IV. THE DISPERSION RELATION

To obtain the dispersion relation connecting ω and k we must substitute f_1 from Eq. (8) into Eqs. (3) and set the determinants formed by the coefficients of F_x and F_y equal to zero. [We note that $E_x=\frac{1}{2}(F_x+F_y)$, $E_y=-i\frac{1}{2}(F_y-F_x)$ in Eqs. (3).] This will give ω as a function of k, and for each value of ω it will be possible to determine the ratio of amplitudes F_x/F_y. In carrying out the procedure it will be necessary to compute the integrals $\int v_xf_1d\mathbf{v}$ and $\int v_yf_1d\mathbf{v}$. We introduce new quantities α, β, γ, δ by

$$\begin{aligned}
\alpha F_x+\beta F_y=&8\pi ei\int v_xf_1d\mathbf{v}\\
=&\frac{4\pi e^2}{m\omega_c}\int_0^\infty\rho^2d\rho\frac{df_0}{d\rho}\int_0^{2\pi}\cos\delta d\delta\int_{-\infty}^{+\infty}dv_z\\
&\times\exp\left(i\frac{k\rho\sin\delta}{\omega_c}\right)\sum_{n=-\infty}^{+\infty}J_n\left(-\frac{k\rho}{\omega_c}\right)\\
&\times\left[\frac{F_xe^{i(n+1)\delta}}{(1+n+\omega/\omega_c)}+\frac{F_ye^{i(n-1)\delta}}{(n-1+\omega/\omega_c)}\right], \quad (9)
\end{aligned}$$

and

$$\begin{aligned}
\gamma F_x+\delta F_y=&8\pi e\int v_yf_1d\mathbf{v}\\
=&\frac{4\pi e^2}{m\omega_c}\int_0^\infty\rho^2\frac{df_0}{d\rho}d\rho\int_0^{2\pi}\sin\delta d\delta\int_{-\infty}^{+\infty}dv_z\\
&\times\exp\left(i\frac{k\rho\sin\delta}{\omega_c}\right)\sum_{n=-\infty}^{+\infty}J_n\\
&\times\left[\frac{F_xe^{i(n+1)\delta}}{i(1+n+\omega/\omega_c)}+\frac{F_ye^{i(n-1)\delta}}{i(n-1+\omega/\omega_c)}\right]. \quad (10)
\end{aligned}$$

In terms of these quantities the dispersion relation becomes

$$(\omega+\alpha)(-\omega^2+c^2k^2+\omega\delta)-(\omega+\beta)(\omega^2-c^2k^2+\omega\gamma)=0. \quad (11)$$

We now compute α, β, γ, δ, making use of the expressions

$$J_{-n}(z)=(1/2\pi)\int_0^{2\pi} e^{+i n\delta} e^{iz\sin\delta} d\delta,$$

$$J_n(-z)=(-)^n J_n(z), \quad J_{-n}(z)=(-)^n J_n(z).$$

Use of the above integral expressions for the bessel function in Eqs. (9) and (10) gives

$$\alpha,\ \beta=(4\pi e^2/m\omega_c)\pi\int_{-\infty}^{+\infty} dv_z \int_0^{\infty} \rho^2 d\rho (df_0/d\rho)$$

$$\times \sum_{n=-\infty}^{+\infty} \frac{J_n(-k\rho/\omega_c)}{(n\pm 1+\omega/\omega_c)}\{J_{n+1\pm 1}+J_{n-1\pm 1}\}. \quad (12)$$

$$\gamma,\ \delta=-(4\pi e^2/m\omega_c)\pi\int_{-\infty}^{+\infty} dv_z \int_0^{\infty} \rho^2 d\rho (df_0/d\rho)$$

$$\times \sum_{n=-\infty}^{+\infty} \frac{J_n}{(n\pm 1+\omega/\omega_c)}\{J_{n+1\pm 1}-J_{n-1\pm 1}\}. \quad (13)$$

To obtain the dispersion relation, one must substitute these expressions in Eq. (11) and solve for ω as a function of k. In general, this is not easy since ω is contained in all the terms of the summation in Eqs. (12) and (13). However, at the limit of $kv_{th}/\omega_c \ll 1$ one can replace the bessel functions by their values at z's and only a small number of terms remain. Thus by direct expansion the dependence of ω on k can be found for long wavelengths and high magnetic field strengths. We shall carry out this expansion later, and in addition we shall represent the series occurring in the above equations by a definite integral which will permit computation of the dispersion relation in the general case.

In investigating Eq. (11) one makes use of what is known about the dispersion relation in absence of random thermal motions. This dispersion relation can be written as

$$(\omega^2-\omega_p^2)(\omega^2-\omega_p^2-c^2k^2)-\omega_c^2(\omega^2-c^2k^2)=0. \quad (14)$$

Solving for ω^2 we find

$$\omega^2-\omega_p^2=\tfrac{1}{2}(\omega_c^2+c^2k^2)\pm\tfrac{1}{2}[(\omega_c^2-c^2k^2)^2+4\omega_c^2\omega_p^2]^{\frac{1}{2}}. \quad (15)$$

In the limiting case of a zero magnetic field there are two types of solutions: $\omega^2=\omega_p^2$ and $\omega^2=\omega_p^2+c^2k^2$. The first is a "plasma-type" solution in which the oscillations are purely longitudinal; i.e., $E_y=0$. The second solution represents transverse electromagnetic waves traveling through the ionized gas; i.e., $E_z=0$. In the limit $ck\gg\omega_p$ the effect of the presence of ionized gas is negligible, and these latter waves become electromagnetic waves in free space. For non-zero magnetic fields one can again easily separate the types of waves, provided $ck\gg\omega_p$ and $ck\gg\omega_c$. We then expect to have two sets of waves: one set at frequencies comparable to ck (electromagnetic) and one set at much lower frequencies (the plasma waves). From Eq. (14) the plasma waves are found by putting $\omega^2-\omega_p^2-c^2k^2\simeq-c^2k^2$ and $\omega^2-c^2k^2\simeq-c^2k^2$. The result is $\omega^2\simeq\omega_c^2+\omega_p^2$. For the electromagnetic type one finds

$$\omega^2\simeq c^2k^2+\omega_p^2/(1-\omega_c^2/c^2k^2)\simeq c^2k^2+\omega_p^2+(\omega_p^2\omega_c^2/c^2k^2).$$

For the general case in which ck is comparable to ω_p or ω_c, the waves cannot be separated into purely longitudinal and purely transverse sets and the dispersion relation becomes complicated (Eq. 15).

Our general dispersion relation can also be simplified in the limit of large ck's. We find that the plasma-type solutions are given by

$$\omega\simeq-\tfrac{1}{2}(\alpha+\beta). \quad (16)$$

This will be evaluated in later sections, and we shall find that Eq. (14) is obtained in the absence of random motions. From Eqs. (3) it is seen that these oscillations are longitudinal. The electromagnetic type solutions are given by

$$\omega^2\simeq c^2k^2+ck(\delta-\gamma). \quad (17)$$

Finally, we discuss the modifications which must be made in Eqs. (3) and (11) in order to take into account the effects of collisions. In the model adopted here $(\delta f/\delta t)_{coll}=(f_0-f)/\tau=-f_1/\tau$, so that one must replace ω by $\omega+i/\tau$ in the Boltzmann equation (3a) and in consequence in the quantities α, β, γ, δ. On the other hand, this replacement for ω must not be made where ω appears explicitly in Maxwell's equations (3b), (3c), and hence in Eq. (11). Thus, the proper procedure is to replace ω by $\omega+i/\tau$ only when ω occurs in α, β, γ, δ. Actually, the model adopted here does not represent collisions but describes a process in which electrons are absorbed by atoms at a rate depending on the prevalent distribution at the given time and are re-emitted at a rate depending on the equilibrium distribution. As a result, in computing the charge density of the system one must take into account the changing net charge of the trapping centers. This charge, however, does not contribute to the currents so that the procedure described above for computing collision effects may be employed. The present model serves only to take into account damping arising from destruction of phase relationships at collisions.

V. DISPERSION RELATION FOR A PEAKED VELOCITY DISTRIBUTION

In this section we study the special plasma treated by Malmfors,[7] an electron gas with a sharp distribution in a plane perpendicular to H_0. We investigate whether excitation is possible, point out the existence of gaps in

the frequency spectrum, and replace Malmfors's results by what we believe to be correct expressions.

Let us take for the velocity distribution

$$f_0(\rho, v_z) = (\rho_0/2\pi v_0)\delta(\rho - v_0)\cdot g(v_z)/g_0,$$

where δ is the Dirac delta-function. Here

$$\int_{-\infty}^{+\infty} g(v_z)dv_z = g_0,$$

v_0 is the absolute velocity of the particles in the plane perpendicular to H_0, and $\rho_0 = \int_{-\infty}^{+\infty} f_0 d\mathbf{v}$ is the density of the ion gas. Then

$$df_0/d\rho = (\rho_0/2\pi v_0)\delta'(\rho - v_0)g(v_z)/g_0,$$

where the δ'-function has the property

$$\int_{-\infty}^{+\infty} f(x)\delta'(x-a) = -f'(a).$$

With these assumptions and with the help of Eqs. (12), (13), and (42), the following expressions for α, β, γ, δ are obtained:

$$\begin{aligned} \alpha, \gamma &= -(\omega_p^2/2\omega_c v_0)(d/dv_0)\{v_0^2(K_0 \pm K_2)\}, \\ \beta, \delta &= -(\omega_p^2/2\omega_c v_0)(d/dv_0)\{v_0^2(L_0 \pm K_2)\}. \end{aligned} \tag{18}$$

As discussed in Sec. IV, one finds the plasma-type solutions for large ck from the simplified dispersion relation $\omega \simeq -\frac{1}{2}(\alpha+\beta)$. The dispersion relation for the plasma-type solutions is

$$\omega = \frac{\omega_p^2}{4\omega_c v_0}\frac{d}{dv_0}\left[v_0^2 \sum_{n=-\infty}^{+\infty} \frac{(J_n + J_{n+2})^2}{(n+1+\omega/\omega_c)}\right].$$

This can be put in the form obtained by Malmfors by writing

$$1 = \frac{\omega_p^2}{4\omega_c^2}\frac{1}{\lambda}\frac{d}{d\lambda}\left[\lambda^2 \sum_{n=-\infty}^{+\infty} \frac{2n}{\lambda}\frac{J_n(J_{n-1}+J_{n+1})}{(\omega/\omega_c)(n+\omega/\omega_c)}\right],$$

where we have put $\lambda = kv_0/\omega_c$ and have used the relation $J_{n-1}(\lambda) + J_{n+1}(\lambda) = 2nJ_n(\lambda)/\lambda$. Finally, we have, using the identity

$$\sum_{n=-\infty}^{+\infty} nJ_n^2(\lambda) \equiv 0,$$

$$1 = -\frac{\omega_p^2}{2\omega_c^2}\frac{1}{\lambda}\frac{d}{d\lambda}\left[\lambda \sum_{n=-\infty}^{+\infty} \frac{J_n(J_{n-1}+J_{n+1})}{n-\omega/\omega_c}\right]. \tag{19}$$

It is to be noted that this dispersion relation differs from that of Malmfors in that a factor i is not present and in addition the sum, rather than the difference, of J_{n-1} and J_{n+1} appears on the right-hand side. It is possible to check the correctness of the above expression if one remembers that in the limit of zero velocity; i.e., $\lambda = 0$, the system becomes a plasma at zero temperature, for which the dispersion relation is $\omega^2 = \omega_p^2 + \omega_c^2$. The above relation reduces to this expression while that of Malmfors does not.

The most interesting feature of Eq. (19) is the behavior when ω is approximately a multiple of ω_c. We shall now show that there is a jump in the frequency in this region. It is particularly easy to study the behavior in the limit $\lambda \ll 1$. We note that in the absence of thermal motions, i.e., $\lambda = 0$, one can always choose ω_p so that ω is a multiple of ω_c; e.g., with $\omega_p^2 = 3\omega_c^2$ one finds $\omega = 2\omega_c$. In the following discussion it will be assumed that $\omega_p^2 \simeq 3\omega_c^2$. One may write Eq. (19) in the form

$$1 = -\frac{\omega_p^2}{\omega_c^2}\frac{1}{\lambda}\frac{d}{d\lambda}\left[\sum_{n=-\infty}^{+\infty} \frac{nJ_n^2}{n-\omega/\omega_c}\right]. \tag{20}$$

Expanding J_n and retaining only powers of λ up to the fourth, one finds

$$1 \simeq -\frac{\omega_p^2}{\omega_c^2}\frac{1}{2}\left[\frac{1}{1-\omega/\omega_c} + \frac{1}{1+\omega/\omega_c}\right] - \frac{\omega_p^2\lambda^2}{8\omega_c^2(2-\omega/\omega_c)}.$$

For $\lambda = 0$ this gives $\omega^2 = \omega_p^2 + \omega_c^2$. With $\omega \simeq 2\omega_c$ the equation simplifies to

$$1 \simeq \frac{\omega_p^2}{\omega_c^2}\frac{1}{(\omega^2/\omega_c^2 - 1)} - \frac{\omega_p^2}{\omega_c^2}\frac{1}{8}\frac{\lambda^2}{(2-\omega/\omega_c)}. \tag{21}$$

When ω/ω_c is less than 2, the second term on the right-hand side is large and negative; when ω/ω_c is greater than 2, it is large and positive. The first term on the right-hand side is slowly varying so that the dispersion relation can be satisfied only if ω/ω_c does not pass through the value 2. We can show that ω/ω_c jumps discontinuously as ω_p is varied continuously. Let us put $\omega/\omega_c = 2 + \epsilon\lambda$ and expand $\omega^2/\omega_c^2 - 1$. The dispersion relation becomes

$$\omega_c^2 \simeq \tfrac{1}{3}\omega_p^2 - \tfrac{4}{9}\omega_p^2\epsilon\lambda + \tfrac{1}{8}(\omega_p^2\lambda/\epsilon).$$

Thus, as ω_p^2 varies continuously in the vicinity of 3, the dispersion relation can be satisfied by taking $\epsilon = \pm(\frac{9}{32})^{\frac{1}{2}}$. The magnitude of the jump in ω is $\Delta(\omega/\omega_c) \simeq (\frac{9}{8})^{\frac{1}{2}}\lambda$ and is proportional to the velocity of the beam. A similar behavior occurs when λ is no longer small; but, in this case, many terms of the same order of magnitude enter in the dispersion relation so that it is more difficult to find an expression for the magnitude of the gap.

It might be thought possible to satisfy Eq. (20) by letting ω be a complex number, representing damping or instability of the oscillations. We shall now show that, at least for $\lambda \ll 1$, this cannot be done. In examining complex solutions one writes $\omega = \omega_R + i\sigma$, where ω_R and σ are real, and one separates the real and imaginary parts of Eq. (20). For $\lambda \ll 1$ and $\omega/\omega_c \simeq 2$ one can use

Eq. (21) instead. One finds for the imaginary part

$$-\frac{\omega_p^2}{3\omega_c^2}\frac{1}{(\omega_R/\omega_c-1)^2+(\sigma^2/\omega_c^2)}$$

$$-\frac{\omega_p^2}{8\omega_c^2}\frac{\lambda^2}{(2-\omega_R/\omega_c)^2+(\sigma^2/\omega_c^2)}=0.$$

With $\omega_R/\omega_c=2$ one obtains $\sigma^2=-\frac{3}{8}\lambda^2$, showing that it is not possible to satisfy the dispersion relation with real values of σ. We have not undertaken a complete study of the dispersion relation (20), but the same type of consideration would seem to hold for all values of λ.

The behavior of the dispersion relation for a plasma in a magnetic field is similar to the behavior of the energy-wave vector relation for an electron moving in a solid. It will be remembered that the permissible values for the energy of the electron lie in bands, the edges of the bands corresponding to wavelengths at which Bragg reflection of the electron waves occurs. It is possible to have energy values in the forbidden region only by allowing k to take on complex values. This behavior refers to the experimental situation in which electrons of the forbidden energies are reflected from the surface of the solid. One is therefore led to expect that electromagnetic waves impinging on a plasma in a magnetic field wili be reflected in selective frequency regions. Since the width of the gap depends on the temperature of the electrons of the plasma, it is possible that the theory may be useful in analyzing plasma. It is to be realized that in actual practice one may have to take into account effects of varying plasma density and absorption because of electron-atom collisions. The latter effect can be treated by the methods developed in this paper. It is to be noted that the underlying reason for the band structure is the same for the plasma as for the solid. In the solid-state problem one studies the propagation of an electron wave in the periodic field of the lattice, while in the plasma one studies the propagation of waves in an electron gas in which all electrons are rotated with a period equal to the cyclotron period.

VI. DISPERSION RELATION FOR A SMOOTH, MAXWELLIAN DISTRIBUTION

The maxwellian distribution for the unperturbed system is particularly important in comparing the exact method with the transport solutions. The distribution function is

$$f_0=N_0(m/2\pi\kappa T)^{\frac{1}{2}}\exp[-(m/2\kappa T)(v_z^2+\rho^2)].$$

In the Appendix expressions are given for α, β, γ, δ. These enable one to study the general dispersion relation. Here we confine our discussion to the plasma-type solutions ($ck\gg\omega_c, \omega_p$), and find for the dispersion relation:

$$\omega=-\frac{1}{2}\cdot\frac{4\pi e^2}{m}\frac{\pi}{\omega_c}\int_{-\infty}^{+\infty}dv_z\int_0^\infty\rho^2 d\rho\frac{df_0}{d\rho}\times\sum_{n=-\infty}^{+\infty}\frac{(J_n+J_{n+2})^2}{n+1+\omega/\omega_c}. \quad (22)$$

Substituting the maxwell distribution for f_0, and using the identity $2nJ_n(z)/z\equiv J_{n+1}+J_{n-1}$, one obtains

$$\omega=+4\omega_p^2\frac{\omega_c}{k^2}\left(\frac{m}{2\kappa T}\right)^2\int_0^\infty\rho\exp\left[-\frac{m}{2\kappa T}\rho^2\right]d\rho\times\sum_{n=-\infty}^{+\infty}\frac{n^2J_n^2}{n+\omega/\omega_c}.$$

With $\lambda=k\rho/\omega_c$, $1/\mu=m\omega_c^2/\kappa Tk^2$, this can be put in the form:

$$\omega=4\omega_p^2\frac{\omega_c^3}{k^4}\left(\frac{m}{2\kappa T}\right)^2\int_0^\infty\lambda\exp\left(-\frac{\lambda^2}{2\mu}\right)d\lambda\times\sum_{n=-\infty}^{+\infty}\frac{n^2J_n^2(\lambda)}{n+\omega/\omega_c}. \quad (23)$$

We shall study this dispersion relation in the two limits $\mu\ll1$ and $\mu\gg1$. The first case corresponds to the limit of low temperatures and long wavelengths, while the second case represents the behavior in the limit of weak magnetic fields.

(A) When $\mu\ll1$

To see how to handle this case we first evaluate Eq. (23) in the limit $T\to0$, using the expressions for the bessel functions of small argument,

$$J_0(\lambda)\simeq1-\tfrac{1}{4}\lambda^2,\quad J_n(\lambda)\simeq\lambda^n/2^n n!,$$

$$\omega=\frac{\omega_p^2}{2\omega_c}\left\{\frac{1}{1+\omega/\omega_c}+\frac{1}{-1+\omega/\omega_c}\right\},\quad\text{or}\quad\omega^2=\omega_p^2+\omega_c^2.$$

The dispersion relation at low temperatures can be found by carrying out the expansion so that the dispersion relation contains terms of the order of μ. The result is

$$\omega^2=\omega_p^2+\omega_c^2+\left(\frac{\kappa Tk^2}{m\omega_c^2}\right)\frac{\omega_p^2\omega_c}{\omega}\left(\frac{\omega^2}{\omega_c^2}-1\right)\cdot\frac{1}{8}\left(\frac{1}{-3+\omega/\omega_c}-\frac{2}{-1+\omega/\omega_c}+\frac{2}{\omega/\omega_c}-\frac{3}{1+\omega/\omega_c}+\frac{2}{2+\omega/\omega_c}\right). \quad (24)$$

This equation is still quite complicated; and one must take care not to introduce irrelevant roots, i.e., roots which do not tend to the correct values as $T\to 0$. To obtain the information which interests us we study several special cases by substituting the value $\omega^2\simeq\omega_p^2+\omega_c^2$ in the last term of Eq. (24). We find that

$$\omega^2=\omega_p^2+\omega_c^2+\tfrac{1}{2}\omega_c\omega_p(\kappa Tk^2/m\omega_c^2) \quad \text{for} \quad \omega_p\gg\omega_c, \tag{25}$$

$$\omega^2=\omega_p^2+\omega_c^2-\tfrac{1}{2}\omega_c^2(\kappa Tk^2/m\omega_c^2) \quad \text{for} \quad \omega_p\simeq\omega_c, \tag{26}$$

$$\omega^2=\omega_p^2+\omega_c^2-\tfrac{1}{2}\omega_p^2(\kappa Tk^2/m\omega_c^2) \quad \text{for} \quad \omega_p\ll\omega_c. \tag{27}$$

We see from these examples that the coefficient of $\kappa Tk^2/m$ depends, in general, on the parameters ω_p and ω_c. As we shall see later, the transport treatments give results of the correct general form; but the coefficients are fixed numbers. The same type of difference can be found if one does not restrict the discussion to the plasma-type solutions, but considers the strongly coupled waves when $ck\simeq\omega_c$, ω_p, for which it is necessary to use the complete dispersion relation (11).

In addition to the above-mentioned discrepancies between the transport and the exact theories, there is a more serious difference when ω is approximately a multiple of ω_c. As in the previous section, this will always occur, since ω_p varies continuously and gives rise to discontinuous jumps for ω at multiples of ω_c. We find from Eq. (24), with the help of the analysis of Sec. V, that the gap width when $\omega\simeq 3\omega_c$ is $\Delta\omega=(16/9)^{\frac{1}{3}}(\kappa T/m)^{\frac{1}{2}}k$. This is proportional to the mean velocity of the plasma electrons and to the wave vector.

(B) When $\mu\gg 1$, (i.e., $m\omega_c^2/k^2\kappa T\ll 1$)

This case represents the limit of a weak magnetic field and we should be able to recover the dispersion relation for plasma oscillations in the absence of a magnetic field when $\omega_c=0$. We notice that in this case ω_c/ω is also expected to be very small. If this occurs in such a way that $m\omega^2/k^2\kappa T\gg 1$, we obtain the ordinary expression, $\omega^2=\omega_p^2+(3\kappa Tk^2/m)$; but if $m\omega^2/k^2 2\kappa T\simeq 1$ we should find that ω is heavily damped,[2,13] expressing the fact that waves shorter than the Debye length cannot exist.

Our starting point is Eq. (23). This equation may be transformed by using the identity

$$\sum_{n=-\infty}^{+\infty}\frac{n^2J_n^2(\lambda)}{n+\omega/\omega_c}\equiv\frac{\omega^2}{\omega_c^2}\sum_{n=-\infty}^{+\infty}\frac{J_n^2(\lambda)}{n+\omega/\omega_c}-\frac{\omega}{\omega_c}\sum_{n=-\infty}^{+\infty}J_n^2(\lambda),$$

where

$$\sum_{n=-\infty}^{+\infty}J_n^2(\lambda)=1.$$

If we introduce the quantity $\Lambda=4\omega_p^2\omega_c^2/k^4(m/2\kappa T)^2$, Eq. (23) becomes

$$\left(\omega+\frac{\omega}{\omega_c}\Lambda\mu\right)=\Lambda\frac{\omega^2}{\omega_c^2}\int_0^\infty\lambda\exp\left(-\frac{\lambda^2}{2\mu}\right)d\lambda\sum_{n=-\infty}^{+\infty}\frac{J_n^2}{n+\omega/\omega_c}.$$

With the help of the methods developed in Appendix 1 we may write

$$\sum_{n=-\infty}^{+\infty}\frac{J_n^2(\lambda)}{n+\omega/\omega_c}=\frac{i}{\exp(i\omega 2\pi/\omega_c)-1}\int_0^{2\pi}J_0\times(\sqrt{2}\lambda[1-\cos\gamma]^{\frac{1}{2}})\exp\left(i\frac{\omega}{\omega_c}\gamma\right)d\gamma. \tag{28}$$

If we invert the order of integration in Eq. (28) and make use of the expression

$$\int_0^\infty J_0(at)\exp(-\rho^2t^2)dt=(1/2\rho^2)\exp(-a^2/4\rho^2),$$

we find the dispersion relation

$$\left(\omega+\frac{\omega}{\omega_c}\Lambda\mu\right)=\mu\Lambda\frac{\omega^2}{\omega_c^2}\frac{i}{\exp(i\omega 2\pi/\omega_c)-1}\times\int_0^{2\pi}\exp\left(i\frac{\omega}{\omega_c}\gamma\right)\cdot e^{-\mu(1-\cos\gamma)}d\gamma. \tag{29}$$

This form of the dispersion relation holds, of course, for μ small as well as μ large; and, if we wished, we could derive the formulas of the previous case by expansion of the integral in powers of μ. However, the main interest in the present form lies in the fact that it is possible to derive asymptotic expansions for the integral when ω_c/ω and $1/\mu$ are small.

The integral

$$I=\int_0^{2\pi}\exp[i(\omega/\omega_c)\gamma]e^{-\mu(1-\cos\gamma)}$$

is studied in Appendix 2. For $\omega_c^2/\omega_p^2\ll 1$ and $(\kappa T/m)(k^2/\omega_p^2)\ll 1$, one finds for the dispersion relation

$$\omega^2=\omega_p^2+\omega_c^2+(3\kappa T/m)k^2+9(\omega_c^2\kappa T/\omega_p^2m)k^2+(6/\omega_p^2)(\kappa Tk^2/m)^2. \tag{30}$$

Thus, in first approximation one finds that the contributions from the magnetic field and thermal motions are not coupled, while in second approximation they are. The case where $(\kappa T/m)(k^2/\omega_p^2)\simeq 1$ leads to complex values for ω, representing heavy damping of waves near the Debye length. The expression for the damping is that found by Landau,[13] slightly modified by the effects of the magnetic field (see Appendix 2).

VII. TRANSPORT EQUATIONS

Finally, we discuss the macroscopic treatments of the plasma oscillation problem and compare them with the exact solution of the Boltzmann equation. The transport treatments aim at taking into account effects of random motions, i.e., finite temperature, using a set of equations for the moments of the distribution function. Physically, these equations represent continuity,

momentum, and energy transport equations, etc. The infinite set is terminated after a few equations by assuming some expression for the highest moments in terms of the lower ones. This termination makes the equations a determined set, and should be accomplished according to a definite procedure so that higher approximations can be carried out. It will develop that if one restricts himself to a low order of approximation, these treatments give qualitatively correct results in many cases, although quantitative accuracy cannot be expected. The advantage of the macroscopic treatments is that they can be applied to many cases in which the exact solution of the Boltzmann equation cannot be obtained, particularly when this contains the integral terms resulting from considering collisions. It is therefore of interest to check the results of the macroscopic treatment with the exact solution when the latter can be found.

The first step in the transport method is to write the correct Boltzmann equation for the problem under discussion. For our problem this is Eq. (1), where in the present analysis we neglect collisions. The moments of f (density, mean velocity, etc.) are defined as

$$\rho(\mathbf{x},t)=\int f d\mathbf{v}, \quad \rho\langle v_i\rangle=\int v_i f d\mathbf{v}, \quad \rho\langle v_i v_j\rangle=\int v_i v_j f d\mathbf{v}.$$

We then take the zero and first moments of Eq. (1). This gives

$$\frac{\partial\rho}{\partial t}+\frac{\partial}{\partial x}(\rho\langle v_x\rangle)=0, \tag{31a}$$

$$\frac{\partial}{\partial t}(\rho\langle v_x\rangle)+\frac{\partial}{\partial x}(\rho\langle v_x^2\rangle)-\frac{eE_x}{m}\rho-\omega_c\rho\langle v_y\rangle=0, \tag{31b}$$

$$\frac{\partial}{\partial t}(\rho\langle v_y\rangle)+\frac{\partial}{\partial x}(\rho\langle v_x v_y\rangle)-\frac{eE_y}{m}\rho+\omega_c\rho\langle v_x\rangle=0, \tag{31c}$$

$$\frac{\partial}{\partial t}(\rho\langle v_z\rangle)+\frac{\partial}{\partial x}(\rho\langle v_x v_z\rangle)=0. \tag{31d}$$

Equation (31a) is the equation of continuity and Eqs. (31b, c, d) are the equations of momentum transfer. Instead of writing the second moment equations separately, we shall find it sufficient to obtain an expression for $\partial[\rho\langle v_x^2+v_y^2+v_z^2\rangle]/\partial t$. Using Eq. (1) and introducing the quantity $T(x,t)$ by means of the definition $\frac{3}{2}\kappa T(x,t)=\frac{1}{2}m\langle(v_x^2+v_y^2+v_z^2)\rangle$, we have

$$\frac{\partial}{\partial t}\left(\rho\frac{3\kappa T}{m}\right)+\frac{\partial}{\partial x}[\rho\langle v_x^3+v_x v_y^2+v_z v_z^2\rangle]$$
$$-\frac{2e}{m}E_x\bar{v}_x\rho-\frac{2e}{m}E_y\bar{v}_y\rho=0. \tag{31e}$$

It will be noticed that the magnetic field terms do not occur in Eq. (31e), and that this equation contains third moments, so that there are too many unknowns.

We shall describe two different methods of treating the above set of equations. The first is equivalent to the use of the maxwell transfer equations and was first used to describe plasma oscillations by the Thomsons.[14] It has recently been extended by Bailey[8] to describe excitation of plasma oscillations in the presence of static electric and magnetic fields. For the discussion of small amplitude oscillations we may write Eqs. (31) as

$$\frac{\partial\langle v_x\rangle}{\partial t}+\frac{\partial}{\partial x}\langle v_x\rangle^2+\frac{v_x^2}{\rho_0}\frac{\partial\delta\rho}{\partial x}-\frac{eE_x}{m}-\omega_c\langle v_y\rangle=0, \tag{32a}$$

$$\frac{\partial\langle v_y\rangle}{\partial t}+\frac{\partial}{\partial x}\langle v_x v_y\rangle+\frac{\langle v_x v_y\rangle}{\rho_0}\frac{\partial\delta\rho}{\partial x}-\frac{eE_y}{m}+\omega_c\langle v_x\rangle=0, \tag{32b}$$

with $\rho=\rho_0+\delta\rho$. If one now assumes with the Thomsons that $\langle v_x^2\rangle$ is a constant equal to $\kappa T_0/m$ (since $\frac{1}{2}m\langle v_x^2\rangle=\frac{1}{2}\kappa T_0$), where T_0 is the constant temperature of the plasma and assume with Bailey that $\langle v_x v_y\rangle=0$, Eqs. (31a), (32a), and (32b) become a determined set of equations. For if we note that E_x and E_y are determined in terms of ρ, $\langle v_x\rangle$, $\langle v_y\rangle$ with the help of Maxwell's equations (3b) and (3c), we see that we have three equations to solve for the unknowns ρ, $\langle v_x\rangle$, $\langle v_y\rangle$.

If we set all quantities proportional to $e^{i(kx-\omega t)}$, we easily find the dispersion relation

$$(\omega^2-\omega_p^2-k^2\kappa T_0/m)(\omega^2-\omega_p^2-c^2k^2)-\omega_c^2(\omega^2-c^2k^2)=0. \tag{33}$$

In comparing this with our previous results we note first that the exact treatment indicates that this type of relation cannot hold for large values of k when damping effects become appreciable in the linear approximation. Second, the term $\kappa T_0k^2/m$ replaces our previous terms in Eqs. (25), (26), (27), and (30) in the limit $ck\gg\omega_p$, ω_c. This shows that for long wavelengths the transport dispersion relation has only semiquantitative accuracy. One can see the reason for this discrepancy most easily in the case treated by the Thomsons, i.e., plasma oscillations in the absence of magnetic fields. Then the assumption was that to first-order terms the term $\partial\langle v_x^2\rangle/\partial x$ is negligible compared to the other terms in Eq. (7). With the help of the distribution function

$$f=f_0(v)+[eE_x/mi(kv_x-\omega)]\partial f_0 e^{i(kx-\omega t)}/\partial v_x,$$

we see that this is not the case and that the contribution of this term is, in general, of the same order as those of the terms retained by the Thomsons. We remark in passing that the transfer treatment corresponds to the lowest approximation in the method of treating thermal

[14] J. J. and G. P. Thomson, *Conduction of Electricity in Gases* (Cambridge University Press, London, 1933), Vol. 2, p. 353.

motions by expanding the distribution function in spherical harmonics, but a study of the effects of higher approximations has not yet been carried out. Although the complexity increases greatly for the higher approximations, this procedure is still easier than finding exact solutions.

The second method of solving the transport equations is an adaptation of the Hilbert-Enskog zero approximation and is somewhat more systematic though more complicated. In this method one uses Eqs. (2) through (6) and takes the distribution function to be of the form

$$f=\rho(m/2\pi\kappa T)^{\frac{1}{2}}\exp(-m/2\kappa T)[(v_x-\langle v_x\rangle)^2+(v_y-\langle v_y\rangle)^2+(v_z-\langle v_z\rangle)^2], \quad (34)$$

where ρ, T, $\langle v_x\rangle$, $\langle v_y\rangle$, $\langle v_z\rangle$ are functions to be determined by Eqs. (2) through (6). One can easily verify, by forming moments with the above distribution function, that these are the same as those used in setting up Eqs. (2) through (6). Furthermore, the above distribution function allows one to express the higher moments in terms of the five unknown functions, so that Eqs. (2) through (6) become a determined set of five equations in five unknowns. We have, in fact,

$$\rho\langle v_iv_k\rangle=\rho\langle v_i\rangle\langle v_k\rangle+\delta_{ik}\rho\kappa T/m, \quad (35a)$$

$$\rho\langle v_xv_y^2\rangle=\rho\langle v_x\rangle\langle v_y\rangle^2+\rho\langle v_x\rangle\kappa T/m, \quad (35b)$$

$$\rho\langle v_z^3\rangle=\rho(\langle v_z\rangle)^3+3\rho\kappa T\langle v_x\rangle/m. \quad (35c)$$

If we substitute these equations into Eqs. (31), put $\rho=\rho_0+\delta\rho$, $T=T_0+\delta\tau$, and simplify the equations for the case of small oscillations, we find the dispersion relation

$$[\omega^2-\omega_p^2-(5\kappa T_0k^2/3m)](\omega^2-\omega_p^2-c^2k^2)-\omega_c^2(\omega^2-c^2k^2)=0. \quad (36)$$

This differs from the previous treatment in that $\kappa T_0k^2/m$ is multiplied by 5/3. Comparing these results with the discussion given in Sec. VI, we see that the transport treatments do not predict bands of forbidden frequencies and a variation with magnetic field of the coefficient of the temperature term. The precise value of this coefficient will be important in all questions where the group velocity of the waves is significant. These results lead us to expect only qualitative accuracy in treating the excitation of plasma-type oscillations in a plasma with static electric fields as has been done by Bailey.[8]

The author is happy to express appreciation for the interest and encouragement of Professor A. von Hippel. He is also indebted to Professor D. Bohm for several stimulating discussions.

APPENDIX 1

Let us now evaluate the series occurring in Eqs. (12) and (13). We have to deal with series of the types

$$K_p=\sum_{n=-\infty}^{+\infty}\frac{J_{n+p}(a)J_n(a)}{n+1+\omega/\omega_c},\qquad L_p=\sum_{n=-\infty}^{+\infty}\frac{J_{n+p}J_n}{n-1+\omega/\omega_c}. \quad (37)$$

We start from the addition theorem for bessel functions[15]

$$J_p(c)e^{ip\beta}=\sum_{n=-\infty}^{+\infty}J_{p+n}(a)J_n(b)e^{in\gamma}. \quad (38)$$

This relation is valid if the five quantities a, b, c, β, γ are all real and are restricted by the relation $ce^{i\beta}=a-be^{-i\gamma}$. For our purposes we shall want to put $a=b$ and to let γ range along the real axis from 0 to 2π. Then, if c and β are to be real for all γ, we must have $c^2=2a^2(1-\cos\gamma)$ and $e^{i\beta}=(1-e^{-i\gamma})/\sqrt{2}(1-\cos\gamma)^{\frac{1}{2}}$, or $\tan\beta=\sin\beta/(1-\cos\gamma)$. Equation (38) becomes

$$\frac{J_p(\sqrt{2}a[1-\cos\gamma]^{\frac{1}{2}})(1-e^{-i\gamma})^p}{(\sqrt{2})^p([1-\cos\gamma]^{\frac{1}{2}})^p}=\sum_{n=-\infty}^{+\infty}J_{p+n}(a)J_n(a)e^{in\gamma}. \quad (39)$$

To sum a series of type K_p we multiply both sides by $\exp\{i[(\omega/\omega_c)+1]\gamma\}$ and integrate γ from 0 to 2π. The result is

$$K_p=\frac{i}{\exp(i\omega 2\pi/\omega_c)-1}\times\int_0^{2\pi}\frac{J_p(\sqrt{2}a[1-\cos\gamma]^{\frac{1}{2}})(1-e^{-i\gamma})^p\exp\{i[(\omega/\omega_c)+1]\gamma\}d\gamma}{(\sqrt{2})^p(1-\cos\gamma)^{p/2}}. \quad (40)$$

Series of type L_p may be summed by multiplying by $\exp\{i[(\omega/\omega_c)-1]\gamma\}$ and integrating. Since we are concerned only with L_0, we find

$$L_0=\frac{i}{\exp(i\omega 2\pi/\omega_c)-1}\times\int_0^{2\pi}J_0(\sqrt{2}a[1-\cos\gamma]^{\frac{1}{2}})\exp\left[i\left(\frac{\omega}{\omega_c}-1\right)\gamma\right]d\gamma. \quad (41)$$

In the present notation the expressions for α, β, γ, δ are

$$\left.\begin{aligned}\alpha,\gamma&=\frac{4\pi e^2}{m\omega_c}\pi\int_{-\infty}^{+\infty}dv_z\int_0^{\infty}\rho^2d\rho\frac{df_0}{d\rho}(K_0\pm K_1),\\ \beta,\delta&=\frac{4\pi e^2}{m\omega_c}\pi\int_{-\infty}^{+\infty}dv_z\int_0^{\infty}\rho^2d\rho\frac{df_0}{d\rho}(K_2\pm L_0).\end{aligned}\right\} \quad (42)$$

For the case where f_0 is maxwellian it is possible to simplify the preceding expressions. This procedure is illustrated in Sec. VI for the special case of the plasma-type solutions (Eq. (28)), and consists of inversion of the orders of integration and subsequent use of the relation

$$\int_0^{\infty}J_\nu(at)\exp(-p^2t^2)t^{\nu+1}dt=\frac{a^\nu}{(2p^2)^{\nu+1}}\exp\left(\frac{-a^2}{4p^2}\right). \quad (43)$$

The resulting expressions are

$$\alpha,\gamma=-\frac{\omega_p^2}{\omega_c}\frac{i}{\exp[i2\pi(\omega/\omega_c)]-1}\int_0^{2\pi}d\gamma\exp\left[i\left(\frac{\omega}{\omega_c}+1\right)\gamma\right]\times[(d/d\mu)(\mu e^{-\mu(1-\cos\gamma)})\pm\tfrac{1}{2}\mu(1-e^{-i\gamma})^2e^{-\mu(1-\cos\gamma)}], \quad (44a)$$

$$\beta,\delta=-\frac{\omega_p^2}{\omega_c}\frac{i}{\exp[i2\pi(\omega/\omega_c)]-1}\int_0^{2\pi}d\gamma\exp\left[i\left(\frac{\omega}{\omega_c}+1\right)\gamma\right]\times[\tfrac{1}{2}\mu(1-e^{-i\gamma})^2e^{-\mu(1-\cos\gamma)}\pm e^{-2i\gamma}(d/d\mu)(\mu e^{-\mu(1-\cos\gamma)})]. \quad (44b)$$

APPENDIX 2

Let us consider the integral

$$I=\int_0^{2\pi}\exp[i(\omega/\omega_c)\delta]\exp[-\mu(1-\cos\delta)]d\delta,$$

where ω is assumed to be real. We find that the stationary points (in the complex plane) of $i(\omega/\omega_c)\delta-\mu(1-\cos\delta)$ are given by $\delta_0=i\phi_0+m\cdot 2\pi$, where $\sin\phi_0=\omega/\omega_c\mu$, so that ϕ_0 is real and positive. In our problem $\mu=(k^2/\omega_c^2)\kappa T/m$, so that $\omega/\omega_c\mu=(m/\kappa T)(\omega\omega_c/k^2)\to 0$ as $\omega_c\to 0$ and $\omega^2/\omega_c^2\mu=(m\omega^2/\kappa Tk^2)$ is constant. The next step is to look for contours along which the imaginary part of the argument is constant. For the contours passing through the first saddle point and the origin we have

[15] E. Jahnke and F. Emde, *Tables of Functions* (Dover Publications, New York, 1945), p. 144.

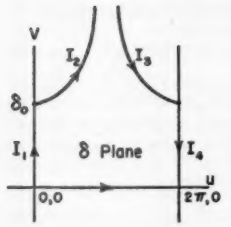

FIG. 1. Paths of constant imaginary argument.

$I[i(\omega\delta/\omega_c)-\mu(1-\cos\delta)]=0$. With $\delta=u+iv$ this becomes $(\omega u/\omega_c)-\mu\sin u\sinh v=0$. By Cauchy's theorem we may deform the path from 0 to 2π to pass along the paths of constant imaginary argument indicated in Fig. 1. On the portions I_1 and I_3 the value of the imaginary argument is zero, while on I_2 and I_4 the value is $2\pi i\omega/\omega_c$. Thus, the integration along I_2 and I_4 gives $-\exp[2\pi i(\omega/\omega_c)](I_1+I_3)$. Furthermore, the contribution to the integral is greatest near the origin and decreases as one proceeds along I_1 and I_3. As a result, the main contribution comes from the integrals along the straight portions I_1 and I_4. We now study I_1 in more detail. For $\omega_c/\omega\ll 1$

$$I_1=i\int_0^{\omega/\omega_c\mu}\exp[-(\omega/\omega_c)\phi]\exp[-\mu(1-\cosh\phi)]d\phi.$$

Putting $\zeta=\omega_c\phi/\omega$, we find

$$I_1=i\frac{\omega}{\omega_c}\int_0^{\omega^2/\omega_c^2\mu}e^{-\zeta}\exp\left[-\mu\left(1-\cosh\frac{\omega_c}{\omega}\zeta\right)\right]d\zeta.$$

We now note that the factor $e^{-\zeta}$ starts at 1 and decreases to $\exp(-\omega^2/\omega_c^2\mu)$ at the upper limit, while the other factor starts at 1 and increases to only $\exp[\frac{1}{2}(\omega^2/\omega_c^2\mu)]$ when ω_c is small. One can therefore evaluate I_1 by expanding the second factor in a convergent series about $\zeta=0$ and integrating term by term. The result is

$$I_1=i\frac{\omega_c}{\omega}\int_0^{\omega^2/\omega_c^2\mu}e^{-\zeta}\left[1+\frac{\mu\omega_c^2}{\omega^2}\frac{\zeta^2}{2!}+\frac{\mu\omega_c^3}{\omega^3}\left(\frac{\omega_c}{\omega^3}+\frac{3\mu\omega_c^3}{\omega^3}\right)\frac{\zeta^4}{4!}+(\mu+15\mu^2+15\mu^3)\frac{\omega_c^6}{\omega^6}\frac{\zeta^6}{6!}+\cdots\right]d\zeta. \quad (45)$$

The upper limit gives rise to terms of order $\exp(-m\omega^2/\kappa Tk^2)$; and if one is not interested in studying the behavior of the frequency for waves of the Debye length, such terms may be neglected by letting the upper limit tend to infinity. The sum of the contributions along the two straight portions then becomes

$$I_1+I_4=i(\omega_c/\omega)[1-\exp(2\pi i\omega/\omega_c)]\times\left\{1+\frac{\mu\omega_c^2}{\omega^2}+\frac{\omega_c^4}{\omega^4}(\mu+3\mu^2)+\frac{\omega_c^6}{\omega^6}(\mu+15\mu^2+15\mu^3)\right\}. \quad (46)$$

When this value is substituted in the expression (29), one finds the dispersion relation

$$\frac{\omega^2}{\omega_p^2}=1+\frac{\omega_c^2}{\omega^2}+\frac{3}{\omega^2}k^2\frac{\kappa T}{m}+\frac{\omega_c^4}{\omega^4}+15\frac{\omega_c^2}{\omega^4}\left(\frac{\kappa T}{m}k^2\right)+\frac{15}{\omega^4}\left(\frac{\kappa T}{m}k^2\right)^2. \quad (47)$$

Equation (47) can be solved by successive approximations when ω_c^2/ω_p^2 and $(\kappa T/m)(k^2/\omega_p^2)$ are small. In the first approximation one puts $\omega=\omega_p$ on the right-hand side and obtains $\omega^2=\omega_p^2+(3\kappa Tk^2/m)+\omega_c^2$. This reduces to the formula for the frequency of plasma oscillations in the absence of a magnetic field. The second approximation to the frequency may be found by substituting the first approximation into the right-hand side. It is

$$\omega^2=\omega_p^2+(3k^2\kappa T/m)+\omega_c^2+(9\omega_c^2\kappa Tk^2/\omega_p^2m)+6/(\kappa Tk^2/m)^2\omega_p^2. \quad (48)$$

We must now consider the contribution of the curved portions to the integral I. As one proceeds along the curve out from the saddle-point δ, the contribution to the integral rapidly becomes negligible, so that one may use the first approximation in the method of steepest descents.[16] We note that since we are integrating along a path in the complex plane, we are to expect a contribution which will make ω complex. The contribution to I is

$$I_2+I_3=\left[1-\exp\left(2\pi i\frac{\omega}{\omega_c}\right)\right]\frac{(2\pi)^{\frac{1}{2}}}{2}\frac{e^{[i(\omega\delta_0/\omega_c)-\mu(1-\cos\delta_0)]}}{\mu^{\frac{1}{2}}(\cos\delta_0)^{\frac{1}{2}}}. \quad (49)$$

If this expression is inserted in the dispersion relation (29), one finds for the imaginary part of $\omega=\omega_R+i\sigma$,

$$\sigma=-\frac{\pi}{2}\frac{\omega_p^4}{(2\pi)^{\frac{1}{2}}k^3}\left(\frac{m}{\kappa T}\right)^{\frac{1}{2}}\frac{\exp(-m\omega^2/2\kappa Tk^2)}{(1+\omega^2\omega_c^2m/k^2\kappa T)^{\frac{1}{2}}}. \quad (50)$$

By a comparison with Eq. (19) of reference 1 we see that this is only the Landau damping slightly modified by the presence of the magnetic field. It is to be emphasized that these results hold only for the case of small damping and small magnetic fields. If ω has a sizable imaginary part, the assumption that ω is real which has been made in evaluating I will break down.

---

[16] H. and B. S. Jeffreys, *Methods of Mathematical Physics* (Cambridge University Press, London, 1946), p. 473.

The Density of States in Light Nuclei

CHARLES L. CRITCHFIELD AND SOPHIE OLEKSA*
Department of Physics, University of Minnesota, Minneapolis, Minnesota
(Received December 26, 1950)

The number of states of energy less than 25 Mev is calculated for a simple model of a nucleus of 20 nucleons. Kinetic energy and the effect of symmetry on the potential energy were considered to be the only systematic contributions to the excitation. A method of classification of states by supermultiplets, using mainly their projections on the S–T plane, is presented. An empirical formula for level density in light nuclei is deduced.

I. INTRODUCTION

THE neutron scattering measurements of Barschall *et al.* at Wisconsin and of the group at Minnesota[1] have made valuable additions to our knowledge of the energy levels in light nuclei. These results, combined with those on proton capture and the well-known frequency of resonance capture of slow neutrons in heavy elements, provide a considerable body of empirical information on the density of energy levels in nuclei, at least for relatively low angular momentum.

Unfortunately, the empirical evidence cannot be considered to be complete, except in limited instances, because of practical difficulties in the resolution of individual peaks and in the identification of the angular momenta of the resonance levels. Moreover, the statistical theories are not wholly adequate to an interpretation of most of the more precise information since this covers a range of intermediate mass numbers, $20 \leq A \leq 40$, in which such theories barely apply, even for low angular momenta.

In order to assist in the study of nuclear energy levels, we have undertaken a computation of the level distribution in a model nucleus. For this purpose, we have chosen $A=20$ as a compromise between feasibility and a reasonable representation of light nuclei. The work, thus, goes farther than the previous study by Bardeen and Feenberg[2] in that it relates the kinetic and potential energies to an explicit nuclear model, with more recent estimates of the importance of the potential energy, and, therefore, leads to a more complete description of the angular momenta and parities of the levels. The underlying assumption remains the same; namely, that the over-all density of levels in the true nucleus with $A=20$ is essentially the same as that calculated in the model which considers the kinetic energy and the effect of symmetry on the potential energy to be the main systematic contributions to the energy of excitation. It is also assumed that spin-orbit splitting, correlations, coulomb energy, etc., remove the degeneracy left by considering only kinetic and symmetry effects, except, of course, that a state of total angular momentum (nuclear spin) j is $(2j+1)$-fold degenerate. No claim is made concerning the exact location of any individual level.

A secondary purpose of this work is to enlarge upon a calculational scheme which may be adapted to machine computations for more complex nuclei, either for level densities or for ground-state calculations. The $A=20$ results are also used to derive a rough empirical formula for level density which may be applicable to light nuclei. Qualitatively, the results of the work presented here are similar to those of reference 2.

II. MODEL OF THE NUCLEUS $A=20$

The calculations below are similar to those made on lighter nuclei by Feenberg and Phillips[3] and by Motz and Feenberg.[4] It is assumed that the nuclear wave function can be written as a sum of products of individual particle wave functions. The individual nuclear waves are taken to be the stationary states of definite n, l, and m for a particle moving freely in a spherical potential of finite depth[5] inside the radius R:

$$\psi_{n,l,m}(\mathbf{r}) = c(\pi/2k_n r)^{\frac{1}{2}} J_{l+\frac{1}{2}}(k_n r) P_l^m(\theta) e^{im\phi}, \quad r<R \quad (1)$$

$$= c'(\pi/2k_n r)^{\frac{1}{2}} H_{l+\frac{1}{2}}^{(1)}(\kappa_n r) P_l^m(\theta) e^{im\phi}, \quad r>R$$

$$H_{l+\frac{1}{2}}^{(1)}(\kappa_n R) J_{l+\frac{1}{2}}(k_n R)' - J_{l+\frac{1}{2}}(k_n R) H_{l+\frac{1}{2}}^{(1)}(\kappa_n R)' = 0, \quad (2)$$

and $J_{l+\frac{1}{2}}(k_n r_i)=0$ for $n-l$ values of $|r_i|<R$. If the potential energy of the well is zero for $r>R$ and

$$v_0 = -\hbar^2 k_0^2/2\mu, \quad r \leqq R, \quad (3)$$

then $\kappa_n^2 = k_0^2 - k_n^2$, with μ as the reduced mass of the nucleon.

The determination of the solution for k_n and κ_n of Eqs. (2) and (3) was effected by graphical methods and by using recursion relations to determine the functions. Thus Eq. (2) is readily proved to be equivalent to

$$\xi_l(kR) + \eta_l(\kappa R) = 0, \quad (4)$$

with

$$\xi_l(x) = xJ_{l-\frac{1}{2}}(x)/J_{l+\frac{1}{2}}(x), \quad \eta_l(y) = iyH_{l-\frac{1}{2}}^{(1)}(iy)/H_{l+\frac{1}{2}}^{(1)}(iy),$$

$$\xi_0(x) = x\cot x, \quad \eta_0(y) = y,$$

$$\xi_l(x) = x^2/(2l-1-\xi_{l-1}), \quad \eta_l(y) = y^2/(2l-1+\eta_{l-1}).$$

* In partial fulfillment of the requirements for the doctoral degree.

[1] Hornyak, Lauritsen, Morrison, and Fowler, Revs. Modern Phys. **22**, 291 (1950); R. K. Adair, Revs. Modern Phys. **22**, 249 (1950).

[2] J. Bardeen and E. Feenberg, Phys. Rev. **54**, 809 (1938).

[3] E. Feenberg and M. Phillips, Phys. Rev. **51**, 597 (1937).

[4] L. Motz and E. Feenberg, Phys. Rev. **54**, 1055 (1938).

[5] H. Margenau, Phys. Rev. **46**, 613 (1934).

The value of the nuclear radius assumed here is that deduced for the ground states by Wigner's analysis,[6]

$$R=1.45A^{\frac{1}{3}}\times10^{-13}\text{ cm}$$
$$=3.07\times10^{-13}\text{ cm for } A=20. \quad (5)$$

In this model the depth of the potential is assumed to be the same for neutrons and protons. Since the value chosen for the depth is an arbitrary matter, we have chosen such a depth that 16.8 Mev is required to remove a neutron, leaving the residual nucleus in its lowest state. A description in terms of individual nucleons probably is better served by such a choice than by matching the total binding energy. The effective depth for protons may be a little lower, but the exact choice of V_0 is a minor detail which need not be considered too closely.

Wigner's analysis[6] is also used to obtain the magnitude of the effect of symmetry on the potential energy. A state belonging to the supermultiplet (STY) has a positive potential energy V_m (in addition to a constant negative potential):

$$V_m=\tfrac{1}{2}L[S(S+4)+T(T+2)+Y^2],$$
$$L=40/A \text{ Mev}, \quad S\geq T\geq Y. \quad (6)$$

It is in this description of the potential energy that the method of this paper and that of reference 2 departs from the earlier statistical analyses of Bethe[7] and of van Lier and Uhlenbeck.[8] In those papers the number of states was computed for a given number of neutrons and protons without counting the multiplicity of states that can be obtained by exchanging charge between neutrons and protons. Hence, they approximate the effect of symmetry by implying infinite Heisenberg forces.

III. CALCULATION OF SYMMETRY CHARACTERS

The kinetic energy of a given configuration is determined by the number of particles in each of the individual orbits; $1s$, $2p$, $3d$, $2s$, $4f$, etc. The next step is to determine the number of states of given orbital angular momentum that can be obtained for a given configuration. This is done without reference to whether a nucleon is a neutron or proton, or to its spin orientation. A given configuration has a certain maximum value M for the sum over individual quantum numbers m, which is obtained by putting as many nucleons into the highest m orbits as possible but no more than four to an orbit. The number of ways of selecting individual orbits in order to obtain sums over m_i lower than M is then determined by inspection. In principle these sums run from M, $M-1$, $\cdots$ to $-M$ but the determination is stopped at $\Sigma m_i=0$ because of the symmetry in positive and negative values of Σm_i. When $\Sigma m_i<M$, there are, in general, a number of possible arrangements of nucleons each of which is characterized by a number, ν_4 of orbits filled by four nucleons, ν_3 by three nucleons, ν_2 by two, and ν_1 by one. It is convenient to denote each such arrangement by the symbol $\{\nu_4\nu_3\nu_2\nu_1\}$. However, a given set of values ν_4, ν_3, ν_2, ν_1 may occur more than once for a given Σm_i if there are alternate ways of distributing the nucleons among distinct orbits of distinct n, l, m quantum numbers.

After one determines the number of ways a value of Σm_i can be achieved in terms of the $\{\nu_4\nu_3\nu_2\nu_1\}$ distributions, the next point of interest is the number of ways in which a particular $\{\nu_4\nu_3\nu_2\nu_1\}$ can be achieved with a given number of neutrons and protons and a given net spin. Each distinct arrangement of charge and spin represents, of course, a distinct wave function, and functions of definite symmetry type are linear superpositions of them. It is to be noted first that ν_4 orbits, which are occupied by four nucleons, have no freedom as to composition. Furthermore, substitution into any of the ν_3 orbits, occupied by three nucleons, is restricted by the Pauli principle so that the freedom of choice is the same as in a singly occupied orbit so far as spin and charge are concerned. The third zeta-component, $Y_\zeta=\frac{1}{2}\Sigma s_z\tau_\zeta$ in Wigner's notation,[9] differs in sign for threefold and singly occupied orbits, but the necessity for taking this into consideration is so rare among the lower supermultiplets that it is convenient to ignore it except in the special cases in which it is decisive. This means that we are interested primarily in distributing N neutrons and P protons among which occur α upward spins and β downward spins in $\nu_1+\nu_3$ singly occupied spaces and ν_2 doubly occupied spaces. The numbers N and P are not true neutron and proton numbers, nor are α and β true spin numbers, but rather "excess" numbers related to the ν's and to spin component S_z and isotopic spin component T_ζ by

$$N+P=\alpha+\beta=\nu_1+\nu_3+2\nu_2,$$
$$T_\zeta=\tfrac{1}{2}(N-P), \quad S_z=\tfrac{1}{2}(\alpha-\beta). \quad (7)$$

Let p be the number of orbits (n, l, m) occupied by two protons and n the number occupied by two neutrons; then ν_2-n-p is the number occupied by one neutron and one proton. By combinatorial analysis, one readily computes the number of arrangements in a given $\{\nu_4\nu_3\nu_2\nu_1\}$ and given n and p. The total number of wave functions occurring with particular values of S_z and T_ζ is a sum over all n and p.

$$f_{S_zT_\zeta}(\nu_2, \nu_1+\nu_3)=\sum_n\sum_p\binom{\nu_2}{n}\binom{\nu_2-n}{\nu_2-n-p}$$
$$\times\binom{\nu_1+\nu_3}{P-\nu_2-p+n}\binom{N+P-2n-2p}{\alpha-n-p}, \quad (8)$$

where $\binom{x}{y}=x!/y!(x-y)!$.

[6] E. Wigner, *University of Pennsylvania Bicentennial Conference* (University of Pennsylvania Press, Philadelphia, 1941).
[7] H. A. Bethe, Phys. Rev. **50**, 332 (1936).
[8] C. van Lier and G. E. Uhlenbeck, Physica **4**, 531 (1937).
[9] E. Wigner, Phys. Rev. **51**, 106 (1937).

TABLE I. Reduction of space arrangements.

$\{\nu_4\nu_3\nu_2\nu_1\}$	$\Sigma a_w(STY)_w$
{2000}	(000)
{1101}	(110)+ (000)
{1020}	(200)+ (110)+ (000)
{1012}	(211)+ (200)+2(110)+ (000)
{0210}	(21–1)+ (200)+2(110)+ (000)
{1004}	(222)+3(211)+2(200)+3(110)+ (000)
{0202}	(220)+ (211)+ (21–1)+ (200)+4(110)+2(000)
{0121}	(310)+ (220)+2(211)+2(21–1)+3(200)+5(110) +2(000)
{0113}	(321)+2(310)+ (222)+3(220)+3(21–1)+6(211) +5(200)+9(110)+3(000)
{0105}	(332)+4(321)+5(310)+5(222)+6(220)+15(211) +5(21–1)+10(200)+15(110)+4(000)

The numbers fs_sT_t form a matrix in the S–T space with elements corresponding (in our case of 20 particles) to positive and negative integral values of S_s and T_t. They are the sums of the numbers of arrangements of the nucleons and indicate nothing concerning the symmetry of the wave function. Since the potential energy of the nucleus is assumed to depend strongly on the symmetry character, the next step is to determine the composition of a given arrangement $\{\nu_4\nu_3\nu_2\nu_1\}$ as a sum of arrangements having definite symmetry. The most convenient manner of designating states of definite symmetry is the (STY) formalism of Wigner. The substates for a given (STY) are readily computed, as shown in reference 9, by expanding those for the four-valued spin in terms of the substates of the three-valued spin and expanding the latter in terms of the ordinary two-valued spin. All substates of supermultiplets used in this work were determined by this method. Summing over the Y_t, one gets the projection of a given (STY) on the S–T plane

$$(S_sT_t)_w=\sum Y_t(S_sT_tY_t)_w, \tag{9}$$

where the subscript w refers to a given supermultiplet, $(STY)=w$. The problem is, then, one of reducing the matrix with elements given by Eq. (8) to

$$fs_sT_t=\sum_w a_w(S_sT_t)_w, \tag{10}$$

thereby reducing all arrangements $\{\nu_4\nu_3\nu_2\nu_1\}$ to sums over supermultiplets w with multiplicity a_w. The results for the arrangements used in this work are given in Table I. In most instances the expansion of fs_sT_t, Eq. (10), is unique. There are exceptions, however, since the projection on the S–T plane of (211) and (21–1) are identical, and also the projections of (222) and (220) are linearly related through lower supermultiplets, *vis.*[10]

$$\text{Projection}[(222)+(211)+(200)] = \text{Projection}[(220)+(110)+(000)]. \tag{11}$$

Actually, the ambiguity in (211) and (21–1) is unimportant so far as the energy is concerned, Eq. (6). The method used for resolving the ambiguities was to examine in detail the distributions of charge and spin corresponding to a $\{\nu_4\nu_3\nu_2\nu_1\}$. Suppose we have an f-matrix containing (STY) projections for which $S>3$ so that we need to determine how many (222) and how many (220) supermultiplets are contained in it. We consider the total of all distributions with $\{\nu_4\nu_3\nu_2\nu_1\}$ that can be achieved with $N-P=4$ and $\alpha-\beta=4(S_s=T_t=2)$ and calculate Y_t for each. There will be so many states, q_2, for $Y_t=2$. Of these a certain number, r_2, will be substates of supermultiplets with $S>2$, which we have determined by Wigner's method cited earlier. Hence, the number of (222) supermultiplets must be q_2-r_2. As mentioned previously, the number of examples requiring such explicit consideration is so small as to make the method of expanding in terms of projections on the S–T plane convenient.

[10] The next such relation is Projection$[(330)+(211)+(200)]$ = Projection$[(332)+(310)+(000)]$.

IV. CLASSIFICATION OF STATES

The lowest state of 20 nucleons is assumed to be a $(1s)^4(2p)^{12}(3d)^4=s^4p^{12}d^4$ configuration. All other configurations obtained by promoting nucleons into orbits of higher kinetic energy and having a total increase of kinetic energy less than 25 Mev were determined. The number of ways of constructing states of given L_s and the supermultiplet composition of each was determined by the method described above. If the sum of the $(STY)_i$ for a certain L_s be denoted by $\eta(L_s)$, the number of states of definite L is $\eta(L)$,

$$\eta(L)=\eta(L_s)-\eta(L_s+1).$$

States of $L=0, 1, 2\cdots$ are designated S, P, $D\cdots$, respectively, in the customary way. The potential energy of each supermultiplet was calculated from

TABLE II. Classification of states of excitation less than 25 Mev.

Configuration	Kinetic energy (Mev)	Potential energy (Mev)	Total energy (Mev)	Supermultiplet	L states
$s^4p^{12}d^4$	0	0	0	(000)	$SD^2G^2H^1L$
$s^4p^{12}d^3s$	5.4	0	5.4	(000)	$SDFGI$
$s^4p^{12}d^4$	0	8.0	8.0	(110)	$P^3D^3F^2G^2H^2I^1K$
$s^4p^{12}d^3s^2$	10.8	0	10.8	(000)	SDG
$s^4p^{12}d^4$	0	12.0	12.0	(200)	$S^3D^2FG^2I$
$s^4p^{11}d^5$	12.8	0	12.8	(000)	$S^3P^4D^4F^3G^{11}H^{10}I^6K^4L^2M^2N$
$s^4p^{12}d^3s$	5.4	8.0	13.4	(110)	$SPD^2F^2G^2HI$
$s^4p^{12}d^2f$	14.5	0	14.5	(000)	$SP^2D^2F^2G^2H^2I^2K^2LM$
$s^4p^{12}d^4$	0	16.0	16.0	(211)	P^3DF^2GH
$s^4p^{12}ds^3$	16.2	0	16.2	(000)	D
$s^4p^{12}d^3s$	5.4	12.0	17.4	(200)	PD^2FGH
$s^4p^{11}d^4s$	18.2	0	18.2	(000)	$S^3P^1D^2F^1G^{10}H^2I^2K^2L^2M$
$s^4p^{12}d^3s^2$	10.8	8.0	18.8	(110)	$SPDFG$
$s^4p^{12}d^2s^2f$	19.9	0	19.9	(000)	$P^3D^2F^2G^2H^2IK$
$s^4p^{11}d^5$	12.8	8.0	20.8	(110)	$S^3P^{14}D^{17}F^{16}G^{20}H^{20}I^{15}K^{13}L^7M^3N$
$s^4p^{12}d^3s$	5.4	16.0	21.4	(211)	$P^3D^2F^2GH$
$s^4p^{12}s^4$	21.6	0	21.6	(000)	S
$s^4p^{12}d^2f$	14.5	8.0	22.5	(110)	$S^3P^1D^2F^1G^{10}H^2I^2K^1L^2M$
$s^4p^{12}d^2s^2$	10.8	12.0	22.8	(200)	SDG
$s^3p^{12}d^5$	23.1	0	23.1	(000)	$SP^2D^2F^2G^2H^2I^2K^2LM$
$s^4p^{11}d^2s^2$	23.6	0	23.6	(000)	$SP^2D^2F^2G^2H^2I^2K$
$s^4p^{12}d^4$	0	24.0	24.0	(222)	D
$s^4p^{12}ds^3$	16.2	8.0	24.2	(110)	D
$s^4p^{11}d^5$	12.8	12.0	24.8	(200)	$S^3P^{10}D^{14}F^{14}G^{15}H^{13}I^9K^5L^2M$

TABLE III. Double multiplet composition.

(STY)	$(2T+1)(2S+1)$
(000)	11
(110)	13 31 33
(200)	11 15 33 51
(211)	13 31 33 35 53
(220)	11 13 31 $(33)^2$ 35 53 55
(222)	11 33 55
(310)	13 15 17 31 $(33)^2$ $(35)^2$ 37 51 $(53)^2$ 55 71 73
(321)	13 15 31 $(33)^2$ $(35)^2$ 37 51 $(53)^2$ $(55)^2$ 73 75 57
(332)	13 31 33 35 53 55 57 75 77

Eq. (6) and added to the kinetic energy of excitation. Restriction of the total excitation to 25 Mev eliminates most of the states that have any appreciable kinetic energy because of the high potential energy of states of low symmetry. The results on symmetry character and L values are given in Table II.

The remaining step in the calculation is the combination of the possible spins in each (STY) with the orbital angular momenta in order to form states of definite total angular momentum, j. For this purpose it is convenient to use the "double multiplet" expansion[11] of the (STY); i.e., express the projections, Eq. (9), as sums of products of the isotopic and ordinary spin multiplets $(T, T-1, \cdots, -T)\times(S, S-1, \cdots, -S)$ and designate them by the double number $(2T+1)\times(2S+1)$. The components of (STY) of interest are shown in Table III. In applying the results in Table III to Ne^{20*}, all spin values are to be used and added vectorially to the L's with which each occurs in Table II

TABLE IV. Number of states of particular J value at a given excitation.

Configuration	Total energy (Mev)	$J=0$	$J=1$	$J=2$	$J=3$	$J=4$	$J=5$	$J=6$
$s^4p^{12}d^4$	0	1		2		2	1	1
$s^4p^{12}d^3s$	5.4	1		1	1	1		1
$s^4p^{12}d^4$	8.0	4	10	16	17	16	12	9
$s^4p^{12}d^2s^2$	10.8	1		1		1		
$s^4p^{12}d^4$	12.0	6	7	14	12	13	7	6
$s^4p^{11}d^5$	12.8	2	6	9	11	11	10	8
$s^4p^{12}d^3s$	13.4	3	11	15	16	12	9	5
$s^4p^{12}d^3f$	14.5	1	3	3	5	4	4	3
$s^4p^{12}d^4$	16.0	7	16	22	21	18	11	5
$s^4p^{12}ds^3$	16.2			1				
$s^4p^{12}d^3s$	17.4	3	9	13	12	10	7	3
$s^4p^{11}d^4s$	18.2	2	7	9	11	10	9	6
$s^4p^{12}d^3s^3$	18.8	3	7	7	7	5	2	
$s^4p^{12}d^2sf$	19.9		2	2	3	2	2	1
$s^4p^{11}d^5$	20.8	43	122	177	204	200	173	131
$s^4p^{12}d^2s$	21.4	8	20	27	25	19	11	5
$s^4p^{12}s^4$	21.6	1						
$s^4p^{12}d^2f$	22.5	16	43	63	71	70	59	44
$s^4p^{12}d^2s^2$	22.8	3	3	6	4	5	2	1
$s^4p^{12}d^5$	23.1	1	2	3	4	4	3	3
$s^4p^{11}d^2s^2$	23.6	1	5	6	7	5	4	2
$s^4p^{12}d^4$	24.0	1	2	3	2	1		
$s^4p^{12}ds^2$	24.2		2	3	2			
$s^4p^{11}d^5$	24.8	33	99	138	157	145	121	85

[11] F. Hund, Z. Physik **105**, 202 (1937); H. A. Jahn, Proc. Roy. Soc. (London) **201**, 516 (1950).

(the exponents in Table II mean the number of distinct states of given L), since all isotopic multiplets contain $T_t=0$. In F^{20} (and Na^{20}), however, $T_t=1$ and the isotopic singlets cannot contribute. In O^{20} (and Mg^{20}), only the isotopic quintets and higher contribute. The resulting numbers of levels at each excitation in Ne^{20} are shown in Table IV for j values 0 to 6. In Fig. 1 we plot the total number of levels with $j=0$ and excitation equal to or less than U. For comparison, the experimental value for Ne^{20} is shown as a point (25 levels) at 15 Mev and the prediction of Bethe's statistical theory[7]

$$I_B(U)=\int_1^U \rho_B(x)dx,$$
$$\rho_B(U)=0.6S^{-4}e^S, \quad S=(AU/2.30)^{\frac{1}{2}}. \tag{12}$$

The agreement between theory and the experimental point in Fig. 1 is partly accidental, inasmuch as it cannot be claimed either that all levels in Ne^{20} below 15 Mev have been found experimentally, or that all

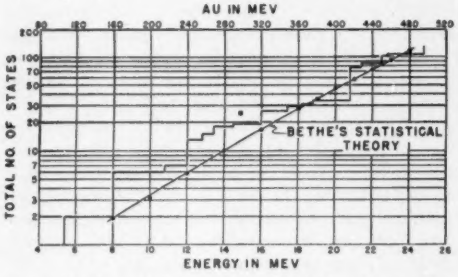

FIG. 1. Total number of states in Ne^{20} for $j=0$ and both parities. The point (■) indicates the total number of levels observed to date.

the levels which have been found have $j=0$. The two deviations, however, tend to cancel rather than add. The agreement between our results and Bethe's calculation for $j=0$ is also astonishingly good, indicating that disregarding the charge exchange is a reasonable device for allowing for symmetry effects in level density.

On the other hand, the statistical theory predicts a factor $(2j+1)$ in the level density of higher j, and, as found in the previous work of Feenberg *et al.*, the actual ratio of the number for $j=0$ is much less for high j and low excitation. One is usually interested in the total number of levels up to a certain value of j. Hence, we present in Table V the ratio of the total number of levels of j less than or equal to j_{max} to the total number of $j=0$ for several energies of excitation.

In using the information in Table V for the interpretation of nuclear reactions one must bear in mind the influence of potential barriers in favoring certain angular momenta and parity.

TABLE V. Ratio of total number at levels with $j \leq j_{max}$ to number with $j=0$.

AU	$j_{max}=0$	1	2	3	4	5	6
200	1.0	2.0	4.1	6.0	8.0	9.0	9.9
280	1.0	3.8	7.6	11.7	15.2	17.8	19.4
360	1.0	4.1	8.1	12.2	15.6	18.1	19.4
440	1.0	3.7	7.6	11.9	16.0	19.4	21.9
∞	1.0	4.0	9.0	16.0	25.0	36.0	49.0

V. APPLICATION TO NUCLEI IN GENERAL

The computations for Ne^{20} have been made in the hope that they might serve as a model for the interpretation of other nuclei. The same detail can be presented, of course, on the basis of the work above, for F^{20} and O^{20}. We present, however, only a comparison between total numbers of levels with $j=0$ and both parities at various excitations in Table VI. It will be noted that F^{20} has a higher level density than Ne^{20} or O^{20}. This effect was shown first by Bardeen and Feenberg.[2] It might be thought, off hand, that the omission of the isotopic singlet states in the enumeration for F^{20}, and both singlets and triplets for O^{20}, would reduce the number of levels below that of Ne^{20}. Actually, this effect is counterbalanced by the fact that the lowest states in F^{20} and O^{20} have lower symmetry than does that of Ne^{20}. Hence, a given excitation falls in a region accessible to higher supermultiplets and greater multiplicity.

We shall generalize the application to nuclei for which the ground state is not a (000) state in the following way. If the ground state is $(S_0T_0Y_0)$, the over-all level density is related to that for a (000) nucleus by adding the Majorana potential to the excitation in the latter and finding $\rho_0(U')$ instead of $\rho_0(U)$, where

$$U'=U+(20/A)[S_0(S_0+4)+T_0(T_0+2)+Y_0^2]. \quad (13)$$

On the other hand, the true level density is less than $\rho_0(U')$, because the lower double multiplets no longer contribute. Let us approximate the relative number of double multiplets by the factor

$$\exp\{-\lambda(S_0^2+T_0^2)/AU'\}, \quad (14)$$

where λ is an unknown, constant energy. The expected order of magnitude of λ is several hundred Mev, since

TABLE VI. Comparison of $j=0$ level numbers for isobars.

Excitation (Mev)	Ne^{20} $T_z=0$	F^{20} 1	Na^{20} -1	O^{20} 2	Mg^{20} -2
		Total number of states			
0	1	2		2	
8	6	11		5	
12	13	14		11	
16	26	56		16	
20	34	114		72	
24	108	255		163	

with $A=20$ the double multiplets are significantly reduced in number if $U'<30$.

As for an empirical form for $I_0(U)$, we have assumed the following

$$\ln[I_0(U)]=a+b\ln U+cU^{\frac{1}{2}} \quad (15)$$

and have determined the best fit to the step-curve in Fig. 1, by the method of least squares. The resulting values are

$$a=-2.06, \quad b=-1.31, \quad c=2.21.$$

In order to generalize Eq. (15) to nuclei of other values of A and (000) ground states we note that Bethe's result for I_B for the case $j=0$ [Eq. (12)] is A^{-1} times a function of the product AU. We assume $I_0(U)$ to have the same functional dependence and obtain

$$\ln[I_0(U)]=4.87-1.31\ln AU+0.49(AU)^{\frac{1}{2}}-\ln A. \quad (16)$$

Generalizing to other values of A and other than (000) ground states, we substitute U' from Eq. (13) for U and add the term given in Eq. (14). We determine λ to give a reasonable fit to the calculations for F^{20} and O^{20}. The result is

$$\ln[I(U)]=4.87-1.31\ln AU'+0.49(AU')^{\frac{1}{2}}-\ln A-200(S_0^2+T_0^2)/AU'. \quad (17)$$

We estimate the validity of Eq. (17) to be restricted to values of $AU'<800$. The total number of levels with $j=0$ and with a given parity is then $\frac{1}{2}I(U)$, and the total number with higher j is to be estimated by use of Table V. Finally, the empirical formula for the density of levels of $j=0$ and given parity is

$$\rho(U)=\frac{1}{2U'}\left[0.245(AU')^{\frac{1}{2}}+200\frac{(S_0^2+T_0^2)}{AU'}-1.31\right]I(U). \quad (18)$$

Energy Levels of B^{11} from the $B^{10}(d,p)B^{11*}$ Reaction*

D. M. Van Patter, W. W. Buechner, and A. Sperduto
Physics Department and Laboratory for Nuclear Science and Engineering, Massachusetts Institute of Technology, Cambridge, Massachusetts

(Received December 20, 1950)

The proton groups from enriched B^{10} bombarded by 1.51-Mev deuterons have been investigated by means of a magnetic spectrograph of high resolution. Eleven proton groups were assigned to the reaction $B^{10}(d,p)B^{11}$, corresponding to the ground state and ten excited states of B^{11}. Five of these excited states have not been previously reported. At 6.8-Mev excitation of B^{11}, a doublet was observed with a level spacing of 50.0±2.0 kev. The range of excitation of B^{11} covered in these experiments was from 0 to 10.2 Mev.

I. INTRODUCTION

THE first investigation of the proton groups from natural boron bombarded by deuterons was made by Cockcroft and Walton.[1] Using range measurements, they found three groups which they attributed to the B^{10} isotope on the basis of mass considerations. Their measurements at 0.55-Mev bombarding energy were repeated with improved accuracy by Cockcroft and Lewis[2] who measured Q-values of 9.14±0.10; 7.00 ±0.10; and 4.71±0.05 Mev,[3] corresponding to the ground state of B^{11} and levels at 2.14 and 4.43 Mev.

Pollard, Davidson, and Schultz[4] bombarded natural boron targets with 3.1-Mev deuterons and found four proton groups by range measurements. They reported Q-values of 9.22±0.2; 7.30±0.3; 5.00±0.2; and 2.39 ±0.2 Mev, corresponding to the ground state of B^{11} and excited states at 1.92, 4.22, and 6.83 Mev.

While the present experiments were in progress, Bateson[5] reported the results of his investigation of the proton groups from enriched B^{10} targets bombarded by 3.8-Mev deuterons. Using range measurements, he found seven groups which he assigned to the $B^{10}(d,p)B^{11}$ reaction, the Q-values being 9.18±0.05; 7.03±0.06; 4.70±0.06; 4.15±0.06; 2.26±0.07; 1.36±0.07; and 0.70±0.10 Mev. This work confirmed the earlier results and indicated new levels in B^{11} at 5.03±0.06; 7.82 ±0.08; and 8.48±0.10 Mev.

The assignment of the proton group with Q-value of 9.2 Mev to the ground-state $B^{10}(d,p)B^{11}$ reaction was shown to be correct by Thirion[6] from his p-γ coincidence measurements on the $B^{10}(d,p)$ proton groups. The excitation curve for the ground-state protons has been measured by Phillips[7] from 0.7- to 2.0-Mev bombarding energy at observation angles of 0, 90, and 135 degrees. Angular distributions of the ground-state protons have been reported by Redman[8] at bombarding energies of 1.06, 1.50, 1.71, 2.36, 3.06, and 3.68 Mev.

Additional information concerning the excited states of B^{11} has been found from other reactions. Ortner and Protiwinsky[9] have reported transitions to the 2.25- and 4.45-Mev levels of B^{11} from the $N^{14}(n,\alpha)B^{11*}$ reaction. Fulbright and Bush[10] have investigated the inelastic scattering of 15.6-Mev protons from natural boron. They found proton groups corresponding to levels at 2.2±0.3; 4.8±0.4; 6.5±0.3; and 7.8±0.4 Mev which could be associated with either B^{10} or B^{11}.

The gamma-radiation from natural boron bombarded by deuterons was first studied by Crane, Delsasso, Fowler, and Lauritsen[11] using a cloud chamber. Improved measurements were later made by Gaerttner, Fowler, and Lauritsen[12] who reported gamma-rays with energies of 1.5±0.2; 2.2±0.3; 4.4±0.3; 6.9±0.4; and 9.1±0.4 Mev at 550- to 850-(peak) kev bombarding energy. Halpern and Crane,[13] also using a cloud chamber, reported gamma-rays of 1.4, 2.4, 4.2, 6.0, and 8.6 Mev at 700-kev bombarding energy.

While the present experiments were in progress, Terrell[14] reported his measurements using a pair spectrometer on the gamma-rays from natural boron and enriched B^{10} bombarded by 1.56-Mev deuterons. He measured gamma-rays of 4.52±0.10; 6.74±0.13; and 9.11±0.18 Mev, assigned to $(B^{10}+d)$, and of 4.5±0.1 Mev, assigned to $(B^{11}+d)$. The thick-target yields of these gamma-rays were approximately 7.2, 7.2, 3.7, and 3.6×10^{7} quanta per microcoulomb, estimated for targets of 100 percent separated isotopes. The asymmetrical shape of the peaks of the two lower $(B^{10}+d)$ gamma-rays indicated the possible existence of weaker unresolved gamma-rays of slightly higher energy. The gamma-rays of 1.5 and 2.2 Mev, reported by earlier workers, would probably not have been detected by Terrell because of the low efficiency of the pair spectrometer at these energies.

* A report of these measurements was given at the 1950 meeting of the Physical Society in Washington, D. C.

[1] J. D. Cockcroft and T. S. Walton, Proc. Roy. Soc. (London) **A144**, 704 (1934).

[2] J. D. Cockcroft and W. B. Lewis, Proc. Roy. Soc. **A154**, 246 (1936).

[3] Corrected by M. S. Livingston and H. A. Bethe, Revs. Modern Phys. **9**, 245 (1937).

[4] Pollard, Davidson, and Schultz, Phys. Rev. **57**, 1117 (1939).

[5] W. O. Bateson, Phys. Rev. **78**, 337 (1950).

[6] J. Thirion, Comptes rend. **229**, 1007 (1949).

[7] G. C. Phillips, Phys. Rev. **79**, 240 (1950).

[8] W. C. Redman, Phys. Rev. **79**, 6 (1950).

[9] G. Ortner and G. Protiwinsky, Nature **142**, 807 (1938).

[10] H. W. Fulbright and R. R. Bush, Phys. Rev. **74**, 1323 (1948).

[11] Crane, Delsasso, Fowler, and Lauritsen, Phys. Rev. **46**, 1109 (1934).

[12] Gaerttner, Fowler, and Lauritsen, Phys. Rev. **55**, 27 (1939).

[13] J. Halpern and H. R. Crane, Phys. Rev. **55**, 415 (1939).

[14] J. Terrell, private communication. Also, Bull. Am. Phys. Soc., 26, 12 (1951).

The high ground-state Q-value of 9.2 Mev for the $B^{10}(d,p)B^{11}$ reaction permits the investigation of the excited states of B^{11} over a large region of excitation. Previous investigations of this reaction have indicated the existence of many levels in this region of excitation. It was decided to investigate with a magnetic spectrograph the protons group from B^{10} bombarded by 1.51-Mev deuterons, since this would establish the position of the excited states of B^{11} over the region from 0- to 10-Mev excitation and might indicate some pattern to the level structure. In addition, the high resolution of the magnetic spectrograph would make possible the detection of fine structure of any of the excited states that would not have been resolved by the earlier range measurements.

II. APPARATUS AND EXPERIMENTAL PROCEDURE

The apparatus and experimental procedures were essentially the same as those described in previous papers[15,16] except for some improvements in stabilization and the calculation of Q-values. A beam of deuterons was accelerated by an electrostatic generator and then deflected through 90° by means of a magnet. After passing through a narrow slit, the deuteron beam was directed at a target placed between the pole faces of a large annular magnet. A fraction of the charged particles, emitted from the target in a plane normal to the incident beam, was deflected through 180° in the magnetic field of the annular magnet and recorded on nuclear-track plates. Each plate covered a range in particle momentum of 6 percent, so that, in order to survey a complete spectrum of charged-particle groups, a series of plates was necessary, each plate being exposed at a different field strength.

The momentum of the charged-particle groups was determined from measurements of the magnetic field and their radii of curvature. The magnetic field measurements were calibrated from the measured radius of curvature of polonium alpha-particles. The value of Hr for polonium alpha-particles, used as an absolute standard, was 3.3159×10^5 gauss cm[17,18] (absolute emu), which is accurate to 0.02 percent. The incident deuteron energy was determined from the observation of deuteron groups elastically scattered from C^{12} and O^{16} nuclei in a thin Formvar target.

Several small corrections[19] were applied to the Q-values calculated for a 90° angle of observation. These corrections took into account:

(1) A small measured departure of the median angle of observation from 90°;

(2) The effect of the finite angle of acceptance

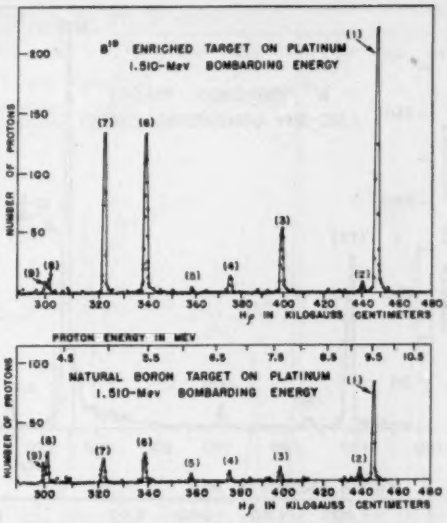

FIG. 1. Proton groups observed from targets of enriched B^{10} and natural boron bombarded by 1.51-Mev deuterons.

($\pm0.2°$ about the median angle) of the detector and the finite size of the deuteron beam striking the target;

(3) The approximation in using the nonrelativistic Q-equation for calculation;

(4) The effect of increased mass of residual nucleus when in an excited state.

The targets used for the $B^{10}(d,p)$ reaction were prepared by the evaporation from a carbon crucible of metallic boron onto 10-mil platinum sheets. Both natural boron and boron enriched to 96 percent B^{10} were used. (The enriched boron was obtained from the Stable Isotopes Division, AEC, Oak Ridge.) These targets had an effective thickness of about 10 kev for the $B^{10}(d,p)B^{11}$ ground-state reaction.

The survey of the proton groups at 90° from these targets was made at 1.51-Mev bombarding energy. In order to observe proton groups with energies of less than 3 Mev, it was necessary to eliminate the deuterons elastically scattered from the platinum backing of the target. This was accomplished by covering the nuclear-track plates with an aluminum foil sufficiently thick to stop the deuterons but thin enough to allow the protons to be recorded. However, this method had some disadvantages. Any variation in the effective thickness of the aluminum foils caused a large variation in the residual range of the proton tracks. This meant that the selection of tracks to be counted could not be so strict, and, therefore, tracks caused by alpha-contamination on the plates could not be eliminated so readily. In addition, any pinholes in the foils allow small numbers of deuterons to be recorded, and these also could not be completely eliminated from the counting

[16] Buechner, Strait, Stergiopoulos, and Sperduto, Phys. Rev. **74**, 1569 (1948).
[16] Buechner, Strait, Sperduto, and Malm, Phys. Rev. **76**, 1543 (1949).
[17] G. H. Briggs, Proc. Roy. Soc. **A157**, 183 (1936).
[18] W. B. Lewis and B. V. Bowden, Proc. Roy. Soc. **A145**, 250 (1934).
[19] Strait, Van Patter, Buechner, and Sperduto, Phys. Rev. **81**, 747 (1951).

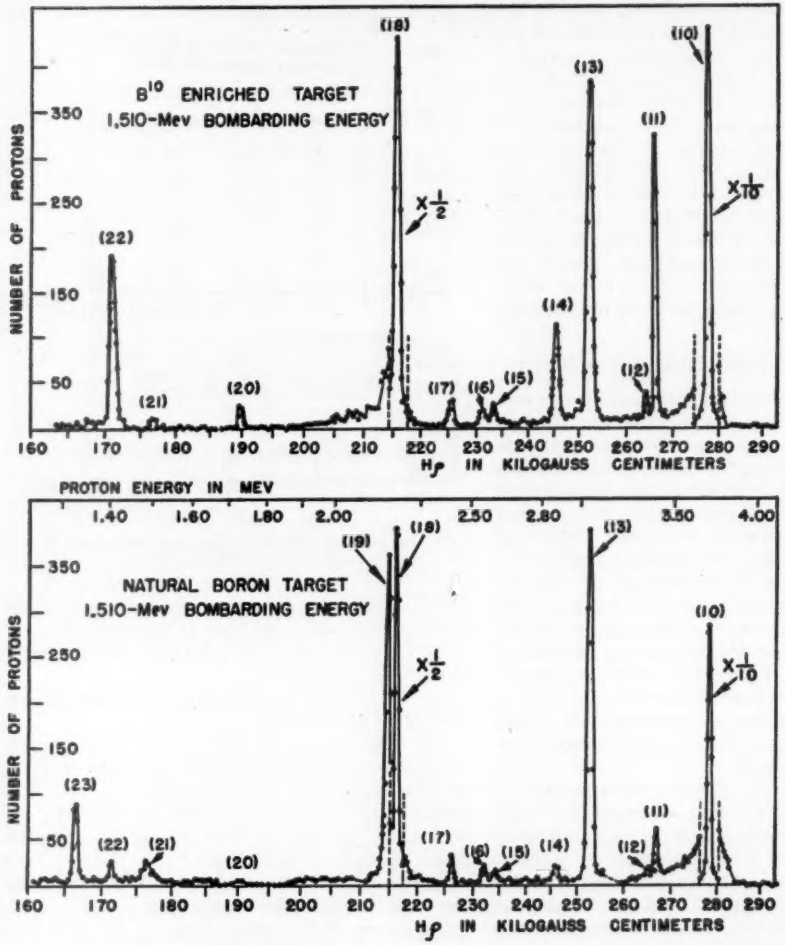

FIG. 2. Proton groups observed from targets of enriched B^{10} and natural boron bombarded by 1.51-Mev deuterons.

of the proton tracks. The result of these effects was an appreciable background between proton peaks. It was found to be impracticable to use this method for the detection of proton groups with energies of less than 1.3 Mev.

In order to investigate proton groups with energies less than 1.3 Mev, targets were prepared by the evaporation of natural boron and enriched B^{10} onto a thin film of Formvar. This type of target with a thin backing has the advantage that the full length of the proton tracks can be recorded and is particularly useful for the investigation of proton groups which occur at Hr values lower than any of the deuteron groups elastically scattered from the nuclei of the target and backing. Such a target was not used for the original survey, because it was considered doubtful that it would withstand beam bombardment. However, it was found that boron targets evaporated onto Formvar films did survive for long exposures to the beam. Proton groups in the energy range from 0.45 to 1.45 Mev were investigated with these targets. It was also possible to observe the deuteron groups elastically scattered from the B^{10} and B^{11} nuclei in these targets.

In this work, a number of alpha-particle groups was also observed. Studies of these groups are reported in separate publications.

III. RESULTS

With the incident deuteron energy held constant at 1.51 Mev, a survey was made of the proton groups of energies 1.3 to 10.5 Mev emitted from targets of enriched B^{10} and natural boron on platinum backings.

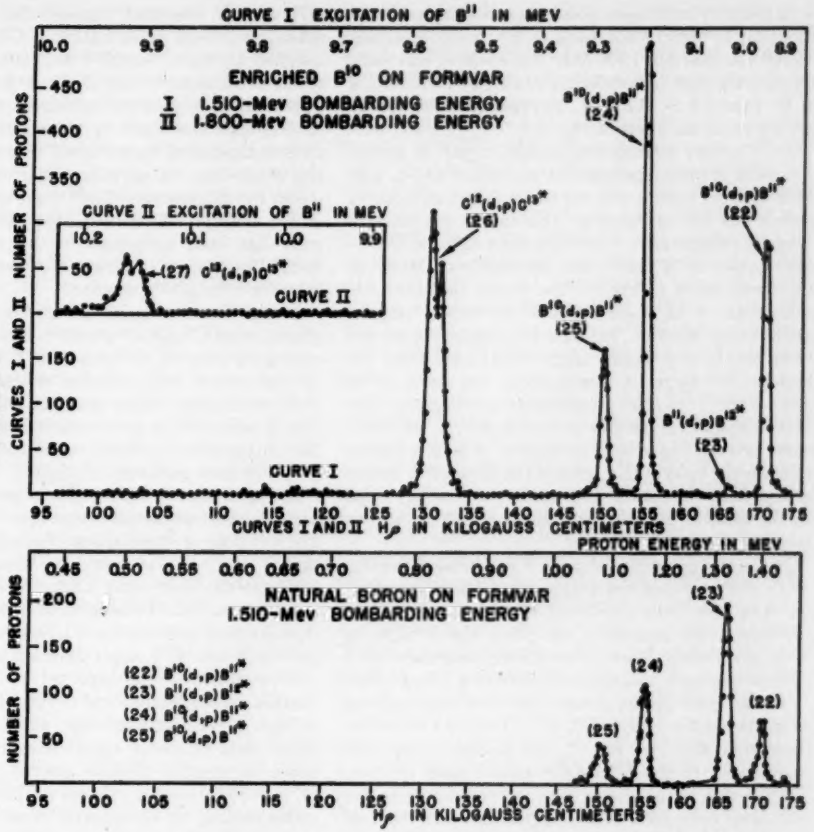

FIG. 3. Proton groups observed from targets of enriched B^{10} and natural boron on Formvar backings bombarded by 1.51- and 1.80-Mev deuterons.

The proton groups with energies 1.3 to 3.0 Mev were observed by means of nuclear-track plates covered with thin aluminum foils. The results of this survey are shown in Figs. 1 and 2. The yields of the proton groups from the two boron targets have been normalized to the same beam bombardment and area counted on the nuclear-track plates.

The enriched B^{10} and natural boron targets were prepared by similar evaporations, and it was expected that the two targets would be about equal in thickness. To verify this, the yield of the $B^{10}(d,p)B^{11}$ ground-state proton group was measured from each target and was found to be a factor of 4.5 greater from the enriched B^{10} target (96 percent B^{10}) than from the natural boron target (19 percent B^{10}). The ratio of the isotopic abundances of B^{10} in the two targets was 5.0. Hence, the thicknesses of the two boron targets were found to be equal within 10 percent. The target thickness was estimated from the half-widths of the lower energy proton groups (20), (22), and (23) and was found to be approximately 10 kev for the $B^{10}(d,p)B^{11}$ ground-state reaction.

The survey was extended to lower proton energies using an enriched B^{10} target evaporated onto a thin film of Formvar. This survey covered a range of proton energies from 1.45 to 0.45 Mev at a bombarding energy of 1.51 Mev, which corresponded to a region of excitation of B^{11} from 8.9 to 10.0 Mev. The results are shown in the upper curve of Fig. 3. From the half-widths of the observed proton peaks, the target thickness was calculated to be 9 kev for the $B^{10}(d,p)B^{11}$ ground-state group. It can be seen that the background between peaks has been reduced considerably compared with the survey of Fig. 2. This improvement was made possible by the use of thin Formvar backing, which eliminated the necessity of using aluminum foils to observe the proton groups. The survey of Fig. 3 was not extended below a proton energy of 0.45 Mev, because at this energy the proton track length became so short that it was difficult to distinguish the proton tracks from the continuous background on the nuclear-track plates.

In order to investigate possible proton groups corresponding to higher excitations of B^{11}, the bombarding energy was raised to 1.800 Mev, and a survey was made for proton groups corresponding to a region of excitation of B^{11} from 9.9 to 10.2 Mev. The results of this survey are shown in the insert of Fig. 3.

At 1.51-Mev bombarding energy, a partial survey was made of proton groups with energies of 1.05 to 1.45 Mev emitted from a natural boron target evaporated onto a thin film of Formvar. This survey was made to verify the assignment of proton groups (24) and (25) to the reaction $B^{10}(d,p)B^{11*}$, and the results are shown in the lower curve of Fig. 3. The target thickness was calculated to be about 14 kev for the $B^{10}(d,p)B^{11}$ ground-state reaction. In order to compare the results from the natural boron target with those from the enriched B^{10} target, a measurement was made of the yield of the $B^{10}(d,p)B^{11}$ ground-state proton group from both targets. The proton groups shown in the lower curve of Fig. 3 have been normalized in such a way as to make the ratio of the yields of the $B^{10}(d,p)B^{11}$ proton groups from the natural and enriched B^{10} targets equal to the ratio of isotopic abundances of B^{10} in the two targets.

In the surveys shown in Figs. 1–3, a total of twenty-seven proton groups was distinguished. Of these groups, fourteen have been attributed to various target contaminants; the remainder, to either the $B^{10}(d,p)$ or $B^{11}(d,p)$ reactions. The evidence for the assignment of all of these groups is outlined in the following paragraphs.

The fourteen proton groups that have been assigned to contaminants of C^{12}, C^{13}, N^{14}, O^{16}, and Si^{28} will be considered first. In Fig. 2, the intense group (10) corresponds to the $C^{12}(d,p)C^{13}$ ground-state reaction. The Q-value of this group from the boron targets was calculated to be 2.712 Mev, in agreement with the most recent Q-value of 2.716 ± 0.005 Mev for the $C^{12}(d,p)C^{13}$ reaction.[19] The yield of this group was a factor of about 1.5 greater from the enriched B^{10} target, indicating the presence of slightly more carbon contamination on this target. The high intensity of this group (a factor of 10 greater than any other observed group) was possibly due to the fact that the boron targets were evaporated from a carbon crucible. However, it has been found that carbon occurs as a surface contamination on all targets and usually increases with beam bombardment.

In Fig. 3, the proton groups (26) and (27), observed from the enriched B^{10} target on Formvar, had measured Q-values of -0.366 and -0.969 ± 0.010 Mev when assigned to the reaction $C^{12}(d,p)C^{13*}$. Both of these groups are double, evidently arising from a layer of carbon on the surface of the target and from the carbon in the thin Formvar backings. The Q-value of group (26) agreed with the published value[16] of -0.370 ± 0.003 Mev for the proton group corresponding to the 3.10-Mev level in C^{13}.

In the previous investigation of the $C^{12}(d,p)C^{13*}$ reaction made in this Laboratory,[16] the proton group (27) was not observed, because that survey did not extend to so high an excitation of C^{13}. If this group is assigned to the $C^{12}(d,p)C^{13*}$ reaction, it would correspond to an excited state of C^{13} at 3.686 ± 0.011 Mev. This result is in excellent agreement with the value of 3.677 ± 0.005 Mev found by Malm and Buechner[20] from an investigation of the $N^{15}(d,\alpha)C^{13*}$ reaction. However, this result does not agree with the value of 3.91 Mev report by Heydenburg *et al.*[21] from their investigation of the $C^{12}(d,p)C^{13*}$ reaction. This discrepancy apparently has been accounted for by recent results of Rotblat[22] who finds two levels in C^{13} at 3.7 and 3.9 Mev from the $C^{12}(d,p)C^{13*}$ reaction.

In Fig. 1, proton group (4) has been assigned to the ground-state $C^{13}(d,p)C^{14}$ reaction. This group evidently originated from the 1.1 percent of C^{13} occurring in the natural carbon contamination of the targets, and its yield was slightly higher from the enriched B^{10} target. The Q-value of this group was calculated to be 5.940 Mev, in agreement with the value[23] of 5.948 ± 0.014 Mev measured from enriched C^{13} targets.

In Fig. 2, the two intense proton groups (13) and (18) occur from all targets and have been attributed to O^{16}. The Q-values of these groups from the boron targets agreed within 5 kev with the measured values of 1.917 ± 0.005 Mev[19] and 1.049 ± 0.007 Mev[19] for the $O^{16}(d,p)$ reaction. These groups had about equal intensities from both the boron targets, in agreement with the assignment to a target contaminant.

In addition to the expected proton groups from contaminants of carbon and oxygen, the surveys shown in Figs. 1 to 3 indicated eight additional weak groups which were of about equal intensity from both the boron targets. Six of these groups, (2), (8), (9), (16), (17), and (21) were attributed to the $N^{14}(d,p)$ reaction, corresponding to the ground state and five excited states of N^{15}. The assignment of these groups was aided by the recent accurate measurements[24] of the $N^{14}(d,p)$ proton groups. The Q-values of all the six groups from the boron targets agreed within 8 kev with the results found by Malm and Buechner. The ratio of the yield of these groups from the enriched B^{10} and natural boron targets varied from 0.5 to 1.5, indicating approximately equal amounts of nitrogen contamination on both targets. In the lower curve of Fig. 1, the N^{15} doublet, peaks (8) and (9), is clearly resolved and corresponds to a level separation of 26 ± 2 kev, in agreement with the value previously reported.[24] It has been found that $N^{14}(d,p)$ and $N^{14}(d,\alpha)$ groups are observed from all targets, and their possible presence must always be considered, particularly for investigations of reactions with low yields.

[20] R. Malm and W. W. Buechner, Phys. Rev. **81**, 519 (1951).
[21] Heydenburg, Inglis, Whitehead, and Hafner, Phys. Rev. **75**, 1147 (1949).
[22] R. G. Thomas, private communication.
[23] Sperduto, Holland, Van Patter, and Buechner, Phys. Rev. **80**, 769 (1950).
[24] R. Malm and W. W. Buechner, Phys. Rev. **80**, 771 (1950).

The remaining two weak proton groups (5) and (15) have been assigned to the $Si^{28}(d,p)Si^{29*}$ reaction. The presence of these groups was unexpected, and at first it was thought that they originated from a small amount of silicon (less than 2 percent) in the boron material. However, recent investigations of other reactions have indicated silicon contamination on all targets. It is now considered probable that the silicon contamination appears during the evaporation of the targets, evidently from the silicon oil used in the vacuum system of the evaporator.

The proton groups (5) and (15), if assigned to the $Si^{28}(d,p)Si^{29*}$ reaction, have measured Q-values of 4.95 ± 0.02 and 1.31 ± 0.02 Mev. These values are in agreement with the recent values of 4.97 ± 0.01 Mev and 1.31 ± 0.01 Mev measured from SiO_2 targets.[25]

In their investigations of the $N^{14}(d,p)$ reaction at 1.420-Mev bombarding energy, Malm and Buechner[24] also found $Si^{28}(d,p)$ groups, the most intense of which were those corresponding to peaks (5) and (15). It is certain that other $Si^{28}(d,p)$ groups were present in the surveys covered in the three figures; however, they were evidently not sufficiently intense to be detected.

The proton group (15) was a factor of 1.7 more intense from the enriched B^{10} target; and, since it occurred in a region corresponding to the Q-value of 1.35 ± 0.07 Mev reported by Bateson[5] for the $B^{10}(d,p)B^{11*}$ reaction, it was considered necessary to eliminate the possibility that part of this peak might be a $B^{10}(d,p)B^{11*}$ group. In order to do this, the bombarding energy was lowered from 1.508 to 1.197 Mev, and the change in proton energy of group (15) was measured as 281.5 ± 2.5 kev. The expected shift in energy of a $Si^{28}(d,p)$ group would be 279.6 ± 2.7 kev, while a $B^{10}(d,p)$ group would shift 232.8 ± 2.3 kev. Since no proton group appeared at a position expected for a $B^{10}(d,p)$ group at 1.197-Mev bombarding energy, it was concluded that the assignment of group (15) to the $Si^{28}(d,p)Si^{29*}$ reaction was correct.

It might appear that the presence of as many as fourteen groups due to contaminants could jeopardize the investigation of the $B^{10}(d,p)$ groups. However, the high resolution of the magnetic spectrograph enabled the proton groups to be well separated and permitted accurate comparison of the Q-values of these groups to known Q-values. In addition, the ratio of the yield of these groups from the enriched B^{10} and natural boron targets was never greater than a factor of 1.7, while all the groups assigned to the $B^{10}(d,p)$ reaction were 3 to 6 times more intense from the natural boron target.

The remaining thirteen proton groups found in the surveys were attributed either to the $B^{10}(d,p)$ or the $B^{11}(d,p)$ reactions. Of these, groups (19) and (23) were much more intense from the natural boron target and were assigned to the isotope B^{11}, as has been previously reported.[26] The remaining eleven proton groups (1), (3), (6), (7), (11), (12), (14), (20), (22), (24), and (25) were approximately a factor of 5 more intense from the enriched B^{10} target (96 percent B^{10}) than from the natural boron target (19 percent B^{10}) and were attributed to the B^{10} isotope.

In Fig. 1, the intense proton group (1) had a measured Q-value of 9.235 ± 0.011 Mev, in agreement with the value of 9.24 Mev predicted from masses[27] for the $B^{10}(d,p)B^{11}$ ground-state reaction and with previous measured values[2,4,5] of 9.14 ± 0.10; 9.22 ± 0.2; and 9.18 ± 0.05 Mev. An additional confirmation of this assignment was obtained from the measurement of the shift in energy of this proton group when the bombarding energy was changed from 1.380 to 1.506 Mev. The observed energy change was 91 ± 2 kev, compared to the value of 95 ± 5 kev expected for a $B^{10}(d,p)$ proton group.

The positions of groups (3) and (6) agreed with $B^{10}(d,p)B^{11*}$ proton groups already reported by previous workers. Both of these groups were a factor of 4 to 5 more intense from the enriched B^{10} target. These groups corresponded to excited states at 2.138 ± 0.014 and 4.459 ± 0.014 Mev, in agreement with the values of 2.15 ± 0.06 and 4.48 ± 0.06 Mev reported by Bateson.[5]

The next proton group (7) shown in Fig. 1 was 5 times more intense from the enriched B^{10} target and had a measured Q-value of 4.201 ± 0.008 Mev, corresponding to an excited state of B^{11} at 5.034 ± 0.014 Mev. This measurement confirms the result of Bateson,[5] who found a previously unreported proton group corresponding to a level in B^{11} at 5.03 ± 0.06 Mev.

In Fig. 2, two proton peaks (11) and (12) were assigned to the $B^{10}(d,p)B^{11*}$ reaction and correspond to a doublet in B^{11} with a level spacing of 50.0 ± 0.6 kev. Both of these groups were 3 to 4 times more intense from the enriched B^{10} target; however, this ratio was subject to uncertainty in the case of peak (12), because of its weak intensity compared to the background in this region. The more intense group (11) corresponds to an excited state in B^{11} at 6.758 ± 0.013 Mev, which has already been reported[4,5] at 6.83 ± 0.2 and 6.92 ± 0.08 Mev. The proton group (12) was a factor of 10 less intense than group (11) at 1.51-Mev bombarding energy and has not been previously reported. This doublet would not have been resolved by the range measurements used by earlier investigators. Because of theoretical interest in such doublets,[28] it was important to be certain of the identification of proton group (12). Further investigations were made of this group which resulted in the unambiguous assignment of group (12) to the reaction $B^{10}(d,p)B^{11*}$. These results will be described in detail in a succeeding section.

The next proton group, (14), assigned to the $B^{10}(d,p)B^{11*}$ reaction, was a factor of 5 more intense from the enriched B^{10} target. This group has a Q-value

[25] Endt, Van Patter and Buechner, Phys. Rev. **81**, 317 (1951).
[26] Buechner, Van Patter, Strait, and Sperduto, Phys. Rev. **79**, 262 (1950).
[27] W. F. Hornyak and T. Lauritsen, Revs. Modern Phys. **20**, 191 (1948).
[28] D.R. Inglis, Phys. Rev. **78**, 616 (1950).

TABLE I. Energy levels in B^{11}.

Peak number	Reaction	Ratio of yields[a]	Approx[b] $d\sigma$	Q-value (Mev)	Level in B^{11} (Mev)
(1)	$B^{10}(d,p)B^{11}$	4.9	2.	9.235±0.011	0
(3)	$B^{10}(d,p)B^{11*}$	3.7	0.4	7.097±0.009	2.138±0.014
(6)	$B^{10}(d,p)B^{11*}$	5.2	1.2	4.776±0.008	4.459±0.014
(7)	$B^{10}(d,p)B^{11*}$	4.9	1.0	4.201±0.008	5.034±0.014
(11)	$B^{10}(d,p)B^{11*}$	3.8	2.	2.477±0.007	6.758±0.013
(12)	$B^{10}(d,p)B^{11*}$	3.	0.2	2.427±0.007	6.808±0.013
(14)	$B^{10}(d,p)B^{11*}$	5.0	1.2	1.937±0.006	7.298±0.012
(20)	$B^{10}(d,p)B^{11*}$	6.	0.3	0.667±0.005	8.568±0.012
(22)	$B^{10}(d,p)B^{11*}$	3.6	5.	0.309±0.005	8.926±0.012
(24)	$B^{10}(d,p)B^{11*}$	4.4	8.	0.045±0.005	9.190±0.012
(25)	$B^{10}(d,p)B^{11*}$	4.1	4.	−0.041±0.005	9.276±0.012
	$B^{10}(d,d)B^{10}$	—	35.	0	
	$B^{10}(p,p)B^{10}$		57.	0	

[a] Ratio of yields from enriched B^{10} and natural boron targets.
[b] Approximate differential cross section at 90° in millibarns per atom per steradian.

of 1.937±0.006 Mev, corresponding to an excited state at 7.298±0.012 Mev. Bateson[5] has reported a $B^{10}(d,p)$ group with a Q-value of 1.36±0.07, which is considerably lower than our value. However, Bateson was not able to resolve his $B^{10}(d,p)$ proton group from the $O^{16}(d,p)O^{17*}$ proton group with a Q-value of 1.049. In view of the otherwise excellent correspondence between the present results and those of Bateson, it appears possible that group (14) was not observed in his experiments. At the 3.8-Mev bombarding energy used in his work, the energy of the proton group from $O^{16}(d,p)O^{17*}$ ($Q=1.049$ Mev) would be such as to give a Q-value of 1.42 Mev if mistakenly assigned to $B^{10}(d,p)B^{11}$. It appears possible that the presence of such a $O^{16}(d,p)O^{17*}$ group in Bateson's range measurements could account for the above discrepancy in Q-values.

In Fig. 2, the weak proton group (20) was assigned to the reaction $B^{10}(d,p)B^{11*}$. The yield of this group was about 6 times greater from the enriched B^{10} target; however, this ratio was not very accurate because of its very low intensity from the natural boron target. The Q-value of this group was measured as 0.667±0.005 Mev, in good agreement with a $B^{10}(d,p)$ Q-value of 0.70±0.10 Mev first reported by Bateson.[5] Additional evidence for the assignment of this group was obtained from a measurement of the change of proton energy when the bombarding energy was changed from 1.507 to 1.800 Mev. The observed shift in proton energy was 218.1±1.2 kev. The expected shift is 219.1±2.1 kev for a $B^{10}(d,p)$ group, whereas the expected shifts for $Be^{9}(d,p)$ and $B^{11}(d,p)$ groups are 212±2 and 225±2 kev, respectively. This result shows that this proton group can be assigned only to a target of mass 10.

In Figs. 2 and 3, there is indicated an intense proton group (22) assigned to $B^{10}(d,p)B^{11*}$. This group was found to be 3 to 6 times more intense from enriched B^{10} targets as compared with natural boron targets. The Q-value of this group was calculated to be 0.309±0.005 Mev, corresponding to an excited state of B^{11} at 8.926 ±0.012 Mev. Prior to these experiments, this $B^{10}(d,p)$ group had not been reported. However, since the first report[29] of these results, Bateson[30] has found a $B^{10}(d,p)$ group with a Q-value of 0.32±0.10 Mev, in excellent agreement with the present work.

The remaining two intense proton groups (24) and (25), shown in Fig. 3, were a factor of 4 to 5 more intense from the enriched B^{10} target on Formvar. In addition, these proton groups were single, as compared with the two $C^{12}(d,p)$ groups (26) and (27) which were double, indicating that proton groups (24) and (25) originated from the target material. In view of this evidence, these groups were assigned to the $B^{10}(d,p)$ reaction, with Q-values of 0.045±0.005 and −0.041 ±0.005 Mev, corresponding to excited states in B^{11} at 9.190±0.012 and 9.276±0.012 Mev. These two $B^{10}(d,p)$ groups have not been reported previously and would not have been observed by Bateson, as they would have been obscured by elastically scattered deuterons.

The results of the surveys indicated the presence of eleven $B^{10}(d,p)$ groups, corresponding to the ground state of B^{11}, and ten excited states, five of which have not been previously reported. These results are summarized in Table I. The position of the levels found agreed with earlier results, while the proton groups corresponding to the new B^{11} levels would not have been observed by earlier workers (except for the group with a Q-value of 0.309 Mev which has been confirmed by Bateson). In the region of excitation of B^{11} from 0 to 6.31 Mev, no additional groups were found with an intensity greater than 0.1 the intensity of the ground-state group. Only 3 percent of the total region was obscured for groups of this intensity by the intense $C^{12}(d,p)$ and $O^{16}(d,p)$ contaminant groups, since none of the groups had a half-width greater than 30 kev. It is considered improbable that any $B^{10}(d,p)$ groups that had an intensity greater than 0.05 the intensity of the ground-state group were missed in the surveys.

As was previously mentioned, the doublet of proton groups (11) and (12) was investigated further in order to make certain of the assignment of the weak group (12) to the $B^{10}(d,p)B^{11*}$ reaction. The doublet was observed at bombarding energies of 1.510, 1.649, and 1.811 Mev, and the results are shown in Fig. 4. From these curves, it was first possible to check the assignment of the intense member of the doublet (11) from the observed change in proton energy of 225.1±2 kev for a change in bombarding energy of 301±3 kev. The expected change in proton energy for a $B^{10}(d,p)$ group would be 225.5±2.1 kev, indicating that the assignment of group (11) to the $B^{10}(d,p)B^{11*}$ reaction was correct.

Once the assignment of group (11) to the $B^{10}(d,p)B^{11*}$ reaction was established, measurement of the spacing between groups (11) and (12) at the three bombarding energies provided a sensitive method of establishing the

[29] W. W. Buechner and D. M. Van Patter, Phys. Rev. 79, 240 (1950).
[30] W. O. Bateson, private communication. Also, Phys. Rev. 80 982 (1950).

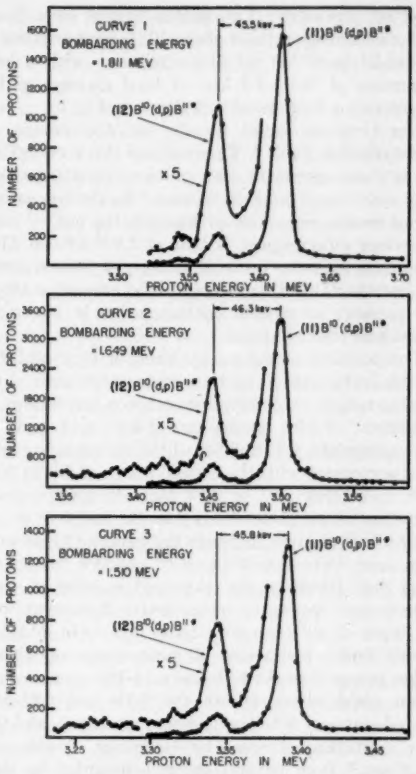

FIG. 4. $B^{10}(d,p)B^{11*}$ doublet observed at bombarding energies of 1.51, 1.65, and 1.81 Mev.

target mass responsible for the less intense group (12). The difference in proton energy of groups (11) and (12) was measured as 45.8±2.0; 46.3±2.0; and 45.5±2.0 kev at bombarding energies of 1.509, 1.649, and 1.811 Mev. These results indicated that the spacing remained constant within 0.5±2.0 kev. If the target mass responsible for group (12) had been one unit different than that responsible for group (11), then the spacing between groups would have changed by 6 to 7 kev when the bombarding energy was changed from 1.509 to 1.811 Mev. It is concluded that both groups (11) and (12) could be assigned unambiguously to the $B^{10}(d,p)B^{11*}$ reaction. In the curves of Fig. 4, there is some evidence for proton groups with intensities less than 0.01 the intensity of group (11); however, none of these groups remained at a constant spacing from the doublet members at the different energies. Hence, there was no evidence for additional structure to the doublet with an intensity greater than 0.09 the intensity of the weaker member (12). At the three bombarding energies, group (11) was a factor of 10, 10, and 8 more intense than group (12). The separation of these two proton groups corresponds to a level separation in B^{11} of 50.0±2.0 kev.

The three $B^{10}(d,p)$ proton groups (22), (24), and (25) correspond to excited states in B^{11} at 8.93, 9.19, and 9.28 Mev, all of which are above the threshold at 8.64 Mev for alpha-emission to Li^7. The half-widths of these proton groups in the surveys shown in Figs. 2 and 3 were about 15 kev, which were attributed chiefly to the effects of target thickness. This assumption was shown to be correct when proton groups (22) and (23) were measured from a much thinner target of natural boron on Formvar, as shown in the upper curve of Fig. 5. In addition, the deuteron groups scattered elastically from the B^{10}, B^{11}, and C^{12} nuclei in the target backing were observed, as shown in the lower curve of Fig. 5. From this curve, the target thickness was estimated to be 2.8 kev for the $B^{10}(d,d)B^{10}$ process, and 2.0 kev for the $B^{10}(d,p)B^{11*}$ proton group (22). The observed half-width of the $B^{10}(d,p)$ group (22) was 5.9 kev. After subtraction of the spreads due to target thickness and instrumental factors, an upper limit of 3.7 kev was found for the natural width of proton group (22). This result indicates an upper limit of 4 kev for the 8.93-Mev excited state of B^{11}.

From the surveys shown in Figs. 1, 2, and 3, it was possible to estimate the relative intensities of the

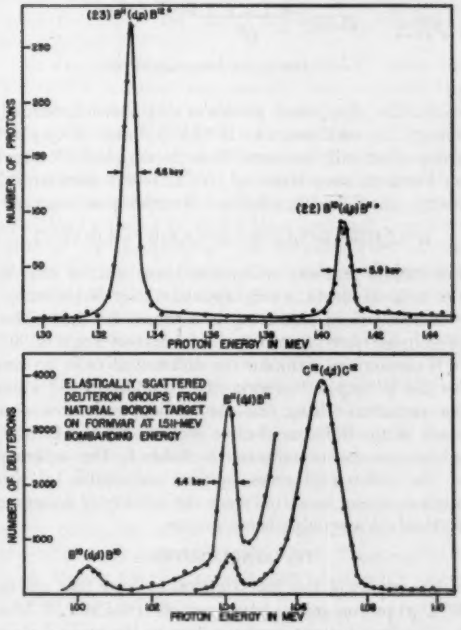

FIG. 5. Proton and deuteron groups observed from a thin target of natural boron on a thin Formvar backing bombarded by 1.51-Mev deuterons.

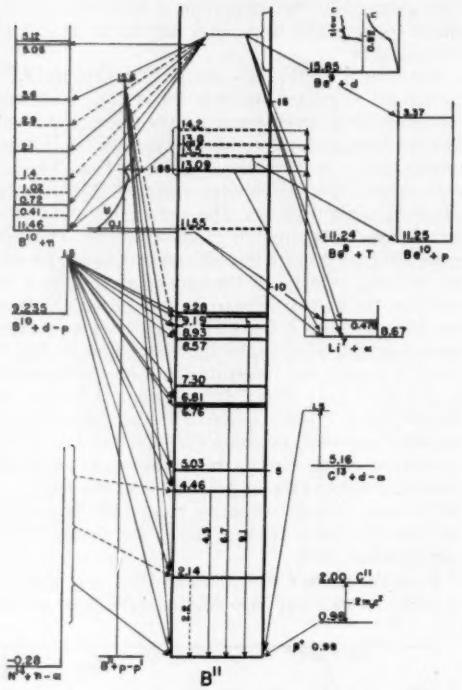

FIG. 6. Energy-level diagram for B^{11}.

various $B^{10}(d,p)$ proton groups at 1.51-Mev bombarding energy. In addition, the $B^{10}(d,d)B^{10}$ and $B^{10}(p,p)B^{10}$ groups elastically scattered from the enriched B^{10} target on Formvar were observed. At 1.51-Mev bombarding energy, the following relative intensities were observed:

$$B^{10}(d,p)B^{11}:B^{10}(d,d)B^{10}:B^{10}(p,p)B^{10}=1.0:17:27.$$

For various reasons, we consider these relative intensities to be accurate to only approximately 50 percent.

If Rutherford scattering is assumed for 1.510-Mev protons scattered from B^{10} at a laboratory angle of 90°, it is possible to estimate the differential cross section for the $B^{10}(p,p)B^{10}$ process as 57 millibarns per atom per steradian. Using this assumption, estimates were made of the differential cross sections for the $B^{10}(d,p)$ proton groups, as indicated in Table I. The accuracy of the differential cross sections calculated by this method cannot be stated since the validity of assuming Rutherford scattering is not known.

IV. CONCLUSIONS

The results of this investigation indicate that eleven $B^{10}(d,p)$ proton groups have been observed at 1.51-Mev bombarding energy, corresponding to the ground state and ten excited states of B^{11}. Five of these excited states at 6.81, 7.30, 8.93, 9.19, and 9.28 Mev have not been reported previously. Two proton groups were found with an intensity ratio of about 10:1, corresponding to a doublet in B^{11} at 6.8-Mev excitation with a level separation of 50.0±2.0 kev. A level diagram of B^{11}, incorporating these results, is shown in Fig. 6.

The Q-values found for the $B^{10}(d,p)$ groups are summarized in Table I. The results of this investigation are in good agreement with previous results, particularly with recent work of Bateson.[5] In the comparison of our results with those of Bateson, the only Q-value in serious disagreement is that of 1.937±0.006 Mev, compared with the value of 1.36±0.07 Mev reported by Bateson. This discrepancy can be accounted for by the presence of oxygen contamination in the range measurements of Bateson.

The positions of the energy levels of B^{11} established by this investigation can be used to assign some of the gamma-radiations observed from boron bombarded by deuterons.[12–14] The gamma-rays of 4.52, 6.74, and 9.11 Mev, assigned by Terrell[14] to $(B^{10}+d)$, appear to be in good agreement with the excited states of B^{11} at 4.46, 6.76, and either 8.93 or 9.19 Mev. It appears probable that these gamma-rays can be assigned to the $B^{10}(d,p)B^{11*}$ reaction, although the possibility that some may arise from the $B^{10}(d,n)C^{11*}$ reaction cannot be ruled out. However, the measured energies of these gamma-rays appear to be in better agreement with the levels of B^{11} than with those of C^{11}. In addition, Terrell found indications of gamma-rays of slightly higher energy than the 4.41- and 6.74-Mev gamma-rays, which could correspond to the 5.03- and 6.81-Mev excited states of B^{11}. The gamma-rays of 6.9- and 9.1-Mev excitation, observed by Gaerttner, Fowler, and Lauritsen,[12] from natural boron bombarded by deuterons were previously ascribed to the $B^{11}(d,n)C^{12*}$ reaction. In view of the above results, it appears that these gamma-rays should be assigned to the $B^{10}(d,p)B^{11*}$ or $B^{10}(d,n)C^{11*}$ reactions. This assignment is in agreement with the observation of Hudspeth and Swann[31] that most of the radiations greater than 2 Mev from $(B+d)$ are from B^{10} rather than from B^{11}. The gamma-ray of 4.4 Mev, observed by Gaerttner *et al.*,[12] from $(B+d)$ can be assigned to both $B^{10}(d,p)$ and $B^{11}(d,n)$ inasmuch as Terrell finds a gamma-ray of 4.5±0.1 Mev from $(B^{11}+d)$ in addition to the gamma-ray of 4.46 Mev from $(B^{10}+d)$. The gamma-ray of 2.2 Mev, observed by Gaerttner *et al.*, can be assigned to both the $B^{10}(d,p)$ and $B^{10}(d,n)$ reactions.

The positions of the levels of B^{11} established in this investigation are shown in the level diagram of Fig. 6. There was no indication of additional $B^{10}(d,p)$ proton groups with an intensity greater than 0.1 the intensity of the ground-state $B^{10}(d,p)B^{11}$ group in a region of excitation of B^{11} from 0 to 10.22 Mev. The intense $C^{12}(d,p)$ and $O^{16}(d,p)$ groups obscured 3 percent of the total region for groups of intensity less than 0.1 the

[31] E. L. Hudspeth and C. P. Swann, Phys. Rev. **76**, 1150 (1949).

intensity of the ground-state $B^{10}(d,p)$ group. The levels of B^{11} found by this investigation appear to be in four groups, with a wide separation of about 2.3 Mev between groups.

For increasing excitation of B^{11}, the number of excited states in each group increases in order from one to four with an over-all spread of about 0.5 to 0.7 Mev for the components of the three higher groups. The fact that no additional levels of B^{11} were found for excitations of 9.3 to 10.2 Mev is in agreement with this pattern.

The next higher level occurs at 11.5-Mev excitation, corresponding to a possible resonance[32] in the $B^{10}(n,\alpha)Li^7$ reaction at a neutron energy of 0.1 Mev. This excited state could correspond to a component of a fifth group of excited states. It would be of interest to examine the yield of the $Li^7(\alpha,\gamma)B^{11}$ reaction starting at low alpha-energies,[33] since resonances would be expected corresponding to the levels of B^{11} at 8.93, 9.19, and 9.28 Mev. An extension of this experiment to higher alpha-energies might establish the position of the next higher excited state of B^{11}.

The background between the $B^{10}(d,p)$ proton groups, corresponding to excited states of B^{11} at 8.93, 9.19, and 9.28 Mev, was less than 0.03 the intensity of these proton groups and could be accounted for by a small amount of alpha-contamination on the nuclear-track plates. In addition, an upper limit of 4 kev was found for the half-width of the 8.93-Mev level of B^{11}, although no proton groups were found corresponding to a region of excitation of 950 kev above the 9.28-Mev level. Therefore, there was no indication of any overlapping of levels or of uniform spacing of levels up to an excitation of B^{11} of 10.2 Mev.

It is of interest to compare the excited states of mirror nuclei of odd mass number. The mirror nuclei, Li^7 and Be^7, each have one low-lying state at 478 and 431 kev, respectively, the positions of which appear to correspond. The mirror nuclei, C^{13} and N^{13}, have excited states at 3.10, 3.68, and 2.34 and 3.52 Mev, respectively. Although the positions of these states do not agree experimentally,[34] their comparison is complicated by the fact that the two excited states of N^{13} are virtual to proton emission, while those of C^{13} are not. Thomas[35] has taken this fact into account and, by a theoretical analysis, has shown that the levels of C^{13} and N^{13} do, in fact, correspond.

A comparison of the mirror nuclei of B^{11} and C^{11} is

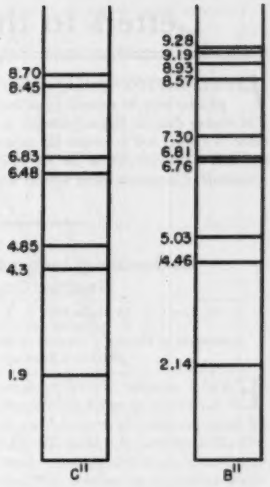

FIG. 7. Comparison of the excited states of C^{11} and B^{11}.

not thus complicated. All excited states of B^{11} below 8.6-Mev excitation are bound, while those up to 11.2 Mev are not virtual to proton or neutron emission. Similarly, excited states of C^{11} below 7.5 Mev are bound, while those below 8.7 Mev are not virtual to proton emission. It is of particular interest to compare the states excited by the mirror reactions of $B^{10}(d,p)B^{11}$ and $B^{10}(d,n)C^{11}$.

An extensive survey of the states of C^{11} from the $B^{10}(d,n)C^{11}$ reaction has recently been reported by Johnson,[36] who finds levels at 1.90, 4.30, 4.85, 6.48, 6.83, 8.45, and 8.70 Mev. A comparison of these C^{11} levels with the levels of B^{11} reported here is shown in Fig. 7, where the striking similarity of the two level schemes can be seen. A doublet in C^{11} of 50 kev, corresponding to that of B^{11} at 6.8 Mev, could not have been resolved by Johnson in his measurements of the $B^{10}(d,n)C^{11}$ neutron groups. The levels of C^{11} are consistently lower by about 0.2 Mev (except in one case where the difference is 470 kev). This could be accounted for by the additional coulomb energy in C^{11}. A discussion of the level schemes of mirror nuclei has been recently presented by Richards.[37] It is concluded that the level schemes of B^{11} and C^{11}, as known at present, correspond up to 9-Mev excitation and that the result provides the best example to date of the agreement of the excited states of two mirror nuclei.

We are glad to acknowledge the generous cooperation of our colleagues at the High Voltage Laboratory. We are particularly indebted to Mr. W. A. Tripp and Mrs. C. A. Bryant for their careful work in counting on the photographic plates.

[32] Goldsmith, Ibsen, and Feld, Revs. Modern Phys. **19**, 259 (1947).

[33] Since this manuscript was prepared for publication, Toppel, Roys, and Bennett, Phys. Rev. **81**, 316 (1951) have reported the observation of three resonances in the thick-target yield curve of the gamma-radiation from Li^7 bombarded by alpha-particles. The positions of these resonances are in excellent agreement with the three levels in B^{11} as determined in the present experiment.

[34] D. M. Van Patter, Phys. Rev. **76**, 1264 (1949).

[35] R. G. Thomas, Phys. Rev. **80**, 136 (1950).

[36] V. R. Johnson, Phys. Rev. **81**, 316(A) (1951).

[37] H. T. Richards, Phys. Rev. **81**, 308 (1951).

Letters to the Editor

PUBLICATION of brief reports of important discoveries in physics may be secured by addressing them to this department. The closing date for this department is five weeks prior to the date of issue. No proof will be sent to the authors. The Board of Editors does not hold itself responsible for the opinions expressed by the correspondents. Communications should not exceed 600 words in length.

Radioactivity Induced in Iridium by Neutron Capture*

J. M. CORK, J. M. LEBLANC, A. E. STODDARD, W. J. CHILDS, C. E. BRANYAN, AND D. W. MARTIN
Department of Physics, University of Michigan, Ann Arbor, Michigan
(Received February 23, 1951)

EARLY studies[1] of iridium showed the presence of two long-lived induced radioactivities of half-lives about 19 hours and 70 days, presumably derived from the two stable isotopes of mass 191 (38.5 percent) and mass 193 (61.5 percent). Further investigations[2] have identified the longer-lived activity, now found to be 78 days, as due to radioactive Ir^{192}, and the 19-hour activity as due to Ir^{194}.

Spectrometric studies showed the presence of many electron lines associated with the 78-day activity, and from an evaluation of the gamma-rays a tentative nuclear level scheme had been proposed. With the increased neutron flux of the Argonne pile, a source of much higher specific activity has now been obtained and found to yield many previously unobserved electron lines. It is evident that certain of the long-lived electron lines have K–L–M differences characteristic of osmium ($Z=76$) and are thus emitted following K-capture in Ir^{192}. The remainder, except for six weak lines, have K–L–M differences of platinum ($Z=78$) and hence are emitted following the competing beta-decay. While the electron energies are in many cases very close to the previously reported values, the many new lines and the present interpretation lead to a considerable change in the nuclear level scheme.

TABLE I. Summary of electron lines.

Electron energy (kev)	Relative intensity	Interpretation	Gamma-energy (kev)	Electron energy (kev)	Relative intensity	Interpretation	Gamma-energy (kev)
49.9	1	$A(\alpha-L)$ 76		229.6	7	K^8 78	307.7
52.6	W	$A(\alpha-L_I)$ 78		237.9	10	K^9 78	316.0
55.0	W	$A(\alpha-L_{III})$ 78		282.0	4	L_I^7 78	295.6
57.5	2	$A(\beta-L)$ 76		284.1	2	L_{III}^7 78	295.6
		and K^4 78	135.6	292.5	1	M^7 78	295.6
60.5	1	$A(\alpha-M)$ 76		294.4	3	L^8 78	308.0
63.4	W	$A(\alpha-M)$ 78		301.0	5	L_I^9 Pb	316.8
68.0	W	$A(\beta-M)$ 76		302.5	5	L_I^9 78	316.1
77.5	W	K^3 76	151.0	304.7	1	L_{III}^9 78	316.2
		or K^3 78	156.0	313.0	3	M^9 78	316.3
97.5	W	K^3 76	169.0	315.4	W	N^9 78	316.1
		or K^4 78	173.0	322.0	W	K^{10} 76	396.0
122.4	2	L_I^1 78	136.0			or K^{10} 78	400.0
124.6	W	L_{III}^1 78	136.1	337.0	1	K^{11} 78	415.1
127.2	2	K^4 76	201.0	360.3	W	K^{12} 76	434.0
131.9	6	K^5 76	205.7			or K^{12} 78	438.0
133.5	W	M^1 78	136.8	380.2	4	K^{13} Pb	467.8
135.5	W	N^1 78	136.1	389.3	4	K^{13} 78	467.4
188.6	W	L^4 76	201.2	402.7	W	L^{11} 78	416.6
193.1	4	L_I^5 76	205.7	410.3	2	K^{14} 76	484.0
195.1	W	L_{III}^5 76	206.0	454.0	3	L^{13} 78	467.6
198.0	W	M^4 76	201.1	464.7	2	M^{13} 78	468.0
200.6	W	N^4 76	201.1	466.8	W	N^{13} 78	467.5
202.9	1	M^5 76	206.0	510.5	1	K^{16} 78	588.6
206.1	W	N^5 76	206.7	525.6	2	K^{16} 78	603.7
207.8	9	K^7 Pb	295.4	533.1	1	K^{17} 78	611.2
209.2	W	K^6 76	283.0	574.5	W	L^{15} 78	588.1
216.8	9	K^7 78	294.9	590.7	W	L^{16} 78	604.3
220.2	7	K^8 Pb	307.8	599.5	W	L^{17} 78	613.1
227.9	10	K^9 Pb	315.5				

Legend: A—Auger; α—K_{α_1} x-ray; β—K_β x-ray; 10—very strong. 1—weak, W—very weak.

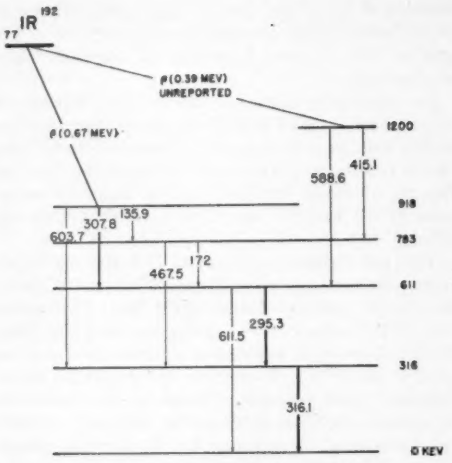

FIG. 1. Proposed nuclear energy levels in $_{78}Pt^{192}$ following β-emission from Ir^{192}.

In all, about 45 electron lines are observed in the energy range from 49 kev to 600 kev, as shown tabulated in column 1, Table I. In addition to the internal conversion electrons, photoelectrons from a lead radiator were also observed. An estimate of the relative intensity of each line is given in column 2. The proposed identifica-

TABLE II. Summary of gamma-rays.

Arbitrary designation	Gamma-energy (kev) $Z=76$	$Z=78$	Arbitrary designation	Gamma-energy (kev) $Z=76$	$Z=78$
1		135.9	10	396 or	400
2	151 or	156	11		415.1
3	169 or	173	12	434 or	438
4	201.1		13		467.4
5	205.7		14	484	
6	283		15		588.6
7		294.9	16		603.7
8		307.7	17		611.2
9		316.1			

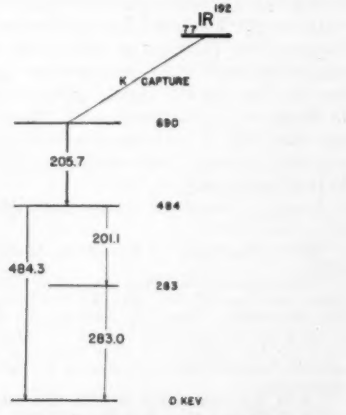

FIG. 2. Proposed nuclear energy levels in $_{76}Os^{192}$ following K-capture in Ir^{192}.

tion of each electron line is presented in column 3 and the resultant gamma-energies in column 4. Arbitrary superscripts are used to denote the gamma-rays increasing in order with the energy. Seven of the low energy electron lines are of Auger origin, as noted in column 3. A summary of the energies of the gamma-rays associated with each process is offered in Table II.

It is now possible to arrange a scheme of 6 levels for the excited platinum 192 nucleus as shown in Fig. 1, which is satisfied remarkably well by 10 of the observed gamma-rays. A proposed level scheme for the osmium 192 nucleus is portrayed in Fig. 2. The K-capture process is also substantiated by the presence of Auger lines characteristic of osmium. Six of the weaker electron lines do not enter in K–L combinations and are assumed to be K lines for either osmium or platinum. A choice is made for the two gamma-rays designated as 6 and 14, since their energies fit satisfactorily in Fig. 2.

The early exposures of the freshly irradiated specimen showed a few electron lines which did not appear on later photographic plates, indicating that they were associated with the 19-hour radioactivity in Ir^{194}. From the electron energies, a single gamma-ray of energy 327.5 kev is indicated for the Pt^{194} nucleus. A similar energy has been known to exist in the K-capture decay of Au^{194}.

* This project was made possible by the joint support of the ONR and AEC.

[1] J. Cork and R. Thornton, Phys. Rev. **51**, 59 (1937); McMillan, Kamen, and Ruben, Phys. Rev. **52**, 375 (1937).

[2] M. Deutsch, Phys. Rev. **64**, 265 (1943); J. Cork, Phys. Rev. **72**, 581 (1947); M. Levy, Phys. Rev. **72**, 352 (1947); R. Hill and W. Meyerhof, Phys. Rev. **73**, 812 (1948).

On Some Recent Calculations on Cascade Shower Theory

H. MESSEL

School of Theoretical Physics, Dublin Institute for Advanced Studies, Dublin, Ireland

(Received March 5, 1951)

THERE have recently appeared a number of works[1–3] on the electron-photon cascade theory. In each case the authors were concerned with the solution of the diffusion equations of the cascade theory of electron showers when the ionization loss term was included. Bhabha and Chakrabarty[4] developed an elegant and simple series solution of the diffusion equations and showed that the first two terms of the series gave results which were quite satisfactory for all practical purposes. It was also pointed out by Jánossy and Messel[5] that the solutions given by B.C. could be quickly and easily evaluated. Their solutions have also the added advantages:

(a) the first-order correction for the effects of ionization loss is expressed as a shift of the energy spectrum by an amount of the order of the critical energy,

(b) the series may be used either to evaluate the number of electrons $[N(E, t)]$ or photons $[\gamma(E, t)]$ above a specified energy E (and this is the physically important quantity), or to evaluate the total number of electrons $[N(0, t)]$ or photons $[\gamma(0, t)]$ at various depths t.

In the meantime Snyder[2] developed solutions of the cascade equations using a different approach. He showed that the solution of the cascade equations could be reduced to the solution of certain difference equations. The method is fairly long and is far from yielding solutions which lend themselves to easy computation. In fact, the solutions given by Snyder are of practical value only for computing the total number of electrons or photons for $E=0$, at various depths. In order to obtain results for any other value of E, the evaluation of a triple complex integral is required. This in itself is a serious drawback. Snyder also pointed out that his solutions yielded values for $N(0, t)$ at the cascade maximum which were about 35 percent higher than those obtained by B.C., who used the first two terms of their series. Hence, it was concluded that the results of B.C. were inaccurate. At the same time Snyder pointed out that for a shower initiated by an electron of energy E_0

$$\int_0^t N(0, t)dt = E_0/\beta, \tag{1}$$

where β is the ionization loss. He then mentioned that the first two terms of the B.C. solution contribute only 70 to 85 percent of E_0/β and hence these authors did not use a sufficient number of terms of their series. B.C. had given in their paper a very satisfactory explanation for the above, which appears to have been overlooked by both Snyder and Bernstein.[3] We quote from reference 1.

"From the physical point of view, however, Eq. (1) must be taken with caution, especially in substances of high atomic number where the critical energy is low. It is not true that all the energy of a cascade is dissipated by the collision loss of cascade electrons alone. A good deal of energy is lost in the form of quanta of energy less than $2mc^2$ which are incapable of further pair creation. Thus the complete series for $N(0, t)$ must give too many cascade electrons of low energy at large thicknesses, and the first two or three terms of the series may well give a truer picture of the physical process in substances of high atomic number."

Bernstein lately has taken Snyder's solution and applied to it a correction by means of a perturbation method. He used a more refined approximation to the Bethe-Heitler cross sections than had hitherto been used. The method employed by Bernstein is straightforward but naturally even more tedious than that of Snyder—and again of the same limited applicability. From Bernstein's results there evolves an interesting feature. He finds that Snyder's results give a value for $N(0, t)$ which is much too high at the cascade maximum. We have plotted in Figs. 1 and 2 the results

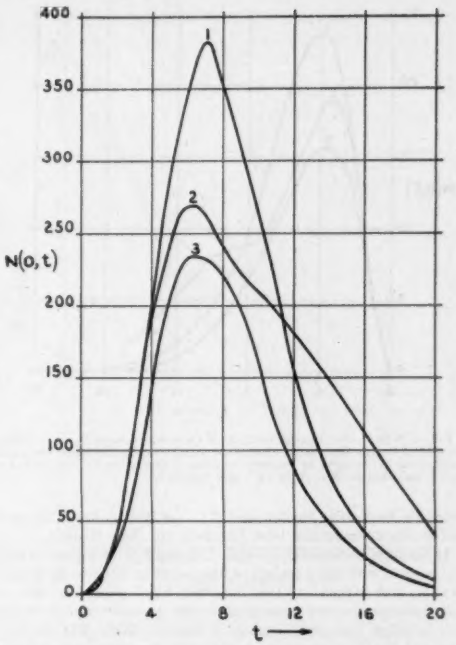

FIG. 1. $N(0, t)$, the average number of electrons induced by an incident electron of energy E_0, plotted against the depth t in cascade units. We have marked the curve given by Snyder's solution 1, that given by Bernstein for lead 2, and that by B.C. 3. In each case $\ln E_0/\beta = 8$.

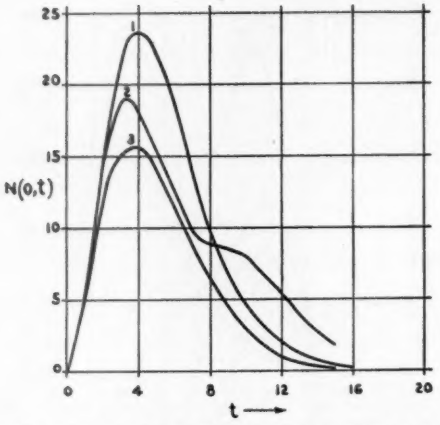

FIG. 2. $N(0,t)$, the average number of electrons induced by an incident electron of energy E_0, plotted against the depth t in cascade units. We have marked the curve given by Snyder's solution 1, that given by Bernstein for lead 2, and that by B.C. 3. In each case $\ln E_0/\beta=5$.

found by Bernstein, Snyder, and B.C. for $N(0,t)$ for $\ln E_0/\beta=8$ and 5. The curves taken from Bernstein are those for lead.

It becomes immediately evident that the B.C. solutions (which can be used with ease) are not as inaccurate as hitherto made out. We also wish to point out that Bernstein, like Snyder, has failed to take into account the facts given in the quotation above. When this is taken into consideration, it appears likely that the pronounced "tail" of the curves given by Bernstein, beyond the cascade maximum, will be decreased to a value close to that given by B.C. It thus now appears that the series solution of B.C. can be used with confidence.

I am indebted to Professor H. J. Bhabha for valuable discussion of the above.

[1] H. J. Bhabha and S. K. Chakrabarty, Phys. Rev. **74**, 1352 (1948).
[2] H. S. Snyder, Phys. Rev. **76**, 1563 (1949).
[3] I. B. Bernstein, Phys. Rev. **80**, 995 (1950).
[4] Reference 1, henceforth shortened to B.C.
[5] L. Jánossy and H. Messel, Proc. Phys. Soc. (London) **A64**, 1 (1951).

Photonuclear Stars in Emulsions*

RICHARD D. MILLER
Radiation Laboratory, Department of Physics, University of California, Berkeley, California
(Received January 23, 1951)

ILFORD C2 emulsions, 200 microns thick, were exposed in the collimated x-ray beam from the Berkeley 322-Mev synchrotron. Exposures were made at synchrotron energies of 322, 242, and 161 Mev, and the monitor ionization chamber was calibrated relative to pair production cross sections at each of the three energies by the method described by Blocker, Kenney, and Panofsky.[1]

The complete area covered on each plate by the beam (½-in. circle) has been scanned for stars with two and more prongs. Because of the impossibility of distinguishing between a two-prong star and a scatter in the track of a single particle in a large number of cases, two-prong stars were classified as either possible or probable. Because of the arbitrariness and the difficulty of setting sufficiently precise criteria for this distinction, the two-prong data are regarded as essentially qualitative. All events within 5.5 microns of either surface of the emulsion after processing were discarded, and the minimum prong range counted was 3 microns.

TABLE I. Relative yields of stars.

No. prongs \ X-ray energy	322 Mev	242 Mev	161 Mev
possible 2	73±7	81±8	34±5
probable 2	91±8	70±7	36±5
3	137±6	109±9	39±5
4	88±5	57±6	29±4
5	37±3	14±3	8±2
6	13±2	3.6±1.6	0.6±0.6
7	3±1		
8	0.9±0.5		
≥3	280±9	184±12	77±9
≥5	54±4	18±4	9±2

The yields of stars with various numbers of prongs are shown in Table I. The 322-Mev yields are normalized to an emulsion thickness before processing of 200 microns, and to an exposure of 10^8 "equivalent quanta," or 322×10^8-Mev total energy in the complete bremsstrahlung spectrum. The yields at the other energies are normalized to the same thickness and to exposures that contain the same number of quanta per Mev interval at 32 Mev. The uncertainties indicated in the table are the standard deviations due to counting statistics only. The prong spectrum of the 322-Mev yield is similar to that reported by Kikuchi;[2] the difference in the minimum prong length counted probably accounts for the discrepancies.

Using the nominal partial densities of emulsion elements given by the manufacturer, and assuming that star production cross sections are proportional to mass number, the 322-Mev yield of 3 and more prong stars gives a cross section for silver, integrated over the bremsstrahlung spectrum, of 6.5×10^{-27} cm² per "equivalent quantum." This figure is reduced to 5.6×10^{-27} if the cross section is assumed proportional to $A^{\frac{1}{2}}$.

The energy distribution of the quanta responsible for the differences in yields from the different energy exposures is shown in Fig. 1. Also shown, at one-tenth the scale for the difference

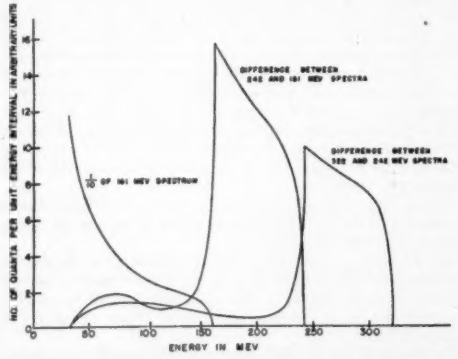

FIG. 1. Differences between spectral distributions of bremsstrahlung from electrons of 322, 242, and 161 Mev, when the spectra have been normalized to contain the same number of quanta per unit energy interval at 32 Mev. The 161-Mev bremsstrahlung spectrum is shown at one-tenth the ordinate scale for the difference spectra.

spectra, is the spectrum of 161-Mev bremsstrahlung. Because most of the difference quanta are in the energy range between the two upper limits of the bremsstrahlung spectra, it is possible to calculate a cross section averaged over this energy interval. Estimating that that part of the yield due to the low energy tail in the 161- to 242-Mev difference spectrum is 10 percent of the 161-Mev yield, and making similar corrections for the yield from the tail in the 242- to 322-Mev difference spectrum, the average cross

TABLE II. Meson photoproduction cross sections of silver, integrated over 322-Mev bremsstrahlung, in units of 10^{-27} cm² per equivalent quantum.

π^+	0.7
π^-	1.1
π^0	4.0
sum	5.8

sections of silver for the production of three or more prong stars are

$$\int_{242}^{322}\sigma(E)N_{322}(E)dE\Big/\int_{242}^{322}N_{322}(E)dE=(8\pm1)\times10^{-27}\text{ cm}^2,$$

$$\int_{161}^{242}\sigma(E)N_{242}(E)dE\Big/\int_{161}^{242}N_{242}(E)dE=(7\pm1)\times10^{-27}\text{ cm}^2,$$

where $N_{322}(E)$ is the number of quanta per Mev in 322-Mev bremsstrahlung, etc.

The integrated meson production cross sections of silver listed in Table II have been calculated from the measured carbon cross sections,[3,4] assuming the A^{-1} dependence of the yield per nucleon found for π^+ meson production.[5] It seems likely that some of the stars observed are associated with meson production. The star yield is probably too large to be accounted for by this process alone, however, since only about $\frac{1}{3}$ of the low energy π^- mesons found which were produced in the emulsion had as many as 3 other prongs associated with their production.

Another possible mechanism for star production by high energy photons is suggested by the π^+ meson relative yield data of Mozley.[5] The implication of the A^{-1} dependence of the yield per nucleon is that only the surface nucleons are effective in producing mesons. Since none of the known photonuclear reactions have cross sections comparable to nuclear area at these energies, this effect is probably not due to nuclear opacity to photons. If, however, this effect is due to nuclear opacity to mesons, one might expect that there should be stars produced by meson production and reabsorption in the same nucleus, with cross sections several times that for meson production.

I wish to thank Professor E. M. McMillan for suggesting this problem and for his helpful discussions, Mrs. W. R. Gaffey for assistance in scanning the plates, Dr. R. S. Christian for calculations of the bremsstrahlung spectra, Mr. R. Kenney and Mr. W. Blocker for the use of equipment and assistance in calibration of the ionization chamber, and Mr. G. C. McFarland and the synchrotron crew for assistance in making the exposures.

* This work was performed under the auspices of the AEC.
[1] Blocker, Kenney, and Panofsky, Phys. Rev. **79**, 419 (1950).
[2] S. Kikuchi, Phys. Rev. **80**, 492 (1950).
[3] Peterson, Gilbert, and White, to be published.
[4] Steinberger, Panofsky, and Steller, Phys. Rev. **78**, 802 (1950).
[5] R. F. Mozley, Phys. Rev. **80**, 493 (1950).

An Interpretation of Nuclear Cross Sections for High Energy Neutrons*

ROBERT JASTROW
Radiation Laboratory, University of California, Berkeley, California
(Received March 2, 1951)

RECENTLY, Dejuren and Moyer have extended the measurements of neutron cross sections to fill in the energy region up to 280 Mev[1] and find two interesting features, illustrated by their data for aluminum in Fig. 1:

1. The cross sections are constant at high energies, above 150 Mev.

2. The drop to these high energy levels occurs very sharply at intermediate energies.

The constancy of the cross sections at high energies is in contrast to the continued decrease with increasing energy which would be expected if the interaction between the neutron and the particles in the nucleus were weak. It suggests the presence of a singularity in the n-n and n-p interactions, presumably the same singularity

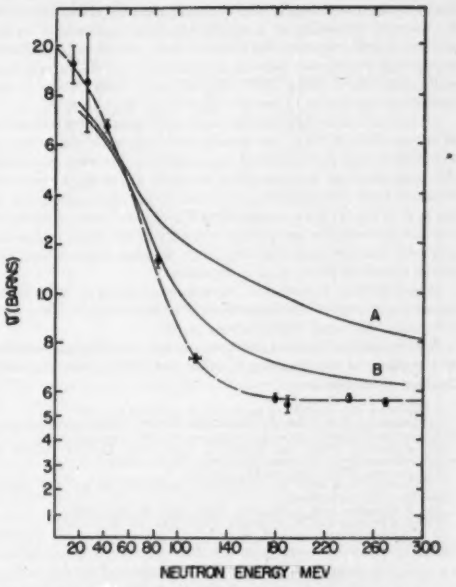

FIG. 1. Cross section of Al for high energy neutrons. The dashed curve is fitted to the experimental points of Dejuren and Moyer. Curves A and B are calculated from the optical model with and without, respectively, a central repulsion in the nucleon-nucleon interaction.

for which evidence is provided in the p-p interaction by the nearly energy-independent p-p cross section at correspondingly high energies.[2,3]

In order to test this interpretation of the energy-independent cross sections we have carried out calculations based on an optical model in which nuclear matter is described by an index of refraction and an absorption coefficient.[4] The cross section is then composed of an incoherent contribution depending only on the absorption coefficient and a coherent contribution depending on the index of refraction. The absorption coefficient is given by

$$K=\tfrac{1}{2}\rho(\sigma_{nn}+\sigma_{np}), \tag{1}$$

where ρ is the nucleon density, and σ_{nn} and σ_{np} are the total n-n and n-p cross sections. For the index of refraction, n, we have (assuming equal numbers of protons and neutrons)

$$n=1+(\pi\rho/k^2)\{f_{nn}(0)+f_{np}(0)\}, \tag{2}$$

where k is the neutron wave number and $f_{nn}(0)$ and $f_{np}(0)$ are the forward scattering amplitudes, all in the laboratory system.

If we assume that n-n and p-p forces are identical, we may insert the measured n-p and p-p cross sections in (1). The forward scattering amplitudes occurring in (2), however, are not unambiguously determined by experiment, even under the assumption of identical n-n and p-p forces, but must be calculated from the particular nucleon-nucleon interaction assumed. We have substituted in (2) scattering amplitudes derived from potentials fitted to n-p and p-p scattering by Christian and Hart[5] and by Christian and Noyes[6] and obtained the neutron cross section given by curve A of Fig. 1. This result does not reproduce the rapid fall in Dejuren's measurements at intermediate energies.

Since the absorption coefficient and the incoherent cross section are fixed by experiment, the origin of the discrepancy must lie in the coherent contribution and, therefore, in the values used for the scattering amplitudes in (2). One sees that a description of the neutron cross sections requires a nucleon-nucleon potential such

that $f(0)$ decreases rapidly with increasing energy above 100 Mev. A potential consisting of a strong repulsion surrounded by an attractive well possesses this characteristic, owing to the circumstance that interference between the repulsion and the surrounding well causes the S phase shift, and hence its contribution to the scattering amplitude, to become negative at high energies.

An interaction of this type, containing a singlet central repulsion of radius 0.60×10^{-13} cm, has already been suggested[3] in connection with high energy p-p scattering measurements. We have calculated the neutron cross sections using forward scattering amplitudes obtained from this potential, with results for aluminum given in curve B of Fig. 1. We conclude from Fig. 1 that if one is restricted to a simple model for the nucleon interaction, the sharp drop in the observed neutron cross section at high energies requires that this model contain a strong central repulsion.

It is important to note that this argument sheds no light on the tensor component of the interaction, since tensor forces of any kind will make only small contributions to $f(0)$.

A more detailed account is in preparation, including a discussion of the effect of the presence of other nucleons on the two-body nucleon cross sections.

* This work was carried out under the auspices of the AEC.
† J. Dejuren and B. J. Moyer, Phys. Rev. **81**, 919 (1951); also University of California Radiation Laboratory Report No. 887 (unpublished).
[3] Chamberlain, Segrè, and Wiegand, Phys. Rev. **81**, 284 (1951); O. Chamberlain and C. Wiegand, Phys. Rev. **79**, 81 (1950).
[4] R. Jastrow, Phys. Rev. **81**, 165 (1951).
[5] R. Serber, Phys. Rev. **72**, 1114 (1947); Fernbach, Serber, and Taylor, Phys. Rev. **75**, 1352 (1949).
[6] R. S. Christian and E. W. Hart, Phys. Rev. **77**, 441 (1950).
[6] R. S. Christian and H. P. Noyes, Phys. Rev. **79**, 85 (1950).

The $T+T$ Reactions

K. W. Allen,* E. Almqvist, J. T. Dewan, T. P. Pepper, and J. H. Sanders†
Atomic Energy Project, National Research Council of Canada, Chalk River, Ontario, Canada
(Received February 26, 1951)

THE interaction of tritons with tritons may lead to three nuclear reactions:

$$T+T\rightarrow He^4+2n+\ 11.3\ \text{Mev} \quad (1)$$

$$\rightarrow He^5+n\ +\sim 10.5\ \text{Mev} \quad (2)$$

$$\downarrow$$

$$He^4+n\ +\sim 0.8\ \text{Mev}^1$$

$$\rightarrow He^4+n^2. \quad (3)$$

The first reaction is a 3-body disintegration resulting in continuous energy distributions for the α-particles and neutrons. The second reaction is a two-stage process recognizable by a neutron group at $\sim$8.8 Mev. Reaction (3) postulates the formation of a di-neutron which, if its lifetime were sufficiently great, would be accompanied by an α-particle group of small energy spread. To distinguish these reactions measurements have been made of the energies of the disintegration products emitted at 90° to the triton beam.

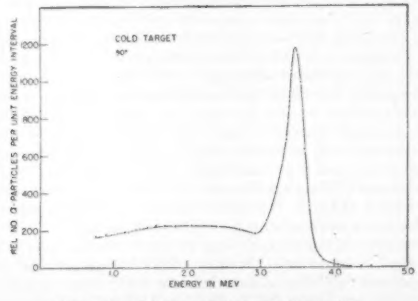

FIG. 1. The $T+T$ α-particle energy distribution. Triton energy = 220 kev.

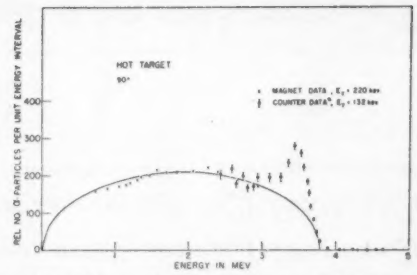

FIG. 2. The $T+T$ α-particle energy distribution. The solid line is the theoretical distribution based on classical statistical mechanics. Probable errors are indicated. E_T is triton energy.

The momentum distribution of the α-particles was investigated using a 90° analyzing magnet[3] with a resolution of 3 percent in momentum. The α-particles were detected by their scintillations in a ZnS screen. Sufficient intensity was obtained by bombarding a brass block with a 200 μa unresolved beam containing 10 percent tritons, some of which were absorbed on the brass and acted as a target. The bombarding energy was 220 kev. The relative number of α-particles per unit energy interval in the range 0.7–4.5 Mev is shown in Fig. 1. Scattered tritons from the beam prevented measurements below 0.7 Mev. The intensity of low energy α-particles has been corrected for the effect of charge exchange in the target.[3] Superimposed on the continuous distribution from reaction (1) is a group of α-particles at 3.5 Mev from the $T+D$ reaction. The high intensity of this group can be explained by the large yield of this reaction at low energies[4] and the natural deuterium content in the beam and in traces of oil on the target.

As the $T+D$ peak might obscure a small group of α-particles associated with the formation of an unstable di-neutron, it was necessary to reduce the deuterium contamination. Best results were obtained by bombarding a metal strip, maintained at a dull red heat, with a resolved beam of mass 5 ions [$H\ H\ T^+$]. Heating the target prevented deposition of oil vapor. An extended investigation of the upper portion of the α-particle distribution was made under these conditions with a proportional counter and thirty-channel pulse analyzer.[5] The complete energy distribution is shown in Fig. 2.

The α-particle distribution shows no group corresponding to the formation of a di-neutron, unless such a group coincides in energy with that of the $T+D$ α-particles. The absence of an α-particle group at an energy greater than 3.8 Mev, the energy corresponding to a di-neutron of zero binding energy, leads to the conclusion that a bound state of the di-neutron, if it exists at all, is formed in fewer than 1 percent of the disintegrations. If the di-neutron exists in a virtual state with a mass exceeding that of two neutrons by an amount equivalent to an energy E, an α-particle group with energy $3.8-E/3$ Mev will be observed whose width will depend on the lifetime of the state. For $E\leq0.6$ Mev an upper limit of 1 percent of the disintegrations may be placed on the existence of an α-particle group of width $\sim$0.2 Mev corresponding to a di-neutron of lifetime $\sim3\times10^{-21}$ sec.

The neutron energy distribution shown in Fig. 3 was obtained from measurements of proton recoils in Ilford C2 100μ-emulsions placed at 90° to the triton beam. A light target assembly was used to reduce the neutron scattering. Since no correction has been made for the small effect of scattering, the distribution may be distorted so as to increase the apparent number of low energy neutrons. Recoil protons from monoenergetic 14-Mev $T+D$ neutrons were observed, but have not been included in Fig. 3. There is some evidence for a peak at $\sim$8.8 Mev corresponding to

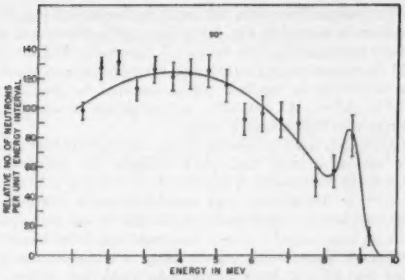

FIG. 3. The $T+T$ neutron energy distribution. Triton energy = 220 kev. Probable errors are indicated.

the formation of He^5 in its unstable ground state. Owing to its short lifetime, this nucleus disintegrates while in motion. This results in an energy spread of its disintegration products; the neutron energy lies between 0.05 and 1.93 Mev, the associated α-particle energy between 0.6 and 2.5 Mev. These particles are not resolved from the 3-body distribution from reaction (1).

The neutron measurements at 90° indicate that either the yield of reaction (2) is small or the neutron and the He^5 are emitted at angles near 0° or 180° to the beam. In the latter case only a few of the breakup α-particles can be observed at 90° owing to the large momentum of the He^5 nucleus. Thus, in either case, the observed α-particle energy distribution is due largely to the 3-body disintegration. Within the present experimental error, the α-particle energy distribution indicates the partition of energy among the products of the 3-body disintegration to be in fair accord with classical phase space considerations,[6] although there is some slight evidence for an angular correlation favoring emission of both neutrons in the same hemisphere.

In conclusion we should like to express our thanks to Dr. R. F. Taschek and his colleagues for valuable discussion of the Los Alamos experiments on the $T+T$ reactions.[7]

* Now at Liverpool University, Liverpool, England.
† Now at the Clarendon Laboratory, Oxford, England.
[1] Williams, Shepherd, and Haxby, Phys. Rev. **51**, 888 (1937).
[2] W. E. Burcham and J. Freeman, Phil. Mag. **40**, 807 (1949).
[3] G. H. Briggs, Proc. Roy. Soc. (London) **A114**, 341 (1927).
[4] D. L. Allan and M. J. Poole, Nature **164**, 102 (1949).
[5] Moody, Howell, Battell, and Taplin, Chalk River Report CREL-464 (1950) (unpublished).
[6] T. D. Newton, as yet unpublished.
[7] Los Alamos Scientific Laboratory, Phys. Rev. **79**, 238(A) (1950).

Solidification of He^3

D. W. OSBORNE, B. M. ABRAHAM, AND B. WEINSTOCK
Argonne National Laboratory, Chicago, Illinois
(Received March 2, 1951)

WE have recently succeeded in solidifying He^3 and have determined a portion of the melting curve by the blocked capillary technique.[1] The melting pressure was found to change from 40.5 atmos at 1.02°K to 56.6 atmos at 1.51°K.

A schematic diagram of the apparatus is shown in Fig. 1. In order to perform the experiment with the amount of gas available (190 cc STP) it was necessary to keep the volume of the system small. This was accomplished by filling the Bourdon gauges (B and G) with mercury and by using 0.1-mm i.d. stainless steel tubing for the U-tube (D) in the helium cryostat (E)[2] and 0.5-mm i.d. tubing for the connections outside the cryostat. The other U-tubes (C and F) were immersed in liquid nitrogen to prevent mercury from plugging the smaller tubing in the cryostat. The apparatus was evacuated and filled through the high pressure valves (A and J). The gas in the reservoir (H) was compressed

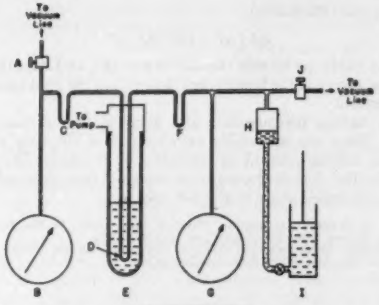

FIG. 1. Solidification apparatus (schematic).

with mercury displaced by means of the hydraulic system (I). The Bourdon gauges, which had 1-lb/in.[2] graduations and a range of 0 to 1000 lb/in.[2], were calibrated with a pressure balance while filled with mercury.

As the pressure in the system was slowly increased, at a constant cryostat temperature, the two gauges gave the same reading until the solidification pressure was reached, and then gauge (G) continued to rise while gauge (B) remained constant. Upon lowering the pressure the gauge readings again became equal at the solidification pressure. A single measurement was made with He^4, and the solidification pressure was found to be 25.2±0.1 atmos at 1.09°K, in satisfactory agreement with the more accurate value of 25.10 atmos found by Swenson.[3] The data for He^3 are plotted in Fig. 2. The equation of the curve in this figure is

$$P=27.0+13.0T^2 \text{ atmos (1.02 to 1.51°K)}, \qquad (1)$$

and it represents the He^3 melting pressure in the range of the measurements with a mean deviation of 0.1 atmos.

With the aid of Eq. (1) an upper limit can be calculated for the volume change on melting, ΔV, by substituting the entropy of the liquid in equilibrium with the vapor[3] for the entropy of melting, ΔS, in the relation

$$dP/dT=\Delta S/\Delta V. \qquad (2)$$

It is assumed that the thermal coefficient of expansion of liquid He^3 is positive, and hence that the entropy of the liquid decreases when the liquid is compressed from the vapor pressure to the melting pressure. The result is $\Delta V<1.2$ cc/mole at 1°K. This is smaller than the volume change of 2.1 cc/mole for He^4 at this temperature[3] but is reasonable because of the higher melting pressure of He^3.

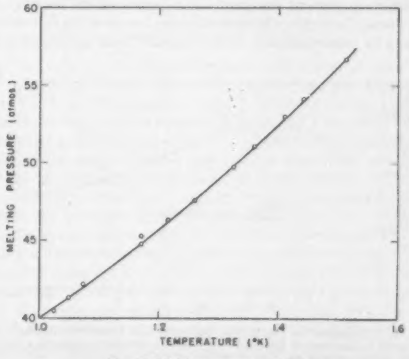

FIG. 2. Melting pressure of He^3.

Also, from the relation

$$\Delta U/\Delta V = T dP/dT - P \tag{3}$$

and Eq. (1) it can be seen that ΔU is zero at 1.44°K and that the internal energy of the liquid is less than that of the solid below this temperature.

The melting pressure data also point to another interesting result. Since any reasonable extrapolation of the data gives a positive melting pressure at absolute zero, it appears likely that He^3, like He^4, does not have a triple point and that the liquid is the stable condensed phase at absolute zero.

[1] W. H. Keesom, Communs. Physical Lab. Univ. Leiden No. 184b (1926); *Helium* (Elsevier, Amsterdam, 1942), p. 180.
[2] Abraham, Weinstock, and Osborne, Phys. Rev. **80**, 366 (1950).
[3] C. A. Swenson, Phys. Rev. **79**, 626 (1950).

Line Breadths of the Fine Structure of the Microwave Spectrum of Oxygen*

ROY S. ANDERSON,† WILLIAM V. SMITH, AND WALTER GORDY
Department of Physics, Duke University, Durham, North Carolina
(Received March 5, 1951)

IN a previous paper[1] we have reported on preliminary measurements of the widths of three fine structure lines of oxygen. These lines arise from reorientations of the oxygen electron spin vector $S(=1)$ with respect to the rotational angular momentum vector K, which is constant for the microwave transitions observed. It has since been possible to extend the determinations of the line-width parameter to include fourteen lines over the range of significant population.

The apparatus for detection of the lines is essentially that cited earlier.[1] To make the measurements more precise, a lattice of frequency markers of 5.70 megacycles spacing has been superimposed on the recorder trace. This superposition results in an individually calibrated recorder trace for each record made. With the detecting system used, the shape of the recorder tracing of an absorption line represents the second derivative of the line contour. Thus, it is easily demonstrated that the distance between the negative minima of the recorder trace is the full width ($2\Delta\nu$) of the line measured at half intensity.

Measurements on each of the lines have been made for at least three different pressures in the range 0.1 to 10 mm Hg. As in the earlier work, measurements at a constant pressure were made for successively decreasing modulations. Each time the measured widths were extrapolated to obtain the width for zero modulation. Since the modulating fields employed were of the order of the earth's field, it was necessary to orient the absorption cell along the earth's field and apply a dc current of proper direction and magnitude to prevent significant broadening of the lines by the earth's field. Corrections have been made, however, for broadening the lines by inhomogeneity of the magnetic field surrounding the cell. The observed line width parameter $\Delta\nu/c$ expressed in cm^{-1} per atmosphere is plotted in Fig. 1 together with a theoretical curve discussed subsequently. The data are in agreement with the single $K=11$ line reported by Gokhale and Strandberg,[2] and are of the same magnitude as the line widths observed by Beringer and Castle[3] for $\Delta J=0$, $\Delta K=0$, $\Delta M=\pm 1$ transitions occurring in the 3-cm region at high magnetic fields.

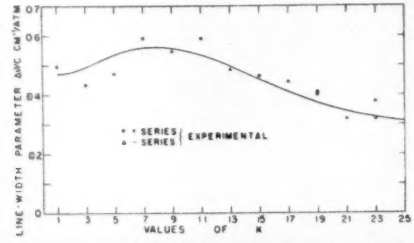

FIG. 1. Comparison of theoretical formula with experimental data. The solid curve is the plot of Eq. (2). The points represent measured values of the line-width parameter. The + series refers to transitions $J=K+1\rightarrow K$ and the − series refers to transitions $J=K-1\rightarrow K$.

Since oxygen lacks an electric dipole moment, interactions between molecules must take place through the mechanism of shorter range forces such as quadrupole ($V\sim 1/r^5$), polarizability ($V\sim 1/r^6$), or still shorter range nonelectric forces. The magnetic dipole interaction is sufficiently small that it can be neglected despite its long range ($V\sim 1/r^3$). Anderson[4] and Mizushima[5] have investigated, respectively, polarizability and quadrupole interactions for $\Delta K=0$. Both interactions yield line widths that decrease fairly rapidly with increasing K, the quadrupole line width decreasing as K^{-4} for high K,[6] while the polarizability line width decreases somewhat more rapidly for low K, and attains a constant plateau for K greater than 15. The still shorter range nonelectric forces may be expected to be essentially independent of K, so that a combination of all three interactions (for $\Delta K=0$) may be expected to yield a line shape of the approximate form,

$$\Delta\nu_{\Delta K=0} = C_1 + C_2 K^{-4}. \tag{1}$$

The observed variation in $\Delta\nu$ with K shows an unmistakable peak about $K=7$. Since $K=7-9$ corresponds to the peak of the thermal population for room temperature, this suggests that resonance interactions contribute an important fraction of the line widths for these states. Both polarizability and quadrupole interactions have an angular $\cos^2\theta$ variation, where θ is the angle between the intermolecular distance r and the asymmetry axis of the molecule. This angular variation gives large matrix elements for $K\rightarrow K+2$ transitions. Since only odd K values are permitted for oxygen (spin $O^{16}=0$; $^3\Sigma^-$ ground state), the population of $(K\pm 2)$ states near the thermal maximum is particularly high with 28 percent of all molecules in $K=7$ or $K=11$ states. These facts suggest that the total line width should be of the form

$$\Delta\nu_{\text{tot}} = C_1 + C_2 K^{-4} + C_3[f(K-2)+F(K+2)], \tag{2}$$

where $f(K)$ is the fractional population of the Kth rotational state, and the resonance interaction has been assumed independent of K to a first approximation. Figure 1 is a plot of Eq. (2) for $C_1=0.027$, $C_2=0.012$, and $C_3=0.090$ cm^{-1} per atmosphere. The fit is seen to be satisfactory. The best fit of the data yields a fairly low value of C_3, which, moreover, includes part of the polarizability interaction along with the quadrupole interactions. Mizushima's expression for the quadrupole interaction alone is

$$\Delta\nu \text{ cm}^{-1}/\text{atmos} = 2.24\times 10^{18} Q K^{-4}, \tag{3}$$

where Q is defined (as in Smith and Howard[7]) as the average Q of the rotating oxygen molecule (=Margenau's Θ/e).[8] Arbitrarily assigning 3/4 of C_2 to a quadrupole interaction gives a value of $Q=0.04\times 10^{-16}$ cm^2 for oxygen. This value is in agreement with the upper limit of $Q\leqq 0.09\times 10^{-16}$ cm^2 deduced from the broadening of ammonia by oxygen.[7]

We wish to thank Professor Mizushima for sending us a prepublication copy of his paper. We have also benefited from correspondence with Dr. P. W. Anderson.

* Research supported and sponsored by the Geophysical Research Directorate of the Air Force Cambridge Research Laboratories. It is published for technical information only and does not represent recommendations or conclusions of the sponsoring agency.
† The material in this paper is a part of the author's thesis submitted in partial fulfillment of the requirements for the degree of Doctor of Philosophy at Duke University.
[1] Burkhalter, Anderson, Smith, and Gordy, Phys. Rev. **79**, 651 (1950).
[2] B. V. Gokhale and M. W. G. Strandberg, Phys. Rev. **82**, 327 (1951).
[3] R. Beringer and J. G. Castle, Jr., Phys. Rev. **81**, 82 (1951).
[4] P. W. Anderson, Harvard Ph.D. thesis (1949).
[5] M. Mizushima, privately communicated.
[6] Small differences between the $J=K+1\rightarrow K$ and $J=K-1\rightarrow K$ interactions have been neglected, since the observed difference is within the experimental scatter of the data.
[7] W. V. Smith and R. Howard, Phys. Rev. **79**, 132 (1949).
[8] H. Margenau, Revs. Modern Phys. **11**, 1 (1939).

Cosmic-Ray Nucleon-Nucleon Collisions in Photographic Emulsions

E. Pickup and L. Voyvodic
Division of Physics, National Research Council, Ottawa, Canada
(Received March 2, 1951)

We have so far found four events in Ilford G5 emulsions exposed at about 85,000 feet[1] which show only relativistic or near relativistic singly charged particles with a typical forward shower cone, and none of the usual low energy nuclear disintegration products. It seems plausible to regard these events as being due to multiple production of mesons by primary protons in single nucleon-nucleon collisions.

All four events show an incoming singly charged particle, and Table I gives the number of shower particles (N) and their angular distribution with respect to the direction of the primary. Event B is illustrated in Fig. 1. From multiple scattering measurements the particle shot backwards appears to be a meson with energy ~400 Mev in the laboratory system, corresponding to a fairly high energy emission in the CM system for a nucleon-nucleon collision. Although only a few particle energies can be measured, we are attempting to compare these, the angular distributions and multiplicities, with the theories of multiple meson production.[2] A similar event with 7 emitted particles was shown by Camerini

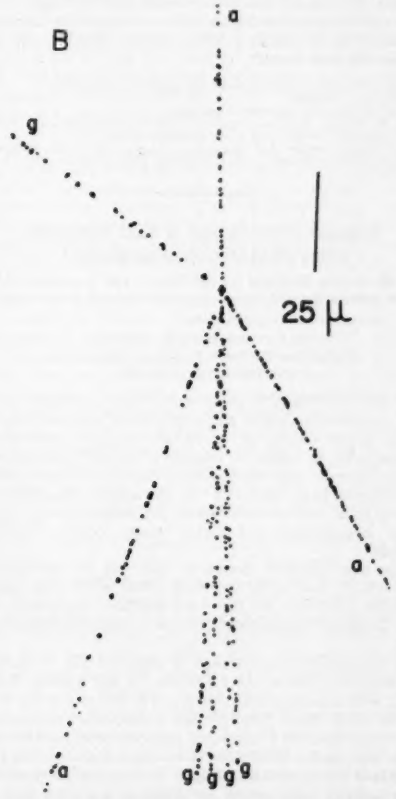

Fig. 1. Projection tracing of event B. The tracks marked a go to the air and those marked g go to the glass backing of the emulsion.

Table I. Angular distribution of shower particles.

Event	N	θ (deg)—Polar angle with primary direction 0–5	5–10	10–20	20–30	30–50	50–90	90–180
A	6	1	2		1	1	1	
B	7	3	1	1		1		1
C	12	6	4			2		
D	13	3	1	5	2		1	1

et al.,[3] and Lord, Fainberg, and Schein[4] have discussed a very high energy event with 17 particles emitted, including 15 in narrow cones.

We might expect single nucleon-nucleon interactions in a collision between an incoming proton and a hydrogen nucleus or a nucleon in a heavier nucleus in the emulsion. Some observations can be made on the basis of conservation of charge. In a purely p-p (or anti p-p) collision this requires that there be an even number of emitted charged particles, whereas for a p-n collision the number would be odd. Thus, it would appear that our events B and D, and the events of Camerini *et al.* and of Lord, Fainberg, and Schein cannot represent collisions of a proton with a hydrogen nucleus, but could be p-n or possibly p-p collisions with the target nucleon in a heavy nucleus. Furthermore, event A can only represent a collision with a hydrogen nucleus or with part of a heavier nucleus in the emulsion. A complete breakup of a carbon nucleus (next lightest to hydrogen in the emulsion) would require at least 7 emitted charged particles in the event, even with the very improbable assumption of no meson production. It seems likely, therefore, that most of the events observed so far represent partial collisions with the heavier nuclei in the emulsion, although A and C could be p-hydrogen collisions.

In addition to A, B, C, and D, we have observed several events with up to 20 shower particles and with only one or two low energy disintegration products. These may represent events of a similar nature to those described above rather than the more frequent high energy disintegrations involving pluro-multiple meson production, and large numbers of low energy products.

[1] The emulsions were exposed through a collaborative program of cosmic-ray investigations by the Bartol Research Foundation and the National Research Council of Canada with the cooperation of the ONR project, "Skyhook."
[2] E. Fermi, Prog. Theor. Phys. **5**, 570 (1950); W. Heisenberg, Nature **164**, 65 (1949); Lewis, Oppenheimer, and Wouthuysen, Phys. Rev. **73**, 127 (1948).
[3] Camerini, Fowler, Lock, and Muirhead, Phil. Mag. **41**, 413 (1950).
[4] Lord, Fainberg, and Schein, Phys. Rev. **80**, 970 (1950).

Meson Production Accompanying Uranium Fission*

H. Bradner and J. K. Bowker
Radiation Laboratory, Department of Physics, University of California, Berkeley, California
(Received February 27, 1951)

The 160 to 200 Mev released in the fission of uranium is sufficient to make the production of a pi-meson energetically possible. The process seems unlikely, however, and was not considered seriously until the event shown in Fig. 1 was discovered[1] in a uranium loaded plate exposed by Al-Salam to cyclotron mesons.[2] Here is definitely a 5-Mev meson (a) coming from a fissioning nucleus and leaving the emulsion just before coming to rest. It is not possible to determine the charge of the meson, since it does not end in the emulsion. Track (b), which stays in the emulsion for 2.4 mm, is a proton of energy 115±20 Mev as determined by grain count and scattering measurements. A nonuniform development of the plate makes it impossible to say with certainty whether this proton was entering or leaving the fission.

If the proton was entering the uranium nucleus, then the meson must have been produced as a result of the fission, since the threshold energy for direct production is greater than 150 Mev. If the proton was leaving the uranium nucleus, the event was

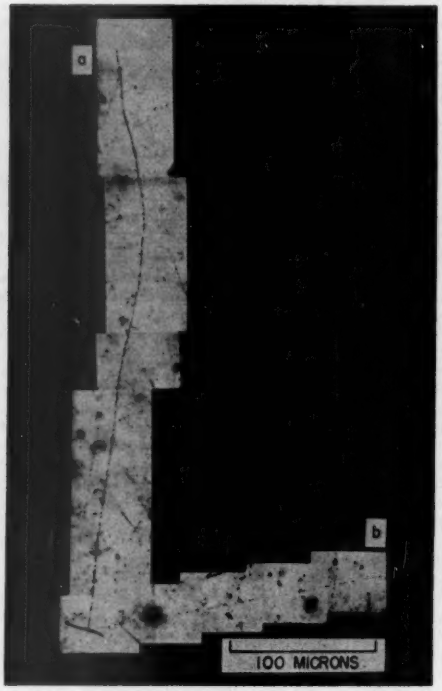

FIG. 1. Photomicrograph of a meson associated with uranium fission.

probably caused by a fast neutron which ejected a meson and a proton from a nucleus which subsequently fissioned.

Following the discovery of this event, two experiments were performed to search for mesons produced in uranium fission.

I. For the first experiment, C2 and G5 emulsions were placed next to a 6-mm×30-mm×0.4-mm sheet of 94 percent U^{235} and exposed for 40 hours to neutrons from a Po-Be source, moderated by 7 in. of paraffin.[3] The source produced 1×10^6 neutrons per sec. Three normal ρ-mesons and two faded ρ-mesons, but no σ-mesons or π-μ-decays, were observed in 340 mm³ of emulsion. One other meson left the emulsion a few microns before coming to rest. All possible meson energies could have been detected in the emulsion.

Assuming a maximum of one π-meson per 340 mm³ (though the ρ-mesons observed were almost certainly due to cosmic-ray background), and assuming a flat distribution in range of the mesons coming from the U^{235} sheet, the probability for producing mesons is less than 8×10^{-7}. A cross section of 500 barns[4] for slow neutron fission of U^{235} was used for this calculation.

II. The second experiment gave a much weaker limit on the cross section for meson production, but achieved high initial nuclear excitation by using the decay energy of π^- mesons. The total energy released is greater than twice the rest mass of a π-meson. A high probability of meson production would be particularly significant in this case, since Al-Salam's measurements[2] indicate that every π^- meson captured in uranium results in fission. A beam of π^- mesons produced in a conventional channel arrangement inside the 184-in. Berkeley cyclotron was stopped in a ½-in. thick slab of ordinary uranium metal. Secondary mesons up to approximately 30 Mev produced in the slab could be observed in a C2 emulsion embedded in absorber beyond the uranium. The total meson flux into the uranium was computed by making runs of the same length, and counting the number of mesons stopping in an emulsion behind a triangular absorber. Background runs were made by replacing the uranium with lead, and by blocking the meson channel with a lead plug. Results are given in Table I.

TABLE I. Experimental results.

Run		Primary	Number of Mesons Secondary (all directions) σ	π-μ	ρ	Secondary (from slab) σ	π-μ	ρ	Area scanned cm²
1	U	4440/cm²	4	3	7	0	0	0	5
2	Pb	4440/cm²	2	5	10	1	0	1	5
3	channel blocked	—	2	2	8	0	0	0	5

It is evident that few if any of the secondary mesons were produced in the uranium, since none came from the direction of the uranium slab, and the number of randomly directed events was statistically no different from the background runs. Assuming that, at most, one of the mesons was produced via fission, it can be estimated that no more than one meson per 172 captured in uranium will produce a secondary meson with energy under 30 Mev.

It can be inferred that the original event observed was a "direct production" of a meson from a fast neutron striking a nucleon in uranium, and was not directly associated with the fission.

The authors wish to thank the other members of the film group, particularly F. M. Smith, J. Willat, and H. Heckman, for their work on this experiment.

* This work was performed under the auspices of the AEC.
[1] Found by J. Willat.
[2] S. G. Al-Salam (private communication).
[3] W. H. Barkas (private communication) had independently made a similar qualitative experiment using unseparated uranium.
[4] B. Feld, in *Science and Engineering of Nuclear Power*. Editor, C. Goodman, Addison-Wesley Press, Cambridge, Massachusetts (1947), Vol. I.

Angular Distribution of Fast Neutrons from Deuteron Bombardment*

K.-H. SUN, D. HARRIS, F. A. PECJAK, AND B. JENNINGS
Westinghouse Research Laboratories, East Pittsburgh, Pennsylvania
AND
A. J. ALLEN AND J. F. NECHAJ
University of Pittsburgh, Pittsburgh, Pennsylvania
(Received February 19, 1951)

MEASUREMENTS[1] have been made previously of the angular distribution and total yield of fast neutrons from various targets bombarded by 15-Mev deuterons and 30-Mev alpha-particles, in which the reaction $S^{32}(n, p)P^{32}$ was used as a threshold detector responding to neutrons over 0.95 Mev. Further measurements have been made on the angular distribution of neutrons from 15-Mev deuterons on Be, using improved experimental arrangements and higher energy neutron threshold detectors.

These new threshold detectors made use of the reactions $Al^{27}(n, \alpha)Na^{24}$, $Ta^{181}(n, 2n)Ta^{180}$, and $F^{19}(n, 2n)F^{18}$ with neutron thresholds at 2.4 Mev, 7.7 Mev,[2] and 10.8 Mev, respectively. The higher thresholds automatically reduce the effective thickness of target.

The experimental arrangement is shown in Fig. 1. Ribbons (¼-in. wide) of 0.0003-in. Al, 0.00025-in. Ta, and 0.006-in. Teflon, $(CF_2)_n$, were simultaneously placed in a holder at a radius of 3.9 cm from the Be target. The activities of these foils were measured after bombardment as a function of angle, and thus yield information on the angular distribution of neutrons of energy above the threshold of the individual detectors. To eliminate the possibility of any activity being caused by deuterons scattered from the cyclotron beam, a lead shield was placed around the target. The effect of this shield and of the cooling water in the Be target on the

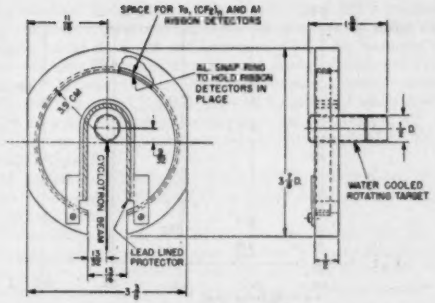
SPACE FOR Ta, $(CF_2)_n$ AND Al RIBBON DETECTORS
AL. SNAP RING TO HOLD RIBBON DETECTORS IN PLACE
3.9 CM
CYCLOTRON BEAM
WATER COOLED ROTATING TARGET
LEAD LINED PROTECTOR

FIG. 1. Arrangement for angular measurement of neutrons above 7.7 and 10.3 Mev from deuteron bombardment.

neutron distribution were found to be negligible. Two ribbons of each detector material were used to prevent recoil contamination. After bombardment, the foils were cut in segments corresponding to angles of from 2° to 5° and counted in an end window Geiger counter. The counts were always recorded with respect to a UX_2 standard. One hour after bombardment, the activities in Ta and Teflon were found to be those expected, namely, Ta^{180} and F^{18} with observed half-lives 8.2 hr and 112 min, respectively. The activities from C in Teflon were short lived and did not interfere. A small amount of the 115-day Ta^{182} activity, about 1 percent of that of Ta^{180} in the forward direction and independent of angular location, was also observed and attributed to the presence of a relatively uniform slow neutron flux. A similar 15.1-hr Na^{24} activity due to Na impurities in Teflon, with an intensity about 0.1 percent of that of F^{18} in the forward direction, was also noticed. These activities were easily corrected for. For $Al^{27}(n, \alpha)Na^{24}$ detector, the activities of the relatively long-lived Na^{24} were measured the day after bombardment when the 15.1-hr half-life was clearly observed.

The results were corrected for decay time and normalized with respect to the activities in the forward directions for Al- and Ta-detectors and to one of the two peak-activities for F-detector. The results are shown in Fig. 2. Figure 2 is a polar plot of all data, including the early ones with S-detector.[1] All angles are in laboratory coordinates. For each detector about 80 experimental points were obtained covering angular regions up to ±160°. Although only the points for F-detector are shown, those for other detectors fall on the curves very well and are omitted from the figure to avoid confusion. The Geiger counter counts extrapolated to the time immediately after a 1½-hr bombardment were 4.2, 2.1, and 1.5 c/sec/μa-hr deuterons/mg of Al, Ta, and $(CF_2)_n$, respectively, for the detectors located at 0° and 3.9 cm from the Be target. These were due to radioactivities from Na^{24}, Ta^{180}, and F^{18}, respectively. The same Geiger counter gave, on the average, 100 ct/sec for a UX_2 standard which is known to disintegrate at a rate of 640/sec.

As shown in Fig. 2 the shape of the angular distributions for Al- and Ta-detectors is similar to that of S-detectors. For the F-detector, the double peaks are clearly resolved. Some indications of multi-peak effect were noted previously[1] with detectors placed at a great distance from the target. Falk[3] observed this same effect with a proton recoil telescope. Ammiraju,[4] however, found only a single peak for neutrons from a thick Be target bombarded with 18-Mev deuterons using the 11-Mev threshold detector, $Cu^{63}(n, 2n)Cu^{62}$. This may be due either to the poor angular resolution of his detector or to higher bombarding deuteron energy. Preliminary results using $Cu^{63}(n, 2n)Cu^{62}$, which has a neutron threshold of 10.3 Mev, also indicated the presence of double peaks.

Since the neutrons from $Be(d, 2n)B^{9}$ have energy less than 8 Mev for 15-Mev deuterons, they are not detected by Ta- and F-detectors. It may be pointed out that the cross sections for the detecting reactions, $(n, 2n)$, (n, α), and (n, p), vary with impinging neutron energies. This is a drawback in the present experiment, in addition to the use of a thick target. The multiple-peak effect has been found in a clear-cut experiment on (d, p) reactions involving single quantum states by Burrows, Gibson, and Rotblat[5] and Holt and Young,[6] and has been interpreted by Butler.[7] The latter treated the (d, p) and (d, n) reactions as a stripping process and related the angular peaks to the spins and parities of the target and product nuclei. It is not unlikely that the double peaks noted here may be ultimately connected with the same cause suggested by Butler.

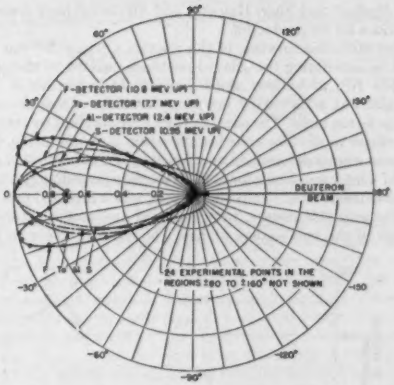
S-DETECTOR (10.8 MEV UP)
Ta-DETECTOR (7.7 MEV UP)
Al-DETECTOR (2.4 MEV UP)
S-DETECTOR (0.95 MEV UP)
DEUTERON BEAM
24 EXPERIMENTAL POINTS IN THE REGIONS ±80 TO ±160° NOT SHOWN

FIG. 2. Relative angular yield of fast neutrons from 15-Mev deuterons on a thick beryllium target.

* Assisted by the joint program of the ONR and AEC.
[1] Allen, Nechaj, Sun, and Jennings, Phys. Rev. 81, 536 (1951).
[3] McElhinney, Hanson, Becker, Duffield, and Diven, Phys. Rev. 75, 542 (1949).
[3] C. E. Falk, Carnegie Institute of Technology thesis, July, 1950.
[4] P. Ammiraju, Phys. Rev. 76, 1421 (1949).
[5] Burrows, Gibson, and Rotblat, Phys. Rev. 80, 1095 (1950).
[6] J. R. Holt and C. T. Young, Proc. Phys. Soc. (London) 63, 833 (1950).
[7] S. T. Butler, Phys. Rev. 80, 1095 (1950).

Excitation Function of $C^{14}(\alpha, p)N^{17}$*

K.-H. SUN, B. JENNINGS, AND W. E. SHOUPP
Westinghouse Electric Corporation, East Pittsburgh, Pennsylvania
AND
A. J. ALLEN
University of Pittsburgh, Pittsburgh, Pennsylvania
(Received March 5, 1951)

IMMEDIATELY after the California group[1] discovered the delayed neutron emitter N^{17} by bombarding neighborhood-elements above oxygen with 195-Mev deuterons, the present authors[2] were able to induce the same activity by the reaction $C^{14}(\alpha, p)N^{17}$, using alphas from a low energy cyclotron. Since then, Alvarez[3] and Hayward[4] have determined the energy relationship in the $\beta^{-}-n$ decay process of N^{17}, and Charpie, Sun, Jennings,

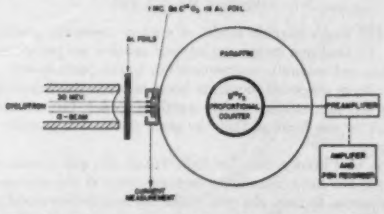

FIG. 1. Experimental arrangement for the excitation study of $C^{14}(\alpha, p)N^{17}$.

and Nechaj[5] and Sher, Halpern, and Stephens[6] have found new reactions for its production.

The excitation function of the reaction $C^{14}(\alpha, p)N^{17}$ was measured by monitoring the delayed neutrons, emitted by the product nuclide N^{17}, at various alpha-energies. The variation in alpha-energies was achieved by inserting 0.0005-in. aluminum foils in the cyclotron beam. The energy values were obtained by measuring the ranges in air. The experimental setup is shown in Fig. 1. The neutron counts determined as a function of time exhibited a half-life of 4.6±1 sec. The counts in 20 seconds immediately after the bombardment (0.02 μamp and 30 sec), which included practically all the available counts, were recorded and plotted against the energy of the bombarding alphas. The result is shown in Fig. 2.

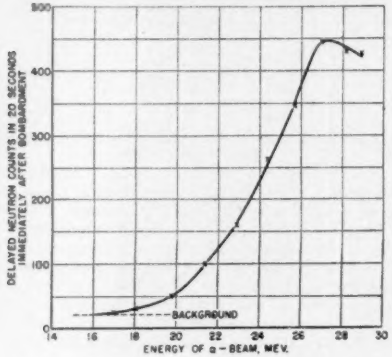

FIG. 2. Relative excitation function of $C^{14}(\alpha, p)N^{17}$.

The threshold of the reaction, based on data from Alvarez's work,[3] should be 12.4 Mev. It was not possible for us to determine this threshold experimentally because of the slow increase in the yield due to the potential barrier for the outgoing protons, and because of the presence of a moderate neutron background. The decrease in yield after 27 Mev is probably due to the competing reaction $C^{14}(\alpha, 3n)O^{15}$ which sets in at an alpha-threshold of about 27.6 Mev. The cross section of the $C^{14}(\alpha, p)N^{17}$ for 27-Mev alpha-particles was estimated to be about 6×10^{-26} cm².

* Assisted by the joint program of the ONR and AEC.
[1] Knable, Lawrence, Leith, Moyer, and Thornton; Chupp and McMillan; L. W. Alvarez; Phys. Rev. **74**, 1217 (1948).
[2] Sun, Jennings, Shoupp, and Allen, Phys. Rev. **75**, 1302 (1949).
[3] L. W. Alvarez, Phys. Rev. **75**, 1127 (1949).
[4] E. Hayward, Phys. Rev. **75**, 917 (1949).
[5] Charpie, Sun, Jennings, and Nechaj, Phys. Rev. **76**, 1255 (1949).
[6] Sher, Halpern, and Stephens, Phys. Rev. **79**, 241 (1950).

Nuclear Magnetic Moments and Similarity between Neutron and Proton States in the Nucleus*

A. L. SCHAWLOW AND C. H. TOWNES
Columbia University, New York, New York
(Received March 2, 1951)

THE single particle model of nuclear moments assumes that all nucleons except the last odd particle are paired and that the spin and magnetic moment are due to this particle only. Actual nuclei have magnetic moments lying between the Schmidt limits given by the extreme single particle model, but usually near enough to one limit so that the state of the odd particle can be assigned.

It is well known that for light atoms the nth proton usually occupies the same angular momentum state in the nucleus as the nth neutron. In fact, the spin of the nucleus having n odd protons (and an even number of neutrons) is the same as that of the nucleus with n odd neutrons in every case up to $n=41$ with the sole exception of the O^{17}, F^{19} pair.[1] The values of the magnetic moments of the odd proton and odd neutron nuclei indicate a still closer similarity between neutron and proton wave functions. If the deviation from the Schmidt limits is caused by an admixture of the two states with the same I ($I=l+\frac{1}{2}$, $I=l-\frac{1}{2}$) and if the proton and neutron wave functions are very similar, the mixture should be the same for the two cases. Then, the moments may be expected to lie at the same fractional distance between the appropriate $I=l+\frac{1}{2}$ and $I=l-\frac{1}{2}$ Schmidt limits. Thus, if the value of the moment of a certain odd proton nucleus places it 10 percent of the distance from its $l+\frac{1}{2}$ limit, the corresponding odd neutron nucleus will have a moment lying about 10 percent of the distance from its $l+\frac{1}{2}$ limit to the $l-\frac{1}{2}$ limit. Some other[2] explanations of deviations from the Schmidt limits should give essentially the same behavior as long as neutron and proton wave functions are very similar.

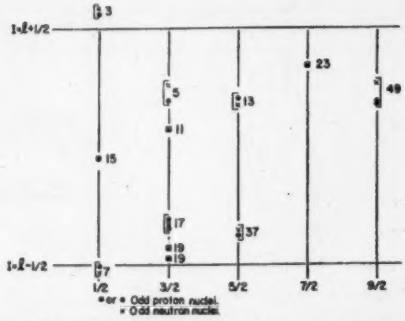

FIG. 1. Comparison of magnetic moments of odd-proton and odd-neutron nuclei. The upper line represents the Schmidt limit $I=l+\frac{1}{2}$ for either neutrons or protons, and the lower line the Schmidt limit for $I=l-\frac{1}{2}$. Ordinate for a nucleus of spin I and magnetic moment μ is $(\mu-\mu_{I-\frac{1}{2}})/(\mu_{I+\frac{1}{2}}-\mu_{I-\frac{1}{2}})$, where $\mu_{I+\frac{1}{2}}$ and $\mu_{I-\frac{1}{2}}$ are the magnetic moments for the two Schmidt limits and for the appropriate spin I. Ordinates are therefore the fractional distance from the $I=l-\frac{1}{2}$ Schmidt limit. Numbers beside points are the number of odd particles in the nuclei. Cases with equal numbers of odd protons or odd neutrons are bracketed.

Figure 1 shows the extent of agreement with these expectations. The upper horizontal line represents the Schmidt limit for the magnetic moment of an odd proton or odd neutron nucleus for $I=l+\frac{1}{2}$, and the lower one for $I=l-\frac{1}{2}$. The ordinate is the fractional distance from the $l-\frac{1}{2}$ Schmidt limit. It may be seen that odd neutron and odd proton nuclei of a given number of odd particles fall very close together on this diagram, as expected, indicating a close similarity of wave functions. The worst deviations are for $n=5$, which corresponds to Be^9 and B^{11} and hence to a rather large fractional difference in nuclear size, and for $n=49$,

TABLE I. Predicted nuclear magnetic moments. Nuclear spins which have not been definitely established are in parentheses.

Number of odd particles	Odd-proton nuclei: Element	Spin	μ observed (nuclear magnetons)	Odd-neutron nuclei: Element	Spin	μ predicted (nuclear magnetons)
11	$_{11}Na^{23}$	3/2	+2.21711	$_{10}Ne^{21}$	3/2	−0.60
15	$_{15}P^{31}$	1/2	+1.13165	$_{14}Si^{29}$	(1/2)	−0.53
19	$_{19}K^{39}$	3/2	+0.391	$_{16}S^{33}$	3/2	+1.00
	$_{19}K^{41}$	3/2	+0.215			
23	$_{23}V^{51}$	7/2	+5.1478	$_{20}Ca^{43}$	(7/2)	−1.38
25	$_{25}Mn^{55}$	5/2	+3.4681	$_{22}Ti^{47}$	(5/2)	−1.79
27	$_{27}Co^{59}$	7/2	+4.6484	$_{22}Ti^{49}$	(7/2)	−0.96
29	$_{29}Cu^{63}$	3/2	+2.22617	$_{24}Cr^{53}$	(3/2)	−0.67
	$_{29}Cu^{65}$	3/2	+2.3845			
31	$_{31}Ga^{69}$	3/2	+2.0167	$_{26}Fe^{57}$	(3/2)	−0.66
	$_{31}Ga^{71}$	3/2	+2.5614			
33	$_{33}As^{75}$	3/2	+1.4	$_{28}Ni^{61}$	(3/2)	+0.10
41	$_{41}Cb^{93}$	9/2	+6.1659	$_{32}Ge^{73}$	9/2	−1.30
51	$_{51}Sl^{121}$	5/2	+3.7	$_{40}Zr^{91}$	5/2	−0.99

where coulomb forces probably are of importance. Other points in Fig. 1 represent odd proton nuclei for which the corresponding odd neutron nuclei have not yet been measured. The moments of these odd neutron nuclei may then be predicted with some assurance to lie near those for the corresponding odd proton nuclei.

On this basis predictions of magnetic moments of odd neutron nuclei are given in Table I. Judging from the deviations in Fig. 1, the accuracy of these predictions should be approximately ±0.1 nuclear magneton.

All nuclear moments used in Fig. 1 and Table I are taken from Mack's review article,[3] except S^{33} and Mg^{25} which are from more recent publications.[4,5]

Considerations of this general type are probably not new, but it seems worthwhile to examine the agreement with experiment now that some odd neutron nuclei moments are being measured. The predicted values may be of use in searching for unknown moments by the nuclear induction method.

* Work supported by the AEC.

[1] The O^{17} spin is 5/2 according to F. Alder and F. C. Yu, Phys. Rev. **81**, 1066 (1951). A spin of 5/2 is also indicated by recent work at Columbia University.

[2] A. Bohr, Phys. Rev. **81**, 134 (1951).

[3] J. E. Mack, Revs. Modern Phys. **22**, 64 (1950).

[4] Eshbach, Hilliger, and Jen, Phys. Rev. **80**, 1106 (1950).

[5] We are grateful to F. Alder and F. C. Yu for communicating their value of the Mg^{25} moment to us before publication. This value is consistent with, but more precise than, the spectroscopic value quoted by Mack.

The Magnetization Process in Ferrites

J. J. Went and H. P. J. Wijn
Philips Research Laboratories, N. V. Philips' Gloeilampenfabrieken, Eindhoven, Netherlands

(Received February 19, 1951)

It is known how the initial permeability μ_0 of ferrites[1] changes with frequency:[2] μ_0 is constant at relatively low frequencies and drops to very low values in a frequency range where resonance phenomena take place. Snoek ascribes this drop to the resonance of the magnetic spins caused by the rf magnetic field in the constant internal anisotropy fields. A close relationship between the value of this resonance frequency and the expected strength of the internal anisotropy fields, as deduced from the value of the initial permeability, has been well proven.[3] In Snoek's theory, it is assumed that the magnetization of ferrites in a small external field is caused by the simultaneous rotation of the electron spins, and not by the reversible Bloch-wall displacements, which are believed to be the cause of the magnetization of ferromagnetic metals in small fields.[4] Therefore, we wish to draw attention to some experiments we performed which shed some light on the magnetization process of ferrites, also at higher inductions.

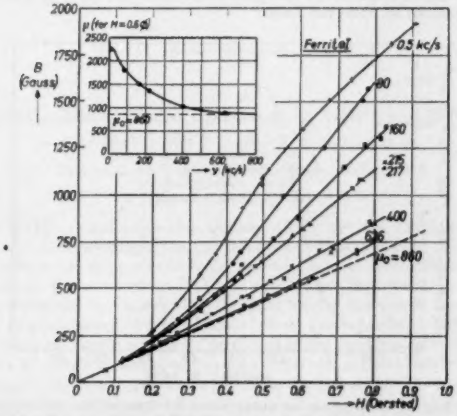

FIG. 1. Initial magnetization curve of ferrite I as a function of frequency.

TABLE I. Composition of ferrites.

Ferrite No.	Composition in mol. % (balance Fe_2O_3) MnO	NiO	ZnO	Density	Gyromagnetic resonance frequency* in Mc/sec
I	43.5	—		4.70	1
IIA	—	25	25	4.55	14
IIB	—	27	23	5.21	10

* The frequency for which μ'' has a maximum ($\mu_0 = \mu' - j\mu''$).

The initial magnetization curve of some ferrites has been measured as a function of frequency by applying a sinusoidal magnetic field of amplitude H_{max} to a toroidal ferrite core with a rectangular cross section. The maximum of the nonsinusoidal induction B_{max} in the core has been determined from the emf induced in a second winding on the core and rectified by a Gratz circuit. Precautions were taken to avoid partial short-circuiting of the primary and the secondary of the transformer.

For the manganese-ferrous-ferrite I (see Table I), Fig. 1 shows the behavior of the initial magnetization curve as a function of frequency. All ferrites with a high permeability have similar frequency-dependent magnetization curves. From Fig. 1 it is clear that here we have two different magnetization processes. The first, which is independent of frequency below the gyromagnetic resonance frequency, determines μ_0, while for field strengths approximately equal to the coercive force the other gives an additional magnetization which already disappears for a frequency below the gyromagnetic resonance frequency of the ferrite (see the straight line $B = \mu_0 H$ for the magnetization curve of ferrite I at 626 kc/sec). The frequency-dependence of the latter process can be described with a single relaxation time.

Another fact seems to give an indication of the kind of magnetization process involved. When two ferrites of about the same composition (IIA and IIB, see Table I) are fired at 1200°C and 1400°C, respectively, the magnetization curves are very different

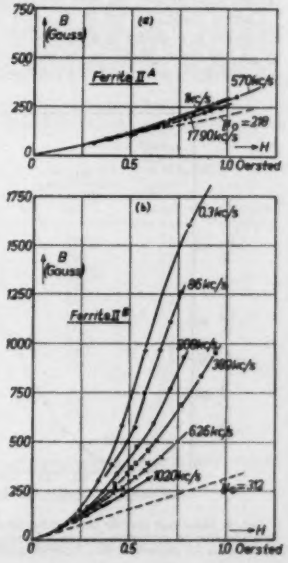

FIG. 2. Initial magnetization curves of ferrites IIA and IIB as functions of frequency.

(Figs. 2a and 2b). The additional magnetization of the ferrite IIB is frequency-dependent, similar to that of ferrite I.

Distortion measurements have also been carried out on transformers having these ferrite cores. The distortion gradually decreases with frequency and reaches zero at the frequency where B is a linear function of H.

From these results it is concluded that in ferrites with a high permeability, at magnetic field strengths of about H_s, an additional magnetization process occurs which (a) is frequency-dependent already below the gyromagnetic resonance frequency, (b) takes place at a lower field strength as the density of the ferrite is greater, (c) is irreversible (since Rayleigh's law holds in small fields).

The initial permeability and the permeability at high frequencies, which is independent of the field strength, are, in our opinion, related to a pure rotational process. In contrast to the magnetization process giving rise to the above-mentioned permeabilities, the additional process is to be ascribed to irreversible Bloch-wall displacements in the ferrite. These results are contradictory to the conclusions reached by Rado *et al.*,[5] that the initial permeability of ferrites is determined by reversible Bloch-wall displacements. A detailed paper on these experiments will be published shortly.[6]

[1] See J. L. Snoek, *New Developments in Ferromagnetic Materials* (Amsterdam, New York, 1947).
[2] J. L. Snoek, Physica **14**, 207 (1948).
[3] D. Polder, Proc. Inst. Elec. Engrs. **97**, II, 246 (1950).
[4] C. Kittel, Revs. Modern Phys. **21**, 541 (1949).
[5] Rado, Wright, and Emerson, Phys. Rev. **80**, 273 (1950).
[6] J. J. Went and H. P. J. Wijn, Physica, to be published.

Cross Section for the Reaction $C^{12}(\gamma, n)C^{11}$

R. N. H. Haslam, H. E. Johns, and R. J. Horsley
Department of Physics, University of Saskatchewan, Saskatoon, Saskatchewan, Canada
(Received March 5, 1951)

THE cross-section curve for the reaction $C^{12}(\gamma, n)C^{11}$ has been determined by Baldwin and Klaiber.[1] However, in view of the discrepancy in the results obtained by these authors and the workers in our laboratory[2] for the reaction $Cu^{63}(\gamma, n)Cu^{62}$, the carbon cross section has been redetermined.

Carbon disks, 1.5 cm in diameter and 1.27 mm thick, were irradiated in a cavity in a Lucite block. The dose was monitored by an "r" meter placed in the same position. The resulting 20.6-min activity was counted in a fixed geometry. Figure 1 shows the saturated specific activity as a function of maximum betatron energy. Corrections for back-scattering, self-absorption, isotopic abundance, and geometry have been applied. The threshold for this reaction, assumed at 18.7 Mev,[3,4] has been used as a calibration point for the betatron energy scale. No attempt has been made to show the portion of the activity curve between 18.7 and 20 Mev, although the contribution of this portion has been considered in the cross-section determination. The experimental points on the activity curve represented by circles were determined with the integrator circuit previously reported.[2] The points marked with a cross were determined by the betatron panel meter. The two sets of results were brought into agreement by determining overlapping activity curves in the region 22 to 24 Mev.

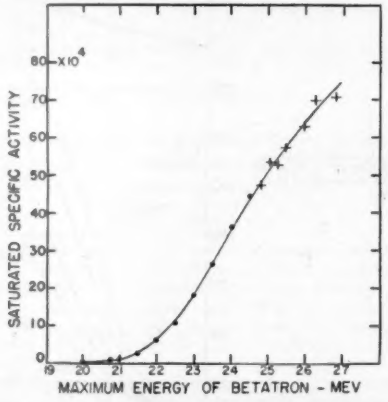

FIG. 1. Saturated specific activity in disintegrations per gram per 100 r as a function of maximum betatron energy, for the reaction $C^{12}(\gamma, n)C^{11}$. Corrections for geometry, etc., have been applied.

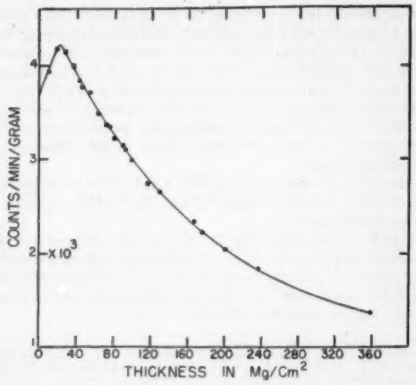

FIG. 2. Self-absorption curve for the positron activity of C^{11}.

As a check on some of the corrections applied in finding the saturated specific activity of carbon, copper and carbon samples were irradiated simultaneously at 23.5 Mev and counted in the same geometry. In determining the carbon activity, use was made of the results previously reported for copper[2] (lowered by 10 percent in agreement with more recent determinations). This latter method yielded a value for the saturated specific activity of carbon 5 percent higher than is reported here. This agreement is very satisfactory when one considers the possible errors involved.

The saturated specific activity curve has been used to determine the neutron yield at 22 Mev. The value obtained, 7.5×10^8 neutrons/mole/r, is in good agreement with the value 6.7×10^8 obtained by Price and Kerst.[5]

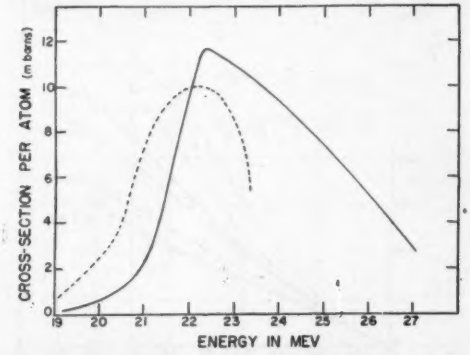

FIG. 3. Cross section as energy curve for $C^{12}(\gamma, n)C^{11}$. The dotted curve shows the shape of the corresponding curve for $C^{12}(\gamma, p)B^{11}$ (reference 12).

Figure 2 is a self-absorption curve for the positron activity of C^{11}. Filter paper was used as a source of carbon for the points corresponding to small thickness (solid squares). The neglect of the bending-over of the curve would have led to an error of 20 percent in determining the activity at zero sample thickness. Similar, though larger, corrections were required for copper.

In Fig. 3 is shown the cross-section curve obtained from the activity curve by the method of analysis previously reported.[2] The cross-section curve has a peak value of 11.6 millibarns at 22.4±0.5 Mev. The width at half-maximum is 4.25 Mev, and the integrated cross section is 0.047 Mev-barn. The ratio of the integrated cross sections of $Cu^{63}(\gamma, n)Cu^{62,6}$ and $C^{12}(\gamma, n)C^{11}$ is 0.63/0.047 = 13.4. This is in satisfactory agreement with ratios of the yields of these reactions produced by betatron x-rays of maximum energy 50 and 100 Mev (15.2, 14.4, respectively),[7] and also with the ratio 14 given by Helmholz and Strauch[8] for 335-Mev x-rays. This would be expected if the cross sections for these reactions were negligible above 50 Mev. Our value of 0.047 Mev-barn for the integrated cross section is considerably lower than that obtained by Lawson and Perlman,[9] who, however, assumed a sharp resonance occurring at approximately 30 Mev.[1]

The average energy for the x-rays producing the $C^{12}(\gamma, n)C^{11}$ reaction, as obtained from absorption coefficient measurements, is given as 22.1±1.5 Mev by Koch, McElhinney, and Cunningham[10] and 25.3±1.5 Mev by Marshall.[11] Although the peak of our cross-section curve lies at 22.4 Mev, the median ordinate lies at 23.5 Mev, and this probably corresponds more closely to the "average" photon energy obtained by the above authors.

The dotted curve of Fig. 3 shows the shape of the cross-section curve for the (γ, p) reaction in the same nuclide, as determined by Mann and Halpern.[12] It has been normalized to their minimum peak value of 1×10^{-28} cm². It is interesting to note that the maxima of the two curves occur at nearly the same energy.

The authors wish to thank Mr. A. Quinton for his assistance with many of the measurements involved. This work is supported by grants from the National Research Council and the National Cancer Institute of Canada. One of the authors (R.J.H.) is indebted to the Ontario Research Council for financial assistance.

[1] G. C. Baldwin and G. S. Klaiber, Phys. Rev. **73**, 1156 (1948).
[2] Johns, Katz, Douglas, and Haslam, Phys. Rev. **80**, 1062 (1950).
[3] Katz, McNamara, Forsyth, Haslam, and Johns, Can. J. Research **A28**, 113 (1950).
[4] McElhinney, Hanson, Becker, Duffield, and Diven, Phys. Rev. **75**, 542 (1949).
[5] G. A. Price and D. W. Kerst, Phys. Rev. **77**, 806 (1950).
[6] B. C. Diven and G. M. Almy, Phys. Rev. **80**, 407 (1950).
[7] M. L. Perlman and G. Friedlander, Phys. Rev. **74**, 442 (1948).
[8] A. C. Helmholz and K. Strauch, Phys. Rev. **73**, 86 (A) (1950).
[9] J. L. Lawson and M. L. Perlman, Phys. Rev. **74**, 1190 (1948).
[10] Koch, McElhinney, and Cunningham, Phys. Rev. **81**, 318 (A) (1951).
[11] L. Marshall, Phys. Rev. **82**, 300 (1951).
[12] A. K. Mann and J. Halpern, Phys. Rev. **80**, 470 (1950).

Photoneutron Cross Sections of Fe^{54}, Ni^{58}, and Zn^{64}

L. KATZ, H. E. JOHNS, R. G. BAKER, R. N. H. HASLAM, AND R. A. DOUGLAS
Betatron Group, University of Saskatchewan, Saskatoon, Saskatchewan, Canada
(Received March 5, 1951)

THE photoneutron cross sections of Fe^{54}, Ni^{58}, and Zn^{64} have been investigated in this laboratory with the method outlined by the authors in an earlier paper.[1] The cross section *versus* energy curves are shown in Fig. 1, and the pertinent results are summarized in Table I. The threshold for the reaction in iron was also checked and was found to be in good agreement with values previously reported. Corrections to the observed activity for K capture amounted to 7 percent in the case of Zn^{64},[2] 100 percent in the case of Ni^{58},[3] and 3 percent in the case of Fe^{54}. The last correction was estimated from the theoretical curves of Feenberg and Trigg,[4] assuming the transition to be allowed.

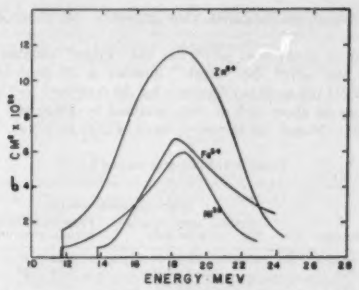

FIG. 1. Cross sections of Fe^{54}, Ni^{58}, Zn^{64} for (γ, n) reactions as a function of energy.

An examination of all published (γ, n), (γ, p), and (γ, d) cross sections would seem to indicate considerable similarity among them. For example, they all have half-widths of about 6 Mev, and their maximum cross sections, as previously pointed out by Katz and Penfold,[5] occur about 6 Mev above the threshold (see also Table II). Fluctuations from this value are generally less than 1.5 Mev. Cameron[6] analyzes the published neutron yield data on the basis of this similarity to obtain some interesting results. In addition, we would like to draw attention to the shape of the $Fe^{54}(\gamma, n)Fe^{53}$ and $C^{12}(\gamma, n)C^{11}$ curves. (See Haslam *et al.*[7] for the latter curve.) These cross sections rise more steeply than the other curves; and after passing through a maximum value, they drop off relatively slowly, resulting in a long tail. We might infer from the behavior of these two isotopes that the relative position of the cross-section maximum and the threshold are not necessarily

TABLE I. Photoneutron cross-section data.

Parent isotope	Threshold Mev	Energy at peak cross section Mev	Maximum cross section barn	Half-width Mev	Integrated cross section Mev-barn
Fe^{54}	13.7±0.2	18.3	0.067±0.006	5.7	0.42
Ni^{58}		18.5	0.050±0.006	4.6	0.33
Zn^{64}		18.5	0.12 ±0.01	7.1	0.83

TABLE II. Summary of photoneutron cross-section data.

Isotope and reaction	Threshold Mev	Energy at peak cross section Mev	Energy of peak cross section above threshold Mev	Reference
$C^{12}(\gamma, n)C^{11}$	18.7	22.4	3.7	a
$C^{12}(\gamma, p)B^{11}$	16	22.2	6.2	b
$Al^{27}(\gamma, n)Al^{26}$	14	19.6	5.6	c
$P^{31}(\gamma, n)P^{30}$	12.4	19	6.6	d
$S^{32}(\gamma, np)P^{30}$	19.1	25.8	6.4	d
$Fe^{54}(\gamma, n)Fe^{53}$	13.8	18.3	4.5	
$Ni^{58}(\gamma, n)Ni^{57}$	12.0	18.5	6.5	
$Cu^{63}(\gamma, n)Cu^{62}$	10.9	17.5	6.6	e
$Cu^{65}(\gamma, n)Cu^{64}$	10.7	19.0	8.5	e
$Zn^{64}(\gamma, n)Zn^{63}$	11.6	18.5	6.9	
$Ag^{109}(\gamma, n)Ag^{108}$	9.3	16.0	6.7	f
$Ag^{109}(\gamma, p)Pd^{108}$	6.1		6.5	f
$Sb^{121}(\gamma, n)Sb^{120}$	9.3	14.5	5.2	e
$Sb^{123}(\gamma, n)Sb^{122}$	9.3	14.5	5.2	e
$Ta^{181}(\gamma, n)Ta^{180}$	8.0	13.5	5.5	e
			Average 6.0	

a Reference 7.
b A. K. Mann and J. Halpern, Phys. Rev. **80**, 470 (1950).
c To be published.
d Reference 5.
e Reference 1.
f B. C. Diven and G. M. Almy, Phys. Rev. **80**, 407 (1950).

related; though as indicated, they generally fall about 6 Mev apart.

It is to be noted that $_{26}Fe^{54}$ has the "magic" number of 28 neutrons and $_{28}Ni^{58}$ the "magic" number of 28 protons. The neutron yield per mole per roentgen for the 6 percent Fe^{54} isotope is found to be about 3/5 of that obtained by Price and Kerst[8] (Table III). Nickel, on the other hand, which is "magic" in all

TABLE III. Photoneutron yields.

Isotope	Neutrons/mole/roentgen: Present work indicated isotope only	Price and Kerst natural element
Fe^{54}	1.01×10^6	1.64×10^6
Ni^{58}	1.12×10^6	1.04×10^6
Zn^{64}	2.82×10^6	2.35×10^6

isotopes, is found to give the same yield, within experimental error, for the 68 percent isotope Ni^{58} as for the natural element. We find about 20 percent more neutron yield from the 50 percent isotope Zn^{64} than Price and Kerst found for the natural element. This difference may still be within the combined experimental error. These measurements substantiate the neutron yield from nickel found by Price and Kerst, which was about one-half of that from the other elements in this region of the periodic table.

The absolute neutron yields are based on a maximum cross section for Cu^{63} of 0.10 barn. This value is 10 percent less than our previously published result[1] and is believed to be more accurate.

[1] Johns, Katz, Douglas, and Haslam, Phys. Rev. **80**, 1062 (1950).
[2] Huber, Medicus, Preiswerk, and Steffan, Helv. Phys. Acta **20**, 495 (1947).
[3] Friedlander, Perlman, Aiburger, and Sunyar, Phys. Rev. **80**, 30 (1950).
[4] E. Feenberg and G. Trigg, Revs. Modern Phys. **22**, 399 (1950).
[5] L. Katz and A. Penfold, Phys. Rev. **81**, 815 (1951).
[6] A. G. W. Cameron, Phys. Rev. **82**, 272 (1951).
[7] Haslam, Johns, and Horsley, Phys. Rev. **82**, 270 (1951).
[8] G. A. Price and D. W. Kerst, Phys. Rev. **77**, 806 (1950).

Interpretation of Photoneutron Yields

A. G. W. CAMERON
Department of Physics, University of Saskatchewan, Saskatoon, Saskatchewan, Canada
(Received March 5, 1951)

"RESONANCE" cross-section curves for several (γ, n) reactions have recently been determined by activation measurements in this laboratory.[1-3] These resonances are of the type predicted for nuclear dipole transitions by Goldhaber and Teller[4] and by Levinger and Bethe.[5] The curves are so similar in relative shape (except for Fe^{54} and C^{12}, which rise steeply owing to high (γ, n) thresholds) that it is possible to use their average cross-section shape in an analysis of the photoneutron yields obtained for 53 elements by Price and Kerst.[6]

TABLE I. Characteristics of (γ, n) cross-section curves.

Reaction	Energy of maximum Mev	$E_m - Q$ Mev[a]	Maximum σ barn	Half-width Mev	Integrated cross section, Mev-barn
$P^{31}(\gamma, n)P^{30}$	17.0	4.6	0.017	7.6	0.13
$Ni^{58}(\gamma, n)Ni^{57}$	18.5	6.8	0.060	4.5	0.33
$Cu^{63}(\gamma, n)Cu^{62}$	17.5	6.6	0.10[b]	5.8	0.63[b]
$Zn^{64}(\gamma, n)Zn^{63}$	18.5	6.7	0.12	7.2	0.83
$Sb^{121}(\gamma, n)Sb^{120}$	14.5	5.2	>0.21	5.4	>1.2
$Sb^{123}(\gamma, n)Sb^{122}$	14.5	5.2	0.34	5.5	2.0
$Ta^{181}(\gamma, n)Ta^{180}$	13.5	5.5	>0.078	4.5	>0.39
Average	—	6.0	—	5.5[c]	—

[a] Energy of peak maximum above threshold.
[b] A 10 percent correction has been applied to the values of reference 1.
[c] This is not the mean of the above values, because the shape averaging was carried out vertically rather than horizontally.

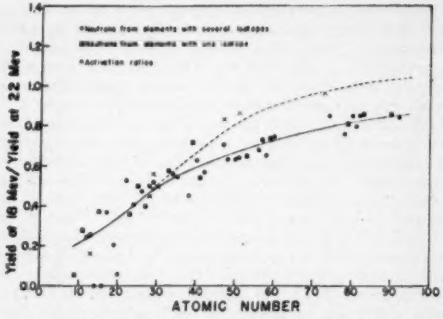

FIG. 1. Ratio of photoneutron yields with 18- and 22-Mev x-rays.

The essential characteristics of the cross-section curves are shown in Table I. An average of the curves was obtained by normalizing them at their peaks in arbitrary cross-section and energy position.

Steinwedel *et al.*[7] predict that the resonance peak energies should vary as $A^{-1/3}$, whereas Goldhaber and Teller predict a variation as $A^{-1/6}$. With the peak position data of Table I and the values for (γ, n) reactions in Cu^{65} (19.0 Mev), Fe^{54} (18.5 Mev),[3] Ag^{109} (16.5 Mev),[3] Al^{27} (19.6 Mev),[3] and C^{12} (22.4 Mev),[10] the best fit to the above type of relationship is

$$E_m = 36A^{-0.18}, \tag{1}$$

where E_m is the peak energy in Mev. This favors the prediction of Goldhaber and Teller. However, the empirical relationship

$$E_m = 21.5\exp(-0.00274A) \tag{2}$$

fits the data much better and has been used in the following considerations.

With the peak energies as calculated from Eq. (2), the average cross-section shape as determined above, and the Schiff x-ray spectrum,[1] the ratio of photoneutron yields for 18 and 22 Mev x-rays was calculated as a function of atomic number. This is plotted as the broken line in Fig. 1. The crosses are the activation ratios which fundamentally determine the curve. The data of Price and Kerst are also plotted in this figure, and the solid curve is the empirical fit to their points. Elements with one or many isotopes are represented, respectively, by solid squares or solid circles. Both types of points fit the empirical curve equally well, indicating that the resonance peak energies for the isotopes in a given element are not appreciably different.

Figure 1 shows that above $Z=30$ there are more neutrons at 22 Mev than can be accounted for from (γ, n) reactions. From threshold considerations these neutrons can only arise from $(\gamma, 2n)$ and (γ, pn) reactions. The ratio of the broken to the solid curve diverges from unity at $Z=30$ and reaches a fairly constant value of 1.22 at $Z=50$. This indicates that the resonance peak energy for $(\gamma, 2n)$ and (γ, pn) reactions falls below 22 Mev at about $Z=40$. Since there are fewer photons at this peak than at the (γ, n) peak, it may be estimated that the sum of the $(\gamma, 2n)$ and (γ, pn) integrated cross sections is of the order of 30 percent of that for (γ, n) reactions (assuming equal contributions from each multiple reaction).

With the above assumptions as to peak shape and energy, the maximum and integrated (γ, n) cross sections were computed directly from the photoneutron yield data. The 22-Mev data were used up to $Z=30$; beyond that, the 18-Mev data were used so as to minimize the contribution from multiple reactions. For the average resonance curve, the integrated cross section (Mev-barns) is related to the peak cross section σ_m (barns) by the expression

$$\int \sigma_{\gamma n} dW = 6.05\sigma_m. \tag{3}$$

These quantities are plotted to relative scales in Fig. 2 as a func-

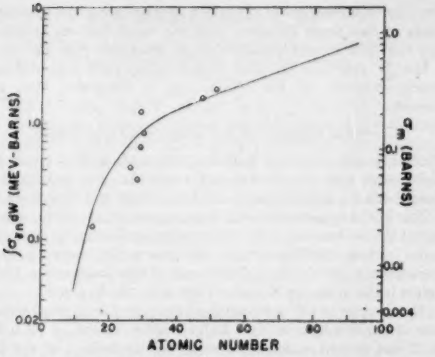

FIG. 2. Maximum and integrated (γ,n) cross sections as a function of atomic number. The curve is derived from photoneutron yields; the points are independent activation measurements of the integrated cross section.

tion of atomic number. Since the absolute cross-section values of Table I were not used in the computation of the average shape, these points and the other values from references 1, 3, and 8 are plotted in Fig. 2 and constitute a satisfactory independent check on the general curve.

Only one (γ, pn) and no $(\gamma, 2n)$ reactions have yet been investigated in detail. The integrated cross section for $S^{32}(\gamma, pn)P^{30}$ is 0.003 Mev-barns,[2] or 2 percent of the integrated (γ, n) cross sections in that region of the periodic table. This may indicate that $(\gamma, 2n)$ reactions are more important than (γ, pn) reactions, or that the extra neutron yields are much less in light elements.

I am indebted to Dr. L. Katz for valuable discussions.

[1] Johns, Katz, Douglas, and Haslam, Phys. Rev. **80**, 1062 (1950).
[2] L. Katz and A. S. Penfold, Phys. Rev. **81**, 815 (1951).
[3] Katz, Johns, Baker, Haslam, and Douglas, Phys. Rev. **82**, 271 (1951).
[4] M. Goldhaber and E. Teller, Phys. Rev. **74**, 1046 (1948).
[5] J. S. Levinger and H. A. Bethe, Phys. Rev. **78**, 115 (1950).
[6] G. A. Price and D. W. Kerst, Phys. Rev. **77**, 806 (1950).
[7] Steinwedel, Jensen, and Jensen, Phys. Rev. **79**, 1019 (1950).
[8] B. C. Diven and G. M. Almy, Phys. Rev. **80**, 407 (1950).
[9] Recently measured in this laboratory.
[10] Haslam, Johns, and Horsley, Phys. Rev. **82**, 270 (1951).

New Superconducting Borides and Nitrides

J. K. HULM AND B. T. MATTHIAS[a]
Institute for the Study of Metals, University of Chicago, Chicago, Illinois
(Received March 5, 1951)

THE pronounced metallic character of many borides, carbides, and nitrides of the transition metals is evident from the fact that the electrical resistivity of these compounds has a positive temperature coefficient in the neighborhood of room temperature and is, in several cases, less than the resistivity of the constituent metal.[1] Meissner[2] found that many of these compounds show superconducting behavior, the carbides of molybdenum and tungsten being of special interest in this respect, since the metals themselves appear to be nonsuperconducting down to very low temperatures (<1°K). A knowledge of the extent to which such apparently nonsuperconducting elements form superconducting compounds is obviously important for a satisfactory theory of superconductivity; but, on reviewing the available data against the general background of the periodic system, one is struck by the large number of interesting compounds which have so far not been tested, little having been done since the pioneer work of Meissner. This situation led us to embark some time ago on an experimental survey of metallic compounds, the object being to throw more light on the chemical and structural conditions governing the occurrence of superconductivity. We have adopted a magnetic detection method, which, as pointed out by Shoenberg,[3] provides a direct measure of the amount of superconducting material present, and avoids the difficulty occurring in electrical resistance measurements that a small quantity of superconducting impurity may shunt the bulk of the specimen, thus producing a large but spurious effect. Although we have so far examined only about 60 semimetallic and intermetallic compounds down to 1.3°K, it seems worthwhile to describe 4 new superconductors which have recently been found in the boride and nitride groups.

TABLE I. Experimental results. Superconducting compounds are shown in boldface type together with their transition temperatures. The numbers in parentheses represent the lowest temperatures of measurement for those compounds which did not become superconducting.

	Nb	Ta	Mo
B	**NbB 6°** Nb_3B_4 (1.27°) NbB_2 (1.27°)	TaB (1.29°) Ta_3B_4 (1.30°) TaB_2 (1.32°)	**MoB 4.4°** Mo_2B_5 (1.32°)
N	**NbN 14.7°** Nb_2N (9.5°)[a]	**TaN (1.88°)**[a] Ta_2N (9.5°)[a]	**Mo_2N 5°** **MoN 12.0°**

[a] See reference 7.

Superconductivity was observed in the monoborides of *niobium* and *molybdenum*, with the transition temperatures[4] shown in the first row of Table I. X-ray analyses for these compounds and also for other borides which did not become superconducting down to the lowest temperatures of measurement (shown in parentheses in Table I) were in good agreement with the recent structural data of Kiessling,[5] who found NbB orthorhombic and MoB tetragonal. It is interesting to note that the only other previously reported superconducting boride, ZrB, tested by Meissner[2] in electrical resistance measurements, is, according to Kiessling,[5] nonexistent. The latter evidence, coupled with the uncertainty of the resistance method, throws considerable doubt on the superconductivity of ZrB, so that NbB and MoB must be regarded as the only borides at present definitely known to be superconducting.

Superconductivity was also observed in two nitrides of *molybdenum*, with the transition temperatures shown in the lower part of Table I. The x-ray analyses were in these cases in agreement with the results of Hägg,[6] who assigns a face-centered cubic structure (with N/2 missing) to Mo_2N and a hexagonal lattice to MoN. In the preparation of Mo_2N by nitriding molybdenum metal, the formation of some mononitride can hardly be avoided. The magnetization of a mixed specimen of about 85 percent Mo_2N, 10 percent MoN, and 5 percent Mo is plotted against temperature in Fig. 1; and from the relative heights of the two plateau regions we conclude that while Mo_2N becomes normal at about 5°K, MoN remains superconducting up to 12.0°K. In the latter, remarkably high transition temperature, which was studied in detail by surrounding the specimen with solid hydrogen, MoN is second only to NbN,[7] a situation seen to be even more striking

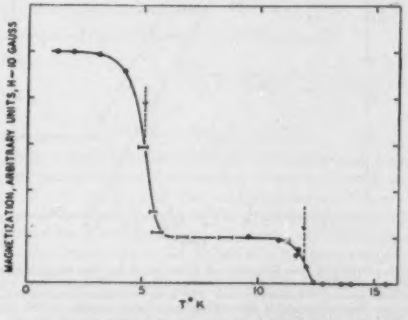

FIG. 1. Temperature variation of low field-strength magnetization of mixed molybdenum nitride specimen.

in the light of Shoenberg's[8] observation that molybdenum metal is itself nonsuperconducting down to 0.3°K.

Measurements on compounds of other transition metals together with details of preparations, analyses, and apparatus will be reported later.

* On leave of absence from Bell Telephone Laboratories, Murray Hill, New Jersey.

[1] K. Moers, Z. anorg. Chem. **198**, 262 (1931).
[2] Meissner, Franz, and Westerhoff, Z. Physik **75**, 521 (1932).
[3] D. Shoenberg, Nature **159**, 303 (1947).
[4] The transition temperature is taken to be the temperature at which the low field strength magnetization attains half its maximum value (e.g., dotted lines, Fig. 1); owing to poor thermal equilibrium, temperatures between 4° and 10°K are at present known only to about one degree.
[5] H. Kiessling, Acta Chemica Scandinavica **1**, 893 (1947); **3**, 90 and 603 (1949).
[6] G. Hägg, Z. Physik. Chem. **B12**, 33 (1931).
[7] F. H. Horn and W. T. Ziegler, J. Am. Chem. Soc. **69**, 2762 (1947); Aschermann, Friederich, Justi, and Kramer, Physik. Z. **42**, 349 (1941).
[8] D. Shoenberg, Proc. Cambridge Phil. Soc. **36**, 84 (1940).

The Beta-Spectrum of Cl^{36}

H. W. Fulbright* and J. C. D. Milton
Palmer Physical Laboratory, Princeton University, Princeton, New Jersey†
(Received February 19, 1951)

It was pointed out by Longmire, Wu, and Townes[1] that the Fermi theory of beta-decay fails to account for the D_3 shape of the Cl^{36} beta-spectrum found by Wu and Feldman,[2] unless a mixture of interactions is assumed. The arguments were based upon the measured[3] spin of two for Cl^{36}, and upon the assumption of a spin of zero for A^{36}. It was shown that the observed spectrum could be accounted for by use of any one of three different mixtures of interactions: $(2S, 2T)$; $(2V, 2T)$; or $(2V, 2A)$.

We have examined the Cl^{36} beta-spectrum by use of a high pressure argon-filled proportional counter[4] and have obtained experimental results which disagree with those mentioned above.

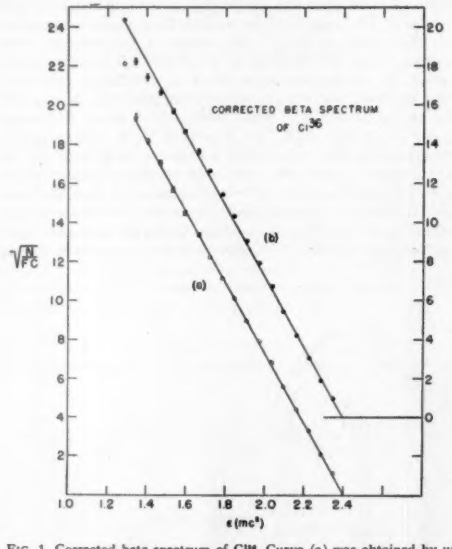

Fig. 1. Corrected beta-spectrum of Cl^{36}. Curve (a) was obtained by use of the C_{2T} correction factor. Curve (b) was obtained when the D_3 correction factor was applied to the same data. The error symbols represent standard deviations. Resolving power corrections have been applied to the original data, but their chief effect is to raise the end point energy slightly. The average thickness of the finely divided KCl source used here was 1.2 mg/cm². The backing was 0.2-mg/cm² Al foil.

The chief disagreement is at the low energy end of the spectrum, where we find fewer electrons, with the result that our points lie very near to a second forbidden tensor spectrum. (See Fig. 1.)

The $2T$ spectrum involves contributions from two different matrix elements. In the terminology of Longmire, Wu, and Townes,

$$C_{2T} = a(T_{ij}^2 \text{ shape}) + b(A_{ij}^2 \text{ shape}) - c(T_{ij}A_{ij} \text{ shape}),$$

where a, b, and c are real numbers, with $a \geq 0$, $b \geq 0$, $c^2 \leq 4ab$. We have found a fit for $c^2 = 4ab$ and $b = 25.73a$. The quantities in parenthesis are defined exactly by Konopinski and Uhlenbeck.[5]

The initial experiment has been repeated six times over a period of six months, with the proportional counter operating under various conditions, and with source thicknesses varying from 0.2 mg/cm² to 5.0 mg/cm²; each of the distributions found agrees better with the $2T$ shape than with the D_3 shape.

The samples of Cl^{36} were obtained by a careful chemical separation of chlorine from an Oak Ridge irradiation unit of KCl. The KCl was treated with concentrated sulfuric acid, and the HCl given off was collected and reconverted into KCl. This procedure should be quite effective in separating chlorine from any radioactive impurity expected to be present. The chief radioactivity in the raw unit was S^{35}. Traces of S^{35} in the final sample could not have affected our results seriously, because of the low (170-kev) energy limit of the S^{35} beta-rays and because any ordinary radioactive impurity would have caused the intensity of the low energy end of the spectrum to be raised, not lowered.

Our method, although relatively new, has faithfully reproduced a number of known spectra such as those of Y^{91} and Be^{10}. (See Fig. 2.) (The Be^{10} and Cl^{36} spectra shown here were obtained within

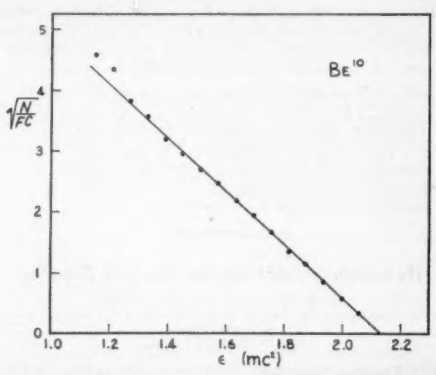

Fig. 2. Corrected beta-spectrum of Be^{10} for comparison with the Cl^{36} spectrum. The plot of this D_3 beta-spectrum is straight down to about 1.3 mc². BeO crystalline source of average thickness about 1.9 mg/cm² on 0.2-mg/cm² Al foil. Coulomb corrections have been applied to both spectra.

a few hours of each other under identical operating conditions.) We have acquired some confidence in its use, both from those results and from an analysis of its operation. A detailed description of the method will be published later.

We conclude that it may well be possible to account for the shape of the Cl^{36} beta-spectrum by means of a single interaction, $2T$ (or $2V$).

We wish to acknowledge the interest of Professor R. E. Marshak in this work. We are indebted to Mrs. Elizabeth Karplus for the chemical separation of the chlorine sample.

* Now at the University of Rochester, Rochester, New York.
† This work was supported in part by the joint program of the ONR and AEC.

[1] Longmire, Wu, and Townes, Phys. Rev. **76**, 695 (1949).
[2] C. S. Wu and L. Feldman, Phys. Rev. **76**, 693 (1949).
[3] C. H. Townes and L. C. Aamodt, Phys. Rev. **76**, 691 (1949).
[4] H. W. Fulbright and J. C. D. Milton, Phys. Rev. **76**, 1271 (1949).
[5] E. J. Konopinski and G. E. Uhlenbeck, Phys. Rev. **60**, 315 (1941).

The Disintegration of As^{74}

STIG JOHANSSON, YVETTE CAUCHOIS,* AND KAI SIEGBAHN
Nobel Institute of Physics, Stockholm, Sweden
(Received February 23, 1951)

THE 17.5-day activity of As^{74} is known to emit positrons, negatrons and γ-radiation.[1] Recently, Mei, Mitchell, and Huddleston[2] found that the negatron spectrum was complex, having the components $E\beta_2^-{}_{max}=0.82$ Mev and $E\beta_1^-{}_{max}=1.45$ Mev. The difference between the two β^- components (0.63) Mev did not agree with the observed γ-energy (0.593±0.003 Mev), but this could possibly be explained from inaccuracies in the Fermi analysis. This circumstance, however, had also been observed in our laboratory together with the peculiar fact that not only the negatrons but also the positrons were accompanied by γ-radiation, in spite of the fact that only one γ-ray was known to exist. A detailed investigation of the disintegration was therefore performed.

The β^- spectrum of the 17.5-day activity was found to be complex, the upper limits for the two components being 0.69 Mev (49 percent) and 1.36 Mev (51 percent), respectively. In the β^+ spectrum a new hard component (1.53 Mev) of small intensity (11 percent) was found besides the main component of 0.92 Mev (89 percent). $\beta^-\gamma$- and $\beta^+\gamma$-coincidence spectra were also run in the spectrometer and it was found that the two softer components were followed by γ-radiation. The γ-spectrum (lead converter) taken with moderate resolution is given in Fig. 1 (upper curve).

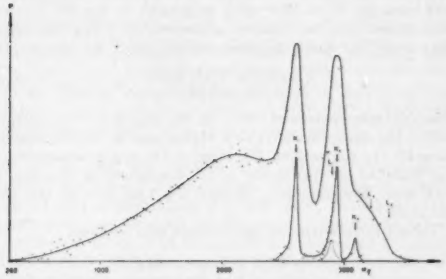

FIG. 1. Photoelectron spectrum of As^{74}. The lower curve was taken by means of the double-focusing spectrometer.

The intensity of the γ-line compared with the annihilation line is, however, far too great to be due to a transition from the soft β^- component to the ground state in Se^{74} as assumed before, but could instead be due to a transition from the soft β^+ component to the ground state in Ge^{74}. A new run with increased resolving power by means of the double-focusing spectrometer was made, with the result given below in Fig. 1. The line split up into two lines, having the energies 0.5963±0.0010 Mev and 0.6352±0.0010 Mev, respectively, with the intensity ratio of 4:1. The small intensity line is certainly emitted in the β^- decay and the high intensity line in the β^+ decay.

A disintegration scheme satisfying our data is presented in Fig. 2. By means of the measured intensities of the β^- and β^+ components and the two γ-lines the branching ratio of K-capture to β^+ for the excited level in Ge is calculated to be 1.5, in good agreement with the theoretical value of 1.3.

The ft value of the hard β^- component is 4×10^8, and the value of $(W_0^2-1)ft=0.5\times10^{10}$ brings this transition into the class of spectra of uniquely forbidden shape ($\Delta L=1$; $\Delta I=2$) according to Shull and Feenberg.[3] The Fermi analysis accordingly shows that the original S-shaped curve is transformed into a straight line when the α-factor is introduced in the analysis. The ft value of the hard, faint β^+ component is 5×10^8 and $(W_0^2-1)ft=0.8\times10^{10}$, which brings this transition into the same class of forbidden spectra.

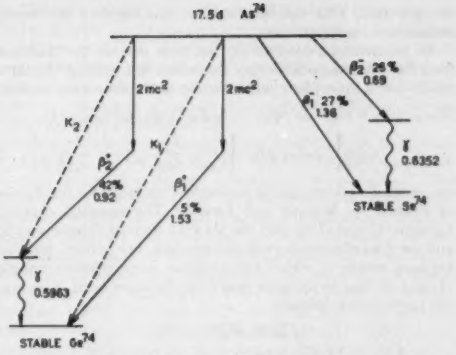

FIG. 2. Disintegration scheme of As^{74}. Energies are in Mev. The percentages shown do not include the K-branches.

The odd 33rd proton and the 41st neutron of the ground state in As^{74} may, according to the spin orbit coupling scheme of the nuclear shell model, be assumed to be in $f_{5/2}$ and $g_{9/2}$ states, respectively. The angular momenta of the odd proton and neutron may then add to form a resultant angular momentum of $2\cdots7$, the state having odd parity. According to Nordheim[4] one should expect that the minimum resultant spin of 2 is preferred here, since the intrinsic spins of the odd particles have different orientations relative to the orbital momenta. These rules agree with the present spin and parity assignment for the ground state of As^{74} based on the β-selection rule for the uniquely forbidden spectra and the fact that the end nuclei are of even-even type having even parity and zero spin.

* On leave from Laboratoire de Chimie-Physique de la Faculté des Sciences de Paris, France.

[1] For a complete list of references see G. T. Seaborg and I. Perlman, Revs. Modern Phys. 20, 585 (1948).
[2] Mei, Mitchell, and Huddleston, Phys. Rev. 79, 19 (1950).
[3] F. Shull and E. Feenberg, Phys. Rev. 75, 1768 (1949).
[4] L. Nordheim, Phys. Rev. 78, 294 (1950).

Retarded Nuclear Interaction

S. T. MA
Institute for Nuclear Studies, University of Chicago, Chicago, Illinois
(Received March 2, 1951)

THE canonical transformation applied by Van Hove[1] to the pseudoscalar meson theory yields, for pure pseudoscalar coupling, the following interaction between a proton and a neutron in an arbitrary coordinate system:

$$H_{n_1n_2,m_1m_2}=-\tfrac{1}{2}f^2\chi_{n_1}(1)\dagger\rho_2\chi_{m_1}(1)\chi_{n_2}(2)\dagger\rho_2\chi_{m_2}(2)\times\left\{\frac{1}{\epsilon_k^2-(\Delta E_1)^2}+\frac{1}{\epsilon_k^2-(\Delta E_2)^2}\right\},\quad(1)$$

where

$$\Delta E_i=E_{n_i}-E_{m_i}\quad(i=1,2).$$

Like Møller's formula for the electrons, (1) involves only Lorentz-invariant quantities, and it is tempting to take it as the potential energy of two nucleons in the energy-momentum space. The presence of the recoil energies in the denominators accounts for the retardation of the meson field. The usual way of dealing with the retarded interaction is the method of the lagrange expansion. The first approximation corresponds to the Yukawa potential $\exp(-\mu r)/r$. The second approximation has been evaluated by Toyoda.[2] For distances comparable with $1/\mu$ the result turns out to be of the same order of magnitude as the first approximation. For this reason it is desirable to treat (1) exactly without resorting

to expansion. This can be done by working with the energy-momentum representation.

An interaction similar to (1) has been derived by Matthews[3] from the Tomonaga-Schwinger formalism. Integrating Matthews' result over a hyperplane perpendicular to the time-axis, we find

$$H_{p_1'p_2',p_1p_2}=-\tfrac{1}{2}f^2(2\pi)^4\psi_{p_1'}(1)\dagger\rho_2\psi_{p_1}(1)\psi_{p_1'}(2)\dagger\rho_2\psi_{p_2}(2)$$
$$\times\exp\left[i(\Delta E_1+\Delta E_2)t\right]\left\{\frac{1}{\epsilon_k^2-(\Delta E_1)^2}+\frac{1}{\epsilon_k^2-(\Delta E_2)^2}\right\}, \quad (2)$$

where the ψ's are creation or destruction operators for the nucleons as defined by Watson and Lepore.[4] The essential difference between (1) and (2) is that the χ's are c-number column-matrices and the ψ's are q-number column-matrices. For a direct transition between states in which the nucleons have positive energies, (1) and (2) lead to the same result. On the other hand, if we apply the perturbation formula

$$\Sigma_c H_{ac}H_{cb}/(E_a-E_c) \quad (3)$$

for indirect transitions with H given by (1) and (2), respectively, it is easily seen that (1) and (2) do not lead to the same result when negative energy states are involved in the intermediate states. This example shows that Dirac's relativistic equation for two particles, which deals with particles with energies of both signs, does not always agree with the hole theory, in which the negative energy states are correlated to pair creation. The situation here is similar to the situation in Weisskopf's calculation of the self-energy of the electron.

When all the states a, b, c in (3) are positive-energy states, (1) and (2) give the same result. This result diverges logarithmically, owing to the cancellation of ϵ_k^2 with $(\Delta E_i)^2$, both of which vary as k^2 at high energies. This divergence is independent of the magnitude of the coupling constant f, and has nothing to do with the question of the convergence of the Born approximations.

It is instructive to compare this divergent result with the finite result obtained by Watson and Lepore[4] from the Feynman-Dyson formalism for the S-matrix due to the exchange of two mesons (reference 4, Sec. IIC). Nambu[5] has suggested the use of the difference between Watson and Lepore's result and the result that follows from (3), with H given by the potential energy of the second order, to define the potential energy of the fourth order. The above consideration shows that the potential energy of the fourth order thus obtained diverges if (1) or (2) is taken to be the potential energy of the second order. This seems to show that the retarded interaction (1) or (2) is unsuitable as the potential energy of the second order.

[1] L. Van Hove, Phys. Rev. **75**, 1519 (1949).
[2] T. Toyoda, Phys. Rev. **77**, 853 (1950).
[3] P. T. Matthews, Phys. Rev. **76**, 1657 (1949).
[4] K. M. Watson and J. V. Lepore, Phys. Rev. **76**, 1157 (1949).
[5] Y. Nambu, Prog. Theor. Phys. **5**, 614 (1950).

Radioactive Hg^{203} and Hg^{205}

W. S. Lyon
Analytical Chemistry Division, Oak Ridge National Laboratory, Oak Ridge, Tennessee[*]
(Received February 19, 1951)

ASSIGNMENTS of the 46-day mercury activity to the Hg^{203} nuclide and the five-minute mercury activity to the Hg^{205} nuclide have been reported previously in the literature.[1,2] Using electromagnetically separated Hg^{202} enriched to 97 percent and Hg^{204} enriched to 89 percent, these mass assignments have been verified, the radiation from Hg^{205} studied, and the thermal neutron activation cross sections for the reactions,

$$Hg^{202}(n,\gamma)Hg^{203}, \quad (1)$$
$$Hg^{204}(n,\gamma)Hg^{205}, \quad (2)$$

with pile neutrons determined.

A 2.37-mg sample of enriched Hg^{202} was irradiated in the ORNL reactor for three weeks together with a cobalt monitor. The decay of portions of the activated sample was followed on both a high pressure ion chamber and a conventional thin end window G-M counter. These data indicate all the activity to have a 46.5-day half-life. Aluminum absorption and coincidence counting data are in accord with the accepted disintegration scheme of a 0.20-Mev β followed by one gamma-ray of 0.280 Mev.[3] Using a total conversion coefficient of 25 percent for the 0.28-Mev gamma, the activity of this source was determined using the high pressure ion chamber and the method described by Overman and Jones.[4] Agreement between this value and that obtained through absolute beta-counting was within 5 percent.

Utilizing the average flux calculated from the Co^{60} activity produced in the cobalt monitor, the isotopic cross section for production of Hg^{203} with pile neutrons was calculated. σ (isotopic) was found to be 3.8 barns; σ (atomic) is thus 1.1 barns. Way and Haines,[5] in the only other available work on the production of Hg^{203}, list σ (isotopic) as 2.4 barns.

A 23.8-mg sample of Hg^{204} was dissolved in dilute HNO_3 and suitable aliquots of this material taken for activation. Active aliquots were evaporated on watch glasses and the decay was followed for several days on a G-M counter equipped with a scaler and continuous recorder. Upon subtraction of the long-lived weak activities due to contaminants in the diluent, the Hg^{205} was found to exhibit a half-life of 5.6 min. Cross sections for neutron capture were obtained by exposing aliquots of Hg^{204}, together with a Mn monitor, in the ORNL reactor for 1190 seconds. Beta-activity of the Hg^{205} was determined by absolute beta-counting. Total Mn^{56} activity induced in the Mn monitor was assessed from ion chamber measurements. Using this figure, the average flux during exposure was calculated. For reaction (2)

$$\sigma\ (\text{isotopic})=0.47\ \text{barn},$$
$$\sigma\ (\text{atomic})=0.032\ \text{barn}.$$

The only other published value for the constant, σ (atomic), is 0.023.[6] The absorption curve data were treated by Feather analysis using P^{32} as a comparator. The range of the simple beta-spectrum was found to be 813 mg/cm² of Al, corresponding to a β_{max} of 1.75 Mev. Krishman and Nahum[7] list 1.62 Mev as the beta end point.

Table I summarizes the experimental data obtained.

TABLE I. Summary of data.

	Hg^{203}	Hg^{205}
$T_{\frac{1}{2}}$	46.5 days	5.6 min
β_{max}	···	1.75 Mev
σ (isotopic)[a]	3.8 barns	0.47 barn
σ (atomic)[a]	1.1 barns	0.032 barn

[a] Pile neutrons.

[*] Based on work performed under the AEC.
[1] H. Slätis and K. Siegbahn, Phys. Rev. **75**, 318 (1949).
[2] R. S. Krishman and E. A. Nahum, Proc. Cambridge Phil. Soc. **36**, 490 (1940).
[3] D. Saxon, Phys. Rev. **74**, 849 (1948).
[4] J. W. Jones and R. T. Overman, AECD-2367 (1948) (unpublished).
[5] K. Way and G. Haines, MonP-405 (1947) (unpublished).
[6] T. I. Taylor and W. W. Havens, Jr., Nucleonics **6**, No. 4, 54 (1950).

Empirical Correlation for a Thermoelectric Property of Superconductors

M. C. Steele and Jules de Launay
Naval Research Laboratory, Washington, D. C.
(Received February 23, 1951)

THE recently published[1] results of the thermoelectromotive force existing at the superconducting-normal junction of a metal showed that the data for tin and thallium fell on the same line when E was plotted as a function of $1-(T/T_c)^2$ on a log-log basis. E is the thermoelectromotive force of the superconducting-normal junction of the same metal, T is the absolute temperature, and T_c is the superconducting transition temperature for zero

magnetic field. The results for tin and thallium suggested that one should seek other properties that are very nearly alike for these two elements with the hope that some general empirical relation might be obtained. It was found that the ratio of T_c/Θ, where Θ is the Debye characteristic temperature, was very nearly the same for tin and thallium. Combining this information with the relation previously given by Steele[2]

$$E_0=\gamma T_c^3/3\epsilon \tag{1}$$

(where γ is the electronic specific heat in the normal state, ϵ is the electronic charge, and E_0 is the value of E at the absolute zero of temperature) suggested that

$$E_0\sim(T_c/\Theta)^2 \tag{2}$$

and

$$\gamma\sim\Theta^{-2}. \tag{3}$$

The γ appearing in Eq. (1) may not be identical to the γ determined from equilibrium phenomena such as specific heat.[1]

The correlation indicated by Eq. (2) can be tested by the recent thermoelectric data. In Table I the pertinent data is given for

TABLE I. Data for the superconductors.

Element	$E_0\times10^4$ volts	T_c°K	Θ°K	$(E_0\Theta^2/T_c^2)\times10^4$ volts
Lead	59.0	7.26	90[a]	9.1
Indium	10.4	3.41	106[b]	10.0
Tin	5.5	3.72	150[c]	9.0
Thallium	5.5	2.40	96[a]	8.8

[a] J. de Launay and R. L. Dolecek, Phys. Rev. 72, 141 (1947).
[b] Value calculated from data of J. R. Clement and E. H. Quinnell, Phys. Rev. 79, 1028 (1950), by assuming that the specific heat in the normal state can be represented by a T^3 law plus a linear term in T.
[c] Value calculated from the combined data of W. H. Keesom and P. H. Van Laer, Physica 5, 193 (1938); and W. H. Keesom and J. N. Van den Ende, Proc. Acad. Sci. Amst. 35, 143 (1932); by assuming that the specific heat can be represented by a T^3 law plus a linear term in T.

lead, indium, tin, and thallium. It is seen that the values of $E_0\Theta^2/T_c^2$ for the particular elements are less than 10 percent different from the mean value of 9.2×10^{-4} volt. In the light of the experimental limitations on the value of E_0 (reported[1] as subject to an error of the order of 10 percent) and the spread in possible values of Θ, it is felt that the data for these four elements substantiates the correlation given by Eq. (2).

Preliminary measurements with mercury ($T_c=4.16$°K) have shown that E_0 for that element is about 250×10^{-4} volt. In order that this be consistent with the results for the other elements and the relation given by Eq. (2), it is necessary that Θ for mercury should be about 25°K. Although this Θ is very much smaller than the value obtained from specific heat measurements ($\Theta=96$°K), it is in fair agreement with the value given by resistance measurements ($\Theta=37$°K).

Additional thermoelectric measurements are needed to test Eq. (2) further. For example, aluminum, with a $\Theta\sim400$°K, would have $E_0\sim10^{-3}$ volt if Eq. (2) were applicable. Such measurements are now in progress at this Laboratory. The results will be reported at a later date.

[1] M. C. Steele, Phys. Rev. 81, 262 (1951).
[2] M. C. Steele, Phys. Rev. 78, 308 (1950).

Further Search for Nuclear Transitions with Lifetimes between 3×10^{-9} sec and 10^{-7} sec*

W. E. Wright† and M. Deutsch
Laboratory for Nuclear Science and Engineering and Department of Physics Massachusetts Institute of Technology, Cambridge, Massachusetts
(Received February 26, 1951)

THE method of delayed coincidences has been utilized in a search for nuclear metastable states with lifetimes less than 10^{-7} sec. Scintillation counters, using stilbene or anthracene with RCA 5819 photomultiplier tubes, were used with wide band amplifiers of a design due to Elmore and a fast electronic coincidence circuit. Under favorable circumstances a half-life of 3×10^{-9} sec could be detected with this apparatus. In most cases studied, the lifetimes were too short to be measured by this apparatus, and only upper limits could be set. Typical curves of coincidence counting rate vs delay and some of the results have been reported previously.[1]

Coincidence absorption studies were undertaken in order that an upper limit on the half-life of a specific transition might be set, even though only prompt coincidences were observed. The detectors were so arranged that both single- and double-channel coincidence absorption experiments could be conducted. Electromagnetic radiation was identified by comparing the observed half-thickness values with the curves published by Glendenin.[2] For the identification of electronic radiation, an empirical range-energy curve was constructed from the observed absorption curves for Dy^{165}, Re^{186}, and Au^{198}. These isotopes were selected because of the simplicity and well-known character of their decay schemes, and because of the wide range in energy of their radiations. In most cases, a determination of the energy and reference to the literature permitted a differentiation between the preceding and succeeding radiations.

The results are summarized in Table I. Column 1 lists the

TABLE I. Observed upper limits on the half-life of excited states.

Daughter isotope	Energy (kev)	Observed $T_{\frac{1}{2}}\times10^9$ sec
Ba^{135}	37	<4
Xe^{131}	82	<4
	284	
Gd^{152}	120	<3
	370	
Ho^{165}	91	<5
W^{183}	114	<4
	310	
Os^{189}	160	<5
Pt^{192}	240	<3
Hg^{199}	160	<3

daughter isotopes of the decays investigated. Column 2 lists the energy in kev of the transition observed. Where two energies are listed for a single isotope, it has not been possible to differentiate between the preceding and succeeding radiation. Column 3 gives in units of 10^{-9} sec the upper limits for the half-life observed for the transitions listed in columns 1 and 2.

The authors wish to thank Professor J. W. Irvine, Jr., and the members of the MIT Cyclotron Group for their advice and assistance in the preparation of the radioactive sources required for these studies.

* This work was supported in part by the joint program of the AEC and ONR.
† Now at ONR Washington, Washington 25, D. C.
[1] M. Deutsch and W. E. Wright, Phys. Rev. 77, 139 (1950).
[2] L. E. Glendenin, Nucleonics 2, No. 1, 12 (1948).

Delayed Coincidence Angular Correlations

Stuart P. Lloyd
Department of Physics, University of Illinois, Urbana, Illinois
(Received February 26, 1951)

WE consider the directional correlation of successive particles emitted in the nuclear cascade $j_1\rightarrow j\rightarrow j_2$, where the j's are the angular momenta of the nuclear levels, when the source is placed in a constant homogeneous magnetic field. The existence of remarkable nuclear spin phase memory phenomena[1] in nonparamagnetic solutions leads one to believe that it might be possible to determine the gyromagnetic ratio of the intermediate

nucleus by observing the angular correlation of the emitted particles as a function of time.[2] One would expect a correlation to persist to times of the order of the total spin relaxation time T_2 of the intermediate nuclei j in the sample, perhaps milliseconds or better.[3] We show here how the theoretical delayed coincidence correlation function describing the effect of the magnetic field is to be obtained from the usual correlation function.

The equations of the Weisskopf-Wigner treatment of the decay[4] can be made to yield a function $W(\Omega_1;\Omega_2;t-t')$ which can be interpreted as the rate (steradian^{-2} sec^{-1}) at which particles of the second transition are emitted at time t with direction $\Omega_2=\theta_2,\varphi_2$ when the preceding particle in the cascade was emitted at time t' with direction $\Omega_1=\theta_1,\varphi_1$, the initial nuclei j_1 being randomly oriented at time zero. As indicated, this rate comes out to be a function of $t-t'$ only, and we refer to it as the delayed coincidence angular correlation function.[5] If ω_0 is the circular Larmor frequency of the intermediate nucleus j in the external magnetic field (along the z-axis), then the delayed coincidence correlation is given by

$$W(\theta_1,\varphi_1;\theta_2,\varphi_2;t)=4\pi\tau_1\exp(-t/\tau)\times\Sigma_{mm'}X_{mm'}(\theta_1,\varphi_1;\theta_2,\varphi_2)\exp(i\omega_0(m-m')t), \quad (1)$$

where

$$X_{mm'}(\theta_1,\varphi_1;\theta_2,\varphi_2)=(2j_1+1)^{-1}(2\pi/\hbar)^3\rho_1\rho_2\delta\Sigma_{m_1m_2}\times[(j_2m_2|\Omega_2,\sigma_2|jm)(jm|\Omega_1,\sigma_1|j_1m_1)\times(j_2m_2|\Omega_2,\sigma_2|jm')^*(jm'|\Omega_1,\sigma_1|j_1m_1)^*]. \quad (2)$$

In Eq. (1), τ_1 and τ are the lifetimes of the initial and intermediate nuclei, respectively, and in Eq. (2), δ is the invariant summation over the spin coordinates σ_1 and σ_2 of the emitted particles, and ρ_1 and ρ_2 are densities-in-energy of the states of the emitted particles. The usual instantaneous angular correlation[6] is

$$W(\theta_1,\varphi_1;\theta_2,\varphi_2)=\tau W(\theta_1,\varphi_1;\theta_2,\varphi_2;0)=4\pi\tau\tau_1\Sigma_{mm'}X_{mm'}(\theta_1,\varphi_1;\theta_2,\varphi_2), \quad (3)$$

normalized to $\int W(\theta_1,\varphi_1;\theta_2,\varphi_2)(d\Omega_1/4\pi)d\Omega_2=1$. It is actually a function only of the angle θ between Ω_1 and Ω_2, of course.

The transformation properties of the nuclear matrix elements[7] can be used to obtain

$$X_{mm'}(\theta_1,\varphi_1;\theta_2,\varphi_2)=X_{mm'}(\theta_1,\varphi_1;\theta_2,\varphi_2+\alpha)\exp(i\alpha(m'-m))$$

for rotations of Ω_2 by angle α around the z-axis. If this is substituted into Eq. (1) with $\alpha=\omega_0 t$, one discovers that

$$W(\theta_1,\varphi_1;\theta_2,\varphi_2;t)=(1/\tau)\exp(-t/\tau)W(\theta_1,\varphi_1;\theta_2,\varphi_2+\omega_0 t). \quad (4)$$

The delayed coincidence angular correlation pattern is just the instantaneous pattern precessing with the intermediate nucleus around the external field.[8] If the instantaneous correlation is given as a power series in $\cos\theta$, the corresponding delayed coincidence correlation is obtained as a fourier series in $\omega_0 t$ by transforming the instantaneous correlation to a Legendre series:[9] $W(\theta)=\Sigma\gamma_l P_l(\cos\theta)$, and then applying the spherical harmonic addition theorem[9] to

$$P_l(\cos\theta)=P_l(\cos\theta_1\cos\theta_2+\sin\theta_1\sin\theta_2\cos(\varphi_1-\varphi_2)).$$

For example, the instantaneous correlation $W(\theta)=1+r\cos^2\theta=1+(r/3)+(2r/3)P_2(\cos\theta)$ gives the delayed coincidence correlation (omitting the decay and normalization factors):

$$W(\theta_1,\varphi_1;\theta_2,\varphi_2;t)=1+(r/3)+(r/6)(3\cos^2\theta_1-1)(3\cos^2\theta_2-1)+(r/2)\sin2\theta_1\sin2\theta_2\cos(\varphi_1-\varphi_2-\omega_0 t)+(r/2)\sin^2\theta_1\sin^2\theta_2\cos2(\varphi_1-\varphi_2-\omega_0 t). \quad (5)$$

In general, the odd harmonics of $\omega_0 t$ drop out if either counter is in the equatorial plane, θ_1 or $\theta_2=90°$; and there are no oscillating terms at all if either counter is on the axis, θ_1 or $\theta_2=0°$ or 180°. The relative amplitudes of the various harmonics are complicated functions of θ_1 and θ_2, in general, and the best position for the counters has to be worked out for each case separately. For the correlation (5), one maximum of the first harmonic amplitude relative to the non-oscillating terms occurs when both counters are on the cone:

$$\cos^2\theta_1=\cos^2\theta_2=(1/2)-(r/(8+6r))+O(r^2).$$

It is to be noted that both the instantaneous correlation and the gyromagnetic ratio of nucleus j can be determined by measuring the distribution of pulses in time in one counter; e.g., if the counter is in the equatorial plane, $W(90°,\varphi;90°,\varphi;t)=(1/\tau)\exp(-t/\tau)W(\omega_0 t)$, where $W(\theta)$ is the instantaneous correlation.

If the highest power of $\cos\theta$ in the instantaneous correlation is $\cos^L\theta$, the delayed correlation contains harmonics up to $\cos(L\omega_0 t)$, and the total gate width Δt should be narrow enough so that these harmonics are not washed out by averaging over the gates: if $L\omega_0\Delta t\geq1$, gate width correction factors must be introduced. For the same reason, the variation $(T_2^*)^{-1}$ of the Larmor frequency due to inhomogeneities in the applied magnetic field should be kept small compared to $(L\tau)^{-1}$.

I wish to thank Professor A. T. Nordsieck for a discussion of the Weisskopf-Wigner method and Dr. C. P. Slichter for discussions on the nature of the fields in material media.

[1] E. L. Hahn, Phys. Rev. 80, 580 (1950). The spin echo effect involves free Larmor precessions of protons in water of up to 10^6 revolutions at 30 Mc.
[2] Sunyar, Alburger, Friedlander, Goldhaber, and Scharff-Goldhaber, Phys. Rev. 79, 181 (1950).
[3] Bloembergen, Purcell, and Pound, Phys. Rev. 73, 679 (1948).
[4] V. Weisskopf and E. Wigner, Z. Physik 63, 54 (1930).
[5] G. Goertzel deals essentially with $\int_0^\infty W(\Omega_1;\Omega_2;t)dt$ in his investigation of the effect of hyperfine structure interactions in $\gamma-\gamma$-angular correlations; Phys. Rev. 70, 897 (1946). We assume that there are no such fields at the nucleus in the liquid sample.
[6] D. L. Falkoff and G. E. Uhlenbeck, Phys. Rev. 79, 323 (1950).
[7] S. P. Lloyd, Phys. Rev. 80, 118 (1950).
[8] This was suggested by Professor M. Goldhaber (private communication).
[9] The necessary formulas can be found in W. E. Byerly, *Fourier Series and Spherical Harmonics* (Ginn and Company, 1893), pp. 179, 211, 199.

Electron Density and Light Intensity Decay in Cesium Afterglows*

P. Dandurand† and R. B. Holt
Department of Physics, Harvard University, Cambridge, Massachusetts
(Received February 20, 1951)

THE decay of the electrodeless discharge through purified cesium has been studied by the previously described techniques[1] of microwave electron density, optical spectrographic, and optical light intensity measurements as a function of time after termination of the exciting fields. In the pressure range 0.02 to 0.1 mm, we found that the electron density, n, decays exponentially with a time constant, τ_1, increasing with pressure from 0.4 millisecond at 0.02 mm to about 1 millisecond at 0.1 mm. A minimum in the light intensity is found at 40 microseconds after cut-off, followed at about 80 microseconds by a broad maximum. The ratio I_{max}/I_{min} is about 8 at the lowest pressure and decreases with pressure. Higher input power during the discharge moves the maximum to shorter times. After the maximum, the light intensity decay is exponential with an associated time constant τ_2 consistently closely equal to $\tau_1/2$, which shows that the light intensity is proportional to n^2. Spectrograms show an intense line spectrum during the discharge, the usual CsI spectrum coexisting with a great number of other lines belonging to the excited cesium ion. In the afterglow, however, the spectrum is practically a pure band spectrum, which was not analyzed in detail, but which shows up in the same wavelength range as the bands found previously in absorption in cesium vapor.[2]

The low pressure electron density data follows the behavior expected for ambipolar diffusion quite well. In order to compare the ion mobility data for cesium ions through cesium vapor with previous measurements[3] of the mobility of cesium ions through rare gases, the electron temperature at moderate times in the afterglow at a pressure of 0.036 mm was estimated by a standard kinetic theory calculation as 1400°K. On this basis, our data gives a value of the mobility, k_0, of about 50 cm^2/volt-sec calculated for 1-mm pressure and 0°C. This value is rather surprising, since the measured values of the mobility of cesium ions through rare

gases are on the order of 10^9. The formation of molecular ions and the possibility of some mechanism such as charge exchange may be used to explain the low observed value of the effective mobility of cesium ions in cesium.

Above about 0.3-mm pressure, electron density decay follows the recombination law, $dn/dt=-\alpha n^2$, very well. The recombination coefficient, α, has a value of the order of 10^{-7} cm³/ion-sec. At constant temperature this coefficient is found to be pressure dependent. At 270°C, for instance, α varies from 3.5×10^{-7} at 0.32-mm pressure to 1.2×10^{-6} at 0.68 mm. At 285°C α varies from 3.5×10^{-7} at 1 mm to 1.45×10^{-6} at 2.6 mm. At times in the afterglow greater than 400 microseconds the light intensity is again found to be proportional to the square of electron density. At shorter times, however, this relationship does not hold, indicating that recombination is initially somewhat slower. The use of simple optical filters shows that the red portion of the spectrum decays initially somewhat faster than the violet. Spectrograms show much less of the cesium ion line spectrum during the discharge than was found at low pressures. The afterglow spectrum is again almost purely molecular.

Our data are in agreement with the following mechanism for recombination-type electron removal in the afterglow. Cesium molecular ions are formed in triple collisions between an atomic ion and two neutral molecules. This is followed by recombination between molecular ions and electrons. This process results in the formation of excited molecules which radiate a band spectrum in the afterglow, thus making dissociative recombination an unlikely explanation for the high values of recombination coefficient observed. The initial maximum of the light intensity as observed at low pressure would then correspond to the initial increase of molecular ion concentration (since the concentration of such ions during the discharge is probably small, as evidenced by the line spectrum observed) followed by a decrease due to diffusion to the walls and recombination. It is quite possible that some equilibrium ratio between the density of atomic and molecular ions develops in the afterglow. This ratio would depend on pressure, a larger proportion of the ions being molecular at higher pressures. This would explain the observed pressure variation of α if we assume also that the recombination coefficient for molecular ions is the limiting value observed at high pressure and that the recombination coefficient for atomic ions is much smaller.

No dependable values for the absolute light intensity were obtained in this work (as have been obtained in this laboratory for several other gases), because the spectrograms showed that most of the energy was concentrated in the infrared, beyond the range of our photomultiplier equipment.

* Assisted by the ONR.
† Present address: 52 rue Vancau, Paris 7, France.
[1] Holt, Richardson, Howland, and McClure, Phys. Rev. **77**, 239 (1950).
[2] F. W. Loomis and P. Kusch, Phys. Rev. **46**, 292 (1934).
[3] C. F. Powell and L. Brata, Proc. Roy. Soc. (London) **A138**, 129 (1932).

Charge Renormalization in the Hartree Approximation*

HARTLAND S. SNYDER
Brookhaven National Laboratory, Upton, Long Island, New York
(Received February 28, 1951)

THE field equations and canonical commutation relations of the Dirac-Maxwell fields are

$$[\gamma_\mu[(\partial/\partial x_\mu)-ie_0A_\mu^0/\hbar]+\kappa]\psi(x)=0, \quad (1)$$

$$\Box A_\mu^0=J_\mu^{0\,\mathrm{ext}}(x)+\tfrac{1}{2}ic_0[\psi^+(x),\gamma_\mu\psi(x)], \quad (2)$$

$$[\psi^+(\mathbf{r},t),\psi(\mathbf{r}',t)]_+=\gamma^4\delta(\mathbf{r}-\mathbf{r}'), \quad (3)$$

$$[A_\mu^0(\mathbf{r},t),\partial A_\mu^0(\mathbf{r}',t)/\partial t]=i\hbar\delta(\mathbf{r}-\mathbf{r}'), \quad (4)$$

in which $J_\mu^{0\,\mathrm{ext}}(x)$ is the external charge and current distribution. If one uses the Hartree approximation of replacing the electron-positron current operator $J_\mu^0(x)=\frac{1}{2}ic_0[\psi^+(x),\gamma_\mu\psi(x)]$ by its expectation value $\langle J_\mu^0(x)\rangle$ in Eq. (2), one obtains

$$\Box A_\mu^0=J_\mu^{0\,\mathrm{ext}}(x)+\langle J_\mu^0(x)\rangle. \quad (5)$$

Any covariant gauge invariant evaluation of $\langle J_\mu^0(x)\rangle$ for the "vacuum" state[1] gives the following form:

$$\langle J_\mu^0(x)\rangle_{\mathrm{vac}}=-a\Box A_\mu^0(x)-\int K^0(x-x')\Box' A_\mu^0(x')dx' \quad (6)$$

for the parts of $\langle J_\mu^0(x)\rangle$ which are linear in the field strength, and we will neglect all nonlinear effects. In Eq. (6) $K^0(x-x')$ is an invariant function of $(x-x')$ which describes the Uehling effect and which is not as singular as a δ-function. Combining Eq. (5) and Eq. (6), one obtains

$$(1+a)\Box A_\mu^0+\int K^0(x-x')\Box A_\mu^0(x')dx'=J_\mu^{0\,\mathrm{ext}}(x). \quad (7)$$

Carrying out a charge and field renormalization, one obtains

$$\begin{aligned} &A_\mu=(1+a)^{\frac{1}{2}}A_\mu^0, && e=(1+a)^{-\frac{1}{2}}e_0,\\ &J_\mu^{\mathrm{ext}}(x)=(1+a)^{-\frac{1}{2}}J_\mu^{0\,\mathrm{ext}}, && K(x-x')=(1+a)^{-1}K^0(x-x'),\\ &J_\mu(x)=(1+a)^{-\frac{1}{2}}J_\mu^0(x). \end{aligned} \quad (8)$$

Under this renormalization, Eqs. (1) and (5) remain unaltered in form apart from the Uehling terms, but e_0 is replaced by e, and $e_0A_\mu^0$ is replaced by eA_μ. Equation (3) remains unaltered, while (4) becomes

$$[A_\mu(\mathbf{r},t),\partial A_\mu(\mathbf{r}',t)/\partial t]=i\hbar(1+a)\delta(\mathbf{r}-\mathbf{r}'). \quad (9)$$

The fact that these equations maintain the same form shows that a charge renormalization will not change the energy levels of atomic systems except for the Uehling terms implied by $K(x-x')$, if the experimental value of $e^2/\hbar$ is used. However, by Eq. (9) we see that the value of Planck's constant for the electromagnetic field will be larger than the Planck's constant of the matter field by the factor $1+a=(e_0/e)^2$. We thus see that charge renormalization is not consistent with the canonical formalism, at least in the Hartree approximation. We note, however, that if one insists on evaluating a so that it is nonvanishing, the error introduced by this can be corrected by reducing the electromagnetic field commutators by the factor $1/(1+a)$.

If the commutator relation Eq. (9) is to remain consistent in time with the equations of motion, Eq. (7), one may infer that $\Box A_\mu(x)=J_\mu^*(x)$, in which $J_\mu^*(x)$ is the experimental external current distribution. Thus, one obtains

$$J_\mu^*(x)+\int K(x-x')J_\mu^*(x')dx'=J_\mu^{\mathrm{ext}}(x). \quad (10)$$

We now note that the conventional evaluation[2] of $K(x-x')$ is such that $J_\mu^*(x)$ is not uniquely determined by the fictitious external charge and current distribution $J_\mu^{\mathrm{ext}}(x)$, because Eq. (10) has nonvanishing solutions when $J_\mu^{\mathrm{ext}}(x)$ is put equal to zero. Since it is $J_\mu^*(x)$ which determines the energy levels of atomic systems, it is convenient to arrange the calculation of the ambiguous quantity $\langle J_\mu(x)\rangle_{\mathrm{vac}}$ so that its parts, which are linear in the field strengths, vanish identically. This can be done.[3]

* Research carried out at Brookhaven National Laboratory, under the auspices of the AEC.
[1] R. Serber, Phys. Rev. **48**, 49 (1935).
[2] J. Schwinger, Phys. Rev. **75**, 651 (1949).
[3] H. S. Snyder, Phys. Rev. **79**, 520 (1950).

Diffuse X-Ray Scattering by Disordered Binary Alloys

WILLIAM J. TAYLOR
Department of Chemistry, Ohio State University, Columbus, Ohio
(Received February 23, 1951)

THE x-ray scattering from binary alloys of the substitutional type shows two effects due to the degree of order (or disorder): (1) Sharp superlattice reflections when long range order is present; and (2) diffuse scattering which depends on the degree of short range order. Theoretical intensity formulas for these two types of scattering have been given by MacGillavry and Strijk[1]

for body- and face-centered cubic lattices. In the present note a general method of treatment is outlined which introduces the short range order parameters in a particularly straightforward way. For this purpose we introduce a parameter $\mu_k{}^L$ which has the value $+1$ if an A atom is at the kth site in the Lth cell, and the value -1 if a B atom is at this site. This is a device similar to that used in the statistics of the Ising lattice.[2] The atomic structure factor at the k, L site can then be represented as

$$f_k{}^L = \tfrac{1}{2}(f_A+f_B)+\tfrac{1}{2}(f_A-f_B)\mu_k{}^L, \tag{1}$$

where f_A and f_B are the structure factors for the two types of atoms. The mean value of $\mu_k{}^L$ is

$$\bar{\mu}_k = (1/N)\sum_L \mu_k{}^L = x_A{}^k - x_B{}^k, \tag{2}$$

where $x_A{}^k$ and $x_B{}^k$ are the fractions of the N sites of type k which are occupied by A and B atoms, respectively. $\bar{\mu}_k$ is obviously a measure of the long range order in the kth sublattice. The mean structure factor at the kth type of site is

$$\bar{f}_k = (1/N)\sum_L f_k{}^L = f_A x_A{}^k + f_B x_B{}^k, \tag{3}$$

while the *fluctuation* at the k, L site may be written in the form,

$$\phi_k{}^L = (f_k{}^L - \bar{f}_k) = \tfrac{1}{2}(f_A-f_B)(\mu_k{}^L - \bar{\mu}_k). \tag{4}$$

We now follow closely the method of Zachariasen[3] to obtain the following formula for the intensity of diffuse scattering,

$$I_D = \tfrac{1}{4}NI_e(f_A-f_B)^2\sum_{k,k'}\exp[i\mathbf{s}\cdot(\mathbf{r}_k-\mathbf{r}_{k'})] \times\sum_M \alpha_{kk'}{}^M \exp(-i\mathbf{s}\cdot\mathbf{A}_M). \tag{5}$$

(I_e = scattering by a single electron; $\mathbf{A}_M = M_1\mathbf{a}_1+M_2\mathbf{a}_2+M_3\mathbf{a}_3$ = direct lattice vector; $\mathbf{r}_k$ = position vector of kth site; $\mathbf{s} = 2\pi(\mathbf{k}-\mathbf{k}_0)$ = Bragg vector).[3] In the present case $\mathbf{s}$ is to be regarded as a continuously variable vector in reciprocal space. The intensity I_D is periodic in reciprocal space provided the sites, k, k', $\cdots$, occur at rational positions in the unit cell (e.g., body or face centering). The fourier coefficients of the diffuse scattering, $\alpha_{kk'}{}^M$, are related to the $\mu_k{}^L$'s as follows,

$$\alpha_{kk'}{}^M = \mu_{kk'}{}^M - \bar{\mu}_k\bar{\mu}_{k'}, \tag{6}$$

$$\mu_{kk'}{}^M = (1/N)\sum_L \mu_k{}^L\mu_{k'}{}^{L-M}. \tag{7}$$

These parameters will fall into equivalent sets if the crystal has nontrivial symmetry. $\mu_{kk'}{}^M$ has the properties of a short range order parameter. In fact, if the fraction of the N pairs of sites, k, L and k', $L-M$ (all L), which are occupied by *like* atoms (AA or BB, as opposed to AB or BA) is denoted by $z_{kk'}{}^M$, it is obvious that

$$\mu_{kk'}{}^M = z_{kk'}{}^M - (1-z_{kk'}{}^M) = 2z_{kk'}{}^M - 1. \tag{8}$$

For $M=0$, $k=k'$, $\mu_{kk}{}^0=1$, and $z_{kk}{}^0=1$. For *perfect* long range order, $\alpha_{kk'}{}^M=0$, $\mu_{kk'}{}^M=\pm1$, and $z_{kk'}{}^M=0$ or 1, depending on the pair of sites in question. The diffuse scattering, I_D, vanishes identically for a perfectly ordered lattice.[4] The limiting values of these parameters as $|M|\to\infty$ are: $\alpha_{kk'}{}^\infty=0$; $\mu_{kk'}{}^\infty=\bar{\mu}_k\bar{\mu}_{k'}$; and $z_{kk'}{}^\infty = x_A{}^k x_A{}^{k'} + x_B{}^k x_B{}^{k'}$. These are also their *average* values (over M).

In the absence of long range order $x_A{}^k$, $x_A{}^{k'}$, and $x_B{}^k$, $x_B{}^{k'}$, may be replaced by x_A and x_B, the over-all fractions of A and B atoms, in all the preceding formulas. In addition, all sites are then usually equivalent, so that a primitive cell containing a single site may be selected. Setting $k=k'=1$, Eq. (5) then reduces to

$$I_D = \tfrac{1}{4}NI_e(f_A-f_B)^2\sum_M \alpha_{11}{}^M \exp(-i\mathbf{s}\cdot\mathbf{A}_M). \tag{9}$$

Inversion of Eq. (9) yields

$$\alpha_{11}{}^M = (4V/N)\int (I_D/I_e)(f_A-f_B)^{-2}\exp(i\mathbf{s}\cdot\mathbf{A}_M)d\mathbf{s}, \tag{10}$$

where the integration is over a single "phase cell" surrounding any reciprocal lattice point[3] (V = volume of primitive cell in direct lattice).

A detailed investigation of diffuse x-ray scattering by the disordered alloy Cu_3Au (face-centered cubic lattice) has been carried out by Cowley.[5] Cowley's interpretation of the fourier coefficients of the diffuse scattering is not entirely in accord with that arrived at here. A consideration of his method of normalization indicates that his α_{lmn} (as tabulated in Table I of reference 5) are equal to $(\alpha_{11}{}^M/\alpha_{11}{}^0)$ in the present notation. From the preceding equations, $\alpha_{11}{}^0=\frac{1}{4}$, and $\alpha_{11}{}^M = 2(z_{11}{}^M - z_{11}{}^\infty)$. Therefore, the quantities tabulated in the last three columns of Cowley's Table I need only be multiplied by $\frac{1}{2}$ to obtain $z_{11}{}^M - z_{11}{}^\infty$, the fluctuation of $z_{11}{}^M$ about its limiting (or average) value. The latter is $z_{11}{}^\infty = \frac{3}{8}$, in this case (in the absence of long range order). As an example, at 405°C $z_{11}{}^M$ has the values 0.568 for nearest neighbors, and 0.695 for next-nearest neighbors, as compared with the limiting value 0.625, and the values $\frac{1}{2}$ and 1, respectively, for perfect order.[6]

[1] C. H. MacGillavry and B. Strijk, Physica **11**, 369 (1946).
[2] G. H. Wannier, Revs. Modern Phys. **17**, 50 (1945).
[3] W. H. Zachariasen, *Theory of X-Ray Diffraction in Crystals* (John Wiley and Sons, Inc., New York, 1945), pp. 213–216.
[4] Other forms of disorder scattering may occur, of course (e.g., that due to thermal vibrations). The intensity I_D of Eq. (5) does not include the superlattice reflections which may appear if long range order is present, and which are essentially as sharp as ordinary Laue-Bragg reflections (in the absence of complicating factors, such as *anti-phase* domains). The intensities of these reflections may be calculated from the *mean structure factors* of Eq. (3).
[5] J. M. Cowley, J. Appl. Phys. **21**, 24 (1950).
[6] The fractional value $\frac{1}{2}$ is not inconsistent with the previous statement that $z=0$ or 1 for perfect order. Inspection of the ordered Cu_3Au structure will show that in averaging over all pairs of nearest neighbors, like pairs ($z=1$) and unlike pairs ($z=0$) occur with equal frequency, leading to the average value $\frac{1}{2}$.

Emulsion Studies of Cosmic-Ray Stars Produced in Metal Foils*

IAN BARBOUR
Kalamazoo College, Kalamazoo, Michigan
(Received March 5, 1951)

WE have described, and given preliminary results[1] from, a method in which cosmic-ray induced disintegrations of nuclei of several elements are studied with metal foils "sandwiched" between pairs of G5 emulsions placed face-to-face. After high altitude exposure, removal of foils, and development, the original alignment of the plates is reconstructed so that they can be scanned, and groups of tracks originating in disintegrations of foil nuclei can be projected back to common centers between the emulsions. Hodgson has recently reported[2] analysis of stars from disintegration of nuclei of a lead foil in contact with a single photographic plate. Advantages of the "sandwich" method, besides the doubled probability for a particle to enter the emulsion, are (a) elimination of frequent spurious coincidences of unrelated cross tracks; (b) lower probability of missing a star, since the scanner not only looks for converging tracks, but also, in the case of every track seen, looks for its continuation in the opposite emulsion which would eliminate it from consideration as a possible member of a foil disintegration; (c) the probability that a particle from an observed foil star not be detected (because it stops in the foil or strikes the emulsion too far from the field-of-view) is almost independent of the point within the foil at which the disintegration occurs, since the increased detection probability for tracks in the plate nearer the disintegrating nucleus is compensated for by the decreased detection probability in the further plate.

Figure 1 summarizes the uncorrected cross-section data to date for six elements ranging in atomic weight from 27 to 197. Typical statistical probable errors are indicated at intervals for each element. The differential distributions (given by the *slopes* of the curves in Fig. 1) are of the form ϵ^{-kn} in the region of larger stars ($n>Z/4$), where for $Z>40$, $k\sim0.2$, increasing for low Z to perhaps twice that value for Al; for smaller n the differential distributions tend to level off to about the same value for all the elements, though correction for stars completely missed would somewhat increase the values for small stars, especially $n=3$ and 4. In Fig. 2

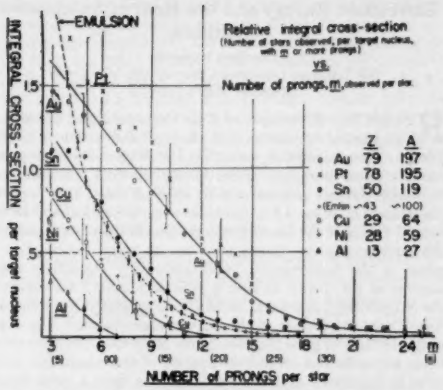

FIG. 1. Relative integral cross sections (number of stars observed, per target nucleus, with m or more prongs) are plotted for several elements against m, the number of prongs observed. Data for emulsion stars are plotted on a scale of n, the number of prongs actually leaving the disintegrating nucleus (see text).

the data have been replotted against atomic weight for stars of different sizes. The slopes of the lines are indicated, decreasing as smaller stars are included, and probable errors are shown for stars of 4 or more observed prongs. Estimated extrapolation to include stars of *all* sizes indicates a total cross section close to $A^{2/3}$.

Emulsion stars are shown in Fig. 1 for comparison; while their statistical errors are small, for 1630 stars were analyzed, uncertainties exist in (a) the ordinate, which depends on the assumed thickness of the emulsion, and its effective number of atoms per cm[3]. For the latter we have used the *equivalent* number of atoms of atomic weight 100 (intermediate between Ag and Br) that would give the same cross section as the emulsion constituents, assuming the manufacturer's analysis and a dependence on atomic weight as discussed above. (This equivalent number is not very sensitive to the exponent.) (b) For comparison with the foil curves, the emulsion stars should be plotted on an abscissa of n, the actual number of prongs in the disintegration. The probability, m/n, of detecting a particle from the observed disintegration of a foil nucleus depends on the stopping power and thickness of the foil and the diameter of the field of view, and varies slightly with the position of the disintegrating nucleus in the foil and with the size of the star; but for these foils calculations of this ratio did not vary greatly from an average value of about 2/3.

The resulting emulsion curve approximates, for $n>6$, that which one might expect for $A=100$. The greater number of smaller stars can readily be accounted for by the known percentages of lighter elements in the emulsion. The average slope of the integral distribution of emulsion stars of 4, 5, and 6 prongs is about 3 times that of the line obtained by projecting to small n the emulsion curve for larger stars (that is, the curve which one would anticipate for $A=100$ by comparison with the foil curves). This would indicate that of the small stars found in emulsion, approximately twice as many can be attributed to the lighter elements present as to Ag and Br. There is, however, considerable uncertainty in this value, because the data for small stars in the foils are less reliable; a differential prong distribution will be given upon completion of scanning and rechecking and more careful analysis of corrections. There will also appear an analysis of measurements made on the energy of each particle in the foil stars and the angular distribution to determine their dependence upon atomic weight as compared with theoretical calculations. Only a few "showers" of minimum-ionization particles, usually interpreted as mesons, have been observed, but these yield some information concerning the variation with atomic weight of meson-production

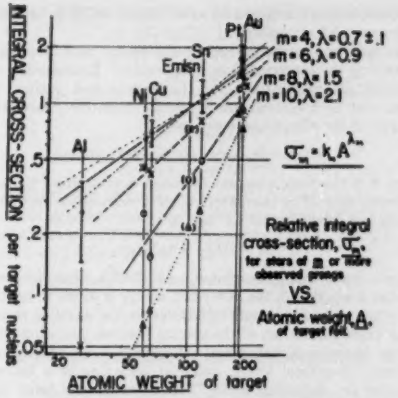

FIG. 2. Integral cross sections σ_m atomic weight of foil for stars of m or more prongs are shown on a double-log plot for four values of m.

cross sections at these energies. Several students have assisted in this work: James Bailey, Milton Meux, Mel Reed, and Dick Wilson.

* This work has been aided by a Cottrell Grant from the Research Corporation.

[1] J. Barbour and L. Green, Phys. Rev. 79, 406 (1950).

[2] P. E. Hodgson, Phil. Mag. 42, 92 (1951).

Natural Spread of the Conic Distribution of the Čerenkov Radiation

YIN-YUAN LI
Physics Department, University of Illinois, Urbana, Illinois
(Received February 26, 1951)

BECAUSE of the existence of a high degree of partial coherence of the wavelets from succeeding free paths, the natural spread of the Čerenkov radiation was very much overestimated in a previous letter.[1] The coherent path length of an electron is much closer to the actual length of travel in the material than it is to the mean free path between emissions of quanta. R. L. Mather of Berkeley has observed with proton beams that the half-breadth of the ray directions is less than the minimum predicted in the letter, when the effects of dispersion are removed. He has also observed a rainbow spectrum.

My sincere thanks are due Professor L. I. Schiff and Mr. R. L. Mather for their kind communications.

[1] Yin-Yuan Li, Phys. Rev. 80, 104 (1950).

Theoretical Low Temperature Spectra of the Thallium Activated Potassium Chloride Phosphor

FERD E. WILLIAMS
General Electric Research Laboratory, Schenectady, New York
(Received March 5, 1951)

A FUNDAMENTAL calculation of the absorption and emission spectra of KCl:Tl has been recently reported.[1] From the properties of the constituent ions the potential energy was computed for $^1S_0$ and $^3P_1{}^0Tl^+$ substituted for K^+ in KCl as a function of a precise configuration coordinate, namely, the Tl^+ nearest Cl^- neighbor distance with the condition that the remainder of the lattice rearranges to minimize the total energy. A classical distribution of atomic configurations characteristic of

the initial state yielded spectra at 80°K and 298°K in satisfactory agreement with experiment.

The quantum-mechanical zero-point energy must be considered in deriving the spectra at low temperatures. Examination of the potential energy contours for the ground and excited states reveal that both systems are harmonic oscillators; therefore, the energies of the vibrational levels are[2]

$$E_n = \hbar(k/M)^{\frac{1}{2}}(n+\tfrac{1}{2}),$$

where k is the force constant obtained directly from the energy contours, and M is the effective mass derived as the following function of the masses of Cl^- and K^+:

$$M = 6M_{Cl^-} + 6\alpha^2 M_{K^+},$$

where α is a coupling constant equal to 0.4264. With the quantum number n equal to 0, the zero-point energy is found to be 0.00830 ev for the ground state and 0.00513 ev for the emitting state.

An exact calculation of the spectra involves summing over the matrix elements for all initial vibrational levels combined with all final vibrational levels, weighted according to a Boltzmann function for the initial levels. This calculation is being investigated. However, because the accessible final vibrational levels involve n of the order of 50, the final state may be considered classically by the correspondence principle, and only the initial state need be considered quantum mechanically. The absorption spectrum is

$$P(\Delta E) = C \sum_{n=0,1,2\ldots} \frac{\exp(-E_n/kT)}{2^n n!} |H_n(\xi_n)|^2 \exp(-\xi_n^2) \frac{\partial a_n}{\partial \Delta E},$$

where C is a normalization constant, ΔE is the transition energy from the nth initial level to the potential energy contour for the final state, $H_n(\xi_n)$ is the nth hermite polynomial of ξ_n, and

$$\xi_n = (Mk)^{\frac{1}{4}}\hbar^{-\frac{1}{2}}(a_n - a_0),$$

where a_n is the configuration of the nth initial level yielding the transition energy ΔE, and a_0 is the equilibrium configuration of the ground state.

The computed absorption spectra at 4°K, 80°K, and 298°K are shown in Fig. 1. The spectra at 80°K and 298°K differ only

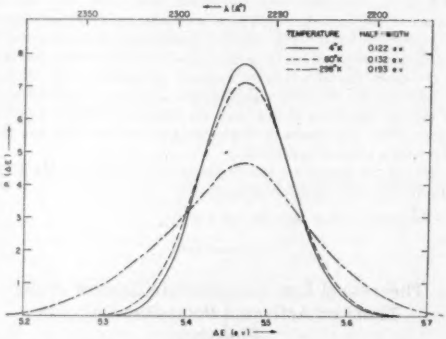

FIG. 1. Theoretical absorption spectra of KCl:Tl at 4°K, 80°K, and 298°K.

slightly from the classical results.[1] It is predicted that reducing the temperature of KCl:Tl below 80°K will not appreciably narrow the absorption band. Similar considerations apply to emission. Experimental measurements are in progress in this laboratory to test these predictions. The author is indebted to M. H. Hebb for helpful discussions.

[1] F. E. Williams, Phys. Rev. 80, 306 (1950); J. Chem. Phys. 19, 457 (1951).
[2] Eyring, Walter, and Kimball, *Quantum Chemistry* (John Wiley and Sons, Inc., New York, 1944), p. 75.

Correlation Energy and the Heat of Sublimation of Lithium

CONYERS HERRING
Bell Telephone Laboratories, Murray Hill, New Jersey
(Received March 5, 1951)

RECENTLY Silverman and Kohn[1] have published a quantum-mechanical calculation of the heat of sublimation of metallic lithium. This calculation, based on the Wigner-Seitz approach, corrects some numerical errors in the previous literature and introduces further refinements. In spite of these, they report a discrepancy of about 4 kcal/mole between theoretical and experimental values of the binding energy. One is therefore faced with the question: is the discrepancy due to some combination of errors in the experimental value and easily correctible shortcomings of the theory, or does it indicate a basic inadequancy of the Wigner-Seitz approach, as has been suggested by Kuhn and Van Vleck[2] in the case of the heavier alkali metals? The object of this letter is to show that the former is the case, the discrepancy being primarily due to underestimation of the correlation energy term in the theory and to adoption of too large a value for the experimental heat of sublimation.

In the Wigner-Seitz method one obtains a solution of the self-consistent field problem for an assembly of electrons moving in the superposition of the potential fields of all the ions of the crystal.[3,4] The correlation energy may be defined as the difference between the energy of this self-consistent field solution and the true ground-state energy of an assembly of electrons moving in the given ion core fields. In the past it has usually been assumed that the correlation energy for metal electrons is the same as for a free electron gas of the same density, for which fairly reliable estimates are available.[5,6] However, if the electrons in the metal have an effective mass m^* appreciably different from the true electron mass m, it is obviously more correct to use the correlation energy for a gas of free particles of mass m^*. This procedure must be correct in the limiting case of a hypothetical metal with a very small number of electrons per atom, since the coulomb matrix elements and energy differences among pairs of low energy determinantal wave functions will be asymptotically the same as for free particles of charge e and mass m^*, and since Macke[6] has shown that a quite satisfactory value of the correlation energy can be derived from a variational expression involving only the matrix elements and energy differences between states whose excitation energy is of the same order as the Fermi energy per particle. Since electrons with energies$\gg$those of the first Brillouin zone behave on the average as expected for mass m, the correlation energy for a half-filled zone may be expected to be intermediate between the values for m and for m^*, probably closer to the latter. For mass m^*, Wigner's[5] expression for the correlation energy becomes $0.58/(r_s+5.1m/m^*)$ rydbergs per electron, where r_s is the radius of the sphere equivalent to an atomic cell. For lithium, $m/m^*=0.727$[1], and the correlation expression just written exceeds the free electron value by 0.014 rydbergs per atom or 4.3 kcal/mole.

The coulomb and exchange energies, for which Silverman and Kohn also assumed the free electron values, differ from these values by amounts which, though smaller than the above, are worth mentioning for completeness. Seitz[4] has shown that the former exceeds the value for a uniform charge distribution by only about 0.6 kcal/mole. The difference between the exchange energy and that of free electrons of the same density is a little larger: a rough calculation by a formula due to Hill and the author[7] gives a value which is numerically smaller by about 2.2 kcal/mole than for free electrons. As was shown in reference 7, this formula is asymptotically valid for low electron densities, but for the density actually occurring it undoubtedly underestimates the exchange energy. This error tends to compensate the error in the correlation estimate of the preceding paragraph. The exchange correction calculated in this way has the opposite sign from that computed by Seitz.[4] The latter involves a computational error, since the

dominant term in Seitz' expression arises from the second term in his Eq. (25), which can be shown to vanish identically.

On the experimental side, the heat of sublimation can be deduced from the vapor pressure data in the literature,[8] either by using the slope of a vapor pressure plot or by using the third law of thermodynamics together with estimated specific heats for the solid and liquid phases. The two methods do not quite agree, and the second, which gives the lower value, is probably the more accurate. By this method Kelley[9] has obtained a value of 36.1 kcal/mole at 0°K; a more recent but as yet undocumented estimate of 36.5 kcal/mole has been given by the Bureau of Standards.[10]

Table I summarizes the comparison of the theoretical and

TABLE I. Contributions to the binding energy of lithium.

Theoretical, Silverman and Kohn*	34.5 kcal/mole
Coulomb correction	−0.6
Exchange correction	−(2.1 or less)
Correlation correction	+(4.3 or less)
Total	36.1
Experiment, 0°K	36.5

* See the accompanying erratum by Silverman and Kohn; following a suggestion of Professor Brooks a correction for zero point energy amounting to −0.9 kcal/mole has been added.

experimental binding energies. The agreement is closer than the uncertainty in either.

I am indebted to Mr. R. A. Silverman for correspondence relating to these calculations and for communication of the corrected results used in Table I.

[1] R. A. Silverman and W. Kohn, Phys. Rev. **80**, 912 (1950).
[3] T. S. Kuhn and J. H. Van Vleck, Phys. Rev. **79**, 382 (1950).
[8] E. Wigner and F. Seitz, Phys. Rev. **43**, 804 (1933); **46**, 509 (1934).
[4] F. Seitz, Phys. Rev. **47**, 400 (1935).
[5] E. Wigner, Phys. Rev. **46**, 1002 (1934), Trans. Faraday Soc. **34**, 678 (1938).
[6] W. Macke, Z. Naturforsch. **5a**, 192 (1950).
[7] C. Herring and A. G. Hill, Phys. Rev. **58**, 132 (1940), Eq. (55).
[8] H. Hartmann and R. Schneider, Z. anorg. u. allgem. Chem. **180**, 275 (1929); M. Maucherat, J. phys. radium **10**, 441 (1939).
[9] K. K. Kelley, U. S. Bureau of Mines Bulletin 383 (1935).
[10] National Bureau of Standards, *Selected Values of Chemical Thermodynamic Properties* (1950).

Erratum: On the Cohesive Energy of Metallic Lithium

[Phys. Rev. **80**, 912 (1950)]

R. A. SILVERMAN
Physics Department, Harvard University, Cambridge, Massachusetts
AND
W. KOHN
Carnegie Institute of Technology, Pittsburgh, Pennsylvania

(Received March 5, 1951)

THE calculations of the letter referred to above were found to contain a numerical error. The corrected Table I of values for the cohesive energy of metallic lithium should now read:

TABLE I.

Method used	Cohesive energy (kcal/mole)
Experimental	36.5
Power series to order k^4	35.2
Variable coefficients using (4)	34.5
Power series to order k^4	35.7
Variable coefficients using (5)	35.4

For the source of the changed experimental value see the letter of Herring in this issue.[1] Furthermore, the theoretical value of Seitz should be changed to 34.5 kcal/mole.

[1] C. Herring, Phys. Rev. **82**, 282 (1951).

Erratum: Remarks on the Nuclear Resonance Shift in Metallic Lithium

[Phys. Rev. **80**, 913 (1950)]

W. KOHN
Carnegie Institute of Technology, Pittsburgh, Pennsylvania
AND
N. BLOEMBERGEN
Harvard University, Cambridge, Massachusetts

(Received March 5, 1951)

CORRECTION of the same numerical error[1] which affected the letter of Silverman and Kohn, Phys. Rev. **80**, 912 (1950), changes the value of P_F to 0.22. The relevant ratio P_F/P_A is thus changed from 1.4 to 1.0.

[1] R. A. Silverman and W. Kohn, Phys. Rev. **82**, 283 (1951).

Beta-Alpha-Correlation in the Disintegration of Li^8

J. W. GARDNER
School of Theoretical Physics, Dublin Institute for Advanced Studies, Dublin, Ireland

(Received February 9, 1951)

BY negative β-decay, Li^8 transforms to Be^8 which is unstable against disintegration into two α-particles. The energy liberated by the entire disintegration $Li^8 \rightarrow 2He^4 + e^- + \nu$ is about 15.8 Mev, and the maximum β-energy (W_0) is about 12.5 Mev.[1] Less than 2 percent of the β-disintegrations go straight to the ground state of Be^8, the rest going to an excited state or states of energy around 3 Mev.[2] There is evidence[2-5] for both the values 0 and 2 for the spin of the Be^{8*}, but the level width is so great (1–2 Mev) that one cannot be entirely certain that there are not two levels present, or, on the other hand, that the properties of a single level of this width need be uniquely defined. Although the two values for the Be^{8*} spin may not be mutually exclusive, however, it would be useful to see what information the $\beta-\alpha$-angular correlation can give on this point, and, incidentally, on the forbiddenness of the β-transition (whether first or second forbidden).

Any evidence of spin 0 would be of a negative character, since it is a general result of angular correlation theory[6] that an intermediate state of spin 0 means a spherically symmetric angular distribution. It remains therefore to examine what predictions can be made about the $\beta-\alpha$ correlation for a Be^{8*} spin of 2 and an assignment of the remaining spins and parities, and of the β-forbiddenness, consistent with the experimental evidence. Bearing in mind that Be^8 must have even parity in both the excited state (spin 2) and the ground state (spin 0), and that the transition to the ground state is clearly more forbidden than the transition to the excited state, we are led to conclude that the only likely β-decay schemes for $Li^8 \rightarrow Be^{8*}$ are:

(1) $0+ \rightarrow 2+$, second forbidden (axial vector interaction);
(2) $3- \rightarrow 2+$, first forbidden (axial vector or tensor interaction).

Each of these schemes would be associated with a third forbidden transition to the ground state of Be^8. Of the two possibilities, one would prefer the first, since it assigns even parity[7] to the Li^8, and a second forbidden transition would seem quite consistent with the "ft" value[8] of 2.8×10^8 for this disintegration, when its exceptionally high energy is taken in account.

The $\beta-\alpha$-angular correlation for schemes (1) and (2) has been investigated by the methods of Falkoff and Uhlenbeck;[6] (1) gives a distribution $I_1(\theta) \sim 1 + A_1 \cos^2\theta + B_1 \cos^4\theta$, and (2) a distribution $I_2(\theta) \sim 1 + A_2 \cos^2\theta$. By a general result of reference 8, both distributions must become isotropic for the low energy β-particles, and must show greatest anisotropy as the β-energy W approaches W_0. The coefficient A_2 cannot be evaluated explicitly, since it involves the ratio of unknown nuclear matrix elements; A_1 and B_1, however, involve only one nuclear matrix element, which may be dropped as a common factor. These coefficients

therefore have been evaluated as explicit functions of W, and tabulated; in the notation of reference 8, $A_1=1/\mu_1(W)$, $B_1=\mu_2(W)/\mu_1(W)$. For $W=W_0$, $I_1(\theta)\sim\cos^2\theta-\cos^4\theta$, and, in fact, even for W down to $\frac{1}{4}W_0$, $I_1(\theta)$ still approximates to a $\cos^2\theta-\cos^4\theta$ distribution in that it has a pronounced maximum near 45° (and 135°). For example, when $W=9.4$ Mev the maximum occurs at 42° and $I_1(0°):I_1(42°):I_1(90°)=2.3:4.9:1.0$. Thus, if only the high energy β-particles are used in the $\beta-\alpha$-correlation experiment, the occurrence of a maximum near 45° in the angular distribution will be a definite criterion for the applicability of scheme (1), since $1+A_2\cos^2\theta$ can never have a maximum between 0° and 90°. If the distribution is anisotropic, but with no maximum between 0° and 90° (at high energies), then we know that scheme (2) applies. An isotropic experimental distribution would, as we have seen, be evidence for an excited Be^8 state of spin 0; it would not be quite conclusive evidence, however, for it could be that we have scheme (2) with the anisotropy of $I_2(\theta)$ too small to be detected. By selecting only the highest energy β-particles for the correlation, experiment, this latter possibility would be reduced to a minimum. Summarizing, then, we conclude that if the $\beta-\alpha$-angular distribution at high β-energies shows any correlation at all, the Be^{8*} has spin 2, and either scheme (1) or scheme (2) applies according as the distribution does, or does not, have a maximum between 0° and 90°. An isotropic distribution probably, but not certainly, means spin 0 for the Be^{8*}.

The work reported above was begun at the Atomic Energy Research Establishment, Harwell, England, in connection with proposed experiments on the $\beta-\alpha$-correlation in the Li^8 disintegration; the writer is indebted to Messrs. J. M. Cassels and T. H. R. Skyrme of Harwell for valuable discussion.

[1] D. S. Bayley and H. R. Crane, Phys. Rev. **52**, 604 (1937).
[2] W. E. Burcham, Proceedings of Harwell Nuclear Physics Conference, 1950.
[3] E. J. Konopinski, Revs. Modern Phys. **15**, 209 (1943).
[4] J. A. Wheeler, Phys. Rev. **59**, 27 (1941).
[5] S. Devons and G. R. Lindsey, Proc. Phys. Soc. (London) **63A**, 1202 (1950).
[6] C. N. Yang, Phys. Rev. **74**, 764 (1948).
[7] G. Breit and E. Wigner, Phys. Rev. **50**, 1191 (1936).
[8] D. L. Falkoff and G. E. Uhlenbeck, Phys. Rev. **79**, 334 (1950).

The Problem of Using Scintillation Crystals as Proportional Counters for High Energy Particles*

FRANCIS X. ROSER† AND THEODORE BOWEN
Department of Physics, University of Chicago, Chicago, Illinois
(Received January 22, 1951)

UP to about 10 Mev, close proportionality between the energy of incident particles and light output in scintillation counters is now a well established fact.[1] In the present investigation an attempt has been made to determine whether this proportionality still holds for high energy μ-mesons and whether the energy loss of these particles in the crystal would fit the theoretical formula of Bethe and Bloch.

Lead absorbers were used to select two energy ranges below the energy of minimum ionization including all particles (a) from 29 to 48 Mev, and (b) from 48 to 170 Mev. Particles with energies from 170 Mev upwards constituted a separate group. These energy ranges were selected to give an increase in the energy loss in equal steps (0.7 Mev/g/cm²).

The coincidence pulses of the fourfold Geiger-Müller counter telescope (Fig. 1B) initiated the sweep of an oscilloscope. The pulses from two RCA 5819 photomultipliers, viewing a cylindrical anthracene crystal (both diameter and length 1½ in.), were delayed and appeared on the sweep together with delayed pulses from Geiger-Müller trays, which determined the range of the mesons through the lead absorbers. Geiger-Müller trays on each side of the telescope prevented shower particles from triggering the sweep.

The aperture of the arrangement was 0.08 steradians, giving an average counting rate of 8 pulses per hour. An additional 16.5-in. lead absorber on top was used to cut off μ-mesons below 580 Mev, thus increasing the counting rate in the ranges for low energies.

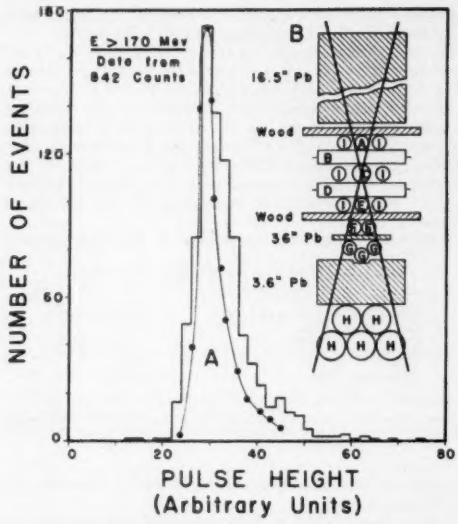

FIG. 1. (A) The histogram shows the distribution of pulse heights found for μ-mesons of energy greater than 170 Mev passing through the phosphor. The smooth curve is the distribution expected on the basis of Landau's theory. (B) Experimental arrangement.

As shown in Fig. 1A, μ-mesons of energy greater than 170 Mev (minimum ionization) passing through the crystal give rise to a pulse height distribution strongly peaked around the mean value of 30.3 Mev. Two conclusions can be drawn:

(1) Because of the rather small spreading out of the pulse height distribution (half-width 20 percent), it is immediately obvious that α-particles and other multiply-charged nuclei should be completely separable from mesons, protons, and electrons.

(2) A possible relativistic increase in energy loss for high energy mesons cannot be deduced directly, because of statistical fluctuations in the ionization process which, according to calculations performed by Landau,[2] are by no means negligible, mainly on account of δ-ray production. This impresses a characteristic skewness on the distribution curve, thus masking the relativistic effect which also tends to produce an appreciable asymmetry. However, some preliminary indication for such an increase might be deduced from the fact that Landau's curve, normalized to pulse height as shown in Fig. 1A, is definitely narrower than the actual distribution obtained by experiment. The difference between the two distributions beyond the maximum (for high energy losses) is quite outside the experimental error of the measurements.

This discrepancy cannot be explained by fluctuations only in the multiplicative effect of the phototubes, which under good conditions for light collection amount to about 5 percent and would certainly affect the distribution equally on either side of the maximum. However, such a difference can be satisfactorily explained on the basis of the Bethe-Bloch formula for ionization loss as corrected by Wick for the density effect, taking into account Wilson's energy spectrum for cosmic rays.

Further experiments are under way to separate, in more direct form, the statistical fluctuations from the expected relativistic rise in ionization. Some indication of an increase up to about 10 percent was reported in photographic plates.[3]

The pulse height distributions in the ranges below minimum ionization energy are broader (Fig. 2), owing to the fact that they result from the superposition of a great many curves similar to

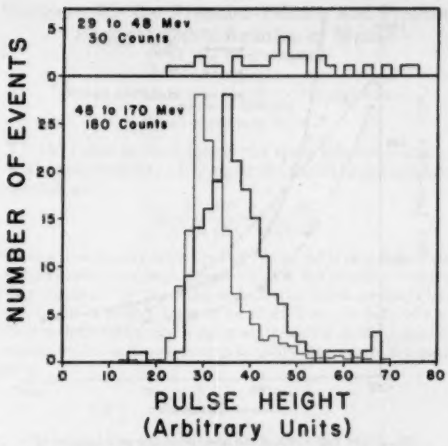

FIG. 2. Upper histogram: the distribution of pulse heights for μ-mesons of energies between 29 and 48 Mev [range (a)]. Lower histogram: the heavy curve shows the distribution of pulse heights for meson energies between 48 and 170 Mev [range (b)]. The light curve is the distribution of Fig. 1A, which is shown for comparison.

the one of Fig. 1A. This is a consequence of the continuous increase in energy loss throughout each energy range.

On the basis of the Bethe-Bloch ionization curve the mean increase in energy loss for μ-mesons (relative to the loss at minimum ionization) should be 20.5 percent for range (b) and 61 percent for range (a). As shown in Fig. 2, the experimental mean values are 22.8±2 percent and 54±7.5 percent above the experimental mean value for minimum ionization, for ranges (b) and (a), respectively. The corresponding shift of the distribution histograms in Fig. 2 to higher values of pulse height is clearly visible.

Knock-on electrons, accompanying μ-mesons and triggering the counter telescope, are necessarily in the range of minimum ionization energy. The pulses of minimum ionization, as shown in the top histogram of Fig. 2, are obviously due to such knock-ons.

In view of these results and by considering the energy range (b) as the most reliable one, proportionality between energy and pulse height within a limit of less than 5 percent seems to be strongly indicated for μ-mesons up to 170 Mev. This further indicates that for other particles one should also expect proportionality up to the respective energies of minimum ionization.

We are greatly indebted to Professor Marcel Schein for his constant interest in this investigation.

* Assisted by the joint program of the ONR and AEC.
† On leave from Universidade Catolica, Rio de Janeiro, Brazil.
[1] W. J. Jordan and P. R. Bell, Nucleonics 5, 30 (1949). R. Hofstadter and J. A. McIntyre, Nucleonics 7, 32 (1950). R. W. Pringle, Nature 166, 11 (1950). S. A. E. Johansson, Ark. Fys. 2, 177 (1950).
[2] L. Landau, J. Phys. U. S. S. R. 8, 201 (1949).
[3] E. Pickup and L. Voyvodic, Phys. Rev. 80, 89 (1950).

The Effect of Electron-Neutron Interaction on Spectral Isotope Shifts

LAWRENCE WILETS* AND LEE C. BRADLEY, III
Palmer Physical Laboratory, Princeton University, Princeton, New Jersey
(Received February 20, 1951)

HAVENS, Rainwater, and Rabi[1] have reported an electron-neutron interaction potential $V=5300\pm1000$ ev, assuming a square well of radius $r_0=2.8\times10^{-13}$ cm. This interaction may be expected to contribute to the isotopic displacement of spectral lines, particularly among the heavier atoms where the large nuclear charge results in a considerable electron density for s electrons at the nucleus.

The relativistic density for s electrons near a point charge Ze is given by[2,3]

$$P(r)=\frac{2(1+\rho)\psi^2(0)}{[\Gamma(2\rho+1)]^2}\left(\frac{2Zr}{a_0}\right)^{2\rho-2}=Ar^{2\rho-2},$$

where

$$\rho=(1-Z^2\alpha^2)^{\frac{1}{2}}$$
$$\alpha=e^2/\hbar c$$
$$a_0=\hbar^2/mc^2$$

and $\psi(0)$ is the nonrelativistic Schroedinger wave function for the electron at $r=0$. If one assumes that the additional neutrons of a heavier isotope are to be found primarily near the edge of the nucleus, then the contribution to the isotopic displacement for an s electron is

$$\epsilon=4\pi nAR^{2\rho-2}r_0^3V,$$

where R is the nuclear radius and n is the difference in atomic weight.

This may be compared with the isotope shift due to the change in nuclear radius.[3-6] If one assumes a uniform charge distribution throughout the nucleus, this shift is given by

$$\delta\Delta W=\frac{12\pi AZe^2}{(2\rho+1)(2\rho+3)}R^{2\rho-1}\delta R.$$

Upon inserting the values for r_0 and V, and using the empirical formula for the nuclear radius $R=1.5\times10^{-13}A^{\frac{1}{3}}$ cm, the ratio between the two contributions to the shifts is given by

$$\epsilon/(\delta\Delta W)\approx0.0122(2\rho+1)(2\rho+3)A^{\frac{1}{3}}/Z\ \text{cm}^{-1}.$$

For zinc ($A=64$, $Z=30$) this ratio is about 0.024; it decreases with increasing atomic number. In deuterium, the 2S level would be shifted by 0.36 Mc due to the interaction.

The above calculations have not considered the distortion of the wave function due to the departure of the potential from a coulomb field. This effect has been treated in the case of the displacements due to the change in nuclear radius,[3,6] and has been found to reduce the shifts by a factor possibly as small as 0.5. A similar correction factor would be expected in the case of the electron-neutron interaction.

* AEC Predoctoral Fellow.
[1] Havens, Rainwater, and Rabi, Proc. Am. Phys. Soc. 26, Nos. 1, 58 (1951).
[2] G. Racah, Nature 129, 723 (1932).
[3] J. E. Rosenthal and G. Breit, Phys. Rev. 41, 459 (1932); G. Breit, Phys. Rev. 42, 348 (1932).
[4] M. F. Crawford and A. L. Schawlow, Phys. Rev. 76, 1310 (1949).
[5] E. K. Broch, Archiv. f. Mat. o. Nat. 48, 25 (1945).

Magnetic Resonance Absorption in Antiferromagnetic Materials

TOSHIHIKO OKAMURA, YOSHIARU TORIZUKA, AND YUZO KOJIMA
Research Institute for Scientific Measurement, Sendai, Japan
(Received January 24, 1951)

THE microwave resonance absorption technique at 3.2-cm wavelength has been used to study the magnetic resonance absorption in MnS, MnO, and MnSe, which have Curie points at −75°C, −151°C, and −123°C,[1] respectively.

In the present experiment the specimen, in a form of a thin disk, was mounted at the bottom of a rectangular resonant cavity, which forms one arm of the microwave bridge and is made of transparent quartz plate, whose inside surface is coated with silvered thin copper plate. The relative magnetic absorption was obtained by observing the Q-value of the cavity, changing the dc magnetic field which was applied orthogonally to the rf magnetic field by an electromagnet.

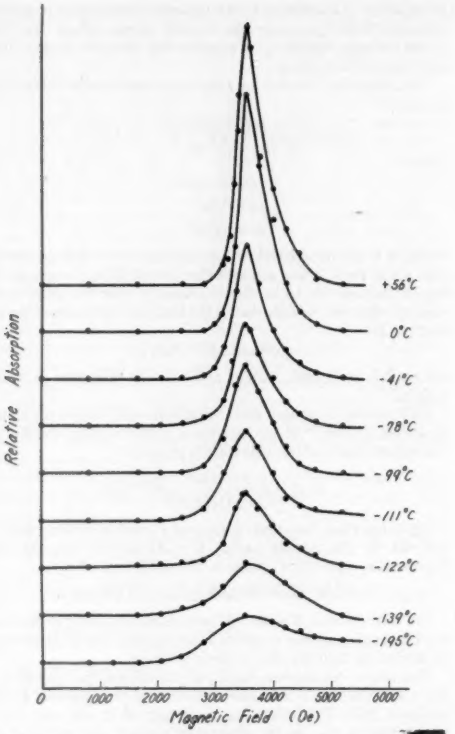

FIG. 1. The curve of resonance absorption *versus* dc magnetic field for MnS at various temperatures.

Figure 1 shows the curve of resonance absorption *versus* dc magnetic field for MnS at various temperatures ranging from −195°C to 60°C. The height of the resonance absorption decreases and the absorption line becomes broader with decreasing temperature, especially below the Curie temperature. The position of the maximum was found to be at a constant magnetic field of 3510 oe throughout this temperature range. The half-width of the absorption line and the height of the absorption peak for MnS, MnO, and MnSe were obtained as functions of the temperature, as illustrated in Figs. 2 and 3, respectively. These temperature dependences are quite contrary to those of the ferromagnetic materials—namely, nickel, supermalloy,[2] and ferromagnetic ferrites;[3] and it seems to suggest the existence of strong local magnetic fields in antiferromagnetic materials.[4,5] The maximum resonance field of 3510 oersted was found for all samples at the frequency of 9311 Mc.

These results may be compared with other studies of magnetic resonance in antiferromagnetic materials. Trounson and his coworkers[4] reported the result of a resonance experiment for Cr_2O_3. They found a second peak appearing at a lower magnetic field below the Curie temperature, and the position of the second peak was found to change with varying temperatures. However, we have not found such phenomena for MnS, MnO, and MnSe. On the contrary, a broadening which might be ascribed to a second peak seems to appear at low temperatures on the higher magnetic field side of the main peak.

A resonance condition for antiferromagnetic materials was given by S. Nakajima and S. Simizu[6] using a model proposed by

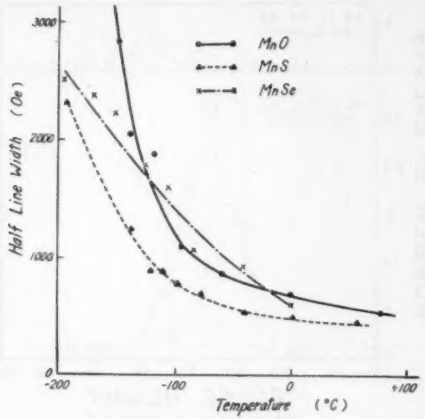

FIG. 2. The half-width of the absorption line as a function of temperature for MnO, MnS, and MnSe.

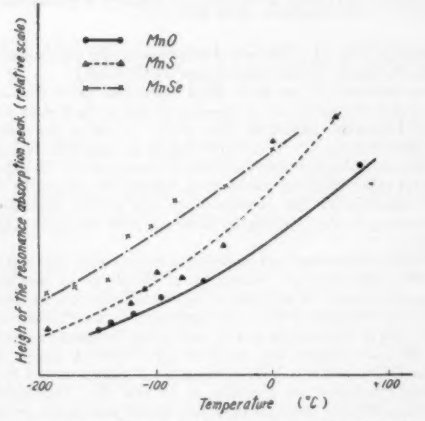

FIG. 3. The height of the absorption peak as a function of temperature for MnO, MnS, and MnSe.

Van Vleck;[7] they find that when $T<T_c$, the resonance frequency ω_1 is given by

$$\omega_1=\gamma\left[1-\frac{2T_c}{T_c+(1-4S_0^3)^{-1}T}\right]H_0,$$

where S_0 is the mean component of an atom's spin in the direction of the antiferromagnetic spontaneous field. If we assume ω_1 to be constant in this formula, the resonance field in this formula becomes infinite at $T=T_c$, and the resonance condition at $T=0°K$ becomes $\omega_1=\gamma H_0$, the usual expression for paramagnetic resonance. Although it is difficult to explain the aforementioned results by this formula, we intend to examine the resonance absorption at higher magnetic fields.

[1] P. W. Anderson, Phys. Rev. **79**, 705 (1950).
[2] N. Bloembergen, Phys. Rev. **78**, 572 (1950).
[3] T. Okamura and Y. Torizuka, recently published.
[4] Trounson, Bleil, Wangsness, and Maxwell, Phys. Rev. **79**, 542 (1950).
[5] D. F. Bleil and R. K. Wangsness, Phys. Rev. **79**, 227 (1950).
[6] S. Nakajima and S. Shimizu, unpublished.
[7] J. H. Van Vleck, J. Chem. Phys. **9**, 85 (1941).

Erratum: On the Pressure-Volume and Pressure-Compressibility Relation of Metals

[Phys. Rev. 72, 1123 (1947)]

P. GOMBÁS
Physical Institute of the University for Technical Sciences, Budapest, Hungary

(Received February 19, 1951)

IN the Letter to the Editor of the above title the formula for the compressibility κ is incorrect and should be replaced by the following one:

$$\frac{1}{\kappa}=\frac{1}{12\pi R}\frac{d^2U}{dR^3}-\frac{1}{6\pi R^2}\frac{dU}{dR}$$

where U denotes the lattice energy of the metal and R the radius of the elementary sphere. Accordingly, in the pressure-compressibility diagrams for the alkali and alkaline earth metals (Figs. 2 and 3) the ordinates have to be divided by $1+\frac{1}{2}\kappa P$, where P denotes the pressure and κ the compressibility at the pressure P represented in the pressure-compressibility diagrams of the quoted paper.

Mirror Levels in Li^7 and Be^7

BEN R. MOTTELSON
Institute for Theoretical Physics, University of Copenhagen, Denmark

(Received March 5, 1951)

THE recently discovered[1] level in Be^7, which appears to be the mirror level of the well-known 478-kev level in Li^7, has an excitation of 429 kev above the ground state. If we assume that $(n-n)$ and $(p-p)$ nuclear forces are exactly equal, we must account for this 49-kev level shift in terms of the different electromagnetic properties of neutron and proton. The customary treatment of energy levels in mirror nuclei has considered only the effect caused by the differing neutron and proton charge. However, it seems that shifts of just the magnitude of that observed in Li^7-Be^7 can occur as a result of the electromagnetic spin-orbit interaction.

The electromagnetic interactions associated with acceleration of spin (Thomas effect) and magnetic interactions (spin-orbit and spin-spin interaction) are well known from atomic systems and must certainly be expected to be present in nuclei. These interactions are very sensitive to the coupling scheme used and so may give information about nuclear structure. In the Li^7-Be^7 mirror system the effect has been calculated assuming that the two levels are $^2P_{3/2,1/2}$ (the ground state has $I=3/2$). The three p-state nucleons are assumed to be coupled together in the spatially symmetric P-state required by the Wigner theory of nuclear structure.[2] Gaussian radial dependence is assumed, and the parameter which determines the range of the wave function is fixed by the experimental coulomb energy difference of the Li^7-Be^7 ground states. For these wave functions only the electrostatic Thomas effect and the magnetic spin-orbit effect contribute, and the calculated amount by which the Li^7 doublet energy should exceed Be^7 is 36.8 kev. A radial dependence which has a greater variation at the origin than the gaussian can be used to get the full 49-kev observed shift. If a wave function is constructed from the $j-j$ coupling model with $[(p_{3/2}p_{3/2})_0p_{1/2}]_{1/2}$ ground state,[3] and $[(p_{3/2}p_{3/2})_0p_{1/2}]_{1/2}$ excited state, the calculated shift is 81.5 kev.

A $j-j$ coupling model for Li^7 has been discussed by Inglis[4] in which the ground state is a mixture of $[(p_{3/2}p_{3/2})_0p_{3/2}]_{3/2}$ and $[(p_{3/2}p_{3/2})_2p_{3/2}]_{3/2}$, while the excited state is $[(p_{3/2}p_{3/2})_2p_{3/2}]_{1/2,3/2,5/2,7/2}$. In this case the level shift in the excited state is attributed to a change in the coulomb energy. However, the lifetime for the γ-decay of the excited state is uniquely determined by the coupling scheme, since it is a magnetic dipole transition, and the half-life predicted on this model[5] is several times the experimentally observed value.[6] The coupling schemes discussed above both give half-lives in agreement with experiment.

A more complete description of these calculations will appear in the *Communications of the Danish Academy*.

The writer is pleased to express his appreciation to Professor Niels Bohr and the Institute for Theoretical Physics for their hospitality and stimulation and to Harvard University for a Parker Traveling Fellowship.

[1] Brown, Chao, Fowler, and Lauritsen, Phys. Rev. 78, 88 (1950).
[2] E. Feenberg and E. Wigner, Phys. Rev. 51, 95 (1937).
[3] We use the following notation: For Li^7 we give first the quantum numbers of the neutrons and their coupling, then the quantum state of the proton, and finally the total angular momentum; for Be^7 interchange neutron and proton.
[4] D. R. Inglis, Phys. Rev. 77, 724 (1950).
[5] In accord with the angular distribution of the γ-rays, we assume that only $[(p_{3/2}p_{3/2})_2p_{3/2}]_{1/2}$ is found in appreciable amount. The amount of admixture of $[(p_{3/2}p_{3/2})_2p_{3/2}]_{3/2}$ to the ground state is fixed by the magnetic moment of Li^7.
[6] L. G. Elliott and R. E. Bell, Phys. Rev. 76, 168 (1950).

Angular Distributions of Shower Particles as a Function of Depth*

L. EYGES AND S. FERNBACH
Radiation Laboratory, University of California, Berkeley, California

(Received February 19, 1951)

WE were nearing the completion of some calculations on the angular distribution of shower particles when we found that, in a recent journal, Borsellino[1] had duplicated independently some of the first stages of our work. We therefore present our results here, insofar as they go beyond Borsellino's.

We have calculated the angular distributions of high energy electrons and photons in air showers as a function of depth in the shower. To do this, we first calculated the moments of these functions and then reconstructed the distribution functions from the moments. Let $\pi(E_0, E, \theta, t)2\pi\theta d\theta dE$ be the number of electrons of energy E to $E+dE$ in the solid angle $2\pi\sin\theta d\theta\cong 2\pi\theta d\theta$ at thickness t (radiation lengths) due to an electron[2] of energy E_0 at $t=0$. The nth moment, $\langle\theta^n\rangle$, of this distribution function is defined by

$$\langle\theta^n\rangle=\frac{\int_0^\infty \pi(E_0, E, \theta, t)\theta^n\theta d\theta}{\int_0^\infty \pi(E_0, E, \theta, t)\theta d\theta}.$$

These moments can be calculated by an extension of the method used to calculate the moments at the maximum of the shower.[3] It turns out that the moments depend on E_0 and t only through the characteristic parameter s of shower theory.[4] For example, one gets, for electrons,

$$\langle\theta^n\rangle_{\text{electrons}}=(E_s/E)^n\delta_n(s),$$

where $\delta_n(s)$ is a certain function of s. The expressions we have obtained for $\delta_n(s)$ agree with those of Borsellino.[1] E_s in these equations is the "characteristic scattering energy," equal to about 21 Mev.

In addition, we have calculated the angular distribution of electrons, which we call $P(E\theta/E_0, s)$, from these moments. If we call $\pi_{\text{long.}}(E_0, E, t)$ the usual longitudinal one-dimensional distribution function and let $x=E\theta/E_s$, then $P(x, s)$ is defined by

$$\pi(E_0, E, \theta, t)2\pi\theta d\theta dE=\pi_{\text{long.}}(E_0, E, t)dE\,P(x, s)2\pi\theta d\theta. \quad (1)$$

We have calculated $P(x, s)$ for $s=0.6$ and $s=1.5$; we have previously calculated it for $s=1.0$. If $s=1.0$ corresponds to the shower maximum, $t_{\max}$, then $s=0.6$ corresponds to about half $t_{\max}$, and $s=1.5$ to twice $t_{\max}$. The shape of $P(x, s)$ is a slowly varying function of s, as one would expect from physical considerations. Our values are given in Table I.

Any method such as ours for reconstructing a function from a finite number of moments does not give the behavior near the origin very accurately; our values for x less than about 0.3 may not be reliable. For larger x, they are probably accurate to within several percent.

We call the angular distribution function for photons $Q(y, s)$,

TABLE I. The electron angular distribution function $P(x, s)$ defined by Eq. (1). Normalization such that $\int_0^\infty P(x, s)xdx=1$.

s	$P(x, 0.6)$	$P(x, 1.0)$	$P(x, 1.6)$
0	13	9.3	6.1
0.1	9.1	7.1	5.0
0.2	6.3	5.3	4.1
0.4	3.10	2.78	2.60
0.6	1.48	1.52	1.58
0.8	7.10×10^{-1}	8.20×10^{-1}	9.00×10^{-1}
1.0	3.45	4.46	5.10
1.2	1.66	2.32	2.75
1.4	8.00×10^{-2}	1.18	1.50
1.6	3.80	6.00×10^{-2}	8.00×10^{-2}
1.8	1.80	2.90	4.18
2.0	8.20×10^{-3}	1.46	2.18
2.2	3.70	7.13×10^{-3}	1.12
2.4	1.58	3.56	5.60×10^{-3}
2.6	6.7×10^{-4}	1.74	2.75
2.8	2.7	8.29×10^{-4}	1.38
3.0	1.12	3.92	6.50×10^{-4}

where $y=W\theta/E_0$, and W is the photon energy. $Q(y, s)$ is defined analogously to $P(x, s)$.

$Q(y, s)$ is singular at the origin. For $s=1$, $Q(y, 1)$ appears to go as $1/y$ for small y.[3] Our method of moments is particularly unreliable in determining the behavior of the function at the origin if the function is singular. For $s=0.6$ and $s=1.5$ a $1/y$ singularity for $Q(y, s)$ is consistent with our results, although it seems clear that for $s=0.6$ the singularity should be stronger than for $s=1.5$. Mainly for ease in expressing the normalization, we have assumed that the singularity is exactly $1/y$ for $s=0.6$ and $s=1.5$. Our results are given in Table II, where we tabulate

TABLE II. The photon angular distribution function $Q(y, s)$. Tabulated values are $yQ(y, s)$. Normalization such that $\int_0^\infty Q(y, s)ydy=1$.

y	$yQ(y, 0.6)$	$yQ(y, 1.0)$	$yQ(y, 1.5)$
0	4.7	3.4	2.1
0.1	2.9	2.4	1.8
0.2	1.8	1.7	1.5
0.4	6.50×10^{-1}	8.76×10^{-1}	1.00
0.6	2.61	4.61	6.42×10^{-1}
0.8	1.18	2.21	3.83
1.0	5.06×10^{-2}	1.18	2.22
1.2	2.28	5.47×10^{-2}	1.19
1.4	1.03	2.74	6.28×10^{-2}
1.6	4.80×10^{-3}	1.38	3.30
1.8	2.25	6.87×10^{-3}	1.66
2.0	1.06	3.44	8.44×10^{-3}
2.2	4.83×10^{-4}	1.72	4.02
2.4	2.25	8.59×10^{-4}	1.89
2.6	1.05	4.32	8.90×10^{-4}
2.8	5.15×10^{-5}	2.18	4.12
3.0	2.43	1.07	1.91

$yP(y, s)$. We would like to emphasize that the accuracy of our relative values for y greater than about 0.3 does *not* depend on our assumption as to the singularity at the origin, and that these values are probably good to within several percent.

* This work was supported by the AEC.

[1] A. Borsellino, Nuovo cimento **7**, 700 (1950).

[2] We discuss an incident electron for the sake of definiteness, although our results hold equally well for an incident photon, provided the energy E one is interested in is much less than the energy of the incident particle.

[3] L. Eyges and S. Fernbach, Phys. Rev. **82**, 23 (1951).

[4] See the second of Eqs. (2.55) to (2.60) in B. Rossi and K. Greisen, Revs. Modern Phys. **13**, 284 (1941).

Radial Distribution of Shower Electrons as a Function of Depth*

SIDNEY FERNBACH
Radiation Laboratory, University of California, Berkeley, California
(Received February 19, 1951)

THE radial distribution of shower electrons can be determined in the same way as the angular distribution.[1] The procedure is somewhat more involved in that one must calculate the mixed radial and angular moments before obtaining the radial moments alone. Let the number of electrons of energy E to $E+dE$ in the annular ring between r and $r+dr$ at depth t (r and t measured in radiation lengths) be $(E_0, E, r, t)2\pi rdrdE$ when the initiating particle is an electron of energy E_0 at $t=0$. We define the mth moment as

$$\langle r^m\rangle=\int_0^\infty \pi(E_0, E, r, t)r^m rdr \Big/ \int_0^\infty \pi(E_0, E, r, t)rdr.$$

These moments are calculated by an extension of the method previously described.[2] In this case one obtains $\langle r^m\rangle$ as a function of the parameter s, where s is determined from E_0 and t by use of the relation

$$\log(E_0/E)+\lambda_1'(s)t=0.$$

$\lambda_1'(s)$ is tabulated in Rossi and Greisen's[3] article.

The moments are most simply written as

$$\langle r^m(s)\rangle=(E_s/E)^m\rho_m(s).$$

Figure 1 shows $\rho_m(s)$ plotted for $m=2$, 4, and 6.

From these moments we calculate the distribution function $P_r(Er/E_s, s)$, where $P_r(Er/E_s, s)rdr$ is proportional to the number of electrons of energy E at a depth corresponding to s in an annular ring between r and $r+dr$. The normalization is taken as $\int_0^\infty P_r(x, s)xdx=1$, where $x=Er/E_s$, E_s being as usual approximately 21 Mev.

In a previous paper,[2] we discussed this calculation for the shower maximum. This corresponds to an $s=1$. In addition, we have now calculated the two cases $s=0.6$ and $s=1.5$ which correspond approximately to half and twice the depth at the shower maximum, respectively.

The radial distribution is singular at the origin, this singularity being of order $r^{-1/3}$ at the shower maximum, if we assume Moliere's[4] calculations to give an accurate picture of the shower spread for small r. In calculating the present distribution function we again assume the functions singular, but have no way of specifying the order of the singularity. This means that we have to guess the behavior of the function for small r. Since the major contribution to the area under the distribution function, namely $\langle r^0\rangle$, comes from small r, the amplitude of the function is not

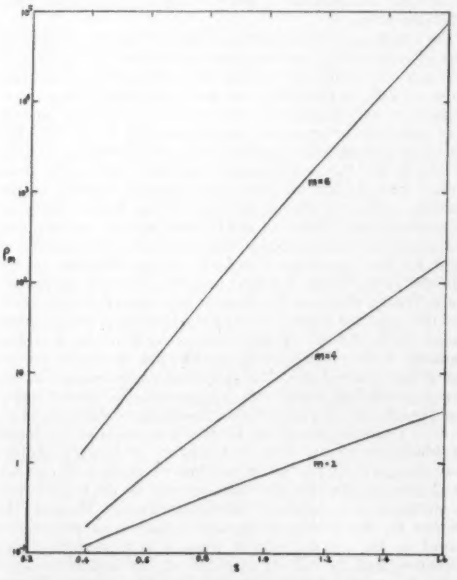

FIG. 1. Radial moments of electron distribution as function of shower depth.

TABLE I. Radial distribution of electrons for $s=0.6$, 1.0, and 1.5.

x	$P_r(x, s)$ $s=0.6$	$s=1.0$	$s=1.5$
0.2	11.	7.6	5.0
0.4	2.85	2.74	2.00
0.6	8.00×10^{-1}	1.01	1.08
0.8	2.30	4.84×10^{-1}	6.10×10^{-1}
1.0	8.50	2.52	3.75
1.2	4.00	1.47	2.40
1.4	2.18	8.72×10^{-2}	1.60
1.6	1.22	5.36	1.14
1.8	7.40×10^{-2}	3.49	8.20×10^{-2}
2.0	4.50	2.26	6.00
2.2	2.90	1.53	4.50
2.4	2.00	1.02	3.50
2.6	1.37	7.20×10^{-3}	2.75
2.8	9.50×10^{-3}	5.16	2.15
3.0	6.70	3.73	1.70
3.5	3.00	1.74	9.80×10^{-3}
4.0	1.36	8.72×10^{-4}	6.00
4.5	6.20×10^{-4}	4.52	3.65
5.0	2.99	2.51	2.35
5.5	1.39	1.46	1.47
6.0	6.90×10^{-5}	8.80×10^{-5}	9.80×10^{-4}
7.0	1.58		4.70

greatly changed at large r so long as we continue the curve back towards the origin smoothly and make $\langle r^0\rangle$ unity. The shape of the function for large r is correct, since it depends only on the higher moments and not at all on the type of singularity. The amplitude, however, does depend to a slight extent on how well we have guessed the behavior at the origin. The normalization, therefore, may be off by several percent. In Table I we present our results for $x>0.2$, but we do not believe the value for $x=0.2$ to be very reliable.

* This work was sponsored by the AEC.

[1] L. Eyges and S. Fernbach, Phys. Rev. **82**, 287 (1951).
[2] L. Eyges and S. Fernbach, Phys. Rev. **82**, 23 (1951).
[3] Rossi and Greisen, Revs. Modern Phys. **13**, 285 (1941).
[4] G. Moliere, *Cosmic Radiation*, ed. Heisenberg (Dover Publications, New York, 1946).

The Quadrupole Moment Ratio of Cl^{35} and Cl^{37} from Pure Quadrupole Spectra*

RALPH LIVINGSTON
Chemistry Division, Oak Ridge National Laboratory, Oak Ridge, Tennessee
(Received February 23, 1951)

RESONANCE absorption lines due to nuclear quadrupole splittings were first observed by Dehmelt and Krüger[1] for chlorine in *trans*-dichloroethylene at 90°K. The splitting is caused by the interaction of the chlorine nuclear electric quadrupole moment with the gradient of the electric field at the nucleus. The electric field gradient can be considered to arise from charge distribution within the molecule and from other charge distributions in the crystal lattice.

Resonance absorptions similar to the above have been observed at this laboratory in several compounds. These are listed in Table I. A frequency modulated regenerative oscillator was used, and the absorption lines were viewed on an oscilloscope. In making frequency measurements, markers formed by harmonics from a Signal Corps type BC-221 frequency meter were superposed on the lines. The meter was calibrated with harmonics from a 1-Mc crystal oscillator which in turn was calibrated against radio station WWV at 10 Mc. The measured frequencies in Table I should be accurate to 0.01 percent; however, the frequency ratios may be somewhat better, because the harmonics selected for the Cl^{37} and Cl^{35} measurements were such that only a small part of the frequency meter dial travel was used. All frequencies listed are the average of eight measurements. Approximately 25-cc samples were used, and all observations were made at liquid nitrogen temperature (80°K). The relative intensities of the Cl^{35} and Cl^{37} lines agreed satisfactorily with the isotopic abundance ratio. In some cases two absorption lines were seen for each isotope. A similar effect has been observed by Dehmelt[2] for the iodine resonance in SnI_4. The effect was ascribed by him to crystallographically different sets of iodines in the lattice. Each set of iodine nuclei thus experiences its own particular electric field gradient. The splittings observed here could be caused by the same effect. In forming the frequency ratios of Table I, the higher Cl^{35} frequency (higher electric field gradient) line has been associated with the higher Cl^{37} frequency.

TABLE I. Measured frequencies and ratios for solid chlorine compounds.

Compound	$\nu(Cl^{35})$ Mc	$\nu(Cl^{37})$ Mc	$\nu(Cl^{35})/\nu(Cl^{37})$
$SOCl_2$	32.0908	25.2935	1.26874
	31.8874	25.1331	1.26874
$POCl_3$	28.9835	22.8432	1.26880
	28.9378	22.8067	1.26883
CH_2Cl_2	35.9912	28.3673	1.26876
$CHCl_3$	38.3081	30.1921	1.26881
	38.2537	30.1500	1.26878
C_6H_5Cl	34.6216	27.2872	1.26879

The frequency ratios in Table I should be the nuclear quadrupole moment ratio of Cl^{35} and Cl^{37}. The average gives

$$Q(Cl^{35})/Q(Cl^{37})=1.26878\pm0.00015.$$

All of the eight ratios agree to within ±0.00005.

Dehmelt and Krüger's value for the moment ratio using *trans*-dichloroethylene was 1.2661 ± 0.0002.

Geschwind, Gunther-Mohr, and Townes[3] have recently summarized published values of quadrupole coupling ratios and shown that in many cases the values for the ratio determined by different investigators varied outside of estimated experimental errors. The variation, at least in part, depended on the molecule used. This was also true for the three accurately remeasured values by the above authors for CH_3Cl, ClCN, and GeH_3Cl, which gave ratios of 1.2691 ± 0.0003, 1.2682 ± 0.0006, and 1.2670 ± 0.0005, respectively. These measurements were made by observing quadrupole splittings in rotational transitions in the microwave region. Gunther-Mohr, Geschwind, and Townes[4] considered that a reasonable explanation of the variation in experimental values on different molecules could be made by assuming a nuclear polarization by the external electric field. This effect is absent in the measurements reported here.

* This work was performed for the AEC.

[1] H. G. Dehmelt and H. Krüger, Naturwiss. **37**, 111 (1950).
[2] H. G. Dehmelt, Naturwiss. **37**, 398 (1950).
[3] Geschwind, Gunther-Mohr, and Townes, Phys. Rev. **81**, 288 (1951).
[4] Gunther-Mohr, Geschwind, and Townes, Phys. Rev. **81**, 289 (1951).

On Einstein's Unified Field Theory

BEHRAM KURŞUNOĞLU
Fitzwilliam House, Cambridge, England
(Received December 8, 1950)

SOME of the most general implications of Einstein's new theory[1] are considered in a paper to appear elsewhere. The results obtained are described in the following shortened version.

By neglecting the cubes and higher orders of antisymmetric field variables a simple expression for the affine field is found in terms of the generalized nonsymmetric tensor $g_{\alpha\beta}=\underset{\sim}{g}_{\alpha\beta}+\underset{\sim}{g}_{\alpha\beta}$ $=A_{\alpha\beta}+\Phi_{\alpha\beta}$, and its first-order partial derivatives $g_{\alpha\beta,\gamma}$, where $A_{\alpha\beta}=\underset{\sim}{g}_{\alpha\beta}=\underset{\sim}{g}_{\beta\alpha}$ and $\Phi_{\alpha\beta}=\underset{\sim}{g}_{\alpha\beta}=-\underset{\sim}{g}_{\beta\alpha}$. I am indebted to the referee of *The Physical Review* for directing my attention to a solution of the Γ-field obtained by Ingraham[2] in a slightly different way from ours.

The antisymmetric part of the Γ-field is given by

$$\Gamma^{\alpha}_{\beta\gamma}=-\tfrac{1}{3}\Gamma^{\alpha}_{\beta\gamma}+A^{\alpha\rho}\Phi_{\beta\gamma|\rho} \qquad (1)$$

subject to the four conditions:

$$\Gamma^{\alpha}_{\alpha\gamma}=\Gamma_{\gamma}=A^{\alpha\rho}\Phi_{\alpha\gamma|\rho}=0, \qquad (2)$$

where the stroke (|) implies covariant differentiation with respect to the Christoffel symbols of the $\mathbf{A}_{\alpha\beta}$-tensor, and

$$I_{\alpha\beta\gamma}=\epsilon_{\alpha\beta\gamma\delta}J^{\delta} \quad (J^{\delta}=4 \text{ "current density" vector}),$$

and

$$\Phi_{\alpha\beta,\,\gamma}+\Phi_{\beta\gamma,\,\alpha}+\Phi_{\gamma\alpha,\,\beta}=I_{\alpha\beta\gamma}. \tag{3}$$

The complete solution for the Γ-field is (approximately)

$$\overline{\Gamma}^{\alpha}_{\beta\gamma}=\{{}^{\alpha}_{\beta\gamma}\}_{\mathbf{A}}-\tfrac{1}{2}\mathbf{A}^{\alpha\rho}(\Phi_{\beta\rho}I^{\nu}_{\gamma\mu}+\Phi_{\gamma\gamma}I^{\nu}_{\mu\beta})$$
$$+\mathbf{A}^{\nu\rho}\mathbf{A}^{\alpha\mu}(\Phi_{\beta\nu}\Phi_{\gamma\mu|\rho}+\Phi_{\nu\gamma}\Phi_{\mu\beta|\rho})+\mathbf{A}^{\alpha\rho}\Phi_{\beta\gamma|\rho}-\tfrac{1}{2}I^{\alpha}_{\beta\gamma}.$$

The contravariant tensor densities $\mathbf{G}^{\alpha\beta}=(-g)^{\frac{1}{2}}\underline{g^{\alpha\beta}}$ and $\mathbf{G}^{\alpha\beta}_{\circ}=(-g)^{\frac{1}{2}}g^{\alpha\beta}_{\circ}$ were obtained by Schrödinger[3] in the form

$$\mathbf{G}^{\underline{\alpha\beta}}=\frac{(-\mathbf{A})^{\frac{1}{2}}[\mathbf{A}^{\alpha\beta}(1+\Omega)-\Phi^{\alpha\mu}\Phi^{\beta}_{\cdot\mu}]}{(1+\Omega-\Lambda^{2})^{\frac{1}{2}}}, \tag{4}$$

$$\mathbf{G}^{\alpha\beta}_{\circ}=\frac{(-\mathbf{A})^{\frac{1}{2}}(\Phi^{\alpha\beta}-\Lambda\Phi^{\alpha\beta})}{(1+\Omega-\Lambda^{2})^{\frac{1}{2}}}, \tag{5}$$

where

$$\overset{*}{\Phi}{}^{\alpha\beta}=\frac{1}{2(-\mathbf{A})^{\frac{1}{2}}}\epsilon^{\alpha\beta\mu\nu}\Phi_{\mu\nu}$$

$$\Lambda=\tfrac{1}{4}\overset{*}{\Phi}{}^{\alpha\beta}\Phi_{\alpha\beta}$$

and

$$\Omega=\tfrac{1}{4}\Phi^{\alpha\beta}\Phi_{\alpha\beta}.$$

From the field equations $\mathbf{G}^{\alpha\beta}_{\circ\,,\beta}=0$, and from Eq. (3) we have

$$((-\mathbf{A})^{\frac{1}{2}}\overset{*}{\Phi}{}^{\alpha\beta})_{,\beta}=-\mathbf{J}^{\alpha}, \quad \mathbf{G}^{\alpha\beta}_{\circ\,,\beta}=0,$$
$$(\mathbf{A}=\mathrm{Det}\mathbf{A}_{\alpha\beta}, \quad g=\mathrm{Det}g_{\alpha\beta}). \tag{6}$$

In this form Eqs. (6) may be compared with Born's[4] electrodynamics.

With the assumed approximation for the Φ's and identifying the $\mathbf{A}_{\alpha\beta}$-field as in a "Minkowski world," in the absence of gravitation we find that the field equations

$$R_{\alpha\beta}=0, \quad \mathbf{G}^{\alpha\beta}_{\circ\,;\gamma}=0, \quad \Gamma_{\alpha}=0, \quad \mathbf{G}^{\alpha\beta}_{\circ\,,\beta}=0$$

reduce to

$$\Gamma^{\alpha}_{\beta\gamma,\,\alpha}=0, \quad \mathbf{G}^{\underline{\alpha\beta}}_{\cdot\,,\beta}=-\mathbf{G}^{\mu\beta}\Gamma^{\alpha}_{\mu\beta}, \quad \Phi^{\alpha\beta}_{\cdot\,,\beta}=0. \tag{7}$$

(The equations $\Gamma_{\alpha}=0$, $\mathbf{G}^{\alpha\beta}_{\circ\,,\beta}=0\dotplus\Phi^{\alpha\beta}_{\cdot\,,\beta}$ are equivalent, and they represent the vanishing of the magnetic current density in Maxwell's electrodynamics.)

In a particular Lorentz frame (x, y, z, ct), the first and the third sets of equations of (7) can be put into a vector form as

$$\left.\begin{aligned}\nabla^{2}\mathbf{H}-\frac{1}{c^{2}}\frac{\partial^{2}\mathbf{H}}{\partial t^{2}}&=-\tfrac{1}{2}\nabla\times\mathbf{J}\\ \nabla^{2}\mathbf{E}-\frac{1}{c^{2}}\frac{\partial^{2}\mathbf{E}}{\partial t^{2}}&=\tfrac{1}{2}\left(\frac{\partial\mathbf{J}}{\partial t}+\nabla\rho\right)\end{aligned}\right\}, \tag{8}$$

$$\left.\begin{aligned}\nabla\times\mathbf{E}+\frac{1}{c}\frac{\partial\mathbf{H}}{\partial t}&=0\\ \nabla\cdot\mathbf{H}&=0\end{aligned}\right\}. \tag{9}$$

The second set of equations of (7) lead to

$$[\eta^{\alpha\beta}\tfrac{1}{4}\Phi_{\mu\nu}\Phi^{\mu\nu}-\Phi^{\alpha\mu}\Phi^{\beta}_{\cdot\,\mu}]_{,\beta}=[\eta^{\alpha\beta}\tfrac{1}{4}\overset{*}{\Phi}_{\mu\nu}\overset{*}{\Phi}{}^{\mu\nu}-\overset{*}{\Phi}{}^{\alpha\mu}\overset{*}{\Phi}{}^{\beta}_{\cdot\,\mu}]_{,\beta}$$
$$=-\overset{*}{\Phi}_{\alpha\beta}J^{\beta} \tag{10}$$
$$(\eta_{ij}=-\delta_{ij}, \quad \eta_{i4}=\eta_{4i}=0, \quad \eta_{44}=1, \quad i,j=1,2,3).$$

Equations (10) could be regarded as a proof for the compatibility of the field equations only if the R.H.S. were proportional to the four vector $d^{2}x^{\alpha}/ds^{2}$; this, on the other hand, is to be looked for in the field equations $R_{\alpha\beta}=0$.

In the above we took

$$(\Phi_{23}, \Phi_{31}, \Phi_{12}; \Phi_{41}, \Phi_{42}, \Phi_{43})=(E_1, E_2, E_3; H_1, H_2, H_3).$$

The factor $(\frac{1}{4})$ in (8) is due to the fact that gravito-electromagnetic units are not introduced.

[1] A. Einstein, *The Meaning of Relativity* (1950).
[2] Ingraham, Ann. Math. **52**, 743 (1950).
[3] E. Schrödinger, Proc. Roy. Irish Acad. **A LI**, 213 (1948).
[4] M. Born, Nature **132**, 282 (1933). M. Born and L. Infeld, Proc. Roy. Soc. (London) **A144**, 425 (1934).

Intensity Distribution of the First Negative ($B^{2}\Sigma\rightarrow X^{2}\Sigma$) Band System of N_2^+

R. G. Turner and R. W. Nicholls
Department of Physics, University of Western Ontario, London, Ontario, Canada
(Received March 5, 1951)

THE theoretical work associated with a laboratory investigation of the mechanisms of excitation of $N_2^+(B^2\Sigma)$ in discharge tubes has required the calculation of the fractional transition probabilities of the vibrational bands of the first negative system of this molecule. The method of calculation employed is in all respects similar to that used in a set of previous calculations for the second positive system of nitrogen.[1] Because the first negative system forms an important part of the auroral spectrum, and from its measured intensity distribution, conclusions may be drawn regarding the state of the upper atmosphere,[2] it has been considered worthwhile to present here the results of these calculations.

The fractional transition probability $f(v', v'')$, shown for each band in Table I, is defined in the expression for the integrated intensity $I(v', v'')$ of a molecular band:

$$I(v', v'')=CN(v')E(V', v'')f(v', v''),$$

where v' and v'' are the vibrational quantum numbers of the two levels involved in the transition. $N(v')$ is the population of molecules in the upper level, and $E(v', v'')$ is the energy separation between the two levels. C, the constant of proportionality is so adjusted that $\Sigma_{v''}f(v', v'')=1$ for each v' sequence.

In order to express the results as fractional transition probabilities, it was necessary to perform calculations for some transitions where bands are not reported to be observed.[3] These are indicated in italics. With the exception of $f(5, 3)$ each of the $f(v', v'')$ values in italics is small enough to suggest that the respective band would, in fact, be difficult to observe. The fact that (5, 3) is not reported in spite of its high $f(v', v'')$ value perhaps may be explained by its calculated wavelength (λ3274.24) lying between those of the (3, 3) (λ3285.3) and (4, 4) (λ3268.1) bands of the second positive system. Possibly, development of the rotational structure of these bands may tend to overlap and obscure (5, 3). Experimental work on this point is in progress.

Comparison between the aforementioned calculations and a less extensive previous set[4] shows fair agreement.

[1] R. W. Nicholls, Phys. Rev. **77**, 421 (1950).
[2] D. R. Bates, Proc. Roy. Soc. (London) **A196**, 562 (1949).
[3] T. R. Merton and J. G. Pilley, Phil. Mag. **50**, 195 (1925).
[4] D. R. Bates, Proc. Roy. Soc. (London) **A196**, 223 (1949).

TABLE I. Fractional transition probabilities, $f(v', v'')$. Transitions where bands are not reported to be observed are indicated in italics.

v' \ v''	0	1	2	3	4	5	6	7	8	9	10	11
0	0.701	0.223	0.047	0.024	0.006							
1	0.334	0.266	0.266	0.067	0.037	*0.028*	*0.002*					
2	0.058	0.435	0.078	0.242	0.089	0.048	0.043	*0.006*				
3	*0.001*	0.147	0.438	0.011	0.175	0.083	0.064	0.070	*0.011*			
4		*0.001*	0.220	0.395	0.000_2	0.115	0.075	0.069	0.085	*0.038*	*0.001*	
5			*0.005*	*0.306*	0.334	*0.007*	*0.07*	0.058	*0.065*	*0.094*	*0.06*	0.000_2

Proceedings of the American Physical Society

Minutes of the 1951 Annual Meeting Held at New York, February 1–3, 1951

THE 303rd meeting of the American Physical Society, being the 1951 Annual Meeting, was held in the buildings of Columbia University in New York City on Thursday, Friday, and Saturday, February first, second, and third, 1951. With respect to the number of contributed (ten-minute) papers this meeting set a new record (291, as against 273 at the Washington meeting of the previous spring). With respect to registration it slumped to 1730 from the previous high of 2070; this is ascribed to chaotic conditions on the railroads. How much of this diminished registration is to be credited to the American Association of Physics Teachers (AAPT), convening simultaneously in Barnard College, we cannot know. There were twenty-eight invited papers, the givers and the titles of which are shown in the following pages commingled with the abstracts of the ten-minute papers. Most of these were in the field of nuclear physics; one group was provided by Brookhaven National Laboratory, and afforded an excellent conspectus of its work and its opportunities; another came in the main from Nevis Laboratory. Aside from nuclear physics, there were half-day symposia of our Divisions of Electron Physics and of Fluid Dynamics, and papers by W. P. Allis, S. Chapman, and J. Bardeen. The labors of the Local Committee, headed as heretofore by W. W. Havens, were beyond all measure and beyond all praise.

The joint session of the two Societies (APS and AAPT) was held in the McMillin Theatre on the Friday afternoon. It began with the Retiring Presidential Address—under the title "Molecular-Beam Researches in Nuclear and Electronic Researches" by President I. I. Rabi of our Society; continued with the presentation to J. W. Hornbeck of the Oersted Medal of the AAPT, and was concluded by the Richtmyer Lecture of the AAPT, delivered by J. C. Slater under the title "The Electron Theory of Solids."

The banquet of the two Societies was held on the Friday evening in the Grand Ballroom of the Hotel New Yorker. The attendance was three hundred and sixty-seven. The after-dinner speaker was J. R. Oppenheimer, who spoke principally on meson theory.

At the Business Meeting of the American Physical Society (held on the Friday morning) the Tellers of Election reported the elections of the following candidates to the respective offices for the indicated terms: *President*, (1951) C. C. LAURITSEN; *Vice-President* (1951) J. H. VAN VLECK; *Secretary* (1951) K. K. DARROW; *Treasurer* (1951) G. B. PEGRAM; *Managing Editor* (1951–52) S. A. GOUDSMIT; *Councillors* (1951–54) R. F. BACHER and E. M. PURCELL; *Members of the Board of Editors* (1951–53) M. GOLDHABER, R. SERBER, and C. H. TOWNES. The terms of all commenced at the end of this Annual Meeting. Thus, at this moment occurred the transfer of the Managing Editorship to S. A. Goudsmit from E. L. Hill, who had valiantly assumed the burden of this hard and all-important task in December 1949 when John Tate fell suddenly ill, and had carried it very well for all the intervening months. A vote of thanks was tendered by the Society to Dr. Hill for his exemplary services. The headquarters of *Physical Review* has now taken its leave of the University of Minnesota, its generous host for a quarter of a century, and has been established at the Brookhaven National Laboratory.

The Society at its Business Meeting on recommendation of the Council adopted an Amendment to the By-Laws, whereby Section 1 of Article VI is made to read as follows:

"1. Each Member of the Society who has paid his dues in full shall be entitled to receive *Physical Review* published by the Society, except that a member not residing in the United States, Canada, or Mexico shall be entitled to receive *Physical Review* only after payment in addition to dues of an amount to be fixed by the Managing Editor. The Council shall be empowered to fix the terms on which members of the Society shall receive either *Physics Abstracts* or *Engineering Abstracts*."

Be it said in this connection that the subscription price at which *Physics Abstracts* and *Engineering Abstracts* are sold to the Society by the Institution of Electrical Engineers (London) has lately been raised; and the purpose of the amendment to the By-Laws is to enable the Council to levy an extra charge on those members of the Society who desire to receive either Journal (it may also become necessary to offer a subsidy to these Journals to make up for the loss they will sustain if many of our members decline to subscribe). A Committee has been appointed and has been instructed to make recommendations about our future relations with *Science Abstracts*.

At the Business Meeting the Secretary further reported a change in the administration of the Society which had been approved by the Council two days earlier. Our Constitution does not place a ceiling on the size of the Board of Editors; it

merely states that not fewer than nine members of the Board (and the Managing Editor in addition) shall be elected. Some time ago the Council increased the membership of the Board to twenty-four, and appointed nine additional members to serve on *Physical Review* and six to serve on *Reviews of Modern Physics*. Henceforth, all twenty-four shall be elected; and each election-ballot will carry the names of six candidates to the Board who are to serve on *Physical Review* and two more who are to serve on *Reviews of Modern Physics*, the terms being always for three years. The nomination-ballot will afford opportunity for eight nominations to the Board.

The Secretary further reported that the membership of the American Physical Society just before the New York meeting stood at 9472; and should all the candidates elected at that meeting duly enter upon membership before further losses occur through death or otherwise, the membership will rise to 9740. The treasurer reported that during 1950 the income of the Society exceeded its expenditures by about $5000; there is little hope that we shall be so fortunate in 1951.

The Council elected twelve candidates to Fellowship and two hundred and sixty-eight to Membership; their names are appended at the end of these Minutes. The Council nominated I. I. Rabi and S. A. Goudsmit to the Governing Board of the American Institute of Physics, and they have been duly elected in replacement of W. V. Houston and J. T. Tate.

By action of the Council and of the American Institute of Physics, a publication charge of ten dollars is established for "Letters to the Editor of Physical Review" regardless of length. As in the case of the publication charge (otherwise known as "Page charge"), hitherto established for articles, payment of this charge will be asked not from the author but from the institution which employs him; and payment will entitle the author to one-hundred gratuitous reprints.

Those who read the Minutes sedulously will remember that at its meeting in Chicago (November 26, 1950), the Council registered its disapproval of certain proposals as to "scientific manpower," and instructed a Committee to examine the problem. This Committee met in Washington on December 8 and 9, 1950, and consulted with many people who are concerned in this matter. The views which the Committee adopted are those which were formulated by D. W. Bronk, President of the National Research Council, in a letter addressed on December 11, 1950 to R. L. Clark. This letter is reproduced hereunder, and the Council has approved it formally.

According to reports reaching the office of the Society, we have lost through death Hendrik de Wet Botha (South Africa), C. F. Eyring (Provo), Eugene Gardner (Berkeley), William Huppert (Newark), J. R. Loofbourow (Cambridge), C. D. Montgomery (New Haven), and Marcia Keith (Braintree) who was one of the six survivors of the group who met in May 1899 to organize the American Physical Society.

Elected to Fellowship: A. E. Benfield, J. H. Buck, Lee Davenport, V. H. Fraenckel, A. C. Graves, C. P. Keim, D. W. R. McKinley, J. R. Risser, F. W. Sears, Samuel Seeley, Madeline M. Tate, B. E. Watt.

Elected to Membership: William E. Abbot, Clarence E. Albertson, Leland C. Allen, Kessar Alexopoulos, Robert C. Axtmann, Louis L. Bailin, Marvin E. Backman, Russell M. Ball, William P. Ball, Michel J. L. Baranger, William A. Barker, Thomas E. Banks, John H. Barrett, Richard Baskin, Ernest Bauer, Wallace W. Beaver, R. Becker, Joseph G. Berick, Irwin I. Bessen, Norman S. Beyer, Daniel G. Bills, Ronald H. Bingham, Peter M. Bird, Leroy N. Blumberg, Dwain B. Bowen, Raymond F. Boyer, Thomas H. Braid, Charles E. Branyan, Joseph X. Brennan, Robert Brennan, Albert P. Bridges, Bertram N. Brockhouse, Frank J. Broughton, Walter L. Brown, George J. Brucker, Keith A. Brueckner, Bernard F. Burke, David Bushnell, Melvin Calvin, Frederick L. Canavan, Robert S. Carter, Charles C. Cerato, Homero L. Cesar, Claude Cherrier, Eugene D. Clayton, Philip Cohen, Stanley Cohen, Glover S. Colladay, Jr., Glenn D. Collins, Richard V. Collins, Allan M. Cormack, Noel Corngold, Andrew W. Crans, Albert D. Crowell, Benjamin P. Dailey, Walter Daskin, John S. Derr, Jr., Dr. Hl de Vries, Robert W. Dickson David L. Douglas, James E. Draper, Raymond V. Dyba, Wilbur E. Dyer, Joseph T. Eisinger, Robert Elioff, Myron A. Elliott, Frank O. Ellison, Sven Epken, Burton P. Fabricand, Auard F. Fairbanks, Waldon Fickett, Frederick H. Fisher, Herbert Fishman, Charles H. Fletcher, Ping K. Fong, Gilbert C. Ford, Wilson J. Frank, Stanley C. Freden, Ephraim H. Frei, Herbert M. Freid, Gordon B. Gaines, Charles G. B. Garrett, John D. Garrison, Herbert Glazer, Per Gloersen, Leon P. Goldberg, Mark Goldsmith, Lester K. Goodwin, Harold L. Greenwald, Roger Grismore, Harold Gruen, Alfred S. Gutman, Clarence R. Haave, Eugene Haddad, Richard W. Hales, John W. Handin, Harry E. Handler, Lester B. Hanson, Eugene R. Hardwick, Jr., Nicolas J. Harrick, Don R. Harris, Clifford J. Heindl, James W. Henderson, Walter H. Higa, Peter Hillman, Joseph F. Hook, Hilda H. T. Hsieh, Kun Huang, Leonard Hubscher, Watts S. Humphrey, John L. Hundley, Angus L. Hunt, Richard G. Inskeep, Taturo Inui, Ralph E. Jamison, Clark E. Johnson, Jr., Richard A. Johnson, Walter H. Johnson, Herbert W. Jones, Sister Mary Joseph, I.H.M., Arnold H. Kahn, Harmut P. Kallmann, Hildegard K. Kallmann, Herbert Kanner, Nisbet S. Kendrick, Jr., John F. Kephant, Leroy T. Kerth, Edward J. King, Robert H. Kingston, Jerome Kraitchman, John W. Kress, Victor E. Krohn, Jr., Murray A. Lampert, Joseph E. Lannutti, John M. LaRue, Gordon J. Lasher, Mother Lorraine Lawrence, Dent I. Lay, Tsung D. Lee, Robert K. Lewis, Robert A. Levy, Paul R. Liller, Gunnar Lindström, Theodore A. Litovitz, William O. Lock, Duncan H. Looney, John L. Lundberg, Charles A. Lundquist, John E. MacDonald, Malcolm H. MacGregor, James E. Mapes, Basil Markow, Charles R. Marotta, Ursula M. Martius, Robert D. Maurer, Charles E. McCain, Philip T. McCormick, Harold V. McIntosh, George L. Meyer, Robert F. Meier, William G. Mikel, Richard C. Mockler, Walter J. Mordarski, Harry A. Morewitz, Minoru P. Nakada, Robert Nathans, Samuel M. Neamtan, Howard W. Neill, William B. Nelligan, Lester L. Newkirk, Steven Obuhanich, Jr., Daniel J. O'Connor, Chester T. O'Konski, Michael J.

Ozeroff, Frank R. Pomilla, Miriam Paul, Rolf Pauli, Melvin Pavalow, William W. Piper, Robert G. Pohl, Robert L. Powell, Edwin A. Power, Robert L. Poynter, George W. Pratt, Jr., Ruggero Querzoli, Karl H. Puechl, Giulio Racah, Peter D. Randolph, Ronald L. Reed, Sidney G. Reed, Jr., Erich Regener, Alfred J. Reis, Walter J. Rhein, Rex E. Richards, Richard P. Riesz, Thomas F. Rogers, Harold E. Rorschach, Jr., John Ross, Stefan Rozental, Arthur Y. Sakakura, George Salzman, Richard H. Sands, Rolf P. Scharenberg, William C. Schupp, Nick A. Schuster, Ruth F. Schwarz, Ralph E. Segel, Karl A. Sense, Williard M. Sessler, Subrahmaniyan Shanmugadhasan, James W. Shearer, Marvin Silver, Howard E. Singhaus, Mriganka S. Sinha, Lars Sjoquist, Arnold G. Skrivseth, James R. Smith, Walter J. Smith, Wesley R. Smith, William B. Smith, William C. Sneed, Robert K. Soberman, Jack A. Soules, Reginald K. Squires, Sidney Standil, Alexander Stieber, William P. Stinson, Julian Stone, Simon Stopek, Hinko H. Stroke, Alexander V. Stuart, Edward F. Sturcken, Charles Süsskind, John L. Symonds, James H. Talboy, Jr., Katsumi Tanaka, William E. Taylor, Lee R. Tepley, Frederick R. Tesche, William J. Thaler, Joseph A. Thie, Sigvard Thulin, Hendrik A. Tolhoek, Kazuhisa Tomita, Vanna C. Tongiorgi, Björn Trumpy, Sidney Van den Bergh, Johannes Van der Mark, James J. Vasa, William M. Venable, David H. Volman, John F. Waddell, Lawrence D. Walker, John M. Walsh, Rudolf W. Waniek, Douglas M. Warschauer, George D. Watkins, John S. Waugh, Charles R. Whitsett, Jack W. Wild, James P. Wittke, Bertram Wolfe, Robert L. Wolke, William W. Wood, Peter E. Wynter, Philip H. Yuster, Henry Zeldes, Paul F. Zweifel, Alfred J. Zmuda.

KARL K. DARROW, *Secretary*
American Physical Society
Columbia University
New York 27, N.Y.

NATIONAL ACADEMY OF SCIENCES

11 December 1950

Mr. Robert L. Clark
Director, Manpower Office
National Security Resources Board
Washington 25, D. C.

My dear Mr. Clark:

In response to your request of September 7, 1950, to advise you on the question of scientific manpower, conferences have been held by various scientific organizations, including a group convened by the National Research Council. Their reports disagree in certain details regarding their more extreme features, but essential agreement appears to have emerged on the first and most urgently necessary steps. As representing this common denominator of agreement, I feel justified in sending you the following recommendations; I believe furthermore, that they represent the attitude of many scientists with whom I have conferred and the Council of the National Academy of Sciences and the Chairman of the Divisions of the National Research Council. In order, however, to give these recommendations official status I am requesting a formal vote of the Council of the Academy and am asking Dr. Whitaker, Chairman of our National Research Council, to poll the Chairmen of the Divisions of the Council. The recommendations are:

1. That a National Scientific Personnel Board (NSPB) be established promptly.
2. The Board (NSPB) should operate under the guidance and authority of the NSRB, as its decisions will have cumulative effects on many sectors of our economy.
3. The Board (NSPB) should be authorized and directed to establish a Register of professionally qualified scientists and engineers in critical fields and students if they are not provided for by other mechanisms.
4. The Board (NSPB) should establish criteria of "professional qualifications" and should be empowered to include in the Register related groups other than natural scientists and engineers if such should prove desirable.
5. Directives should be issued requiring each Local Draft Board to assign to the NSPB (with credit against its quota) any draftee who can qualify for the Register; NSPB should be authorized to decide whether the draftee is to be assigned to one of the military services or released under appropriate controls to special civilian work and classified as "in Essential Scientific Service." Any draftee so classified should not be free to enlist or accept military status, but may appeal to the NSPB for review of his case.
6. This Board (NSPB) should be asked to examine continuously the problems relating to professional and scientific manpower and to advise the NSRB and the President regarding the effective use of those available and the maintenance of a continued supply of trained personnel.

The National Academy of Sciences-National Research Council will be glad to give advice in formulating the functions and composition of the NSPB should the NSRB desire such assistance.

It is my belief that this action would pave the way for further steps if and when these should become necessary.

Yours sincerely,
(SIGNED) Detlev W. Bronk, President

Errata for abstracts will be found on page 346.

PROGRAMME

THURSDAY MORNING AT 10:00

McMillin

(C. E. MANDEVILLE presiding)

Cosmic-Ray Particles; Nuclear Scattering

A1. Origin and Behavior of Cosmic Rays Observed at 1600 M. W. E. Underground. K. GREISEN, G. COCCONI, AND L. M. BOLLINGER, *Cornell University.*—In a salt mine under 600 meters of earth, 93 counters were disposed in crossed telescopes of large area ($\frac{1}{2}$ m²) but small angular resolution ($\pm 7°$), containing 14 in. Pb and followed by 21 in. Pb with a double counter row underneath. Particles crossing the telescopes triggered master pulses which registered, on a hodoscope, coincidences with the individual counters underground, and with 80 unshielded counters (total surface 3 m²) placed on the surface of the ground at vertices of a 43-meter square. The observed correlation of particles underground with air showers increases from zero at large zenith angles to 14 percent in the vertical direction, agreeing with the interpretation that all the particles underground were contained in extensive showers having more than 500 electrons at the surface. The absolute frequency of particles underground agrees with that of surface air showers with more than 500 electrons. The absorption in 21 in. Pb is (1.3 ± 0.26) percent, slightly exceeding the absorption in equivalent rock overhead, indicating that the penetrating particles are mostly mesons, probably accompanied by occasional penetrating secondaries. Underground, penetrating showers are observed in the hodoscope records; also groups of parallel particles which appear to be μ-mesons in cores of large air showers.

A2. A Study of the Proton Content of the Low Energy Hard Component at Sea Level.* G. W. MCCLURE, *Bartol Research Foundation.*—By interposing between the coincidence counters of an anticoincidence absorption telescope a fourfold coincidence train of low pressure (so-called "inefficient") counters, it has been possible to estimate the percentage of protons contained in the low energy end of the penetrating component spectrum. As the sea-level radiation capable of penetrating 10 cm Pb is chiefly nonelectronic and consists mainly of mesons for which the momentum spectrum is well known, a measurement of the counting efficiency of the low pressure train for *all* radiation penetrating 10 cm Pb allows an accurate calculation of the efficiency for particles of any mass and range. A determination of the efficiency for counting only the relatively low energy radiation absorbed in 5.5 cm Pb below the low pressure train leads to the conclusion that a very small fraction of the stopped component consists of particles heavier than μ-mesons. If in fact the absorbed radiation (range between 10 and 15.5 cm Pb consists solely of mesons and protons, the percentage of the latter is 4 ± 5 percent. Systematic uncertainties which could affect this result by a few percent will be discussed.

* Assisted by the joint program of the ONR and AEC.

A3. Decay Processes Observed in a Multiple Plate Cloud Chamber at 10,600 Feet.* H. BRIDGE, F. HARRIS, AND B. ROSSI, *M.I.T.*—In an experiment designed primarily to study the secondary particles from nuclear interactions, we have obtained several pictures showing decay processes. In one series of measurements the cloud chamber was triggered by a penetrating shower detector immediately above it. With this arrangement several pictures were obtained in which decay occurs either in the gas or in one of the plates. Some of these events are inconsistent with the known $\pi \rightarrow \mu$ or $\mu \rightarrow e$ decay processes. In one such event a slow particle ionizing several times minimum originates in a nuclear event, penetrates 1.7 g cm^{-2} Al and decays in the gas giving a charged product at about 90 degrees. The decay product goes back to the Al plate where it is strongly scattered or else suffers a further interaction. The event is consistent with the decay of a particle of mass $\approx 900\ m_e$ into a π-meson.

* Assisted by the joint program of the ONR and AEC.

A4. Boundary Effects in Cosmic-Ray Neutrons at a Water Surface.* Author Unknown.—The energy and spacial distributions of the neutron component of the cosmic radiation were investigated on and below the surface of Echo Lake in Colorado. Ten enriched BF_3 counters connected in parallel were used as the neutron detector. The associated circuitry was placed on a platform which was erected in the middle of the lake. The detector and preamplifier were placed in a watertight box which was supported by lever arms attached to the platform. The thermal neutron density was measured at different depths by employing tin and cadmium shields about the detector. The thermal neutron density was measured at different depths by employing tin and cadmium shields about the detector. The thermal neutron density decreased down to a depth of 30 cm in agreement with the theoretical predictions made by Bethe, Korff, and Placzek.[1] The thermal neutron density remained constant below a depth of 30 cm. The production rate of 4.2×10^{-4} neutrons per gram per second and the absorption depth of 138 grams per cm² were calculated from the data obtained 50 cm below the surface. These results are found to be consistent with the idea that nuclear disruptions are the main source of neutrons in the cosmic radiation at 10,600 feet.

* This work was supported by the ONR and AEC.
[1] Bethe, Korff, and Placzek, Phys. Rev. **57**, 573 (1940).

A5. Some Observations on the New Unstable Cosmic-Ray Particles.* W. B. FRETTER, *University of California, Berkeley.*—A large cloud chamber containing several lead plates has been used to observe the unstable particles already reported.[1,2] The probability of observation has been increased by making the distance between the lead plates two inches instead of 0.75 inch as in our previous experiments. Twenty cases have been seen at sea level where a neutral particle changed into two charged particles in the gas and three cases of sudden changes of direction in the gas have been observed. In one event produced by a neutral, one of the secondary particles was heavily ionizing (estimated at about 4x minimum), passed through a 0.25-inch lead plate without noticeable change in ionization or scattering, and thus must have had a mass larger than that of a π-meson. These events all occur in penetrating showers and the findings of the previous observers are generally confirmed.

* Assisted by the ONR and AEC.
[1] G. D. Rochester and C. C. Butler, Nature **160**, 855 (1947).
[2] Seriff, Leighton, Hsiao, Cowan, and Anderson, Phys. Rev. **78**, 290 (1950).

A6. A New Method of Energy Determination of Heavy Primaries of the Cosmic Radiation. B. PETERS, H. L. REY-

NOLDS,* AND D. M. RITSON, *University of Rochester.*—Preliminary measurements have been made on a stack of plates exposed at 90,000 feet for 8 hours at Minnesota. Part of the stack consisted of 20 plates, each separated by 3 mm of brass. Some of the heavy tracks traced through are observed to break up into showers of protons, alphas, and heavier fragments, which can also be followed through the stack. Relative scattering measurements have been made for the alphas and heavier particles by measuring their separations in successive plates and taking second differences. The velocities of the alphas and heavy fragments should be similar to that of the incident primary initiating the shower on the assumption that they could not have experienced appreciable deceleration without breaking up. Spurious scatterings can be introduced by errors in plate alignment and separation; these systematic errors can be eliminated by statistical analysis with showers of more than three particles. The highest energy measured to date is 26±5 Bev per nucleon (potassium or calcium giving a shower of 1 boron, 3 alphas, and 8 protons). The method should work up to energies of 100 Bev per nucleon. This work was supported by the joint program of the ONR and AEC.

* AEC Predoctoral Fellow.

A7. Multiple Scattering Calibration for Cosmic-Ray Energy Determinations. L. VOYVODIC AND E. PICKUP, *National Research Council, Canada.*—Measurements have been made on the multiple Coulomb scattering of electron pairs produced in photographic emulsions which were exposed to the 14- and 17-Mev (p, Li) gamma-rays. This experimental scattering calibration will be shown to be in approximate agreement with the detailed theories of E. J. Williams and others, and the resolution of the multiple scattering technique will be discussed. Examples of scattering measurements and energy determinations for high energy cosmic-ray particles will be shown.

A8. Scattering of Protons at 31.5 Mev from Be, C, Al, Pb. ROY BRITTEN,* *Princeton University.*—The 31.5-Mev protons from the Berkeley linear accelerator were used to bombard foils of beryllium, polystyrene, aluminum, and lead. The charged particle spectra resulting have been observed at 90° and 160° using a sodium iodide crystal[1] and photo-multiplier as detector. For beryllium, excitation of the known 2.4-Mev level was observed, as well as broad or composite levels at higher excitation. For carbon, excitation of the known levels at 4.3, 7.1, and 9.5 Mev was observed as well as broad or composite levels between 10 and 19 Mev. In addition, the deuteron group from the reaction $C^{12}(p, d)C^{11}$ was observed. The proton groups corresponding to the 4.3- and 9.5-Mev levels were strongly anisotropic but no evidence for anisotropy was found for the other groups from carbon. The cross sections for elastic scattering at 160° ran from 0.15(Be) to 0.64(Pb) millibarn per steradian and the ratio of the elastic scattering cross section at 90° to that at 160° ran from 8.8(Al) to 10.8(Pb). Calculations indicate that no simple model can explain these results. A description will be given of a rapid manual method for the analysis of pulse-height distributions recorded on film.

* Public Health Service Fellow.
[1] Franzen, Peele, and Sherr, Phys. Rev. 79, 742 (1950).

A9. 240-Mev Proton-Proton Scattering.* C. L. OXLEY, R. D. SCHAMBERGER, AND O. A. TOWLER, JR. *University of Rochester.*—Proton-proton scattering cross sections have been measured in the angular range from 90 to 27.5 degrees cg by two previously described methods. One method[1] uses coincidence scintillation counters within the cyclotron tank. The other[2] distinguishes p-p scattering by magnetic deflection and photographic detection. Absolute cross-section values in either case are derived from the beta-activity of the polyethylene target and the cross section for the $C^{12}(p, pn)C^{11}$ reaction.[3] The cross section shows little variation throughout the angular range studied. An absolute cross section of 4.5±0.5 millibarns per steradian is found. Data at smaller scattering angles will be presented.

* Assisted by the joint program of the AEC and ONR.
[1] C. L. Oxley, Phys. Rev. 76, 461 (1949).
[2] A. O. Towler and C. L. Oxley, Phys. Rev. 78, 326 (1950).
[3] Aamodt, Peterson, and Phillips, Phys. Rev. 78, 87 (1950).

A10. n-D Scattering at 1.4 Mev.* A. M. THORNDIKE AND A. W. WOTRING,† *Brookhaven National Laboratory.*—Neutrons of 1.35–1.50 Mev were produced by deuteron bombardment of carbon with the Brookhaven Van der Graaff. A beam defined by a paraffin collimator passed through a deuterium-filled cloud chamber, and the angular distribution of recoil deuterons was observed. Background was reduced by shielding the cloud chamber. 374 recoil tracks from a total of 1027 had position, range, and angle within acceptable limits. For these tracks the background correction was from 4 to 20 percent. The data show frequent backward scattering in the center-of-mass system and are consistent, within statistical uncertainties, with the ordinary force curve of Buckingham and Massey.[1] The same result has been found at higher energies,[2,3] but these results do not rule out the possibility of agreement with improved exchange force calculations.[3]

* Work performed under the auspices of the AEC.
† Now at Columbia University, New York City.
[1] R. A. Buckingham and H. S. W. Massey, Proc. Roy. Soc. A179, 123 (1941).
[2] J. F. Darby and J. B. Swan, Austral. J. Sci. Research 1, 18 (1948); Hamouda, Halter, and Scherrer, Phys. Rev. 79, 539 (1950); E. Wantuch, Phys. Rev. 79, 729 (1950); and others.
[3] Martin, Burhop, Alcock, and Boyd, Proc. Phys. Soc. (London) 63A 884 (1950). (See note added by Buckingham.)

A11. Nuclear Energy Level in Be^9. KENNETH E. DAVIS, *Reed College.*—Because of its apparent sharpness and clear separation from near neighbors the energy level observed in the nucleus[1] of Be^9 seemed particularly appropriate for the study of the angular dependence of inelastic scattering of protons. A modified form of a scattering camera developed by Wilkins[2] was used to obtain intensity values for scattering angles between 20° and 165° at ten-degree intervals. Preliminary results indicate a variance with the results predicted by Longmire from a simplified model, but the difference is readily explainable. The apparent narrowness of the level even though it is a virtual one has been of particular interest and further study of this characteristic was indicated. An attempt has been made to narrow the energy spread of the incident beam for this purpose and some success was achieved. This work was initiated and carried to near completion at the University of Rochester with the assistance of the University and the Research Corporation.

[1] K. E. Davis and E. M. Hafner, Phys. Rev. 73, 1473 (1948).
[2] T. R. Wilkins and G. Kuerti, Phys. Rev. 55, 1134 (1939).

A12. Elastic Scattering of Gamma-Rays. ROBERT R. WILSON, *Cornell University.*—Gamma-rays may be scattered elastically by atoms in several ways: (a) by Thompson scattering from the nucleus; (b) by Rayleigh scattering from the tightly bound electrons; (c) by nuclear resonance scattering; and (d) by Delbruck scattering from the electric field of the nucleus through virtual pair formation. In the hope of measuring the last process, a large NaI–Th scintillation detector has been used to study the elastic scattering of the gamma-rays of Co^{60} and ThC″ from a lead target. It is possible to distinguish the small elastic scattering from the overwhelming elastic Compton scattering because of the good energy resolution of the detector. Preliminary measurements have been

made at various angles from 45° to 135°. At 135°, the cross section for the 1.3-Mev Co^{60} gamma-ray is 0.2 mb, and for the 2.6-Mev ThC″ gamma-ray it is 0.1 mb. These are higher than those calculated by Bethe* on the basis of Thompson and Rayleigh scattering alone, particularly for 2.6 Mev where the theoretical value is not higher than 0.03 mb. The measurements are being extended to other elements to exclude the remote possibility that the large experimental result is due to nuclear resonance scattering.

* H. A. Bethe, private communication.

THURSDAY MORNING AT 9:30

Horace Mann

(EDWARD TELLER presiding)

General Theory; Electromagnetic Theory; Gaseous Diffusion

B1. Matrix Formalism for Fields of Arbitrary Spin. D. C. PEASLEE,* *Washington University.*—Equations of the form $(\beta_\mu{}^{2s}\partial_\mu+\mathfrak{M})\psi=0$ are investigated, where $\beta_\mu{}^{2s}=\gamma_\mu{}^1+\cdots+\gamma_\mu{}^{2s}$ and the γ^i are commuting Dirac matrices. The β^{2s} are reducible, and one of the irreducible representations has a ψ for which there are $(2s+1)$ "large" components in the rest system and hence describes a particle of spin s. The operators for extracting this representation are expressible in terms of the general $\beta_\mu{}^{2s}$. The equivalent Klein Gordon equation contains only one rest-mass. The β-matrices provide natural bases for constructing the intrinsic n-pole electromagnetic tensor of the particle, q^n. From the commutation relations of the β^{2s} it follows immediately that $n\leq 2s$. The β^{2s} formalism is directly related to those of Dirac and Bhabha; it contains implicitly the auxiliary conditions found necessary by Pauli and Fierz.

* Assisted by the joint program of the ONR and AEC.

B2. The Partition Function in Quantum Statistics. M. DRESDEN, *University of Kansas,* AND R. L. PETRITZ, *Catholic University.*—An attempt has been made, to obtain an alternate mathematical formulation of quantum statistics. One starts in close analogy to the Gibbs ensemble, with a postulate concerning the probability $P(n_1\cdots n_i\cdots)$ of a given set of occupation numbers n_i in the energy states ϵ_i. The expression for P is similar to the conventional one, except for a combinatorial factor which characterizes the statistics. Then employing the technique of generating functions, one obtains for any statistics, the partition function as a single complex integral. For Bose statistics one obtains

$$\exp(-\psi/kT)=\frac{1}{2\pi i}\oint\frac{dz}{z^{N+1}}\prod_i\frac{1}{(1-z\exp-\epsilon_i/kT)^{g_i}}.$$

The poles of the integrand are determined by the energy levels of the system, their multiplicity is determined by the weight of the levels. The classical partition function follows exactly from this expression, the customary expressions for the other statistics follow only after a saddle point integration. This approximation is not always legitimate as was observed for the case of an ensemble of oscillators.[1]

[1] N. H. V. Temperley, Proc. Roy. Soc. (London) **199**, 361 (1949).

B3. On Criticisms of Generalized Boson Theories. ALEX E. S. GREEN, *University of Cincinnati.*—Podolsky's electrodynamics, the writer's work in meson theory[1] and the closely related or equivalent work of Bopp, Bhabha, DeBroglie, Born and Green, Thirring and others have been criticized in various papers by Pais, Feynman, Mathews, Feldman, Pais and Uhlenbeck[2] and others who apparently tend to the conclusion that it is impossible to give a realistic interpretation to a generalized boson theory. We consider the content of the critical papers and show that some of the arguments contain serious defects. We further show that the totality of these arguments does not furnish a substantive basis for any significant conclusion whatsoever. Thus the theories need not yet be relegated simply to the role of a powerful convergence securing device. The theories have been used formally in this manner with skill and success by Feynman, Pauli, and Villars and others but without regard for basic problems.

[1] A. Green, Phys. Rev. **73**, 26, 519 (1948); **75**, 1926 (1949).
[2] A. Pais and G. Uhlenbeck, Phys. Rev. **79**, 145 (1950). See this paper for other references.

B4. On the Theory of Thermal Fluctuations, or Generalized Noise.* HERBERT B. CALLEN AND THEODORE A. WELTON,† *University of Pennsylvania.*—The Nyquist equation for the voltage fluctuations ("Johnson noise") in electrical impedances is generalized. The resulting theorem relates the fluctuations of the intensive thermodynamic parameters of an equilibrium system to appropriate kinetic coefficients relevant to irreversible processes which may occur in the system. Thus every generalized impedance function implies a fluctuating "force," related to the real part of the impedance by an equation formally identical to the Nyquist relation. Several applications are made of the theorem. The law of viscous drag of a fluid on a moving body (e.g. Stokes' law) implies a fluctuating force and yields the law of Brownian motion. The radiation impedance for the electromagnetic radiation from an oscillating charge implies a fluctuating electric field in the vacuum and yields the Planck radiation law. The acoustic radiation impedance of a gaseous medium similarly yields an expression for the pressure fluctuations in a gas.

* This work was supported in part by the ONR.
† Now at Oak Ridge National Laboratory, Tennessee.

B5. Element Formation in a Nonstatic Cosmological Model.* R. A. ALPHER AND R. C. HERMAN, *The Johns Hopkins University.*—The problem of element formation in the early stages of an expanding universe has been examined according to the neutron capture theory.[1] Numerical results have been obtained on the SEAC (Bureau of Standards Eastern Automatic Computer) for a variety of initial conditions. The observed universal relative abundance—atomic weight distribution can be reproduced theoretically in general trend if the neutron-proton ratio is taken as 4:1 at the start of the capture process ($t\sim 130$ sec in the expansion), and the density of matter $\rho_m=\rho_0 t^{-\frac{1}{2}}$, $\rho_0\sim 4\times 10^{-4}$ g/cm³. The effect of initial neutron-proton ratio on the density required to fit the observed abundance distribution will be discussed.

* Supported by the U. S. Navy, Bureau of Ordnance.
[1] R. A. Alpher and R. C. Herman, Revs. Modern Phys. **22**, 153 (1950).

B6. Electromagnetic Induction in Matter of Astronomical Dimensions.* W. F. G. SWANN, *Bartol Research Foundation.*—On account of induced currents, a highly conducting body of

large size finds great difficulty in experiencing a change of magnetic flux through any portion of it, so that, indeed, a perfect conductor of any size, large or small, can experience no change of flux. However, since mechanical forces due to the currents invite alteration of dimensions of the matter, it becomes possible to realize changes of magnetic flux through areas fixed in space and therefore to realize acceleration of cosmic-ray particles. A particular case comprising a conducting ring of matter which is allowed to expand under the self-repulsion of its current elements is worked out in detail, showing that if t is the time for the radius of the ring to increase from r_0 to R, then $t<Mr_0^{\frac{1}{2}}(R-r_0)/2^{\frac{1}{2}}N^{\frac{1}{2}}$, where M is the mass of the ring and N is the initial magnetic flux through it. The time actually decreases with increase of N. While the flux through the ring as a whole remains constant with the time, the flux through a fixed area decreases with the time.

* Assisted by the Joint Program of the ONR and AEC.

B7. Mode Representations in Uniformly Stratified Regions. N. MARCUVITZ, *Polytechnic Institute of Brooklyn.*—Representations of the electromagnetic field in regions possessing a symmetry axis can be expressed in terms of guided waves travelling parallel or perpendicular to the symmetry direction. Such representations, which have different rates of convergence, require the solution of an eigenvalue problem yielding in general both a discrete and continuous spectrum. The complete set of eigenfunctions may be determined by contour integration of a characteristic Green's function via the methods of Weyl, Titschmarsh, *et al.* Complete mode representations for dielectric slab regions that comprise both discrete (surface waves) and continuous modes will be presented.

B8. Multipole Radiation from Oscillating Systems. P. R. WALLACE, *McGill University.*—We develop a systematic approach to the analysis of the radiation from a given oscillating system of charges and currents, without the use of approximations. Using a simple vector identity, the vector potential is separated into irrotational and solenoidal parts. The field may be expressed in terms of the latter alone. A second vector identity involving the operator L also introduced by Franz* enables us to separate the field into parts for which the radial components of electric and magnetic field, respectively, vanish identically. Expansion in spherical harmonics then gives rise to magnetic and electric multipoles of all orders. Introduction of "tensor spherical harmonics"† permits the exhibition of these radiations in terms of natural multipoles (derivatives of $1/r$) in a manner invariant under Cartesian coordinate transformations. The angular momenta and radiation patterns of the various multipoles may be readily obtained. The fields are determined without restriction as to size of radiating system (compare wavelength), in the induction as well as the radiation region.

* W. Franz, Z. Physik **127**, 363–370 (1950).
† P. R. Wallace, Can. J. Research **A26**, 99–114 (1948).

B9. Radiation from a Nonmetallic Wave Guide. ROBERT M. WHITMER, *Rensselaer Polytechnic Institute.*—In an earlier paper[1] it was shown that a part of the field about a dielectric guide cannot be described by modes, but is given by a branch-cut integral. For a line source in a plane guide, this integral has been calculated at a point far distant from the source. The nonmodal field behaves like $H_1^1(kr)\sin\alpha$, where k is the propagation factor in the medium surrounding the guide, and α is measured from the axis of the guide. This field is radiated, not guided. Comparisons of radiated and guided power will be discussed.

[1] Robert M. Whitmer, Proc. IRE **36**, 1105 (1948).

B10. Random-Flight Treatment of Gaseous Diffusion. PAUL PITKANEN, *Rice Institute*, AND W. H. FURRY, *Harvard University.*—If one constituent of a gas mixture is present in very small concentration, the diffusion coefficient D_{12} can be found by solving the problem of random flights for a single molecule. The random-flight picture has ordinarily been used with the assumption that successive free paths are entirely independent, but a formulation can be obtained that takes complete account of correlations of speed and direction. The determination of D_{12} is made to depend on the solution of an integral equation, and a procedure of solution by successive approximations suggests itself rather naturally. The results for the first two approximations are obtained without undue labor and agree with the results of the standard Enskog-Chapman theory. That the agreement would hold in all approximations is evident from the fact that the same integral equation can be obtained from the standard formalism in the given case of infinitesimal concentration. The random-flight approach provides both a derivation of the key equation from simple physical considerations and a method of solution considerably less complicated than that of the traditional treatments.

B11. A Simplified Treatment of Gaseous Diffusion for Arbitrary Concentration. W. H. FURRY, *Harvard University.*—When the constituents of a mixture of gases are present in comparable concentrations, the random-flight picture cannot be used to give a reliable account of diffusion. Correlations between the effects of collision on the two colliding molecules and between the diffusion of one constituent and that of the other make it impossible to base an adequate treatment on a description of the prolonged wandering of a single molecule. It is then natural to proceed by considering the distribution of velocities of molecules in a volume element as accounted for by the place of each molecule's last previous collision and its fate in that collision. To make the resulting equations manageable, one must assume a stationary case with all quantities independent of two of the rectangular coordinates. The treatment is in its geometrical structure somewhat reminiscent of crude "mean free path" arguments, but is entirely accurate within the usual assumptions of gas theory. It leads to a pair of integral equations that are also contained in the Enskog-Chapman formalism, and that can be treated by a fairly simple method to obtain the known approximate results.

B12. Effect of Turbulence in Thermal Diffusion Columns.* JOHN DONALDSON AND W. W. WATSON, *Yale University.*—Contrary to the specification of the Furry, Jones, and Onsager theory that the gas flow in thermal diffusion isotope separation columns must be lamellar, we find that some turbulence improves markedly the separation factor and transport. Our measurements are made with hot-wire columns 3 meters long, power input ~725 watts, using argon gas. At pressures three times that for onset of general turbulence the separation factor q_s is still 1.5. When spacers consisting of pairs of 40-mil Ni wires are attached to the vertical hot wire every 10 cm along its length, q_s for optimum pressure rises from 9.1 to 27.5, while spacers every 5 cm increases q_s further to 36. The optimum pressure at the same time increases from 0.17 atmos (no spacers) to 0.28 atmos. For a similar column with a plain hot wire but having constrictions every 15 cm in the cold wall wall q_s is 26.6. Analysis of our data shows that the coefficient of remixing by convection drops by a factor of 3 when the wire carries 10-cm spacers. Since for each of these operations equilibrium is attained in about the same time (6 hours), this introduction of regularly spaced swirls in the gas produces a decided increase in efficiency.

* Assisted by the AEC.

B13. Self-Diffusion in Capillaries at Low Pressures.* SIDNEY VISNER, *Carbide and Carbon Chemicals Division.*—The self-diffusion coefficient of xenon was measured in capillaries of 0.0025 and 0.025 cm radius, using Xe-131 grown from I-131, as a tracer. Pressures ranged from 0.003 to 15.8 mm Hg,

corresponding to radius to mean free path ratios, r/λ, from 0.001 to 65. Capillaries were investigated of half-length to radius ratio, L/r, of 65, 9.8, and 2.7. Two chambers were connected by capillaries and the relative concentration in each chamber was measured directly with counters. The results from capillaries of L/r 65 but not from L/r 9.8 agree with the Pollard-Present[1] theory in which θ (mean molecular velocity), r/λ, and L/r are the only parameters. However, in the limit of zero pressure, the coefficients for all tubes, $0.64\theta r$, $0.55\theta r$, and $0.43\theta r$, agree with Clausing.[2] The extrapolation to $0.66\theta r$ for infinite length tubes agrees with Knudsen's diffusive flow coefficient. The coefficient extrapolated to 76 mm Hg pressure is 0.058 cm²/sec±2 percent at 27.3°C, 25 percent higher than reported elsewhere[3] but in agreement with calculations.[4]

* Work performed under contract with AEC.
[1] W. G. Pollard and R. D. Present, Phys. Rev. **73**, 762 (1948).
[2] P. Clausing, Physica **9**, 65 (1929).
[3] W. Groth and P. Harteck, Z. Electrochem. **47**, 167 (1941).
[4] Hirschfelder, Bird, and Spotz, Chem. Revs. **44**, 205 (1949).

B14. Hydrodynamic Equations of Diffusion. M. H. JOHNSON, *Naval Research Laboratory*.—The interdiffusion of ionized and neutral gases in a magnetic field has been treated by kinetic theory methods.[1] The problem can also be handled with a phenomenological definition of the diffusion coefficients as a starting point.[2] The assumption that each gas satisfies the ideal gas law then leads to the conception of a frictional force, exerted by one gas on another, which is proportional to their relative velocity and is inversely proportional to their diffusion coefficient. The hydrodynamic equations, which follow from the equilibrium of forces on each gas, determine the diffusion currents when the external forces are known. Explicit solutions for the diffusion currents are the previously found relations[1] between the currents and the diffusion coefficients of the various pairs of gases. Moreover, the hydrodynamic equations show that, in the absence of external forces, the motion is adiabatic and that, if external forces are present, the work done appears as heat generated by the friction of relative motion.

[1] T. G. Cowling, Proc. Roy. Soc. (London) **A183**, 453 (1945).
[2] M. H. Johnson and E. O. Hulburt, Phys. Rev. **79**, 802 (1950).

B15. Calculation of Vibrational Relaxation Times for Gases and Gas Mixtures. R. N. SCHWARTZ, *U. S. Naval Ordnance Laboratory*.—Using the method previously described by the author,* the vibrational relaxation times for gases such as O_2, N_2, Cl_2, Br_2, and gas mixtures such as Cl_2-N_2, Cl_2-H_2, Cl_2-H_e, Cl_2-CO, N_2-O_2, N_2-H_2, N_2-CO, N_2-A, O_2-H_2, O_2-CO, and O_2-A have been computed. The intermolecular force field was approximated by an exponential form. The numerical constants appearing in this form were derived from viscosity and diffusion data. The calculated values of the relaxation times agree well with experimental values, where such values are available. The case of Cl_2-CO, where the agreement is not so good, is discussed as an example of a class of impurities that is different from the others listed above. The method of calculation presented can be applied to polyatomic molecules.

* R. N. Schwartz, Phys. Rev. **79**, 546 (1950).

THURSDAY MORNING AT 9:30

Pupin 301

(W. W. BUECHNER presiding)

Reactions of Transmutation and Nuclear Energy Levels (Lighter Elements Mostly)

C1. Gamma-Ray Energy Measurement of the Tritium (p, γ) Reactions.* R. S. ROCHLIN AND B. D. MCDANIEL, *Cornell University*.—A preliminary measurement has been made of the energy of the gamma-radiation[1] from the reaction $T^3(p, \gamma)He^4$. Tritium absorbed in a zirconium target was bombarded by 0.94±0.06-Mev protons from the Cornell cyclotron. The gamma-rays emerging at 38° in the laboratory system were detected by a pair spectrometer,[2] which indicated a line of mean energy 19.9±0.6 Mev. Considering the proton energy and Doppler effect, this corresponds to a Q value of 19.2±0.6 Mev available from the mass change, which is to be compared with the value $Q=19.78\pm0.07$ Mev obtained from mass tables.[3] The observed line width at half-maximum, approximately 8 percent, is no greater than the probable resolution width of the spectrometer, in which a 0.003-in Pb radiator was used. More precise measurements are planned.

* Assisted by the ONR.
[1] Argo, Gittings, Hemmendinger, Jarvis, and Taschek, Phys. Rev. **78**, 691 (1950).
[2] R. L. Walker and B. D. McDaniel, Phys. Rev. **74**, 315 (1948).
[3] H. A. Bethe, *Elementary Nuclear Theory* (John Wiley and Sons, Inc., New York, 1947).

C2. Angular Distribution of the Ground-State Deuteron Peak from the $Be^9(p, d)Be^8$ Reaction.* J. A. HARVEY, *M.I.T.*—The intensity of the ground-state deuteron peak from a thin beryllium target has been measured from 20°–140° at proton energies of 8, 7, 6, and 5 Mev. The protons were obtained from the M I.T. cyclotron and the deuterons detected by a triple proportional counter as previously reported.[1] Preliminary results indicate that the differential cross sections at these 4 proton energies are the same within 20 percent, both in absolute value and in angle. The angular distributions are approximately isotropic from 140°–70° and rise rapidly in the forward direction; the intensity at 20° is 15 times that at 70°. The differential cross section at 90° is approximately 2 millibarns/steradian. Previously reported work with proton energies from 0.6 to 1.0 Mev show the distribution to be more strongly forward for the higher energy. The observed similarity of the distribution between 5 and 8 Mev is not in agreement with a simple pick-up process. A similar forward distribution has been observed in the $Be^9(d, t)Be^8$ reaction with 14-Mev deuterons by H. E. Gove.

* This work has been supported in part by the joint program of the ONR and AEC.
[1] Livingston, Boyer, Gove, Harvey, and Deutsch, Phys. Rev. **78**, 344 (1950).

C3. The Alpha-Spectrum from the Deuteron Bombardment of Beryllium. R. W. GELINAS AND S. S. HANNA,* *Johns Hopkins University*.—In the search for excited states of Li^7 by means of magnetic analysis of the $Be^9(d, \alpha)Li^7$ reaction, previous investigators[1,2] have covered a region up to an excitation energy in Li^7 of about 3.5 Mev. The investigation made by Inglis[2] revealed the rise of a broad peak or plateau of alpha-particles above $E_{ex}=2.5$ Mev, which was attributed to the three-particle reaction $Be^9(d, 2\alpha)H^3$. We have continued this

investigation, covering a region up to $E_{ex}=5.6$ Mev, and have confirmed the presence of this reaction which produces a strong continuum throughout the region analyzed above the threshold. Between $E_{ex}=3.2$ and 4.5 Mev the intensity is fairly constant; between $E_{ex}=4.5$ and 5.1 Mev the observations are obscured by Li^{+++} recoils which cannot easily be distinguished from alphas at the particular bombarding energy employed (680 kev); above $E_{ex}=5.1$ Mev the intensity of the continuum appears to diminish. The possibility that a homogeneous group of alpha-particles might be obscured in the continuum (or the Li recoils) will be discussed.

* Assisted by a contract with the AEC.
[1] W. W. Buechner and E. N. Strait, Phys. Rev. 76, 1547 (1949).
[2] D. R. Inglis, Phys. Rev. 78, 104 (1950).

C4. Angular Distribution of High Energy Neutrons from Targets Bombarded with 110-Mev Protons.* KARL STRAUCH,† *Harvard University.*—The well-known carbon detection method[1] has been used to measure the angular distribution of neutrons of energies above 20 Mev emitted from Be, C, Al, Cu, and Pb targets bombarded with 110-Mev protons. The targets were situated at a radius of 40 inches inside the cyclotron tank and polystyrene detectors were placed at various locations on the tank wall behind Dural absorbers. An angular range from 0° to 63° (with gaps due to obstructions) could be covered. Preliminary results give similar neutron distributions from Be, Al, Cu, and Pb targets with full widths at half-intensity from 54° to 59° in the center-of-mass system. The angular distribution from C has a flat peak possibly because of the high threshold energy of the (p, n) reaction. The influence of neutrons originating from sources other than the target will be discussed and the results compared with similar data taken with 340-Mev protons.[2]

* Assisted by the joint program of the ONR and AEC.
† Society of Fellows.
[1] Helmholz, McMillan, and Sewell, Phys. Rev. 72, 1003 (1947).
[2] Miller, Sewell, and Wright, UCRL 753.

C5. Angular Distributions of Fast Neutrons from Deuteron Bombardment.* K. H. SUN, D. HARRIS, F. A. PECJAK, AND B. JENNINGS, *Westinghouse Research Laboratories,* AND A. J. ALLEN AND J. F. NECHAJ, *University of Pittsburgh.*—The angular distribution of neutrons from Be bombarded by 15-Mev deuterons was measured using the $F^{19}(n, 2n)F^{18}$ and $Ta^{181}(n, 2n)Ta^{180}$ reactions, with thresholds at 10.8 and 7.7 Mev, respectively, as detectors. Some 0.8-cm strips of 0.006-in. Teflon (C_nF_{2n}) and 0.0003-in. tantalum were supported on a 7.84-cm diameter ring surrounding the target. The neutron distribution was obtained by cutting the strips into 3° to 9° segments and measuring the activities of the F^{18} and Ta^{180}. The distribution, using a Ta-detector, was a single forward peak with a width at half-intensity of 54° similar to that found with the low threshold (0.97 Mev) $S^{32}(n, p)P^{32}$ detector.[1] Using the F-detector, two well resolved forward peaks with a separation of 30° were found. Because of the high neutron threshold of the F-detector only neutrons from Be(d, n) and none from Be$(d, 2n)$ were detected. The thicknesses of the Be-targets in these experiments were effectively reduced on account of the characteristics of the high threshold detectors used.

* Assisted by the joint program of the ONR and AEC.
[1] Allen, Nechaj, Sun, and Jennings, Phys. Rev. 76, 188 and 463 (1949); Phys. Rev. 77, 752 (1950).

C6. Slow Neutrons from the Deuteron Bombardment of Light Elements.* E. B. TUCKER,† *Yale University.*—A BF_3 proportional counter has been used to determine neutron thresholds in several (dn) reactions. Results for $C^{13}(dn)N^{13}$ show that only the resonance levels of the compound nucleus N^{14} are observed. Deuteron bombardment of the elements Li, Be, B, and F gives thresholds which indicate the existence of a number of levels which are assigned to the various final nuclei. Be^9 targets yield the previously reported level[1–3] at a bombarding energy of 0.92 Mev as well as another level at 2.3 Mev. The $Li^7(dn)Be^8$ reaction yields thresholds at deuteron energies of 0.75 and 2.1 Mev; $B^{11}(dn)C^{12}$ at 1.1, 1.9, and 3.4 Mev; $F^{19}(dn)Ne^{20}$ at 1.3 Mev. No thresholds which could be attributed to $B^{10}(dn)C^{11}$ were observed. The energy determinations involved the stopping power of helium relative to air, and a determination of this quantity agreed with Mano's[4] results.

* Supported by the joint program of the ONR and AEC.
† Now at University of Minnesota, Minneapolis, Minnesota.
[1] Evans, Malich, and Risser, Phys. Rev. 75, 1161 (1949).
[2] Bonner, Butler, and Risser, Phys. Rev. 79, 240 (1950).
[3] W. D. Whitehead and C. E. Mandeville, Phys. Rev. 77, 732 (1950)
[4] Mano, J. phys. radium 5, 628 (1934).

C7. The Angular Distribution of $Li^6(n, \alpha)H^3$ for 270-kev Neutrons. JAMES H. ROBERTS, LILLIAN DARLINGTON, AND JACK HAUGSNES, *Northwestern University.*—The angular distribution for $Li^6(n, \alpha)H^3$ for 270-kev neutrons is being determined by track measurements in Li^6 loaded 100μ C2 emulsions. The angle between the direction of neutron incidence and the triton tracks is measured for all tracks meeting geometrical selection criteria. The plates wrapped in cadmium were exposed by J. Morris Blair to $Li^7(p, n)Be^7$ neutrons from the Argonne electrostatic generator. About 1500 tracks have been measured and divided into 15° intervals in the center-of-mass system. The tracks produced by epithermal neutrons are resolved from the main group for three angle intervals around the forward direction. These may be used to calculate the epithermal background for all intervals assuming these tracks to be distributed isotropically. The distribution is highly asymmetric. The triton yield is highest in the forward direction, has a large dip near 90°, and rises to a moderate height in the backward direction. The data has been fit to a cosine series indicating a predominance of p-neutron capture with a small contribution from s-neutrons.

C8. Relative Angular Distribution of the 17.6- and 14.8-Mev Lithium Gamma-Rays.* M. B. STEARNS AND B. D. MCDANIEL, *Cornell University.*—Earlier measurements of the relative angular distribution of the 14.8- and 17.6-Mev gamma-rays from lithium are in disagreement. Devons and Hine using a pair spectrometer and a 10-kev target,[1,2] obtained the result that to an accuracy of 20 or 30 percent no variation of the relative intensities exists. H. Waffler,[2] using the reaction $C^{13}(\gamma, 3\alpha)$ for the detection of the gamma-rays in photographic plates, obtained a ratio of about 2.7 for the relative intensities at 90° and 0°, and about 1.8 for the ratio at 45° and 0°. Using a pair spectrometer and bombarding a thick target with 500-kev protons, we have made measurements at 0, 35, and 70 degrees. Defining R to be the ratio of intensities of the 17.6- to the 14.8-Mev lines, we obtained the values $R_{35}/R_0=1.06\pm0.05$ and $R_{70}/R_0=1.01\pm0.05$. This would indicate that the protons producing the narrow resonance at 440 kev are s-protons. Measurements are also being made bombarding a thin target with 1-Mev protons. This should produce evidence as to whether the ground state and the 3-Mev level of Be^8 have the same angular momentum.

* Assisted by the ONR.
[1] S. Devons and M. G. N. Hine, Proc. Roy. Soc. (London) A199, 56–73 (1949).
[2] Proc. of the Harwell Nuclear Physics Conf., September 1950.

C9. Energy Levels in Li^7. H. E. GOVE AND J. A. HARVEY,* *M.I.T.*—The spectra of inelastically scattered protons, deuterons, and alphas of incident energies 8, 14, and 31 Mev, respectively, from lithium and the alpha-spectrum from $Be^9(d, \alpha)Li^7$ have been studied using the M.I.T. cyclotron and apparatus previously reported.[1] In all four reactions a group corresponding to a level in Li^7 with a mean value of 4.77 ± 0.10 Mev has been observed. In addition, an alpha-group from $Be^9(d, \alpha)Li^7$ has been observed which would correspond to a

level in Li^7 at 7.54±0.17 Mev. This agrees with the observations of Blair.[2] Recent work by Adair[3] indicates an alternative interpretation of the results found by Blair and this point will be discussed. Aside from the well-known level at 480 kev and the ones reported here no additional levels in Li^7 have been found.

* This work has been assisted by the joint program of the ONR and the AEC.
[1] Livingston, Boyer, Gove, Harvey, and Deutsch, Phys. Rev. 78, 344 (1950).
[2] J. M. Blair, quoted by Goldsmith, Ibser, and Feld, Revs. Modern Phys. 19, 259 (1947).
[3] R. K. Adair, Phys. Rev. 79, 1018 (1950).

C10. The Excitation Function for $B^{10}(d, \alpha)Be^8$. W. D. WHITEHEAD,* *Bartol Research Foundation.*—The excitation function for the $B^{10}(d, \alpha)Be^8$ ground-state group and the first excited level have been determined by bombarding thin targets of isotopically enriched boron (96 percent B^{10}) with deuterons from the Bartol Van de Graaff generator and observing the α-particles with an argon-filled proportional counter at 90° to the beam. The bombarding energy was varied from 0.5 Mev to 1.6 Mev in 0.1-Mev intervals; and both curves have evidence of a resonance at 1.05 Mev, which gives a level in C^{12} at 26.1 Mev.

* Sponsored by a joint program of the ONR and AEC.

C11. Gamma-Rays from Deuteron Bombardment of B^{10}, B^{11}, N^{14}, and F^{19}.* JAMES TERRELL,† *Rice Institute.*—A pair spectrometer has been used to analyze the high energy gamma-ray spectra produced by bombarding thick targets of natural boron, enriched boron (96 percent B^{10}), nitrogen, and fluorine with 1.56-Mev deuterons. The resolution used was about 10 percent. The $B^{10}+D$ spectrum shows gamma-rays of 4.52, 6.74, and 9.11 Mev, with possible unresolved lines between these values. The spectrum from $B^{11}+D$, partially masked by the strong $B^{10}+D$ gamma-rays, shows a single 4.5-Mev gamma-ray, ascribed to the level of that energy in C^{12}; this is identical with the Po-Be gamma-ray spectrum[1] from C^{12*}. The nitrogen target produced strong gamma-rays of energy 5.35, 7.48, and 8.51 Mev, with some indication of unresolved lines at 4.4 and 6.5 Mev. The $F^{19}+D$ spectrum shows high energy gamma-rays of energy 8.1, 9.4, and 11.7 Mev. In any of these spectra lower energy gamma-rays may be present though undetected, because of the large variation of spectrometer sensitivity with energy.

* Assisted by the joint program of the ONR and AEC.
† AEC Predoctoral Fellow; now at Western Reserve University, Cleveland, Ohio.
[1] J. Terrell, Phys. Rev. (to be published).

C12. High Energy Photo-Protons from Carbon.* D. WALKER, *Cornell University.*—Protons with energies up to more than 120 Mev have been observed to be emitted by a carbon target under bombardment by bremsstrahlung γ-rays from an electron synchrotron operated at 190 Mev. These high energy protons are emitted preferentially in the forward direction. The relative numbers of protons with energies exceeding 90 Mev, emitted per steradian at angles to the γ-ray beam of 30°, 60°, 90°, and 135° in the laboratory system, are approximately 3.5:2:1:0.2. For 90-Mev protons emitted at 30°, the nuclear cross section per steradian per Mev of proton energy per Q is of the order of a micro-barn, where Q is the total energy in the γ-ray beam divided by the maximum γ-ray energy. The number of protons exceeding an energy E decreases at least as rapidly as E^{-4} for E in the vicinity of 100 Mev. These results cannot be explained by a compound nucleus model. They are, however, in qualitative agreement with a two-nucleon model.[1]

* This work was performed under contract with the ONR.
[1] J. Levinger (see following abstract).

C13. High Energy Nuclear Photo-Effect.* J. S. LEVINGER, *Cornell University.*—The production of high energy protons[1] (40 to 250 Mev) by the nuclear photo-effect has been estimated using Heidmann's two-nucleon model[2] for the nuclear wave function. The cross section for the nuclear photo-effect has an energy dependence, and an angular dependence, similar to that for the deuteron photo-effect.[3] In the deuteron photo-effect there will be an upper limit E_0 to the proton energy spectrum, corresponding to the maximum photon energy. The energy spectrum of protons produced by a bremsstrahlung photon spectrum varies roughly as E^{-6}, for E less than E_0. For E greater than E_0, the energy spectrum decreases more rapidly. High energy protons have a strongly forward angular distribution in the laboratory system. The differential cross section for production of 90-Mev protons from carbon, at 30° in the laboratory system, is estimated as the order of 30 microbarns/steradian per photon (of 180 Mev), or 0.3 microbarn/steradian Mev, per Q.

* This work was performed under contract with the ONR.
[1] D. Walker, previous abstract.
[2] J. Heidmann, Phys. Rev. 80, 171 (1950).
[3] L. I. Schiff, Phys. Rev. 78, 733 (1950); J. Marshall and E. P. Guth, Phys. Rev. 78, 738 (1950).

C14. Photo-Proton Yields. ARNE LUNDBY AND LEONA MARSHALL, *University of Chicago.*—Protons from (γ, p) reactions[1] produced by betatron bremsstrahlung have been studied in a coincidence arrangement. The photon beam was collimated to 1.5 cm at 4 meters from the target. The protons were generated in thin foils oriented at 45° to the beam, and observed at 90° with two successive para-terphenyl crystals (~15 mg/cm). The scintillations were recorded by two 1P21 photo-multipliers in a fast coincidence circuit.[2] This arrangement was unable to detect protons of kinetic energy less than 3.5 Mev. The variation of coincidence rate with maximum energy showed the expected threshold characteristics. The identification of the detected particles as protons was made certain by measuring their time of flight between the two scintillators. This was done by examining the variation of coincidence rate with delay of the pulses from one photomultiplier. The yield of protons normalized to unit photon flux increases from the threshold to a maximum, and then falls off with increasing maximum energy. This behavior is similar to that of the photo-neutron process. For aluminum, the integrated photo-proton cross section $\sim 10^{-26}$ Mev cm². The integrated cross section was found to be roughly proportional to A.

[1] B. C. Diven and G. M. Almy, Phys. Rev. 80, 407 (1950); A. K. Mann and J. Halpern, Phys. Rev. 80, 470 (1950).
[2] Arne Lundby, Phys. Rev. 80, 477 (1950).

C15. Properties of (γ, n) Cross Sections. L. MARSHALL, *University of Chicago.*—The mean energies[1] of photons producing the reactions $Cu_{63}(\gamma, n)Cu_{62}$, $Zn_{64}(\gamma, n)Zn_{63}$, and $C_{13}(\gamma, n)C_{11}$, have been found by measuring the absorption coefficient per electron[2] for many values of Z. Monitor and detector were made of the element investigated. The absorbers were Be, C, Al, Ti, Fe, Ni, Cu, Zn, Se, Mo, and Sn. Less than 1 percent of the radiation striking the detector originated in the absorber. In this geometry the absorption cross section per electron is a linear function of Z. Its slope is Z^{-1} x pair production cross section of the screened nucleus. Its intercept is Z^{-1} x Compton cross section plus pair production cross-section of an electron. The experimental curves were linear for all three detectors. The slopes were evaluated with the Bethe-Heitler formula, yielding the mean energies 17.6±0.7 Mev for Cu_{63}, 16.7±0.7 Mev for Zn_{64}, and 25.3±1.5 Mev for C_{13}. The values from the intercepts agreed but had larger errors. Since no self-absorption was evident above the limit of experimental error, it followed from the assumption of a Breit-Wigner shape, that $\sigma_{\gamma n}(E_R) < 0.30 \times 10^{-24}$ for Cu_{63}, $< 0.44 \times 10^{-24}$ cm² for Zn_{64}, and $< 0.065 \times 10^{-24}$ cm² for C_{13}.

[1] Koch, McElhinney, and Cunningham, Phys. Rev. 81 (to be published).
[2] Blocker, Kenney, and Panowsky, Phys. Rev. 79, 419 (1950).

C16. Absolute Integrated (γ, n) Cross Section for Cu^{63}. A. H. ROSENFELD, L. MARSHALL, AND S. C. WRIGHT, *University of Chicago.*—We have measured the energy flux of the Chicago betatron at 46 Mev by a method similar to that of Blocker *et al.*, corrected for the deviation from the pair-production cross section calculated with the Born approximation. The method requires the examination of the initial slope and total area of the bremsstrahlung transition curves by measurement or the ionization produced in a thin-walled ion chamber as a function of depth in absorbers of various Z. The current from a monitor chamber was balanced against the current from the detector chamber to eliminate the effect of intensity fluctuations. The photon beam was collimated to 2.3×10^{-4} steradian and electron contamination was removed with a magnet. The relation of energy flux to roentgen per minute as measured on a victoreen ion chamber in a Pb cylinder with $\frac{1}{2}$-in thick walls is 2.6×10^{7} Mev sec^{-1} cm^{-2} $rimm^{-1}$ at 46 Mev. The measurement of the energy flux allowed the absolute determination of the Cu^{63} integrated photo-neutron cross section. Cu foil (6 mg cm^{-2}) was irradiated by the entire flux accepted by the intensity calibration system. Its activity was measured on a calibrated counter. The correction for self-absorption was shown to be negligible. Taking the value of 17.6 Mev for the mean energy of photons (see previous abstract, we calculate $\int\sigma_{\gamma n}(E)dE=(0.71\pm0.15)\times10^{-24}$ Mev cm^2 in the line for Cu_{63}.

THURSDAY MORNING AT 10:00

Pupin 428

(J. W. LISKA presiding)

High Polymer Physics; Biophysics

D1. The Relation between the Theory of Rubber and the Theory of Liquids. AUTHOR UNKNOWN.—It is usually assumed that rubber is formed of a network of non-interacting chain molecules. This paper is concerned with the extension of the statistical theory to interacting chains. Analogies can be developed between the theory of interacting chains and the various theories of liquids. The theory of liquids of Lennard-Jones and Devonshire[1] on the one hand and Kirkwood[2] on the other, each yield Waals' equation at high temperatures when used for models of rubber. At low temperatures only the latter will give a reasonable explanation of embrittlement. Both can explain the incompressibility. The behavior of rubber at low temperatures can be compared to that of a network with intermolecular forces comparable to those in a liquid. The increase in modulus observed at low temperatures is apparently due to these van der Waals interactions. No treatment of the stiffening of the chain at low temperatures is given although this stiffening may be an important factor in embrittlement.

[1] Lennard-Jones and Devonshire, Proc. Roy. Soc. (London) **A163**, 53.
[2] J. G. Kirkwood, J. Chem. Phys. 3, 300 (1935).

D2. Short-Time Stress Relaxation Properties of Plastics. M. T. WATSON, W. D. KENNEDY, AND G. M. ARMSTRONG, *Tennessee Eastman Corporation.*—An apparatus is described for the measurement of stress as a function of time following elongation of a plastic specimen to a predetermined strain. Rapid elongation is effected by release of a compressed, massive spring which extends the specimen until the motion is stopped. The load is measured by means of a tubular weighbar employing bonded-wire strain gauges; recording is done by means of oscillographs. Elongation requires about three milliseconds, and decay of stress for the subsequent two to five seconds is observed; the experiments thus cover a time zone for which little data have been reported in the literature. For practical applications, this time range corresponds to rates of stressing often encountered in use of plastic articles. It is found that plastics, depending upon their constitution, the temperature, and the strain, vary both in their rates of stress decay and in the ultimate amount of decay from a few percent to nearly 100 percent. The stress-time functions are not simple exponentials; in many cases, the stress is found to be approximately linearly dependent upon the logarithm of the time. Experimental results for a number of plastics are presented.

D3. Flow Figures and Delayed Plastic Flowing in Polymeric Film. JOHN KAUFFMAN, *University of Illinois,* AND WALLER GEORGE, *Naval Research Laboratory.*—Configurations of flow markings (generalized Lüders bands) are observed to form prior to the development of local necking (plastic shock waves) in polymeric films subjected to dead weight loading. Initially, the markings appear "bound" to free edges, or internal imperfections. Subsequent elapse of time under load allows further "growth" of the markings. Several typical types of development will be illustrated, including "reflection" from a free edge. Repeated loading experiments suggest that the time interval during which the flow marking is "bound" is less than about ten seconds in commercial polyamide film, at 3500 psi initial stress. When loadings for this duration are followed by sufficiently long rest periods, the effect of the initial localization disappears, and the specimen behaves on subsequent loading as a previously unloaded specimen. Time intervals under load greater than ten seconds, even when followed by reasonable "rest" periods, appear to induce irreversible localizations, which after a sufficient number of repetitions, lead to the formation of plastic shocks. In these cases the total time under load prior to shock formation is essentially the same as the delay time for shock formations under uninterrupted dead weight loading.[1]

[1] J. Kauffman and W. George, Phys. Rev. **77**, 761(A) (1950); Phys. Rev. **78**, 357(A) (1950).

D4. Specific and Apparent Specific Volumina of Polystyrene and their Significance. ARTHUR C. THOMPSON AND WILFRIED HELLER, *Wayne University.*—Apparent specific volumina of polystyrene are determined in chlorobenzene and bromobenzene, at 25.00°C, and are discussed on the basis of recent density measurements on bulk polystyrene by Flory and Fox. At least three percent of the volume of solid bulk polystyrene at room temperature consists of cavities. Its volume would be nearly the same as that of polystyrene dissolved in a good solvent if the apparent second-order transition could be avoided. It is proposed to characterize the apparent second-order transition by an alternation of configurational probability in neighboring volume elements. The resulting "microstrain" and cavitation allow a simple explanation of phenomena associated with the apparent second-order transition, such as brittleness. A comparative discussion of the new data and of scant data available

in the literature shows that the number of vacant sites within a polystyrene molecule in solution is small in good solvents—where conceivably a slight solvation exists—and is very large in poor solvents. In the latter case, the free volume may exceed that found in solid bulk polystyrene at room temperature. A correlation suggests itself between apparent (partial) specific volume and intrinsic viscosity of polymers supporting the view that the degree of solvent drainage across freely kinking polymer molecules is an important factor in their rheological behavior.

D5. Adsorption Isotherms and Fractional Adsorption of Polyethyleneglycols. WILFRIED HELLER AND WARREN TANAKA, *Wayne University.*—Previous work has shown that the adsorbability, on norit and on alumina, of PEG 6000 (polyethyleneglycol of molecular weight $M=6000$) is larger than that of PEG 600. The effect of the solvent-adsorbent combination upon the magnitude of the difference agreed with the rule of Freundlich and Heller. Separation of the above fractions from a mixture—by differential adsorption—was found to be feasible and practical. The detailed adsorption characteristics of ethyleneglycol and of PEG 300, 600, 1540, and 6000 were now determined (norit, aqueous solution). The specific adsorption increases very strongly with $\bar{M}$ below $\bar{M}=600$; it changes little at higher $\bar{M}$, particularly between 1540 and 6000, less the higher the equilibrium concentration. Claesson, on investigating other polymers within a range of much higher molecular weights, found the opposite effect of $\bar{M}$. A maximum adsorbability must therefore be assumed for an intermediate $\bar{M}$. An increase with $\bar{M}$—above a certain $\bar{M}$—in the amount of internal surface area inaccessible to the polymer molecules, would account for the above facts. A decision requires additional experiments with nonporous adsorbents. The formation of monomolecular polymer films at the adsorbent is indicated by the fact that the higher members of our fractions give Langmuir isotherms. The character of the rate curves agrees with that to be expected for diffusion of polymer molecules into a porous adsorbent.

D6. Effect of Primary Ionization on Tobacco Mosaic Virus. ERNEST POLLARD, *Yale University,** AND A. E. DIMOND, *Connecticut Agricultural Experiment Station.*—Preliminary studies have shown that tobacco mosaic virus in the dry state loses its infectivity relatively slowly. The loss of infectivity is dependent on temperature and at room temperature and below it can be held dry for several days. When bombarded by deuterons in the dry state, the action of radiation is predominantly at the locale of primary ionization, since secondary effects do not travel many atom radii. Using this fact a study has been made of the effect of varying the deuteron energy, and hence the relative separation of primary ionizations. The results show that tobacco mosaic virus presents a target of cross section 23×10^{-12} cm², which remains constant as the ionization density changes by a factor of two. If it is supposed that the virus has dimensions $50\times150\times2700$A, the results can be explained on the basis that one primary ionization produced anywhere in the virus causes inactivation. This is in striking contrast to similar experiments on bacterial viruses. The conclusion drawn is therefore that this one plant virus is essentially a single molecule.

* Assisted by the U. S. AEC.

D7. Irradiation of Viruses with Soft X-Rays. W. R. GUILD,* *Yale University.*—An x-ray tube and target chamber combination has been constructed for the purpose of irradiating viruses with very soft x-rays (500–3500 volts). The tube is designed for maximum current with minimum heating. Cathode, anode, and specimen holder are watercooled to prevent heat inactivation of the virus. The geometry is such that the specimen (inside the vacuum chamber) does not see the hot filament except by secondary diffuse reflection. The data so far show that the *T*-1 bacteriophage of *E. coli* is inactivated rather easily by these x-rays, the 37 percent dose at 2000 volts and 40 ma tube current requiring only about 20 minutes. The 37 percent dose varies with wavelength, and the object of the experiment is to study this variation to see whether the effects of absorption by particular elements can be determined as the x-ray spectrum crosses the absorption edges of the particular elements.

* AEC Predoctoral Fellow.

D8. Cyclotron Bombardment of Enzymes.* R. B. SETLOW, *Yale University.*—The technique, developed previously,[1] for the inactivation of dry enzymes and viruses by a cyclotron deuteron beam has been used to bombard the enzymes urease and catalase. These molecules are approximately spherical and have molecular weights 480,000 and 250,000, respectively. The enzymatic activity was determined by the rate of splitting of urea and hydrogen peroxide. For the two enzymes the cross section for inactivation by 3.8-Mev deuterons was found to be about ten times smaller than the geometrical cross section. When the ionization density along the deuteron path was increased by use of foils, the inactivation cross section rose, but still failed to reach the geometrical cross section. Thus, a primary ionization, which liberates about 90 ev within the molecule, does not inactivate the molecule as a whole. The mechanism of radiation inactivation and the internal structure of urease and catalase will be discussed in the light of these results.

* Assisted by the AEC.
[1] E. Pollard and F. Forro, Jr., Phys. Rev. **78**, 335 (1950).

D9. Cyclotron Bombardment of Hemoglobin.* R. K. APPLEYARD, *Yale University.*—Dried samples of human and dog carboxy hemoglobin have been irradiated by fast deuterons from the cyclotron, using the technique of Pollard and Forro.[1] The irradiated material is redissolved in buffer solution and is examined spectrophotometrically. Cross sections have been measured for the depression of the visible and soret absorption bands. These cross sections are lower than the known average area of the molecule per heme group, but rise with increasing ion density. The variation of the apparent cross sections with *p*H of the redissolved material show that destruction of heme groups is negligible. Oxidation of the iron atom to form methemoglobin is negligible, in striking contrast to the results of irradiation experiments carried out upon hemoglobin in aqueous solution.[2] The mechanism of the action of ionizing radiation upon dried conjugated proteins will be discussed on the basis of the experiments on hemoglobin.

* Assisted by the AEC.
[1] E. Pollard and F. Forro, Jr., Phys. Rev. **78**, 335 (1950).
[2] H. Fricke and B. W. Petersen, Am. J. Roentgenol. Radium Therapy **17**, 611 (1927).

D10. The Dependence of Photo-Reactivation of a Virus on the Wavelength of the Ultraviolet Used for Inactivation. DONALD J. FLUKE, *Yale University.*—The sensitivity of organisms to inactivation by ultraviolet light may usually be expressed in terms of a probability cross section. Plotted *versus* wavelength of the inactivating radiation, this cross section gives an inactivation spectrum for the organism. A number of organisms have been shown to recover from ultraviolet inactivation upon subsequent irradiation by wavelengths in the blue and near ultraviolet. This effect, called photo-reactivation, takes place for bacteriophages to a survival curve similar in shape to the over-all survival curve, but of shallower slope.[1] The inactivation cross section may be considered as consisting of two sectors, one photo-reactivable and the other not. The work reported in this paper concerns the relation between these two sectors for various wavelengths of inactivating radiation, that is, the effect of photo-reactiva-

tion on the inactivation spectrum. From 2400 to 2900A, where bacteriophage are most sensitive to ultraviolet, the two sectors are about equal for the virus T-1. The photo-reactivable sector appears to be proportionally lowest where over-all ultraviolet sensitivity is highest. Inactivation by wavelengths longer than 3000A appears at present to be almost completely photo-reactivable.

[1] R. Dulbecco, J. Bact. 59, 329 (1950).

D11. The Inactivation of Protein Monolayers with Deuterons.* FRANKLIN HUTCHINSON, *Yale University.*—Samples of bovine serum albumin to be inactivated by irradiation were prepared by transferring monomolecular films of the albumin from a water surface to a chromium-coated glass slide by the Blodgett-Langmuir technique. After bombardment with 1- to 3.7-Mev deuterons the percentage inactivation was determined by measuring the decrease in ability of the protein to react specifically with the homologous antibody. This binding capacity could be assessed by measuring the thickness of antibody which was adsorbed by the protein monolayer, the thickness of antibody being determined to better than 1A by an ellipsometer.[1] The fundamental advantages of this method of preparation of the irradiated sample are that very thin, uniform targets may thus be obtained, and that only very small amounts (less than micrograms) of material are needed. The cross sections for inactivation depend strongly on the deuteron energy, showing that the molecular dimension perpendicular to the plate is probably small compared to the spacing of ionization along the deuteron track. The cross section is about 100A² for 3.7-Mev deuterons, compared with our estimated 2500 A² for the normal globular albumin molecule.

* This work was supported by the AEC.
[1] A. Rothen, Rev. Sci. Instr. 16, 26 (1945).

D12. The Inactivation of Dry Protein Deposits with Deuterons.* W. P. MCNULTY, JR.† AND FRANKLIN HUTCHINSON, *Yale University.*—Using a colorimetric microanalysis, one may determine the percent survival of a protein antigen, bovine serum albumin, following bombardment with 3.7-Mev deuterons. The method depends on precipitation of antigen with homologous antibody, resolution, and color development with the Folin-Ciocolteau reagent.[1] In these experiments an aqueous solution of antigen was dried on foil disks prior to bombardment. The effective cross section of around 500 A² is five times larger than that found by irradiation of bovine albumin deposited in a monomolecular layer from a water surface. It is highly unlikely that such a difference can be due to an orientation effect among molecules in the monolayer. This is therefore direct evidence that there is a change in the spatial arrangement of the protein molecule when deposited in monolayer. Despite this change, the power of combining specifically with homologous antibody is retained.

* Supported by AEC.
† James Hudson Brown Junior Fellow.
[1] M. Heidelberger, and C. F. C. McPherson, Science 97, 405; 98, 63 (1943).

D13. Absorption and Action Spectra of Bacillus Subtilis. HAROLD J. MOROWITZ,* *Yale University.*—Ultraviolet absorption spectra have been taken for pure spore preparations of the bacterium, *Bacillis subtilis.* Ground preparations were used to eliminate scattering anomalies. Absorption maxima were found at 2770A, 2700A, and 2620A. The 2620A peak may be identified with nucleic acid and the 2770A peak may be identified with protein. Definite classification may not be made for the 2700A peak. The ultraviolet action spectrum (cross section for lethal effects as a function of wavelength) has been determined for the same organism. A strong peak was found in the 2700A region, and another maximum was found in the 2800A region. These may be correlated with the 2700A and 2770A absorption maxima. Relative quantum efficiencies may be obtained as a function of wavelength. The general similarity between action spectra and absorption spectra for the whole cell indicates that photons absorbed in most of the cell components are capable of causing lethal effects. The specific differences in the spectra indicate selectively high efficiencies for some of the absorbers.

* AEC Predoctoral Fellow.

THURSDAY AFTERNOON AT 2:00

Pupin 301

(C. C. LAURITSEN presiding)

Reactions of Transmutation and Nuclear Energy Levels, (Heavier Elements Mostly)

DA1. Energy Levels in F^{20} from the $F^{19}(d, p)F^{20}$ Reaction.* HUGH A. WATSON, D. M. VAN PATTER, AND W. W. BUECHNER, *M.I.T.*—The excited states of F^{20} have been investigated using the $F^{19}(d, p)F^{20}$ reaction with incident deuteron energies of 1.5 and 1.8 Mev. Proton groups from thin layers of PbF_2 on a platinum backing have been analyzed at 90 degrees using a 180-degree focusing annular magnet. The investigation has so far been carried over a range from the ground state to an excitation energy of about 2 Mev. Proton groups corresponding to the following Q-values were observed: 4.37, 3.72, 3.55, 3.39, 3.32, 3.06, 2.40, and 2.33. These correspond to excitation energies of 0, 0.65, 0.82, 0.98, 1.05, 1.31, 1.97, and 2.04 Mev. The levels at 0.82, 1.05, and 2.04 Mev have not previously been reported; the others are in agreement with the results of Allen and Rall.[1] Other proton groups have also been observed, and it is expected that some of these may be identified with the above reaction.

* This work has been assisted by the joint program of the AEC and ONR.
[1] R. C. Allen and W. Rall, Phys. Rev. 78, 337 (1950).

DA2. Nuclear Electron Pairs from $F^{19}(p, \alpha)O^{16}$. G. C. PHILLIPS AND N. P. HEYDENBURG, *Carnegie Institution of Washington.*—Scintillation counters and fast coincidence techniques have been used to examine the excitation function for the emission of pairs of electrons by the reaction $F^{19}(p, \alpha)^*O^{16}$ in the range of bombarding energies 0.8 to 2.0 Mev. The electrostatic generator of the Department of Terrestrial Magnetism was used to bombard thin targets of CaF_2 with protons monoenergetic to 0.1 percent. Six resonances due to levels in Ne^{20} that decay to the 6.052-Mev pair emitting level in O^{16} were observed. The resonant widths which range from 23 to 450 kev are slightly narrower than previously reported, and are in general wider than the Ne^{20} levels for the competing processes of gamma-ray emission. Angular correlations of the two members of the electron pair have been investigated and a search has been made for pairs of gamma-rays. The angular correlation data can be fitted reasonably well with a function $A+B\cos\theta$. No positive evidence for pairs of gamma-rays has been obtained.

DA3. Stacked Foil Technique for Nuclear Reactions With the Internal Cyclotron Beam.* N. M. HINTZ, *Harvard University.*—The stacked foil technique for obtaining nuclear excitation functions has been used with the internal 110-Mev proton beam of the Harvard cyclotron. The foils and absorbers are placed 1 inch above or below the plane of the circulating beam. Protons are scattered into the foils by multiple Coulomb scattering in a few mils of Ta placed in the median plane at 180° or 360° from the targets. The 180° arrangement is necessary when good energy resolution is desired as the cyclotron beam has been found to have a spread in energy of 12 Mev at 120 Mev.[1] The 180° position gives roughly ½ percent of the primary beam to $\frac{1}{16}$ in. diam foils; the 360° position about five percent as particles of all energies and angles in the horizontal plane are refocused at the target radius. Preliminary curves will be shown for the reactions $Al^{27}(p, 3pn)Na^{24}$ and $Al^{27}(p, 5p5n)F^{18}$. The proton flux at the foils has been monitored with the $C^{13}(p, pn)C^{11}$ reaction,[2] giving approximate absolute values to these cross sections.

The threshold for F^{18} is near 45 Mev, indicating the ejection of α-particles or heavier fragments from the nucleus.

* Assisted by the joint program of the ONR and AEC.
[1] N. Bloembergen and P. J. Van Heerden, paper presented at this meeting.
[2] Aamodt, Peterson, and Phillips, UCRL-526 (1949).

DA4. Excitation Functions for Proton Reactions With Sodium and Magnesium.* R. B. HOLT AND J. W. MEADOWS, *Harvard University.*—Proton bombardment at energies up to 120 Mev have been carried out on the Harvard University cyclotron using targets of $Na^{23}NO_3$, $Mg^{24}O$, $Mg^{26}O$, and ordinary MgO. A stacked sample and absorber technique was employed, using the formation of C^{11} from interleaved polyethylene foils as a monotor.† The internal scattered beam at positions 185° and 360° from the scatterer was used, the 185° position giving better energy resolution but lower intensity than the 360° position. For Na^{23}, the thresholds and absolute excitation curves for the reactions forming F^{18} and Na^{22} have been obtained. For Mg^{25} and Mg^{26}, the reactions to form Na^{24} and F^{18} have been studied. For Mg^{24}, the formation of F^{18} has been measured. Excitation function curves for these various reactions will be presented.

* Assisted by the joint program of the ONR and AEC.
† Aamodt, Peterson, and Phillips, University of California Radiation Laboratory Report 526 (1949).

DA5. Energy Levels in Na^{24} from $Na^{23}(d, p)Na^{24}$.* A. SPERDUTO AND W. W. BUECHNER, *M.I.T.*—The proton groups from $Na^{23}(d, p)Na^{24}$ have been analyzed with a magnetic spectrometer. Thus far, at a deuteron energy of 2.0 Mev, eight groups have been measured. The results are in general agreement with previous work[1] on this reaction, except that two of the reported levels in Na^{24} appear to be double. The Q-values obtained in the present work are 4.73, 4.26, 4.17, 3.39, 2.89, 2.86, 2.17, and 1.32 Mev.

* This work has been assisted by the joint program of the AEC and ONR.
[1] W. D. Whitehead and N. P. Heydenburg, Phys. Rev. 79, 99 (1950).

DA6. Magnetic Analysis of the $Si^{30}(d, p)Si^{31}$ Reaction.* D. M. VAN PATTER, H. ENGE, AND W. W. BUECHNER, *M.I.T.*—The proton groups from silicon-dioxide targets (with the Si^{30} content enriched to 64 percent) bombarded by 1.8-Mev deuterons have been analyzed at 90 degrees with a magnetic spectrometer. From a comparison with the proton groups observed from natural silicon-dioxide targets (3 percent Si^{30}), three proton groups were identified with the $Si^{30}(d, p)Si^{31}$ reaction. The measured Q-values of these groups were 4.367 ±0.010; 3.604±0.009; and 2.666±0.006 Mev, corresponding to the ground state of Si^{31} and excited states at 0.763±0.011 and 1.701±0.010 Mev. No additional $Si^{30}(d, p)Si^{31}$ proton groups were observed with an intensity greater than 0.15 the intensity of the group with Q-value of 4.367 Mev in an energy range corresponding to Q-values from 4.25 to 4.95 Mev. The Si^{31} levels recently reported by Motz and Humphreys[1] at 0.73±0.15 and 1.73±0.15 Mev are therefore confirmed; however, no evidence has been found for the level that they reported at 1.23±0.15 Mev. A search for proton groups corresponding to higher excited states of Si^{31} is being continued. An investigation of the $Si^{29}(d, p)Si^{30}$ reaction is also in progress. (The enriched silicon isotopes were obtained from the Isotopes Division, AEC, Oak Ridge.)

* This work has been assisted by the joint program of the AEC and ONR.
[1] H. T. Motz and R. F. Humphreys, Phys. Rev. 80, 595 (1950).

DA7. Proton Gamma-Ray Coincidence Study of the Excited States of the Si^{30} and B^{11} Nuclei. H. H. LANDON, *Yale University.**—The excited states in the energy level spectra of the Si^{30} and B^{11} nuclei were studied by means of a proton-gamma-ray coincidence technique for the purpose of determining the nature of the gamma-ray decay scheme. The nuclei were formed under cyclotron bombardment using the $Al^{27}(\alpha p)Si^{30}$ and $B^{10}(dp)B^{11}$ reactions. The gamma-rays from each state were selected using the coincidence technique and the energies of each gamma-ray were estimated where possible using an absorption coefficient measurement. A proton-gamma-gamma-coincidence experiment was performed to assist in establishing the nature of the decay when a cascade transition was suspected. The transitions from the first two excited states of Si^{30} are directly to the ground state while the transition from the third excited state takes place by means of a cascade to the second state and then to the ground state. The decay scheme in the B^{11} nucleus is most likely the same as for the Si^{30} nucleus for the first two excited states, while the third and the prolific fifth, and sixth states show cascade transitions as most probable.

* Assisted by the ONR and AEC.

DA8. The Reactions $S(p, \gamma)Cl$. T. D. HANSCOME AND C. W. MALICH, *Naval Research Laboratory.*—Gamma-radiation from proton capture by sulfur has been observed in targets of normal isotopic composition. The Naval Research Laboratory Van de Graaff accelerator has been used to explore these reactions over a proton energy interval of 0.9 to 2.1 Mev. There seem to be numerous narrow resonances, many of which are not well resolved with the energy resolution of one percent used in the preliminary survey. The more prominent resonances occur at about 1.37, 1.61, 1.69, 1.8, and 1.86 Mev. Relatively intense resonances above 1.9 Mev have not been resolved. Work at higher resolution is in progress. No induced activity comparable to the yield has been observed in the target indicating that S^{32} has a small proton capture cross section at these energies compared to the other isotopes. A careful check of this is planned. Present estimates of gamma-ray energy are as expected from calculated Q-values, with some cascade transitions probable. It is hoped that precise gamma-ray energy measurements will give additional information.

DA9. Protons from Deuteron Bombardment of Chlorine.* W. W. ENNIS, *Yale University.*—Natural chlorine in the form of gaseous HCl has been bombarded with 3.5-Mev cyclotron deuterons. Observation at 90° yielded 10 proton groups, with Q-values 0.44, 0.69, 1.18, 1.84, 2.40, 2.76, 3.03, 3.46, 3.94, and 6.26 Mev. Of these the seventh, eighth, and tenth agree with previous work.[1] Assignment of levels to isotopes will be made on further work with specimens enriched by thermal diffusion; these are now being prepared. The Q-value corresponding to the highest proton energies is most probably due to $Cl^{35}(dp)Cl^{36}$. Assuming this to be the case the mass difference $Cl^{36}-Cl^{35}$ is 0.9998±0.0001. This agrees reasonably with presently accepted mass values. If it is assumed to be due to $Cl^{37}(dp)Cl^{38}$ the discrepancy is 2.7 Mev. Hence the value for

the mass differences quoted above is very probably right within the experimental error.

* Assisted by the joint program of the ONR and AEC.
[1] E. F. Shrader and Ernest Pollard, Phys. Rev. 59, 277 (1941).

DA10. The $Mn^{55}(p, n)Fe^{55}$ Neutron Spectrum.* P. H. STELSON AND W. M. PRESTON, *M.I.T.*—A thin (20-kev) target of manganese on a tantalum backing was bombarded by monoenergetic protons of 2.97, 3.42, and 3.77 Mev from the Rockefeller electrostatic generator. Nuclear emulsion plates (Eastman NTB, 200 microns thickness) were mounted 15 cm from the target at 0° and 90° with respect to the incident proton beam. The resulting neutron spectra, obtained from the analysis of about 2500 proton recoil tracks, show well-defined groups which correspond to excited states in Fe^{55} at 0.42, 0.94, 1.36, and 2.08 Mev. The *Q*-value for the ground state reaction was measured to be -1.05 ± 0.03 Mev which is not in good agreement with the value -1.15 Mev obtained from the threshold measurement reported by Smith and Richards.[1] Levels in Fe^{55} at 0.935 and 1.41 Mev have been found by Deutsch and Hedgran[2] from the study of the decay scheme of Co^{55}. These levels correspond closely to two of the levels reported here.

* Jointly supported by the ONR and the Bureau of Ships.
[1] R. V. Smith and H. T. Richards, Phys. Rev. 74, 1257 (1948).
[2] M. Deutsch and A. Hedgran, Phys. Rev. 75, 1443 (1949).

DA11. Gamma-Rays from Proton Bombardment of the Elements Mn to Ga. C. W. MALICH, *Naval Research Laboratory.*—A survey has been made of the gamma-radiation from thick targets of Mn, Fe, Co, Ni, Cu, and Zn bombarded by protons of 1 to 2 Mev, using a coincidence counter arrangement for detector. With an energy resolution of about one percent, the yields from Mn and Fe indicate numerous narrow resonances; those from Co and Ni increase approximately exponentially with bombarding energy, with some evidence for resonances; those from Cu and Zn increase nearly exponentially with no apparent resonances. At 1.5 Mev, the relative yields are approximately 8:5:15:1:4:1 for equivalent detector geometry; on this scale, a thick Al target gives a yield of 100. Preliminary energy measurements give half-intensity absorber thicknesses ranging from 0.45 g/cm² of aluminum to 0.60 g/cm²; the spectra appear to be complex.

DA12. Triton Bombardment of C, O, Al, Fe, Ge, and Bi. M. L. POOL, D. N. KUNDU, P. E. WEILER AND T. W. DONAVEN, *Ohio State University.*—Tritium gas was introduced into the cyclotron and resonance obtained so as to produce tritons of 6.5 Mev. The triton beam impinged upon various selected internal probes. Hilger carbon gave an extremely long half-life activity which presumably is C^{14} by the (t, p) reaction. Confirmation was made by absorption measurements. The $O(t, n)$ reaction is a very strong one. The presence of small amounts of oxygen on all substances gives a prominent 1.87-hr F^{18} activity. The introduction of two neutrons or a di-neutron into Al produces a strong 6.7-min activity according to the reaction, $Al(t, p)$. With higher bombarding energies, up to 10.5 Mev, the $Al(t, He^3)$ reaction predominates. Triton bombardment of enriched Fe^{58} indicated a (t, d) reaction. Enriched Ge^{73} showed several activities. The (t, n^3) reaction seems to have a cross section much larger than the (t, n) or (t, p) reaction. The activity produced by $Ge^{72}(t, p)$ was also observed. For triton energies of 6.5 Mev no (t, p) reaction in Bi was observed on an alpha-counting equipment.

DA13. Bombardment of Cu and Ag with Tritons. D. N. KUNDU AND M. L. POOL, *Ohio State University.*—6.5-Mev tritons obtained by introducing tritium gas into a cyclotron were made to impinge upon stacks of 0.001-in. Cu and 0.0006-in. Ag foils in a special internal target for 2 and 3 hours respectively. The foils were shielded on all sides except for a small slot at the entrance of the beam. The decay curves of the various foils were followed under the same geometry along with absorption measurements. In every case the neutron activation was estimated and corrected for. From Cu, the reactions $Cu^{63}(t, d)$ and $Cu^{65}(t, p)$ are established with cross-section ratios 1:1. This may be interpreted to mean that it is as easy to introduce a di-neutron into a Cu nucleus as a single neutron. The reactions $Cu^{63}(t, n)$ and $Cu^{65}(t, He^3)$ were also observed, the latter only in the first foil with a small relative yield as is to be expected. From Ag, the reactions $Ag^{109}(t, d)$, $Ag^{109}(t, p)$ and $Ag^{109}(t, He^3)$ have been observed. The reaction $Ag^{107}(t, n)$ must be very low in comparison. The O—P process was strongly in evidence in both Cu and Ag. The introduction of di-neutrons into nuclei was not traced beyond the range of the tritons.

DA14. Electron Excitation of Cd^{111*}. B. WALDMAN AND W. C. MILLER, *University of Notre Dame.*—The electron excitation of Cd^{111*} has been studied from 1.2 to 2.3 Mev. The excitation curve obtained rises monotonically, contrary to the results of Wiedenbeck,[1] and is similar in character to the electron excitation curve[2] of In^{115*}. The excitation is a composite of direct electron and x-ray excitations. It is possible to determine from the excitation curve two activation levels at 1.33 ± 0.02 Mev and 1.75 ± 0.05 Mev. The cross section for electron excitation at 1.5 Mev is of the order of 10^{-34} cm². This research has been supported by the Research Corporation and the joint program of the ONR and AEC.

[1] Wiedenbeck, Phys. Rev. 67, 92 (1945).
[2] Waldman, Miller, and Gideon, Phys. Rev. 76, 181 (1949).

DA15. Photo-fission of Bismuth. RICHARD L. GARWIN, *University of Chicago.*—Early results have been obtained confirming the photo-fission of bismuth reported by Sugarman.[1] The fission rate observed for bismuth in this experiment (~1 fission/gram *R*) for 71-Mev maximum bremstrahlung energy is in essential agreement with Sugarman's value—1.8 fissions/gram *R*—when corrected to his energy of 86 Mev. Incipient failure of the betatron limited the total running time at 71 Mev to one hour, several limiting the data obtained. Details of the experiment will be presented, including the hydrogen-filled electron-collection fission chamber, the x-ray-operated gate circuit to eliminate electrical noise pulses, and the other techniques necessary to enable the chamber to count fissions unambiguously in an instantaneous x-ray flux of 10^7 *R*/min. Under normal betatron operation this would correspond to an average intensity of 5000 *R*/min. More extensive results on bismuth and other elements, including energy dependence of the fission reaction, will be forthcoming after the betatron is rebuilt. This work was supported in part by the ONR and AEC.

[1] N. Sugarman, Phys. Rev. 79, 532 (1950).

THURSDAY AFTERNOON AT 2:15

Horace Mann

(I. I. RABI presiding)

Invited Papers

E1. Nuclear Hyperfine Structure of Paramagnetic Resonance. M. H. L. PRYCE, *Oxford University.* (40 min.)

E2. On the Physical Interpretation of the Scattering Matrix in Quantum Electrodynamics. M. FIERZ, *University of Basel.* (40 min.)

E3. Radioactive Decay of the Neutron. J. M. ROBSON, *Chalk River Laboratory.* (25 min.)

THURSDAY AFTERNOON AT 2:15

McMillin

(R. E. MARSHAK presiding)

Cosmic-Ray Showers and Stars

EA1. Meson Showers in Cosmic Rays. E. PICKUP AND L. VOYVODIC, *National Research Council, Canada.*—Details will be given concerning showers of mesons produced in nuclear disintegrations in photographic emulsions at about 90,000 feet. The angular distribution and, in some cases, the energies of shower particles will be discussed. The stars, which are initiated by protons and heavier nuclei, are of various types. They range from 60-pronged stars with ~35 shower particles to stars with large and small showers, which have associated with them only one or two heavily ionizing evaporation products. In particular some events will be described which are characterized by showing none of the usual evaporation products, but only relativistic or near relativistic tracks. These are thought to result from collisions of incoming protons with one or two nucleons near the periphery of a nucleus. There appears to be some tendency for pairs of lightly ionizing tracks to be emitted.

EA2. Penetrating Showers Associated with Air Showers.* R. L. COOL AND O. PICCIONI, *Brookhaven National Laboratory.*—In extensive air showers at mountain altitudes we have observed, as have several authors, a component exhibiting similar properties to the so-called *N*-component. Observing directly hodoscope photographs and using large lead screens, we confirm that the observed penetrating showers are not of electronic nature. Using 80 counters as a hodoscope to observe the electron density, we find (A) the frequency of extensive penetrating showers with electron density $>\Delta$ is proportional to $\Delta^{-0.5}$ over a density interval of more than a factor of 100. This shows that associated penetrating showers are not produced by two or more *independent* particles, and that the *N*-density is proportional to the electron density. (B) The frequency of extensive penetrating showers changes less than 20 percent for $\Delta \geq 15$ m^{-2} in moving the electron density detector from 5 meters to directly above the penetrating shower detector, while it increases rapidly for smaller densities. (C) The density of the supposed *N*-component decreases, between 14,000 and 5000 ft, following closely the decrease in density of the electronic component. This suggests that the *N*-component might be generated by the high energy photo-electronic component.

* Research carried out under the auspices of the AEC.

EA3. Absorption Measurements on the Neutral Radiation Producing Penetrating Showers.* H. W. BOEHMER AND H. S. BRIDGE, *M.I.T.*—We are reporting preliminary results of an experiment at Echo Lake, Colorado, elevation 10,600 feet, investigating the production of penetrating showers by neutral particles in the cosmic radiation. The equipment consists of a penetrating shower detector covered with a 3.5-inch lead producing layer and a highly efficient anticoincidence tray above the producer. Preliminary measurements using lead and carbon absorbers above the anticoincidence tray have been completed. The results for lead give a mean free path for the neutral particles, which varies from about the value corresponding to the geometric cross section (165 g-cm^{-2}) to about 215 g-cm^{-2} depending on the multiplicity of particles required in the penetrating shower. The corresponding result for carbon varies between 85 and 105 g-cm^{-2}. In both lead and carbon the mean free path approaches closer to the value expected from the geometric cross section as the multiplicity in the penetrating shower increases.

* Assisted by the joint program of the ONR and AEC.

EA4. Decoherence of Extensive Air Showers at Airplane Altitudes.* H. L. KRAYBILL, *Yale University.*—The rate of simultaneous discharge of two Geiger counter telescopes as a function of their horizontal separation has been measured in a B-29 airplane at altitudes of 25,000 ft and of 32,000 ft, near 55°N geomagnetic latitude. The airplane was furnished by the U. S. Air Force. Separations varying from 360 cm to 30 cm were used. The coincidence rate increases by a factor of 2.0 $\pm$0.1 between 360-cm and 30-cm separation at 32,000 ft. The corresponding factor at 25,000 ft is 1.4. Comparison will be made with similar measurements[1] at 11,500 ft. The altitude variation of the decoherence will be discussed. Data obtained µsing thin lead absorber at 25,000 ft indicate that approximately four-tenths of the showers responsible for the rise in counting rate at small separations st this altitude are absorbed by 3 mm of lead.

* Assisted by the joint program of the ONR and AEC.
[1] J. Wei and C. G. Montgomery, Phys. Rev. **76**, 1488 (1949).

EA5. General Theory of Cascade Showers,* W. T. SCOTT,† *Brookhaven National Laboratory.*—A general approach to the stochastic problem of cascade showers is presented, using a simplified model for illustration. The work of Bhabha[1] is extended to show how all statistical information about a shower may be found in principle from the average energy spectrum. Jánossy's method of generating functions[2] is used, in connec-

tion with Friedman's adjoint theory using the energy spectrum as a Green's function,[3] to summarize these results. An appropriate foundation is thus presented for further work on the problem of the distribution in number of particles at a given depth in the shower.

* Work performed in part under the auspices of the AEC.
† Author now at Smith College.
[1] H. J. Bhabha, Proc. Roy. Soc. (London) **A202**, 301 (1950).
[2] F. L. Friedman, M.I.T. Lab for Nuclear Sci. and Eng., Tech Rpt. 31 (1949).
[3] L. Jánossy, Proc. Phys. Soc. (London) **A363**, 241 (1950).

EA6. Angular Distribution of Particles in Cascade Showers. L. EYGES AND S. FERNBACH, *University of California, Berkeley.*—The angular distribution of high energy electrons and photons in cascade showers has been calculated as a function of depth in the shower. This has been done by first calculating the moments of the distributions as a function of depth, and then using these moments to reconstruct the functions, in a way explained previously.[1] The moments are found in terms of contour integrals which are evaluated by saddle-point integration for large t, and by series expansions for small t. Blatt[2] and Borsellino[3] have previously calculated the second moments (mean squares); we have, in addition, calculated the fourth, sixth, and eighth moments, and these fix the distribution functions with sufficient accuracy.

[1] L. Eyges and S. Fernbach, Phys. Rev. (to be published).
[2] John Blatt (unpublished).
[3] A. Borsellino, Nuovo Cimento **7**, 323 (1950).

EA7. Cascade Showers Produced by 200-Mev Electrons.* ANATOLE M. SHAPIRO,† *Cornell University.*—The gamma-ray beam from the Cornell synchrotron has been converted into pairs in the gamma-ray spectrometer, and positive and negative electrons of 200±10 Mev have been allowed to enter a twelve-inch cloud chamber. The cloud chamber is triggered by a counter telescope which selects electrons of the proper energy, and pictures are then taken of the cascade showers produced in the lead plates in the chamber. The average number of electrons as a function of the depth in lead is thus obtained, and also the fluctuations in this number. These results are compared with Monte Carlo calculations of cascade showers[1] and the standard shower theory. It is found that the average number of electrons is considerably less than that predicted by the Monte Carlo calculations unless the multiple scattering of the electrons in the lead is considered. Multiple scattering calculations are now being made to extend the Monte Carlo method and these will be described.

* Supported in part by the ONR.
† AEC Predoctoral Fellow.
[1] R. R. Wilson, Phys. Rev. **79**, 204 (1950).

EA8. Production of Stars by 240-Mev Protons.* ALFRED M. PERRY,† *University of Rochester.*—Two-hundred-micron Ilford G-5 plates have been exposed to 240-Mev protons in the circulating beam of the Rochester cyclotron. In a preliminary survey 281 stars of one or more prongs were found. The mean free path in the emulsion for the production of stars is 82 cm ±15 percent. There are 142 stars which have one or two "gray" prongs (protons ≥30 Mev, deuterons ≥60 Mev). Of the 167 "gray" prongs, 96 percent are in the forward hemisphere relative to the incident protons. Of 705 "black" prongs (lower energy protons and deuterons, all alpha-particles). 60 percent are in the forward hemisphere. The average number of prongs per star is 3.1. The frequency of stars with various numbers of prongs is as follows:

Number of prongs:	1	2	3	4	5	6	7
Percentage of all stars:	4.6	32.0	30.2	17.8	11.4	3.6	0.4

An energy distribution of the prongs will be given.

* Work supported by the AEC.
† AEC Predoctoral Fellow.

EA9. Stars Induced by 350- to 400-Mev Protons.* S. J. LINDENBAUM, G. BERNARDINI, AND E. T. BOOTH, *Columbia University.*—G-5 plates were directly exposed to the proton beam of the Nevis cyclotron and 404 stars were analyzed. The prong and angular distributions of black (>6 times minimum), sparse black (between 3 and 6 times minimum), and gray (<3 times minimum) prongs will be presented and discussed. The mean free path for all interactions involving at least one prong (less than three times minimum) has been obtained by track length sampling and based upon 404 stars is 56±9 cm, corresponding to an average cross section of 45±8 percent geometric indicating considerable nuclear transparency. A correction for zero prong stars (phenomenalogically large angle scattering or disappearance of a proton in flight) is being determined by scanning along individual tracks. Preliminary results seem to add about 10 percent of geometric cross section, which is about the expected extrapolated value. A Goldberger[1] type calculation of the interaction of 400-Mev nucleons with a nucleus of mass number 100 is in progress and a comparison of preliminary results with experiment will be made. The experimental results seem to be consistent with the general behavior predicted by such a model.

* This project was jointly supported by the Office of Naval Research and the Atomic Energy Commission.
[1] M. L. Goldberger, Phys. Rev. **74**, 1269 (1948).

EA10. Neutron Stars in Oxygen, Neon, and Argon. J. K. BØGGILD AND F. H. TENNEY, *University of Rochester.*—An 8-in. Wilson cloud chamber has been exposed to neutrons produced in the forward direction by 240-Mev protons bombarding Cu or Be targets in the Rochester cyclotron. Measurements were made on 807 stars from O, Ne, and A gases. Lightly ionizing tracks were counted as protons or alpha-particles depending on the delta-ray count. Heavily ionizing tracks were counted as alpha-particles although in some cases recoiling residual nuclei or protons of 5 Mev or less are included. All three gases showed a similar prong distributon up to 5 prongs. The alpha-to-proton ratios computed in the above fashion were found to be:

	2-prong stars	3-prong stars	4-prong stars
O	2.68	1.57	2.82
Ne	2.14	1.35	1.30
A	0.88	0.98	0.84

The alpha-to-proton ratio decreases with atomic number as expected except for 2-prong Ne stars and 4-prong O stars, which will be discussed separately.

EA11. Emulsion Studies of Cosmic-Ray Stars in Metal Foils.* IAN BARBOUR AND LAWRENCE GREENE,† *Kalamazoo College.*—Cosmic-ray induced disintegrations of nuclei of several elements are studied with metal foils "sandwiched" between face-to-face Ilford G5 emulsions exposed at balloon altitudes to investigate the dependence upon atomic weight of the star-production cross sections for stars of various sizes and types. After exposure, removal of the foils, development, and accurate re-alignment of each pair of emulsions, the plates are scanned for groups of tracks which can be projected back to common centers between the emulsions, and thus are attributable to disintegrations of foil nuclei. The preliminary results reported[1] have been extended to include Au, Pt, Sn, Cu, Ni, and Al, giving a range of Z from 13 to 79, and allowing a check between foils of different thickness and density. The total cross section per target nucleus for stars of any size follows quite closely an $A^{\frac{1}{3}}$ law. An analysis of groups of minimum-ionization particles interpreted as meson showers has also been undertaken.

* This work has been aided by a Cottrell Grant from the Research Corporation.
† Now at Ohio State University.
[1] I. Barbour and L. Greene, Phys. Rev. **79**, 406 (1950).

THURSDAY AFTERNOON AT 2:15

Pupin 428

(W. P. ALLIS presiding)

Symposium of the Division of Electron Physics

F1. Recent Studies of Electron Collision Cross Sections at Low Energies. S. C. BROWN, *M.I.T.* (35 min.)

F2. Distinguishing Atomic from Molecular Ions: A Review of Positive-Ion Mobilities in the Noble Gases. J. A. HORNBECK, *Bell Telephone Laboratories.* (35 min.)

F3. Recent Improvements in the Non-Magnetic Mass Spectrometer. W. H. BENNETT, *University of Arkansas.* (40 min.)

FRIDAY MORNING AT 9:00

McMillin

(I. I. RABI presiding)

Business Meeting of the American Physical Society

FRIDAY MORNING AT 10:10

Havemeyer 309

(GREGORY BREIT presiding)

Nuclear Theory

G1. Mass Evidence for the Doubly-Magic Character of Sn^{120} and Ce^{140}.* HENRY E. DUCKWORTH, GEORGE S. STANFORD, AND JOHN M. OLSON, *Wesleyan University.*—It has been pointed out[1] on the basis of recent atomic mass measurements that major transition points in the packing fraction curve appear to coincide with nuclides which, in the scheme of Maria Mayer, contain closed shells of both protons and neutrons, that is, they are "double magic." Four such nuclides are $_{14}Si_{14}^{28}$, $_{28}Ni_{32}^{60}$, $_{40}Zr_{50}^{90}$ and $_{82}Pb_{126}^{208}$. New mass comparisons will be described which lead to mass values for Sn^{122}, Sn^{124}, Te^{128}, Te^{125}, Te^{130}, Nd^{140}, W^{182}, W^{183}, and W^{184}. These results, when combined with previously reported mass values, indicate that abrupt changes in the slope of the packing fraction curve occur at $_{50}Sn_{70}^{120}$ and $_{58}Ce_{82}^{140}$, both of which are double magic according to the Mayer scheme. Some remarks will be made concerning the usefulness of mass data in the identifying of closed shell configurations in the nucleus.

* This work has been done under Contract with the AEC.

[1] H. E. Duckworth and R. S. Preston, New England Section, Am. Phys. Soc., November 4, 1950.

G2. Nuclear Energy Surface. DAVID L. HILL, *Vanderbilt University.*—Many data acquired in recent years enable us to fill in new detail in the surface passing through the masses of the stable and the radioactive nuclei. Interpreting the empirical surface in terms of the liquid drop model, we may assess the adequacy of the "parabola assumption" for isotopic spin energy at various parts of the surface, and we may determine the isotopic spin energy density as a function of atomic number. Associated with variations in this energy density are variations in the effective surface tension energy and in the mean mass density in the nucleus. We may further indicate an approximate connection between these quantities and the windings in the valley or the locus of stable nuclei.

G3. Polarization Effects Due to *LS* Coupling in $n-p$ Scattering. LINCOLN WOLFENSTEIN, *Carnegie Institute of Technology.*—A spin-orbit coupling in the interaction between nucleons provides the possibility that nucleons may be polarized in nucleon-nucleon scattering. This coupling may be due either to the tensor force, for which case the polarization effect has been discussed previously,[1] or to a direct spin-orbit interaction, which has been suggested[2] in recent analysis of scattering data. For both of these cases polarization effects vanish in the Born approximation. To estimate this effect for the second case, a rough calculation has been made for $n-p$ scattering at 90 Mev using the Case-Pais *LS* coupling (scattering amplitude calculated to the Born approximation) plus a central force (Yukawa potential with "even" exchange: scattering amplitude calculated exactly). While the *LS* coupling contributes only 12 percent to the unpolarized cross section for scattering angles near 90°, it produces a polarization of more than 40 percent. This corresponds to a left-right asymmetry of about 2.5 in the 90° scattering of a completely polarized neutron beam. This polarization effect is symmetrical about 90° in contrast with that due to the tensor force.[1] Possible experiments will be discussed.

[1] L. Wolfenstein, Phys. Rev. **76**, 541 (1949).
[2] K. M. Case and A. Pais, Phys. Rev. **80**, 203 (1950).

G4. Effects of Nuclear Spin and Parity on the $N^{14}(n, p)$ and (n, α) Reactions.* BERNARD T. FELD,† *Nuclear De-*

velopment Associates.—Recent measurements by Johnson and Barschall[1] of the $N^{14}(n, p)$ and (n, α) cross sections show: (1) two sharp (n, p) resonances below 1 Mev; (2) two sharp resonances between 1 and 2 Mev, of which the first is predominantly (n, p) and the second (n, α). The (n, α) reaction, threshold ~0.3 Mev, should not be strongly excited below ~1 Mev. The devision, above 1 Mev, of the compound nucleus levels into p- and α-emitting levels may be explained (following a suggestion of J. M. Blatt) by the limitation, due to angular momentum and parity selection rules, of the possible l-values of the protons and α-particles emitted from a given N^{14} level. The level widths and peak cross sections are determined by the barrier penetrability of the neutron, proton, and/or α-particle involved in the reaction. The data on the lowest resonances are consistent with known nuclear spins and the assignment of opposite parities to C^{14} and N^{14}. This result is of interest for the problem of the β-decay of C^{14}. The large thermal (n, p) cross section requires a relatively close, heretofore unobserved (possibly negative) resonance.

* Work supported by the AEC.
† Work done while on summer leave from M.I.T.
[1] R. K. Adair, Revs. Modern Phys. 22, 249 (1950).

G5. Neutron Capture Gamma-Rays. BERNARD MARGOLIS, *M.I.T.*—Assuming electric quadrupole radiation (which gives correct estimates for radiation widths), the gamma-rays emitted by atomic nuclei after thermal neutron capture have been studied theoretically. Maxima for the distribution in energy of the gamma-rays from nuclei with high energy level densities lie at about 3 Mev. As the level densities decrease (i.e., for nuclei with less level structure) the position of the maximum moves to higher gamma-ray energies. The form of level density assumed in the above is $w(E) = C\exp(aE)^{\frac{1}{2}}$. A study of gamma-cascades reveals that the average number of gamma-rays emitted in the decay of the compound nucleus for cases of high energy level density is about three or four. This agrees with experiments by Muehlhause.[1] A nucleus with either widely or equally spaced levels radiates almost entirely to the low lying levels making the average number of emitted gamma-rays not much more than one.

[1] C. O. Muehlhause, Phys. Rev. 79, 277 (1950).

G6. Inelastic Scattering of Neutrons.* W. HAUSER, *M.I.T.* AND H. FESHBACH,† *Nuclear Development Associates.*—It has been pointed out that the application of statistical theory to inelastic neutron processes does not necessarily lead to isotropic angular distribution of the emergent neutrons.[1] The angular distribution and total cross section are calculated here under the assumption, valid for all but the light nuclei, that the statistical model may be applied to the compound nucleus. The schematic theory of nuclear reactions[2] then leads to definite predictions which are dependent only on the nuclear radius and the properties of the excited levels of the target nucleus. Results are sensitive to the parity and angular momenta of the excited levels and thus emphasize the usefulness of this type of experiment for nuclear spectroscopy. Tables have been prepared from which one may easily obtain the angular distribution and total inelastic scattering for arbitrary nuclear spin and parity changes but for incident and emergent neutrons of angular momenta $l \leq 2$. Specific calculations have been carried through for some nuclei having isomeric levels.

* This work supported in part by the AEC.
† This work done while on summer leave from M.I.T.
[1] L. Wolfenstein, private communication.
[2] H. Feshbach and V. F. Weisskopf, Phys. Rev. 76, 1550 (1949).

G7. On the Directional Correlation of Successive Nuclear Radiations. GIULIO RACAH,* *Institute for Advanced Study.*—Using the algebra of tensor operators[1] the summations over the magnetic quantum numbers which appear in the expressions of the angular correlations are carried out explicitly for the most general case (including polarization, multipole interference, $\beta-\gamma$-correlations, etc.). For non-polarized beams the angular correlation function has the form

$$W(\theta) = \Sigma_k C_k P_k(\cos\theta),$$

where the C_k are products of four functions, two of them depending on the angular momenta of the emitted radiation and of the nuclear states involved in each transition, and two on the kind and polarization properties of the emitted particles. For polarized beams the expression of the angular correlation function contains spherical harmonics instead of Legendre polynomials if one beam is polarized and the eigenfunctions of the symmetrical top if both beams are polarized.

* On sabbatical leave from the Hebrew University, Jerusalem, Israel.
[1] G. Racah, Phys. Rev. 62, 438 (1942), Sec. 3.

G8. Deuteron Photo-Disintegration with Noncentral Forces. NORMAN AUSTERN, *University of Wisconsin.*—It is well known that noncentral nuclear interactions must lead to characteristic effects in the deuteron photo-disintegration cross section. The most striking effect is an isotropic term in the angular distribution, arising in photoelectric transitions. It has recently been shown[1] that the isotropic photomagnetic cross section can be closely estimated, so it is now reasonable to make careful calculations on the electric isotropic term. The effects of noncentral forces strongly involve the nuclear interaction in the P states. Thus, the photo-angular distribution may provide a measure of the P wave interaction that is independent of scattering experiments and does not require accurate total cross sections. Results will be presented for calculations on tensor force effects for potentials which are near "half-exchange." The influence of velocity dependent interactions will also be discussed.

[1] N. Austern, Phys. Rev. (to be published).

G9. On the Bhabha Potential. HARRY SCHIFF, *McGill University.*—From a generalized wave equation of the fourth order, Bhabha derived a static potential for two nucleons which can be written

$$V = Ae^{-Hr} + B(e^{-Hr}/Hr)[-\tfrac{1}{4}(\sigma_1\cdot\sigma_2)(Hr-2) - \tfrac{1}{4}(Hr+1)S_{12}]$$

and does not contain the $1/r^3$ divergence that the previous static potentials, based on the generalized wave equation of the second order were supposed to have had. The symmetric meson theory version of this potential was considered, as applied to the deuteron. Calculations were made for $A=0$, with unsatisfactory results. Inspection then showed that the inclusion of A required that A and B be negative. These parameters were adjusted so that the singlet and triplet deuteron states were satisfied. Calculations with the resulting triplet variational wave functions yielded a quadrupole moment that was more than twice as large as the experimental value, and a triplet effective range that was about 20 percent too great. The results indicated that the symmetric form of the Bhabha potential did not yield values in accord with experiment.

G10. A Relativistic Equation for Bound State Problems. H. A. BETHE AND E. E. SALPETER, *Cornell University.*—The relativistic S-matrix formalism of Feynman is applied to the bound state problem for two interacting particles. An integral equation is obtained with a kernel in the form of an expansion in powers of $g^2/\hbar c$, the dimensionless coupling constant for the interaction. Each term in this expansion gives a Lorentz invariant equation. In nonrelativistic approximation and to lowest order in $g^2/\hbar c$ the equation reduces to the appropriate Schrödinger equation. This integral equation is applied to the deuteron ground state using scalar mesons, with scalar coupling, of mass $\mu = 275\ m_e$ for a binding energy of 2.23 Mev. For neutral mesons the value obtained for $g^2/\hbar c$ differs only

by a fraction proportional to $(\mu/M)^3$ from that obtained by using a phenomenological Yukawa potential, $g^2/\hbar c = 2.39(\mu/M) = 0.358$. For charged mesons a larger correction term is obtained due to the fact that a nucleon can emit, or absorb, positive and negative mesons only alternately. $(g^2/\hbar c)$ is increased by a fraction of $1.1(\mu/M)$ or 16 percent.

G11. Nuclear Forces in the Pseudoscalar Theory According to the Strong Coupling Approximation. J. V. LEPORE, *Indiana University.*—The pseudoscalar coupling of the pseudoscalar meson field has not been investigated in the strong coupling limit. This is due to the fact that the pseudoscalar γ_5 has no clear meaning in terms of two component wave functions. One must characterize the source by a four component wave function. It seems of some interest to investigate this case in order to gain insight into the solution of field problems. Also, recent experimental results qualitatively support the pseudoscalar character of the pi-meson and weak coupling approaches for this theory always yield $f^2/4\pi > 1$. The Tomonaga method is employed. The Hamiltonian may be diagonalized if the kinetic energy of the nucleons is neglected. The source size and coupling constant are related. For the single-nucleon problem, part of the energy can be interpreted as a mass renormalization of the bare nucleon. The rest represents the usual "self-field." Nuclear forces appear similar to those yielded by a scalar theory although this conclusion may be altered by a more refined investigation which is in progress. Thanks are due Professor Serber, who suggested the problem.

G12. On the Relation between the Neutron-Neutron Force and the γ-Ray Spectrum Resulting from π^- Meson Capture in Deuterium. K. M. WATSON AND R. N. STUART, *University of California, Berkeley.*—The radiative capture of slow π^- mesons in deuterium leads to a final state containing two slow neutrons, causing the γ-ray spectrum to depend sensitively on the nature of the $n-n$ force.[1] It is shown that to a good approximation the γ-ray spectrum (near its high energy limit) is independent of the detailed mechanism of the meson absorption process and can be expressed directly in terms of the ^1S phase shift, δ, for $n-n$ scattering by means of a multiplicative factor, $\sin^2\delta$. The finer details of the spectrum depend on the deuteron wave function essentially outside the range of the $n-p$ force and on the details of the absorption in hydrogen—for which an appeal is made to experimental results on the inverse process of photo-meson production. The analysis leads to a means of deducing the effective range and scattering length for the singlet $n-n$ potential.

[1] This effect has been noted by S. Tamor and R. E. Marshak, Phys. Rev. **80**, 766 (1950) and by Brueckner, Serber, and Watson, Phys. Rev. (to be published).

FRIDAY MORNING AT 9:30

Schermerhorn 501

(J. H. MCMILLEN presiding)

Fluid Dynamics

GA1. Aerodynamics of Blasts. L. TING AND H. F. LUDLOFF, *New York University* (Introduced by S. A. KORFF).—The pressure and density fields behind blasts passing over surfaces of arbitrary flat structures are obtained in explicit analytic form. Taking into account the rotationality of flow, due to curvature of the shock, it turns out that disturbance pressure δp obeys a wave equation. Moreover, the usual condition on the structure surface, and the conservation laws across the disturbed shockfront are fulfilled. In this way a boundary value problem for δp results. To obtain an analytic solution, the following is important: (1) No cone field transformations are used, as previously, because that restricts the generality of results. Instead: (2) Lorentz transformation of coordinate system is introduced. (3) "Reflection" of the boundary condition is carried out. (4) Some "lost boundary conditions" are considered. The resulting expressions for pressure and density are explicit and simple; moreover valid for *any* surface, not only for wedges. Since the rotationality of flow is restricted to a triangular domain behind the shock, a plot of isobars and isopycnics shows how suddenly each isopycnic splits off from the corresponding isobar after traversing the "demarcation line." Thus, a "slipstream" is derived, in accordance with W. Bleakney's interferograms.

GA2. An Experimental Investigation of Transonic and Accelerated Supersonic Flow by the Hydraulic Analogy. E. V. LAITONE, *University of California, Berkeley.*—The fundamentals and the experimental technique for the analogy between the gravity waves propagated on the free surface of a shallow body of liquid and the two-dimensional flow of a compressible gas are briefly reviewed. The experimental investigation is then devoted to the transonic problem of detached shock waves in front of a wedge moving at varying supersonic speeds. The first part of the report is mainly concerned with the experimental location of the detached shock wave as a function of the free stream Mach number in steady flow and a correlation with existing theories. The second part of the report provides an experimental study of the effect of acceleration and deceleration on the shape and location of detached and attached shock waves. This is the most important development since no other method can so easily yield as much information on the effect of acceleration on the formation of attached and detached bow shock waves. The experimental data are correlated on the basis of a non dimensional acceleration parameter and several hypothesis are advanced for predicting the behavior of shock waves in accelerated flow.

GA3. Oblique Shock Wave Theory with Heat Exchange and Change of State. FREDERICK W. ROSS, *University of Detroit.*—Theory is presented for oblique shock waves involving (1) heat exchange, k_1, (2) transfer of part of the compressible fluid, k_2, to an incompressible state, and (3) change in specific heat ratios, k_3. By matching mass flow, momentum, and energy relations across an oblique finite disturbance it is shown that these additional conditions introduce new terms in the solution of the form $k_i u_1/(u_1 - u_2)$. For k_i not zero a minimum shock angle is found which always exceeds the Mach angle by a definite increment. For air-flow at u_1/a^* of 1.5 with dew point $-20°$F this increment is calculated as 3.1 degrees. For expansion about a corner such flow differs from the Prandl-Meyer type and in supersonic nozzles, for example, oblique shock waves are predicted which can explain anomalous pressure losses and the presence of extraneous waves. Hodographs of the velocity solution include a doubly infinite set of curves, one, the usual set, introduced by Mach number as parameter and the other by k_i. The theory includes physi-

cally possible normal and oblique flows involving increase of supersonic velocities, and subsonic shock waves of which oblique flame fronts are indicated as one form.

GA4. Some Results Obtained with a Hot Wire Anemometer and a Shock Tube.* R. BETCHOV, *University of Maryland.*—A hot wire anemometer and a small shock tube were used to study the time lag of the wire and its behavior in a supersonic flow. Some information was also obtained on the transient phenomena in a shock tube. The electrical resistance of the wire was kept constant by a special feed-back amplifier, this made it possible to determine whether the time lag of the wire T_I when the current changes, is equal or not to the time lag T_v when the air flow is modified. The differences are certainly smaller than the effect predicted by a simple theory of the wire based on a linear differential equation (King's formula, heat conduction in the metal and linear relation between resistivity and temperature). By introducing a nonlinear term (completed King's formula and parabolic relation between resistivity and temperature) we can explain this very favorable property of the hot wire.

* Supported by the Office of Air Research.

GA5. A Study of Flows in a Shock Tube.* R. K. LOBB, *University of Maryland.*—An investigation of the flows in a shock tube has been carried out, with emphasis on the high Mach number flows between the contact surface and the rarefaction wave. Theory predicts an unlimited Mach number in this region as compared to a maximum Mach number of 1.89 (for air) in the region between the contact surface and the shock wave. This flow is less uniform than in the latter region. However, it does have a much higher density and Reynolds number. Two transient shock waves decreased the duration of the steady state flow below that predicted by theory. The Mach numbers of the steady flow diverge sharply from theory for diaphragm pressure ratios over 300 and approach a maximum of 5.0. This suggests further experiments to check the one-dimensional nonstationary rarefaction wave theory[1] for extreme expansions.

* Sponsored by the Institute of Aerophysics, University of Toronto.
[1] R. Courant and K. O. Friedrichs, *Supersonic Flow and Shock Waves* (Interscience Publishers, Inc., New York, 1948).

GA6. Refraction of Shock Waves. R. G. STONER, *The Pennsylvania State College.*—Experimental study of shock wave refraction at a gas interface[1] has been extended to the interaction of plane shocks with a plane boundary between two different gases. A shock tube of rectangular cross section, 1¾ by 7½ inches, has been constructed. A test section allows a plane soap film extending across the narrow dimension of the tube to be drawn to a length of about 6 inches, closing off a small changer into which the second gas is introduced by flow. This mechanism is mounted between Lucite disks which form the observation windows, and which can be rotated about an axis lying in the tube wall to change the angle of incidence between the shock front and the interface from 0° (head-on) to about 60°. Spark shadowgraphs are taken, from which the orientation of reflected and refracted shocks can be obtained. Preliminary series of pictures have been taken of shocks traveling from air into several other gases, at shock strengths ξ between 1.0 and 0.65. Extension to stronger shocks will require alteration of the test section to allow operation at reduced pressure.

[1] R. G. Stoner and M. H. Glauberman, Phys. Rev. **76**, 882 (1949).

GA7. The General Theory of Linearized Rotational Compressible Flow and Applications. CHIEH-CHIEN CHANG AND BOA-TEH CHU, *The Johns Hopkins University.*—The fundamental equations governing the motion of a steady nonviscous compressible flow can be linearized for a parallel but not necessarily uniform main stream when the disturbances are small. For two-dimensional and axially symmetric flow, these equations can be reduced to the generalized Cauchy-Riemann equations considered by Bers and Gelbart. For general three-dimensional flow, a single second-order partial differential equation is obtained. It is shown that in general, the linearized equation may be applied in the transonic range. For example, transonic flows with different velocity gradients in a parallel channel with wavy walls are solved. For some main stream gradients, simple solutions can be found and the pressure distribution on an arbitrary airfoil in supersonic flight is calculated. In one case, the result can be readily compared with Ackeret's thin airfoil theory—the latter gives only a first approximation for pressure distributions when the main stream velocity gradients in the neighborhood of the airfoil are small. General solutions of the two-dimensional problem are constructed for arbitrary main stream gradients and are applied to study:—(1) Interaction of shock wave and boundary layer with arbitrary velocity profile; (2) Transmission of disturbances across shear layer; (3) Pressure distribution on an arbitrary airfoil.

GA8. Explicit Determination of Contour Integral Representations of General Solutions for One-Dimensional Compressible Fluid Flow.* R. P. SHAW, *New York University.*—By a suitable hodograph transformation the Eulerian (or Lagrangean) equations can be written as linear equations for radial waves in hodograph spaces whose positive (or negative) numbers of dimensions depend on the adiabatic exponent. General solutions in a form exhibiting forward-, and backward-traveling waves can be written as contour (or real) integrals with extremely simple algebraic kernels. The two arbitrary functions f_+ and f_-, appearing in the integrands can then be determined to fit various types of arbitrary initial and boundary data. If two arbitrary simple waves interact, each function is determined by data from one of the waves. If a simple wave is reflected from the open end of a tube (constant pressure condition), f_- is determined by the wave and f_+ is a functional transform of f_-. For air, f_+ satisfies a modification of Bessel's equation with an inhomogeneous term depending only on f_-.

* The work described in this paper was done with the support of the ONR, Department of the Navy, and the Office of Air Research, Department of the Air Force.

GA9. The Pressure Field Associated with the "Spinning" Detonation.* A. J. MOORADIAN, S. A. HOSHOWSKY, AND W. E. GORDON, *University of Missouri.*—Previous workers have observed from photographs of detonating gas mixtures that the luminous zone follows an helical path near the walls of the tube.[1] We have found that there is associated with this "spinning" detonation an oscillating pressure field which has helical symmetry, and which persists with decreasing amplitude for some distance behind the detonation front. The wavelength of the spin, computed as the product of the period and the detonation velocity, is equal to the observed pitch of the helical path. The phenomenon has been found in a number of hydrogen-oxygen mixtures with various diluents, and it is always present near the detonation limits (both pressure and composition limits). Curiously, spin is present both in lean and rich mixtures, but is absent from certain intermediate compositions. Certain regularities have been observed in the dependence of the wavelength on the composition and the pressure. No satisfactory theoretical explanation has been found.

* This work was carried out under ONR Contract.
[1] Campbell and Finch, J. Chem. Soc. 2094 (1928). Bone and Fraser, Phil. Trans. Roy. Soc. **A230**, 373 (1931). Bone, Fraser, and Wheeler, Phil. Trans. Roy. Soc. **A235**, 29 (1935).

GA10. An Analysis of a Stokesian Fluid. K. M. SIEGEL, *University of Michigan.*—When the Reynolds number is less than one, the incompressible Navier-Stokes Equation reduces

to the equation of Stokes. The resulting equation is a linear fourth-order partial differeatial equation. A method based on the separation of variables solution for the Stokes stream function for an ideal flow yields nontrivial solutions to the Stokesian Fluid Equation for a viscous flow. An observation is made that three constants of the motion remain unchanged when one goes from the ideal flow solution to the Stokesian fluid solution for the same body or similar type bodies (ones which are finite in extent and are contour surfaces of separable Laplacian Coordinate Systems, such as a sphere or an ellipsoid). These constants are associated with boundary conditions which have remained unchanged between the ideal fluid and the Stokesian Fluid. They are the ones which require the normal velocity at the surface to be equal to zero and the disturbances due to the body to tend to zero as one approaches infinity.

GA11. Skin Friction in Supersonic Rarefied Gas Flow. S. A. SCHAAF AND F. S. SHERMAN, *Berkeley.*—Experimental and theoretical results are presented relating to the drag coefficient C_D for a flat plate at zero angle of attack in a supersonic air stream of such low density as to introduce slip effects. Drag data were obtained in a low density supersonic wind tunnel over a Mach number M range of 2.2 to 3.5. The Reynolds number R, based on length of flat plate, was varied both by using plates of different length and by changing the air stream pressure level and extended over a range of 30 to 2000. An extension of the classical Rayleigh flat plate viscous flow theory to include the effects of slip was developed and lead to a relation in the form $C_DM=f(M^2/R)$. The experimental data confirms this theory over the range of values tested within a mean scatter of ±5 percent. This work was performed under an ONR contract.

GA12. The Response of Water to Spherical Missiles Entering at Supersonic Speeds.* R. L. KRAMER AND J. H. MCMILLEN, *U. S. Naval Ordnance Laboratory.*—One-eighth-inch diameter steel spheres were shot vertically downward into water at velocities up to 7000 ft/sec and the impact and penetration investigated shadowgraphically. Evidence was obtained indicating that very high temperatures are produced upon impact at supersonic speeds. Photographic records showed that supersonic impacts are accompanied by the emission of a short flash of light. Also the shadowgraphs show the presence of highly agitated masses of air or water vapor near the point of impact. Shadowgrams were obtained of the supersonic missiles during the flight through water using photographic films placed only two sphere diameters from the missile. The resulting reduction in optical refraction gave improved position records and permitted an estimate of the drag coefficient for spheres. The measured values ranged from 0.3 to 0.7 and were larger than the coefficient of 0.3 for subsonic speeds and smaller than the coefficient of 1.0 for air at the same Reynolds and Mach number. By tracing individual spark beams through the shock wave configuration just behind the front the ratio of radial to tangential gradients of the density was inferred.

* Partially supported by the ONR.

GA13. Dependence of the Water-Entry Cavity on the Surface Condition of a Missile Model.* ALBERT MAY, *U. S. Naval Ordnance Laboratory.*—Heretofore the scaling of water-entry events has been investigated principally by varying the velocity, size, or density of the entering missile, or the constants of the gas above the water. Since, at low speeds (20 ft/sec), vertically-entering spherical missibles do not form cavities as readily when the missile surface is clean as when contaminated by handling or greasing, a search was made for the scaling law applicable to the cavity-formation threshold. For a given entry speed, however, whether a cavity will be formed seems to depend little on the size or specific gravity of the sphere, or the choice of a particular contaminant. Clean steel and Duralumin spheres with diameters from ½ to 3 in. formed cavities for speeds above 18 to 21 ft/sec, and greased spheres above 10 to 13 ft/sec. Our cavity-threshold scaling investigations do not indicate a predominant effect of surface forces. The use of still smaller steel spheres has given some evidence of Froude scaling of the threshold.

* Partly supported by the ONR.

GA14. Some Aspects of Air Condensation in Hypersonic Wind Tunnels. S. G. REED, JR., *U. S. Naval Ordnance Laboratory.*—Recent data obtained with the Naval Ordnance Laboratory hypersonic wind tunnel indicates that condensation of air, with little change in entropy, is probably occurring around the extrapolated dew-point for air. Some consequences of assuming that the condensation of one-component systems is isentropic were examined. It is shown that upper limits can be assigned for the quantity condensed in such expansions. The deviation of the slope of the static pressure *versus* volume curve from the extrapolated perfect gas curve and from the dew-point line is calculated. These results indicate that the deviation of the static pressure values from the perfect-gas isentrope values will be small when the point of condensation occurs on the flat portion of the pressure-volume curve of the expansion. In actual experiments, the slight gain in entropy and the real gas properties both tend to make the effect of condensation on measured pressure values even smaller. Applications of these results to some hypersonic wind tunnel measurements are discussed.

GA15. Hydrodynamical Theory of Slider Bearing Lubrication. A. CHARNES AND E. SAIBEL, *Carnegie Institute of Technology.*—The usual method of solving the slider bearing problem is to start from the equation giving the approximate solution, developed by Reynolds,[1] and to assume the thickness of the oil film to be a linear function of the coordinates. This leads to an equation which is awkward to solve, consequently series solutions for a limited range of the parameters involved have been developed[2] and approximate solutions have also been given.[3] In this paper, an exact solution is developed for a slider with or without side leakage having an oil film of thickness equal to an exponential function. The result is a tractable solution in the form of a rapidly convergent series over the complete range of the parameters for pressure, maximum pressure, total load, and center of pressure. The results compare favorably with the exact solution extant for the linear slider and the proposed solution may be used as either an approximation to the linear slider or as an exact solution for a slider of exponential form in its thickness.

[1] O. Reynolds, Trans. Roy. Soc. (London) **177**, pt. 1, 157–234 (1886).
[2] Muskat, Morgan, and Meres, J. Appl. Phys. **11**, 208–219 (1940).
[3] C. R. Boegli, J. Appl. Phys. **18**, 482–488 (1947).

GA16. The Physical Properties of Active Nitrogen and its Application to the Study of Low Density Flow. JAMES M. BENSON, *Langley Aeronautical Laboratory.*—The physical properties of active nitrogen have been investigated experimentally in low density flow at velocities extending into the supersonic region. The results indicate that active nitrogen may be used for observations of flow at low density without introducing excessive disturbances in the stream. The positions of shock waves are correctly indicated by afterglow, but it appears that the afterglow should be observed through a suitable filter to obtain correct indications of density in the flow. The experimental results will be discussed briefly to show that they are inconsistent with Mitra's theory of the afterglow and that a metastable molecular state having energies adjoining those of the B state appear to be required to explain the response of the afterglow to a shock wave. Experi-

mental methods will be described for the study of supersonic flow at low density by the use of the Lewis-Rayleigh afterglow in shock tubes. The methods are applicable also to a more detailed analysis of the Lewis-Rayleigh afterglow and its transient response throughout the spectrum to the step-function changes associated with a shock wave.

FRIDAY MORNING AT 10:10

McMillin

(W. F. G. SWANN presiding)

The Nevis Laboratory; Cosmic Rays

H1. The Cyclotron at Nevis. E. T. BOOTH, *Columbia University.* (30 min.)
H2. Meson Reactions in Hydrogen and Deuterium. R. E. MARSHAK, *University of Rochester.* (30 min.)
H3. Nuclear Interaction of Negative Pi-Mesons. G. BERNARDINI, *Columbia University.* (30 min.)
H4. The Production of Mesons by Protons. J. STEINBERGER, *Columbia University.* (30 min.)

FRIDAY MORNING AT 9:30

Pupin 301

(P. P. EWALD presiding)

Non-Metallic Crystals

HA1. Theory of Antiferroelectric Crystals. C. KITTEL, *University of California, Berkeley.*—An antiferroelectric crystal will be defined as a crystal in which lines of ions or cells are spontaneously polarized, but with adjacent lines polarized in antiparallel directions. The antiferroelectric state is known to be more stable than the ferroelectric state for dipoles arranged at the lattice points of *bcc*, *fcc*, and simple cubic lattices, when only dipolar interactions are considered. The theory has been developed on the supposition that the transition is of the second order. The dielectric susceptibility is *not* expected to follow a $C/(T+\theta)$ law as in antiferromagnetism; but may rather on passing through the Curie point remain nearly constant, and at a not particularly high value. The anomaly in the heat capacity should be similar to that observed in ferroelectrics, and x-ray superstructure lines should also be observed. $AC/(T+\theta)$ susceptibility variation as reported in $SrTiO_3$ is suggestive of a ferroelectric above an effective negative Curie or transition temperature; the Curie temperature in this case could perhaps be made positive by the application of a large hydrostatic pressure, although in $BaTiO_3$ pressure has the opposite effect.

HA2. The Ionic Displacement in Barium Titanate. H. C. SCHWEINLER, *M.I.T.*—Slater's method of treating the Lorentz correction in a crystal[1] has been applied to a model of barium titanate in which both the titanium ions and the oxygen ions can experience appreciable displacements. To explain the experimental observations of Kaenzig[2] on the ionic displacements, we must assume that the titanium ion is seven times as strongly bound to its equilibrium position as is the oxygen ion. The local fields are in the ratio $E_{Ba}:E_{Ti}:E_{O_1}:E_{O_2}:E_{O_3}::0.40:1.67:0.34:0.34:1.05$, where O_3 are the oxygens in line with the titaniums and the applied field and O_1, O_2 are the remaining oxygens. This last shows clearly the inadequacy of an "average field" assumption.

[1] J. C. Slater, Phys. Rev. **78**, 748 (1950).
[2] W. Kaenzig, Phys. Rev. **80**, 94 (1950).

HA3. $BaTiO_3$ Single-Domain Crystals at Low Temperature.* WALTER J. MERZ, *M.I.T.*—Blunt and Love[1] found for $BaTiO_3$ ceramics at about 70°K a peculiar peak in the dielectric loss. Hulm[2] found for multi-domain crystals a strong increase of the coercive field-strength when lowering the temperature and was unable to polarize the crystals completely below 20°K. Since this situation might indicate a new low temperature transition of $BaTiO_3$, we investigated it on single domain crystals.[3] The dielectric constant decreases linearly below the transition at about 180°K and reaches the value of about 130 at liquid helium temperature. We could not find any anomaly in the dielectric loss. A strong increase in the coercive field-strength occurs below 90°K, but using good crystals we were able to saturate them even at helium temperature. The spontaneous polarization stays almost constant from ~180°K down to 4.2°K with a value of $P_s \simeq 8.5 \times 10^{-6}$ coul/cm^2. The coercive field-strength increases from about 250 volts/cm at 180°K to about 10,000 volts/cm at 4.2°K, but $BaTiO_3$ stays ferroelectric without any additional transition.

* Sponsored by the ONR, the Army Signal Corps, and the Air Force.
[1] R. F. Blunt and W. F. Love, Phys. Rev. **76**, 1202 (1949).
[2] J. K. Hulm, Proc. Phys. Soc. (London) **63A**, 1184 (1950).
[3] Walter J. Merz, Phys. Rev. **76**, 1221 (1949).

HA4. Optical and Electrical Measurements on Rutile Single Crystals.* DONALD C. CRONEMEYER, *M.I.T.*—The intrinsic conductivity for plates cut both parallel and perpendicular to the *c*-axis has an activation energy of 1.5 ev (from $\sigma = \sigma_0 e^{-\epsilon/kT}$). This activation energy is maintained over a temperature range, 350 to 850°C. The optical transmission shows an absorption rising toward 4100A. This absorption moves toward the ultraviolet at low temperatures and simultaneously increases in steepness. Near 4°K the threshold of absorption lies near 4100A, and the absorption is so sharp that the optical density changes from 0.3 to 3 over a wavelength change of 20A. On the other hand, the position of the absorption peak moves slightly towards longer wavelengths

as the temperature decreases below 100°K. The optical activation energy of 3.0 ev should correspond to the thermal activation energy of 1.5 ev.

* Sponsored by the ONR, the Army Signal Corps, and the Air Force.

HA5. Shear Modes of Vibration in Thick Plates.* VIRGIL E. BOTTOM, *Colorado A. and M. College.*—By means of the piezoelectric effect many inharmonic overtones of thickness shear modes may be excited in a quartz plate. Series relationships exist between the frequencies of these modes.[1] An approximate treatment of the origin and nature of these modes has been carried out by neglecting the nonisotropy of the medium and the coupling to other modes of vibration. The treatment consists of solving the three-dimensional wave equation for the boundary conditions applicable to a thick circular plate which is rigidly clamped around the periphery and vibrating in thickness shear. In spite of the approximations, several features of the overtone spectrum are explained, and fair agreement between the observed and calculated overtone frequencies is obtained.

* This work supported by Signal Corps contract.
[1] Bever, Bottom, and Weber, Phys. Rev. **74**, 1562 (1948).

HA6. A Comparison of Internal Viscosities of Natural and Synthetic Quartz.* KARL S. VAN DYKE, GARY D. GORDON, GEORGE F. FISHER, AND WILLIAM F. PALMER, *Wesleyan University.*—Q's of the order of 5×10^6 are measured for 300 kc, half-inch rings of both synthetic and natural quartz. No significant difference is found between the viscosities of a clear natural sample and a clear synthetic sample. The decay method of earlier reports[1] is used, which yielded Q's to 6×10^6 kc for a 6.3-cm ring of natural quartz. Mounting losses are kept at a minimum by use of a basket-like suspension on three single silk fibers. The surfaces of the rings are etched and they vibrate in vacuum. Experimental data are not available for comparing the internal viscous properties of the present samples of quartz with that sample which earlier gave Q's in the millions for a very large ring. A series of geometrically similar rings covering a wide range of diameters and all cut from the same crystal of quartz is in preparation and Q-measurements on these are expected to provide a basis for such a comparison. Two samples of synthetic quartz are under study, one grown by the Brush Development company, the other by the Bell Telephone Laboratories.

* This work is supported by the U. S. Army Signal Corps.
[1] Waltz, Maynard, and Van Dyke, J. Acoust. Soc. Am. **19**, 732 (1947).

HA7. Deviations from the Cauchy Relations in NaCl- and CsCl-Type Crystals. E. BURSTEIN, P. L. SMITH, AND D. L. ARENBERG, *Naval Research Laboratory and U. S. Naval Air Development Center.*—Recent measurements have made available additional information on the factors which lead to deviations from the Cauchy relations.[1] In crystals made up of ions with rare gas configurations the contribution from the "many-body" forces associated with overlapping of the ions is positive for c_{44} and negative for c_{12}, so that $c_{44}/c_{12}>1$.[2] Thus, in LiF, NaF, and MgO, where the overlapping between ions is appreciable, the experimental values at room temperature for c_{44}/c_{12} are 1.4, 1.2, and 1.8, respectively. The c_{44} and c_{12} values are roughly equal for NaCl, NaBr, KCl, KBr, KI, RbCl, and CsBr where the overlapping of ions is smaller. In crystals where the cations do not have a rare gas configuration, the experimental data indicate that $c_{44}/c_{12}<1$. Thus, in AgCl, AgBr, TlCl, and TlBr, the c_{44}/c_{12} values are 0.18, 0.22, 0.50, and 0.51, respectively. The deviations from the Cauchy relations in these crystals may be attributed to contributions from exchange and correlation energies and deformation of the ions. These contributions are presumably larger than those from the overlapping of ions in PbS where the c_{44}/c_{12} value is 0.8.

[1] Smith, Burstein, and Arenberg "The elastic properties of cubic crystals." (to be published).
[2] Per-Olov, Löwdin, Arkiv Mat., Astron. Fysik **35**, No. 30 (1948).

HA8. Electrical Breakdown Paths in Asymmetrical Crystals. JAMES W. DAVISSON AND ELIAS BURSTEIN, *Naval Research Laboratory.*—Electrical breakdown paths in $NaClO_3$, $NaBrO_3$, ADP, and KDP follow the equivalent direction scheme prescribed by the class symmetry of the cyrstal. The paths are found to be unidirectional, in agreement with the fact that the equivalent directions in crystals which lack a center of symmetry are not centrosymmetric. This property manifests itself as follows. Imagine the crystal section divided into four quadrants. Then the path pattern obtained from a negative point electrode placed at the center will normally yield paths that lie in two quadrants that are diagonally situated, while a positive point electrode yields paths that lie in the remaining two quadrants. The orientation of the paths is dependent upon temperature and voltage. In addition, the positive and negative patterns are generally not equivalent. In ADP and KDP the positive and negative patterns, unlike those in $NaClO_3$, NaBrO and the alkali halides,[1] are actually confined to different set of planes in their variation with temperature. Thus, an essential polarity effect exists. The polarity effect is especially marked in ADP at low temperatures, where the positive and negative patterns both lie within the same two quadrants.

[1] J. W. Davisson, Phys. Rev. **73**, 1194 (1948).

HA9. Growth of Single Crystals of BaO by Vapor Phase Deposition on MgO Crystals at High Temperature.* WILLIAM C. DASH, *Cornell University.*—A seeding technique has been developed in connection with experiments on vapor phase growth of BaO at this laboratory.[1] A single MgO crystal slab 1 cm³ is placed into a 1 cm³ cavity inside a cylinder of compressed BaO powder. The cylinder is then enclosed in platinum and crystalline MgO and surrounded by three independently powered molybdenum heaters in a vacuum furnace. The temperature of the cylinder is slowly raised to about 1400°C with a gradient maintained across the cavity in such a direction as to prevent condensation on the MgO at temperatures where surface mobility is low. Then the temperature gradient is reversed and held at 20° to 30° across the cavity, thereby evaporating BaO onto the MgO. Occasionally crystals as large as 1 cm×1cm×1.5 mm are obtained in 48 hours of growth. The top of the crystal frequently exhibits terraces with parallel planes whose normal is perpendicular to the MgO surface. The other axes are sometimes parallel to the MgO axes, sometimes at 45° to the MgO axes; and frequently there are macroscopic regions of each of these orientations.

* Work supported by ONR and the Research Corporation.
[1] "Preparation and some electrical properties of barium oxide crystals." Technical Report No. 2. ONR Contract N6-ori-91.

HA10. Oriented Overgrowths of Alkali Halides on Calcite. L. G. SCHULZ, *University of Chicago.*—Thin films of alkali halides formed on cleavage surfaces of calcite were examined with electron diffraction. Relative to the long diagonal, *LD*, of a face of the cleavage rhomb the following orientations were observed. (1) Deposits of NaCl, KCl, KBr, KI, and RbI grown from the vapor had the [001] direction normal to the substrate with the [110] direction perpendicular, or parallel, to *LD*. NaCl, KCl, and KBr had the same orientation when grown from solution. (2) Deposits of KI and RbI grown from solution had the [111] direction normal to the substrate with the $[1\bar{1}0]$ direction parallel to *LD*. (3) Deposits of LiF grown from the vapor and from solution had a [741] direction normal to the substrate and the $[12\bar{1}]$ direction approximately parallel to *LD*. (4) Deposits of CsCl and CsBr grown from solution had the [110] direction normal to the substrate and the $[1\bar{1}0]$ direction parallel to *LD*. When grown from the vapor, these two salts had an abnormal NaCl structure with orientation (1). A discussion will be given of the probable reason for each orientation.

HA11. The Structure of Ammonium Chloride by Neutron Diffraction. G. H. GOLDSCHMIDT AND D. G. HURST.—The positions of the deuterium in ND_4Cl have been determined by neutron diffraction. Powdered crystal measurements at −180°C and 23°C with neutrons of wavelength 1.07A gave observed structure factors which were compared with those calculated for various arrangements of deuterium in the known lattice. Very good agreement was found at low temperature for a T_d^1 lattice in which the deuterons lie on cube diagonals at a distance of 1.03A from the nitrogen. The same type of lattice occurs at room temperature. At neither temperature is there any evidence for disorder or rotation. Owing to lattice energy, the deuterons do not appear as points, but occupy a finite space. The results indicate a spherical cloud for the deuteron at low temperature, and a spreading out transverse to the diagonal at room temperature. The room temperature motions can be interpreted in several ways, among them is an angular oscillation of the tetrahedron about the nitrogen as center, or a precession around the diagonals. On the assumption of Gaussian distributions of density and negligible inelastic scattering, the characteristic radius of the spherical cloud is 0.28A and the characteristic angle from the diagonal is about 17 degrees.

HA12. The Cohesive Energy of Solid NH_3. ROBERT L. HELLENS, *Yale University*.—In previous calculations of the forces between NH_3 molecules the second virial coefficient has been used, in conjunction with optical dispersion data and the known dipole moment, to determine the interaction energy. Exact inclusion of the effect of the higher multipole terms in the potential energy is difficult in this type of treatment. In the present work the cohesive energy of solid NH_3 has been computed for a face-centered cubic lattice, taking account of the multipole forces as far as the dipole-octupole term. The energy of the crystal assumes a minimum value when the face-centered lattice is slightly distorted, corresponding to rigid displacements of the four interpenetrating cubic lattices which comprise the face-centered lattice. Since the existence and position of this minimum depend critically on the higher multipole terms, the lattice deformation found by x-ray measurements may be used to determine the one disposable parameter in the multipole expansion, and thus the quadrupole and octupole moments. One part of the dipole-octupole term depends on the positions of the hydrogen atoms in the crystal and therefore displays properties usually associated with the presence of hydrogen bonds.

HA13. The Dielectric Polarization of Ice. J. A. SCHELLMAN AND W. KAUZMANN, *Princeton University*.—The dielectric constant of ice is interpreted in terms of the Kirkwood theory, assuming that the relative configuration of neighboring molecules is chiefly determined by electrostatic interactions. This calculation leads to configurations unfavorable to a large dielectric constant. Assuming the validity of the Kirkwood equation, either of two conclusions can be drawn from this: (1) the electric dipole moment is greatly increased by hydrogen bond formation; or (2) intermolecular forces stronger than electrostatic forces cause crystalline ice to exist in an electrostatically unfavorable average configuration. The mechanism of dielectric polarization of ice is now generally explained in terms of proton transfer rather than molecular rotation. It is usually assumed that ice can, by transfer of protons, assume a state of polarization interpretable in terms of the orientation of dipoles. Our investigation shows that this mechanism can only result in the ordinary polarization of a conductor, which is consistent with experimental data. Alternate mechanisms will be discussed.

HA14. The Dielectric-Strain Constant at Radar Frequencies.* C. W. HORTON AND C. S. MCCLESKY, JR., *The University of Texas*.—Measurements are being made of the dependence of the dielectric constant of glass, polystyrene, and other plastics on the stress and strain. The sample is mounted in a section of a rectangular wave guide which is excited in the $TE_{1,0}$ mode. Measurements made on polystyrene show that when the applied force is parallel to the electric vector, the fractional change of the dielectric constant, $\Delta\epsilon/\epsilon$, is proportional to the principal strain for strains as large as 0.014. The constant of proportionality is 1.12. The stress-strain curve for polystyrene is not linear over this range, so that the fractional change of the dielectric constant is not proportional to the stress. Similar measurements have been made when the applied force is perpendicular to the electric vector and to the axis of the wave guide. In this case the applied force is parallel to the critical dimension of the wave guide and the change in the geometry dominates the measurements. Satisfactory corrections for these effects have not been made yet. Measurements are made at 3.2 centimeters by comparing the phase of the wave that passes through the test sample with that of a standard reference signal.

* The work described in this paper was done at Defense Research Laboratory under the sponsorship of the Bureau of Ordnance, Navy Department.

HA15. Propagation of Excitation in Certain Insulating Crystals. WILLIAM R. HELLER, *University of Illinois*.—On the basis of the customary scheme for discussion of the propagation of excitations in insulating crystals,[1] it is shown that two modes of transport may be contrasted in crystals *without* large overlap of electronic wave functions of the crystal constituents. When the oscillator strength for optical absorption is small, the exciton is shown to have a very large effective mass, and propagation (analogous to sensitized fluorescence) is a diffusion phenomenon.[2] When the oscillator strength approaches unity, the frequency of excitation tunneling will exceed the frequencies of internal motion of the crystal constituents, and one should observe "resonance" propagation with an appropriate wave number.

[1] F. Seitz, *Modern Theory of Solids* (McGraw-Hill Book Company, Inc., New York, 1940), p. 413.
[2] T. Förster, Ann. Physik (2), 55 (1947).

FRIDAY MORNING AT 9:45

Horace Mann

(L. J. HAWORTH presiding)

Apparatus of Nuclear Physics

I1. Current Loading in Ion Accelerating Tubes. J. L. MCKIBBEN AND KEITH BOYER, *Los Alamos Scientific Laboratory*.—Experiments have shown that "electron loading"* phenomena in accelerating tubes is a by product of a positive ion−negative ion chain reaction. The 45-section accelerating tube used was 8 inches i.d. and 22½ inches long and was mounted

without ion source in a small Van de Graaff. The threshold for discharge between the ends of the tube increased from 0.6 to 1.8 Mev as: (a) the pressure was increased to 0.1 micron, (b) a bias voltage was applied to the cathode surface. The upper limit was imposed by breakdown between individual electrodes. The cathode surface was then moved 1½ feet further from the accelerating tube by use of a screen lined Lucite tube. The application of a magnetic field which prevented electrons but not negative ions from returning to the anode surface did not change the threshold voltage for the discharge. Furthermore, it eliminated x-rays. The electron current from cathode to the screen inside the Lucite tube was 50 times the positive ion−negative ion current. The probability of an electron releasing a positive ion was found to be 1.2×10^{-4} from 0.7 to 1.7 Mev in another experiment. Analysis of positive ions in a fourth arrangement showed that they were mostly hydrogen.

* C. M. Turner, Bull. Am. Phys. Soc. 25, No. 5, 17 (1950).

I2. Van de Graaff Injector for Brookhaven Cosmotron. R. G. HERB, *University of Wisconsin*; J. G. TRUMP, *M.I.T.*; J. L. DANFORTH, AND E. A. BURRILL, *High Voltage Engineering Corporation*.—A 4-Mev proton accelerator has been installed for use as an injector to the proton synchrotron at Brookhaven National Laboratory. This electrostatic accelerator follows the Herb design, and is housed in a steel pressure tank 8 feet in diameter and 25 feet long. A set of tracks permits the tank and high potentials shells to be rolled away from the column. Pulsed, analyzed proton beams have been reliably obtained with over 0.3-ma intensity, 4-Mev energy, homogeneous in energy to about 1 part in 500. Stability is obtained by regulation of corona current from a continuous-beam signal obtained from the Mass-2 analyzer portal. Unusual mechanical and control flexibility has been incorporated for ease in adapting the injector to the needs of the Cosmotron. Design features and performance characteristics of this Van de Graaff accelerator will be discussed.

I3. Operation of the M.I.T. Rockefeller Electrostatic Generator. W. M. PRESTON AND CLARK GOODMAN, *M.I.T.*—This generator is housed in a vertical tank fifteen feet high, normally pressurized at 160 lb. The accelerating and differential pumping tubes have 108 one-inch sections, each consisting of a glass ring and an aluminum electrode. The ion source is a 30-Mc/sec electrodeless discharge in a two-inch diameter glass bottle. The ion beam is focused beneath the generator on a slit system; it is then bent through 90 degrees by a magnet and refocused on a second or analyzing pair of slits. The magnetic field is stabilized by a tunable proton resonance device to one part in 20,000. The generator voltage is regulated by a varying corona load controlled by an error signal from the analyzing slits. As an example of resolution, we have obtained a $Li^7(p, n)$ neutron yield "rise curve" at threshold of about 1 kev in 2 Mev, with a 5-microampere proton beam on the target. The limit thus far has been about 4 Mev. Construction of the generator started with a Rockefeller grant; it has been completed under the M.I.T. Neutron Shielding Group.*

* Jointly supported by the ONR and the Bureau of Ships.

I4. Effect of Ducts on the Attenuation of Neutrons and Gamma-Rays in the M.I.T. Cyclotron Shield. J. W. CRAWFORD, JR.,* E. E. KINTNER,* AND CLARK GOODMAN, *M.I.T.*—Most shielding studies consider only attenuation of radiation by bulk materials. Nearly every shield must be perforated to some degree and leakage may constitute the major uncertainty in the shield design. The effects of 6-inch ducts in concrete have been investigated using the M.I.T. cyclotron as a source. Concrete blocks containing the ducts were located on the vertically movable section of the cyclotron shield which serves as a door. The major uncertainties are the energy spectra and the distribution of the sources. The attenuations through the ducts of thermal, resonance, and fast neutrons were measured by In, Cd-In-Cd, and P foils. Gamma-rays were measured with a small G-M tube. Further work is in progress using tanks of water perforated by ducts of 4, 6, and 8-inch diameter. This work was partially supported by ONR and BuShips.

* Now at Code 390 BuShips.

I5. Range-Energy Curve for Alpha-Particles in the Kodak NTB Emulsion.* O. GAILAR, *Purdue University*.—The range-energy curve for α-particles in the Kodak NTB plates, emulsion No. 434, 313-9, has been measured for energies between 3 and 19 Mev. Th, Po, and U are used for energies less than 9 Mev, and α-particles from the Purdue cyclotron, for energies greater than 7 Mev. The α-particles from the cyclotron are scattered through 90° by a 0.0001-in. gold foil, and impinge on a NTB plate. The energy of these particles is both measured and varied by a rotating Al foil holder, patterned after Kelly.[1] The experimentally determined curve agrees very well with one calculated by integrating the Bethe stopping power equation, and is close to the range-energy curve in the Ilford Bl emulsion. Apparatus for measuring the range of Po α-particles used for calibrating the various batches of emulsions is also described.

* Supported by the ONR and an Eastman Kodak fellowship.
[1] E. L. Kelly, Phys. Rev. 75, 1006 (1949).

I6. The Experimental Range-Energy Relation for Protons from 50 to 110 Mev.* N. BLOEMBERGEN† AND P. J. VAN HEERDEN, *Harvard University*.—The energy distribution of the proton beam of the Harvard synchrocyclotron has been analyzed by putting photographic plates along a radius inside the tank a few inches below the plane in which the particles are accelerated. After having been scattered by a tungsten target, the protons are separated according to their energy and focused by the cyclotron magnet at approximately 180° onto the plates. The width of the energy distribution is about 12 Mev. Both target and plates could be moved in radially to cover a wider range of energies. The use of Al, Cu, and Pb absorbers of varying thickness, put in front of the plates, allows the determination of many points of the range-energy curve with less than 0.5 percent error. Preliminary data fit the recently calculated curves[1] with this accuracy. Data on straggling will also be presented.

* Assisted by the joint program of the ONR and AEC.
† Society of Fellows.
[1] Aron, Hoffman, and Williams, *Range-Energy Curves* (Second Revision 1949), AECU-663, UCRL-121.

I7. A High Performance Beta-Ray Spectrometer.* A. A. BARTLETT AND K. T. BAINBRIDGE, *Harvard University*.—The construction and performance of an electron spectrometer of the Siegbahn and Svartholm[1] double-focusing type will be described wherein a cone of electrons is focused at $\pi\sqrt{2}$ radians from the source. The principal departure from prior designs is that the return flux path in iron is at the circumference of the instrument, outside of the exciting coil located at the root of the working gap. The main advantages are (1) that all parts of the iron circuit are operated at low flux densities thus minimizing changes in focal properties often encountered from saturation of the "core". (2) The coil can be shaped as was done in this case to eliminate the need for shims where the gap is greatest. The field can be used up to the largest radius permitted by the coil form. (3) The profile of the poles is calculable and only one machining job was necessary. The radius of the equilibrium orbit is 30.0 cm, the maximum acceptance angle for electrons is 0.8 percent of a sphere, and the detection is by a side window counter. Under these conditions, the resolution (full width at half-height) of the 2.62

Mev ThC″-D conversion electrons from a source 1-mm wide was 0.32 percent.

* This work was supported by the ONR and AEC under ONR contract.
[1] K. Siegbahn and N. Svartholm, Nature 157, 872 (1946).

I8. A Uniform Solenoidal Magnetic Field Beta-Ray Spectrometer. F. H. SCHMIDT, G. L. KEISTER, D. I. MEYER, AND W. E. GROSS, *University of Washington.*—A beta-ray spectrometer has been constructed which focuses the electrons on a ring slit which is concentric with the instrument axis. The existence of the ring focus was first shown by Witcher. Frankel pointed out the improved resolution at large emission angles. Persico and Du Mond[1] have discussed the theory. The water-cooled solenoid is 12¾ in. i.d. and 42 in. long. End correction is provided by coils at the extremities of the solenoid. The field is uniform axially within 0.4 percent and azimuthally within 0.03 percent. The baffle system permits a central emission angle of 35°; the fraction of total solid angle transmitted is adjustable up to 5 percent. The ring focus slit is adjustable to obtain optimum resolution for the desired transmission. The entire baffle system is mounted on wheels and may be rolled out of the vacuum tank to facilitate access. The instrument has been calibrated with ~2μc Thorium *B* source of negligible thickness deposited on a thin Nylon backing. A measured momentum resolution (full width at half-maximum) $\Delta p/p$ of 0.95 percent has been obtained on the "*F*" and "*I*" internal conversion lines. The baffle was set for a transmission of 3 percent. The theoretical momentum resolution for this baffle setting is 0.86 percent. This work is partially supported by the AEC.

[1] J. W. M. Du Mond, Rev. Sci. Instr. 20, 160 (1949).

I9. A Unique-Response Gamma-Ray Scintillation Spectrometer. F. C. MAIENSCHEIN AND JOE KEAGY BAIR, *NEPA Division, Fairchild Engine and Airplane Corporation.*—Spectral measurements with continuous gamma-ray spectra would be greatly facilitated by using a spectrometer giving rise to a single peak for a monoenergetic gamma-ray. A single sodium-iodide crystal does not have this property. However, a Hofstadter type two-crystal spectrometer does give a single peak for each gamma-ray with an energy less than about 1.5 Mev. Above this energy, annihilation quanta from pair production produce coincidences which give rise to additional peaks. Therefore, for measurements above 1.5 Mev, the above instrument was converted into a pair spectrometer by the addition of a third crystal in coincidence with the first two. In this instrument, the electron pair is captured in the initial crystal, while the two annihilation quanta trip the two auxiliary crystals. High energy measurements were also made by connecting the third crystal of the pair spectrometer in anticoincidence with the first two. Such an arrangement discriminates against pair coincidences. While the discrimination is not complete, this method may be useful as an aid in untangling complicated spectra. All measurements were made with both collimated and uncollimated sources. The resolutions obtained were around 10–15 percent full width at half-maximum, which is about the limit of the initial crystal. Sensitivities were obtained of the order of 2×10^{-3} counts/sec per unit gamma-ray flux incident on the initial crystal.

I10. Some Phosphor-Plastic Systems as Scintillation Counters. W. S. KOSKI, *The Johns Hopkins University.*—The scintillation properties of anthracene and stilbene dissolved in Lucite, Paraplex, and polystyrene have been investigated using gamma-rays from Co[60]. The systems involving Lucite and Paraplex were poor γ-ray counters, however, 2 percent anthracene or stilbene in polystyrene gave results that were comparable to those of single crystals of anthracene or stilbene. The emission spectra of these solid solutions are essentially the same as those of pure stilbene or anthracene. There is, however, a slight shift in wavelength. The spectral data suggests a mechanism for the energy transfer from the polystyrene to the phosphor and this will be discussed.

I11. Energy Response of Liquid Scintillation Counters. GEO. T. REYNOLDS, F. B. HARRISON AND D. HILL, *Princeton University.*—Experiments have been performed to determine the dependence of pulse height per unit energy loss upon velocity of ionizing particle in fast scintillation solutions.[1] By means of a differential discriminator the pulse height, corresponding to an α-particle with a given energy loss in the solution, has been determined for various residual energies of α-particles. Included also was the pulse height corresponding to α-particles from Po dissolved in the scintillating solution. These pulse heights were compared with those corresponding to the Cs^{137} 625-kev electron. The extent of the nonuniformity of energy response observed in these organic scintillators is indicated by the fact that an α-particle losing 5 Mev in the solution gives rise to a pulse that is only 0.8 that obtained from a 0.6-Mev electron. The observed velocity dependence will be discussed.

[1] Reynolds, Harrison, and Salvini, Phys. Rev. 78, 488 (1950); G. T. Reynolds, Nucleonics, May, 1950; F. B. Harrison and G. T. Reynolds, Phys. Rev. 79, 732 (1950); H. Kallman and M. Furst, Phys. Rev. 79, 857 (1950).

I12. Measurements of the Timing of Cloud-Chamber Operation. MONROE F. RICHMAN, *Syracuse University.*—A simple device has been designed permitting continuous registration of the pressure change during expansion of a cloud chamber. The displacement of a membrane is transferred onto the shaft of a RCA 5734 electromechanical transducer tube, whose amplified output, mixed with signals corresponding to triggering pulse, cleaning field switch, light flash etc. is traced on an oscilloscope. Some results of a systematic investigation on the optimum operating conditions of a large square cloud chamber will be presented.

I13. A Theoretical Discussion of Diffusion Cloud Chambers.* R. P. SHUTT, *Brookhaven National Laboratory.*—In his article on continuously sensitive cloud chambers, A. Langsdorf[1] proved theoretically that by letting vapor diffuse from a hot to a cold surface the supersaturation necessary for drop formation on ions can be obtained. In order to enable one to predict the "ideal" temperature distribution necessary to maintain the proper supersaturation through a given depth of a chamber an attempt has been made to formulate theoretically the condensation phenomena not considered by Langsdorf. Drop growth and the motion of the drops through the chamber have been taken into account. Because the temperature of a growing drop adjusts itself almost instantaneously to its environment the problem can be treated as semi-stationary. By impressing the ideal temperature distribution for given conditions one would make the most economical use of the available vapor and thus one might be able to obtain track formation through a greater depth in a chamber. Ideal temperature distributions for different conditions are to be discussed and limiting gas pressures above which the operation of diffusion chambers may become impractical will be given.

* Work done at Brookhaven National Laboratory under the auspices of the AEC.
[1] A. Langsdorf, Rev. Sci. Instr. 10, 91 (1939).

I14. Operation of Diffusion Cloud Chambers at High Pressures.* D. H. MILLER, E. C. FOWLER AND R. P. SHUTT, *Brookhaven National Laboratory.*—High pressure cloud chambers are well suited for the study of nuclear interactions in gases. Since high pressure expansion chambers cannot be cycled frequently enough for efficient utilization of accelerators a continuously sensitive chamber for pressures up to 20 atmospheres has been constructed from a stainless steel cylinder. Methanol vapor has been used almost exclusively so far. With

air or argon at pressures above 3 atmospheres it becomes increasingly difficult to provide sufficiently large temperature gradients to obtain track formation through an acceptable depth of the chamber. With vapor diffusing downward in helium or hydrogen gases the chamber becomes stable only at pressures of several atmospheres, depending on the temperature distribution. For example, with hydrogen at 15 atmospheres, with an average temperature gradient of 6°C per cm, and with a bottom temperature of −60°C, the temperature of the evaporating liquid must be kept below 10°C. Under these conditions the track sensitive layer is only 1¼ in. deep. A small amount of argon (less than ½ atmosphere) added to the hydrogen stabilizes the chamber sufficiently to permit raising the liquid temperature to 30°C, increasing the depth of the sensitive layer to 2½ in.

* Work done at Brookhaven National Laboratory under the auspices of the AEC.

FRIDAY MORNING AT 10:30

Pupin 428

(S. C. BROWN presiding)

Discharge in Gases

IA1. Decay Processes in the Krypton Afterglow.* JOHN M. RICHARDSON†, *Harvard University.*—Previously described techniques[1] for the investigation of atomic and molecular decay processes in pulsed discharge afterglows have been applied to samples of krypton which unavoidably contained traces estimated of the order 0.1 to 0.01 mole percent xenon. It is found that such quantities of xenon profoundly enter into the afterglow processes of recombination and radiation, the degree increasing with pressure in the range 6 to 25 mm Hg. The effect does not occur at low pressures where diffusion phenomena prevail. Nevertheless, it has been possible to conclude that both krypton and xenon have recombination coefficients of the same order as recently measured for other gases, and tentative values of 6×10^{-7} cm³/electron-sec and 2×10^{-6} cm³/electron-sec, respectively, are proposed. Correlation of the observed visible light intensity emitted in the immediate afterglow where krypton processes predominate (100 to 200 μsec) with the rate of electron removal accounts for a major portion of the radiant energy released per recombination event as predicted from consideration of the atomic energy states. Therefore, a form of radiative recombination is indicated.

* This work was assisted by ONR.
† AEC Predoctoral Fellow.
[1] Holt, Richardson, Howland, and McClure. Phys. Rev. 79, 239 (1950).

IA2. Plasma Oscillations in a Static Magnetic Field.* E. P. GROSS, *M.I.T.*—A theory of the small-amplitude oscillations of an ionized gas in a static magnetic field is developed, including the effects of temperature motions. The Boltzmann equation is solved for this problem, and exact expressions are obtained for the distribution function and dispersion relation. A general feature of the dispersion relation is the existence of gaps in the spectrum at frequencies which are approximately multiples of $\omega_c=eH/mc$. The magnitude of the gap depends on the temperature of the gas, being proportional to it for long wavelengths. This leads to the prediction of selective reflection of waves impinging on a plasma with frequency in the forbidden range. For $ck\gg\omega_p$, ω_c the waves split into approximately longitudinal plasma waves and transverse waves. Detailed analysis is made of the plasma waves for ω_c small and ω_c large. At long wavelengths the frequency is $\omega^2\simeq\omega_p^2+\omega_c^2+\beta\kappa Tk^2/m$, where β depends on ω_p and ω_c. For waves near the Debye length the waves are heavily damped. Two simpilfied treatments of plasma oscillations based on transport equations are compared with the above treatment. Expressions of the form $\omega^2\simeq\omega_p^2+\omega_c^2+\beta\kappa Tk^2/m$ are obtained where the factor β is independent of ω_c and ω_p. In addition, the transport treatments fail to predict the heavy damping near the Debye length and the existence of gaps in the frequency spectrum.

* Sponsored by the ONR, the Army Signal Corps, and the Air Force.

IA3. Parallel Plate Spark Counters in Magnetic Fields. FRANK L. HEREFORD, *University of Virginia.*—An increase has been observed in the sparking potential of parallel plate counters operated in magnetic fields (up to 2500 gauss) applied in the direction of the discharge channel. Increases up to 200 volts were observed for 0.2-cm plate spacing in pressures of the order of one-half atmosphere. The phenomenon is apparently due to a focusing action decreasing the mean radius of the positive ion sheath remaining at the anode after collection of the avalanche electrons. This results in an increased positive ion space charge field which in accordance with Meek's criterion raises the sparking potential. Normally, the radius of this positive ion concentration is dependent only upon the random diffusion of the avalanche electrons in the lateral direction. Raether's measurements[1] of this diffusion rate have confirmed the applicability of the well known Einstein diffusion theory in this regard. By the method of Ornstein and van Wijk[2] one can obtain a solution of the Einstein equation for the case of a superposed magnetic field. Results of this calculation will be compared with experimental *sparking potential vs field strength* curves.

[1] H. Raether, Z. Physik 107, 91 (1937).
[2] L. S. Ornstein and W. R. van Wijk, Physica 1, 235 (1930).

IA4. Sharpness of the Sparking Potential in Various Gases.* G. A. KACHICKAS AND L. H. FISHER, *New York University.*—Previous observations of the sharpness of the sparking potential (s.p.) in air in uniform fields with a brass cathode[1] have been extended to N_2, A, and O_2. At any given time, the s.p. in air, A, and in slightly impure N_2 is sharp to at least a few volts (out of 10 to 30 kv). In pure N_2 the s.p. varies by about 50v in 30 kv. Definition of the s.p. in O_2 is difficult, since times as long as five minutes may be required before a spark passes. In pure N_2, enormous decreases in the s.p. (up to 23 percent) were obtained with a primary current of 200 electrons/μsec. With this same primary current, the s.p. of slightly impure N_2 is lowered by about one percent, while the s.p. of A is not affected at all. Von Laue distribution plots for time lags of spark breakdown are presented. These plots show a statistical feature in the breakdown of O_2 (negative ion formation); there is no such element in the breakdown of air, N_2 (impure), or A.

* Supported by the ONR and the Research Corporation.
[1] L. H. Fisher and B. Bederson, Phys. Rev. 81, 109 (1951).

IA5. The Philips Gage Discharge. TALBOT CHUBB,* *University of North Carolina.*—The Philips gage is differentiated from other similar cold cathode discharges requiring a magnetic field. Its operation at pressures above a micron is distinguished from low pressure operation by the presence of sufficient positive ion current to permit the formation of a cylindrical plasma at anode potential. The micron-pressure discharge with good secondary emitting cathodes takes place at a few hundred volts, produces ions of low energy spread, possesses a constant voltage *vs* current density and pressure curve and is probably characterized by its cathode electrons losing most of their energy by molecular collisions. The micron pressure discharge with poor secondary emitting cathodes takes place at much higher voltages, produces ions with a high energy spread, and is probably characterized by its cathode electrons failing to dissipate most of their energy in molecular collisions. The low pressure discharge with a ring anode possesses a crudely linear increase of current with with pressure at constant voltage, a big variation in current with cathode material, and a radial electric field. Philips gages can produce oscillation in the kilocycle, megacycle, and kilomegacycle regions.

* Now at the Naval Research Laboratory.

IA6. Space Charge Detector for Alkali Halide Molecular Beams. R. BRAUNSTEIN AND J. W. TRISCHKA, *Syracuse University.*—A potassium chloride beam was directed against the coaxial tungsten filament of a space charge limited cylindrical diode. The positive ions produced by surface ionization were trapped in the potential minimum surrounding the cathode causing relatively large increases in plate current. Amplifications (ratios of change in electron current to ion current) as high at 70,000 were obtained with a diode containing and plates at positive potentials, similar in structure to the "Kingdon Cage." A diode without end plates was also employed yielding amplifications of the order of 10^4. The mechanism of space charge release which seems consistent with our data is that of neutralization of the positive ions at the cathode after several oscillations in the potential minimum. Curves were plotted of amplification as a function of plate voltage at various filament temperatures and beam intensities, in order to delineate the optimum sensitivity of such a detector. Amplification reaches a peak at about 10 percent of the electron saturation current; it increases slightly with increase in filament temperature. The detector is nonlinear, the amplification decreasing with increasing beam intensity. A theory of a simplified model of the space charge release will be discussed.

Post-Deadline Papers, If Any

FRIDAY AFTERNOON AT 2:00

McMillin

(C. C. LAURITSEN presiding)

Joint Ceremonial Session of the American Physical Society and the AAPT

Retiring Presidential Address of the American Physical Society

J1. Molecular-Beam Researches in Nuclear and Electronic Physics. I. I. RABI, *Columbia University.*

(DUANE ROLLER presiding)

J2. Presentation of the Oersted Medal of the AAPT to J. W. Hornbeck.

Richtmyer Lecture of the AAPT

J3. The Electron Theory of Solids. J. C. SLATER, *M.I.T.*

FRIDAY AFTERNOON AT 3:10

Pupin 301

(W. E. LAMB, JR. presiding)

Atomic and General Theory

K1. A Simple Potential for Atomic Calculations, EDWARD H. KERNER, *Wayne University.*—The potential is of the form $(Z-Br)/r(1+Ar)$ and approximates sufficiently well to the Hartree or Fermi-Thomas potentials for many purposes. The parameters A and B depend on Z and on the degree of ionization of the atom. Schrödinger and (with some extra complexities) Dirac wave functions may be found as quickly converging series of hydrogenic functions or as power series in $Ar/(1+Ar)$ or $(1+Ar)^{-1}$, and in other ways. Energy eigenvalues ϵ and expansion coefficients C_j may be readily evaluated using the recurrence formulae for the C_j which follow from the differential equations; the roots of the determinant of the infinite

set of linear equations defined by these formulas give the ϵ. They may be found with arbitrary accuracy using a simple numerical procedure which amounts to calculating successively the roots of finite determinants of increasingly large order. This appears to be considerably simpler in practice than the usual method of expanding the determinant as a continued fraction. For the Schrödinger equation, the eigenvalue problem is nearly identical with that arising in the well known hydrogen molecule ion problem. The integrals of the WKB approximation may be found explicitly as elliptic integrals.

K2. Configuration Interaction for the Ground State of He I.* L. C. GREEN, M. M. MULDER, *Haverford College*, C. W. UFFORD, E. SLAYMAKER, *University of Pennsylvania*, E. KRAWITZ AND R. T. MERTZ, *Watson Scientific Computing Laboratory*.—In order to estimate the number of configurations which must be taken into account to obtain a ground-state wave function of a given accuracy for He I, the Hylleraas six-term expression for this state has been expanded in series of orthogonal functions. To determine the degree of dependence of the coefficients on the specific function used for the ground state, the Hylleraas three-term expression has also been expanded. One set of orthogonal functions consisted of symmetrized product-type wave functions where the functions of the individual electrons were found from a Hartree self-consistent field without exchange.[1] As a second set of orthogonal functions, variationally determined analytic wave functions were used.[2] The results of the calculation for the six-term expression and the self-consistent field functions give for the square of the coefficient of the $1s^2$ configuration 0.9921, and for the $1s2s$ configuration 0.0013. These results indicated the need for considering a large number of configurations if an accurate wave function is desired.

* This work was supported in part by the ONR and in part by a grant from the Research Corporation.
[1] W. S. Wilson and R. B. Lindsay, Phys. Rev. **47**, 681 (1935).
[2] Morse, Young, and Haurwitz, Phys. Rev. **48**, 948 (1945).

K3. Electron Affinity of Sodium. R. M. THALER* AND A. O. WILLIAMS, JR., *Brown University*.—The self-consistent field calculation of the structure of Na^- neglects the polarization effects of the added electron and yields a negative electron affinity.[1] A better wave function is $\Phi(1+c\rho)$, where Φ is the Hartree wave function for Na^-, ρ is the distance between the two $3s$ electrons, and c is a parameter to be evaluated by the Hylleraas technique. The lengthy integrals arising during calculation of the energy can be approximated by simpler forms and evaluated. Final results for Na^- are a positive electron affinity of 1.2 electron volt (stable ion) and an average angular separation between the $3s$ electrons of 157°. This decrease in energy relative to the Hartree result is mainly due to the increased separation and lowered interaction potential energy of the $3s$ electrons. Since the $4s$ electrons of K^- should show still stronger polarization, the electron affinity for potassium can be estimated to be about +0.7 electron volt.

* Now at Yale University.
[1] D. R. Hartree and W. Hartree, Proc. Camb. Phil. Soc. **34**, 550 (1938).

K4. Klein's Theory and the Coupling of Angular Momenta in Molecules. J. H. VAN VLECK, *Harvard University*.—Klein[1] has observed that when referred to axes mounted on the molecular framework, the components of a molecule's total angular momentum satisfy the usual commutation relations, but with an anomalous sign of i. He has shown that from this fact the Wang secular equation for the asymmetrical top can be deduced very simply. However, neither he nor Casimir exploited the possibilities of this method for deducing the matrices, secular equations, etc., connected with the coupling of electronic orbital and of electronic or nuclear spin angular momenta to the molecular rotation (Hund's cases *a* and *b*, hfs, etc.). These angular momenta all obey commutation relations with the normal sign of i. Hence, they can be subtracted from the total angular momentum by using the ordinary formulas for the addition of angular momenta. As a result, the coupling problems associated with angular momentum in molecules are, with appropriate allowances for differences in notation and interpretation, mathematically equivalent to well-known problems in atomic spectra. Details will probably be published in *Reviews of Modern Physics*.

[1] O. Klein, Z. Physik **58**, 730 (1930); H. B. G. Casimir, "Rotation of a rigid body in quantum mechanics" (Dissertation, 1931).

K5. The Fourth-Order Self-Energy of the Electron. ROBERT M. FRANK,* *Cornell University*.—The self-energy of a free electron is calculated to order e^4. The modification of quantum electrodynamics suggested by Feynman[1] is used to make the matrix elements finite. After mass renormalization, using the self-energy to order e^2, there remain four Feynman diagrams whose matrix elements must be calculated. Two of these represent the two ways in which two virtual quanta may be emitted and absorbed by the electron, both quanta being present at the same time. The third diagram represents the emission of a virtual quantum which creates a virtual pair, the quantum produced by the pair annihilation being absorbed by the electron. The last diagram corresponds to the emission and absorption of a virtual quantum accompanied by a mass renormalization. The matrix elements involve an integration over the momenta of all virtual quanta present in each diagram. These integrals are approximated by assuming that the Feynman cutoff, λ, is large compared to the electron mass. It is found that the result depends upon $(\ln\lambda)^2$, but it is not the square of the second-order self-energy.

* Present address: Florida State University.
[1] R. P. Feynman, Phys. Rev. **76**, 769 (1949).

K6. Some Results on the Quantum Theory of a Finite-Sized Electron. GEORGE YEVICK, *Stevens Institute of Technology*.—Using the Lagrangian formulation of quantum mechanics developed by Feynman, we have been considering general types of interactions between the electron and the electromagnetic field which give the electron a finite structure. These interactions contain higher derivatives of the electron trajectory, e.g., the four-acceleration. We have encountered three basic problems. (1) What quantum mechanically corresponds to these higher derivatives? (2) How does one order quantum mechanically a product which classically contains a number of higher derivatives as factors? (3) How does one evaluate overlapping "slices" in the Feynman perturbation procedure when one has a finite-sized electron? We have solved problems (1) and (2), but we have made little progress on (3). We can show that these overlapping or "contact" terms exist; but we cannot exhibit their explicit form, because of the apparent great labor needed to evaluate many slices in space-time. These contact terms are a significant new feature and mean physically that two or more photons can interact with the electron when the electron's center is at a given point in space-time. Donald Yennie (private communication) has pointed out to us the connection between contact terms with gauge invariance.

K7. Classical Electrodynamical Motion Including Radiative Reaction. GILBERT N. PLASS, *The Johns Hopkins University*, AND JOHN A. WHEELER, *Princeton University*.—An idealized description of radiative reaction—applicable to the quantum world when a correspondence principle description of the motion is legitimate—uses that classical relativistic equation of motion of a charged particle which has been derived in different ways by Dirac and by Wheeler and Feynman. In it appears the third derivative of the displacement. Consequently, the solution contains extra constants to be determined so that the particle will not execute a runaway motion. Eliezer has proven that it is impossible to satisfy this condi-

tion in the case (1) of a particle moving directly towards an attractive Coulomb force. He also concluded that similar difficulties arise in (2) a repulsive Coulomb field and (3) in the field of a thin charged plate. We find on the contrary—accepting the notion of preacceleration—reasonable physical solutions for (2) and (3) and for the harmonic oscillator. We conclude it is reasonable to expect physically acceptable solutions for all nonsingular potentials. The paradox of the divergence for (1) we find can be interpreted and resolved within the framework of the absorber theory of radiation, provided that the idealized absorber envisaged there is considered to contain only a finite number of charged particles.

K8. Radiative Corrections to the Klein-Nishina Formula. L. M. BROWN AND R. P. FEYNMAN,* *Cornell University.*—The corrections to the differential cross section for the Compton effect arising from an additional virtual quantum are computed for unpolarized radiation using the methods developed by one of us.[1] A nonrelativistic approximation has been previously obtained.[2] The terms of the e^4-order transition amplitude are evaluated. The interference of the fourth-order amplitude with the second-order amplitude is found, including explicit integrations over the intermediate momenta and averages over the spin of the electron and the polarizations of the photons. The resulting correction to the cross section contains an infrared catastrophe. To make a comparison with experiment possible, the cross section for the double Compton Effect (absorption of one photon followed by emission of two) is computed and integrated over the energy of one of the photons up to a value small compared to mc^2. The sum of single and double Compton cross sections contains no divergence to order e^4. The final general formula is complicated, so that some numerical results as well as approximate expressions valid under various limiting conditions will be given.

* Now at Northwestern University and California Institute of Technology, respectively.
[1] R. P. Feynman, Phys. Rev. 76, 749 and 769 (1949).
[2] R. Schafroth, Diss. E. T. H. Zurich (1949).

K9. Covariant Diamagnetic Effects in the Vacuum.* T. A. WELTON,† *University of Pennsylvania.*—The elementary theory of holes yields an induced current density proportional to the inducing vector potential, for a slowly varying field. This result is commonly regarded as non-gauge-invariant and the effects of this induced current are systematically ignored by the use of some subtraction formalism. It will be shown that the usual result, following as it does from a gauge-invariant theory, does not in fact represent a failure of gauge invariance. It rather corresponds to the existence of a simple physical property of the vacuum of the positron theory, namely, the diamagnetic susceptibility of a system of free electrons in negative energy states. The expression for this susceptibility can be correctly calculated by the most elementary classical argument. There seems then to be no basis for regarding the photon self-energy as less physical than the charge renormalization and Uehling terms in the vacuum susceptibility. The admission of the photon self-energy as a physically meaningful consequence of the hole theory then clearly necessitates the reformulation of the positron theory to avoid the appearance of the usual reactive polarization effects.

* Supported in part by ONR.
† Now at Oak Ridge National Laboratory, Oak Ridge, Tennessee.

K10. Secondary Constraints in Covariant Field Theories.* JAMES L. ANDERSON, PETER G. BERGMANN, AND ROBERT PENFIELD, *Syracuse University.*—It was shown previously[1] that in any covariant theory there exist a number of so-called constraints between the field variables and the momentum densities completely free of time-differentiated quantities. Just as in quantum electrodynamics, the Poisson brackets (or commutators) between these "primary" constraints and the Hamiltonian must be set equal to zero if the canonical equations are to be satisfied. We call these resulting expressions "secondary constraints." We have examined whether the repetition of this procedure leads to further constraints, with the result that it does not, but that the primary and secondary constraints together with the Hamiltonian form a function group, i.e., that all further Poisson brackets are linear in these expressions and their spatial derivatives. The reason is that certain linear combinations of the primary and secondary constraints form the generators of the most general infinitesimal coordinate transformation in space-time, and these form, of course, a continuous group. From the point of the canonical theory, this group is the group of transformations leaving a certain class of Hamiltonians invariant.

* Supported by ONR.
[1] Peter G. Bergmann, Phys. Rev. 75, 680 (1949).

K11. Conservation Laws in the Hamiltonian Formalism.* JOSHUA GOLDBERG, PETER G. BERGMANN, AND RALPH SCHILLER, *Syracuse University.*—With respect to infinitesimal coordinate transformations generated by a set of arbitrary functions ξ^k, we require that the Lagrangian density change by a complete divergence.[1] This condition leads to the Bianchi identities and hence to the strong conservation laws. If we remain entirely within the Hamiltonian structure, we must formulate the condition of covariance differently. However, if C belongs to a group of generating functionals that leave the Hamiltonian invariant modulo the primary constraints, then C is a constant of the motion. In particular, those generating functionals generating the infinitesimal coordinate transformations belong to that group. We have shown that if such a generating functional is to exist, then four expressions must vanish; they correspond to the Bianchi identities. It is possible to write these identities as total divergences. If the left-hand sides of the field equations satisfy the Bianchi identities, then the right-hand sides must satisfy them, too. We thus obtain total divergences involving the energy, momentum, and matter distribution densities, which must vanish. These relations are the strong conservation laws in terms of canonical variables.

* Supported by ONR.
[1] Phys. Rev. 75, 680 (1949).

K12. On Invariant Canonical Transformations.* PETER G. BERGMANN, *Syracuse University.*—In the two preceding papers, it was shown that the invariance of the canonical formalism with respect to infinitesimal canonical transformations corresponds to the covariance of the underlying Lagrangian theory. In ordinary mechanics, an infinitesimal invariant transformation, defined as leaving the form of the Hamiltonian unchanged throughout the phase space S, is generated by an integral of the motion. In the presence of constraints, only the subspace S_I in which the primary constraints are satisfied corresponds to meaningful Lagrangian situations. The transformation group I that leaves the Hamiltonian unchanged in form in S_I depends on four arbitrary functionals of the canonical coordinates and t; it is this group that corresponds to ordinary coordinate transformations. In the more restricted subspace S_h, in which all constraints are satisfied, the invariant transformation group h depends on eight arbitrary functionals. Because of the known transformation properties of the Lagrangian theory, the group I is better suited for an examination of the structure of the function group consisting of the constraints and H. But from the point of view of the canonical formalism, h appears more natural.

* Supported by ONR.

K13. Time-Reversibility of Quantum Electrodynamics and Commutation Relations. SATOSI WATANABE.—The

author previously showed, in the framework of many-time theory, that the quantum electrodynamics reproduces the time-reversibility of classical electrodynamics, provided the current commutation relations are assumed for the electromagnetic field.[1] The present paper is its generalization to the super-many-time theory, to show that the classical reversibility is guaranteed by the usual commutation relations of the electron field and the electromagnetic field. The argument can be used in the inverse sense to conclude the ordinary commutation relations as necessitated by the requirement of reversibility.* This report will contain: (a) definition of four kinds of tensors (or pseudo-tensors) and four kinds of spinors (or pseudo-spinors) as representations of the most general Lorentz group,[2] (b) introduction of eight component spinors, (c) time-reversibility of nonquantized fields in interaction, (d) time-reversibility of quantized fields in interaction, and (e) reversibility and commutation relations.

[1] S. Watanabe, Sci. Papers Inst. Phys. Chem. Research (Tokyo) **31**, 109 (1937). See especially page 116.
* It is a pleasure of the author to note here that this inversion of the argument has been suggested by news brought to him by Mr. K. Case about the unpublished work of Mr. J. Schwinger.
[2] S. Watanabe, Sci. Papers Inst. Phys. Chem. Research (Tokyo) **39**, 157 (1941).

K14. Information, Measurement, and Quantum Mechanics. JEROME ROTHSTEIN, *Signal Corps Engineering Laboratories.*—Measurement consists in selection of a subset of the ensemble of *a priori* possible results consistent with the defining conditions, thus yielding information as defined in communication theory.[1] Isomorphic abstract formulations of theory of measurement and communication ensue, measurement and defining conditions corresponding to message and specification of stochastic nature of the message source. Quantum mechanics predicts possible results of measurement and their corresponding probabilities of occurrence, with the outcome of single measurements generally unpredictable. Wave functions contain the information obtainable about a system from operational specification of its preparation or measurement and describe ensembles consistent therewith rather than single systems. "Casual anomalies" (discontinuous changes in wave function) resulting from measurement merely indicate changed information. The Einstein-Podolsky-Rosen paradox shows different measurements can yield different information and thus different wave functions and representative ensembles, despite the individual system being physically unaffected by the choice made. The "real" state of a system, being operationally undefined, seems extraneous to quantum mechanics, just as the meaning of messages is irrelevant to communication engineering; reality and meaning are problems of another level, possibly along with casuality. From the present viewpoint, quantum statistics deals with less than maximal information and includes quantum mechanics as its sharpest form rather than constituting a separate discipline.

[1] C. E. Shannon, Bell System Tech. J. **27**, 279, 623 (1948); N. Wiener, *Cybernetics* (John Wiley and Sons, Inc., New York, 1950).

K15. Dimensionless Formulation in the Irreducible Volume Character of Events. B. T. DARLING, *Ohio State University.*—The interaction of spin ½ material processes with the electromagnetic field may be formulated in an entirely dimensionless manner depending only on two pure numbers, the fine structure constant α, and $\beta(=1.61)$. The charge, mass, energy, potentials are all pure numbers. For the charge we have $e=\pm 1$, while the masses are just the roots $z_0, z_1, z_2, \cdots$ of the mass quantization condition. The rest energy is just equal to the rest mass. For example the rest mass of the hydrogen atom in the nth Bohr orbit is $z_0+z_{1s}-\beta/\alpha^2n^2$. The radius of the nth Bohr orbit would be α^2n^2/β. For the purpose of this discussion the Maxwell equations will be used in their usual form.

FRIDAY AFTERNOON AT 3:10

Schermerhorn 501

(P. KUSCH presiding)

Molecular Beams and Microwave Spectra

L1. An Atomic Beam of Helium Atoms in the Metastable $1s\,2s$, $^3S_1$ State. VERNON HUGHES AND GARDINER TUCKER, *Columbia University.*—An atomic beam of helium atoms in the metastable $1s\,2s$, $^3S_1$ state has been produced from a discharge tube source and detected by electron ejection from a cold tungsten wire.[1] The discharge tube had a directly heated cathode and was operated with dc power; the atoms were allowed to escape through a small slit in the discharge tube. The Stern-Gerlach deflection pattern to be expected for atoms with a magnetic moment of 2 Bohr magnetons was observed. Because of the large background of photo-electrons ejected from the detector by the photons from the discharge tube, (this background signal was about 100 times the signal due to the metastable atoms) it was necessary to observe the Stern-Gerlach deflection pattern as a difference curve between the conditions of deflecting field on and off. By the use of two inhomogeneous magnetic fields (A and B fields), the beam of metastable atoms was refocused around a wire stop which blocked photons from reaching the detector. An electron current due to the refocused beam of as high as 5.10^{-14} amp was obtained.

[1] R. Dorrestein, Physica **9**, 433 and 447 (1942).

L2. New Measurements of the Deuteron Electric Quadrupole Moment.* H. G. KOLSKY, T. E. PHIPPS, N. F. RAMSEY, AND H. B. SILSBEE, *Harvard University.*—The molecular beam magnetic resonance method recently proposed by Ramsey[1] has been applied to H_2 and D_2 molecules. Measurements have been made both in high magnetic fields as with previous studies and for the first time in weak fields of less than ten gauss. The latter measurements are particularly effective in increasing the precision of the results since the desired interactions are measured directly instead of superposed on a much larger interaction with an external magnetic field. Curves showing the observed radiofrequency spectra will be presented along with tables of the molecular interaction constants inferred from them. One of these interaction constants is for the quadrupole moment of the deuteron. With the previous notation,[2] $-qQ=(1.2936\pm.006)\times10^{-3}$ cm^{-1}. With Newell's[3] most recent value of q, the deuteron quadrupole moment Q is $+(2.741\pm.016)\times10^{-27}$ cm^2, which is one percent below that inferred by Newell[3] from the best previous data.

* Work partially supported by joint program of ONR and AEC.
[1] N. F. Ramsey, Phys. Rev. **78**, 695 (1950).
[2] Kellogg, Rabi, Ramsey, and Zacharias, Phys. Rev. **57**, 677 (1940).
[3] G. F. Newell, Phys. Rev. **78**, 711 (1950).

L3. The Spin-Orbit Spectrum in Molecular Beams. W. A. NIERENBERG, *University of California, Berkeley.*—If a nucleus of spin one-half is coupled to the molecular rotation, its molecular beam spectrum can be predicted for all values of the magnetic field from the Zeeman to the Paschen-Back region with one closed expression. This expression is valid for large values of rotational quantum number and small rotational g-factor and assumes a Boltzmann distribution of rotational states. The special case of spin one-half is simple because the symmetry permits cosine coupling only and the energy levels are well known for this Hamiltonian. A kind of correspondence principle can be developed for this example which does two things. It shows that the other nucleus in a diatomic molecule has little effect on the spectrum of the first due to the coupling of the second nucleus to the rotation. Second, it permits the extension of the calculation to nuclei of spins greater than one-half when the coupling is predominantly cosine-like. Finally, the restriction to negligible rotational g-factor can be removed to give the approximate energy levels but the spectrum is now more complicated due to the transitions $\Delta M_J = \pm 1$, which are now observable. A simple picture showing the motion of the vectors can be constructed.

L4. Pressure Broadening by Foreign Gases in the Microwave Spectrum of Ammonia. C. A. POTTER, A. V. BUSHKOVITCH, AND A. G. ROUSE, *St. Louis University.*—Half-widths of five pressure-broadened lines of the ammonia inversion spectrum were measured, as a function of total pressure. The perturbing gases were oxygen, helium and nitrous oxide in various mix ratios. The results appear to indicate that the collision cross sections decrease with increasing mix ratio of perturber to absorber.

L5. Millimeter-Wave Spectra. S. J. TETENBAUM, *Yale University.**—A source-modulated spectroscope has been built for study of the microwave absorption spectra of gases in the 5 to 6 millimeter region. Millimeter wave power is obtained as the second harmonic generated by a silicon-tungsten crystal converter driven by a klystron oscillator. The modulation, detection, and display techniques are similar to those in wide use. Frequency measurements are made using a cavity wave meter. The apparatus has been tested with the known $J=3\rightarrow4$ rotational spectrum of OCS. The $J=1\rightarrow2$ rotational spectrum of N_2O has also been observed and the hyperfine structure of this spectrum is now under study. Other molecules are being investigated and results will be presented.

* Assisted by the ONR.

L6. Further Studies of the Microwave Absorption Spectrum of Nitrosyl Chloride.* JOHN D. ROGERS AND DUDLEY WILLIAMS, *The Ohio State University.*—The $J=1$ to $J=2$ transition of NOCl has been studied in more detail than indicated in the earlier report on the subject.[1] Analysis of the experimental data in terms of asymmetric top theory gives the following values for the rotational constants: for $NOCl^{35}$, $A=2.845$ cm^{-1}, $B=0.19141$ cm^{-1}, $C=0.17934$ cm^{-1}; and for $NOCl^{37}$, $A=2.854$ cm^{-1}, $B=0.18682$ cm^{-1}, and $C=0.17534$ cm^{-1}. Analysis of the hyperfine structure of different lines associated with the transition in terms of the theory of Knight and Feld yield consistent values for nuclear quadrupole interactions of the Cl^{35} and Cl^{37} nuclei with the molecular fields. From the Stark patterns observed for $NOCl^{35}$, it is possible to obtain a value for the component of the dipole moment parallel to the axis of least moment of inertia.

* This work was in connection with a contract between the Air Force Cambridge Research Laboratories and the Ohio State University Research Foundation.
[1] Pietenpol, Rogers, and Williams, Phys. Rev. **76**, 690 (1949).

L7. Radiofrequency Spectra of CsCl. R. G. LUCE AND J. W. TRISCHKA, *Syracuse University.*—The radiofrequency spectra of cesium chloride were studied by means of the electric resonance method.[1,2] The four observed lines were identified as $J, m_J \rightarrow J, m_J'$ transitions 2, 0→2, 1; 3, 0→3, 1 and/or 4, 1→4, 2; 5, 1→5, 2; and 4, 0→4, 1. The extremely complex fine structure presumed to be present in the observed lines was not resolved, so that no accurate determination of the nuclear quadrupole coupling constants was possible. However, from the line widths the absolute value of the quadrupole interactions, $|eqQ/h|$, for Cl and Cs were each estimated to be less than 5 mc. The breadth of the lines made it possible to determine from our data the two molecular constants A, the moment of inertia, and μ, the dipole moment, but a value of $\mu^2 A = 42.13\times10^{-78}$ cgs units was obtained. Using an internuclear distance, r, of 3.06×10^{-8} cm ascertained by electron diffraction,[3] a value of $\mu=9.8\pm0.4$ debye was found. This gives an ionic character, μ/er, of 67 percent where e is the charge on the electron.

[1] H. K. Hughes, Phys. Rev. **72**, 614 (1947).
[2] J. W. Trischka, Phys. Rev. **74**, 718 (1948).
[3] Maxwell, Hendricks, and Moseley, Phys. Rev. **52**, 968 (1937).

L8. Microwave Spectrum of CF_3CCH. J. N. SHOOLERY AND R. G. SHULMAN,* *California Institute of Technology (Introduced by* H. Q. NORTH*).*—The $J=3\rightarrow4$ and $J=4\rightarrow5$ transitions of the symmetric top molecule, 1, 1, 1, trifluoropropyne, have been investigated using a Stark-modulation type microwave spectrometer with a recording meter. From accurate frequency measurements of several isotopic species most of the structural parameters have been determined. Considerable splitting of the transitions, attributed to low lying excited vibrational states, has been observed. For the $J=3\rightarrow4$ transition, of the most naturally abundant isotopic species, seven lines due to excited vibrational states have been found near the fundamental at 23,023.6 mc. The value of the dipole moment is being determined and will be presented.

* Present address: Hughes Aircraft Company, Culver City, California.

FRIDAY AFTERNOON AT 3:10

Horace Mann

(C. C. LAURITSEN presiding)

Brookhaven Programme

M1. The Brookhaven National Laboratory. L. J. HAWORTH, *Brookhaven.* (30 min.)
M2. The Brookhaven Reactor. L. B. BORST, *Brookhaven.* (30 min.)
M3. Research in Physics at Brookhaven. T. H. JOHNSON, *Brookhaven.* (30 min.)
M4. Recent Work on Nuclear Structure. MAURICE GOLDHABER, *Brookhaven.* (30 min.)

FRIDAY AFTERNOON AT 3:10

Havemeyer 309

(R. LADENBURG presiding)

Symposium of the Division of Fluid Dynamics

MA1. Magnetohydrodynamics. EDWARD TELLER, *Los Alamos Scientific Laboratory.* (30 min.)

MA2. Some Modern Problems in Classical Hydrodynamics. GARRETT BIRKHOFF, *Harvard University.* (30 min.)

MA3. Recent Trends in Gas-Dynamics Research. Z. I. SLAWSKY, *Naval Ordnance Laboratory.* (30 min.)

MA4. Modern Trends in Shock-Tube Research. G. N. PATTERSON, *University of Toronto.* (30 min.)

Business Meeting of the Division of Fluid Dynamics

FRIDAY AFTERNOON AT 3:10

Pupin 428

(J. H. VAN VLECK presiding)

Nuclear Theory; General Physics

N1. A Phenomenological Treatment of Photo-Meson Production from Deuterons. M. LAX, *Syracuse University;* H. FESHBACH, *M.I.T.;* G. F. CHEW, *University of Illinois;* AND H. W. LEWIS, *University of California, Berkeley.*—A calculation which depends neither on meson theory nor on the strength of meson-nucleon coupling is made of the production of single photo-mesons from deuterons relative to that from free nucleons. The approximations made include (1) neglect of neutron-neutron forces in the final state, (2) neglect of two particle effects such as exchange currents. Both of these are important near threshold where it may be expected that the neutron-neutron resonance will increase the cross section sharply. The meson spectrum at various angles for several photon energies has been obtained, as well as approximate values for the total cross section valid near threshold and for high energy photons. The cross sections obtained are smaller than that of a free nucleon partly because of the effects of binding and partly because of the exclusion principle. The former can be calculated while the second depends upon the probability of a spin change by the nucleon emitting the meson. The latter also determines the behavior of the total cross section near threshold, as well as the shape of the meson spectrum at the high energy end.

N2. Photo-Meson Production from Deuterons. M. L. GOLDBERGER, *University of Chicago,* F. VILLARS AND H. FESHBACH, *M.I.T.*—Starting from pseudoscalar meson theory with pseudoscalar coupling, an effective nonrelativistic meson-nucleon-photon Hamiltonian correct to first order in nucleon momenta is developed. This Hamiltonian is then applied to the production of mesons from deuterium, the meson spectrum at various angles being obtained for a given photon energy. The effect of the nuclear interaction in the final state is included for the S state but not for states of higher angular moment, while the effect of two-nucleon terms in the Hamiltonian is neglected. By examination of magnitude of the cross section for positive meson production near threshold and hear the high energy end of the meson spectrum, relative to that for photo-production in hydrogen, the neutron-neutron interaction may be studied. By comparing positive and negative production at other parts of the meson spectrum a test may be made of the applicability of the effective Hamiltonian to this process. The calculation of the positive to negative ratio is in progress.

N3. Classical Theory of Neutral Photo-Meson Production. KEITH A. BRUECKNER, *Institute for Advanced Study (Introduced by* J. R. OPPENHEIMER).—The observed approximate equality of the cross sections for production by photons of neutral and charged mesons is not easily understood on elementary theoretical grounds. In fact, perturbation theory in the weak coupling limit predicts a much smaller cross section for neutral mesons than for charged mesons for all theories. Only for pseudoscalar theory with pseudoscalar coupling can comparable neutral and charged cross section be obtained by considering contributions of higher order in the meson-nucleon coupling constant. Because of the probable inapplicability of a power series expansion for the pseudoscalar theory, however, these results can be believed only in an extremely qualitative way. The symmetrical theory for pseudoscalar mesons has been applied to this problem in a classical manner similar to that given by W. Pauli and used by K. M. Case and H. W. Lewis for a neutral theory. In this method, it is not necessary to assume that the meson-nucleon coupling is weak. However, the theory is somewhat unphysical in that nucleon recoil is neglected, and the meson field, spin, and isotopic spin are not quantized. The results obtained are in qualitative agreement with experiments on thejproduction of charged and neutral mesons if an unstable nucleon isobar with excitation of 300 to 400 Mev is assumed to exist. Implications of this result for other processes will be discussed.

N4. Neutral Meson Production by γ-Rays. MORTON F. KAPLON, *University of Rochester.*—The cross sections for neutral meson production by γ-rays on nucleons have been calculated to lowest order in the weak coupling approximation for scalar and pseudoscalar theories. For both cases the ratio of neutral to charged production is $\sim(\mu/M)^2$. The calculation was repeated including the Pauli term representing interaction of the nucleon's anomalous moment with the electromagnetic field. This addition makes a negligible contribution to the scalar but strongly increases the pseudoscalar cross section. (The anomalous moment in both cases contributes negligibly to the charged production.) At a photon energy of 250 Mev the total cross section for pseudoscalar π^0 production (excluding the anomalous moment interaction) is $0.39\times10^{-27}(f^2/hc)$ and is a factor of 10 greater if the anomalous moment is included. The excitation function for the latter case varies as the cube of the meson momentum near threshold; the angular

distribution in the laboratory system is roughly isotropic in the backward hemisphere and decreases strongly in the forward. Recent preliminary experiments st Berkeley indicate that the total cross section and excitation function are in fair agreement but give poor agreement with the angular distribution. This work was assisted by the AEC.

N5. Generalization of Forbidden Beta-Decay. GEORGE L. TRIGG,* *Washington University.*—The work of Konopinski and Uhlenbeck,[1] Marshak,[2] and Greuling[3] on forbidden beta-decay has been generalized to the case of an arbitrary mixture of all five invariants in the interaction Hamiltonian. Interference effects between the five terms appear in the general case. Some, but not all, of these disappear if the condition of symmetry between position and negaton emission, proposed by deGroot and Tolhoek,[4] is imposed. The effect of these terms on spectral shapes will be discussed.

* AEC Predoctoral Fellow.
[1] E. J. Konopinski and G. E. Uhlenbeck, Phys. Rev. 60, 308 (1941).
[2] R. E. Marshak, Phys. Rev. 61, 431 (1942).
[3] E. Greuling, Phys. Rev. 61, 568 (1942).
[4] S. R. deGroot and H. A. Tolhoek, Physica 16, 456 (1950).

N6. Some Experimental Indications of the Stresses Produced in a Body by an Exploding Charge. JOHN S. RINEHART, *U. S. Naval Ordnance Test Station.*—When an explosive charge is detonated on the surface of a body, a large amount of energy is introduced into the body in the form of a high intensity compressional stress wave of short duration. The energy in this wave distributes itself within the body and eventually becomes dissipated. The absorbed energy appears, at least in part, in the form of observable inelastic deformations. In some cases, qualitative inferences regarding the probable nature of the stress distribution that must have existed in the body after detonation of the charge can be drawn from the final condition of the material. The effects produced by small cylindrical charges that were detonated on the surfaces of heavy steel plates are discussed. Particular attention is paid to (a) shapes of crater, (b) changes in hardness, (c) flow patterns, (d) fractures, and (e) changes in microstructure. The distribution of stress appears in some respects to correspond to that which might be set up by a static load. The mechanisms of inelastic deformation, however, differ very greatly between the static case and the dynamic case. Dynamic loading produces numerous shock twins and fractures that undoubtedly occur because of the very high strain rates involved.

N7. Development of Ultra Compact, Ultra High Speed Digital Computers. DONALD H. JACOBS AND MICHAEL MAY, *The Jacobs Instrument Company.*—The hitherto untouched field of all-electronic, all-parallel digital computers is being explored systematically by The Jacobs Instrument Company. This paper covers research in this field accomplished between the spring of 1949 and the spring of 1950. The work culminated in the completion of the first computer of this type, called JAINCOMP-A. It is small ($11\times16\frac{1}{2}\times19\frac{1}{2}$ in.), light (40 lb), and simple (103 tubes). It is very reliable because of its simplicity and because no synchronizing or clocking pulses are required. This computer (a study model) has four binary digits plus a sign stage. It is fast, being able to take two numbers out of storage, add them together, and replace them in storage in 18 μsec. (Using newer techniques, it can be increased to 20 binary digits for the same size and weight, and have a much higher operating speed.) JAINCOMP-A can accept fixed inputs (punch cards) and variable inputs (from other machines or equipment). It can be used as a computer or can control other devices. Although this type of computer was originally intended for the special-purpose field, it has excellent potentialities for general purpose work. The computer adds, subtracts, multiplies, takes sines, cubes numbers, etc., and performs a computing program. Other computers embodying major advances in speed, compactness, and simplicity over the techniques used in JAINCOMP-A are under construction.

N8. Basic Theory of the 3-Color Cathode-Ray Tube. JENNY E. ROSENTHAL, *Monmouth Junior College.*—A series of phosphor strips fluorescing with the 3 primary colors, red, green, and blue, are deposited on the face plate of a cathode-ray tube. To cause selective excitation of only one color at a time we use a deflection arrangement similar to that in an electrostatic cathode-ray tube. However, in this case the beam enters the deflecting field at an angle through a slit in one of the plates. Depending on the voltage between the plates it will strike different positions of the plate opposite the one through which it enters. Calculations show that under optimum conditions sufficient resolution can be obtained in this manner to excite the phosphor strips individually. To insure sufficient resolution under standard conditions of operation one of the sets of strips is mounted on suitable supports inside the deflecting plate system. With this arrangement it is possible to obtain a picture in one of the three primary colors by a change of the deflecting voltage alone. Like all electrostatic tubes, this 3-color cathode-ray tube is particularly well adapted for low voltage operation.

N9. Electrostatic Amplification Factor of a Triode with Mixed Geometry. H. S. THOMAS.—An expression for the electrostatic amplification factor, μ, of a triode with cylindrical cathode and grid and plane parallel plates is obtained in terms of a μ calculated from one of the classical formulas for plane parallel geometry and the variation with polar angle of the cathode charge density induced by the plate-cathode field. The potential function for a line charge between two parallel conducting planes is used to compute the approximate variation of the normal component of plate-cathode field intensity, and hence of the surface charge density induced by this field, around the cathode. A simple analytical expression of good accuracy for a cathode diameter of one-half the plate separation or less is obtained by expansion of functions in series to the second order. This expression is used to calculate the μ of several typical tubes. The results are compared with the published data on these types, with which they are found to be in good agreement.

N10. Trajectories in an Axial Focusing Double Lens Spectrometer.* S. C. SNOWDON, *Bartol Research Foundation.*—The third-order zero angular momentum trajectories of an electron starting out in the central plane of a single focusing coil have been computed for a $1/1+x^3$ axial field shape. By suitably matching the above solutions with a set of similar solutions obtained by shifting the origin, it is possible to obtain the complete zero angular momentum trajectories corresponding to the double lens problem in which the axial field shape approximates rather closely one that is physically realizable. Typical trajectories will be discussed.

* Assisted by the joint program of the ONR and AEC.

N11. Mass Spectra of Deuteroacetylenes, Monodeuterobenzene, and Alpha-Monodeuteronapthalene. FRED L. MOHLER AND VERNON H. DIBELER, *National Bureau of Standards.*—Measurements of the mass spectra of C_2D_2 and C_2DH have been repeated with improved precision and spectra of C_6H_5D and alpha-$C_{10}H_7D$ are presented for the first time. In all these compounds it is possible to measure the isotopic purity accurately by measuring the molecule ions at a potential below the appearance potential of the dissociated ions. This gives the basis for computing the spectra of the pure isotopic compounds. There is a marked difference in the probability of removing H as compared with D in the different compounds. For C_2DH the *a priori* probabilities of removing

D and H are equal. However, C_2D^+ is 64 percent of the mass 25 peak of C_2H_2 and C_2H^+ is 33 percent of the C_2H_2 peak. By contrast the $C_6H_4D^+$ peak of C_6H_5D is almost exactly 5/6 of the $C_6H_5^+$ peak of C_6H_6 which is the *a priori* probability of removing H rather than D. Similarly in $C_{10}H_7D$ the $C_{10}H_6D^+$ peak is 7/8 of the $C_{10}H_7^+$ peak of $C_{10}H_8$. The complete spectra of C_6H_5D and $C_{10}H_7D$ can be computed satisfactorily from spectra of C_6H_6 and $C_{10}H_8$ on the assumption that probabilities of removing H and D are equal.

N12. Electrical Currents Produced in the Atmosphere by Thunderstorms. R. E. HOLZER, *University of California, Los Angeles* AND DAVID S. SAXON,* *National Bureau of Standards.*—Assuming that the electrical conductivity of the atmosphere increases exponentially with height, as indicated by balloon flight observations up to about 18 km,[1] calculations have been made of the electrical potential arising from charge distributions of the order of those observed in thunderclouds. From this potential the air-ground current density, the total current flowing upward to the ionosphere and the current generated in the thundercloud itself can be calculated. For a static charge distribution, the role of the conductivity is dominant in determining the potential except, of course, in the immediate neighborhood of the charges. On the other hand, for a time dependent charge distribution, with periods of the order of those actually observed, the conductivity is dominant only in the upper atmosphere. Indeed, below heights of perhaps 10 km, the effect of the conductivity is negligible and the potential satisfies Poisson's equation to a high degree of accuracy. A complete solution, valid everywhere, can be expressed in terms of hypergeometric functions. Preliminary estimates of the calculated current flows indicate at least order of magnitude agreement with those actually observed.

* Presumably on leave from University of California, Los Angeles.

[1] J. A. Fleming (editor) *Terrestrial Magnetism and Electricity* (McGraw-Hill Book Company, New York, 1939), p. 204 ff.

FRIDAY EVENING AT 7:00

Grand Ballroom, Hotel New Yorker

(I. I. RABI AND DUANE ROLLER presiding)

Banquet of the American Physical Society and the AAPT

After-dinner speech by **J. R. Oppenheimer**

SATURDAY MORNING AT 10:00

McMillin

(J. R. ZACHARIAS presiding)

Invited Papers in Nuclear Physics

P1. Neutron Resonances and Cross Sections. JAMES RAINWATER AND W. W. HAVENS, JR., *Columbia University.* (30 min.)

P2. Positron Annihilation. MARTIN DEUTSCH, *M.I.T.* (30 min.)

P3. Work on Nuclear Energy Levels at the California Institute of Technology. C. C. LAURITSEN, *California Institute of Technology.* (30 min.)

P4. Deep Nuclear Energy Levels in Medium-Light Nuclei. E. C. POLLARD, *Yale University.* (30 min.)

SATURDAY MORNING AT 10:00

Pupin 301

(C. H. TOWNES presiding)

Microwave Spectra

Q1. The Microwave Spectra of the Deutero-Ammonias.* M. T. WEISS AND M. W. P. STRANDBERG, *M.I.T.*—Measurements of the inversion-rotation spectra of the deutero-ammonias have been made in the 7000 Mc/sec to 80,000 Mc/sec region. Thirty-five lines of NH_2D and NHD_2 have been measured and identified by means of the Stark effect. As expected, our results show that for these molecules only simultaneous rotational and inversion transitions can be observed. Thus, corresponding to each $J_s \rightarrow J_s'$ transition two absorption lines can be observed separated by either twice the rota-

tional energy separation or twice the inversion splitting of the levels involved. From our observations, the inverstion splittings of the partially deuterated molecules can be calculated and are found to be in good agreement with the Dennison and Uhlenbeck[1] inversion doubling theory. Thus the inversion splittings for the ammonia molecules are approximately as follows: 24,000 Mc/sec for NH_3; 12,000 Mc/sec for NH_2D; 5000 Mc/sec for NHD_2; 2000 Mc/sec for ND_3. Our results are also in agreement with the structural parameters of ammonia as given by Herzberg.[2] The sign of the nuclear quadrupole coupling constant was also measured and found to be negative as expected. The centrifugal distortion for both rotation and inversion states has been experimentally determined.

* This work has been supported in part by the Signal Corps, the Air Materiel Command, and ONR.
[1] D. M. Dennison and G. E. Uhlenbeck, Phys. Rev. 41, 313 (1932).
[2] G. Herzberg, *Infrared and Raman Spectra* (D. Van Nostrand Company, New York, 1945), p. 439.

Q2. The Rotational Magnetic Moment of $^1\Sigma$-Polyatomic Molecules.* J. R. Eshbach and M. W. P. Strandberg, *M.I.T.*—An expression has been derived relating the rotational magnetic moment of a general $^1\Sigma$-molecule to the rotational angular momenta. Previously[1,2] expressions have been given for molecules with high degrees of symmetry. The present result, as well as the previous, depends on the assumption of a rigid nuclear framework with electrons moving in the nuclear potential. Our expression shows the dependence of the magnetic moment matrix on molecular constants and the angular momenta referred to the principle inertial axes. Thus, the magnetic moment matrix may be written for any molecule for which the angular momentum matrices and direction cosine matrices are known. Zeeman measurements on the microwave spectrum on $N^{15}H_3$ substantiate the theory in this particular case. It is shown that rotational moment measurements serve to evaluate the complicated second-order paramagnetic term[3] in the theory of susceptibility of such molecules, and thus the diamagnetic term, which is dependent only on the electronic ground state, becomes known from susceptibility measurements.[4]

* This work has been supported in part by the Signal Corps, the Air Materiel Command, and ONR.
[1] G. C. Wick, Phys. Rev. 73, 51 (1948); Z. Physik 85, 25 (1933).
[2] C. K. Jen, Technical Report No. 114 Cruft Laboratory, Harvard University, August 22, 1950.
[3] J. H. Van Vleck, *Electric and Magnetic Susceptibilities* (Oxford University Press, London, 1932), p. 275.
[4] For a similar evaluation in the case of diatomic molecules, see also N. F. Ramsey, Jr., Phys. Rev. 58, 226 (1940).

Q3. Centrifugal Distortion in Asymmetric Molecules, HDS.* R. E. Hillger† and M. W. P. Strandberg, *M.I.T.*—Using the vibration-rotation matrix elements derived by H. H. Nielsen[1] for the general polyatomic molecule, a method is presented for determining centrifugal distortion correction factors of asymmetric molecules in terms of the general centrifugal distortion matrix elements and the rigid-rotor term values. The necessity of diagonalizing the entire energy matrix for each term value is effectively eliminated. Corrections are obtained specifically for Q branch "a" or "c" type transitions; the extension to P or R branch transitions, while quite straightforward, is considerably more difficult. The distortion dependence is determined explicitly as a function of the usual angular momentum quantum numbers up to $J=5$ and is then extrapolated to higher J terms, resulting in a single functional relation. Twelve rotational absorption lines of HDS^{32} were found in the microwave region, and these were fitted to the centrifugal distortion equation by the method of least squares. The fit is good, and the five distortion coefficients obtained checked with values calculated from vibrational (infrared) data. Calculation of the inertia defect present in planar molecules allowed the effective moments of inertia of HDS to be determined.

* This work has been supported in part by the Signal Corps, the Air Materiel Command, and ONR.
† Now associated with Snow and Schule, Inc., Cambridge, Massachusetts.
[1] H. H. Nielsen, Phys. Rev. 60, 794 (1941).

Q4. Microwave Spectrum of Ketene.* H. R. Johnson, J. G. Ingersoll, and M. W. P. Strandberg, *M.I.T.*—The microwave absorption spectrum of the pentatomic molecule ketene has been investigated. R branch and Q branch transitions of $H_2{}^1C_2{}^{12}O^{16}$, $D^2H^1C_2{}^{12}O^{16}$ and $D_2{}^2C_2{}^{13}O^{16}$ in the ground vibrational state, R branch lines of $H_2{}^1C_2{}^{13}O^{16}$ in three excited vibrational states, and R branch lines of $D_2{}^2C_2{}^{13}O^{16}$ in two excited vibrational states have been measured. Major molecular constants corrected for centrifugal distortion which explain the ground-state lines are

	$(b+c)$ mc	$(b-c)$ mc	δ
$H^1D^2C_2{}^{12}O^{16}$	18,821.67 ±0.05	472.422 ±0.005	0.002633 ±0.00002
$H_2{}^2C_2{}^{13}O^{16}$	20,209.14 ±0.05	377.41 ±0.02	0.001386 ±0.00002
$D_2{}^2C_2{}^{13}O^{16}$	17,673.42 ±0.05	568.138 ±0.005	0.00426479 ±0.0000000

The lines in excited vibrational states will be discussed.

The structure of ketene can be determined from these measurements. The accuracy of locating the carbon atom near the center of gravity is, however, poor. Tentative results, neglecting zero-point vibration, are $r_0(C-H)=1.19A$, $r_0(C=C)+r_0(C=O)=2.62\pm0.01A$, $HCH=106°\pm2°$.

* This work has been supported in part by the Signal Corps, the Air Materiel Command, and ONR.

Q5. Microwave Absorption Spectrum of Oxygen.* B. V. Gokhale and M. W. P. Strandberg, *M.I.T.*—Work on the absorption spectrum of oxygen in the 5 mm wavelength region is continuing in this Laboratory.[1] Pressures in the range 0.5 mm to 5 mm of mercury are used to study the line breath parameters of the individual lines. This information, together with the absorption frequencies,[2] is useful to check the current theories of the absorption process and of pressure-broadening. Some effort is being made to study the effect of nitrogen contamination on line breadth as for example in air. Data are taken with a recording type slow-sweep spectroscope; the absorption is detected by means of a zero-based square-wave Zeeman modulation. This method yields a true picture of the line shapes directly when sufficiently large modulation is used. Special precautions have to be taken to obtain correct results since the line breadths are fairly large at the pressures used, and hence require a wide sweep. The line $K_-=11$ has, for example, a total breadth $(2\Delta\nu)$ of 20 Mc/sec at a pressure of 5.7 mm of mercury.[3]

* This work has been supported in part by the Signal Corps, the Air Materiel Command, and ONR.
[1] For previous work see Strandberg, Meng, and Ingersoll, Phys. Rev. 75, 1524 (1949).
[2] First Wicrowave measurements reported from Duke University, see Smith, Burkhalter, Anderson, and Gordy, Phys. Rev. 79, 651 (1950).
[3] This includes extraneous broadening due to inhomogeneity and residual field effects.

Q6. Microwave Spectrum of CHD_2Cl^{35} and the Structure of Methyl Chloride.* S. L. Miller,† J. Kraitchman, B. P. Dailey, and C. H. Townes, *Columbia University*.—Molecular parameters for methyl chloride computed on the basis of various symmetric isotopic replacements have varied greatly. The uncertainty has been largest in the hydrogen parameters. In an attempt to redetermine these parameters more accurately, the $J=1\rightarrow2$ transition for $K=0$ and $K=1$ has been observed in CHD_2Cl^{35}. The frequency of transition $1_0\rightarrow2_{-1}$ is 45,789 mc; of $1_{-1}\rightarrow2_{-1}$, 46,099.4 mc; of $1_{+1}\rightarrow2_0$, 46,407 mc. CHD_2Cl is a slightly asymmetric top. The two large principal moments of inertia I_B and I_C are almost equal. Line $1_1\rightarrow2_0$ is at frequency $3B+C$ and line $1_0\rightarrow2_{-1}$ at frequency $3C+B$. The separation between these lines $2(B-C)=617.90$ mc gives a very sensitive indication of the position of the hydrogen

atoms in the molecule. On the basis of the above data and previously observed isotopic shifts in the $J=0\rightarrow1$ transition, the following parameters have been determined:

Bond distance	C−Cl	1.781A
Bond distance	C−H	1.098A
Bond angle	H−C−H	110°23′.

* Work supported jointly by the Signal Corps and ONR.
† AEC Predoctoral Fellow.

Q7. Microwave Spectrum and Structure of ReO_3Cl.* E. AMBLE† AND A. L. SCHAWLOW, *Columbia University.*—Rhenium trioxy-chloride has been prepared and some lines in its microwave spectrum have been observed. It is found to be a symmetric rotor. The lines have a half-width of about 60 megacycles because of unresolved vibrational and hyperfine structure, and because of the presence of the two rhenium isotopes. For ReO_3Cl^{185}, $B=2.0933\pm0.0005$ kilomegacycles; for ReO_3Cl^{187}, $B=2.0242\pm0.0005$ kilomegacycles. If tetrahedral bond angles are assumed, i.e. $<$O Re O$=<$O Re Cl, then the Re−Cl distance is 2.23A, and the Re−O distance is 1.69A. These rhenium bond distances are closed to those formed, in similar compounds, by the neighboring elements Os and W. The transitions observed were $J=2\rightarrow3$, $4\rightarrow5$, and $5\rightarrow6$. Higher frequency transitions are being studied in order to measure the separation caused by the rhenium and so to completely determine the structure of the molecule. Work has begun on $ReOF_4$, which should have a simpler hyperfine structure characteristic of the rhenium nuclei.

* Work supported by the Signal Corps and AEC.
† On leave from Oslo University.

SATURDAY MORNING AT 10:00

Schermerhorn 501

(H. A. BOORSE presiding)

Cryogenics

R1. Eddy Currents Become Supercurrents in Superconductors. P. B. ALERS, J. W. MCWHIRTER, AND C. F. SQUIRE, *The Rice Institute.*—A solid sphere of pure metallic tin has been mounted for rotation at speeds from zero to ten revolutions per second. The sphere was placed in a uniform magnetic field of about 10^{-5} Webers/meter^2 and it was placed in a bath of liquid helium at 4.2°K. At this temperature the tin has a high conductivity of about 4×10^{10} mho/meter so that a rotation of 2.5 revolutions/sec produces eddy currents which remove the external magnetic flux passing through the solid tin. Speeds greater than 2.5 revolutions/sec produce almost no greater eddy current and smaller speeds produce smaller eddy currents. The sphere was allowed to rotate at 2.5 revolutions/sec and then cooled to 3.0°K which is below its superconducting transition temperature. The eddy currents then became supercurrents or what has been called "Meissner Currents." We assert this because the magnetic field distribution around the sphere remained unchanged during the cooling below the transition and remained unchanged when we stopped the rotation. We have produced a complete "Meissner Effect" in a large cylinder of pure tantalum by rotating and then slowly cooling below the transition temperature. We have compared the classical theory of magnetic field distribution due to eddy currents with the London Theory of magnetic field distribution due to supercurrents.

R2. Magnetic Properties of a Superconducting Hollow Lead Sphere. JULIUS BABISKIN, *Naval Research Laboratory.*—Measurements have been made to determine the equatorial magnetic field distribution inside and outside a hollow superconducting lead sphere (99.996 percent pure). Bismuth probes were used to measure the magnetic field strengths. These experiments, all performed at 4.2°K, have shown that the sphere is a perfect magnetic shield for applied fields $H_A<\frac{1}{3}H_c$ (where H_c=critical field). In the intermediate state ($\frac{1}{3}H_c<H_A<H_c$), for constant H_A, the internal field increased with time, while the external field decreased with time. On decreasing H_A from $>H_c$ to zero, the internal field decreased with time, while the external field increased with time. At $H_A=0$, a large internal and a smaller reversed external "frozen-in" field was observed. It was found that reapplying fields <100 gauss did not change the internal "frozen-in" field. The "frozen-in" fields can be destroyed by reversing H_A to $-\frac{1}{3}H_c$ and then reducing H_A to zero. Thus, the original conditions of the experiment are restored. Complete internal and external hysteresis loops were observed and will be discussed in detail.

R3. Resistance Minima in Metals.* H. E. RORSCHACH, JR., AND MELVIN A. HERLIN, *M.I.T.*—Work by Serin, Dunnington, and Garfunkel[1] on the low temperature resistance of magnesium indicated a minimum above 4.2°K. A mutual inductance method of measuring resistivity has been employed to extend these measurements. A sample of magnesium has been found to have a definite resistance minimum at approximately 15° with a definite rise in resistance down to 1°K. A bulk sample of gold investigated by this method also showed a definite rise in resistivity below 4.2°K. Some measurements on beryllium showed no minimum.

* This work has been supported in part by the Signal Corps, the Air Materiel Command, and ONR.
[1] Garfunkel, Dunnington, and Serin, Phys. Rev. **79**, 1 (1950).

R4. Electrical and Thermal Conductivities of Pure Aluminum at Very Low Temperatures. R. T. WEBBER, F. A. ANDREWS, AND D. A. SPOHR, *Naval Research Laboratory.*—Measurements have been made of the electrical and thermal conductivities of three specimens of highly pure aluminum (99.995+ percent) at temperatures from 2 to 21°K. The thermal conductivities satisfied the relation of the free electron theory,[1] $w=1/K=1/(AT)+BT^2$, where w=thermal resistance, K=thermal conductivity. The constants A and B, the residual electrical resistivities, ρ_0, and the Lorenz ratios at 4.2°K, $L_{4.2}$, for the three specimens were:

	Al I	Al II	Al III
A [watt cm^{-1} °K^{-2}]	7.04	6.06	4.05
B [cm watt^{-1} °K^{-1}] $\times10^3$	2.70	2.72	2.72
ρ_0 [ohm-cm] $\times10^9$	3.04	3.79	5.51
$L_{4.2}$ [volt^2 cm^2 °K^{-2}] $\times10^8$	2.14	2.30	2.23

The measured values of the constant B yield[1] an effective number of 0.041 electron per atom. The electrical resistances failed to obey the Matthiessen Rule and the temperature-dependent part of the electrical resistance increased much less rapidly than T^5. As predicted by theory,[1] the Lorenz ratios at liquid hydrogen temperatures were appreciably lower than the values at 4.2°K shown in the table above.

[1] R. E. B. Makinson, Proc. Camb. Phil. Soc. **34**, 474 (1938).

R5. Magnetic Dipole Interactions in Crystals Near Absolute Zero.* M. PRINCE AND MELVIN A. HERLIN, *M.I.T.*—

Various authors[1] have made calculations on the magnetic dipole energy in crystals at low temperatures and have been able to predict magnetization curves. All of these calculations include approximations or are valid only under special conditions. Thus the predicted magnetization curves have different shapes according to the different theories. In order to evaluate these theories, we have carried out an extensive set of measurements of magnetization curves. These will be presented and conclusions as to the values of the theories will be discussed.

* This work has been supported in part by the Signal Corps, the Air Materiel Command, and ONR.

[1] J. H. Van Vleck, J. Chem. Phys. **5**, 320 (1937); **6**, 81 (1938); J. A. Sauer and A. N. V. Temperley, Proc. Roy. Soc. **176**, 203 (1940); J. M. Luttinger and L. Tisza, Phys. Rev. **70**, 954 (1946).

R6. Thermoelectromotive Force of Superconducting *Versus* Normal Junctions of the Same Metal. M. C. STEELE, *Naval Research Laboratory.*—Measurements of the thermoelectromotive force of superconducting *versus* normal junctions of the same metal have now been made on lead, tin, indium, thallium, and mercury. The previously proposed relation[1]

$$E = E_0[1-(T/T_s)^3]$$

has been found to fit the data for each of the above-mentioned elements. E is the thermoelectromotive force, T is the temperature of the junction ($T \leq T_s$) and T_s is the normal transition temperature. Current data are summarized below.

Element	T_s°K	(E_0, volts) $\times 10^9$
Lead	7.26	59.0
Mercury	4.16	250.0
Tin	3.72	5.5
Indium	3.41	10.4
Thallium	2.40	5.5

[1] M. C. Steele, Phys. Rev. **78**, 308 (1950).

R7. Barium Titanate at Low Temperatures. ROLAND W. SCHMITT, *Rice Institute.*—We have investigated the dielectric properties of barium titanate ceramic down to liquid helium temperatures by examining the hysteresis loops of the substance. The ferroelectric property persists down to these temperatures but the loops become much smaller in size in a manner which suggests a "freezing-in" of the domains as has been noted by Hulm.[1] The relatively high temperature dependence of the total permittivity of the substance in the liquid helium region suggests that there is the possibility of a measureable electrocaloric effect at these temperatures. Assuming that the processes which occur are reversible and taking a crudely extrapolated value of the specific heat, we find that a simple thermodynamic argument indicates a temperature drop of the order of 0.1°K should occur at 4°K upon adiabatic application of a field of 20,000 volts/cm. We have attempted to observe temperature changes of this sort using a carbon resistance thermometer and no effects even near this order of magnitude have been observed. It seems that irreversible processes may have to be taken into account.

[1] J. K. Hulm, Proc. Phys. Soc. **A63**, 1184 (1950).

R8. Pressure Variation of Second Sound Velocity in Helium II.* R. D. MAURER AND MELVIN A. HERLIN, *M.I.T.*—The velocity of second sound as a function of pressure and temperature has been measured to 0.95°K at pressures to 25 atmos by means of a pulse method. The minimum in velocity goes to lower temperature with increase of pressure. The quantitative dependence of the rise in velocity upon pressure indicates that this rise is a phonon effect.

* This work has been supported in part by the Signal Corps, the Air Materiel Command, and ONR.

SATURDAY MORNING AT 9:45

Horace Mann

(W. SHOCKLEY presiding)

Semiconductors; Photo-Conductivity; Lattice Defects

S1. Efficiency of Alpha-Bombardment Conductivity in Germanium. KENNETH G. MCKAY, *Bell Telephone Laboratories.*—Rectifying barriers in germanium have been use to detect alpha-particles.[1,2] A relevant factor is the efficiency of production by bombardment of electron-hole pairs in the germanium proper. The measurement must exclude current multiplication in the barrier as in point contact barriers. Polonium alphas bombarded the edge of an $n-p$ barrier in a single-crystal germanium rod.[3] Essentially all the energy was dissipated in the barrier itself. Suitable precautions ensured that all the charge of electrons and holes produced in the germanium was measured. A charge of 9.5×10^8 electrons was measured per incident alpha, corresponding to an average energy loss of 5.6 ± 0.3 electron volts per electron-hole pair. Theory[4] and photoelectric measurements[5] demonstrate no current multiplication inherent in a plane $n-p$ junction. Therefore, the measured efficiency is characteristic of the germanium lattice.

[1] J. G. McKay, Phys. Rev. **76**, 1537 (1949).
[2] Orman, Fan, Goldsmith, and Lark-Horowitz, Phys. Rev. **78**, 646 (1950).
[3] G. K. Teal and J. B. Little, Phys. Rev. **78**, 647 (1950).
[4] W. Shockley, Bell System Tech. J. **28**, 435 (1949).
[5] F. S. Goucher (to be published).

S2. Intrinsic Conduction in Germanium. W. C. DUNLAP, JR. *General Electric Research Laboratory.*—An experimental study has been made of the transition of the conduction properties of germanium from the impurity range to the intrinsic range. Among the properties studied were the variation of Hall coefficient and resistivity with magnetic field and the change of these characteristics with temperature, the variation of mobility figure ($10^8R/\rho$) with temperature, for a number of single crystals, both N- and P-type. For high resistivity P-type material a large variation of Hall coefficient with magnetic field has been found. This leads to a reversal of Hall coefficient with increasing magnetic field at temperatures close to the transition point. Above the transition point, the Hall effect increases in magnitude with increasing magnetic field. This effect has been explained qualitatively in terms of the change of mobility of holes relative to that of electrons in a magnetic field. For P-type samples, the variation of mobility figure with temperature was accounted for accurately by the free electron theory of mixed conduction by electrons and holes, assuming a mobility ratio $\mu_e/\mu_h = 1.50$. The magneto-resistance of the P-type samples was greater than that of N-type samples in the impurity range; the magneto-resistance of all samples was the same in the intrinsic region.

S3. Measurement of Semiconductor Impurity Content. C. N. KLAHR, *Westinghouse.*—It is possible to determine the total impurity concentration in a semiconductor (donor centers plus acceptor centers) by electrical measurements alone. Thus

one may distinguish samples of semiconductor with the same resistivity but different mobilities as having different impurity content. This is based on a general theoretical treatment of the effect of the nonadditivity of lattice scattering, ionized impurity scattering, and non-ionized impurity scattering on the resistivity and Hall coefficients of semiconductors with both electron and hole carriers. Formulas for various electrical properties of semiconductors are derived which are generalizations of the usual ones. On the basis of these results it is possible to devise several practical experimental methods to measure total impurity concentration by measuring the resistivity and Hall coefficient of semiconductor samples at high and low temperatures. It is expected that such measurements may facilitate experimental work and the technology of semiconductors.

S4. Mobility of Electrons in High Electric Fields. E. J. RYDER, *Bell Telephone Laboratories*, (*Introduced by* W. SHOCKLEY).—The mobility of electrons in *n*-type germanium has been measured as a function of electric field for gradients as high as 2×10^4 volts/cm. Precautions were taken to minimize both heating and hole modulation. Pulse measurements were made with single-crystal samples of germanium cut into the form of tiny, smooth filaments with relatively massive terminations. The voltage pulses used were of short duration ($\sim10^{-7}$ sec) and low repetition rate. It has been determined that Ohm's law is obeyed at room temperature only up to a field of about 6×10^3 volts/cm, beyond which there is a gradual departure approaching constant current density. At a temperature of -180°C a similar departure takes place at a field of about 2×10^2 volts/cm. The ohmic range is one of constant mobility, whereas the constant current region is one of inversely varying mobility and constant drift velocity of the order of 10^7 cm/sec.

S5. Mobility of Electrons in High Electric Fields: Theory. W. SHOCKLEY, *Bell Telephone Laboratories*.—An electron of mass m and speed v_1 moving in a crystal at temperature T loses energy to the acoustical modes at a rate

$$P_A=(4mc^2v_1/l)[(v_1^2/2v_T^2)-1],$$

provided $v>c$, c being the speed of longitudinal acoustical waves, l the mean free path, and $v_T^2=2kT/m$. The term in $v_1^2/2v_T^2$ agrees with Seitz.[1] Electrons in germanium with energies a few times kT should lose energy chiefly to acoustical modes. A crude mobility theory for high fields is made by equating power loss to power gain $P_E=e\mu E^2$, where E is the field and μ the effective mobility. Assuming $\exp(-mv^2/2kT_e)$ electron distribution, then $P_A=8mc^2v_e(T_e-T)/Tl(\pi)^{\frac{1}{2}}$ and $\mu=v_T\mu_T/v_e$, where $v_e^2=2kT_e/m$ and $\mu_T=4le/mv_T3(\pi)^{\frac{1}{2}}$; for fields higher than $2c/\mu_T$ these give a drift velocity $\mu E=(32/3\pi)^{\frac{1}{2}}(c\mu_TE)^{\frac{1}{2}}$. Assuming a delta-function distribution gives a 20 percent smaller velocity.

[1] Equation (11) F. Seitz, Phys. Rev. **76**, 1376 (1949).

S6. Contact Barrier Breakdown Studies in Germanium.* RALPH BRAY, *Purdue University*.—High resistance barriers are found in germanium at (a) contacts to metals, (b) grain boundaries in high resistivity *N*-type material, and (c) internal $P-N$ boundaries. At high dc voltage, barrier breakdown in the high resistance direction is characterized by a peak voltage followed by a negative dynamic resistance region. Benzer[1] and Taylor,[2] by resorting to millisecond voltage pulses, in cases (a) and (b), respectively, showed the negative resistance to be due to heating. In the present experiments, 2 to 10 microsecond pulses were utilized to reduce heating effects further and also reduce carrier injection from the electrodes. The high voltage characteristic becomes more precisely measureable. The voltage peak is eliminated: for cases (a) and (b) the high barrier resistance decreases greatly—at what may be called the breakdown voltage—to a low dynamic resistance which closely corresponds to the bulk sample resistance. For case (c), a single sample was tested and found to have, even at 1000 volts, a dynamic resistance much greater than the bulk resistance and only slightly lower than the peak resistance value at low voltage.

* Work supported by the Signal Corps.
[1] S. Benzer, J. Appl. Phys. **20**, 804 (1949).
[2] W. E. Taylor and H. Y. Fan, Phys. Rev. **78**, 335 (1950).

S7. Light Emission from SiC. C. ACCARDO, E. JAMGOCHIAN, AND K. LEHOVEC, *Signal Corps Engineering Laboratories*.—Light emitted from silicon carbide $N-P$ type boundaries when current passes in the forward direction was investigated using a photo-multiplier. The emission spectrum extends from 4500–6500 angstroms at room temperature and is found to be nearly independent of current from 0.1 milliampere to 50 milliamperes. The light intensity increases approximately proportionally to current (efficiency about 3×10^{-6} quanta per electron at room temperature). The light is considered as arising from recombination of the injected carriers.

S8. Accelerated Recovery of Selenium Rectifiers after Voltage Pulses by Illumination. K. LEHOVEC, *Signal Corps Engineering Laboratories*.—A voltage pulse when applied to a selenium rectifier in the blocking direction leaves the rectifier in a perturbed state. The perturbance is measured by the deviation of the capacity from the equilibrium value.[1] The rate of recovery can be accelerated by illumination through a transparent electrode. The acceleration of the recovery depends in the same manner on the light intensity and the wavelength as does the photo-current in selenium photo-voltaic cells. The observations are explained as follows: The voltage pulse in the blocking direction pulls out electrons from elevated energy states in the selenium or the selenium surface. The accelerated recovery is due to subsequent filling of these states by photo-electrons. It can be derived from the experiments on the basis of this concept that the number of electrons pulled out from the elevated energy states by the voltage pulses used must be less than 10^{11} per cm^2.

[1] K. Lehovec, Phys. Rev. **78**, 348 (1950).

S9. Photo-Conductivity in Sintered Zinc Oxide.* P. H. MILLER, D. M. WARSCHAUER, AND T. T. REBOUL, *University of Pennsylvania*.—Experiments on the spectral response of the photo-conductivity of sintered zinc oxide at different temperatures when shuttered light was used gave a response linear in voltage and light intensity. The photo-currents were small in comparison with the dark currents. Assuming a value of the mobility of 100 cm^2/volt-sec for single crystals to apply to a sintered specimen and a cross section of 10^{-14} cm^2 for the capture process (similar to *F*-centers), then at the peak of the response 10^4 electrons are freed per incident quantum and the electron remains free about 10^{-7} sec. If Hahn's[1] grain boundary model is used, the above values should be multiplied by $(W/L)^2$ and $(W/L)^{-1}$, respectively, where W is the thickness of the boundary layer and L the edge of the better-conducting cube. High frequency resistance measurements indicate that W/L cannot be less than 10^{-2} and the corrected decay time 10^{-6} sec. An analysis of the shape of the shuttered response indicates a free time of 10^{-2} to 10^{-3} sec. Thus, the grain boundary model gives a somewhat better but a still incomplete picture. The spectral intensity distribution of the visible phosphorescence excited by x-rays has features in common with the photo-condutcivity response, however, the decay times are considerably shorter than 10^{-2} sec.

* This work supported in part by the U. S. Navy.
[1] Hahn, Russell, and Miller, Phys. Rev. **75**, 1631 (1949).

S10. Optical Absorption and Photo-Conductivity in Amorphous and Hexagonal Selenium.* M. ALTEN GILLEO, *M.I.T.*—In amorphous selenium films at room temperature the op-

tical absorption coefficient α is about 2×10^{2} cm^{-1} at 6900A and rises steadily to a maximum of about 5×10^{4} cm^{-1} at 2600A. Photo-conductivity sets in at about 5600A where α has attained $\sim10^{3}$ cm^{-1}. With decreasing temperature the absorption edge and the threshold of photo-conductivity shift toward shorter wavelengths. The temperature dependence of α for wavelengths *ca* 6800A can be related to the thermal excitation of vibrational levels in the chain molecules composing the film. When the amorphous selenium is transformed into the hexagonal ("metallic") modification, α increases in the 5000 to 7200A region. In a film of 0.5-micron thickness photo-conductivity is now observed at wavelengths as long as 7500A and reaches a maximum for an optical density of about one at 6500A. With decreasing temperature the region of maximum response and the absorption edge move together toward shorter wavelengths. This behavior can be explained by a bimolecular law of recombination of charge carriers, if their non-uniform concentration is taken into account.

* Sponsored by the ONR, the Army Signal Corps, and the Air Force.

S11. Transient Photoelectric Currents Produced by Intermittent Illumination of Cadmium Sulfide. J. C. M. Brentano and E. M. Nakaji, *Northwestern University*.—Pulsating illumination of a cadmium sulfide block to which an electric field is applied produces a periodic variation of the photoelectric current.[1] Using 60-cycle pulsating illumination in the visible range we observe during the first few seconds of illumination a gradual decrease of the photo-current variation to a steady value about 1/10 of the initial value, the time rate of decrease depending on intensity and wavelength band. We further observe that on removing the external field and connecting the electrodes over a high resistance pulsating illumination produces a photo-current variation in opposite direction to that observed with the field. This decays with a time constant of a few seconds depending on the intensity of illumination. Only illumination with wavelength 5100A or shorter effectively produces this relaxation current. These two transient phenomena can be interpreted on the ground of a model which foresees a positive hole space charge and filling of the holes via the conduction level.

[1] See R. Frerichs, Phys. Rev. 72, 594 (1947); and J. Appl. Phys. 21, 312 (1950), also for further references.

S12. The Influence of Dislocations on the Easing of Optical Selection Rules. Frederick Seitz, *University of Illinois*.—Under ideal conditions in a perfect solid, the total wave number vector of electrons and light quanta is conserved when electrons are excited by light, provided the reduced wave number scheme is employed. One may expect this rule to be violated when the crystal contains imperfections. Excluding lattice vibrations, the two most interesting types of imperfection are those, such as impurity atoms, which produce a distortion only over a region of the order of atomic dimensions, and dislocations, which produce distortion over a comparatively large region. The influence of both kinds of imperfection on the selection rules for optical transitions are considered. Fourier integrals involving the strain field of dislocations that were evaluated by J. S. Koehler are employed in this analysis. It is concluded that a Taylor dislocation and a line of impurity atoms of the same length have comparable influence on the breakdown of selection rules for cases in which W, the change in total wave number vector during the transition, lies near the boundary of the first Brillouin zone. On the other hand, the dislocation permits many more transitions in which W lies near the center of the zone. The ratio of the transition probability for a line of misfit atoms and for the dislocation, which is equivalent to an extra plane of atoms, is of the order of $(Wa)^4$, where a is the lattice constant. This fact is discussed in relation to the silver halides.

S13. Lattice Defects in Silver Bromide. Chester R. Berry, *Eastman Kodak Company*.—Measurements have been made of the lattice parameter of silver bromide at room temperature and in the range from about 350 to 420 degrees C. The results are compared with the values obtained on the basis of two contrary assumptions: first, that the lattice expansion is identical with the external expansion measured by Strelkow;[1] and, second, that some of the external increase in volume is caused by formation of vacancies, the resultant parameter being that estimated by Lawson.[2] Within experimental error, the measured curve agrees with the first assumption, which is equivalent to the assumption that no Schottky defects have formed. Since it is known from ionic conductivity measurements that there are about 2 percent of defects at temperatures near 420 degrees C, it is concluded that these are Frenkel defects. However, the magnitude of the errors involved in the measurements is such that the existence of a small number (about 10 percent of the total) of Schottky defects cannot be entirely precluded.

[1] P. G. Strelkow, Physik. Sowjetunion 12, 73 (1937).
[2] A. W. Lawson, Phys. Rev. 78, 185 (1950).

S14. Electric Field Surrounding a Dislocation. Rolf W. Landauer, *Lewis Laboratory, NACA*.—An edge-type dislocation is surrounded by a strain distribution which gives a compressed lattice on one side of the slip plane and an expanded lattice on the other side. The width of the filled portion of the conduction band therefore varies in the vicinity of the dislocation. To maintain the electrons in equilibrium, the Fermi level must everywhere be at the same energy, while the bottom of the conduction band must vary. This gives an effective potential in which the electrons move. The potential is just that of a line dipole located along the dislocation axis. The scattering due to this potential has been used to calculate an increase in the resistance of isotropically cold worked copper of $\Delta\rho/\rho=3\times10^{-18}N$ for N dislocations per cm^2. This is about 200 times larger than the scattering produced by the potential, which takes into account only the displacement of screened ions from their normal positions.

S15. Dissociation Energies of Cd^{++} Vacancy Complex and Double-Vacancy in NaCl.* John R. Reitz and J. L. Gammel, *Los Alamos Scientific Laboratory*.—Dissociation energies for two types of lattice imperfection (namely, the impurity-ion vacancy complex and the double-vacancy) have been determined theoretically for NaCl, using the semiclassical model of ionic crystals developed by Born and Mayer. The procedure followed in calculating these energies was based on the method developed by Mott and Littleton[1] for computing the formation energies of single vacancies. The numerical result obtained for the complex, 0.44 ev, is in fair agreement with the value of about 0.3 ev found experimentally by Etzel and Maurer.[2] The dissociation energy of the double-vacancy was calculated to be 0.89 ev.

* Work done under the auspices of the AEC.
[1] N. F. Mott and M. J. Littleton, Trans. Faraday Soc. 34, 485 (1938).
[2] H. W. Etzel and R. J. Maurer, J. Chem. Phys. 18, 1003 (1950).

SATURDAY MORNING AT 9:45

Pupin 428

(GERTRUDE SCHARFF-GOLDHABER presiding)

Beta- and Alpha-Emitters

T1. Source Decharging in Low Energy Beta-Spectroscopy. LEONARD GROSS,* *Princeton University.*—Source charging of thin organic backing films is a serious source of spectrum distortion in low energy beta-spectroscopy. In this paper the relative merit of several methods of source decharging will be discussed. A few results are stated here. A metallic layer of a heavy stable metal (like gold) provides a suitable conducting backing for investigating spectra in the region above about 90 kv. For lower energies, active metallic backings like beryllium are satisfactory, provided the film is not exposed to the atmosphere for more than a few hours; most often this is inconvenient. Filament decharging (heating a tungsten wire placed behind the backing film so that the film draws current from the filament as it charges) has many advantages. Since the emission characteristics of the filament (without flashing or aging, which are undesirable in the presence of the thin film) are not sufficiently stable, the most feasible procedure is to run the filament at several tens of microamperes emission current for about five seconds immediately preceding each determination of a point on the spectrum. This method is applicable to positron emitters as well as electron emitters.

* Now at Research and Development Laboratories, Hughes Aircraft Company, Culver City, California.

T2. The Nuclide P^{33}. L. YAFFE AND F. BROWN, *National Research Council, Canada.*—The nuclide P^{33} has been prepared by the reaction $P^{32}(n, \gamma)P^{33}$. The P^{33} was extensively purified and finally precipitated as ferric phosphate, yielding 150 *mC* P^{33}. Inactive phosphorus P^{31} was treated in an identical manner using the same reagents and techniques. The samples were irradiated separately in the rapid action rabbit of the NRX heavy water pile, and then counted using the proportional counter technique described by Yaffe and Stevens.[1] The irradiated P^{33} sample showed an activity not present in the irradiated P^{31} sample. Successive irradiations showed that the absolute amounts of this activity formed decreased as expected from the half-life of P^{33}. Competing reactions are ruled out. A half-life of 22 ± 5 seconds is proposed for P^{33}.

[1] L. Yaffe and W. H. Stevens, Can. J. Research (to be published).

T3. Sixty-Day Isomer of Columbium 91.* J. OVADIA AND P. AXEL, *University of Illinois.*—A sample of zirconium enriched in the isotope of mass 90 was obtained from Carbide and Carbon Chemicals Division, Oak Ridge National Laboratory, and bombarded with 10-Mev deuterons in the cyclotron of the Washington University of St. Louis. Investigation of the columbium activity with a double thin lens beta-ray spectrometer showed the K and L peaks of a 104.5 ± 0.1-Kev gamma-ray, with $N_K/N_L=2.1\pm0.1$. No other soft radiation was seen. Therefore this is the "150"-Kev gamma-ray reported earlier.[1] The gamma-ray was observed in a NaI crystal and a comparison of the intensities of the x-ray and gamma-ray lead to a conversion coefficient of the order of 50. Critical absorption of the x-ray using an argon-filled proportional counter showed an intense columbium x-ray, together with a much weaker zirconium x-ray. The zirconium x-ray results from the decay of the columbium 91 ground state to zirconium by K-capture with a long half-life. These data clearly establish that the 60-day half-life is due to an isomeric transition and not to K-capture.

* Supported in part by the joint program of the ONR and the AEC.
[1] G. T. Seaborg and I. Perlman, Revs. Modern Phys. 20, 585 (1948).

T4. The Beta-Spectrum of Tc^{99}. C. S. WU AND L. FELDMAN, *Columbia University.*—Tc^{99}, a product of uranium fission, has an unusually long half-life of 10^5-10^6 years. Its comparative half-life, $fT\sim10^{12}$ sec, leads to an empirical classification of second forbidden. Tc^{99} (1.7 μc/mg) was recently procured from the Isotope Division of the AEC, and its β-spectrum was investigated with the solenoidal spectrometer. Several sources were prepared with varying thicknesses from about 0.1 to 0.4 mg/cm² on thin film backings of $\sim$0.020 mg/cm². Although a detergent or insulin was used in all cases, the uniformity of the sources is not as good as desired. Repeated chemical purification and electroplating were both used to ensure purity. The uncorrected Kurie plot is markedly different from a linear allowed shape but is continuously curved concave towards the energy axis. When the Kurie plot is corrected by the unique correction factor for a $\Delta I=3$(no) transition, $D_2=1/30(p^4+10/3p^2q^2+q^4)$, it yields a curve with considerable curvature. Therefore, the D_2 factor can be excluded. However, $\alpha=1/12(p^2+q^2)$, the unique correction factor for a $\Delta I=2$(yes) transition, does give a straight line from the upper energy end down to about 120 kev. The extrapolated end point thus obtained is $W_0=293\pm5$ kev. The correction factor α occurs also in the second forbidden transitions C_{2T} and C_{2V} for $\Delta I=2$(no). A theoretical interpretation with the predictions of the nuclear shell structure model will be presented. This work is supported in part by the AEC.

T5. Gamma-Rays in the Decay of Rh^{106} and Pr^{111}. D. E. ALBURGER, E. DER MATEOSIAN, M. GOLDHABER, AND S. KATCOFF,* *Brookhaven National Laboratory.*—Among long lived fission products, 1 *y* Ru^{106} and 275 *d* Ce^{144} have been found to produce photo-neutrons in Be and D. The photoneutrons are produced by gamma-rays emitted with intensities of the order of 2 percent per β-ray in the decay of the daughters, 30-sec Rh^{106} and 17-m Pr^{144}. In Rh^{106} a 2.9-Mev gamma-ray was found with a scintillation spectrometer. The whole gamma-ray spectrum has been investigated in detail with a lens spectrometer and found to consist of lines with energies of 0.511, 0.621, 0.87, 1.045, 1.55, and 2.9 Mev. The first two are strong and of nearly equal intensity and agree with internal conversion lines found by R. D. Hill. No crossover gamma-ray of 511+621 kev is observed. It is probable that more than one pair of cascade gamma-rays is present, and this may play a role in the analysis of the angular correlation known to exist in Rh^{106}. The gamma-ray spectrum of Pr^{144} has at least three components, 2.185 ± 0.015, 0.700 Mev, and a line of less than 150 kev. The first of these was measured by a direct comparison with the 2.2-Mev line from radium. The weak photo-neutron yield from Ce^{144}+D is probably caused by a higher energy gamma-ray of low intensity.

* Under contract with the AEC.

T6. Memory in Angular Correlation of the γ-Rays Emitted from Excited States of Cd^{111}. D. M. ROBERTS AND R. M. STEFFEN,* *Purdue University.*—Cd^{111} has a metastable state of 247-kev excitation energy which decays with a half-life of 0.08 microsecond to the ground state of spin $\frac{1}{2}$. This transition is preceded by a γ-ray of 173-kev quantum energy. We measured the angular correlation between the 173-kev and the 247-kev γ-rays emitted in the decay of In^{111} to Cd^{111} using a coincidence amplifier with a resolving time of 0.12 microsecond. The measured points follow within experimental error the angular

correlation function $f(\theta)=1-R/Q\cos^2\theta$ with $R/Q=-0.06\pm0.02$. Measurements repeated with the same resolving time but with a 0.13 microsecond delay showed the same result, indicating that the spin orientation of the intermediate 0.08 microsecond state does not change appreciably before the emission of the 247-kev γ-ray. The measured correlation function is characteristic for a dipole and a quadrupole transition between levels of angular momenta 5/2, 3/2, and 1/2. The conversion of the 173-kev and the 247-kev γ-rays indicates a magnetic dipole and an electric quadrupole transition, respectively.

* Supported in part by the AEC.

T7. Isomerism of In^{110}. E. Bleuler, J. W. Blue, and A. C. Johnson,* *Purdue University.*—The $(\alpha, 3n)$ reactions with $Ag^{109,107}$ lead to activities of 66-min and ~5-hr half-life.[1] The former is assigned to In^{110}, the latter to In^{108}. On the other hand, the reaction Cd^{108} $(d, 2n)$ In^{108} results in an activity[2] of ~55 min. The discrepancy has been removed by showing that the longer period belongs to an isomer of In^{110}. The ground state (66 min) decays by positron emission (2.25 Mev) to an excited state of Cd^{110} at 654 kev. The decay of the conversion line emitted from this level was followed in a double coil lens-type spectrometer and found to follow periods of 66 min and 4.9 hr. The latter must be assigned to an isomer. It decays chiefly by electron capture to a highly excited state of Cd^{110}. In addition to the 654-kev γ-ray, conversion lines due to transitions of 937 and 887 in Cd^{110}, known to be in cascade from the decay of Ag^{110}, are found. The isomeric transition to the ground state (119 kev) is very weak and seems to belong to the $l=4$ class. A tentative decay scheme will be given.

* Supported by the ONR and AEC.
[1] S. N. Ghoshal, Phys. Rev. 73, 417 (1948).
[2] E. C. Mallary and N. L. Pool, Phys. Rev. 76, 1454 (1949).

T8. Beta-Gamma Angular Correlation in the Decay of Sb^{124}, I^{131}, and I^{126}. Donald T. Stevenson,* *M.I.T.*—Ridgeway,[1] and Beyster and Wiedenbeck[2] have measured an integral beta-gamma correlation in Sb^{124}. We have measured the energy dependence of this correlation using a lens spectrometer.[3] The correlation near the end point is -0.41 and decreases slightly in absolute value until electrons from the 1.69-Mev spectrum[4] begin to contribute to the coincidence rate. At 1.0 Mev the correlation is -0.15. Possible interpretations will be discussed. We found no gamma-rays in coincidence with the 2.20-Mev positron spectrum in I^{131} in contradiction with the decay scheme of Mitchell, *et al.*[5] Preliminary results indicate that coincidences involving the 1.50-Mev positrons are isotropic. A correlation of about $+0.13$ was found for 460-kev beta-rays in the decay of I^{126}.

* This work was supported in part by the joint program of the ONR and the AEC.
[1] S. L. Ridgeway, Phys. Rev. 78, 821 (1950).
[2] J. R. Beyster and M. L. Wiedenbeck, Phys. Rev. 79, 169 (1950).
[3] The Sb^{124} was obtained from Oak Ridge.
[4] Langer, Moffat, and Price, Phys. Rev. 79, 808 (1950).
[5] Mitchell, Mei, Maienschein, and Peacock, Phys. Rev. 76, 1450 (1949).

T9. Beta-Gamma Angular Correlations in Sb^{122}. I. Shaknov, *Columbia University.*—An investigation of the total and differential angular correlation coefficients in Sb^{122} has been performed in this laboratory. Both beta- and gamma-detectors were anthracene crystal counters with 5819 photo-multipliers. The pulses were amplified with a wide band amplifier, then shaped by shorted delay lines and fed to a fast coincidence circuit. Using a T-junction, the pulses from the beta-counter were branched to a differential pulse height analyzer. The output of this analyzer was used to gate the fast coincidence output, thus accepting only coincidences in which the beta-particle energy fell in the proper energy interval. The sources were placed under vacuum in a Lucite chamber. The apparatus was checked for performance by measuring total correlation coefficients in the following substances: gamma-gamma correlations in Co^{60} and Rh^{104}, beta-gamma correlations in Au^{198}, Na^{22}, Sb^{124}. In all cases results agreed with previous work of other investigators. A thin source of Sb^{122} was prepared by vacuum evaporation onto a thin Formvar film. The total correlation coefficient, assuming $W(\theta)=1+R/Q\cos^2\theta$, was found to be $R/Q=+0.067\pm0.01$, while the coefficient, accepting beta-particles of a narrow energy interval in the high-energy region was $R/Q=+0.157\pm0.02$. This work was supported in part by the AEC.

T10. The Twice-Forbidden Transition of Cs^{137} and the Law of Beta-Decay.* L. M. Langer and R. J. D. Moffat, *Indiana University.*—The shape of the beta-spectrum of the direct 1.17-Mev low intensity transition between the $g_{7/2}$ ground state of Cs^{137} and the $d_{3/2}$ ground level of Ba^{137} has been determined in detail. The measurements were made in the 40-cm radius of curvature magnetic spectrometer with strong (>4.mC) high specific activity sources. Special precautions were taken to preclude any possible instrumental distortions of the momentum distribution. The conventional Fermi plot of the data is convex towards the energy axis. Attempts have been made to fit the data with a forbidden factor appropriate to a transition involving a change of 2 units of angular momentum and *no* parity change. Whereas the axial vector and tensor forms of the theory predict the same spectrum shape for the recently observed once forbidden, $\Delta I=2$, and twice forbidden, $\Delta I=3$, transitions, they yield different forbidden factors for the twice forbidden, $\Delta I=2$, transition of Cs^{137}. It appears that the axial vector and also the combination scalar-axial vector-pseudoscalar forms of interaction are not capable of explaining the data for any possible values of the adjustable parameters. On the other hand, the tensor form of the theory can be made to give good agreement with the experimental spectrum.

* Assisted by a grant from the Frederick Gardner Cott el Fund of the Research Corporation and by the joint program of ONR and AEC.

T11. The Disintegration of Au^{198}. L. G. Elliott and J. L. Wolfson, *Chalk River Laboratory.*—The radiations from Au^{198} have been studied in a magnetic spectrometer at energies above 0.30 Mev with a line width at half maximum of 0.5 percent in electron momentum. The main beta-spectrum ends at 0.957 ± 0.003 Mev. A component with an intensity 10^{-4} of the main spectrum and a maximum energy of 1.37 ± 0.05 Mev corresponds to a beta-transition direct to the ground state of Hg^{198}. There are two γ-rays at energies of 0.6757 ± 0.0015 Mev and 1.0870 ± 0.0020 Mev, having quantum intensities relative to the strong 0.4112 Mev γ-ray of $(4.8\pm1.0)\times10^{-3}$ and $(1.3\pm0.2)\times10^{-3}$, respectively. The measured values of the γ-ray internal conversion coefficients are consistent with the theoretical values of electric quadrupole for the 0.4112- and 1.087-Mev γ-rays and magnetic dipole for the 0.6757-Mev γ-ray. Since also Hg^{198} is an even-even nucleus, it follows that the spins of the ground-state, 0.4112-Mev and 1.087-Mev levels are 0, 2, 2, respectively.

T12. Investigation of the Shape of Beta-Spectra at the Low-Energy End.* R. R. Edwards, P. E. Damon, and H. M. Schwartz, *University of Arkansas.*—Reliable investigation of the low kev region of beta-spectra has only recently become possible, through the use of gaseous sources in proportional counters. Aside from Coulomb effects, the problem of the disposition of the excess atomic binding energy released in negative beta-decay is of interest, particularly at high Z and low maximum beta-energy. According to Hebb,[1] this energy should be carried away by the beta-particle, in which case one would expect the beta-spectrum to have a cut-off at the low energy end, corresponding to this excess energy. The perturbation method employed by Feinberg,[2] however, implies a sharing of the energy between beta-particle and neutrino. Our investigation of the beta-spectrum of Pb^{210} (RaD) as gaseous tetramethyl lead by proportional counter spectrometry indi-

cates a definite deficiency (compared to a normal Fermi distribution) of particles below 15 kev, and a most probable energy greater than half the previously reported maximum of the spectrum (25–29 kev). Investigation of this and other suitable nuclides is continuing.

* Supported in part by the U. S. AEC.
[1] M. H. Hebb, Physica 5, 701 (1938).
[2] E. L. Feinberg, J. Phys. (U.S.S.R.) 4, 424 (1941).

T13. Investigation of the Complex β-Spectrum by the Coincidence Spectrometer. P. A. MACKLIN, L. I. LIDOFSKY, AND C. S. WU, *Columbia University.*—A coincidence technique in conjunction with Columbia's solenoidal spectrometer has been developed to resolve and investigate the β-spectrum of the low energy group from a complex spectrum. An anthracene crystal counter is used as the gamma-ray detector and a G-M counter as the β-detector. The resolution of the spectrometer is set at 10 percent. The Au^{198} β-spectrum (a simple spectrum followed by gamma-emission) was investigated with and without coincidences to check the performance of the system. Complete investigation of the complex spectrum of Rb^{86} and Sb^{122} were completed. All sources were prepared by the vacuum evaporation method. Several different runs on Rb^{86} all gave an α-type spectrum for the high energy group (1760±10 kev) and a spectrum indistinguishable from the allowed shape for the low energy group (670±5 kev). The spectrum of the low energy group could also be fitted by C_{1F} or C_{1V}. This is in good agreement with the results of Muther and Ridgeway.[1] The uncorrected Kurie plot of the low energy group of Sb^{122} also gives a straight line as in the case of Rb^{86}. The extrapolated upper energy limit of this group is 1460±10 kev. The theoretical interpretation and its implication with the β-γ-angular correlation results will be discussed. We are most indebted to Chalk River Laboratory, National Research Council of Canada, for the high specific activity Rb^{86} and to the Isotope Division of the AEC for the Sb^{122} and Au^{198} used in this investigation.

[1] H. R. Muether and S. L. Ridgeway, Phys. Rev. 80, 750 (1950).

T14. The Emission of Pb X-Rays from Po^{210} Sources.* WILLIAM RUBINSON AND WILLIAM BERNSTEIN, *Brookhaven National Laboratory.*—Using a proportional counter pulse analyzer,[1] we have investigated the low energy photons from Po^{210} sources. These were first observed by Curie and Joliot,[2] who interpreted them as Po L and M x-radiations. By comparison of the $L\alpha$ line from the Po^{210} source with the corresponding lines excited by α-particle bombardment of Tl, Pb, and Bi, and by critical absorption measurements on the $L\beta$ line, we have established that the L lines, at least, are characteristic x-ray lines of Pb. The yield, per nuclear decay, is (preliminary measurement): $L\alpha$, $\sim 5.2\times10^{-4}$; $L\beta$, $\sim 2\times10^{-4}$, with an error of perhaps 25 percent. This means, assuming a Pb L fluoresecence yield of $\sim$0.5, that when a Po^{210} nucleus decays, the chance that its electronic cortege emits an L electron is $\sim$0.1 percent. We will also report on the M lines from Po sources, and on the x-radiations arising from the β-decay of P^{32} and S^{35}, and compare these results with the theoretical predictions of Migdal[3] and of Levinger.[4]

* Research carried out under the auspices of the AEC.
[1] Bernstein, Brewer, and Rubinson, Nucleonics 6, 39 (1950).
[2] I. Curie and F. Joliot, J. phys. radium, VII 2, 20 (1931).
[3] A. Migdal, J. Phys. (U.S.S.R.) 4, 449 (1941).
[4] J. L. Levinger, Thesis, Cornell University (June, 1948).

T15. The Half-Life of Ac C′. R. F. LEININGER, E. SEGRÈ, AND F. N. SPIESS,* *University of California, Berkeley.*—Bombardment of lead with 20- to 40-Mev alpha-particles gives rise to several short lived alpha-activities. Of these Ac C (Bi 211) and Ac C′ (Po 211) have been positively identified. A third one is due to an isomer of polonium, most probably 211 or perhaps 210. Ac C′, contrary to the old assumption based on Geiger-Nuttall law, has a half-life of 0.52 second; this has been found by producing Ac C′ with an (α, n) reaction on Pb 208 and confirmed by separating it from its mother substance At 211. The astatine had been prepared by a Bi $(\alpha, 2n)$ reaction and the separation was effected by volatilizing the astatine from a platinum strip. The residue, isotopic with polonium, decayed with a half-life of 0.52 seconds. We saw also the corresponding increase in alpha-activity of At 211, deprived of Ac C′, which occurs while the latter substance regrows to reach radioactive equilibrium with At 211.

* AEC Predoctoral Fellow.

SATURDAY AFTERNOON AT 2:15

Horace Mann

(J. B. JOHNSON presiding)

Invited Papers

U1. Some Phenomena of the Upper Atmosphere. S. CHAPMAN, *Oxford University.* (30 min.)
U2. Report on the Gaseous Electronics Conference of October, 1950. W. P. ALLIS, *M.I.T.* (50 min.)
U3. Supraconductivity and Lattice Vibrations. J. BARDEEN, *Bell Telephone Laboratories.* (30 min.)

SATURDAY AFTERNOON AT 2:00

McMillin

(E. T. BOOTH presiding)

Mesons and Electrons

V1. Experimental Search for the Beta-Decay of the π^+ Meson. HELEN L. FRIEDMAN AND JAMES RAINWATER, *Columbia University.*—Four hundred and six hundred micron Ilford G-5 (beta-sensitive) plates were exposed to fairly monochromatic π^+ mesons inside the chamber of the Columbia University 164-in. cyclotron in a special collimator using magnetic

focusing. Scanning was done at the surface of the plates so only tracks entering the surface in about the expected direction were considered. Such tracks were followed far enough to determine if they were mesons ending in the emulsion. In this way a meson was always recognized well before the $\pi-\mu$-junction was reached. About 40 percent of these entering tracks were mesons of which about 50 percent (for the 600 μ-plates) ended in the emulsion. For any position along the plate about 90 percent of the mesons were within 1 Mev of the mean energy for that position which varied from 11 to 14 Mev. A few meson tracks >9 Mev, which showed no $\pi-\mu$-junction, ended in electrons. However, these all had ranges considerably outside the 90 percent region for the meson ranges. At time of writing the result is zero $\pi-\rho$ events our of 666 $\pi-\mu$-events falling in the 90 percent region. Later results will be presented. This work was supported in part by the ONR and AEC.

V2. Absorption of π^+ Mesons by Deuterons. W. B. CHESTON, *University of Rochester*.—Calculations on absorption of π^- mesons from the K-shell of the meson-deuteron system[1] have led to important information about the properties of the π-meson. For π^+ mesons of several Mev, the same selection rules hold as for π^- absorption. For higher energies, the reaction $\pi^++d\rightarrow p+p$ dominates and a measurement of the absolute cross section and the angular distribution of the emitted protons should throw light on the spin and parity of the π-meson. For 25-Mev π^+ mesons, we find:

Meson-nucleon coupling	S(S)	PS(PV)	V(V)	PV(PV)
$\sigma/g^2/\hbar c\times10^{-27}$ cm^2	1.15	9.45	1.66	9.22
$\sigma(90)$: $\sigma(180)$	0.10	0.85	1.38	1.21

By detailed balancing, the spin 0 total cross sections must be three times as large as the spin one cross sections. Since the cross section[2] for $p+p\rightarrow\pi^++d$ at 340 Mev is several times 10^{-28} cm^2, the π^+ absorption cross section should be about 10^{-26} cm^2 at 25 Mev for π^+ and should provide a unique determination of the spin. This work was assisted by the AEC.

[1] S. Tamor, Phys. Rev. (to be published).
[2] K. Brueckner, private communication.

V3. The Lifetime of the π^- Meson.* L. M. LEDERMAN, G. BERNARDINI, E. T. BOOTH, AND J. H. TINLOT†, *Columbia University*.—The decay process of the 90 Mev π^- mesons produced in the Nevis cyclotron was studied with a cloud chamber.[1] The lifetime of the π^- meson is determined directly from the corrected number of $\pi\rightarrow\mu$-decays observed and the total track length of π^- mesons. A cloud chamber run with a ½-in. lead plate showed that the beam included fast electrons as well as π^- and μ^- mesons. The proportion of electrons was deduced from the fraction of particles in the correct momentum interval stopping in the lead plate after correcting for probable number of meson interactions.[2] The proportion of μ^- mesons was estimated by studying a series of Ilford G-5 nuclear plates exposed behind various thicknesses of carbon during the cloud chamber run. The plates were scanned for ρ and σ-mesons. The data were corrected to give the fraction of μ^- mesons in the proper momentum interval. The preliminary result obtained with 45 events gives for the mean life of the π^- meson at rest the value $2.8\pm0.6\times10^{-8}$ sec.

* Assisted by the joint program of the ONR and AEC.
† Now at the University of Rochester.
[1] Lederman, Tinlot, and Booth, Phys. Rev. (to be published).
[2] Bernardini, Booth, Lederman, and Tinlot, Phys. Rev. (to be published).

V4. The Interaction of π-Mesons with Nuclei.* M. CAMAC, D. CORSON, R. LITTAUER, A. SHAPIRO, A. SILVERMAN, R. WILSON, AND W. WOODWARD, *Cornell University*.—π-mesons created in a target exposed to 300-Mev synchrotron radiation are focused into a monoenergetic beam with a double-focusing magnetic analyzer. The mesons are observed with a counter telescope—cloud chamber combination placed near the focal point. The cloud chamber contains several absorber plates, the total thickness being sufficient to stop the π-mesons but not sufficient to stop μ-mesons of the same momentum. The beam is found to include only a few percent of μ-mesons. The π-mesons are observed to undergo large angle scatterings and to be captured while in flight in aluminum and in copper absorbers. In 1140 traversals of 35–60 Mev π^- and π^+ mesons through ½-inch aluminum plates, 20 such large angle scatterings or absorptions have been observed, giving an interaction cross section consistent with the nuclear geometrical cross section. A preliminary measurement of the production ratio of π^- to π^+ mesons in the energy range 60 to 75 Mev in carbon gives 1.1 ± 0.2.

* This work was performed under contract with the ONR.

V5. Energy Spectrum of Positrons from the Decay of the μ^+ Meson. H. J. BRAMSON AND W. W. HAVENS, JR., *Columbia University*.—The multiple scattering of positrons obtained from meson decay is being measured, using electron sensitive emulsions exposed in the Nevis cyclotron. In previously reported work, the photographic plate has shown increasing promise of minimizing the twofold obstacles inherent in any analysis of the differential energy spectrum: (a) the difficulty in resolution of the energy of the positron, and (b) the few suitable tracts available for desirable statistical weight. The situation since the work of Davies *et al.** has been so improved as to promise a substantial refinement of their results. Artificial meson generators together with the development of an essentially distortionless emulsion 600 micron thick has provided a source of positrons suitable for study. Further, the rapid development of the technique of multiple scattering measurements** has permitted rapid evaluation of energy without sacrificing accuracy. Recent results† casting doubt on the validity of the Williams' theory in this connection necessitated a reevaluation of energy calibration. Results of these measurements will be reported. This work is supported by the ONR and AEC.

* Davies *et al.*, Phil. Mag. 40, 1250 (1949).
** Fowler, Phil. Mag. 41, 169 (1950); Goldschmidt-Clermont, Bull. Centre Phys. Nuc. No. 14 (1950).
† Corson, Phys Rev. 80, 303 (1950).

V6. Neutron Production by Negative Mesons Stopped in Lead. A. M. CONFORTO* AND R. D. SARD, *Washington University*.†—In an investigation of neutron emission resulting from μ-meson capture in various nuclei, data have been obtained for Pb, using a magnetized iron lens to single out neutrons due to negative mesons slowed down by ionization loss alone. At sea-level, under thin roof: counters A, magnetized iron (239 g cm^{-2}), paraffin (6.3 cm), counters B, Pb absorber (87 g cm^{-2}), counters C, neutron detector (paraffin-BF_3). Confirming a previous indication,[1] the $(AB-C:N)$ Pb difference is considerably higher when focusing negatives, $4.04\pm0.29/h$ as against $0.68\pm0.13/h$. The apparent mean neutron multiplicity is 1.4 ± 0.2. As the $(AB-C)$ Pb difference exceeds somewhat the actual meson stopping rate, this figure is in satisfactory agreement with the 1.9 ± 0.2 found underground with apparatus designed for an absolute multiplicity measurement.[2] The absence of dense material overhead, together with the high probability of nuclear energy loss in the *Fe* (which would spoil the focusing), rules out π^- mesons. The data without Pb absorber give a definite indication of neutron production by μ^- capture in the iron supporting members between B and C.

* Now at the University of Rome.
† Assisted by the joint program of the ONR and AEC.
[1] G. Groetzinger and G. W. McClure, Phys. Rev. 74, 341 (1948); G. W. McClure and G. Groetzinger, Phys. Rev. 75, 340 (1949).
[2] M. F. Crouch (private communication).

V7. Nuclear Disintegrations Produced by μ-Mesons. G. COCCONI AND V. COCCONI TONGIORGI, *Cornell University*.—An apparatus consisting of 12 BF_3 counters surrounding a

block of lead 4×18×18 in. was sunk into a lake at depths from 1 to 60 m. The nuclear disintegrations occurring in the lead were detected as showers of two or more neutrons. In the first 5 m of water the radiation producing the nuclear disintegrations is absorbed with a mfp of ~150 g/cm², hence it consists mostly of the tail of the nucleonic component. Beyond 10 m, it is absorbed as the penetrating component, hence μ-mesons must be the primaries of the disintegrations observed there. The absolute intensity of the disintegrations indicates for the μ-mesons a cross section of $\sim 1\times10^{-29}$ cm²/nucleon, practically independent of depth. These events are believed to be mostly induced by the virtual photons accompanying the charged mesons. Analogous processes produced by real photons are 10 times less probable. μ-meson capture and (γ, n) reactions induced by mesons can contribute significantly only to the events with a single recorded neutron. The frequency of single recorded neutrons indicates an average multiplicity of 2 neutrons from each μ-meson captured in lead. Our results are in agreement with those obtained by George and Evans, with photographic plates underground.

V8. The Emission of Slow Positive and Negative Mesons from Nuclear Disruptions Produced by Cosmic Radiation. HERMAN YAGODA, *National Institutes of Health.*—Microscopic examination of 600 micron plates and nuclear emulsion castings[1] of 1200- and 1800-micron thickness exposed in the stratosphere have revealed 101 examples of slow mesons created and terminating in the sensitive layers. As evidenced by $\pi-\mu$-decay 15 of the ejected particles are π^+, and 86 are identified as π^- by the formation of secondary stars at the track terminus. The parent star size permits a rough classification of the events initiated in (Ag+Br) nuclei and those of the gelatin component (H+C+N+O). For the slow π^- mesons the available statistics indicate a heavy to light nuclei ratio of 3.5±0.9, suggesting a production process of the same magnitude as the ration of the geometric cross sections of the respective nuclei. In plates coated 600 microns the observational intensity of the slow meson connected double stars is 9 per cc per day. Owing to the smaller probability of escape from the thick castings the observational intensity is increased to 19 per cc per day. The energy spectrum of the ejected mesons resides between 0.5 to 22 Mev. Data on range distribution and the multiplicity of the secondary stars will be described.

[1] H. Yagoda, Phys. Rev. **79**, 207 (1950).

V9. Analysis of Meson Production in Nucleon-Nucleon Collisions. K. M. WATSON AND K. A. BRUECKNER, *University of California, Berkeley.*—A phenomenological theory of meson production in nucleon-nucleon collisions has been developed and is applied to an interpretation of experimental results obtained at Berkeley.* Since, for present experimental beam energies, most of the initial nucleon kinetic energy goes into the rest-energy of the meson, leaving relatively slow particles in the final state (in the center-of-mass system), the production process is accompanied by large momentum transfers which suggests close distances of approach for the two colliding nucleons. Interpreting this as representing a short range interaction, it seems natural to make a partial-wave analysis of the particles in the final state. This leads directly to relationships between the excitation function, meson spectrum, and angular distribution. Combined with angular momentum and parity conservation the analysis seems capable of leading to a simple interpretation of the experimental results.* Applied to the experimental energy spectra and angular dependence, the center-of-mass angular dependence is deduced to be of the form of a $\cos^2\theta$ distribution for π^+ mesons produced by proton-proton collisions. Implications as to charge symmetry are also considered.

* We are indebted to C. Richman, H. A. Wilcox, W. Cartwright, W. Whitehead, M. Skinner, V. Z. Peterson, H. F. York, and their collaborators for discussions of their experiments and permission to quote their results in advance of publication.

V10. Mean Life of a Positron in Stilbene.* D. C. MOORE, *Rensselaer Polytechnic Institute.*—The theory of Dirac[1] predicts a mean life of 10^{-9} sec for the positron in stilbene. Using a diode-type coincidence circuit and coaxial delay lines, some measurements have been made of the time delay between the stopping of the positrons and the absorption of the annihilation gamma-rays. Tentative data indicate that this mean life is $1.0\pm0.5\times10^{-9}$ sec. These tentative results contrast with the work of Shearer and Deutsch.[2] They find, in general, an experimental cross section which is higher than that predicted by theory. Further measurements are being made. These further measurements, the experimental apparatus, and the method of analysis of the data will be discussed.

* Supported by Rensselaer Polytechnic Institute Research Fund.
[1] P. A. M. Dirac, Proc. Camb Phil. Soc. **26**, 361 (1930).
[2] J. W. Shearer and Martin Deutsch, Phys. Rev. **76**, 462 (1949).

V11. Annihilation of Swift Positrons.* J. W. SHEARER AND M. DEUTSCH, *M.I.T.*—Scintillation counters have been used to study the annihilation of swift positrons in matter. Positrons emitted from a strong Co-56 source are focused by a magnetic lens spectrometer on an anthracene crystal. A differential discriminator selects only the small pulses from this crystal and puts them into coincidence with pulses from a sodium iodide scintillation counter which is used as a γ-ray detector. This second counter can be rotated about the anthracene crystal, and its efficiency as a function of γ-ray energy is known by a previous calibration. The expected coincidence rates as functions of the angle of rotation, the γ-ray energies, and the incident positron energy were calculated by combining the expected small angle scattering with the Bethe-Heitler[1] theory of annihilation. The measurements were taken at average positron energies of 510, 765, and 1020 kev, and the results behaved qualitatively as expected, but were only 60 percent of the predicted coincidence rates. It is not possible to state whether the discrepancy is real or is due to experimental error. Triple coincidences measured using an additional γ-ray counter confirmed that the annihilation process was predominantly two-quantum.

* This work has been supported in part by the joint program of the ONR and AEC.
[1] H. A. Bethe and W. Heitler, Proc. Roy. Soc. **146**, 83 (1934).

V12. A Preliminary Measurement of the Decay of Positrons in Plexiglas.* WALTER E. MILLETT, *University of Florida.*—Positrons from sodium-22 were allowed to be annihilated in gold, lead, and Plexiglas. In the decay of sodium-22 the emission of a positron is followed by the emission of a 1.3-Mev gamma-ray. Preliminary measurements of coincidences between the 1.3-Mev gamma-ray and one of the annihilation gamma-rays have been made with a high resolution coincidence circuit by the method of delayed coincidences. A plot of the logarithm of the coincidence counting rate *versus* time delay gave similar curves when lead and gold were used as absorbers. But this plot of the data obtained when Plexiglas was used as an absorber was broader. The slopes of the "tails" of the curves for both gold and lead were about 9×10^{-10} sec and that for Plexiglas was about 14×10^{-10} sec. It should be emphasized that this work is still in the preliminary stages and further work will be carried out. The pulses used were those obtained using a stilbene crystal and an RCA 5819 photo-multiplier tube. The coincidence circuit used seems to be similar in principle to one discussed by Z.

Bay in the Physical Review **79**, 233 (1950). However, the author is not familiar with the details of Bay's circuit.

* This work was carried out at the California Institute of Technology as an AEC Postdoctoral Fellow. Additional support after the expiration of the Fellowship was provided by the ONR.

V13. The Velocity of Gamma-Rays in Air. M. R. CLELAND AND P. S. JASTRAM, *Washington University*.—The velocity of gamma-rays in air has been measured directly by means of scintillation counters and a delayed-coincidence system. The gamma-rays used were the 0.5-Mev quanta, emitted simultaneously in opposite directions, that result from positron annihilation. The source of positrons was Cu^{64}, which at the start of the experiment had a strength of about 1 curie. The source was placed between two scintillation counters, one of which was left fixed, while the other was varied in position. For five different positions of the second counter, the corresponding delay due to the time of flight of the gamma-ray was determined. The distance between source and counter ranged from 2.5 to 32 5 meters, and was measured to 1 millimeter. Calibration of the coaxial cables used for introducing known delay was accomplished by determining the resonant frequencies of the cables under short-circuit termination, between 2 megacycles and 200 megacycles. The measured value of the gamma-ray velocity, estimated to be accurate to better than one-half percent, is 2.983×10^{10} cm sec^{-1}.

V14. Radiation Loss of Electrons.* L. M. SPETNER AND J. S. CLARK, *M.I.T.*—An experiment is being performed to measure the radiation loss of electrons and positrons on passing through matter. The synchrotron gamma-ray beam impinges upon the glass wall of a magnet cloud chamber producing positron-electron pairs. The energy of each particle is then measured both before and after it traverses a plate in the chamber. Preliminary results have been obtained with about 0.2 radiation lengths of stainless steel and the results do not disagree with the Bethe-Heitler bremsstrahlung theory. An experiment is under way using a carbon plate and it is hoped that the results of this experiment will demonstrate the effect of bremsstrahlung in the field of the atomic electrons. Because of the sharpness of the tracks appearing in the post-expansion photographs, the error in the energy measurement, which depends upon the energy, is a maximum of about two percent. Typical cloud-chamber photographs will be shown.

* Assisted by the joint program of the ONR and AEC.

SATURDAY AFTERNOON AT 2:15

Pupin 428

(A. H. NIELSEN presiding)

Optical Physics, Including X-Rays

W1. High Intensity Spectroscopic Flame Sources.* G. A. HORNBECK AND R. C. HERMAN, *The Johns Hopkins University*.—A high intensity source has been developed which provides a means for studying at high dispersion the polyatomic spectra emitted by flames of hydrocarbons, CO and NH_3. Spectra of these gases burning with O_2 or O_3 with diluents such as N_2, CO_2, and A have been examined from ~2300 – ~9000A. If the fuel/oxygen ratio, ρ, is about stoichiometric, one obtains flames in which diatomic spectra are most prominent. If $\rho\ll1$ or if the concentration of diluents is high, cooler flames result in which diatomic spectra are highly suppressed. To obtain high intensity under these conditions, premixed gases are burned in an open quartz tube heated in a furnace at ~1000°C to stabilize the flame at the high flow rates employed. High dispersion spectrograms have been obtained of the hydrocarbon and CO flame bands and α-bands of the NH_2 flame virtually free from diatomic spectra with relatively short exposures. Exposure times of ~30 sec are required with a medium quartz Bausch and Lomb spectrograph and ~10 min with a 2-meter Baird grating spectrograph (4A/mm) using 25μ slits and II-O plates.

* Supported by the U. S. Navy, Bureau of Ordnance.

W2. Vibration-Rotation Bands of CO in Flame Spectra.* SHIRLEIGH SILVERMAN, *The Johns Hopkins University*, AND W. S. BENEDICT, *National Bureau of Standards*.—The emission of carbon monoxide-oxygen flames has been studied with a 7200-line vacuum grating spectrometer. Between 2.3μ and 2.6μ the vibration-rotation bands of CO appear as a well-developed spectrum, with only slight interferences from other bands (CO_2?) at the long-wavelength end. The 2–0, 3–1, 4–2, and 5–3 bands all appear, and extend to J values above 50. Heads are formed in the R branches at J~50, and are a prominent feature of the spectrum. The positions of the lines of higher v' and J show slight deviations from those calculated according to the constants of Herzberg and Rao.[1] From the observed relative intensities and theoretical transition probabilities, rotational and vibrational "temperatures" may be calculated. These are both about 2000°K±10 percent. This is much lower than the calculated flame temperature (~3000°K) or the observed "temperature" of 2900°K derived from the rotational distribution of levels in the OH radical at 3064A.

* Supported by U. S. Navy, ONR and Bureau of Ordnance.
[1] G. Herzberg and K. N. Rao, J. Chem. Phys. **17**, 1099 (1949).

W3. Vibration-Rotation Lines of OH in Flame Spectra.* W. S. BENEDICT, EARLE K. PLYLER, AND CURTIS J. HUMPHREYS, *National Bureau of Standards*.—The emission from oxy-acetylene and oxy-hydrogen flames has been recorded in the spectral region 1.1μ–2.5μ with a 15,000-line grating spectrometer and PbS detector. Under favorable conditions, slits as narrow as 0.025 mm could be used, affording good resolution of the complex structure, which is principally due to vibration-rotation bands of H_2O. In the region of 16μ, which in the oxy-acetylene flame is relatively free from H_2O emission, numerous vibration-rotation lines of OH have been identified. These include all lines from $P(5)$ to $P(19)$ in the 2–0 band, from $P(4)$ to $P(15)$ in the 3–1 band, and from $P(4)$ to $P(10)$ in the 4–2 band. The spin doublets, and at high K the Λ-doublets are resolved. From the observed relative intensities and theoretical transition probabilities, it is possible to calculate effective rotational and vibrational "temperatures." Preliminary results yield 2600°±200°K by both methods, for the oxy-acetylene flame, at a position in the outer cone where measurements using the ultraviolet band at 3064A normally yield "temperatures" around 3000°K.

* Supported in part by ONR.

W4. The Hyperfine Spectra of Diatomic Molecules. R. A. FROSCH AND H. M. FOLEY, *Columbia University*.—A general theory of the magnetic hfs for diatomic molecules including

relativistic effects has been obtained. Expressions for the energy levels have been worked out for the various cases of angular momentum coupling. In "Hund's case *a*" the diagonal part of the hfs operator has the form $a(\mathbf{I}\cdot\mathbf{J})/J(J+1)$ in zero field. Formulas for the energy levels in "Hund's case *b*" are given for Σ-states and for non-Σ-states. The effect of the relativistic hfs interaction is most apparent in Σ-states, where it gives a nonvanishing hfs for $K=0$, analogous to the hfs in atomic *s* states. The coefficients in the hfs splittings are given explicitly in terms of integrals over the electronic wave functions.

W5. The Infrared Spectrum of Active Nitrogen. LEWIS M. BRANSCOMB, *Harvard University*.—Re-association of two nitrogen atoms in the presence of a third body is generally taken to be the primary source of excitation energy in the Lewis-Rayleigh glow of active nitrogen. A detailed reaction scheme cannot be established until the dissociation energy of N_2 is known. Kaplan[1] has reported an enhancement of the first-positive (0, 0) band at 10,440A, which indicates a very selective population of the $v=0$ level of the $B^3\pi$ state of N_2 in the Lewis-Rayleigh afterglow. This observation was taken to suggest the 7.383-volt value for $D(N_2)$. Our experiment to determine $D(N_2)$ from the infrared spectrum of the "dark modification" of active nitrogen met with failure because our spectra did not indicate that the infrared (0, 0) band was abnormally intense. Forty-eight hour exposures on hypersensitized and pre-fogged I-Z plates show 31 bands of the N_2 first-positive system in the Lewis-Rayleigh glow, including the (0, 0) and (1, 1) bands. There is no indication in these spectra that $v'=0$ is populated in preference to $v'=1$, 2, or 3. The results reported here neither confirm nor contradict the 7.383 volt value for $D(N_2)$. Relations between these observations and the spectra of the air glow of the earth's atmosphere are discussed.

[1] J. Kaplan "The laboratory production of auroral afterglows," *The Emission Spectra of the Night Sky and Auroras* (The Physical Society, London, 1948), p. 118.

W6. Hindered Rotation in CH_3CF_3 and CH_3SiF_3. H. T. MINDEN* AND B. P. DAILEY, *Columbia University*.—The frequencies of certain low lying vibrations, which are inactive in the infrared and Raman spectra, may be roughly determined from the measurement of intensity ratios of vibrational fine-structure lines in the microwave spectrum. The torsional frequencies in the similar molecules CH_3CF_3 and CH_3SiF_3 have been determined to be 234 ± 40 cm^{-1} and 141 ± 30 cm^{-1}, respectively.[1,2] Using the parabolic approximation to a cosine barrier to internal rotation values of 3480 cal/mole for CH_3CF_3 and 1200 cal/mole for CH_3SiF_3 can be calculated. The value for the barrier in CH_3CF_3 is in good agreement with the more precise but less directly determined values calculated from thermodynamic data[3] and from combination and difference frequencies in the infrared spectrum.[4,5] The lower barrier observed for CH_3SiF_3 is apparently a result of the greater distance between interacting groups in this molecule. The change in rotational constant from ground state to excited state of torsion is also smaller for CH_3SiF_3.

* Now with RCA Laboratories Division, Princeton, New Jersey.
[1] Dailey, Minden, and Shulman, Phys. Rev. **75**, 1319 (1949).
[2] Minden, Mays, and Dailey, Phys. Rev. **78**, 347 (1950).
[3] Russel, Golding, and Yost, J. Am. Chem. Soc. **66**, 16 (1944).
[4] H. S. Gutowsky and H. B. Levine, J. Chem. Phys. **18**, 1297 (1950).
[5] Nielsen, Claassen, and Smith, J. Chem. Phys. **18**, 1471 (1950).

W7. The Infrared Spectrum of C_2D_2 Under High Dispersion. R. M. TALLEY* AND A. H. NIELSEN, *University of Tennessee*.—The infrared spectrum of C_2D_2 has been investigated by Stitt[1] and Randall and Barker[2] with prism instruments, and Nielsen[3] reported band centers for two strong bands. The present investigation was made with a grating spectrometer from 500 and 8000 cm^{-1} using path lengths up to 12-meter atmospheres. The infrared fundamentals were remeasured with high accuracy, and the inactive fundamentals were determined accurately for the first time from difference bands. The fundamental frequencies are 2701.84, 1764.9, 2439.10, 511.38, and 536.94 cm^{-1} vacuum in the order used by Herzberg. About 30 combination and difference bands, most of which are new, were measured and assigned. Enough information was available for the calculation of all of the anharmonic constants and the simple harmonic frequencies. All of the rotational and vibration-rotational constants were evaluated for the first time. The average B_0 value was 0.8482_7 cm^{-1} vacuum and B_e was 0.8550_7 gm-cm^2. Some new bands of C_2HD were also measured.

* Now at the U. S. Naval Ordnance Laboratory, White Oak, Maryland.
[1] F. Stitt, J. Chem. Phys. **8**, 56 (1940).
[2] H. M. Randall and E. F. Barker, Phys. Rev. **45**, 124 (1934)
[3] A. H. Nielsen, Phys. Rev. **57**, 346 (1940).

W8. Quenching in Fluorescence in Liquid Solution.* S. GRAND, F. C. COLLINS, *Polytechnic Institute of Brooklyn*, AND G. E. KIMBALL, *Columbia University*.—Equations for the quenching constant, k_Q, as a function of concentration and diffusion constant, have been derived using a diffusion flux equation obtained with a modified boundary condition.[1] Comparison with quenching data for any particular fluorescer leads to a value of the mean lifetime, τ_0, of the excited state in terms of a "virtual quenching radius," R'. R' involves the probability, α, of quenching per encounter as follows: $R'=\alpha R/(\alpha R+\rho)$, where R is the actual quenching radius and ρ is related to the mean diffusional jump length. The dependence of k_Q upon the concentration, c_0, of quencher leads to unique values for τ_0 and R'. Williamson and LaMer's[2] quenching data for fluorescein yield a τ_0 for fluorescein in excellent agreement with that obtained by Perrin[3] from depolarization measurements. τ_0 values for several other fluorescers, for which only quenching data exist, have been predicted. For long τ_0 and small R', k_Q becomes independent of c_0.

* Supported by the ONR.
[1] F. C. Collins and G. E. Kimball, J. Colloid Sci. **4**, 425 (1949).
[2] B. Williamson and V. K. LaMer, J. Am. Chem. Soc. **70**, 717 (1948).
[3] F. Perrin, Ann. Physik (10) **12**, 169 (1929).

W9. Spectroscopy from the Point of View of Communication Theory. Part I. Resolution.* GILBERT W. KING, *Albert D. Little, Inc.*, AND A. G. EMSLIE, *Williams College*.—The following factors which affect resolution, the numerical aperture of the instrument D/f, finite entrance and exit slits ($2d$), absorption of the prism B, and the finite width of the absorption line 2δ, have been treated simultaneously to get the exact relationship between the resolving power $2a$ and slit width. The results are presented graphically for various values of natural line width and the prism absorption. For B, δ, and d/δ large, the relationship can be approximated by a law of quadrature $3a^2=4d^2+(\delta+B)^2$, where a, d, and δ are measured in units characteristic of the diffraction pattern at wavelength λ, $\lambda f/\pi D$. The absorption coefficient in absolute units is multiplied by a quarter of the base of the prism to give B. In the practical range, the law of combination is much stronger, and the resolving power for small δ and B can actually be better than that expected from the geometrical optics of the slits alone.

* This work was done in part under a Grant-in-Aid from the American Cancer Society upon the recommendation of the Committee on Growth of the National Research Council.

W10. Does Circularly Polarized Light Magnetize a Refractive Medium? RICHARD M. BETH AND ANGUS F. BOND, *Western Reserve University*.—An extremely small but possibly detectable effect of circularly polarized light may be inferred as follows. As the light passes a fixed point in a refracting medium of index n, the electric vector of magnitude E describes a circle in a plane perpendicular to the direction of propagation; so does the electric polarization, $P=(n^2-1)E/4\pi$ esu. The mean positions of the displaced negative electrons,

N per cm³, thus described circular paths of mean radius $r=P/Ne$, while the much more massive positive charges remain practically at rest. Considered as amperian currents these electron movements represent a magnetization of $\pi r^2 \nu Ne/c$ emu, where ν is the frequency of the light. The resultant magnetic induction is $B=\nu(n^2-1)^2E^2/4Nec$ gauss in the direction of propagation for right circularly polarized light. With reasonable assumptions the order of magnitude of B is 10^{-13} gauss. Means of detection so far considered do not seem to offer adequate sensitivity.

W11. Further Calculations of X-Ray Diffusion in an Infinite Medium.* L. V. SPENCER AND FANNIE STINSON, *National Bureau of Standards.*—The polynomial expansion method for solving x-ray penetration problems has been applied to the following cases: (1) *Plane monodirectional* 1.33-Mev source in water. Particular attention was paid to the radiation scattered back of the source. The calculation was limited to scattered x-rays with energies above 200 kev. The results show the appearance behind the source of components high enough in energy to indicate that they must have been scattered two or more times. (2) *Point monodirectional* 1.33-Mev source in water. The mean square sideways displacement has been determined as a function of depth of penetration. The calculation has so far been carried out for energies above 730 kev and for penetrations up to about 10 mean free paths of the most penetrating component. (3) Calculations are also being made of the angular distribution of the scattered x-rays as a function of distance from a *point isotropic* Co^{60} source in water.

* Work supported by an ONR grant.

W12. On the Production and Detection of Polarized X-Rays. G. C. WICK AND M. MAY, *University of California, Berkeley.*—It will be shown that the bremsstrahlung emitted at a (small) angle to the direction of the electron beam striking an x-ray target can be quite considerably polarized even at very high energies. Use has been made of the simple Weizsäcker-Williams method, but some checks based on the more accurate Bethe-Heitler formulas will be discussed. The detection of γ-ray polarization by pair-creation has been discussed in a similar manner; the results will be compared with those of Berlin and Madansky.[1] The main difficulties in the application of these ideas seem to arise from multiple scattering of the electrons. An attempt to estimate the effect of multiple scattering in some typical cases has been made.

[1] T. H. Berlin and L. Mandansky, Phys. Rev. 78, 623 (1950).

W13. On the Nonspecular Reflection of Electromagnetic Waves.* VICTOR TWERSKY, *New York University.*—The nonspecular reflection of plane electromagnetic waves of arbitrary polarization and angle of incidence by certain perfectly conducting surfaces, composed of either semicylindrical or hemispherical bosses on an infinite plane, was analyzed. Solutions for the problem of the single boss were extended, subject to the single-scattering hypothesis, to obtain the far field solutions for certain small finite patterned distributions and both small finite and infinite uniform random distributions of bosses of radii small compared with the wavelength. It was found for certain values of the parameters that the reflected radiation consisted only of either the specular or the scattered contributions, while for other values one of the scattered contributions, either the parallel or perpendicular compohent vanished. The results also indicated the occurrence of an extremum in the reflected radiation in the vicinity of the specular angle of reflection, which for certain ranges of the parameters for the small finite distributions was a minimum rather than a maximum. For these cases there was also some critical angle of incidence (not necessarily $\pi/2$, or grazing incidence) for which the reflection at the specular angle was completely specular.

* The research reported in this paper has been made possible through support and sponsorship extended in part by the Geophysical Research Directorate of the Air Force Cambridge Research Laboratories.

SATURDAY AFTERNOON AT 2:15

Schermerhorn 501

(L. W. MCKEEHAN presiding)

Metals

X1. The Interaction of 5*d* Shells in Tungsten. IRVIN ISENBERG, *University of Chicago.*—The contributions of the Fermi energy and electrostatic interaction of different polyhedra to the elastic constants of tungsten are quite small compared to the measured values. If one assumes that the contributions from the energy of the lowest 6*S* state and from the many body forces arising from the non-orthogonality of the wave functions of different ions are also small then the major part of the elastic constants is due to the 5*d* exchange energy. Because of the short range nature of these interactions only nearest and next nearest neighbors need be considered and one can neglect the contribution made by terms involving the first derivative of the second nearest neighbor interaction energy. One can then solve for the first and second derivatives of the nearest neighbor interaction and the second derivative of the next nearest neighbor interaction in terms of the elastic constants. The two second derivatives are positive and roughly equal while the first derivatives are positive and roughly equal while the first derivative is quite small. These values may be interpreted in terms of an antiferromagnetic array in tungsten as proposed by Zener.[1]

[1] C. Zener, Phys. Rev. (to be published).

X2. Perturbed Energy Bands in Transition Alloys. J. E. GOLDMAN, *Carnegie Institute of Technology.*—The electronic specific heat, low temperature magnetic properties, Hall effect, and the electrical resistivity in copper-nickel alloys containing more than 60 percent copper are not readily explained in terms of the usually applied band theory. The latter requires that the 3*d* band in nickel be filled by the 4*s* electrons contributed by copper when the composition reaches 60 percent copper, and that with further additions of copper the alloy behave as a metal with completely closed inner shells. A theory is proposed in which these properties are ascribed to the statistical fluctuations in local concentration of nickel atoms which are calculable for a perfectly random alloy from the binomial coefficients. It is suggested that when a cluster containing an atom and its 12 nearest neighbors is predomi-

nantly nickel (>7 nickel atoms), the resulting perturbation in the periodic potential shifts the band upwards in a manner analogous to that predicted by Slater and by James for the case of impurities in a semiconductor. In the neighborhood of such a cluster, there will exist vacant *d*-states into which electrons can be excited from the highly dense Fermi surface and thereby contribute significantly to the specific heat. Calculations based on this hypothesis and certain simplifying assumptions give good quantitative agreement with specific-heat and magnetic data.

X3. Free Energy Changes in the $\beta_1-\beta^1$ Transformation in the Alloy AuCD.* D. S. LIEBERMAN, T. A. READ, AND L. C. CHANG, *Columbia University.*—Single crystals of AuCd undergo a diffusionless phase transformation from an ordered body-centered cubic structure above the transition temperature to an orthorhombic structure below it. The low temperature orthorhombic phase consists of an aggregate of domains or a single domain depending on the annealing procedure of the sample. The relative orientation of the domains in the aggregate correspond to the various crystallographically equivalent transformation lattice shears.† If a bending moment is applied to the specimen as it is cooled through the transformation temperature, a deformation is produced which remains substantially the same even upon release of the load. On subsequent heating under various loads, the original cubic structure is recovered, as is likewise the original shape of the specimen which had existed above the transformation temperature. Use has been made of this phenomenon to study the free energy difference between the two phases as a function of temperature. The various loads applied upon heating the deformed specimen oppose the transformation. Deflection and hence degree of transformation were observed as a function of temperature and the applied load, and thus the transformation temperatures as a function of the external work done by the sample.

* This work was supported by the AEC.
† L. C. Chang and T. A. Read, J. Metals (January 1951).

X4. Measurements of Atomic Mobility in Binary Alloys by Means of the Pair-Reorientation Effect. A. S. NOWICK, *University of Chicago.*—The anelasticity associated with stress-induced reorientation of pairs of solute atoms[1] is utilized to study atomic mobility in homogeneous substitutional alloys. From the time of relaxation, τ, obtained at each temperature by measurement of elastic after-effect (for $\tau>20$ sec) or of an internal friction peak (for $\tau<1$ sec), the corresponding diffusion coefficient may be obtained. Since the time required for a measurement is of the order of the mean time for a single atomic jump, the atomic mobility may be obtained at temperatures considerably below those at which macroscopic diffusion measurements can be made. The method is applied to silver-zinc and silver-indium alloys; the heat and entropy of activation for the elementary diffusion process are obtained as a function of alloy composition. The data obtained by this method are compared with conventional diffusion data for these alloys.

[1] C. Zener, Phys. Rev. **71**, 34 (1947).

X5. Measurement of Carbon Diffusion in Metallic Carbides. G. C. KUCZYNSKI AND R. W. LANDAUER, *Lewis Laboratory, NACA.*—The rate at which excess metallic inclusions are consumed by carbon diffusing in from a surface, is utilized for measurement of the diffusion coefficients of carbon in metallic carbide lattices. Under certain conditions easily realized in practice a simple solution of the flow equation can be obtained. From the measurements of the average diameter of metallic inclusions as a function of time at a fixed distance from the interface, the diffusion coefficient of carbon at a given temperature can be calculated using the above mentioned solution.

X6. Self-Diffusion in Cobalt. FOSTER C. NIX AND FRANK E. JAUMOT, JR., *University of Pennsylvania.**—The self-diffusion of cobalt has been measured using radioactive Co^{60}. The radioactive Co^{60} was evaporated onto the surface of pure cobalt samples. The absorption coefficient in cobalt of the complex spectrum of the radioactive isotope was required in the mathematical analysis used. This was determined under conditions similar to those present in the diffusion samples. The data at 1050°C, 1150°C, and 1250°C, indicate that the self-diffusion coefficient for cobalt is given approximately by $D=0.37\exp(-67000/RT)$ cm^2 sec^{-1}.

* This work was supported by the ONR.

X7. Inertia of Oscillating Ferromagnetic Domain Walls. GEORGE T. RADO, *Naval Research Laboratory.*—A domain wall driven by a sinusoidal external field, $H=H_0\exp(i\omega t)$, is shown to have the same apparent mass per unit area, m, as that derived by Döring[1] and Becker for the wall in uniform motion, even though in the oscillatory case the spin orientations are found to be functions of $(x-\int v dt)$ and t. Döring's approximation ($K\ll 2\pi M_s^2$) is used. Phenomenological damping torques, assumed by Kittel (to be published) and others in discussing uniformly moving walls, are not now considered. Nonlinearities are avoided by restricting H_0 and ω to the range $\gamma H_0\ll\omega\ll\gamma(2K/M_s)$. The wall velocity, v, is obtained from the "solvability condition" of an inhomogeneous classical eigenvalue equation. If H is applied along $[0, 1, \bar{1}]$, the 90° wall separating two semi-infinite domains (having equilibrium magnetizations along $+y$ and $+z$, respectively) oscillates along the x axis and, as expected, $v=(2^{\frac{1}{2}}M_s/i\omega m)H$. The domain rotations are shown to influence the time-dependent demagnetizing field essential for wall oscillation, but such interactions are negligible here because of the frequency restriction $\omega\ll\gamma(2K/M_s)$. Experimentally identified wall resonances[2] are examined.

[1] W. Döring, Z. Naturforsch. **3a**, 374 (1948).
[2] Rado, Wright, and Emerson, Phys. Rev. **80**, 273 (1950).

X8. The Initial Susceptibility of Nickel under Tension. B. N. BROCKHOUSE,* *University of Toronto.*—The initial susceptibility (χ) of a very pure nickel wire has been measured under various tensional stresses (Z) between room temperature and the Curie point. The results are found to depend upon the structure of the specimen. For annealed nickel the quantity χZ is independent of Z if the stresses are applied in order of increasing magnitude and if no plastic deformation occurs. If boundary movements do not contribute to χ then χZ is independent of the annealing temperature. At temperature below 150°C the temperature variation of χZ is in agreement with the recent theory of Döring.[1] At higher temperatures χZ increases monotonously to the Curie point but at a smaller rate than Döring's low temperature theory predicts. For cold-worked nickel χZ is always smaller than for annealed nickel and has a significantly larger temperature dependence. This fact together with the difference in purity of the specimens used accounts for much of the difference between these results and those of Scharff.[2]

* Now at the Chalk River Laboratories, National Research Council of Canada.
[1] W. Döring, Z. Physik **124**, 501 (1948).
[2] G. Scharff, Z. Physik **97**, 73 (1935).

X9. Heat Treatment of Iron-Silicon Alloys in a Magnetic Field. MATILDA GOERTZ, *Bell Telephone Laboratories. Introduced by* R. M. BOZORTH.—In an investigation of the magnetic properties of iron-silicon alloys it has been found that heat treatment in a magnetic field is effective for alloys containing between two and ten percent silicon. The maximum effect was obtained at about 6.4 percent silicon, in agreement with preliminary work by O. L. Boothby and H. J. Williams. An effect of this kind on lower silicon contents has already been

obtained independently by Mihara.[1] The low crystal anisotropy and the magnitude of the Curie temperature (≈700°C) are favorable for effective magnetic anneal. After annealing in pure hydrogen at 1300°C, the magnetic anneal increases the maximum permeability by a factor of about 5, to 300,000. In a single crystal of 6.5 percent silicon, magnetized parallel to a [100] direction, the hysteresis loop is squared by the magnetic anneal, and the maximum permeability is increased from 50,000 to 3,800,000, the highest ever reported for any material. Heat treating this crystal in a transverse field lowers the permeability to about 40,000 and the shape of the hysteresis loop becomes similar to that for an ordinary anneal.

[1] K. Mihara, unpublished report. See "Magnetic Development in Japan during World War II." U. S. Naval Technical Mission to Japan, pp. 46–55 (1946). ATIS No. 3380.

X10. Formation of Oxide Films on Chromium Steels. H. J. YEARIAN, *Purdue University.*—Electron micrographs of the surface of chromium steels taken after increasing periods of oxidation at temperatures of 500°C to 700°C show that a uniform film of small crystallites is quickly formed; most of the growth thereafter is confined to small localized regions. These regions of local attack form at random positions on the metal surface, growth rapidly at first, then more slowly in the form of nodules; new growth centers are formed continuously. As oxidation proceeds the local growths gradually coalesce to form a continuous scale which may be removed mechanically, leaving a quite uniform oxide film. The density and rate of growth of the nodules increase with increase of time and temperature of oxidation and with decrease of the chromium content of the alloy. X-ray diffraction shows that αFe_2O_3 is the principal component of the nodules, whereas transmission electron diffraction (of stripped films) indicates a high proportion of Cr_2O_3 in the thin film substrate. Experiments to determine the cause of the localized atrack will be described.

X11. Effect of Oxide Films on the Internal Friction of Cadmium Single Crystals.* S. SHAPIRO AND T. A. READ, *Columbia University.*—Andrade[1] and Harper and Cottrell[2] have shown that thin oxide films have an important effect on the plastic behavior of cadmium or zinc single crystals as observed in creep or tension tests. In the present work internal friction measurements have been made by the composite quartz oscillator method[3] on cadmium single crystals which do and do not have oxide films of the type studied by Andrade. The crystals were grown by the Bridgman method from New Jersey Zinc Company 99.999 percent cadmium, and the oxide film was made by immersing the specimen in a 0.1M Cd NO_3 solution for 30 minutes. Preliminary results indicate that the oxide film results in a much more rapid rise in internal friction with increase in vibration amplitude, particularly in the range of amplitude in which an increase in internal friction is produced by the measurement. When the oxide film is removed and the crystal is allowed to recover for several hours, the internal friction behavior returns to that observed before oxidation. It will be pointed out that this result makes it impossible to ascribe the effect of oxide films on plastic properties simply to an inhibiting effect on dislocation formation at the specimen surface.

* This work supported by the ONR.
[1] E. N. DaC. Andrade, Nature **164**, 536 (1949).
[2] S. Harper and A. H. Cottrell, Proc. Phys. Soc. (London) Sec. B 331 (1950).
[3] T. A. Read, Phys. Rev. **58**, 371 (1940).

X12. On a Mechanism Causing a Logarithmic Scale Growth. I. J. EPSTEIN AND K. LEHOVEC, *Signal Corps Engineering Laboratories.*—The rate of growth of a scale on a metal is investigated under the following assumptions: (1) The rate determing step is the diffusion of metal ions through the scale. (2) The equilibrium concentration of electrons in the scale is low compared with that of the diffusing metal ions. Under these conditions there arises a space charge in the scale from the diffusing ions which together with the image charge on the metal gives a potential hindering the movement of the ions. This causes the growth to change from the well-known parabolic law which holds in the initial phases of growth to a logarithmic law:

$$d = 1.2 \times d_0 \ln[(t/t_0)+1] \quad (\text{for } t \gg t_0),$$

where d is the thickness of the scale, t is the time, $t_0 = 2\epsilon\epsilon_0/N_0^2 e v b$ and $d_0 = (2\epsilon\epsilon_0 kT/N_0 e^2)$[1] [$\epsilon_0 = 8.86 \times 10^{-14}$ amp sec/volt cm, k Boltzmann constant, e elementary charge, ϵ dielectric constant, v volume of a scale molecule, N_0 concentration of metal ions in the scale at the metal boundary, b ionic mobility in the scale].

SATURDAY AFTERNOON AT 2:00

Pupin 301

(H. C. TORREY presiding)

Mostly Magnetic Resonance and Nuclear Magnetic Moments

Y1. The Microwave Faraday Effect. G. F. HULL, JR. AND R. G. BARNES, *Dartmouth College.**—The microwave analog of the Faraday effect has been found experimentally at wavelengths in the 3-cm region.[1] Materials which exhibit this effect are paramagnetic salts $MnCl_2.4H_2O$ and $MnSO_4.H_2O$. For these salts the Faraday rotation has been measured from 7850 to 9800 Mc and for various values of magnetic field up to 1350 gauss. The equation for the Faraday effect $\theta = RLH$, where θ is the angular rotation of the plane of polarization, L the path length, H the magnetic field, and R the Verdet constant, is found to be valid. The average value of the Verdet constant for $MnSO_4.H_2O$ is 0.93×10^{-3} min per cm gauss, and 3.46×10^{-3} min per cm gauss for $MnCl_2.4H_2O$. Variation in the Verdet constant with frequency has been found for both salts. Measurements have also been made of the dielectric constant and permeability of $MnCl_2.4H_2O$ over the same frequency band. From these values the index of refraction can be obtained. The variation of index of refraction can then be compared with the variation found theoretically from the Faraday effect measurements.

* Assisted by the ONR.
[1] M. C. Wilson and G. F. Hull, Jr., Phys. Rev. **74**, 711 (1948).

Y2. The Magnetic Moment of ^{99}Tc. KARL G. KESSLER AND WILLIAM F. MEGGERS, *National Bureau of Standards.*—The hyperfine structure of the 30 strongest lines of ^{99}Tc in the wavelength region 2900 to 5000A has been investigated with a Fabry-Perot interferometer and prism spectrograph. The 2.1 mg sample[1] of ^{99}Tc was excited in a liquid-nitrogen-cooled beryllium hollow cathode discharge tube filled with helium

gas at about 1 mm pressure. A nuclear spin of $9/2\hbar$ has been determined for this isotope.[5] The magnetic moment of the nucleus has been calculated from the splitting of the $4d^6\,(^5D)\,5s\,{}^6D$ terms in the $^{99}_{43}$Tc I spectrum. Calculations using the Goudsmit-Fermi-Segrè formula[3,4] yield a value of 5.2 ± 0.5 nuclear magnetons for the magnetic moment. Additional corrections for the effect of the mass of, and charge distribution in, the nucleus[5] may increase this value 10 to 20 percent, thereby approaching the theoretical Schmidt limit[6] of 6.79 nm for a $^2G_{9/2}$ state.

[1] Loaned by the AEC.
[2] K. G. Kessler and W. F. Meggers, Phys. Rev. **80** (to be published).
[3] S. Goudsmit, Phys. Rev. **43**, 636 (1933).
[4] E. Fermi and E. Segrè, Z. Physik **83**, 729 (1933).
[5] M. F. Crawford and A. L. Schawlow, Phys. Rev. **76**, 1310 (1949).
[6] Th. Schmidt, Z. Physik **106**, 358 (1937).

Y3. The Paramagnetic Spectrum of Ammonium Chrome Alum.* ARTHUR F. KIP, R. MALVANO,† AND CHARLES F. DAVIS, *M.I.T.*—A dynamic method[1] has been used to investigate the paramagnetic resonance spectrum of ammonium chrome alum single crystals below the sharp transition which occurs at about 80°K.[2] A fraction of the usual static magnetic field is 60-cycle modulated, and variation in the paramagnetic absorption with applied field is observed on a CRO. Microwaves in the 1- and 3-cm range have been used. Below the transition, the simple theory of Weiss[3] cannot be used. Difficulties include the presence of at least two Stark splittings,[4] and probably one other; and a large displacement of certain lines from their expected positions. Measurements at various angles determine which lines correspond to which ion in the unit cell. In this chrome alum as well as in all others tested, low intensity lines reported earlier[1] are found and are identified as due to forbidden transitions in which $\Delta m \neq \pm 1$.

* This work has been supported in part by the Signal Corps, the Air Materiel Command, and ONR.
† While on an Italian National Research Fellowship, aided by the Fulbright Fund.
[1] R. Malvano and M. Panetti, Phys. Rev. **78**, 826 (1950).
[2] B. Bleaney and R. P. Penrose, Proc. Phys. Soc. **60**, 395 (1948).
[3] P. R. Weiss, Phys. Rev. **73**, 470 (1948).
[4] B. Bleaney, Phys. Rev. **75**, 1961 (1949).

Y4. The Microwave Spectrum of Ammonium Chrome Alum. JULIAN EISENSTEIN, *University of Wisconsin*.—Problems involved in the theoretical interpretation of the experimental results of Kip, Malvano, and Davis will be discussed. Features of the spectrum which are not well understood are the nonuniform spacing of certain lines and the existence, below the transition temperature, of several different zero-field splittings. The following hypotheses for explaining these features must probably be rejected: existence of small crystalline fields of rhombic symmetry, magnetostriction, local field effects, and inversion of the level scheme.

Y5. Theory of Paramagnetic Resonance Line Breadths in Diluted Crystals. P. W. ANDERSON, *Bell Telephone Laboratories*.—It is shown that Margenau's "statistical theory" of line broadening[1] applies approximately to spin-spin broadening in diluted paramagnetic crystals. Contrary to a current argument, the line breadth varies directly as the concentration, while the center intensity does not vary greatly with concentration. The line shape in the limit of low concentration is dispersion type. An extension of Margenau's work to the problem in which there is a minimum distance of perturbers from the absorbing atom indicates that the center intensity probably varies as $(1+c)$, where c is the fractional concentration; this agrees fairly well with Van Vleck's results[2] which are valid at concentration 1, since the ratio of center intensity as $c\to 0$ to that obtained by Van Vleck is about 1:2.24. It is concluded that experimental results of various laboratories indicating a falling-off of intensity with concentration must be explained on the basis of other mechanisms, such as spin-lattice interaction or exchange effects.

[1] H. Margenau, Revs. Modern Phys. **8**, 22 (1935).
[2] J. H. Van Vleck, Phys. Rev. **74**, 1168 (1948).

Y6. Theory of Magnetic Resonance in $N^{14}O^{16}$.* MAURICE KARNAUGH AND HENRY MARGENAU, *Yale University*.—The methods of Margenau and Henry[1,2] have been applied, with slight modifications, to the calculation of the magnetic resonance spectrum of the lowest state of $N^{14}O^{16}$. This yields a symmetric six-line spectrum arranged in three hyperfine doublets. Values of the applied magnetic field for the resonances corresponding to the six transitions ($\Delta M_J=0$, $\Delta M_J=1$) at the fixed microwave operating frequency have been calculated. These values agree with the microwave absorption data of R. Beringer and J. G. Castle, Jr. (unpublished) to within 0.07 percent. The calculated separations of the doublet components lie within the range of experimental error. Comparison of the coupling energy of the nuclear and orbital magnetic moments in $N^{14}O^{16}$ and $N^{15}O^{16}$ is consistent with the ratio of the magnetic moments of the nuclei of the two nitrogen isotopes as obtained by the nuclear magnetic resonance method.[3]

* This work is supported by the ONR.
[1] H. Margenau and A. Henry, Phys. Rev. **78**, 587 (1950).
[2] A. Henry, Phys. Rev. **80**, 549 (1950).
[3] W. G. Proctor and F. C. Yu, Phys. Rev. **77**, 716 (1950).

Y7. Electron-Nuclear Interactions in Paramagnetic Ions. E. F. CARR AND C. KIKUCHI, *Michigan State College*.—The invariance requirement leads to the expression

$$-a_1\mathbf{L}\cdot\mathbf{I}+a_2\left\{\frac{3\mathbf{I}\cdot\mathbf{r}\mathbf{S}\cdot\mathbf{r}}{r^5}-\mathbf{I}\cdot\mathbf{S}\right\}-a_3\mathbf{S}\cdot\mathbf{I}$$

for the electron-nuclear interaction potential. In the case of atomic hfs, where J is a good quantum number, the interaction potential reduces to $a_J\mathbf{I}\cdot\mathbf{J}$, and experiment gives only the effective coupling constant a_J. For a paramagnetic ion in a crystal, however, the magnitudes of two of the coupling constants can be evaluated from the experimental data, provided a suitable value is assumed for the third constant. The coupling constants for the Cu^{++} ion have been evaluated for various values of the third constant, using Ingram's value[1] $\Delta\nu_{II}/\Delta\nu_{\perp}=8.3$. These constants will be compared with the spectroscopic value. Also their relation to the nuclear specific heat[2] will be discussed.

[1] D. J. E. Ingram, Proc. Phys. Soc. **A62**, 664 (1949).
[2] R. J. Benzie and A. H. Cooke, Nature **164**, 837 (1949); also J. A. Brinkman, Master's thesis, Michigan State College, for the theoretical analysis.

Y8. Dependence of the Magnetic Shielding of Nuclei Upon Molecular Orientation. N. F. RAMSEY,* *Harvard University*.—The theory[1] of the magnetic shielding of nuclei in molecules has been extended to determine the dependence of the magnetic shielding upon the rotational magnetic quantum number of the molecule. With the previous notation[1] and with the subscripts of σ indicating the molecular magnetic quantum number, it is found for diatomic molecules in the first rotational state that

$$\sigma_{m=1}-\sigma_0=\frac{e^2}{10mc^2}\left(0\left|\frac{3z^2-r^2}{r^3}\right|0\right)-\frac{a^3a_3I}{5\mu_{NM}}\left(\frac{2Z\mu_{NM}}{Ia}-\frac{H_r}{MJ}\right).$$

The second term of this expression can be evaluated as in the earlier theory.[1] In principle, $\sigma_{m=1}-\sigma_0$ can be determined experimentally from molecular beam measurements. A measurement of this difference in shielding therefore determines the average value of $(3z^2-r^2)/r^3$ which should provide a check on the electronic wave function used in calculating the similar though different quantity $(3z^2-r^2)/r^5$ that is used in determining the quadrupole moment of the deuteron.

* Work partially supported by joint program of ONR and AEC.
[1] N. F. Ramsey, Phys. Rev. **78**, 699 (1950).

Y9. An Improved rf Spectrometer: g-Factor Ratios Li^7/Li^6 and Cl^{35}/Cl^{37}. G. D. WATKINS AND R. V. POUND, *Harvard University*.—A radiofrequency spectrometer of improved noise figure, similar in principal to one previously described,[1] has been developed. The cathode-coupled 6J6 oscillator is retained but the tank is decoupled from the plate by a resistance equal to the resonance impedance of the tank, and a resistance-loaded "plate" choke is placed in the cathode return. (The first prevents loading of the tank by the tube, the second reduces shot current noise.) A broad band rf amplifier and delayed level stabilization are used. A modulated electronic resistance supplies an artificial "absorption" for absolute calibration. The noise figure, measured at 3 Mc by using this calibrator, is the ideal 2 at low oscillation levels. It rises with level becoming 7 at 0.5 volt rms measured at the tank, and above this rises as the square of the level. With this spectrometer, the nuclear g-factor ratio of Li^7 to Li^6 was measured in an aqueous solution of normal abundance LiCl and found to be 2.64091 ± 0.00001. The nuclear g-factor ratio of Cl^{35} to Cl^{37} in the same solution was measured to be 1.2013 ± 0.0001.

[1] R. V. Pound and W. D. Knight, Rev. Sci. Instr. 21, 219 (1950).

Y10. Nuclear Magnetic Moment Ratios of Isotopic Pairs.* N. I. ADAMS, III, T. F. WIMETT, AND F. BITTER, *M.I.T.*—In view of the importance of accurate determinations of the nuclear moments of isotopic pairs,[1-3] apparatus has been assembled to extend the range and possibly the precision of such measurements. These include: Helmholtz coils producing fields up to 2000 gauss; a new barrel-type electromagnet[4] with usable fields up to 30,000 gauss; stable null circuits; and special "phase lock-in" oscillator circuits[5] which generate the two resonance radiofrequencies from harmonics and subharmonics of a single stable crystal oscillator. The fields in these magnets are sufficiently well controlled so that with the stable circuits developed, the structure of very narrow lines can be studied in detail. A preliminary result for the rubidium isotopes is $Rb^{87}/Rb^{85}=2.033380\pm0.000028$ which is in agreement with previous less accurate determinations.[1]

* This work has been supported in part by the Signal Corps, the Air Materiel Command, and ONR.
[1] A. Bohr, Phys. Rev. 73, 1109 (1948).
[2] F. Bitter, Phys. Rev. 76, 150 (1949).
[3] A. Bohr and V. F. Weisskopf, Phys. Rev. 77, 94 (1950).
[4] F. Bitter, R. L. E. Quarterly Progress Report, M.I.T. p. 37, July, 1950.
[5] L. F. Koerner, Bell Labs Record, February, 1950.

Y11. Integral Relationships Among Nuclear Magnetic Moments. ENOS E. WITMER, *University of Pennsylvania*.—The ratio μ/μ_p has been determined now for a large number of nuclei to a high degree of precision. Using these values and correcting for diamagnetism, it is found that in most cases $\mu=kC$, where C is a constant and k is an integer, which is 1876 for the proton. Thus the values for n^1, H^1, H^2, H^3, Be^9, B^{11}, F^{19}, P^{31}, K^{39}, and Sc^{45} are in reasonable accord with this formula. The correction for diamagnetism was made by the formula $H_s'/H=0.259\times10^{-4}Z^{1/3}$. Evaluating the constant C gives apparently $\mu=k(11\times61)(1-\alpha/2\pi)\mu_N$.

Y12. Ratio of Quadrupole Moments of Cl^{35} and Cl^{37}.* R. GUNTHER-MOHR, S. GESCHWIND, AND C. H. TOWNES, *Columbia University*.—Recent measurements of the ratio of the quadrupole moments of Cl^{35} and of Cl^{37} by several observers using different methods are in disagreement by amounts considerably outside the limits of the quoted experimental errors. Because of these uncertainties we have redetermined the ratio $eqQ(Cl^{35})/eqQ(Cl^{37})$ from the microwave spectra of CH_3Cl, ClCN, and GeH_3Cl. The coupling ratio for CH_3Cl was 1.2691 ± 0.0003, for ClCN was 1.2682 ± 0.0006 and for GeH_3Cl was 1.2670 ± 0.0005. It seems clear that the apparent ratio of quadrupole coupling constants of the two Cl isotopes depends slightly on the molecular environment. The two molecular effects which might change the apparent quadrupole couplings from one molecule to another are the pseudo-quadrupole effect of Foley and the variation of zero point vibration with isotopic mass. Reasonable estimates indicate that these effects are much too small to account for the observed change. A likely explanation of the change in quadrupole coupling ratios with molecular environment is that an anisotopic polarization of the Cl nuclei occurs in the molecular electric fields, giving rise to an anisotropic polarization energy which depends in the same way on the angular momentum quantum numbers as does the quadrupole energy itself. The ocrresponding polarization coupling constant is

$$\tfrac{3}{4}e(\alpha_s-\alpha_z)\left\langle\frac{\rho(3\cos^2\theta_m-1)}{r^4}\right\rangle,$$

which depends on the molecular environment in a different manner than eqQ. Estimates of this effect which are subject to large possible uncertainties also gave a value smaller than that measured.

* Work supported jointly by the Signal Corps and ONR.

Y13. Nuclear Electric Quadrupole Splitting in Crystalline I_2.* R. V. POUND, *Harvard University*.—Resonant absorption of rf magnetic energy occurs in I_2, with no applied static magnetic field, because of interaction between the nuclear electric quadrupole moment of I^{127} and the crystalline and molecular electric field gradient. The resonances of polycrystalline samples can be broadened, and consequently reduced in intensity, by the application of a magnetic field. Apparatus previously described[1] has been modified to obtain improved sensitivity through detection of an audiofrequency component in the cavity output resulting when a magnetic field is applied periodically. The two resonances, $\pm5/2\leftrightarrow\pm3/2$ and $\pm3/2\leftrightarrow\pm1/2$, reported by Dehmelt[2] have been observed at temperatures from 300° to 4°K. The higher line moves from 644.4 to 642.8 Mc whereas the lower one goes from 331.3 to 334.0 Mc, both with decreasing temperature. The breadths increase, from about 35 and 45 kc at 300°K, with decreasing temperature, but at 4°K the relaxation time T_1 is of the order of seconds. The broadening at low temperatures is apparently caused by strains in the sample and depends upon its preparation and past history.

* Supported in part by the joint program of the ONR and AEC.
[1] R. V. Pound, Phys. Rev. 79, 685 (1950).
[2] H. G. Dehmelt, Naturwiss. 17, 398 (1950).

Y14. Investigation of Nuclear Effects in Paramagnetic Salts at Low Temperatures. STEPHEN MALAKER, *Oak Ridge National Laboratory*.—Several ions of the iron group possess a nuclear spin by virtue of which they have a magnetic moment. The hyperfine structure coupling of this nuclear magnetic moment with the magnetic moment of the electron cloud gives rise to a Schottky specific heat anomaly at about 0.1 degree K. in the region where the specific heat goes at T to the -2 one can make specific heat measurements by an ac bridge method without recourse to calorimetry. A single crystal of cobalt ammonium sulfate hexahydrate has been studied and the results show that the nuclear specific heat of CO (divalent) is of the order calculated from microwave absorption measurements.

SATURDAY AFTERNOON AT 2:15

Havemeyer 309

(JAMES RAINWATER presiding)

Neutrons; Nuclear Masses

Z1. Coherent Neutron-Proton Scattering by Liquid Mirror Reflection.* G. R. RINGO AND M. T. BURGY, *Argonne National Laboratory* AND D. J. HUGHES, *Brookhaven National Laboratory.*—A measurement of the coherent neutron-proton scattering amplitude, utilizing total reflection of slow neutrons from a liquid hydrocarbon, has been reported.[1] As the result ($-3.75\pm.03\times10^{-13}$ cm) was significantly different from existing values, the measurement was repeated with a series of liquids and at several neutron wavelengths in order to investigate systematic errors. The repetitions[2] showed no disagreement with the original value and indicated that the accuracy of the method could be increased. Final measurements have now been made utilizing a series of carefully purified hydrocarbon liquids, and a method in which no measurement of neutron wavelength is necessary. The ratio of the amplitude of hydrogen to that of carbon has been determined to 0.3 percent and the final value of the hydrogen amplitude, including the error (0.5 percent) in the carbon amplitude,[3] is $(-3.78\pm0.02)\times10^{-13}$ cm (standard error). This value is the weighted average of the results obtained with purified liquids.

* Under contract with the AEC.
[1] Hughes, Burgy, and Ringo, Phys. Rev. **77**, 291 (1950).
[2] Hughes, Burgy, and Ringo, Phys. Rev. **79**, 227 (1950).
[3] W. W. Havens and L. J. Rainwater, Phys. Rev. **75**, 1296 (1950).

Z2. Coherent Neutron Scattering from Gases.* A. W. MCREYNOLDS AND G. W. JOHNSON, *Brookhaven National Laboratory.*—Neutron coherent scattering lengths for gases have been determined by measurement of the index of refraction using a total reflection method. Well-collimated neutron beams from the Oak Ridge and Brookhaven reactors were reflected from surfaces of aluminum, Lucite, and ethylene glycols at angles of 2 to 5 minutes. Pressures of surrounding O_2, N_2, He, or A were varied from 1 to 150 atmospheres, and neutron indices of refraction of the gases relative to the mirror and to each other determined from variation of reflected intensity with pressure. The results for oxygen were in good enough agreement with the value 4.2 barns from diffraction measurements on solid oxides to verify that the same cross-section is derived from refraction in gases, although atomic binding differs. The cross section of nitrogen was found to be around 10 barns, compared to 4.6 barns (coherent) from diffraction results. Phase of scattering was positive for all four gases.

* Under contract with the AEC.

Z3. The Scattering of Fast Neutrons by Bismuth and Lead. C. E. MANDEVILLE AND C. P. SWANN, *Bartol Research Foundation.*—Scatterers of bismuth and lead have been irradiated by monoenergic fast neutrons of energy 4.3-Mev, produced by the deuteron-deuterium reaction in the Bartol Van de Graaff statitron. Scattered neutrons, elastic and inelastic, were observed by the method of recoil protons and photographic plates. Five thousand acceptable recoils were noted in 50,000 fields of view, examined in binocular microscopes. No neutrons appear to be inelastically scattered by Bi^{209}. If any inelastically scattered neutrons are present in the bismuth data, they must not exceed by more than ten percent the intensity of the elastic group. Two inelastically scattered groups appear in the lead data, corresponding to nuclear energy levels at ~1.3 Mev and ~3.3 Mev in naturally occurring lead. The inelastic cross section in lead for neutrons at 4.3 Mev is less than one-half the elastic cross section. Alternative interpretations of the data for lead will be discussed.

Z4. Neutron Scattering in the Resonance Region, II.* J. TITTMAN, C. SHEER, W. W. HAVENS, JR., AND L. J. RAINWATER, *Columbia University.*†—The slow neutron scattering chamber previously described[1] has been further developed, and used to measure the ratio of scattering to total cross section of gold in the low energy region as a function of neutron energy. The method utilizes "infinitely" thick targets, the scattering from which—for the geometry used—can be shown to be described essentially by a power series in (σ_s/σ_t), provided $(\sigma_s/\sigma_t)\lesssim0.5$ (where σ_s = scattering cross section and $\sigma^3=\sigma_s+\sigma_c$ = total cross section). The measurements are made by taking ratios of the scattered counts from the unknown (gold) target to that of a carbon reference target and comparing to a similar ratio using a standard target in place of the gold. Thick targets of Ni_3B and B_2O_3 were used for the latter and serve to calibrate the instrument since their cross sections are independently known. Detailed measurements on the 4.87-ev gold resonance have been completed and excellent agreement between the theoretical Breit-Wigner one-level formulas and the experimental curve of $(\sigma_s/\sigma_t)_{Au}$ has been obtained. These results in addition to the previously measured values of $\sigma_{so}\Gamma^2$ and the self-indication cross section for gold[1] yield the following parameters for the 4.87-ev excited level of Au^{198}:

J	Γ	Γ_{no}	σ_{pot} (nonresonant spin state)	σ_{pot} (resonant spin state)
1	0.172 ev	0.0211 ev	10.6 barns	13.3 barns

* Tittman, Sheer, Rainwater, and Havens, Phys. Rev. **77**, 748 (1950) will be referred to as I.
† This work was supported in part by the AEC.
[1] O. Frisch, K. Danske Vidensk. Selsk. **14**, No. 12 (1937); M. Goldhaber, private communication.

Z5. Neutron Scattering in the Resonance Region, III. C. SHEER, J. TITTMAN, W. W. HAVENS, JR., AND L. J. RAINWATER, *Columbia University.*—An extension of the slow neutron scattering measurements on gold, as previously reported,[1] into regions of higher energy, has been carried out. Results of these scattering measurements between 30 ev and 500 ev will be reported and compared with transmission data in the same region. Since the cross section of gold in this region is quite low, a thick target is geometrically unfeasible and hence accurate determinations of σ_s/σ_t by this method is impractical. However, the ratio of counts scattered from the gold target to that scattered from a carbon reference target, which is roughly proportional to σ_s/σ_t, will be shown. These measurements indicate that this method is quite sensitive in locating weak levels which have an appreciable percentage of capture. For example, strong dips in the curve of σ_s/σ_t *vs* energy have been found at 75 ev and 300 ev indicating the presence of levels which are so weak that their presence is barely suggested by the transmission curve. The measurement of neutron scattering from silver by this method has been started. Preliminary results for the 5.1-ev and 16-ev resonances will be presented.

[1] Tittman, Sheer, Rainwater, and Havens, Phys. Rev. **77**, 748 (1950) and preceding paper.

Z6. Slow-Neutron Resonance Levels in Separated Tungsten Isotopes. W. SELOVE,* *Argonne National Laboratory.*—The transmission of separated tungsten isotopes has been measured for slow neutrons in the resonance region, with resolution of a few percent up to 50 or 100 ev, and, with rapidly worsening resolution, up into the kev region. Three of the four major isotopes have been investigated—182, 183, and 186. The results show level spacings of the order of 10 to 30 ev in 182, 20 ev in 183, and several hundred ev in 186. These results will be discussed in relation to various factors concerning level densities.

* Now at Harvard University.

Z7. Interaction of Neutrons with Electrons in Liquid Bismuth. W. W. HAVENS, JR., L. J. RAINWATER, AND I. I. RABI, *Columbia University.*—The neutron electron interaction has been determined by measuring the cross section of liquid bismuth as a function of neutron wavelength. This cross section decreases by 3 percent between 0.33A and 1.33A. The change in cross section is caused by (a) neutron capture, (b) liquid scattering, (c) relative velocity effect, (d) neutron electron interaction. The spin dependent scattering is small because the total cross section of solid Bi is less than 0.5 barn at 5.5A. The capture cross section of this Bi is 0.035 barn at 0.026 ev, determined by the pile oscillator. The relative velocity correction is $0.011\lambda^2$. The liquid effect was investigated by Placzek, Nyboer, and Van Hove, who proved that the type of structure did not alter the liquid effect a great deal. The liquid correction used was $0.095\lambda^2$. After applying these corrections the residual change was attributed to the neutron electron interaction. The neutron electron cross section can be expressed in terms of the Born approximation by giving an interaction potential V acting over a volume τ. Assuming τ a spherical volume of radius 2.8×10^{-13} cm, V is (5300 ± 1000) ev. An uncertainty of 650 ev is due to statistical consideration, the additional uncertainty being due to the uncertainty in the corrections applied.

Z8. Thermal Neutron Transport in Water. FRANK J. SISK* AND EDWARD C. CAMPBELL, *Oak Ridge National Laboratory.*—To obtain appropriate values for the thermal neutron transport parameters for water, a detailed experimental study was made of the one-dimensional flux near a black (cadmium) plane. The situation was realized experimentally in the large water tank surmounting the thermal column of the Oak Ridge Graphite Reactor. The flux distribution was determined by activation of small thin In foils spaced axially below a cadmium disk. In each run two of the foils were exposed at constant location for monitoring. By solving the transport integral equation for this problem by the method of numerical iteration, an excellent representation of the experimental data is obtained with the following values of the transport parameters: diffusion length, 2.67 ± 0.02 cm; transport cross section, 75 ± 3 barns per H_2O molecule; absorption cross section, 0.57 ± 0.02 barn per molecule. The measured neutron flux at the Cd plane was found to be 18.6 percent of the extrapolated asymptotic flux at the plane.

* United States Naval Post Graduate School.

Z9. Thermal Neutron Time-of-Flight Velocity Selector. F. G. P. SEIDL, H. PALEVSKY, R. F. RANDALL, AND W. THORNE,* *Brookhaven National Laboratory.*†—An instrument similar to the Argonne "chopper" has been put in operation to separate thermal neutrons from the Brookhaven pile according to their times of flight between a shutter and a detector consisting of one or more $B^{10}F_3$ counters. The associated equipment includes a circuit to introduce a time delay (1 to 16 millisec) between the closing of the shutter and actuation of the gating circuits which consecutively open and close twelve recording channels. Means are provided to collimate and monitor the incident beam and for testing the circuits. Special features are: (1) The shutter design prevents the slowest neutrons of one burst from arriving in the detector simultaneously with the fastest neutrons of the following burst. (2) Each recording channel feeds a scaler of high-resolution which eliminates dead-time corrections at large counting rates. A time-of-flight resolution, i.e. $(t_{max}-t_{min})/t_{av}$, of 5 μsec/m is available from $\sim$0.2 ev to below 0.001 ev. Slides will be presented illustrating details of construction and the performance.

* Member of the firm Thorne-Brown Company, Westport, Connecticut.
† Under contract with the AEC.

Z10. Inelastic Scattering of Low Energy Neutrons in Graphite.* G. W. JOHNSON, H. PALEVSKY, AND D. J. HUGHES, *Brookhaven National Laboratory.*—The velocity selector described in the preceding abstract was used to measure the inelastic cross section in graphite. The measurements were made with wavelengths longer than the Bragg cutoff (6.7A) to avoid coherent scattering. Graphite is suited for checking the existing inelastic scattering theories as it exhibits no spin dependent scattering and the isotopic incoherence is negligible. In addition the correction for neutron capture is small. For room temperature graphite the cross section was measured as 0.8 barn at 7A. In the range 7 to 11A the cross section was proportional to wavelength. The room temperature value, as well as the wavelength dependence of the cross section, is in agreement with the theory of J. Pomeranchuk and A. Akhieser[1] and D. Kleinman.[2] The temperature dependence of the cross section is now under investigation.

* Under contract with the AEC.
[1] A. Akhieser and J. Pomeranchuk, J. Exp. Theor. Phys. USSR 17, 770 (1947).
[2] D. Kleinman, Chicago Physical Society Meeting, Nov. 1950, Paper V8 Bu 11. Am. Phys. Soc. 25, No. 5, 38 (1950).

Z11. Analysis of Neutron Capture Gamma-Radiation Spectra in Heavy Elements. J. DAVID JACKSON, *McGill University,* AND B. B. KINSEY, *National Research Council, Chalk River.*—The spectrum of gamma-radiation from slow neutron capture has been observed for a number of heavy elements ($A>70$) with a coincidence pair spectrometer.[1] These spectra have been analyzed in terms of the evaporation model of the nucleus. In general, the spectra are in excellent qualitative agreement with the evaporation theory, having peaked distributions with the maximum at relati vely low energies (in some cases below the experimental cutoff of about 2.5 Mev). The level densities implied by these spe^{C}tra are, on the whole, in accord with the predictions of a nucle^{a}r model such as a modified Fermi-Dirac gas. However, near $N=50$, 126, the observed spectra change character markedly, having distributions which peak at relatively high energies. This means that the level densities are greatly decreased from "normal" values. On the shell model this decreased level density is to be expected because of the great reduction in the number of degrees of freedom of motion within the nucleus that occurs st the closed shells. Experimental data are not available at present for $N\approx82$, but at $Z\approx50$ there is no evidence for a departure from the normal evaporation model, despite the closed proton shell.

[1] Kinsey, Bartholomew, and Walker, Phys. Rev. 77, 723 (1950); 78, 77, 481 (1950).

Z12. Mass Difference of Rubidium and Potassium Isotopes.* E. E. HAYS, P. I. RICHARDS, AND S. A. GOUDSMIT, *Brookhaven National Laboratory.*—The magnetic time-of-flight mass spectrograph, based on principles described previously,[1] has been assembled. The magnet used is on loan from the Westinghouse Research Laboratories. It was de-

signed several years ago by E. U. Condon and J. A. Hipple and produces a homogeneous field inside a sphere of 19" diameter. Ions from a pulsed ion source move in a helix of about 12.5-cm radius and 12.5-cm height. An electron multiplier ion detector was specially designed by L. G. Smith. A timer, using the general principles of Loran equipment was built by the Electronics Division of our Laboratory. Up to six revolutions can be measured with accuracy. The total time is about 400 μsec for K, and 850 μsec for Rb. By pulse-matching this can be measured to .01 μsec which represents 1 millimass unit. Precision measurements have not yet been possible because of the occurrence of small surface potentials, but it is expected that methods may be developed to correct for their effects. The differences between neighboring masses are not affected by the perturbing electric fields. Preliminary results indicate that the mass difference between Rb^{85} and Rb^{87} is 1.999, and between K^{39} and K^{41} it is 2.000, with an uncertainty slightly over 1 millimass unit.

* Research carried out at Brookhaven National Laboratory, under the auspices of the AEC.
[1] S. A. Goudsmit, Phys. Rev. **74**, 622–623 (1948).

Z13. Microwave Study of Silicon and Sulfur Masses.* S. GESCHWIND AND R. G. GUNTHER-MOHR, *Columbia University.*—From the absolute frequencies of the $J=1\rightarrow 2$ transition in $O^{16}C^{12}S$, corresponding to S^{32}, S^{33}, and S^{34}, which were measured to an accuracy of 5 kc or better, the mass difference ratio $S^{33}-S^{32}/S^{34}-S^{32}$ was calculated, neglecting zero-point vibrations, and was found to be $S^{33}-S^{32}/S^{34}-S^{32}=0.500714\pm0.00003$. This is to be compared with Davisson's[1] value of 0.50060 ± 0.00008 obtained from nuclear reactions. Similarly, the mass difference ratio $Si^{30}-Si^{29}/Si^{30}-Si^{28}$ was determined from the isotopic shift in the $J=1\rightarrow 2$ transition in SiH_3Cl^{35}, and was found to be $Si^{30}-Si^{29}/Si^{30}-Si^{28}=0.49941\pm0.00005$. This is very good agreement with the value 0.499341 ± 0.00006, obtained by Duckworth, *et al.*,[2,3] from mass spectrometer experiments. The agreement between the two sets of results justifies an earlier estimate of the outside limit of the error introduced by neglecting zero-point vibrations.

* Work supported by the Signal Corps and the ONR.
[1] P. W. Davisson, Phys. Rev. **75**, 757 (1949).
[2] Duckworth, Preston, and Woodcock, Phys. Rev. **79**, 188 (1950).
[3] Duckworth and Preston, Phys. Rev. **79**, 402 (1950).

Errata Pertaining to Papers A4, C11, IA3, IA6, K14, L7, N9, Q4, S1, S11, S14, T2, V1, X1, Y11, and Z4

A4, by Author Unknown. Instead of Author Unknown read Martin J. Swetnick, New York University.

C11, by James Terrell. In the title N^{14} should read N^{11}. In footnote 1, Phys. Rev. (to be published) should read Phys. Rev. **80**, 1076 (1950).

IA3, by Frank L. Hereford. In lines 5 and 6, Increases up to 200 volts should read Increases up to 20 volts. In lines 10 and 11, increased positive ion space charge field should read decreased positive ion space charge field.

IA6, by R. Braunstein adn. J. W. Trischka. A footnote * should be added reading, Assisted by the ONR. In lines 9 and 10, with a diode containing and plates at positive, should read, with a diode containing end plates at positive.

K14, by Jerome Rothstein. In line 16, casual anomalies should read causal anomalies. In line 26, casuality should read causality.

L7, by R. G. Luce and J. W. Trischka. A footnote * should be added reading, Assisted by the ONR. In line 12, The breadth of the lines made it possible, should read, The breadth of the lines made it impossible.

N9, by H. S. Thomas. A footnote * should be added reading, Associated with Tung-Sol Lamp Works, Inc.

Q4, by H. R. Johnson, J. G. Ingersoll, and M. W. P. Strandberg. The title should read, **Microwave Spectrum of Ketene.***† H. R. JOHNSON, J. G. INGERSOLL, AND J. W. P. STRANDBERG, *M.I.T.*, AND J. H. GOLDSTEIN, *Harvard University.*‡ Footnote † should read, Preliminary work has been published by Bak, Knudsen, Madsen, Raestrup, and Anderson, Phys. Rev. **79**, 190 (L) (1950). Footnote‡ should read, Now at Emory University, Georgia.

S1, by Kenneth G. McKay. In line 3, use should read used. In reference 1, J. G. McKay should read K. G. McKay.

S11, by J. C. M. Brentano and E. M. Nakaji. A footnote * should be added reading, This paper has been withdrawn before the Meeting, but could not be taken out of the text for technical reasons. The results as given are affected by contact potentials and circuit characteristics. Further experiments are in progress.

S14, by Rolf W. Landauer. In line 14, 3×10^{-13} should read 3×10^{-14}. In line 14, 200 should read 20.

T2, by L. Yaffe and F. Brown. In line 2, the reaction $P^{32}(n,\gamma)P^{32}$ should read, the reaction $P^{32}(n,\gamma)P^{33}$.

V1, by Helen M. Friedman and James Rainwater. In line 20, $\pi-\rho$ events our of, should read, $\pi-e$ events out of.

X1, by Irvin Isenberg. The next to the last sentence should read, The two second derivatives are positive and roughly equal while the first derivative is quite small.

Y11, by Enos E. Witmer. In the last line, $\mu=k(11\times61)(1-\alpha/2\pi)\mu_N$, should read, $\mu=[k/(11\times61)](1-\alpha/2\pi)\mu_N$.

Z4, by J. Tittman, C. Sheer, W. M. Havens, Jr., and L. J. Rainwater. In line 4, previously described,[1] should read, previously described (I). In line 11, $\cdots\sigma^3=\sigma_s+\sigma_s\cdots$, should read, $\cdots\sigma_1=\sigma_s+\sigma_s\cdots$.

Author Index to Papers Presented at the Annual Meeting

Accardo, C., E. Jamgochian, and K. Lehovec—S7
Adams, N. I., III, T. F. Wimett, and F. Bitter—Y10
Alburger, D. E., E. der Mateosian, M. Goldhaber, and S. Katcoff—T5
Alers, P. B., J. W. McWhirter, and C. F. Squire—R1
Allis, W. P.—U2
Alpher, R. A. and R. C. Herman—B5
Amble, E. and A. L. Schawlow—Q7
Anderson, James L., Peter G. Bergmann, and Robert Penfield—K10
Anderson, P. W.—Y5
Appleyard, R. K.—D9
Austern, Norman—G8
Babiskin, Julius—R2
Barbour, Ian and Lawrence Greene—EA11
Bardeen, J.—U3
Bartlett, A. A. and K. T. Bainbridge—I7
Benedict, W. S., Earle K. Plyler, and Curtis J. Humphreys—W3
Bennett, W. H.—F3
Benson, James M.—GA16
Bergmann, Peter G.—K12
Bernardini, G.—H3
Berry, Chester R.—S13
Betchov, R.—GA4
Beth, Richard A. and Angus F. Bond—W10
Bethe, H. A. and E. E. Salpeter—G10
Birkhoff, Garrett—MA2
Bleuler, E., J. W. Blue, and A. C. Johnson—T7
Bloembergen, N. and P. J. van Heerden—I6
Boehmer, H. W. and H. S. Bridge—EA3
Boggild, J. K. and F. H. Tenney—EA10
Booth, E. T.—H1
Borst, L. B.—M2
Bottom, Virgil E.—HA5
Bramson, H. J. and W. W. Havens, Jr.—V5
Branscomb, Lewis M.—W5
Braunstein, R. and J. W. Trischka—IA6
Bray, Ralph—S6
Brentano, J. C. M. and E. M. Nakaji—S11
Bridge, H., F. Harris, and B. Rossi—A3
Britten, Roy—A8
Brockhouse, B. N.—X8
Brown, L. M. and R. P. Feynman—K8
Brown, S. C.—F1
Brueckner, Keith A. and K. M. Watson—V9
Brueckner, Keith A.—N3
Burstein, E., P. L. Smith, and D. L. Arenberg—HA7
Callen, Herbert B. and Theodore A. Welton—B4
Camac, M., D. Corson, R. Littauer, A. Shapiro, A. Silverman, R. Wilson, and W. Woodward—V4
Carr, E. F. and C. Kikuchi—Y7
Chang, Chieh-Chien and Boa-Teh Chu—GA7
Chapman, S.—U1
Charnes, A. and E. Saibel—GA15
Cheston, W. B.—V2
Chubb, Talbot—IA5
Cleland, M. R. and P. S. Jastram—V13
Cocconi, G. and V. Cocconi Tongiorgi—V7
Conforto, A. M. and R. D. Sard—V6
Cool, R. L. and O. Piccioni—EA2
Crawford, J. W., Jr., E. E. Kintner, and Clark Goodman—I4
Cronemeyer, Donald C.—HA4
Darling, B. T.—K15
Dash, William C.—HA9
Davis, Kenneth E.—A11
Davisson, James W. and Elias Burstein—HA8
Deutsch, Martin—P2
Donaldson, John and W. W. Watson—B12
Dresden, M. and R. L. Petritz—B2
Duckworth, Henry E., George S. Stanford, and John M. Olson—G1
Dunlap, W. C., Jr.—S2
Edwards, R. R., P. E. Damon, and H. M. Schwartz—T12
Eisenstein, Julian—Y4
Elliott, L. G. and J. L. Wolfson—T11
Ennis, W. W.—DA9
Epstein, I. J. and K. Lehovec—X12
Eshbach, J. R. and M. W. P. Strandberg—Q2
Eyges, L. and S. Fernbach—EA6
Feld, Bernard T.—G4
Fierz, M.—E2
Fluke, Donald J.—D10
Frank, Robert M.—K5
Fretter, W. B.—A5
Friedman, Helen L. and James Rainwater—V1
Frosch, R. A. and H. M. Foley—W4
Furry, W. H.—B11
Gallar, O.—I5
Garwin, Richard L.—DA15
Gelinas, R. W. and S. S. Hanna—C3
Geschwind, S. and R. G. Gunther-Mohr—Z13
Gilleo, M. Alten—S10
Goertz, Matilda—X9
Gokhale, B. V. and M. W. P. Strandberg—Q5
Goldberg, Joshua, Peter G. Bergmann, and Ralph Schiller—K11
Goldberger, M. L., F. Villars, and H. Feshbach—N2
Goldhaber, Maurice—M4
Goldman, J. E.—X2
Goldschmidt, G. H. and D. G. Hurst—HA11
Gove, H. E., and J. A. Harvey—C9
Grand, S., F. C. Collins, and G. E. Kimball—W8
Green, Alex E. S.—B3
Green, L. C., M. M. Mulder, C. W. Ufford, E. Slaymaker, E. Krawitz, and R. T. Mertz—K2
Greisen, K., G. Cocconi, and L. M. Bollinger—A1
Gross, E. P.—IA2
Gross, Leonard—T1
Guild, W. R.—D7
Gunther-Mohr, R., S. Geschwind, and C. H. Townes—Y12
Hancome, T. D. and C. W. Malich—DA8
Harvey, J. A.—C2
Hauser, W. and H. Feshbach—G6
Havens, W. W., Jr., L. J. Rainwater, and I. I. Rabi—Z7
Haworth, L. J.—M1
Hays, E. E., P. I. Richards, and S. A. Goudsmit—Z12
Heilens, Robert L.—HA12
Heller, Wilfried, and Warren Tanaka—D5
Heller, William R.—HA15
Herb, R. G., J. G. Trump, J. L. Danforth, and E. A. Burrill—I2
Hereford, Frank L.—IA3
Hill, David L.—G2
Hilliger, R. E. and M. W. P. Strandberg—Q3
Hintz, N. M.—DA3
Holt, R. B. and J. W. Meadows—DA4
Holzer, R. E. and David S. Saxon—N12
Hornbeck, G. A. and R. C. Herman—W1
Hornbeck, J. A.—F2
Hornbeck, J. W.—J2
Horton, C. W. and C. S. McCleskey, Jr.—HA14
Hughes, Vernon and Gardiner Tucker—L1
Hull, G. F., Jr. and R. G. Barnes—Y1
Hutchinson, Franklin—D11
Isenberg, Irvin—X1
Jackson, J. David and B. B. Kinsey—Z11
Jacobs, Donald H. and Michael May—N7
Johnson, G. W., H. Palevsky, and D. J. Hughes—Z10
Johnson, H. R., J. G. Ingersoll, and M. W. P. Strandberg—Q4
Johnson, M. H.—B14
Johnson, T. H.—M3
Kachickas, G. A. and L. H. Fisher—IA4
Kaplon, Morton F.—N4
Karnaugh, Maurice and Henry Margenau—Y6
Kauffman, John and Waller George—D3
Kerner, Edward H.—K1
Kessler, Karl G. and William F. Meggers—V2
King, Gilbert W. and A. G. Emslie—W9
Kittel, C.—HA1
Kip, Arthur F., R. Malvano, and Charles F. Davis—V3
Klahr, C. N.—S3
Koisky, H. G., T. E. Phipps, N. F. Ramsey, and H. B. Silsbee—L2
Koski, W. S.—I10
Kramer, R. L. and J. H. McMillen—GA12
Kraybill, H. L.—EA4
Kuczynski, G. C. and R. W. Landauer—X5
Kundu, D. N. and M. L. Pool—DA13
Laitone, E. V.—GA2
Landauer, Rolf W.—S14
Landon, H. H.—DA7
Langer, L. M. and R. J. D. Moffat—T10
Lauritsen, C. C.—P3
Lax, M., H. Feshbach, G. F. Chew, and H. W. Lewis—N1
Lederman, L. M., G. Bernardini, E. T. Booth, and J. H. Tinlot—V3
Lehovec, K.—S8
Leininger, R. F., E. Segrè, and F. N. Spiess—T15
Lepore, J. V.—G11
Levinger, J. S.—C13
Lindenbaum, S. J., G. Bernardini, and E. T. Booth—EA9
Lieberman, D. S., T. A. Read, and L. C. Chang—X3
Lobb, R. K.—GA5
Luce, R. G. and J. W. Trischka—L7
Lundby, Arne and Leona Marshall—C14
Macklin, P. A., L. I. Lidofsky, and C. S. Wu—T13
Maienschein, F. C. and Joe Keagy Bair—I9
Malaker, Stephen—V14
Malich, C. W.—DA11
Mandeville, C. E. and C. P. Swann—Z3
Marcuvitz, N.—B7
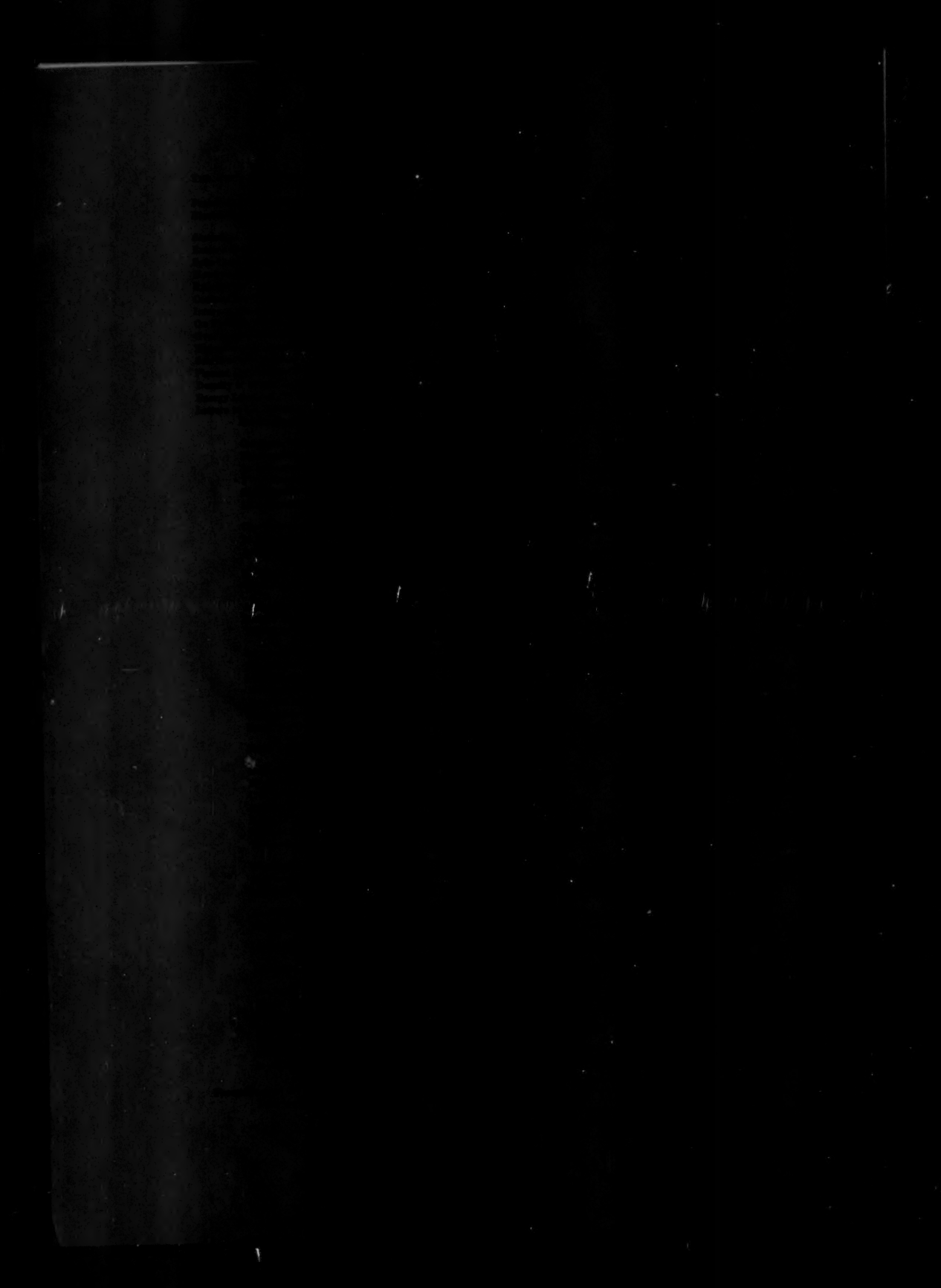
Margolis, Bernard—G5
Marshak, R. E.—H2
Marshall, L.—C15
Maurer, R. D. and Melvin A. Herlin—R8
May, Albert—GA13
McClure, G. W.—A2
McKay, Kenneth G.—S1
McKibben, J. L. and Keith Boyer—I1
McNulty, W. P., Jr. and Franklin Hutchinson—D12
McReynolds, A. W. and G. W. Johnson—Z2
Merz, Walter J.—HA3
Miller, D. H., E. C. Fowler, and R. P. Shutt—I14
Miller, P. H., D. M. Warschauer, and T. T. Reboul—S9
Miller, S. L., J. Kraitchman, B. P. Dailey, and C. H. Townes—Q6
Millett, Walter E.—V12
Minden, H. T. and B. P. Dailey—W6
Mohler, Fred L. and Vernon H. Dibeler—N11
Mooradian, A. J., S. A. Hoshowsky, and W. E. Gordon—GA9
Moore, D. C.—V10
Morowitz, Harold J.—D13
Nierenberg, W. A.—L3
Nix, Foster C. and Frank E. Jaumot, Jr.—X6
Nowick, A. S.—X4
Ovadia, J. and P. Axel—T3
Oxley, C. L., R. D. Schamberger, and O. A. Towler, Jr.—A9
Patterson, G. N.—MA4
Peaslee, D. C.—B1
Perry, Alfred M.—EA8
Peters, B., H. L. Reynolds, and D. M. Ritson—A6
Phillips, G. C. and N. P. Heydenburg—DA2
Pickup, E. and L. Voyvodic—EA1
Pitkanen, Paul and W. H. Furry—B10
Plass, Gilbert N. and John A. Wheeler—K7
Pollard, E. C.—P4
Pollard, Ernest and A. E. Dimond—D6
Pool, M. L., D. N. Kundu, P. E. Weiler, and T. W. Donaven—DA12
Potter, C. A., A. V. Bushkovitch, and A. G. Rouse—L4
Pound, R. V.—Y13
Preston, W. M. and Clark Goodman—I3
Prince, M. and Melvin A. Herlin—R5
Pryce, M. H. L.—E1
Rabi, I. I.—J1
Racah, Giulio—G7
Rado, George T.—X7
Rainwater, James and W. W. Havens, Jr.—P1
Ramsey, N. F.—V8
Reed, S. G., Jr.—GA14
Reitz, John R. and J. L. Gammel—S15
Reynolds, Geo. T., F. B. Harrison, and D. Hill—I11
Richardson, John M.—IA1
Richman, Monroe F.—I12
Rinehart, John S.—N6
Ringo, G. R., M. T. Burgy, and D. J. Hughes—Z1
Roberts, D. M. and R. M. Steffen—T6
Roberts, James H., Lillian Darlington, and Jack Haugsnes—C7
Robson, J. M.—E3
Rochlin, R. S. and B. D. McDaniel—C1
Rogers, John D. and Dudley Williams—L6
Rorschach, H. E., Jr. and Melvin A. Herlin—R3
Rosenfeld, A. H., L. Marshall, and S. C. Wright—C16
Rosenthal, Jenny E.—N8
Ross, Frederick W.—GA3
Rothstein, Jerome—K14
Rubinson, William and William Bernstein—T14
Ryder, E. J.—S4
Schaaf, S. A. and F. S. Sherman—GA11
Schellman, J. A. and W. Kauzmann—HA13
Schiff, Harry—G9
Schmidt, F. H., G. L. Keister, D. I. Meyer, and W. E. Gross—I8
Schmitt, Roland W.—R7
Schulz, L. G.—HA10
Schwartz, R. N.—B15
Schweinler, H. C.—HA2
Scott, W. T.—EA5
Seidl, F. G. P., H. Palevsky, R. F. Randall, and W. Thorne—Z9
Seitz, Frederick—S12
Selove, W.—Z6
Setlow, R. B.—D8
Shaknov, I.—T9
Shapiro, Anatole M.—EA7
Shapiro, S. and T. A. Read—X11
Shaw, R. P.—GA8
Shearer, J. W. and M. Deutsch—V11
Sheer, C., J. Tittman, W. W. Havens, Jr., and L. J. Rainwater—Z5
Shockley, W.—S5
Shoolery, J. N. and R. G. Shulman—L8
Shutt, R. P.—I13
Siegel, K. M.—GA10
Silverman, Shirleigh—W2
Sisk, Frank J. and Edward C. Campbell—Z8
Slater, J. C.—J3
Slawsky, Z. I.—MA3
Snowdon, S. C.—N10
Spencer, L. V. and Fannie Stinson—W11
Sperduto, A. and W. W. Buechner—DA5
Spetner, L. M. and J. S. Clark—V14
Stearns, M. B. and B. D. McDaniel—C8
Steele, M. C.—R6
Steinberger, J.—H4
Stelson, P. H. and W. M. Preston—DA10
Stevenson, Donald T.—T8
Stoner, R. G.—GA6
Strauch, Karl—C4
Sun, K. H., D. Harris, F. A. Pecjak, B. Jennings, A. J. Allen, and J. F. Nechaj—C5
Swann, W. F. G.—B6
Talley, R. M. and A. H. Nielsen—W7
Teller, Edward—MA1
Terrell, James—C11
Tetenbaum, S. J.—L5
Thaler, R. M. and A. O. Williams, Jr.—K3
Thomas, H. S.—N9
Thompson, Arthur C. and Wilfried Heller—D4
Thorndike, A. M. and A. W. Wotring—A10
Ting, L. and H. F. Ludloff—GA1
Tittman, J., C. Sheer, W. W. Havens, Jr., and L. J. Rainwater—Z4
Trigg, George L.—N5
Tucker, E. B.—C6
Twersky, Victor—W13
Van Dyke, Karl S., Gary D. Gordon, George F. Fisher, and William F. Palmer—HA6
Van Vleck, J. H.—K4
Van Patter, D. M., H. Enge, and W. W. Buechner—DA6
Visner, Sidney—B13
Voyvodic, L. and E. Pickup—A7
Waldman, B. and W. C. Miller—DA14
Walker, D.—C12
Wallace, P. R.—B8
Watanabe, Satosi—K13
Watkins, G. D. and R. V. Pound—V9
Watson, Hugh A., D. M. Van Patter, and W. W. Buechner—DA1
Watson, K. M. and R. N. Stuart—G12
Watson, K. M. and K. A. Brueckner—V9
Watson, M. T., W. D. Kennedy, and G. M. Armstrong—D2
Webber, R. T., F. A. Andrews, and D. A. Spohr—R4
Weiss, M. T. and M. W. P. Strandberg—Q1
Welton, T. A.—K9
Whitehead, W. D.—C10
Whitmer, Robert—B9
Wick, G. C. and M. May—W12
Wilson, Robert R.—A12
Witmer, Enos E.—Y11
Wolfenstein, Lincoln—G3
Wu, C. S. and L. Feldman—T4
Yaffe, L. and F. Brown—T2
Yagoda, Herman—V8
Yearian, H. J.—X10
Yovick, George—K6